

ATS-910-012
VOLUME 1

FINAL REPORT

FOR

ATS F&G

(PHASES B & C)

(17 OCTOBER 1969)

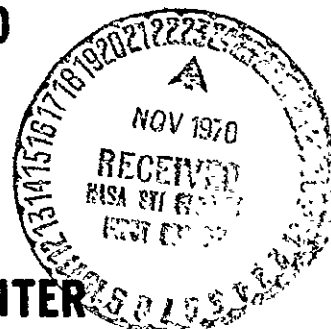
CONTRACT NO. NAS5-11609

PREPARED BY

FAIRCHILD HILLER CORPORATION
GERMANTOWN, MARYLAND

FOR

GODDARD SPACE FLIGHT CENTER
GREENBELT, MARYLAND



N71-10839

(ACCESSION NUMBER)

(PAGES)

CR-11149

(NASA CR OR TMX OR AD NUMBER)

G3

(CODE)

31

(CATEGORY)

FACILITY FORM 002



Reproduced by
**NATIONAL TECHNICAL
INFORMATION SERVICE**
Springfield, Va. 22151

N O T I C E

THIS DOCUMENT HAS BEEN REPRODUCED FROM THE BEST COPY FURNISHED US BY THE SPONSORING AGENCY. ALTHOUGH IT IS RECOGNIZED THAT CERTAIN PORTIONS ARE ILLEGIBLE, IT IS BEING RELEASED IN THE INTEREST OF MAKING AVAILABLE AS MUCH INFORMATION AS POSSIBLE.

RESTRICTED INFORMATION

This document contains information for government purposes which is not to be disclosed in whole or in part, except by authorized representatives of the United States Government, without the prior written consent of Fairchild Hiller Corporation's Space and Electronics Systems Division.

ATS-910-012
VOLUME 1

FINAL REPORT

for

ATS F&G

(PHASES B&C)

(17 OCTOBER, 1969)

Contract Number NAS5-11609

GODDARD SPACE FLIGHT CENTER

Contracting Officer: A. H. Wessels

Technical Officer: A. H. Sabelhaus

Prepared by

FAIRCHILD HILLER CORPORATION

Germantown, Maryland

Project Manager: I. Singer

for

GODDARD SPACE FLIGHT CENTER

Greenbelt, Maryland

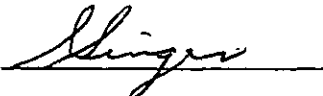
Approved: 

TABLE OF CONTENTS

<u>Paragraph</u>	<u>Title</u>	<u>Page</u>
SECTION I	INTRODUCTION	1-1
SECTION II	PROGRAM CONTROL	2-1
2.1	Schedule Milestones	2-1
2.2	Documentation	2-2
SECTION III	SYSTEMS ENGINEERING	3-1
3.1	Mission Objectives	3-1
3.1.1	Technological Objectives	3-2
3.1.2	Application Objectives	3-6
3.2	Spacecraft Design Description	3-19
3.2.1	Introduction	3-19
3.2.2	Spacecraft Description	3-20
3.2.3	Launch, Separation & Deployment	3-23
3.2.5	Electrical Subsystems	3-33
3.3	ATS-F Experiments	3-36
3.3.1	Instructional Television	3-36
3.3.2	Position Location and Aircraft Communication Equipment	3-41
3.3.3	Data Relay System	3-44
3.3.4	Spacecraft Attitude Maneuvering Optimal Control/Self-Adaptive Precision Pointing Spacecraft Attitude Control (SAMOC/ SAPPSAC)	3-52
3.3.5	Experiment Interfaces	3-58
3.4	Summary of System Characteristics	3-86
3.5	Major System Trade-offs	3-99
3.5.1	One Versus Two Equipment Modules	3-99
3.5.2	Lockheed Versus Goodyear Reflector	3-100
3.5.3	Titan Versus Atlas Centaur Launch Vehicles	3-101

F 111 2

PRECEDING PAGE BLANK NOT FILMED

PRECEDING PAGE BLANK NOT FILMED

TABLE OF CONTENTS

<u>Paragraph</u>	<u>Title</u>	<u>Page</u>
3.5.4	Cylindrical Versus Flat Solar Panels	3-102
3.5.5	Cubic Versus Circular Cross-Section for EVM	3-103
3.5.6	Trade-off Study of Fixed Vs. Rotating S-Band Feed	3-105
3.6	System Reliability	3-107
3.6.1	Reliability Prediction	3-107
3.6.2	Failure Mode, Effects and Criticality Analysis	3-123
3.6.3	Critical Reliability Areas	3-134
3.6.4	ATS Parts Assurance Program	3-142
3.6.5	Preferred Materials List	3-143
SECTION IV	STRUCTURAL SUBSYSTEM	4-1
4.1	Introduction	4-1
4.2	System Design Considerations	4-1
4.3	Structural Subsystem Detail Description	
4.3.1	EVM	4-7
4.3.2	Reflector Support Truss	4-18
4.3.3	Structural Hub	4-23
4.3.4	Solar Array Panels	4-24
4.3.5	Solar Array Panel Supporting Booms	4-24
4.3.6	Adapter, Spacecraft/Launch Vehicle	4-39
4.3.7	Fabrication and Accessibility Evaluation	4-40
4.3.8	EVM Venting	4-40
4.4	Equipment Location	4-40
4.4.1	Subsystem Component Layout	4-40
4.4.2	Experiment Layouts	4-56
4.4.3	Hub Mounted Equipment	4-56

TABLE OF CONTENTS

<u>Paragraph</u>	<u>Title</u>	<u>Page</u>
4.4.4	Alignment Provisions	4-61
4.5	Spacecraft/Adapter Separation Subsystem	4-61
4.5.1	Configuration Description	4-61
4.5.2	Electrical Subsystem	4-63
4.5.3	Instrumentation	4-64
4.6	Solar Array Deployment Subsystem	4-64
4.6.1	Launch Lock at the Release Mechanism	4-64
4.6.2	Deployment Actuation and Locking Mechanism	4-78
4.6.3	Electrical System	4-83
4.6.4	Instrumentation and Power Wiring	4-84
4.7	Materials	4-87
SECTION V	THERMAL CONTROL SUBSYSTEM	5-1
5.1	Thermal Subsystem for EVM	5-1
5.1.1	Thermal Louvers	5-3
5.1.2	Heat Pipes	5-4
5.1.3	Thermal Coatings	5-11
5.1.4	Multilayer Insulation	5-13
5.2	Solar Arrays	5-14
5.3	Reflector Support Truss	5-15
5.4	Reflector Hub Components	5-16
5.5	Ground Cooling	5-17
5.5.1	Laboratory	5-17
5.5.2	Pre-Launch Checkout Testing	5-17
SECTION VI	TRANSPONDER SUBSYSTEM	6-1
6.1	Introduction	6-1
6.2	Transponder Configuration	6-3
6.2.1	Receiver	6-3

TABLE OF CONTENTS

<u>Paragraph</u>	<u>Title</u>	<u>Page</u>
6.2.2	IF Amplifier	6-3
6.2.3	Synthesizer	6-6
6.2.4	Transmitters	6-6
6.2.5	Input-Output Circuitry	6-6
6.2.6	Monopulse Tracking Operation	6-6
6.2.7	Wideband Data Unit	6-6
6.3	RF Receive Section	6-8
6.3.1	Diplexers and Filters	6-8
6.3.2	RF Preamplifiers	6-8
6.3.3	Down-Converter Mixers	6-12
6.3.4	S- and L-Band Power Amplifier	6-13
6.3.5	UHF Transmitter	6-16
6.3.6	Tracking Beacon	6-19
6.3.7	RFI and T&FD Experiment	6-19
6.4	IF Amplifier	6-19
6.4.1	IF Distribution Networks	6-19
6.4.2	IF Amplifier	6-23
6.5	Frequency Synthesizer	6-29
6.5.1	Recommended Configuration	6-29
6.5.2	Circuit Operation	6-29
6.5.3	Phase Lock Loop Configuration	6-29
6.5.4	Reference Oscillator	6-33
6.5.5	Synthesizer Redundancy Switching	6-33
6.6	Monopulse System	6-34
6.6.1	Recommended Configuration	6-34
6.7	Wideband Data Link	6-39
6.7.1	System Configuration	6-39
6.7.2	Voltage Controlled Oscillators	6-39

TABLE OF CONTENTS

<u>Paragraph</u>	<u>Title</u>	<u>Page</u>
6.8	Command, Telemetry and Power Subsystems	6-42
6.8.1	Command, Telemetry and Power	6-42
6.8.2	Power Subsystem Interface	6-51
6.9	Physical Description	6-55
6.9.1	Layout	6-55
6.9.2	Components and Assemblies	6-55
6.9.3	Weight Allocation	6-60
6.9.4	Power Considerations	6-60
SECTION VII	PRIME FOCUS FEEDS	7-1
7.1	Introduction	7-1
7.2	Summary Description	7-2
7.2.1	X-Band Feed and Earth Viewing Horn	7-2
7.2.2	C-Band Feed	7-5
7.2.3	S-Band Feed	7-5
7.2.4	L-Band Feed	7-5
7.2.5	UHF Feed	7-6
7.2.6	VHF Feed	7-6
7.2.7	RF Design	7-6
7.2.8	X-Band Feed	7-6
7.2.9	C-Band Feed	7-12
7.2.10	S-Band Feed	7-12
7.2.11	L-Band Feed	7-27
7.2.12	VHF Feed	7-29
7.2.13	VHF Feed	7-29
7.2.14	X-Band Earth-Viewing Horn	7-32
7.2.15	Expected Performance Summary	7-36
7.3	Mechanical Design/Integration	7-39

TABLE OF CONTENTS

<u>Paragraph</u>	<u>Title</u>	<u>Page</u>
7.3.1	Layout	7-39
7.3.2	Component Design	7-39
7.3.3	Weight Allocation	7-47
SECTION VIII	PARABOLIC REFLECTOR	8-1
8.1	General Description	8-1
8.2	Physical Description	8-10
8.2.1	Hub Assembly	8-10
8.2.2	Rib Assembly	8-12
8.2.3	Reflective Surface Assembly	8-13
8.3	Properties And Characteristics	8-13
8.3.1	General	8-13
8.3.2	Material Properties	8-16
8.3.3	Mass Properties	8-21
8.3.4	Structural Characteristics	8-22
8.3.5	Dynamic Characteristics	8-22
8.3.6	Thermal Characteristics	8-23
8.3.7	Potential Problem Areas	8-23
8.4	Performance	8-24
8.4.1	Deployment And One-G Testability	8-25
8.4.2	Thermal Effects and Surface Deviations	8-25
8.4.3	RF Performance	8-34
8.4.4	Reliability	8-36
8.5	Design Procedure	8-36
8.5.1	General Design Approach	8-36
8.5.2	Design Optimization Process	8-37
8.5.3	Deleted	
8.5.4	Final Design Selection	8-41

TABLE OF CONTENTS

<u>Paragraph</u>	<u>Title</u>	<u>Page</u>
8.6	Manufacturing Procedure	8-41
8.6.1	Component Parts Fabrication	8-41
8.6.2	Reflector Assembly and Alignment	8-41
8.7	Spacecraft Integration	8-42
8.7.1	Spacecraft Interface Requirements	8-42
8.7.2	Reflector Alignment With Spacecraft	8-42
SECTION IX	ATTITUDE CONTROL SUBSYSTEM	9-1
9.1	Functional Description	9-1
9.1.1	Objectives of the ATS-F&G Mission	9-1
9.1.2	Attitude Control Subsystem Functional Performance Requirements	9-1
9.1.3	Review of Attitude Control Subsystem Functional Operation	9-5
9.1.4	Performance Versus Requirements	9-17
9.1.5	Interfaces Between ACS and other ATS Subsystems	9-20
9.1.6	Phase D Program Participants	9-25
9.2	Physical Description	9-26
9.2.1	Attitude Control Subsystem	9-26
9.2.2	Components	9-26
SECTION X	INTERFEROMETER	10-1
10.1	Introduction	10-1
10.1.1	Functional Description	10-3
10.1.2	Performance Summary	10-4
10.1.3	Development Summary	10-6
10.2	Functional Description	10-7
10.2.1	Subsystem Functional Arrangement	10-7
10.2.2	Functional Description, Spacecraft Equipment	10-10

TABLE OF CONTENTS

<u>Paragraph</u>	<u>Title</u>	<u>Page</u>
10.2.3	Performance Analysis Summary	10-18
10.2.4	Operational Modes	10-18
10.2.5	In-Orbit Testing and Operation	10-22
10.3	Subsystem Description	10-24
10.3.1	General Spacecraft Subsystem Description	10-25
10.3.2	Mass Characteristics	10-25
10.3.3	Power Consumption	10-25
10.3.4	Array and Front End Assembly Mechanical/ Thermal Design	10-30
10.3.5	Front End Subassembly Mechanical/Thermal Design Structural Design	10-32
10.3.6	Electronics Receiver/Converter Mechanical/ Thermal Design	10-34
10.3.7	Module Descriptions	10-37
10.3.8	Interface Description	10-48
10.3.9	Ground Transmitter Station	10-52
10.3.10	Ground Data Processor	10-54
SECTION XI	COMMANDABLE GRAVITY GRADIENT SUBSYSTEM	11-1
11.1	Functional Description	11-1
11.1.1	Functional Performance Requirements	11-1
11.1.2	Functional Operation and Performance	11-1
11.1.3	Interfaces	11-8
11.2	Physical Description	11-9
11.2.1	Coggs Layout/Location Mounting Characteris- tics	11-9
11.2.2	Design Characteristics	11-14
11.2.3	Thermal Characteristics	11-23
11.2.4	Power Characteristics	11-23
11.2.5	Mass Properties	11-23

TABLE OF CONTENTS

<u>Paragraph</u>	<u>Title</u>	<u>Page</u>
11.2.6	Reliability	11-26
SECTION XII	AUXILIARY PROPULSION SUBSYSTEM	12-1
12.1	Functional Description	12-2
12.1.1	Functional Performance Requirements	12-2
12.1.2	Component Functional Requirements	12-10
12.2	Functional Operation and Performance	12-13
12.2.1	Overall System	12-14
12.2.2	Components	12-18
12.3	Functional Interface Description	12-24
12.3.1	Spacecraft Interfaces	12-24
12.3.2	Input Interface Signals	12-24
12.3.3	Output Interface Signals	12-26
12.3.4	Telemetry	12-26
12.3.5	Power Interface	12-26
12.3.6	Thermal Interface	12-36
12.4	Physical Description	12-27
12.4.1	Overall APS	12-28
12.4.2	Component Physical Descriptions	12-32
SECTION XIII	TELEMETRY AND COMMAND SUBSYSTEM	13-1
13.1	Introduction	13-1
13.2	T&C Subsystem Description	13-8
13.2.1	Functional Description	13-8
13.2.2	Link Calculations	13-16
13.2.3	FDM-VHF Telemetry Link	13-21
13.2.4	Design Implementation	13-26
13.3	T&C Subsystem Components	13-29
13.3.1	Command Decoder/Distribution (CDD) Unit	13-29

TABLE OF CONTENTS

<u>Paragraph</u>	<u>Title</u>	<u>Page</u>
13.3.2	Data Acquisition and Control Unit	13-39
13.3.3	Spacecraft Clock	13-54
13.3.4	Data Switching Unit	13-58
13.3.5	T&C VHF Equipment	13-61
SECTION XIV	ELECTRICAL POWER SUBSYSTEM	14-1
14.1	Design Objectives	14-1
14.1.1	Voltage and Power Requirements	14-1
14.1.2	Solar Array Panels	14-2
14.1.3	Spacecraft Battery Configuration	14-3
14.1.4	Power Subsystem Performance	14-3
14.1.5	Summary of Design Objectives	14-4
14.2	Design Approach	14-5
14.2.1	Solar Array	14-5
14.2.2	Line Conditioning	14-9
14.2.3	Load Interface Circuits (LIC)	14-10
14.2.4	Summary of Design Approach	14-12
14.3	Selected Design	14-12
14.3.1	Solar Array	14-16
14.3.2	Power Busses	14-21
14.3.3	Battery Disconnect Plugs	14-22
14.3.4	Load Regulators	14-22
14.3.5	Battery Chargers	14-25
14.3.6	Battery	14-25
14.3.7	Summary of Selected Power Subsystem	14-26
14.4	Conditioned Power Profile	14-28
14.4.1	Telemetry and Command Subsystem	14-28
14.4.2	Attitude Control Subsystem	14-28

TABLE OF CONTENTS

<u>Paragraph</u>	<u>Title</u>	<u>Page</u>
14.4.3	Communications Subsystem	14-34
14.4.4	Experiment Packages	14-34
14.4.5	Total Conditioned Power Profiles	14-34
14.4.6	Depth of Discharge	14-47
14.4.7	Battery Charging Rates	14-50
14.5	Commands	14-50
14.6	Telemetry Monitors	14-53
14.6.1	Overall Functions	14-53
14.6.2	Specific Functions	14-54
SECTION XV	HARNES SUBSYSTEM	15-1
15.1	Introduction	15-1
15.1.1	Redundant Wiring	15-2
15.1.2	Shielded Wire Usage	15-4
15.1.3	Twisted Wire Usage	15-4
15.1.4	System Grounding	15-4
15.1.5	General Wire Sizing	15-5
15.1.6	Connector Pin Current Derating	15-6
15.2	Harness Operational Requirements	15-6
15.2.1	Battery Disconnect	15-7
15.2.2	Pyrotechnics System	15-7
15.2.3	Umbilical Interface	15-7
15.3	Harness Subsystem Configuration	15-7
15.3.1	General Earth Viewing Module Harness Layout	15-8
15.3.2	Experiment Module Layout	15-10
15.3.3	Service Module Layout	15-16
15.3.4	Communications Module Layout	15-23
15.3.5	Module Interface	15-25
15.3.6	External Harness Layout	15-25

TABLE OF CONTENTS

<u>Paragraph</u>	<u>Title</u>	<u>Page</u>
15.4	Harness Component Parts	15-29
15.4.1	Connectors	15-29
15.4.2	Wire	15-31
15.4.3	Terminal Junctions	15-33
15.4.4	Harness Weight Analysis	15-33
SECTION XVI	RADIO BEACON EXPERIMENT	16-1
16.1	Introduction	16-1
16.2	Functional Requirements	16-5
16.3	RF Design	16-7
16.3.1	Transmitter	16-7
16.3.2	Antenna Design	16-14
16.3.3	Triplexer Design Description	16-15
16.4	Physical Description	16-18
16.4.1	Layout	16-18
16.4.2	Component and Assemblies	16-18
16.4.3	Weight Allocation	16-21
16.4.4	Power Allocation	16-21
SECTION XVII	GROUND SUPPORT EQUIPMENT	17-1
17.1	Introduction and Summary	17-1
17.1.1	Design Guideline	17-1
17.2	Spacecraft AGE	17-2
17.2.1	Spacecraft Electrical AGE System Test Complex	17-2
17.2.2	Mechanical AGE	17-9
17.3	Attitude Control Subsystem AGE/BTE	17-18
17.3.1	ACS Test Station	17-18
17.3.2	Inertial Reference Assembly Test Station	17-22
17.3.3	Digital Operational Controller Test Station	17-24
17.3.4	Analog Backup Controller Test Station	17-24

TABLE OF CONTENTS

<u>Paragraph</u>	<u>Title</u>	<u>Page</u>
17.3.5	Actuator Control Electronics Test Station	17-26
17.3.6	Inertia Wheel Test Station	17-26
17.3.7	Earth Sensor Test Station	17-29
17.3.8	Star Tracker Test Station	17-29
17.3.9	Sun Sensor Test Station	17-32
17.3.10	Sun Sensor Electronics Test Station	17-35
17.4	Auxiliary Propulsion Subsystem AGE/BTE	17-37
17.4.1	Auxiliary Propulsion Subsystem Test Station	17-37
17.4.2	Thrust Measurement Test Station	17-38
17.5	Interferometer AGE/BTE	17-38
17.5.1	Interferometer Subsystem Test	17-40
17.6	Telemetry and Command	17-40
17.6.1	Subsystem AGE	17-43
17.7	Communication Subsystem AGE/BTE	17-44
17.7.1	Communications Test Set	17-46
17.8	Power Subsystem AGE/BTE	17-46
17.8.1	Switching Mode Regulator (SMR) Test Set	17-49
17.8.2	Battery Charger	17-50
17.8.3	Load Interface Circuit Test Set	17-50
17.8.4	Battery Test Set	17-53
17.8.5	Power Control Unit Test Set	17-53
17.9	Experiment Interface AGE	17-57
17.9.1	Power	17-57
17.9.2	Telemetry and Command	17-59
17.9.3	Experiment Loads	17-59
17.9.4	Test Point Panel	17-60
17.10	Spacecraft Simulators	17-60

TABLE OF CONTENTS

<u>Paragraph</u>	<u>Title</u>	<u>Page</u>
17.10.1	T&C Simulator	17-60
17.10.2	Transponder Simulator	17-65
SECTION XVIII	TEST PLANS	18-1
18.1	Introduction and Summary	18-1
18.1.1	Test Program Objectives	18-1
18.1.2	Test Program Approach	18-1
18.1.3	Test Approach	18-2
18.1.4	Test Program Description	18-7
18.1.5	Engineering Development Test Program	18-7
18.1.6	Integration, Design Verification, and Qualification of the EVM	18-8
18.1.7	Qualification of ATS Spacecraft Assembly	18-9
18.1.8	Flight Acceptance Tests	18-10
18.2	Engineering Development Test Program	18-10
18.2.1	General	18-10
18.2.2	Subsystem Development Tests	18-11
18.2.3	Thermal/Structural Model Tests	18-21
18.3	Qualification Tests	18-22
18.3.1	Subsystem Qualification	18-23
18.3.2	Prototype Spacecraft Qualification	18-32
18.4	Flight Acceptance Tests	18-37
18.4.1	Introduction	18-37
18.4.2	Subsystem Acceptance	18-37
18.4.3	Flight Spacecraft Acceptance	18-38

LIST OF ILLUSTRATIONS

<u>Figure</u>	<u>Title</u>	<u>Page</u>
2-1	Summary Pert Network	2-7
3.1-1	ITV Operational Configuration	3-8
3.1-2	PLACE Experiment	3-9
3.1-3	NIMBUS/AAP Relay DRS	3-10
3.2-1	Spacecraft Deployed Configuration	3-21
3.2-2	Exploded View of ATS-F	3-22
3.2-3	Launch Configuration Profile View	3-24
3.2-4	ATS F&G Launch and Acquisition Sequence	3-25
3.2-5	ATS Launch Configuration	3-26
3.2-6	Separation Sequence	3-27
3.2-7	Deployment Sequence	3-28
3.2-8	Orbital Configuration	3-31
3.2-9	Field of View at 94° Longitude and at 15° E Longitude for 5° Elevation above the Horizon	3-31
3.2-10	ATS F&G Functional Block Diagram	3-34
3.3-1	India Instructional Television	3-37
3.3-2	850 MHz Antenna Beam Coverage of India for ITV	3-40
3.3-3	PLACE Experiment	3-42
3.3-4	NIMBUS/AAP Data Relay DRS	3-46
3.3-5	S-Band Antenna Feed Array Along with Defining Coordinate System of Beams	3-48
3.3-6	Two-Satellite Tracking (NIMBUS/AAP)	3-49
3.3-7	DRS Command Operation Configuration	3-51
3.3-8	SAMOC/SAPPSAC Functional Block Diagram ATS-F On-Board Equipment	3-53
3.3-9	SAMOC/SAPPSAC Operational Configuration	3-57
3.3-10	Experiment Subsystem Block Diagram	3-59

LIST OF ILLUSTRATIONS

<u>Figure</u>	<u>Title</u>	<u>Page</u>
3.3-11	Frame Format for ATS F&G	3-62
3.3-12	ATS F&G Configuration	3-69
3.3-13	Communication Module Equipment Configuration	3-71
3.3-14	Experiment Module Configuration	3-73
3.3-15	EME Field of Views	3-83
3.4-1	Total Conditioned Normal Power	3-97
3.6-1	Reliability Pictorial Diagram State A	3-109
3.6-2	Reliability Pictorial Diagram State B	3-111
3.6-3	Reliability Pictorial Diagram State C	3-117
3.6-4	T&C Subsystem Reliability Diagram	3-125
3.6-5	Simplified Reliability Diagram, RF Interferometer	3-126
3.6-6	Power Subsystem Block Diagram	3-132
4.1-1	Orbital Configuration	4-3
4.1-2	Launch Configuration	4-5
4.3-1	Experiment Module Configuration	4-9
4.3-2	Interferometer	4-11
4.3-3	Service Module Structure	4-15
4.3-4	Communications Module Structure	4-19
4.3-5	Reflector Support Truss	4-21
4.3-6	Structural Hub	4-25
4.3-7	Solar Array	4-29
4.3-8	Solar Array Panel Supporting Booms	4-37
4.3-9	Adapter, Spacecraft/Launch Vehicle	4-41
4.4-1	Subsystem Component Layout	4-43
4.4-2	Subsystem Component Layout	4-45
4.4-3	Subsystem Component Layout	4-47
4.4-4	Subsystem Component Layout	4-51

LIST OF ILLUSTRATIONS

<u>Figure</u>	<u>Title</u>	<u>Page</u>
4.4-5	Component Arrangement-Experiment Module - Design Layout	4-57
4.4-6	Hub Equipment Layout (Proposed Configuration Small EME)	4-59
4.5-1	Electrical Subsystem For Initiating Spacecraft/ Adapter Separation Schematic	4-65
4.6-1	Semi-Cylindrical Solar Array Panels	4-67
4.6-2	Solar Array Release Mechanism	4-73
4.6-3	Solar Panel Deployment Sequenced	4-79
4.6-4	Hinge Lock Configuration	4-81
4.6-5	Pyrotechnic Electrical System	4-85
4.9-1	Shear/Bending Moment Diagrams	4-91
4.9-2	Components of Structural Subsystem	4-92
5.1-1	Earth Viewing Module	5-2
5.1-2	Thermal Louvers	5-5
5.1-3	Thermal Louvers ATS F&G	5-7
5.1-4	Typical Neat Pipe 90° Miter Bend	5-9
5.1-5	Parabolic Dish Model for Millimeter Wave Communications Satellite	5-10
5.1-6	Heat Pipe Development Laboratory	5-12
6.2-1	ATS-F Communication Subsystem Block Diagram	6-4
6.2-2	Simplified IF Amplifier Block Diagram	6-5
6.2-3	Simplified Synthesizer Block Diagram	6-7
6.3-1	Transponder Diplexers and Filters	6-9
6.3-2	Typical TDA Frequency Response	6-11
6.3-3	Solid State S- and L-Band Power Amplifier Configurations	6-14
6.3-4	S- and L-Band Power Amplifier Redundancy Configurations	6-15

LIST OF ILLUSTRATIONS

<u>Figure</u>	<u>Title</u>	<u>Page</u>
6.3-5	Proposed UHF Transmitter Configuration	6-17
6.3-6	UHF Power Amplifier Configuration	6-18
6.3-7	RFI and T&FD Experiment Interface	6-20
6.4-1	Input IF Switching Matrix	6-21
6.4-2	Output IF Switching Matrix	6-22
6.4-3	Proposed IF Amplifier Block Diagram	6-24
6.4-4	IF Signal Output Power With Predetection and Post-detection AGC	6-28
6.5-1	Frequency Synthesizer Configuration	6-30
6.5-2	Synthesizer Phase-Lock Loop Configuration	6-32
6.6-1	Monopulse Receive Portions of Transponder	6-35
6.6-2	UHF Monopulse Modulator	6-36
6.6-3	S-Band and X-Band Monopulse Modulators	6-37
6.6-4	Monopulse Demodulator	6-38
6.7-1	Proposed Wideband Data Unit	6-40
6.7-2	150 MHz Voltage Controlled Oscillator Block Diagram	6-41
6.8-1	Command Interface Details	6-44
6.8-2	Transponder Command Distributor Block Diagram	6-46
6.8-3	Select-One-Of-Four Command Distributor Switching Circuit	6-48
6.8-4	Telemetry Interface With Select-One-Of-Four Circuit	6-49
6.8-5	Relay Driver Schematic	6-50
6.8-6	Typical Digital Telemetry Interface	6-52
6.8-7	Typical Analog Telemetry Interface	6-52
6.8-8	Transponder Prime Power Interface	6-53
6.9-1	EVM Layout Showing Communication Subsystem Location	6-56
6.9-2	Transponder and Feed Integration	6-57

LIST OF ILLUSTRATIONS

<u>Figure</u>	<u>Title</u>	<u>Page</u>
6.9-3	Bottom View of Communication Subsystem Box Showing Transponder Layout	6-58
6.9-4	Transponder Layout	6-59
7.2-1	EVM Layout Showing Composite Feed	7-3
7.2-2	Antenna Feed, RF Schematic	7-4
7.2-3	X- & C-Band Multimode Waveguide Feed	7-8
7.2-4	X-Band Horn Module Configuration	7-9
7.2-5	X-Band Monopulse Comparator	7-10
7.2-6	X-Band Antenna Switching Circuit	7-11
7.2-7	C-Band Polarization Control Network	7-13
7.2-8	S-Band Feed Element Arrangements	7-15
7.2-9	Calculated Secondary Patterns for Single Helical Element Excitation	7-16
7.2-10	Calculated Secondary Patterns for Single Sprial Element Excitation	7-17
7.2-11	Recommended S-Band Feed Distribution Network Using SP4T Pin-Diode Switches	7-21
7.2-12	S-Band SP4T Pin-Diode Switch	7-22
7.2-13	Schematic Diagram of S-Band SP4T Pin-Diode Switch	7-24
7.2-14	S-Band Antenna Feed Network RF Path Configuration	7-25
7.2-15	S-Band Antenna Feed Network, Control Side	7-26
7.2-16	Feed Network for Common L and S Band Radiating Element	7-28
7.2-17	L-Band Feed Switch Network	7-30
7.2-18	On-Axis Turnstile 850 MHz Feed	7-31
7.2-19	VHF Tracking Feed	7-33
7.2-20	Lens-Compensated Horn Gain	7-34

LIST OF ILLUSTRATIONS

<u>Figure</u>	<u>Title</u>	<u>Page</u>
7.3-1	Transponder and Feed Integration	7-40
7.3-2	Composite Feed Assembly (Plan View)	7-41
7.3-3	Composite Feed Assembly (Side View)	7-42
7.3-4	Composite Feed Assembly (Bottom View)	7-43
7.3-5	Crossed - Dipole Detail (Typical for S- and L-Band)	7-45
7.3-6	VHF Element	7-46
8.1-1	Thirty-Foot Parabolic Reflector for ATS F&G	8-3
8.2-1	25X Scale Travis Marquissette No. 635 (Multifilament Yarns Shown as Monofilament)	8-14
8.3-1	Mesh Stress-Strain Curve	8-17
8.3-2	Mesh Coefficient of Thermal Expansion	8-19
8.3-3	Coated Stand (200X)	8-20
8.3-4	Uncoated Stand (1000X)	8-20
8.4-1	Temperature History of Ribs	8-27
8.4-2	Temperature History of Mesh Panels	8-28
8.4-3	Hub Surface Temperature Histories	8-29
8.4-4	Maximum Spanwise Temperature Gradients	8-30
8.4-5	Surface Deviation from Theoretical Paraboloid at Orbit Time Hour 4	8-31
8.4-6	Surface Deviation from Theoretical Paraboloid at Orbit Time Hour 11	8-32
8.4-7	Numbering System of Ribs and Mesh Points	8-33
8.4-8	RMS vs. Orbit Time	8-35
8.5-1	Typical Variable Optimization	8-39
8.5-2	RMS Distortion History	8-40
8.7-1	Parabolic Reflector in Stowed Configuration	8-43

LIST OF ILLUSTRATIONS

<u>Figure</u>	<u>Title</u>	<u>Page</u>
9.1-1	ATS Reference Coordinate System	9-6
9.1-2	Acquisition Control Modes Block Diagram	9-7
9.1-3	Operational Control Modes Block Diagram	9-8
9.1-4	Experiment Modes Block Diagram	9-8
9.1-5	Sun Sensor Configuration	9-11
9.1-6	Power Distribution for ACS	9-20
9.2-1	Digital Operational Controller - Outline Drawing	9-30
9.2-2	Digital Operational Controller - Cutaway View	9-31
9.2-3	Central Processor Block Diagram	9-32
9.2-4	General Format of Instruction Word	9-33
9.2-5	Data Flow Diagram	9-36
9.2-6	Digital Operational Controller Interfaces	9-39
9.2-7	Digital Operational Controller Input/Output Electronics Functional Block Diagram	9-41
9.2-8	A/D - D/A Converter SIO Functional Block Diagram	9-44
9.2-9	Serial Data Register SIO	9-45
9.2-10	Pulse Accumulator SIO Functional Block Diagram	9-46
9.2-11	CDD - SIO Block Diagram	9-47
9.2-12	Telemetry (DACU) SIO Block Diagram	9-47
9.2-13	Basic Plated-Wire Element	9-49
9.2-14	Basic Plated-Wire Bit	9-49
9.2-15	Digital Operational Controller Power Supply Organization	9-53
9.2-16	Digital Operational Controller Program Organization	9-55
9.2-17	Simplified Digital Operational Controller Executive Routine Flow Chart	9-56
9.2-18	Analog Backup Controllers - Outline Drawing	9-60

LIST OF ILLUSTRATIONS

<u>Figure</u>	<u>Title</u>	<u>Page</u>
9.2-19	Analog Backup Controller - Cutaway View	9-61
9.2-20	Analog Backup Controller Functional Block Diagram	9-63
9.2-21	Flight Head Assembly	9-65
9.2-22	Radiance Gain Circuits	9-66
9.2-23	Radiance Processing Block Diagram	9-66
9.2-24	Scan Generator Simplified	9-67
9.2-25	Visor Drive Circuits	9-68
9.2-26	Visor Readout Electronics	9-69
9.2-27	Sun Avoidance Circuits Block Diagram	9-70
9.2-28	Angle Computation Circuits (Single-Channel)	9-71
9.2-29	Power Distribution Circuits	9-71
9.2-30	Scanning Mechanism	9-73
9.2-31	Offset Mirror Assembly	9-75
9.2-32	Bolometer Telescope Parts	9-76
9.2-33	Sun Sensor Subassembly	9-77
9.2-34	Flight Head Assembly with Front Cover Plate Removed	9-78
9.2-35	Polaris Sensor, Conditioning Electronics Simplified Block Diagram	9-81
9.2-36	Polaris Sensor Chassis	9-82
9.2-37	Stray Light Baffle - Second Stage	9-83
9.2-38	Lens Assembly	9-84
9.2-39	Polaris Sensor Assembly - Cutaway View	9-85
9.2-40	Sun Detector Assembly	9-85
9.2-41	Rotary Solenoid Sun Shutter	9-87
9.2-42	Electronic Components Packaging	9-88
9.2-43	Polaris Sensor Alignment References	9-89

LIST OF ILLUSTRATIONS

<u>Figure</u>	<u>Title</u>	<u>Page</u>
9.2-44	Hub Coarse Sun Sensor	9-93
9.2-45	EVM Coarse Sun Sensor	9-93
9.2-46	Fine/Target Sensor Block Assembly	9-94
9.2-47	EVM Electronics 1 and 2	9-94
9.2-48	Hub Electronics	9-95
9.2-49	Coarse Eye Assembly	9-95
9.2-50	Fine Eye/Target Detector Assembly	9-96
9.2-51	Pitch Coarse Sun Sensor Location, Orientation	9-96
9.2-52	Pitch Coarse Sun Sensor Location, Orientation	9-97
9.2-53	Yaw Coarse Sun Sensor Location, Orientation	9-98
9.2-54	Yaw Coarse Sun Sensor Location, Orientation	9-99
9.2-55	Inertial Reference Assembly Outline Drawing	9-102
9.2-56	Inertial Reference Assembly Functional Block Diagram	9-103
9.2-57	Actuator Control Electronics Assembly - Outline Drawing	9-107
9.2-58	Actuator Control Electronics Assembly - Cutaway View	9-108
9.2-59	Load Line Limiting Gate Characteristic	9-110
9.2-60	Block Diagram of ACE Power Flow to APS	9-111
9.2-61	Controlled-Frequency Reaction Wheel Drive System	9-112
9.2-62	Basic Inertia Wheel Configuration	9-114
9.2-63	Cutaway View of Inertia Wheel Rotor and Stator	9-115
9.2-64	Motor Input Power	9-117
10.1-1	Interferometer Functional Diagram	10-2
10.2-1	RF Interferometer System Functional Arrangement	10-8
10.2-2	Basic Equation, Angle Measurement	10-9

LIST OF ILLUSTRATIONS

<u>Figure</u>	<u>Title</u>	<u>Page</u>
10.2-3	Interferometer System Functional Block Diagram	10-11
10.2-4	Phase Coherent Down - Conversion	10-15
10.3-1	Interferometer Installation in Experiments Module	10-26
10.3-2	Interferometer Array Assembly	10-27
10.3-3	Receiver Front End	10-28
10.3-4	Receiver/Converter Electronics Unit (RCEU)	10-29
10.3-5	RF Interferometer Array Assembly	10-31
10.3-6	Installation of Interferometer Antenna Array	10-33
10.3-7	RF Receiver Front End Electronics	10-35
10.3-7A	Receiver Converter Electronic Unit	10-36
10.3-8	Coupler/Switch Module	10-40
10.3-9	Digital Converter and Buffer	10-47
10.3-10	Interferometer Telemetry Outword	10-50
10.3-11	Interferometer Ground Transmitter	10-53
10-3-12	System Block Diagram	10-55
11.1-1	Boom Spacecraft Configuration	11-2
11.1-2	COGGS/ACS Signal Interface Functional Block Diagram	11-5
11.1-3	Pitch and Roll Response to ± 8.5 Degree Attitude Steps	11-7
11.1-4	Pitch and Roll Tracking	11-7
11.1-5	Roll Response to 1-Deg/Min Ramps	11-8
11.2-1	ATS F&G Deployed Configuration	11-11
11.2-2	COGGS Mechanical Layout	11-12
11.2-3	COGGS System Schematic	
11.2-4	COGGS Boom/Deployer Assembly	11-18
11.2-5	RAE Edglock Antenna Element Prior to Heat Treating	11-20

LIST OF ILLUSTRATIONS

<u>Figure</u>	<u>Title</u>	<u>Page</u>
11.2-6	Antenna Element Edglock Zipper	11-20
12.1-1	Ammonia APS Mechanization Diagram	12-7
12.1-2	Location and Redundancy of Attitude Control Thrust Nozzles	12-8
12.1-3	Location of Orbit Control Thrust Nozzles	12-10
12.2-1	Regulated Pressure Feed Assembly	12-18
12.3-1	APS Interface Signals	12-25
12.4-1	Regulated Pressure Feed Assembly - Cylindrical Tanks	12-29
12.4-2	ATS Spacecraft Showing Location of Auxiliary Propulsion Subsystem in Earth Viewing Module	12-31
12.4-3	Major Subassemblies of the APS	12-32
12.4-4	Location and Mounting of Orbit Control Thrusters and Feed Tubing	12-36
12.4-5	Orbit Control Thruster Design (TRW)	12-38
12.4-6	Orbit Control Thruster Design (TRW) Showing Location of Heater Element	12-39
13.1-1	ATS Communication Networks	13-2
13.1-2	T&C Subsystem Functional Block Diagram	13-4
13.2-1	Command Subsystem Functional Block Diagram	13-9
13.2-2	Command Word Format	13-11
13.2-3	Telemetry Subsystem Functional Block Diagram	13-13
13.2-4	Command Address Assignments	13-15
13.2-5	Data Word Address Assignment	13-16
13.2-6	Minor Frame Telemetry Word Assignments	13-17
13.2-7	Subcommutated Telemetry Word Assignments	13-18
13.2-8	FDM Frequency Allocations	13-23
13.2-9	Overview of Interface Requirements of T&C Subsystem	13-28

LIST OF ILLUSTRATIONS

<u>Figure</u>	<u>Title</u>	<u>Page</u>
13.3-1	CDD Logic Flow	13-31
13.3-2	Termination Configuration for Discrete Commands	13-34
13.3-3	Termination Configuration for Data Word Commands	13-35
13.3-4	Command Decoder/Distributor Timing Commands	13-37
13.3-5	DACU Functional Diagram	13-41
13.3-6	Telemetry Format	13-43
13.3-7	DACU Output Signal Timing	13-46
13.3-8	Analog-to-Digital Converter	13-48
13.3-9	A/D Converter Timing	13-49
13.3-10	Status Word Description	13-51
13.3-11	Spacecraft Clock Block Diagram	13-55
13.3-12	DSU Switching Functions	13-59
13.3-13	Antenna Unit	13-63
13.3-14	Composite Antenna Pattern Histogram Deployed Spacecraft (Both VHF Antennas Operational)	13-64
13.3-15	Typical Polar Plot Antenna Pattern	13-65
14.1-1	Power Subsystem Breadboard	14-6
14.2-1	Location and Orientation of Solar Array	14-7
14.2-2	Simplified Block Diagram of Power Subsystem	14-11
14.3-1	ATS Power Subsystem Block Diagram	14-13
14.3-2	Power Subsystem Block Diagram, Experiment LIC's	14-15
14.3-3	Solar Array in Respect to Sun	14-17
14.3-4	Solar Array Replaceable Modules	14-18
14.3-5	Solar Array Voltage vs. Current	14-19
14.3-6	Solar Array Power Derivation Curves	14-19
14.3-7	Solar Array Power Requirement for ITV Experiment	14-20
14.3-8	ATS Power Interface Block Diagram	14-23

LIST OF ILLUSTRATIONS

<u>Figure</u>	<u>Title</u>	<u>Page</u>
14.3-9	Battery Loading for Occult Load	14-27
14.3-10	ATS F&G Power Subsystem Installation Design Layout	14-31
14.4-1	Power Profile Component Summary	14-37
14.4-2	Total Conditioned Normal Power	14-39
14.4-3	Total Conditioned Peak Power	14-41
14.4-4	PLACE and ITV Power Profile for Solstice Launch	14-43
14.4-5	PLACE and ITV Power Profile for Equinox Launch	14-45
14.4-6	Ascent Sequence	14-48
14.6-1	Typical Analog Voltage Monitor Circuit	14-58
14.6-2	Typical Discrete Monitor Circuit	14-58
14.6-3	Typical Temperature Monitor Circuit	14-58
15.3-1	Exploded EVM - Prior to Harness Installation	15-9
15.3-2	Experiment Module Harnessing	15-11
15.3-3	EVM Experiment Module Harness Layout	15-13
15.3-4	EVM Service Module Harness Layout	15-17
15.3-5	Service Module Harnessing	15-19
15.3-6	EVM Communication Module Harness Layout	15-24
15.3-7	ATS-F Spacecraft Configuration and External Harness	15-26
15.3-8	EVM Interface	15-27
16.1-1	EVM Layout Showing Communication Subsystem Location	16-2
16.1-2	Radio Beacon Experiment Functional Block Diagram	16-3
16.3-1	Radio Beacon Transmitter Detail Block Diagram	16-8
16.3-2	Frequency Deviation vs Temperature Curve	16-13
16.3-3	Series and Parallel Triplexer Configuration	16-16
16.4-1	Radio Beacon Equipment Layout	16-19
16.4-2	Transmitter Layout	16-20

LIST OF ILLUSTRATIONS

<u>Figure</u>	<u>Title</u>	<u>Page</u>
17.2-1	System Test Complex	17-4
17.2-2	Spacecraft Shipping Container	17-14
17.2-3	Spacecraft Holding Fixture	17-15
17.2-4	Truss Holding Fixture	17-17
17.3-1	Attitude Control Subsystem Test Station Functional Block Diagram	17-19
17.3-2	IRA Test Station Block Diagram	17-21
17.3-3	DOC Test Station Block Diagram	17-25
17.3-4	ABC Test Station Functional Block Diagram	17-27
17.3-5	Actuator Control Electronics Test Station Functional Block Diagram	17-28
17.3-6	Inertia Wheel Test Station Functional Block Diagram	17-30
17.3-7	Earth Sensor Test Station	17-31
17.3-8	Star Tracker Test Station Functional Block Diagram	17-33
17.3-9	Sun Sensor Test Station Functional Block Diagram	17-34
17.3-10	Sun Sensor Electronics Test Station Functional Block Diagram	17-36
17.5.1	Block Diagram IBTE	17-39
17.6-1	T&C Test Console Block Diagram	17-41
17.6-2	T&C Subsystem Test Configuration	17-45
17.7-1	Communications Test Set Block Diagram	17-47
17.8-1	SMR Test Set Schematic Diagram	17-51
17.8-2	Battery Charger Test Set Schematic Diagram	17-52
17.8-3	Load Interface Circuit Test Set Schematic Diagram	17-54
17.8-4	Battery Test Set Schematic Diagram	17-55
17.8-5	Power Control Unit Test Set Functional Block Diagram	17-56
17.9-1	Experiment Interface Unit Functional Block Diagram	17-58

LIST OF ILLUSTRATIONS

<u>Figure</u>	<u>Title</u>	<u>Page</u>
17.10-1	T&C Simulator Block Diagram	17-61
17.10-2	Transponder Simulator	17-64
17.10-3	Transponder Simulator Block Diagram	17-68
18.1-1	Functional Flow Block Diagram Thermal Structural Model Prototype Spacecraft Integrated Test Program	18-3
18.1-2	Functional Flow Block Diagram Flight Spacecraft Integrated Test Program	18-5
18.2-1	Attitude Control Subsystem Development Test Summary	18-13
18.2-2	APS Development Test Summary	18-14
18.2-3	T&C Subsystem Development Test Summary	18-16
18.2-4	Communication Subsystem Development Test Summary	18-17
18.2-5	Transponder Development Test Summary	18-18
18.2-6	Power Subsystem Development Test Summary	18-20
18.3-1	Attitude Control Subsystem Qualification Test Summary	18-25
18.3-2	APS Qualification Test Flow Diagram	18-26
18.3-3	T&C Subsystem Qualification Test Summary	18-28
18.3-4	Transponder Qualification Test Summary	18-29
18.3-5	Communication Subsystem Qualification Test Summary	18-30
18.3-6	Power Subsystem Qualification Test Summary	18-31
18.3-7	EVM Integration	18-34
18.4-1	Acceptance Test Summary - Attitude Control Subsystem	18-39
18.4-2	Acceptance Test Summary - T&C Subsystem	18-40
18.4-3	Acceptance Test Summary - Transponder	18-41
18.4-4	Acceptance Test Summary - Communication Subsystem	18-41
18.4-5	Acceptance Test Summary - Power Subsystem	18-43

LIST OF TABLES

<u>Table</u>	<u>Title</u>	<u>Page</u>
2.2-1	Periodic Documents	2-2
2.2-2	Technical Documents	2-3
3.1-1	Technical Objectives Applied to ATS F Experiments	3-3
3.1-2	Applications Objective Summary	
3.3-1	Experiment Telemetry Requirements	3-63
3.3-2	Experiment Command Requirements	3-65
3.3-3	GFE Experiment Power Requirements	3-67
3.3-4	Experiment Weight and Volume Summary	3-76
3.4-1	Overall System Characteristics	3-86
3.4-2	ATS F&G Spectrum Utilization	3-88
3.4-3	Summary of Weights	3-89
3.4-4	ATS-F Communication Requirements	3-90
3.4-5	APS Mission Requirements	3-91
3.4-6	APS Propellant Weights	3-92
3.4-7	Telemetry and Command Requirements	3-93
3.4-8	Telemetry Subsystem Parameters	3-94
3.4-9	Command Subsystem Parameters	3-95
3.4-10	RF Interferometer Subsystem Summary	3-96
3.5-1	Weights of Major Structural Components (Oct. 68)	3-100
3.5-2	EVM Circular Versus Cubic Configuration Comparison	3-104
3.5-3	Performance Evaluation Based on Requirements	3-106
3.6-1	Estimated Operating Times	3-108
3.6-2	Redundant Sensors/Controllers/Torques for ACS Modes (3 Sheets)	3-128
3.6-3	APS Component Life	3-141
4.3-1	Area Volume of EVM	4-8
4.9-1	Structural Criteria and Compliance	4-90

LIST OF TABLES

<u>Table</u>	<u>Title</u>	<u>Page</u>
6.1-1	Communication Subsystem Performance Summary	6-2
6.3-1	Microwave Filter Summary	6-10
6.3-2	Comparison of TWTA and Solid State S- and L-Band Power Amplifiers	6-16
6.4-1	Expected Received Signal Levels	6-26
6.5-1	Frequency Synthesizer Performance Requirements	6-31
6.8-1	Summary of Connections	6-43
6.9-1	EVM Heat Loads (Watts)	6-61
6.9-2	Transponder Component Size and Weight	6-62
6.9-3	Communications S/S Thermal Dissipation	6-66
7.2-1	S-Band Feed Performance Comparison	7-18
7.2-2	S-Band Switch Matrix Configuration Summary	7-20
7.2-3	Estimated X-Band Horn Performance Parameters	7-35
7.2-4	Itemized Composite Feed Component Losses (dB)	7-37
7.2-5	Predicted Vs. Required RF Characteristics for ATS F&G 30-Ft. Parabolic Antenna	7-38
7.3-1	Composite Feed Weight Estimate	7-48
8.3-1	Mechanical Properties of Mesh Material	8-16
8.3-2	Transmittance of Mesh vs. Incidence Angle	8-18
8.4-1	Reflector Component Temperatures During Orbit	8-26
9.1-1	Summary of ACS Modes	9-4
9.1-2	Backup Capability - Operational	9-17
9.1-3	ACS Requirements/Performance Summary	9-18
9.1-4	APS Orbit Control Requirements	9-18
9.1-5	ACS Dominant Disturbances	9-19
9.1-6	Controller Requirements/Performance Summary	9-21
9.1-7	Sensor Requirements/Performance Summary	9-22
9.1-8	Torquer Requirements/Performance Summary	

LIST OF TABLES

<u>Table</u>	<u>Title</u>	<u>Page</u>
9.2-1	Mass Property Summary	9-27
9.2-2	Attitude Control Subsystem Power Requirements (watts)	9-28
9.2-3	Controller Physical Data and Reliability	9-29
9.2-4	Instruction Repertoire Summary	9-34
9.2-5	Memory Sector Organization	9-35
9.2-6	Digital Operational Controller Interface Signals	9-40
9.2-7	Special I/O Electronics	9-43
9.2-8	Power Supply Characteristics	9-54
9.2-9	Interferometer Subsystem Weight and Power Summary	9-106
9.2-10	Weights of Inertia Wheels	9-113
10.2-1	Error Sources	10-19
10.2-2	Test Summary	10-23
10.2-3	Ground Station to Interferometer Link Parameters	10-24
10.3-1	Mass Characteristics	10-25
10.3-2	Power Dissipation in Each Assembly	10-30
10.3-3	Summary of Ground Transmitter Capability Requirements	10-53
11.1-1	Basic COGGS Requirements and Corresponding Response	11-3
11.2-1	Key Design Features for COGGS	11-10
11.2-2	Maximum Power Consumption	11-24
11.2-3	Average Power Consumption	11-24
11.2-4	Weight Using a 0.765-Inch-Diameter Boom	11-24
11.2-5	Weight Using a 0.57-Inch-Diameter Boom	11-24
11.2-6	Weight Summary - Gimbal Assembly	11-25
11.2-7	COGGS Boom/Mechanism Weight Breakdown	11-25

LIST OF TABLES

<u>Table</u>	<u>Title</u>	<u>Page</u>
12.1-1	APS Requirement/Performance Summary	12-3
12.1-2	Component Requirement/Performance Summary	12-4
12.1-3	APS Impulse Requirements	12-5
12.1-4	Thrust Levels and Lever Arms	12-6
12.1-5	Thruster Duty Cycle in Control System Operational Modes	12-6
12.1-6	Ammonia Solenoid Valve Functional Requirements	12-11
12.1-7	Ammonia Latching Valve Functional Requirements	12-12
12.1-8	Thrust Level and Response Time for A/C and O/C Thrusters (Including Solenoid Valves)	12-12
12.2-1	Normal Operational Modes	12-13
12.2-2	Operating Modes (With Failed Elements)	12-16
12.2-3	Solenoid Performance Data at 74 ^o F (Model 15457)	12-22
12.3-1	Interface Summary	12-24
12.3-2	Input Interface Signals (From Actuator Control Electronics)	12-25
12.3-3	APS Output Interface Signals to ACE	12-26
12.4-1	APS Weight Breakdown	
13.1-1	Command Subsystem Parameters	13-5
13.1-2	Telemetry Subsystem Parameters	13-6
13.2-1	Command Tone Frequency Assignment	13-10
13.2-2	Telemetry Links	13-19
13.2-3	Normal Command Links	13-20
13.2-4	FDM-VHF (136 MHz) Telemetry Link Calculations	13-22
13.2-5	Power Distribution	13-24
13.2-6	Mass Properties Estimates	13-27
13.3-1	Power Enabling of CDD Elements	13-33
13.3-2	Telemetry Points by Sampling Rates	13-39
13.3-3	Telemetry Points by Function	13-39

LIST OF TABLES

<u>Table</u>	<u>Title</u>	<u>Page</u>
13.3-4	Spacecraft Clock Pin Requirements	13-56
13.3-5	Receiver Characteristics	13-61
13.3-6	Transmitter Characteristics	13-62
14.3-1	Power Subsystem Component Characteristics	14-29
14.5-1	Power Subsystem Commands	14-51
14.6-1	Power Subsystem Telemetry Monitors	14-56
15.4-1	ATS Harness Weight Analysis	15-34
16.1-1	Summary of Electrical Characteristics	16-4
16.2-1	Measurement Parameter Fundamental Relationships	16-6
16.3-1	Master Oscillator Performance Characteristics	16-12
16.4-1	ATS Beacon Weight Table	16-21
16.4-2	DC Power Requirements	16-22
17.2-1	Summary Listing of Electrical AGE and BTE	17-3
17.2-2	Summary of Mechanical AGE	17-10
17.6-1	T&C Test Console Equipment List	17-42
18.2-1	Subsystem/Component Development	18-12

SECTION I
INTRODUCTION

This is a final report submitted to summarize program activities of Fairchild Hiller Corporation and its subcontractors in complying with the requirements of Goddard Space Flight Center Contract NAS 5-11609 for Applications Technology Satellites (ATS) F&G, Phases B and C. The objective of this report is to describe the ATS F&G design as of the conclusion of the contract. Historical details of the design evolution are contained in the monthly progress reports, subsystem reports and other documentation listed in paragraph 2.2 of this report.

The NASA objectives of the ATS F&G program may be summarized as:

1. Demonstration of the feasibility of a 30-foot diameter deployable parabolic spacecraft antenna with good RF performance up to 10 GHz.
2. Provisions of spacecraft fine pointing (0.1 degree), slewing (17.5 degrees in 30 minutes), and tracking capability.
3. Provision of an oriented, stable spacecraft at synchronous altitude for advanced technological experiments.
4. Demonstration of precision interferometer measuring technology for closed loop servo performance.
5. Demonstration of the capability of forming high-gain, steerable antenna beams.
6. Provision of a multi-frequency, multiple access communication system.

The frontpiece of this report is an artist's concept of the Fairchild Hiller design. The lower cubical spacecraft structure, called the EVM for Earth Viewing Module, contains most of the spacecraft electronics, and GFE experiments. On the top of this module are the feeds for the 30-foot diameter parabolic reflector. The top of the reflector support truss is called the hub. A bridge truss across the top of the hub provides the support for the solar array booms, the Commandable Gravity Gradient Experiment and the Environmental Measurements Experiments package. The

ribs of the parabolic reflector are flexible and wrap around the hub in the stowed position for launch. The solar panels are hinged to their deployment booms, and the booms are hinged at the bridge truss so that the solar panel launch position is around the reflector support truss above the EVM. In its design study efforts Fairchild Hiller was supported by three team member subcontractors; Honeywell for the Attitude Control Subsystem and the Auxiliary Propulsion Subsystem; IBM for the RF Interferometer and the Telemetry and Command (T&C) Subsystem; Philco-Ford for the integrated Transponder Subsystem and the Antenna Feed subsystem. The Lockheed Missiles and Space Company design for the parabolic reflector was selected.

The principal features of the Fairchild Hiller design are described in Sections 3 through 16 but are highlighted here. Structurally the spacecraft is attached to the launch vehicle through an adapter truss. The adapter truss is connected directly to the EVM and to the reflector support truss to provide the simplest and most direct load paths. The EVM does not have to carry the full load imposed by the truss and hub members. The EVM is designed for ease of accessibility to all equipment during installation and after final assembly. The simple basic geometry and flat mounting surfaces of the EVM yield maximum packing density. High heat dissipating components are mounted directly to the north and south faces of the EVM. Heat pipes and thermal louvers are attached to these sides and the low temperature gradient between the components and louvered surface provides good control of component temperatures. The modularized EVM design allows for relatively independent integration of the major subsystems, thus reflecting significant cost and schedule savings during spacecraft assembly and test. Design flexibility also is facilitated, as relatively major changes can be accomplished without the need to rework the entire EVM structure. One of the new composite materials, Graphite Fiber Reinforced Plastic, is used for the reflector support truss as its low coefficient of thermal expansion eliminates alignment variations due to temperature change. It also contributes a saving in weight.

The Attitude Control Subsystem utilizes a Digital Operational Controller backed up by a totally redundant duplicate controller, as well as a simplified back-up analog controller with slightly reduced performance. This insures that the critical controller function will continue to sustain operation of the spacecraft even in the event of multiple failures. All sensors and torquers are backed up by means of duplicate components or functionally-redundant components so as to provide redundant coverage for all acquisition and operational modes. The Polaris Star Tracker, the Inertial Reference Assembly and the momentum wheels are all existing, developed components, qualified for similar spacecraft operations. The Earth Sensor, breadboarded and tested during this phase of the program are based upon a previously proven VELA design.

The Auxiliary Propulsion Subsystem provides a gas system for wheel unloading, orbit control and station keeping. It is designed to be mounted to a central plate within the EVM, thus providing an integral structure for fabrication and assembly. As a consequence this subsystem will be assembled, tested and installed as a single package with no breaks in any of the thruster lines, including the orbit control thrusters which are placed on the reflector truss members. Ammonia was selected

as the expellant because of its success in previous flights at the required thrust levels. It has no degrading effects on thermal control coatings or on the copper-coated Dacron mesh used in the reflector. The attitude control thrusters, located at the surface of the EVM are fully redundant in all three axes. The jets are oriented to thrust perpendicular to the mounting surface to avoid any problem of plume impingement.

The Telemetry and Command Subsystem exploits the 30-foot reflector by using the prime focus VHF monopulse feed to transmit the basic spacecraft telemetry data. Three independent dedicated antenna-transmitter-receiver groups provide triple redundant RF systems for the telemetry and command functions without the need for RF switching. The command elements are powered continuously from the solar array with automatic switchover to battery power when required.

The semi-cylindrical solar panels provide constant power output throughout the day, while at the same time maintaining a balanced cross section to solar pressure around the roll and yaw axes. Solar array power is sufficient to support all nominal load requirements without dependence upon the battery. Battery capacity is designed for support of "housekeeping" and critical experiment loads during solar occult conditions. It can also back-up the solar array to carry peak loads when required. Selection of solar array and battery voltages above the desired regulated line voltage avoids the need for boosters anywhere in the system.

The Communications Subsystem transponder design allows for complete cross-strapping of all frequencies and operating modes. The RCS TA 7205 transistor is the basic component of solid state amplifiers at the UHF, L- and S-bands, resulting in weight, cost and schedule savings with improved efficiency and reliability. Two independent low orbit satellites may be tracked throughout most of the visible orbit by controlling the spacecraft Z-axis pointing, and switching to the appropriate S-band beams from the cross shaped feed element array.

The principal communications experiments to be performed are Instructional Television (ITV), Position Location and Aircraft Communication Equipment (PLACE) and the Data Relay System (DRS). The ITV experiment is a special case of the more general TRUST (Television Relay Using Small Terminals) experiment. The purpose of the experiment is to advance space communications techniques by implementing, testing and demonstrating CCIR quality wideband signaling between the ATS spacecraft and inexpensive UHF ground receiving stations. Programming from a centrally located ground station will be transmitted on X-band to ATS and relayed at UHF to two types of ground stations located in India: individual special ground receivers located in villages and conventional receivers in urban areas via VHF rebroadcast facilities. The control of ATS will be provided from a ground station located in Europe, with the spacecraft located over the equator at 15° East.

The PLACE experiment is aimed at developing an improved air traffic control technique. The purpose is to demonstrate the ability to determine continuously the location of all aircraft in the system and to maintain their positions relative to each other. When implemented with the ATS as a synchronous altitude

communications repeater, PLACE will provide two-way voice and digital data communications between all cooperating aircraft and their associated ground control facilities.

The DRS experiment will demonstrate critical aspects of the technology necessary to an operational data relay system between a ground facility and a low altitude satellite via the ATS spacecraft. The specific program goals of DRS include real-time data relay, range and range rate tracking, and low altitude satellite commanding through ATS. Simultaneous tracking of two low altitude satellites will be demonstrated with duplex communication provided to one selected satellite. Data relay with NIMBUS and Apollo Workshop satellites have been selected for the satellite tracking experiments.

The spacecraft design fulfills all of the requirements imposed by the mission objectives and the GSFC design specifications. In addition, the Fairchild Hiller design incorporates many innovations that result in improved performance capabilities beyond basic requirements.

SECTION II

PROGRAM CONTROL

2.1 SCHEDULE MILESTONES

The combined Phase B and C program was basically a design study, supported by breadboard fabrication and testing in critical areas. The output of the program was primarily engineering reports and related documentation. There were 24 such items listed in the contract delivery schedule.

The contract starting date was September 17, 1968 and this report is concerned with the fixed price portion of the contract which concluded on October 17, 1969. There is a holding period, on a cost plus fixed fee basis, which extends from October 17, 1969 to January 31, 1970 with options to extend month by month until Phase D is awarded. Separate reports will be made on tasks performed during the holding period.

At the start of the contract there existed a GSFC document entitled "Preferred Approach for ATS F&G." The first major milestone was to deliver an assessment of the preferred approach on December 17, 1968, three months after contract award. This assessment included recommendations for changes, additions, or deletions to the preferred approach. Major design changes evolved during this period were the change from the Atlas/Centaur launch vehicle to the Titan IIC and the change from the side-hinged petaloid parabolic antenna concept to a flexible-rib design. Approval of the recommended changes resulted in Fairchild Hiller's Final Approach for ATS F&G, Report No. ATS-990-004 dated 25 January 1969. This essentially concluded the Phase B activity and the remainder of the contract period was devoted to development of the design.

The culmination of the Phase C efforts was the delivery of the Proposal for Phase D on September 17, 1969. This proposal included separate volumes giving the technical design details of each subsystem of ATS F&G, and which represent the design study effort of Phase C. Contract changes during this period added the Commandable Gravity Gradient Experiment to the design tasks. After delivery of the proposal the final month of the contract was utilized in preparing the following contractual items for delivery:

- Item 15 Breadboard Test Data
- Item 16 Test Procedures
- Item 17 Specifications and Drawings

- Item 20 Final Report
- Item 22 Materials Report
- Item 24 New Technology Report

The final PERT network which was used to plan and control the program is given in Figure 2-1, Sheets 1 through 4. In this presentation the location of the event circles indicates the planned completion date according to the time scale at the bottom of each sheet. The actual completion date of each event is given in the bottom half of each event circle. Fairchild Hiller delivered all contractual items on time. Of the events on the PERT network which were the responsibility of the contractor, less than 10% were completed later than planned.

2.2 DOCUMENTATION

The results of Fairchild Hiller Corporation's efforts on Phase B and C of the ATS F&G Program were recorded in the many documents that were delivered to NASA-GSFC. The tables below give a complete listing of all of these documents. Table 2.2-1 shows the documents which were delivered periodically during Phase B/C. Table 2.2-2 shows the remaining documents that covered specific aspects of the program.

Table 2.2-1. Periodic Documents

Title	Number	Date
Monthly Progress Report	ATS-910-001 thru ATS-910-011	Tenth day of each month (covering the previous calendar month) Sept., 1968 thru Aug. 1969.
Mass Properties Report	ATS-920-001 thru ATS 920-012	Four working days after the 17th of each month. Oct., 1968 thru Sept., 1969
Power Profile	ATS-930-001 thru ATS-930-012	Four working days after the 17th of each month. Oct., 1968 thru Sept., 1969.
Materials Report	ATS-940-001 (First) ATS-940-002 (Final)	April 17, 1969 Nov. 17, 1969'

Table 2.2-2. Technical Documents

Title	Number	Date
Single Module vs. Dual Module Comparison Study Report	ATS-990-001	Oct. 17, 1969
Assessment of the Preferred Approach	ATS-990-002	Jan. 21, 1969
Breadboard Plan	ATS-990-003	Jan. 20, 1969
Final Approach for ATS F&G	ATS-990-004	Feb. 24, 1969
Electric Power Overload Protection Plan	ATS-990-005	March 10, 1969
Telemetry and Command Logic	ATS-990-006	March 10, 1969
Interim Reliability Report	ATS-990-007	March 10, 1969
AGE/BTE List	ATS-990-008	March 17, 1969
AGE/BTE List	ATS-990-008A	May 19, 1969
ATS-F Phase D Expanded RFI Experiment	ATS-990-009	April 9, 1969
Subsystem Reports	ATS-990-010 thru ATS-990-020	Sept. 17, 1969 (Submitted as Volumes I-A thru I-N of the Proposal)
Commandable Gravity Gradient Subsystem Proposal	ATS-990-021	June 9, 1969
Radio Beacon Experiment Subsystem Proposal	ATS-990-022	June 10, 1969
Configuration Management Plan	ATS-990-023	July 17, 1969
Dynamic Analysis	ATS-990-025	June 27, 1969

Table 2.2-2. Technical Documents (cont)

Title	Number	Date
Structural Analysis	ATS-990-026	July 17, 1969
Orbital Response	ATS-990-027	July 17, 1969
System Thermal Analysis and Design	ATS-990-028	July 17, 1969
Reflector Analyses	ATS-990-029	
EVM Support Structure Thermal Analyses and Design	ATS-990-030	July 17, 1969
Coupling Analysis	ATS-990-031	July 17, 1969
Configuration Management Plan	ATS-990-032	July 17, 1969
Exposure of the Parabolic Reflector Surface	ATS-990-033	July 23, 1969
Load Interface Circuit	ATS-990-034	Aug. 5, 1969
Proposal for ATS F&G (Phase D)	ATS-990-035	Sept. 17, 1969
Attitude Control Subsystem (ACS) Ground Testing Techniques	ATS-990-036	Aug. 18, 1969
Quality Assurance Plan	ATS-990-037	Aug. 18, 1969
Reliability Plan	ATS-990-038	Aug. 18, 1969
Deployment Test Procedure	ATS-990-039	Aug. 18, 1969
Structural Dynamic Analysis	ATS-990-040	Sept. 2, 1969
Additional Studies of Solar Array Boom	ATS-990-041	Sept. 17, 1969
Additional Structural Investigations	ATS-990-042	Sept. 16, 1969
Breadboard Test Data for the Earth Sensor	ATS-990-043	Oct. 17, 1969

Table 2.2-2. Technical Documents (cont)

Title	Number	Date
Breadboard Test Data for the Auxiliary Propulsion Subsystem	ATS-990-044	Oct. 17, 1969
Breadboard Test Data for the Transponder	ATS-990-045	Oct. 17, 1969
Breadboard Test Data for the Antenna Feed	ATS-990-046	Oct. 17, 1969
Breadboard Test Data for the Radio Beacon Experiment	ATS-990-057	Oct. 17, 1969

Proposal for ATS F&G (Phase D)	ATS-990-035	Sept. 17, 1969
Volume I	Program Summary	
Volume I-A	Structure Subsystem	
I-B	Thermal Control Subsystem	
I-C (Books 1 & 2)	Attitude Control Subsystem	
I-D (Books 1 & 2)	Auxiliary Propulsion Subsystem	
I-E	Power Subsystem	
I-F	Transponder	
I-G (Books 1 & 2)	Telemetry & Command Subsystem	
I-H	Parabolic Reflector	
I-I	Prime Focus Feed	
I-J	Harness Subsystem	
I-K (Books 1 & 2)	Interferometer	
I-L	Radio Beacon Experiment	
I-M	Gravity Gradient Experiment	
I-N	Experiments	
Volume II (Books 1 & 2)	Test and Evaluation	
Volume III (Books 1 - 6)	Reliability and Quality Assurance	

Proposal for
ATS F&G (Phase D) (con't)

ATS-990-035

Sept. 17, 1969

Volume IV

Launch and ATSOCC Support

Volume V

Facilities

Volume VI

Work Breakdown Statements

Volume VII

Resumes

Volume VIII

Manufacturing

Volume IX

Business Management

Volume X (Books 1 - 7)

Cost

3. 1. 1 TECHNOLOGICAL OBJECTIVES

The six basic technological objectives previously introduced are discussed in more detail in the following paragraphs. Their potential future applications and their impact on the spacecraft configuration (functional and operational) is presented herein.

3. 1. 1. 1 Demonstration of the Feasibility of a 30-Foot Diameter, Deployable Parabolic Spacecraft Antenna With Good RF Performance up to 10 GHz

During the next decade there will be an increasing demand on the capacity of present communications systems. A desire to transmit more information directly between widely separated geographical locations has already been demonstrated (Intelsat Satellites). Recent technological advances have shown that it is now feasible to provide a communications satellite having high effective radiated power (ERP) in synchronous orbit. Such a satellite makes possible the utilization of small inexpensive terrestrial terminals as space communication relays, rather than the more complex receiving stations used to date. The potential of using receiving stations with substantially lower gain and higher noise figures permits contemplating communication relay links with spacecraft, aircraft, ships, and low cost ground stations.

ATS F&G provide, as an integral part of the basic spacecraft, a 30-foot diameter, deployable parabolic reflector. The design of the antenna and deployment mechanism ensures a high reliability of its deployment in synchronous orbit. The ATS F&G 30-foot reflector, operating in conjunction with recently developed microwave power amplifiers, provides high ERP heretofore not obtainable in frequency bands from VHF to X-Band. In addition, the 30-foot diameter reflector itself represents a significant step forward in spacecraft deployable structures.

As indicated in Table 3.1-1 the feasibility of the 30-foot parabolic reflector will be demonstrated primarily by direct antenna measurements and three candidate ATS F experiments.

- (TRUST) The Television Relay Using Small Terminals - experiment utilizes the high gain of the 30-foot parabolic reflector at UHF to demonstrate the capability of providing direct TV broadcast via satellite relay to selected geographical areas with relatively inexpensive receiving stations.
- (PLACE) The Position Location and Aircraft Communication Equipment - experiment utilizes the high gain of the 30-foot parabolic reflector at L-Band to demonstrate the capability of improving air traffic control techniques by providing direct ground-to-aircraft communications and navigation aids via the satellite over prescribed (North Atlantic Corridor) aircraft flight paths.

SECTION III

SYSTEMS ENGINEERING

3.1 MISSION OBJECTIVES

The Applications Technology Satellite (ATS) Program provides the required stabilized platform for experiments that can be classified, according to the experiment objective, in four basic groups:

- Communications Experiments
- Meteorological Experiments
- Spacecraft Stabilization Experiments
- Scientific Experiments

The ATS F&G satellites incorporate unique technological objectives, that, to a large degree, dictate the spacecraft design and the applications experiments selected for the mission. These NASA objectives, stated in a condensed form, are:

1. Demonstration of the feasibility of a 30-foot diameter deployable parabolic spacecraft antenna with good RF performance up to 10 GHz.
2. Provision of spacecraft fine pointing (0.1 degree) slewing (17.5 degrees in 30 minutes), and tracking capability.
3. Provision of an oriented, stable spacecraft at synchronous altitude for advanced technological experiments to be selected through the Space Science and Applications Steering Committee.
4. Demonstration of precision interferometer attitude measuring technology for closed loop servo performance.
5. Demonstration of the capability of forming high-gain, steerable antenna beams.
6. Provision of a multi-frequency, multiple access communication system.

The following paragraphs discuss these six basic technological objectives and the experiments that demonstrate these objectives. Table 3.1-1 lists the candidate applications provided in the complement of ATS F equipments, categorizing them generally into each of the six technological objectives listed above.

Table 3.1-1. Technical Objectives Applied to ATS-F Experiments

Application	Technological Objective					
	1	2	3	4	5	6
Data Relay Satellite	X	X	X		X	X
Position Location and Aircraft Communication Equipment	X	X	X			X
Television Relay Using Small Terminals	X	X	X			X
Interferometer				X		
SAMOC/SAPPSAC		X	X			
Commandable Gravity Gradient		X	X			
Monopulse		X				
Antenna Pattern Measurement	X	X				
Very High Resolution Camera		X	X			
High Resolution Radiometer			X			
Time and Frequency Dispersion	X	X				
Radio Frequency Interference	X	X				
LASER		X	X			
Millimeter Wave			X			
Radio Beacon			X			
Low Energy Electron Proton			X			
Low Energy Proton			X			
Solar Cosmic Ray			X			
Particle Acceleration			X			
Magnetometer			X			
Auroral Particle			X			
Solar Coroll Radiation			X			

- (DRS) The Data Relay System - utilizes the high gain of the 30-foot parabolic reflector at S-Band to demonstrate the capability of providing an operational data relay between the low earth orbiting satellites and a central data acquisition facility.

A number of other applications experiments, selected by the Space Science and Steering Committee, also make use of the 30-foot parabolic reflector.

3.1.1.2 Provision of Spacecraft Fine Pointing (0.1 Degree) and Slewing (17.5 Degrees in 30 Minutes)

Utilization of high frequency, large aperture antennas require that precision pointing control of the spacecraft be provided for RF beam positioning. There are, in addition, a number of other applications where precision pointing becomes highly desirable as resolution requirements become more stringent. Classified in the second category are high resolution meteorological experiments, as well as the optical (LASER) communication system. The specialized capability of tracking low earth orbit spacecraft is provided by implementation of the spacecraft slewing capability.

The ATS F&G spacecraft provide, as part of the spacecraft attitude control system, the necessary pitch, roll, and yaw sensors, operational controllers, and torquers required to demonstrate the technological objective stated above. Offset pointing of the spacecraft attitude to 0.1 degree can be performed by utilizing prime sensors. Station pointing can be performed by using either the prime sensors or by using the X-Band monopulse. Open loop and closed loop monopulse slewing capability is provided for tracking low earth orbit satellites.

The provision of the fine pointing and slewing capability of the spacecraft will be demonstrated for the most part with the accomplishment of the applications objectives as defined by the TRUST, PLACE, and DRS experiments, in conjunction with operational tests performed using the monopulse and interferometer. The capability of being able to hold the pointing accuracy and slew over the earth disc is a particular technological significance, as is the two year operational life of the three-axis, closed loop attitude control system.

3.1.1.3 Provision of an Oriented, Stable Spacecraft at Synchronous Altitude for Advanced Technological Experiments Selected through the Space Science and Applications Steering Committee

The ability of ATS F&G to establish an earth oriented stable platform at synchronous altitude provides the environment necessary for selected, advanced technological experiments. The objective is usable for and required by a large number of technological and scientific experiments. The applications objectives of those experiments selected by the Space Science and Applications Steering Committee are discussed in Paragraph 3.1.2.

3.1.1.4 Demonstration of Precision Interferometer Attitude Measuring Technology for Closed Loop Servo Performance

Interferometer technology has been well established and the performance parameters associated with interferometer techniques have been tested in a variety of applications; the most notable of these is the Space Tracking and Data Acquisition Network (STADAN) Minitrack System. To date, however, the use of interferometer technology in providing a space qualified sensor has not been demonstrated.

The spacecraft equipments on board ATS F&G include an RF interferometer utilized as a precision spacecraft attitude angle sensor that can work in conjunction with the Attitude Control Subsystem. The output is represented as direction cosines to a ground station transmitting at X-Band. The attitude angles (direction cosines) are measured in the spacecraft, by measuring the phase differences between the signals received by the pairs of antenna elements installed along the spacecraft pitch and roll axes.

The resultant information may then either be telemetered to a participating ground station for reduction of the attitude information or be directly coupled to the spacecraft Attitude Control Subsystem. The interferometer provides attitude information in pitch and roll when a single ground station is utilized. It can also provide information in yaw when two or more stations are in use. The interferometer may be utilized as an on-board functional back-up to the prime earth sensors, providing a ± 12.5 degrees offset pointing capability while maintaining its attitude angle precision of 0.03 degree. In addition to its utilization as a pitch/roll sensor for acquisition and offset pointing, the relatively wide field of view of the interferometer will be operationally useful for precise attitude control during antenna measurements.

The interferometer as a sensor incorporates the inherent capability for further development providing higher accuracies. The ATS-F interferometer thus demonstrates the potential of space-borne interferometer sensors for further applications.

3.1.1.5 Demonstration of the Capability of Forming High-Gain, Steerable Antenna Beams

This technological objective is to demonstrate the feasibility of independently steering high-gain antenna beams over the earth disc without moving the spacecraft. The beam steering will be performed at S-Band, demonstrating the ability to maintain a secondary beam of specified gain and beamwidth. The beams will be steered using electronic antenna switching. The ability to rapidly switch beams between two points can be demonstrated utilizing ground stations or satellites. An important application of this technology is the tracking of multiple orbiting low-earth satellites.

The ATS F&G spacecraft implement an S-Band antenna system to demonstrate the objective of forming high-gain steerable beams. Tracking of single and dual satellites is performed, permitting duplex communication with any single satellite at S-Band. The rapid electronic beam switching capability, coupled with the offset pointing capability of the spacecraft, permits communication with either of two independent satellites.

3.1.1.6 Provision of a Multi-Frequency, Multiple Access Communication Subsystem

The communication technology experiment candidates for ATS F&G involving small ground terminals have dictated that a multi-frequency, multiple access transponder and prime focus feed system be developed for utilization with the 30-foot parabolic reflector. UHF, L, S, and X-Band frequencies have been selected for ATS-F.

ATS-F provides an Integrated Transponder and Prime Focus Feed incorporating features adapted from the requirements specified for performance of selected experiments. PLACE, TRUST, and DRS have, to the greatest degree, determined the particular design of the ATS-F Communications Subsystem and the performance of these experiments will demonstrate the technological objective.

The following paragraphs describe the applications objectives of the ATS spacecraft. Table 3.1-2 tabulates a summary of the objectives. A brief description of the impact of these experiments on the spacecraft design and operational modes is also provided.

3. 1. 2. 1

Instructional Television

The Instructional Television (ITV) experiment is a special case of the more general TRUST (Television Relay Using Small Terminals) experiment. The purpose of the experiment is to advance the state-of-the-art in space communications by implementing, testing, and demonstrating CCIR quality wideband signaling between the ATS-F spacecraft and inexpensive UHF ground receiving stations.

The value of television as an educational tool in underdeveloped nations has been increasingly recognized in recent years. It has been demonstrated as a highly efficient and effective medium for mass instruction of the population of emerging nations. National TV distribution throughout large countries with a dispersed multilingual population can be done economically by using a synchronous satellite system with multiple sound channels to ease language problems that might arise.

Programming from a centrally located ground station will be transmitted on X-Band to ATS-F and relayed at UHF to two types of ground stations located in India: to individual special ground receivers located in villages and to conventional receivers in urban areas via VHF rebroadcast facilities. Figure 3.1-1 depicts an artist's conception of the ITV operational configuration. The basic objective of this experiment is to provide an economical educational television network embodying the following features:

- The ability to distribute CCIR quality educational television to many scattered villages and a few densely populated areas.
- Provision for utilizing a single ground station in India (Ahmadabad) as the central programming facility.
- Provision of the capability for simultaneous transmission of multiple voice channels.
- Utilization of low cost receivers.

Table 3.1-2. Applications Objectives Summary

Experiment	Objective Type	Major Objectives
Very High Resolution Camera	Meteorological	Measure cloud cover Determine wind field
High Resolution Radiometer	Meteorological	Measure cloud cover Determine wind field Ocean temperatures/Earth resources
Time and Frequency Dispersion	Communications	Investigate high data rate digital communications
Radio Frequency Interference	Communications	Investigate C-band terrestrial noise sources (geographical/noise power distribution)
LASER	Communications	Feasibility of the application of wide-band coherent laser communications systems
Millimeter Wave	Communications	Investigation of atmospheric propagation at MMW frequencies. Feasibility of the application of MMW communications systems
Radio Beacon	Scientific	Ionospheric/exospheric electron content measurements. Ionospheric propagation effects
Environmental Measurements Experiment	Scientific	Solar cell degradation. Magnetic field measurement. Particle measurements
SAMOC/SAPPSAC	Spacecraft Stabilization	Investigation of computer controlled attitude control performance optimization
Commandable Gravity Gradient	Spacecraft Stabilization	Investigation of the feasibility of gravity gradient techniques for attitude control
TRUST	Communications	To advance state-of-the-art in space communications by demonstrating CCIR quality wideband signaling between ATS-F and inexpensive ground stations
PLACE	Communications	To develop improved air traffic control techniques
DRS	Communications	To demonstrate technology necessary for an operational data relay system

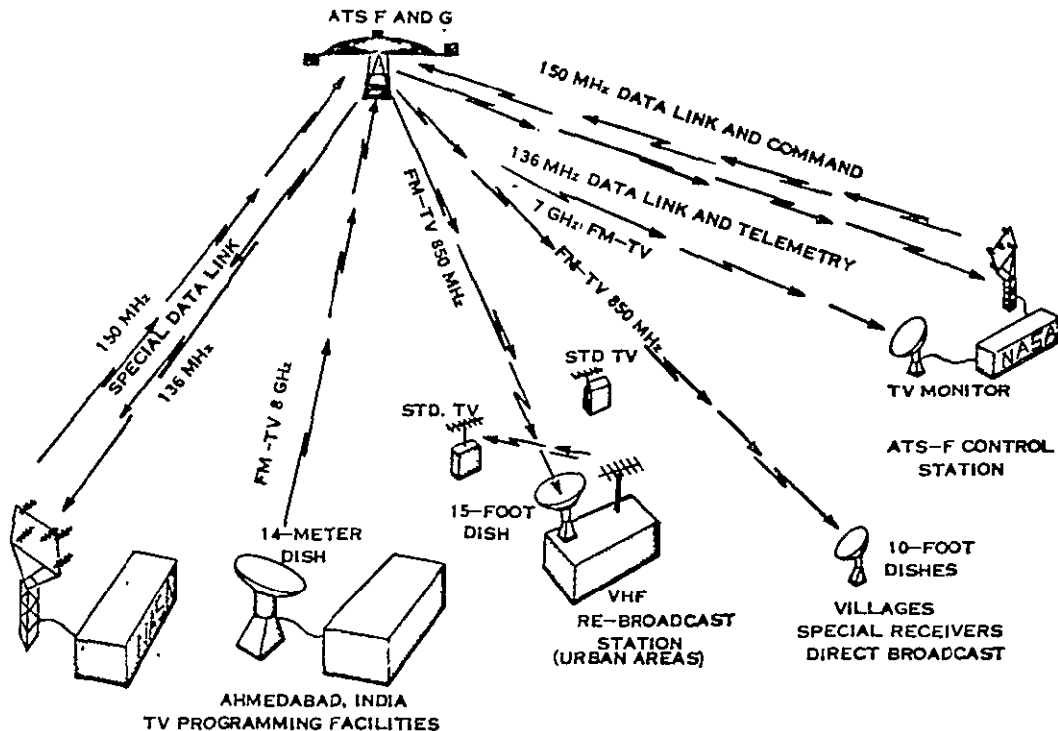


Figure 3.1-1. ITV Operational Configuration

The major requirement of the ATS-F spacecraft for this experiment is the development of an 80-watt X-Band to UHF frequency translating communication repeater. This UHF power amplifier, when used to feed the 30-foot diameter parabolic antenna, must produce an ERP of at least 48 dbw over a 3-degree field of view.

3.1.2.2 Position Location and Aircraft Communication Equipment (PLACE)

The Position Location and Aircraft Communication Equipment (PLACE) experiment is aimed at developing an improved air traffic control technique. The purpose of PLACE is to demonstrate the ability to continually determine the location of all aircraft in the system and to monitor their positions relative to each other. When implemented with the ATS F as a synchronous altitude satellite communications repeater, PLACE will provide two-way voice and digital data communications between all cooperating aircraft and their associated ground control facilities.

Provision of continuous communications between ground control stations and aircraft, coupled with finer resolution navigation measurements will be particularly important with the increase in traffic density coupled with evolution of the "Jumbo Jets" and supersonic transports in the 1970s. The air traffic density over the North Atlantic is already sufficiently high so that less than optimal routes must at times be utilized. The problem is expected to become worse if improved communications and navigation procedures are not developed. The safety of aircraft flight and reaction

to potential emergency situations will be enhanced by improved operational communication and navigation systems. Figure 3.1-2 depicts the links associated with the PLACE experiment.

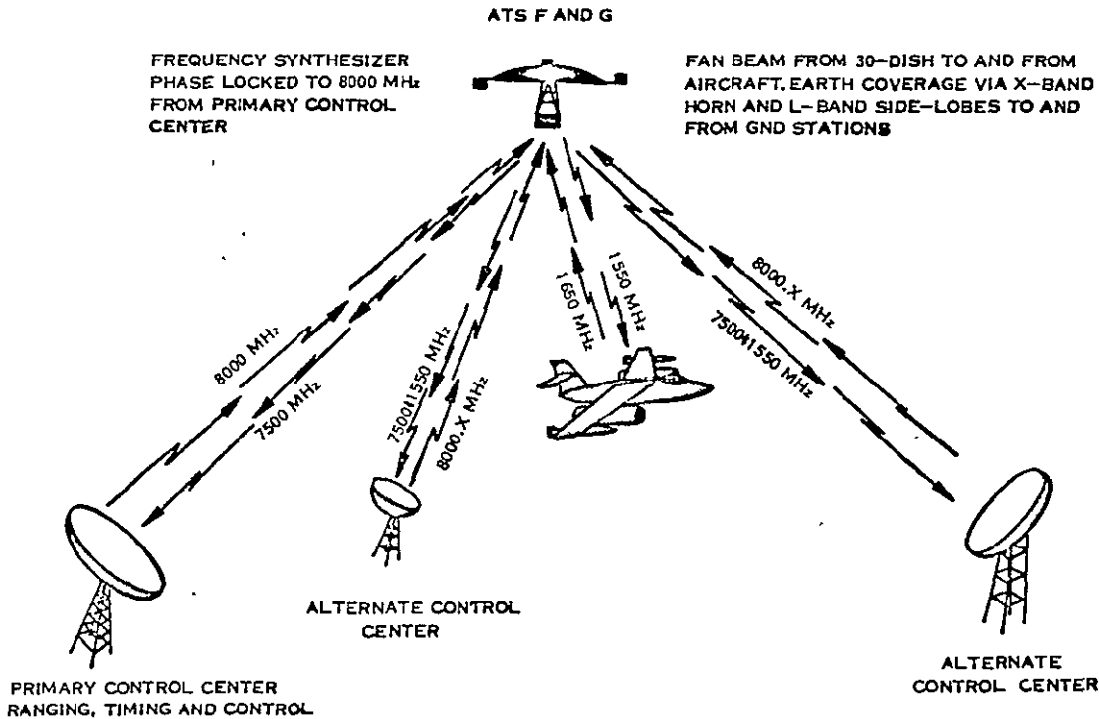


Figure 3.1-2. PLACE Experiment

PLACE communications require duplex RF links through the ATS-F repeater. To accommodate multiple ground control facilities transmitting FM signals on one link and multiple aircraft transmitting SSB signals on the second link, the ATS-F communication transponder must be a frequency-division multiple-access (FDMA) signal processing repeater. On the ground to aircraft link, multiple FM signals must be converted to FM/PM and on the aircraft to ground link SSB signals must be converted to SSB/PM.

In the navigation experiment, utilizing ranging information from the spacecraft to the aircraft, a known altitude and OMEGA information (or information from a VLF station), it is expected that the location of the aircraft can be determined to an accuracy of 1 nautical mile.

3.1.2.3 Data Relay System

The Data Relay System (DRS) experiment will explore, develop and demonstrate critical aspects of the technology necessary to an operational data relay system between a data acquisition facility (DAF) and a low altitude satellite via the ATS-F. The specific program goals of DRS include:

- Real-time data relay
- Range and range-rate tracking, using GRRR and ATS-R systems
- Low altitude satellite commanding through the ATS-F

Simultaneous tracking of two low altitude satellites will be demonstrated with duplex communication provided to one selected satellite. Data relay, with Nimbus and Apollo Workshop satellites in particular, have been chosen for the satellite tracking experiments with ATS-F. Figure 3.1-3 depicts an artist's conception of the operational configuration.

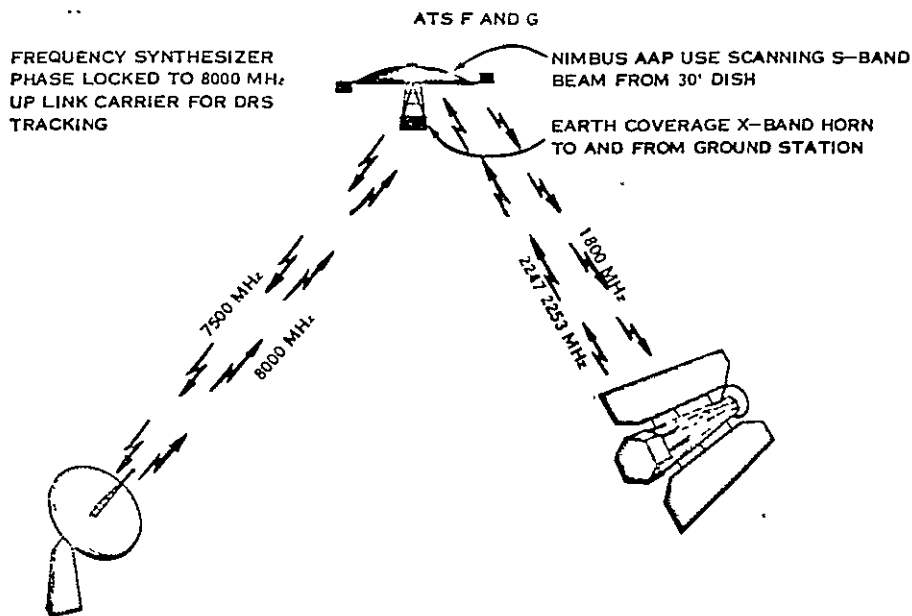


Figure 3.1-3. NIMBUS/AAP Relay DRS

The DRS experiment requires that the ATS-F possess the capability of maintaining S-Band beam tracking of one or two low altitude satellites. Thus the ATS-F to target satellite communications will be based upon high-gain S-band antenna beams; the ATS-F to ground link will be at X-Band using the spacecraft earth coverage horn. Use of the GRRR tracking system requires that the ATS-F master oscillator be capable of phase locking to the carrier component of the X-Band up-link signal so all frequency translation operations in the ATS-F will be phase coherent.

The major design requirement associated with the DRS experiment is in obtaining adequate gain over the required S-Band antenna field of view. Care must be taken to minimize the beam cross-over antenna gain loss and to identify these points so beam switching is accomplished at the correct time during a satellite track.

3. 1. 2. 4

Spacecraft Attitude Maneuvering Optimal Control (SAMOC)/ Self-Adaptive Precision Pointing Spacecraft Attitude Control (SAPPSAC)

The objective of the SAMOC/SAPPSAC experiments is to demonstrate a new control technique for active fine pointing and attitude slewing maneuvers with optimum performance. The SAMOC system demonstrates a control concept for changing the ATS pointing vector in a prescribed manner. The SAPPSAC system demonstrates a control concept for holding a precise pointing attitude in the presence of unknown disturbance torques.

The mathematics for this optimized self-adaptive control system have been determined. It remains, however, to demonstrate the feasibility and practicality of this approach in actual practice. This is the objective of SAMOC/SAPPSAC. To avoid unnecessary complications in the spacecraft, the T&C subsystem will be used in the loop in conjunction with a ground computer.

The most important impact of this experiment is the T&C subsystem which must provide the requisite functions. The Command Subsystem incorporates a timed-tone control mode to provide control of wheels and jets. The Attitude Control Subsystem provides the special interfaces to the wheels and jets to permit time-tone control. As part of the ATS-F system complement of features, attitude data required by SAMOC/SAPPSAC is provided on the PCM telemetry frame.

The SAMOC/SAPPSAC operational configuration will utilize a computer at Goddard Space Flight Center connected in real time to the ATS-F spacecraft through the ATS ground station located at Rosman, North Carolina. Successful execution of the experiment will demonstrate the potential of utilizing adaptive techniques for optimization of performance. When applied to conservation of expendable fuel supplies, the experiment shows particular promise in extending the life of spacecraft utilizing jets for attitude propulsion.

3. 1. 2. 5

Commandable Gravity Gradient System

The objective of the Commandable Gravity Gradient System (COGGS) is to demonstrate the applicability of gravity gradient control techniques for precision attitude control of the spacecraft. On ATS-F the COGGS is being specifically developed for use at synchronous altitude to perform to the following requirements:

- Precision pointing with a maximum error of 0.1 degree up to 10 degrees off the local vertical.
- A slew maneuver capability of 17.5 degrees across the earth disc and settle to 0.1 degree accuracy within 30 minutes.

- A tracking maneuver capability with track angle commands of 1 degree/minute with a maximum error of 0.5 degree. The settling time to a pointing accuracy of 0.1 degree shall be no more than 10 minutes.

When the COGGS is in operation, the ATS-F spacecraft sensors will be utilized to sense attitude angle errors. The operational controller will interface with the sensors and COGGS to provide required roll/pitch gimbal angle commands. Inertia wheels will provide roll and pitch loop damping and yaw control. The ATS -F house-keeping systems will be utilized in support of the COGGS. The most stringent design requirement for COGGS is the development of a boom that will meet the required maximum slew rate, within the given weight constraints. A boom designed to meet the stated requirements would have a low fundamental bending frequency, causing serious dynamic response problems for the Attitude Control Subsystem. It has therefore been proposed to reduce the maximum slew rate capability to 0.5 degree/minute. Deployment of the COGGS boom is scheduled at the end of the mission to ensure the experiment does not interfere with other mission objectives of the spacecraft. Extension of the mission past fuel depletion is therefore possible.

3.1.2.6 Very High Resolution Camera

The objective of the Very High Resolution Camera Experiment is to provide high resolution cloud cover pictures of the earth disc. The camera will also provide means for meteorological investigations and will demonstrate the technology utilized in the development of the high resolution (5000 lines) image dissector camera system. The camera data when correlated with data from the High Resolution Radiometer aboard ATS-F will permit the determination of wind field and cloud altitude as a function of pressure.

The Very High Resolution Camera is supported by housekeeping systems provided as part of the ATS-F spacecraft. A special experiment spacecraft interface is the wide-band high quality data link (at X-Band) provided by the communications subsystem. The camera has also imposed a special requirement on the design of the attitude control subsystem; the need for a very high stabilization mode. A jitter amplitude of .003 degree and jitter rate of .0003 degree per second is required (design goal) to insure a minimum contribution of resolution error from the spacecraft.

Data for the very high resolution camera will be taken at each of the three ATS ground stations. Real time data transfer will be available from Rosman to GSFC for certain tests. The data will normally be recorded at the ground stations and transmitted to GSFC at a later time for processing onto seventy millimeter film by an Electron Beam Recorder. Capability of sector scan pictures, as well as full earth disc pictures will be available to obtain a higher rate of meteorological information of certain areas.

3.1.2.7 High Resolution Radiometer

The objective of the High Resolution Radiometer is to photograph the earth disc from synchronous altitude. Two bands of data are available; one at 10.5 to 12.5 micron (IR) and the other at 0.55 to 0.75 micron (visible). The data will be used for meteorological observations, ocean temperature determination, albedo measurements, and earth resources. In particular, the radiometer cloud temperature data can be used to calculate cloud height and pressure.

The Radiometer is supported by the ATS-F housekeeping systems. Wide-band data from the radiometer is transmitted to ground stations over the high quality X-Band data link provided by the communications system. The Radiometer requires precise stabilization of the spacecraft. The VHR camera, also on board the spacecraft, has a more stringent stabilization requirement than the radiometer and has "sized" the attitude control low jitter mode.

Data from the Radiometer will be taken at each of the three ground stations; real time data transfer will be available from Rosman to GSFC for certain tests. The data will normally be recorded at the ground station and transmitted to GSFC at a later date for processing.

3.1.2.8 Time and Frequency Dispersion

The objective of the Time and Frequency Dispersion Experiment (T&FD) is to provide quantitative data on the time and frequency dispersion of very narrow RF pulses transmitted from ATS-F to the ground. Amplitude and phase measurements will determine the effect of the propagation characteristics of the transmission medium.

T&FD will utilize the 0.1 degree pointing accuracy and slewing capability of ATS-F along with the 30-foot diameter parabolic reflector to obtain necessary data. The housekeeping systems of ATS-F will also be utilized (power thermal control, etc.). A major requirement on the spacecraft design is the modulator interface with the integrated transponder. A design has been developed to accept a $\cos^2 x$ shaped modulating pulse at a signal level of -37 dbm to modulate the drive of the communication subsystem X-Band traveling wave tube amplifier. The pulse width and its repetition rate are selectable.

Data from the T&FD experiment will be taken at the ground stations. The information obtained from the experiment will provide quantitative data as to the applicability of utilizing microwave frequencies (C-Band is of particular interest) for high speed digital data links.

3.1.2.9

Radio Frequency Interference

The objective of the Radio Frequency Interference (RFI) Experiment is to provide data on the mutual interference between satellite and terrestrial telecommunications systems. Specifically the distribution of terrestrial noise power will be measured over a band of 500 MHz about a 6 GHz nominal center frequency to determine the following:

- The geographical and frequency distribution of the 6 GHz interference sources
- The integrated interference noise power
- The practical gain/temperature (G/T) limits for satellites
- The minimum satellite protection ratio of wanted to unwanted carrier ratio (C/X)

The RFI experiment utilizes the supporting systems provided by the ATS-F spacecraft. The major requirement is the design of a 6 GHz Feed with selectable polarization, as part of the prime focus feed assembly. The feed has been positioned on axis and physically integrated with the X-Band feed. When used with the 30-foot diameter parabolic reflector a gain of 48 db is achieved. The 0.1 degree offset pointing accuracy over a ± 10.0 degree slewing range inherent in the ATS-F Attitude Control Subsystem provides the support particularly necessary to achieve the RFI objectives.

Data for the Radio Frequency Interference experiment will be received on the X-Band down-link at the ATS ground station located at Rosman. Supporting housekeeping data (attitude information) will also be available. A number of proposed domestic satellite communications systems have utilized frequencies in the 6 GHz to 4 GHz bands already allocated to terrestrial radio relay systems. The RFI data will help the Federal Communications Commission make decisions on frequency assignments and transmission regulations for domestic satellite systems.

3.1.2.10

LASER Experiment

The objective of the LASER Experiment is to utilize present laser technology to demonstrate the feasibility of optical communications in space. The coherent laser communications system will permit the following:

- Establish the technology required to provide wideband, clear-weather, data channels between ATS-F and the earth.
- Provide equipments to permit a direct comparison of microwave and LASER communication systems.
- Measure the optical propagation characteristics of the atmosphere.

The laser also has a monopulse output that will be utilized to demonstrate the feasibility of using an optical monopulse in a closed loop with the attitude control system.

The ATS-F provides the support systems necessary for performance of the LASER Experiment. In particular, the high pointing accuracy of ATS-F and the high data quality achievable with the supporting microwave communication link are necessary for evaluation of the laser performance.

The LASER experiment will be performed by the Laser ground station located at, and in conjunction with, the ATS Mojave ground station. The modulated signals and microwave link will be supplied from the ATS station. The data obtained will demonstrate the applicability of LASER technology to space applications. The performance characteristics of the laser system will be completely tested under operational conditions.

3.1.2.11 Millimeter Wave Experiment

The scientific objective of the Millimeter Wave Experiment is to obtain data related to the propagation characteristics of the space/earth transmission medium. The data will be taken for the K_a and K_u transmission bands over a wide variation of weather conditions. Several, separated millimeter wave ground stations are to be utilized providing a sample distribution of climatic conditions. The particular propagation parameters of interest are atmospheric absorption, refraction, dispersion, fading, and noise interference. The experiment will demonstrate the technology of space-qualified millimeter wave hardware and the performance of K_a and K_u Band systems, as they may later be applied to communications, navigation, and radio telescopes.

The ATS-F spacecraft provides the housekeeping support systems necessary to achieve the technical objectives of this millimeter wave experiment. A high quality baseband reference signal must be cross-strapped from the ATS-F microwave (X-Band) communication up-link and provided to the millimeter wave experiment. When operating with the support systems and the full X-Band transmission link for comparison purposes, the Millimeter Wave Experiment constitutes one of the highest power loads (404.6 w) for ATS-F.

Data for the Millimeter Wave Experiment will be taken by the millimeter-wave transportable ground station located at Rosman and participating ground stations positioned throughout the continental United States. The ATS ground station at Rosman will support the experiment; transmitting X-Band to the spacecraft, receiving the X-Band return and spacecraft/millimeter wave housekeeping data. Data on weather conditions will be taken for correlation with the Millimeter Wave Experiment performance data. The performance data will be evaluated primarily by measurement of the amplitude and phase characteristics over the receive bandwidth on the carrier or multi-tone spectrum. For one communications experiment an evaluation of the quality of the millimeter wave link will be performed.

3.1.2.12

Radio Beacon Experiment

The objective of the Radio Beacon Experiment is to provide scientific data related to the properties and behavior of the exosphere and ionosphere through measurement of the dispersion of radio signals in those propagation media. The following investigations are planned:

- Ionospheric electron content as a function of ionospheric storms. Rates of production/loss and transport of ionization in the F-region of the ionosphere. Study of the effects of eclipse and gravity.
- Exospheric electron content as a function of solar/geomagnetic activity and diurnal and seasonal changes.
- Measurement of ionospheric scintillations (amplitude and phase).
- Ionospheric absorption measurements.

The Radio Beacon imposes a requirement for almost continuous operation, particularly early in the mission when ATS-F will be located at 94° W longitude in view of the continental United States. The main area of concern in providing the experiment equipments has been the design of an antenna that will maintain the required phase stability and provide the required ERP without interference with the other spacecraft functions.

Data for the Radio Beacon will be taken on the ground by a number of small stations located at various geographical locations. The ionospheric/exospheric investigations will utilize a number of measurements including the Faraday effect, and the group-path method. The group path method measures the phase difference between coherent modulation of two different carrier frequencies. With the Radio Beacon in a geostationary orbit measurements can be made from a position where the influence of the magnetosphere and solar wind environments is easily interpreted. The stationary relationship between the beacon and participating ground stations simplifies data reduction and provides an opportunity to obtain more data at specific latitudes than has been the case for topside sounding equipments on low orbiting satellites. This stationary relationship will permit sufficient data to be taken to predict the average behavior of the ionosphere.

3.1.2.13

Environmental Measurements Experiments

The objective of the Environmental Measurements Experiments (EME) is to make scientific measurements of the space environment at synchronous altitude. The three types of measurements covering seven (7) unique experiments are:

- Solar Cell Degradation
- Magnetic Field
- Particle Measurements (electron, proton, alpha)

The EME Experiment utilizes the support systems of ATS-F in the performance of its functions. The EME will be located on the hub assembly to expose its space-viewing surfaces and therefore must provide its own thermal control. The major impact upon the ATS-F spacecraft by EME is the requirement for an extremely low (0.5 gamma) magnetic field at the location of the magnetometer. The field of view requirements of the experiment will have to be "custom fit" with the spacecraft. Moreover, deployment of the COGGS boom late in the mission will probably interfere with the EME viewing space.

The data from EME is transmitted to the ground on its own PCM wavetrain over the spacecraft VHF link. This data will be recorded at ATS stations, with STADAN support as necessary. Listed below are the specific objectives of the individual EME experiments.

a. Solar Cell Radiation Experiment

The objective of the Solar Cell Radiation Experiment is to measure the degradation of solar cells at synchronous altitude. Current and voltage characteristics will be measured on 80 selected solar cells. Each cell will embody variations in characteristics as to type and kinds of protective coatings.

Solar cells have been and will be used extensively, in conjunction with batteries, as the prime unregulated power source for unmanned spacecraft. The data taken from this experiment will be utilized in the development of solar cell types that optimize radiation damage resistance and optical transparency. The data, of course, must be correlated to the environment (orbit). Performance of the test under laboratory conditions, although it is useful, cannot provide the complex environment actually present in space.

b. Magnetometer Experiment

The objective of the magnetometer is to measure the magnetic field in three orthogonal axes at synchronous altitude. Transient variations will be measured, including diurnal variations due to the solar wind and fluctuations caused by geomagnetic storms.

c. Particle Experiments

The objective of the particle experiments is to make scientific measurements of the orbital environment of ATS-F (synchronous altitude). Electron measurements will be made over a 50 EV to 1 MEV range, proton measurements over a 50 EV to 230 MEV range, and alpha particle measurements over an energy range from 1.3 MEV to 280 MEV. The data will be taken to correlate, with distortions of the magnetosphere, the cause and effect, which is more apparent at synchronous altitude. Auroral effects, cosmic ray effects, diurnal variations due to the solar wind, solar flare effects, all will be studied. Data will then be correlated with ATS-F ephemeris and attitude information.

The magnetometer and particle experiments will provide data enabling a better understanding of high altitude radiation phenomena. This is important when it is considered that the early 1970's promise to be years of increased solar flare activity.

3.2 SPACECRAFT DESIGN DESCRIPTION

3.2.1 INTRODUCTION

The ATS F&G mission requires a spacecraft in an Earth-oriented synchronous altitude, equatorial orbit and stabilized about three axes. The primary requirements have been defined in terms of performance parameters derived from the mission objectives in Section 3.1 of this report.

Primary Mission Requirements:

- Communications Performance
- Attitude and Propulsion Control Performance
- Telemetry and Command Performance
- Experiment Power
- Experiment Weight

The remaining design requirements are self-imposed as the performance of each system element is obtained through commitment of budgeted weight and power resources. The Communications, Attitude Control and Experiment primary requirements demand a large spacecraft with high conditioned dc power.

Certain basic configuration elements which have remained essentially constant throughout the several years of concept, design analyses and trade-off study are summarized below:

- Large Deployable Parabolic Reflector
- RF Feed Module with Earth Viewing Experiments
- Large Deployable Solar Array
- Active 3-axis Control System

The placement of a comparatively large physical structure into synchronous orbit while maintaining a compact and structurally sound configuration during the launch and orbital injection phases of the mission presented some unusual design problems. Not only are the involved physical structures large, but their functional requirements demand a high degree of precision in mechanical alignment and orientation, thus placing additional requirements upon design and deployment techniques. The configuration and techniques evolved by FHC to reliably accomplish these objectives are deceptively simple in nature, yet meet all of the mission requirements and enhance the performance of defined experiments and the other spacecraft subsystems.

The FHC design for the ATS F&G spacecraft is shown in Figure 3.2-1 in the orbital deployed configuration. The spacecraft is stabilized about three axes to provide controlled pointing of the high gain reflector toward a selected portion of the Earth and to permit the experiment to view the Earth of space as required.

3.2.2 SPACECRAFT DESCRIPTION

3.2.2. General Description

As shown in Figure 3.2-2, the spacecraft is functionally separable into six major elements:

- Adapter
- Earth Viewing Module (EVM)
- Reflector Support Truss
- Structural Hub
- Reflector
- Solar Arrays and Supporting Booms

The EVM is mounted to the transtage of the Titan III C launch vehicle at vehicle station 77.0, and is located 5 inches above the transtage by means of an adapter consisting of four independent trusses. Each truss has two tubular legs formed in a V configuration. The points of the V's are attached to the EVM approximately at its mid-height point, and the open ends of the V's are attached to eight points on the Titan III C field joint.

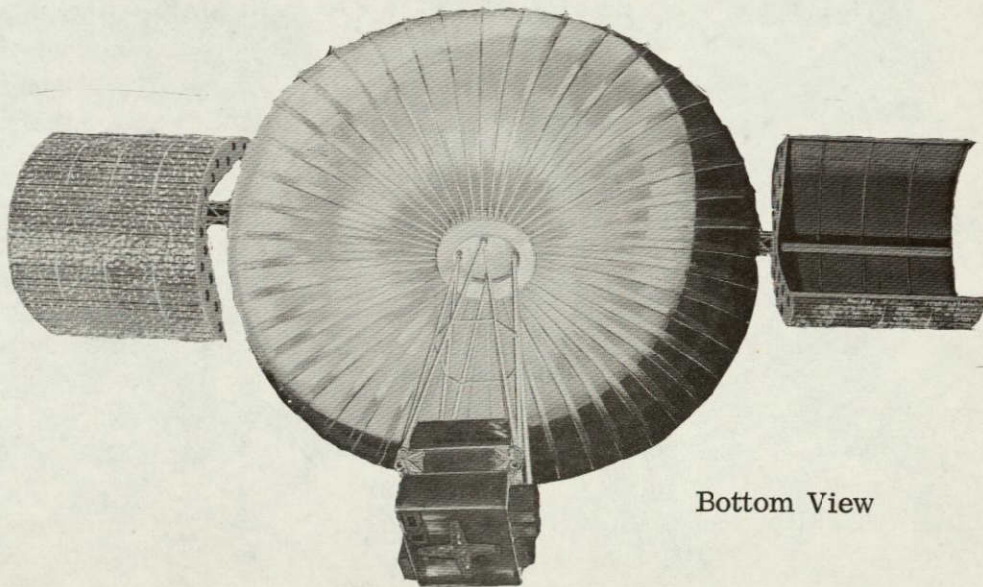
The EVM portion of the spacecraft contains the majority of the electronic equipment including all Prime Focus Feed and Earth Viewing components. The EVM shape is a cube approximately 54 inches along each edge with the upper surface located at the focal point of the 30-foot diameter reflector. This cubical configuration is divided into three separate modules for assembly, integration and test, thereby, providing excellent access to installed equipment during the early portions of spacecraft integration.

The reflector support truss connects the EVM with the structural hub, and maintains accurate alignment and positioning between these elements. The truss consists of eight tubular members arranged in symmetrical A-frame configuration. It supports the orbit control jets of the auxiliary propulsion system and all electrical interconnecting wiring between the hub and the EVM.

The structural hub is a box frame approximately 39 inches square and 6 inches deep. The hub at its four corners supports the 30-foot diameter reflector, while its deep space side (-Z direction) provides a mounting surface for the solar array booms and for experiments that must view deep space. These include an environmental measurements experiments package (EME) and a gravity gradient experiment (COGGS).



Side View



Bottom View

Figure 3.2-1. Spacecraft Deployed Configuration

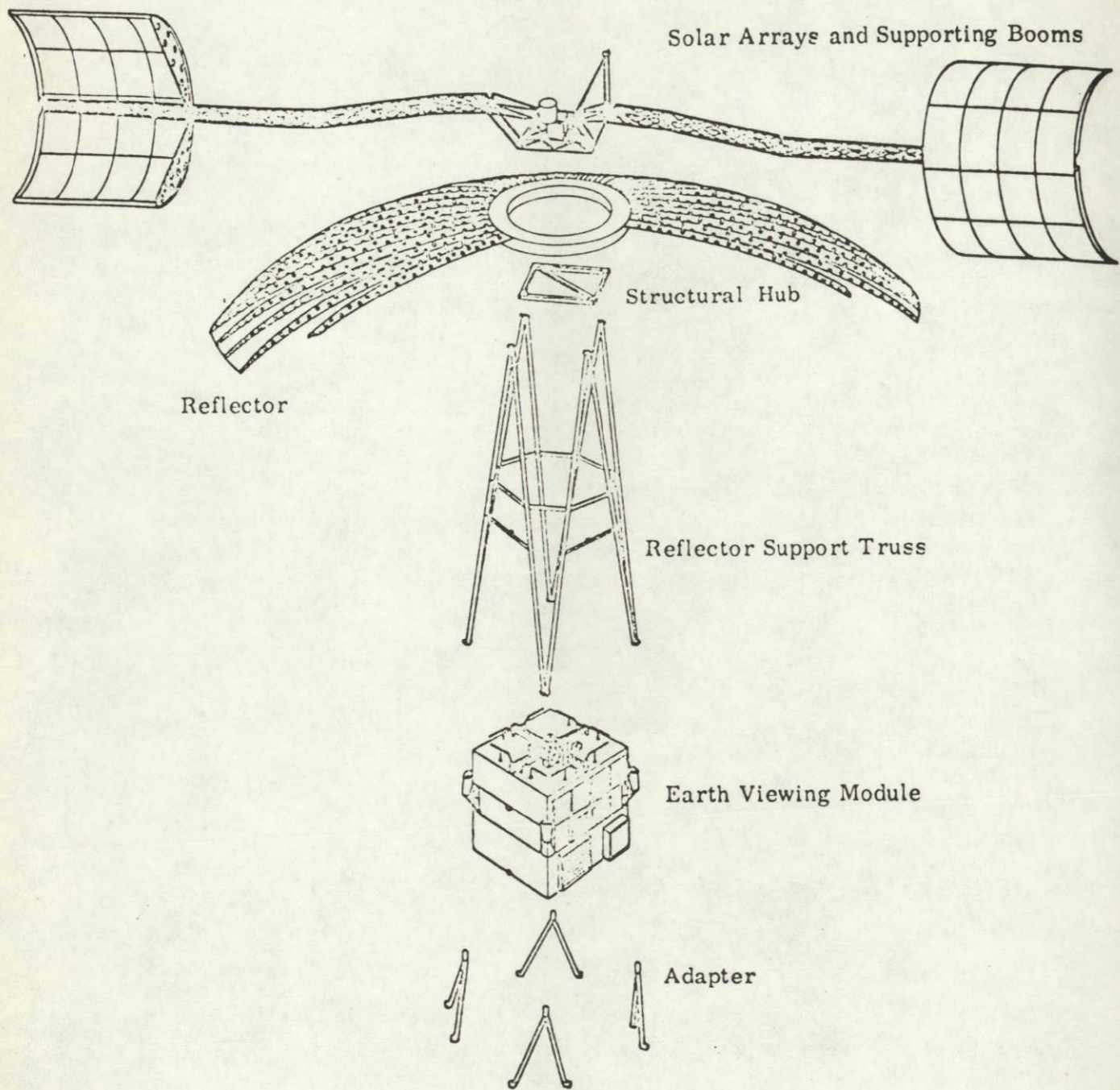


Figure 3.2-2. Exploded View of ATS-F

The reflector embodies the Lockheed "flex-rib" design. It consists of 48 flexible radial ribs covered by a copper and silicone coated Dacron mesh stowed in an annular container. Upon release it deploys into a paraboloidal reflecting surface with an F/D ratio of 0.44. The reflector focuses RF energy toward the earth when illuminated by the feed elements on the EVM.

The solar array consists of two semi-cylindrical panels supported upon deployable booms and arranged with the cylindrical axes approximately normal to the orbital plane. Except for occultation this configuration provides a nearly constant power output throughout the day. The two solar panels each have an outside diameter of 108 inches and a height of 88.5 inches.

3.2.2.2 Stowed Configuration

The designated launch vehicle, the Titan III C, allows a nominal transtage fairing 10 feet in diameter by 30 feet in height. For launch, the reflector is stowed around the structural hub in a toroidal package of approximately 78 inches outside diameter. The solar array booms are folded down at the knee joints that interconnect the booms to the bridge truss structure mounted on the structural hub. The two semi-cylindrical solar array panels are folded back over the booms to form a complete cylinder with its lower edge approximately three inches above the prime focus feed surface of the EVM. Figure 3.2-3 shows the spacecraft in the stowed configuration.

In the launch configuration the solar array panels clear the internal dynamic envelope of the payload fairing by 2.1 inches. The solar array booms at their most forward point have lateral dynamic excursions of approximately 1 inch, which result in a 0.9 inch clearance from the available fairing dynamic envelope.

The height along the "Z" axis of the spacecraft from the bottom surface of the EVM to the most forward point (magnetometer) is 25.3 feet.

3.2.3 LAUNCH, SEPARATION & DEPLOYMENT

3.2.3.1 Launch Sequence

It is desired to place ATS-F into a nominally synchronous equatorial circular (SEC) orbit, initially above the United States at 94 degrees $\pm 4^{\circ}$ west longitude. It is presently planned to launch the spacecraft from the Eastern Test Range aboard a Titan III C at an azimuth of about 93 degrees East. In order to achieve a desired sunrise injection for synchronous orbit, the launch will occur about 0100 hours. The launch window can be extended from ± 0.5 hours nominal to ± 1.25 hours maximum by utilizing the $\pm 11^{\circ}$ pitch offset command for the earth sensor. This ensures that earth acquisition will occur during the roll scan maneuver around the sun line. A schematic representation of the launch trajectory is shown in Figure 3.2-4.

At the second equatorial crossing in the parking orbit, the Transtage (Stage III) will be ignited for about 310 seconds to inject the spacecraft/Transtage into

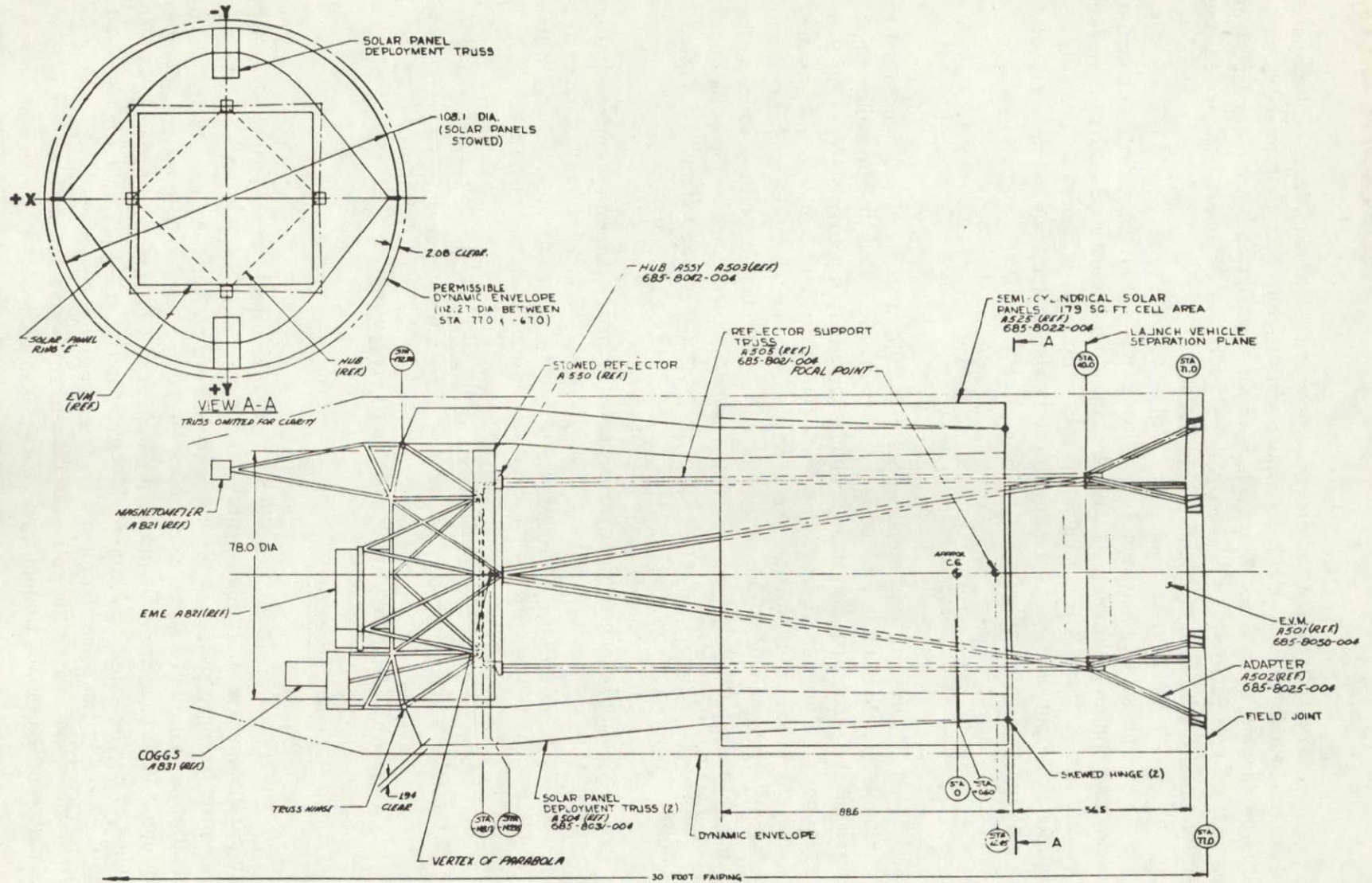
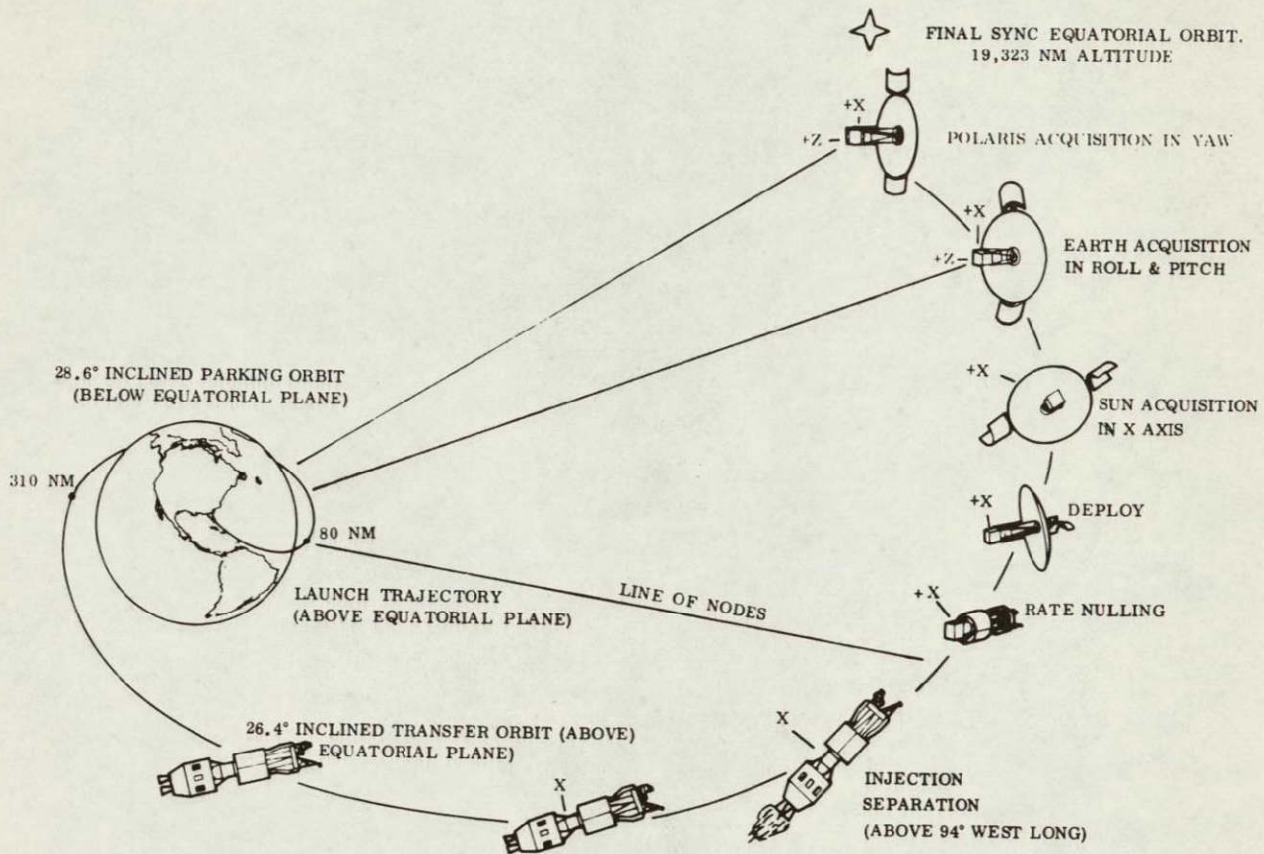


Figure 3.2-3. Launch Configuration Profile View

a transfer orbit with apogee at the synchronous orbit altitude of 19,323 n. mi. by the self contained on-board flight programmer. The transfer orbit inclination is reduced to 26.36 degrees to maximize the payload capability in the final synchronous circular (SEC) orbit. Figure 3.2-5 shows an artists conception of the spacecraft/Transtage during powered flight.



During the 5.3 hour coast in the transfer orbit, the Transtage will position the orientation of the spacecraft so the thermal control louvers will be pointed away from the sun. This will ensure proper operation of the ATS thermal control system during the transfer orbit. The X-axis of the ATS will be aligned with the sun line to enhance solar power generation by the stowed solar panels since elements of the Attitude Control Subsystem and the Telemetry and Command Subsystem (T & C) will be powered during the launch phase.

Following the coast to synchronous altitude, the Transtage will thrust for about 120 seconds to inject the spacecraft into a nominal synchronous equatorial circular orbit. Separation of the spacecraft from the Transtage is automatically triggered following injection by the Transtage Flight programmer, with a backup capability provided by ground command from Rosman via the ATS command

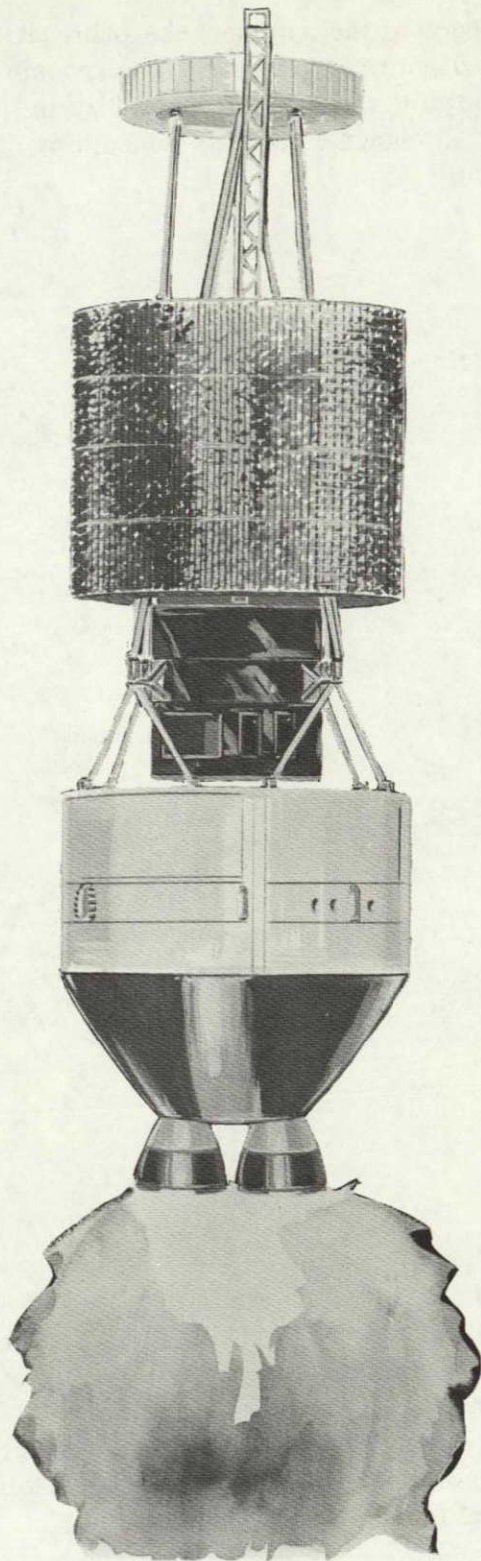


Figure 3.2-5. ATS Launch Configuration

system. Following separation, the Transtage is reoriented to perform a retro maneuver to remove it from the ATS orbit path and preclude any subsequent interference with ATS orbit operations.

3.2.3.2 Separation

After apogee injection, the spacecraft/transtage combination is in a synchronous equatorial orbit and in an inertially stable attitude. At this point the spacecraft is separated from the transtage/adapter assembly. Separation is initiated by signal from the transtage, which fires four totally redundant pyrotechnic separation attachments on both the transtage and the spacecraft sides of the separation plane. A relative separation velocity of 3 ft./second is obtained through the action of four matched springs, one at each of the attachment points. The minimum required separation velocity to prevent spacecraft launch vehicle-adapter interference at a 1°/sec tip off rate is .08 ft./sec. Separation is verified by a 30 inch delay-lanyard operated signal returned through the spacecraft telemetry system. A backup system to initiate separation is provided through the spacecraft command system, in the event of primary system failure.

An illustration of the separation sequence is shown in Figure 3.2-6. Upon separation, the adapter structure remains with the transtage. Guides on the EVM and rollers on the four V-shaped trusses assure that separation is a controlled rectilinear motion with less than 0.05°/sec. tip-off rates.

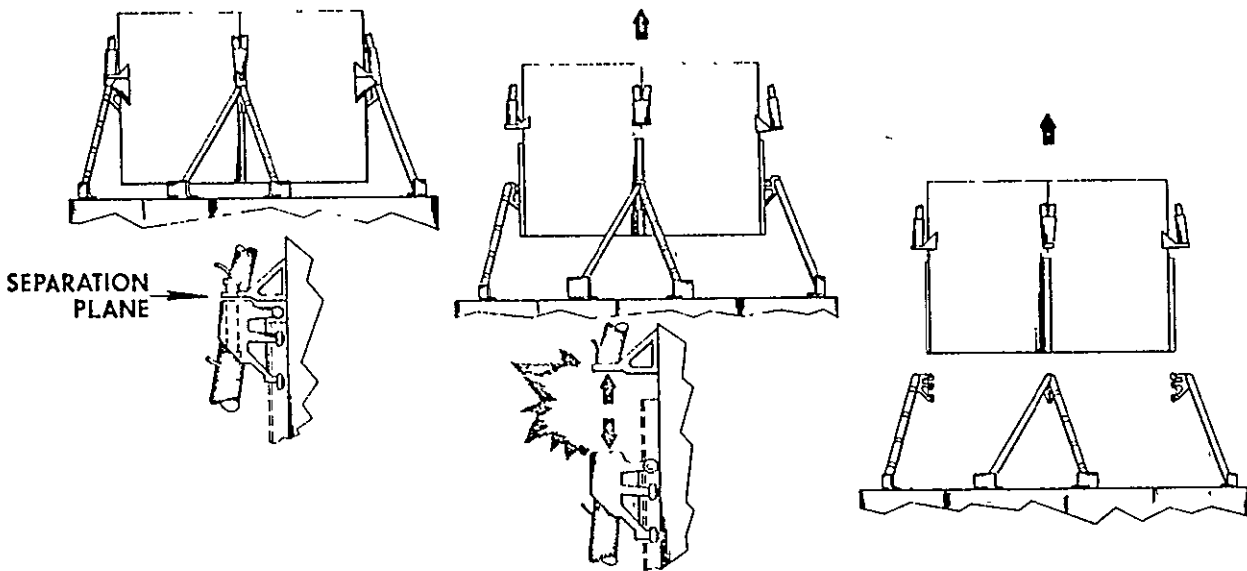


Figure 3.2-6. Separation Sequence

Figure 3.2-7 shows step-by-step the deployment sequence initiated after verification of separation and the nulling of tumbling induced by separation. (1) The solar panels are released from their launch restraint to the EVM. The solar array support booms then rotate (2-3) about simple knee joints connecting them to the structural hub bridge truss until they are in a position 22 degrees above their final position, thus ensuring room for reflector deployment. After lockup of the two knee joints, the solar panels rotate (4-7) about their skewed hinges and assume positions above and outboard of the reflector deployment envelope. The reflector then deploys (8) in a near-radial plane from the hub, and snaps into a paraboloidal shape. The solar array booms are rotated downward about the knee joints through the 22 degree angle, (9) to reach a final position that prevents mutual shadowing of the array and reflector, and that minimizes spacecraft inertias. Only two hinges are involved for each array and positive locks at all joints lock the solar array subsystem into its final orbit configuration. The deployed spacecraft spans 51.9 feet from tip-to-tip of the solar array, 30 feet across the reflector, and 25.3 feet in the Z-direction from the earth viewing side of the EVM to the top of the magnetometer. The spacecraft orbit lies in the equatorial plane.

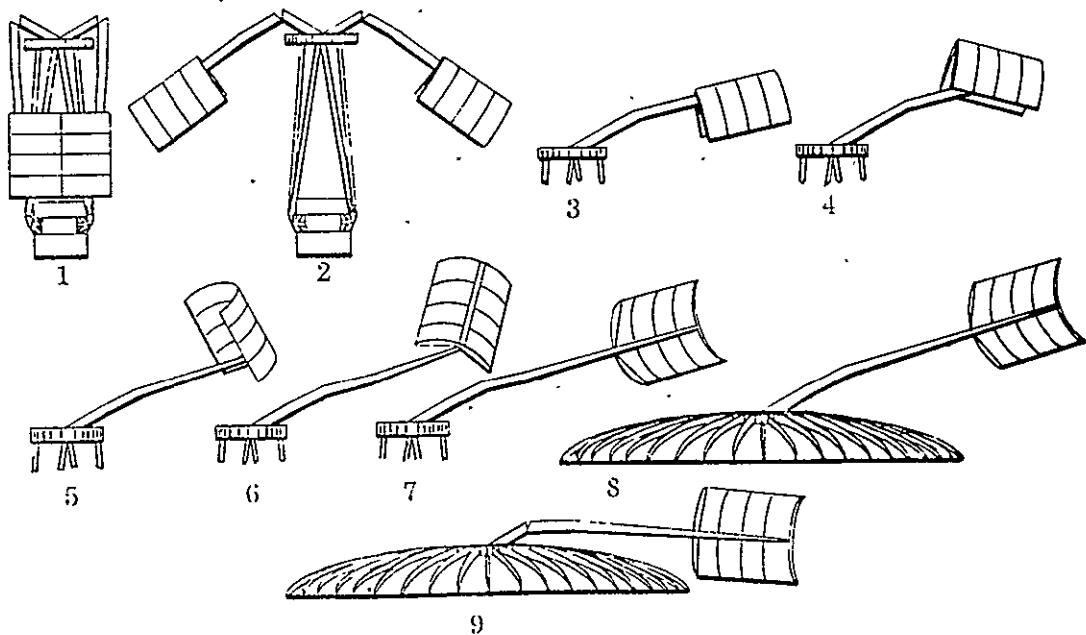


Figure 3.2-7. Deployment Sequence

3.2.3.4 Acquisition of Mission Attitude

Shortly after verification that spacecraft separation from the Titan Transtage has been successfully completed, a command will be sent from Rosman to "Rate Null" the spacecraft. This will reduce any angular rates, imparted by the separation maneuver, about the three spacecraft body axes to less than 1.0 degrees per second. Then commands will be sent to ATS-F to deploy the solar panels and 30-foot parabolic reflector. The 1.0 degree per second rate limit is a conservative design constraint imposed by the deployment mechanism.

Once the solar panels and 30-foot reflector have been successfully deployed and the spacecraft body angular rates are less than 0.05 degrees/sec., sun acquisition can begin. This step can start from any initial spacecraft attitude using the 4 steradian field of view of the coarse sun sensors. Control based on these sensors will bring the sun within the 9 degree acquisition field of view of the fine sun sensor. The spacecraft X-axis can thus be brought within 1 degree of the sun by pitch and yaw control.

Upon completion of sun acquisition, a command is sent to roll the spacecraft about the +X (roll) axis at a $0.25^{\circ}/\text{sec.}$ roll rate. When the earth sensor roll head indicates earth presence, the roll axis control is automatically switched to the earth sensor. When the roll and pitch head indicates earth acquisition (both horizons are in the field of view) the +Y (pitch) axis control is switched to the earth sensor. Earth acquisition is complete when pitch and roll errors are less than 1.0 degree.

Upon completion of earth acquisition, Polaris acquisition begins. Commands are sent to select star intensity threshold settings as well as a roll offset command. This latter command defines the position of Polaris so it can be acquired by a yaw angle maneuver using the IRA as the reference sensor. When the yaw error is less than 2.0 degrees, and the presence of Polaris indicated by the Polaris sensor, control of the +Z (yaw) axis is transferred to the Polaris sensor. Polaris acquisition is complete when the yaw error is less than 0.5 degrees of the line of sight of the star.

With the ACS now nulling the roll and pitch outputs from the Earth Sensor and the yaw output from the Polaris sensor, the spacecraft is maintained in a local vertical orientation. That is, the +Z (yaw) axis is constrained to lie along the local vertical and the Y-Z plane is held on Polaris. A sketch of the deployed spacecraft indicating direction of the reference axes is shown in Figure 3.2-8.

3.2.3.5 Orbit Correction

When the initial orbit of ATS-F has been obtained, satellite ephemeris data will be sent to the DOC. Ground computation will then be made to correct the orbit to the desired synchronous circular orbit. The ACS will be commanded into the orbit control mode to enable the orbit control jets to be used to correct for a maximum orbital velocity error of 30 feet per second or less. It will take the ATS-F 3-millipound

thrusters a maximum of 7 days to increase the spacecraft velocity by that amount. The earth coverage fields of view for the two planned spacecraft locations (94° W and 15° E) are shown in Figure 3.2-9 for antenna angles above 5°.

3.2.4 MECHANICAL SUBSYSTEMS

The functional interactions between the structure thermal control and the parabolic reflector are primarily mechanical in nature, and once deployed assume a semi-passive role in the day to day functional operation of the spacecraft.

3.2.4.1 Structure

The structural subsystem must reliably house and position all components of the spacecraft throughout all phases of the two year mission (five year design goal), supplement and enhance the operation of all subsystems and experiments, be compatible with the launch vehicle, and contribute a minimum weight to the total spacecraft.

In developing the structural subsystem, various candidate configurations were evolved; tradeoffs were conducted among these configurations by considering the detail requirements; including accessibility, system integration, packaging efficiency, electrical harnessing, and thermal control factors. In the final design, all structural components exhibit positive margins of safety, and all natural frequencies exceed the specifications. The selected design is lightweight, structurally sound, and meets all specified static dynamic and reliability criteria.

3.2.4.2 Thermal Control

The ATS F&G thermal control subsystem accommodates the wide fluctuation in the internal power dissipation from the components within the earth viewing module (EVM). During the PLACE experiment, the internal dissipation is 443 watts; in a normal minimum condition (orbit control), this level drops down to 154 watts. In these extremes, the thermal control subsystem must maintain all internal mounting plate temperatures within a 30°C temperature excursion, and must prevent temperature changes that extend to degrade the alignment accuracy of spacecraft subsystems.

The Thermal Control System, which meets all these requirements, includes the use of superinsulation, thermal louvers, heat pipes, passive coatings, a unique cubical spacecraft configuration that lends itself to radiative cooling, and the judicious placement of heat-dissipating components within the structure. The design incorporates a significant degree of redundancy (e.g., 10% of the thermal louver blades and 50% of the heat pipes can fail and still maintain acceptable temperatures), conservatism (e.g., maximum coating degradation has been assumed, as well as worst case solar conditions and "cold condition below the analytical minimum), practicality (e.g., the heat pipe configurations are all in parallel planes, so the system can be tested in a 1-g field), and adaptability to emergency conditions (e.g.,

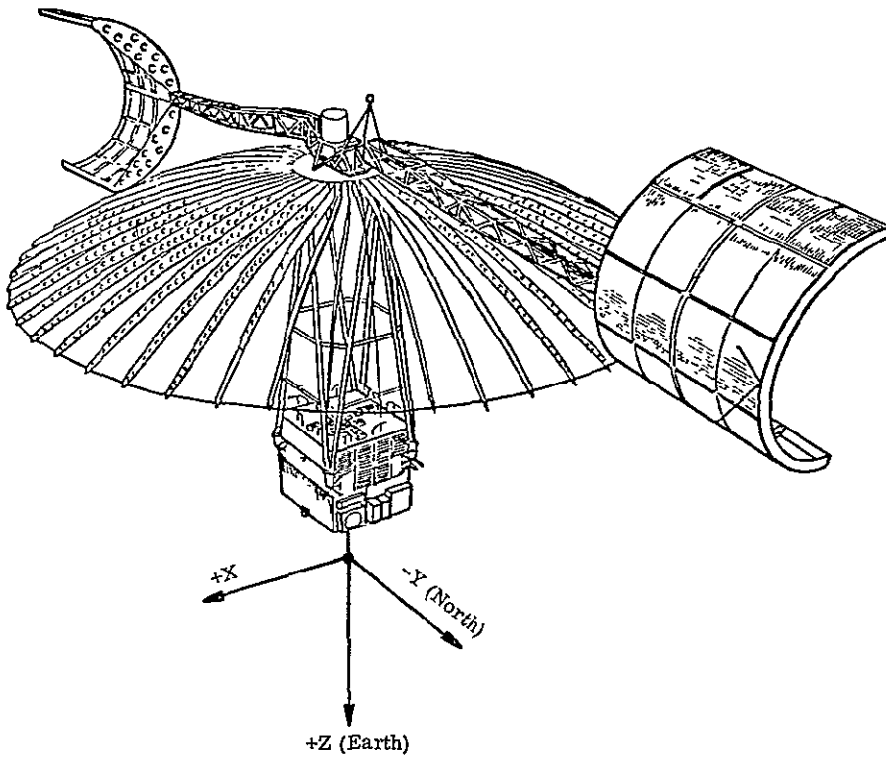


Figure 3.2-8. Orbital Configuration

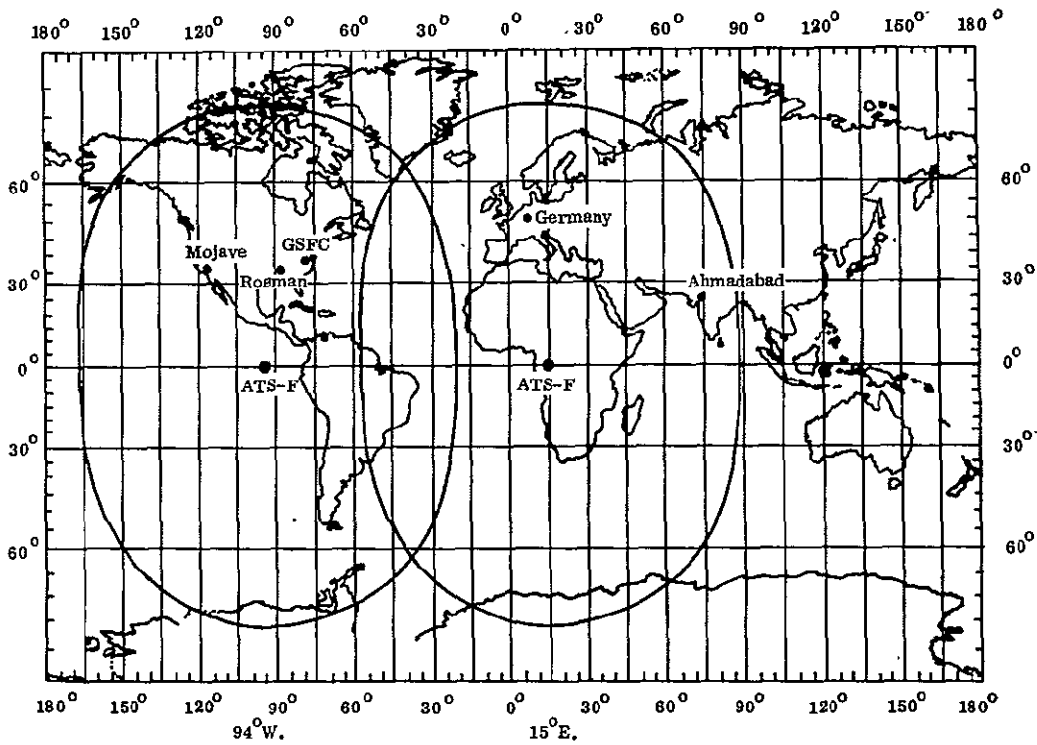


Figure 3.2-9. Field of View at 94°W Longitude and at 15°E Longitude for 5° Elevation Angle Above the Horizon.

large thermal time constants). The system uses hardware elements with which Fairchild Hiller has experience and familiarity, and provides complete temperature control for the spacecraft during ground testing, pre-launch, ascent, and orbital phases.

3.2.4.3 Parabolic Reflector

The basic primary requirements imposed upon the reflector by the ATS F&G mission objectives are the successful deployment in orbit after survival of the spacecraft launch conditions and the achievement of an orbital RF performance that insures an overall antenna system performance in excess of the requirements (50 db minimum gain at X-band) of the ATS F&G system specifications. Additional, secondary requirements established by system design and quality assurance considerations are the capability and facility of the reflector subsystem for integration with the remainder of the spacecraft system, from both the design and the physical assembly point of view, and the testibility of the subsystem under terrestrial conditions for design proof, performance verification and flight qualification purposes. The Lockheed "flex-rib" design has been selected for use on ATS F&G for the following key reasons:

- Deployment Reliability - Simplicity of the release and deployment mechanisms, minimum number of moving parts and redundancy in the deployment mechanism.
- Launch Survival - Rugged, compact launch configuration and efficient, effective load transfer into the structural supports.
- RF Performance - Low values of surface deviations from the theoretical paraboloid. This includes effects of inherent design (flatness) errors, manufacturing and assembly tolerances, repeatability of the contour upon successive depolyments and thermally induced deflections in the orbital environments.
- Spacecraft Integration - Simplicity of physical mounting and structural soundness of the support provisions, accessibility to the reflector itself and to other critical areas of the spacecraft system prior to launch; capability and provisions for proper alignment of the antenna system, minimum weight and low moments of inertia, high natural frequencies and damping in both the launch and the orbital configurations.
- Quality Assurance - Ease of ground handling and low vulnerability to damages during normal handling; capability of deployment testing one-g conditions; capability of proper verification of the predictions of zero-g contours, thermal deflections and the resultant RF performances in orbit.

3.2.5 ELECTRICAL SUBSYSTEMS

The electrical subsystems of the spacecraft are designed to perform the principal operational functions required to fulfill the objectives of the ATS F&G mission. Though identified and described separately in this section, these subsystems are integrated into a functionally coordinated design. The subsystems that comprise the functional operating system are:

- Attitude Control
- Auxiliary Propulsion
- Communication
- Interferometer
- Telemetry and Command
- Power Supply
- Experiments

Figure 3.2-10 illustrates in a highly-simplified block diagram the basic functional signal flow relationships among the operational subsystems. For the sake of simplification, the Power and T&C lines are omitted and more than one component may be represented by a single block in the diagram, so as to emphasize function over packaging considerations.

The communications subsystem consists of the transponder and the prime focus feed with antennas at X-, C-, S, and L-bands, as well as UHF and VHF. The VHF feed is used for the T&C subsystem, while the C-band feed is used by the RFI experiment. The remaining feeds are used with the transponder and RF power amplifiers to support the communications experiments and to provide wide band ground links with the RFI, Millimeter Wave, VHR Camera, Radiometer, and Laser experiments. Monopulse operation is implemented at X-band, S-band, and VHF allowing the spacecraft to self-point to a selected ground station.

The operational controller of the attitude control subsystem accepts attitude sensory inputs from the monopulse detectors of the communications subsystem, as well as the inertial reference assembly, the earth sensors, sun sensors, and Polaris Sensors. Additional attitude sensing inputs are derived from the interferometer subsystem and the Laser experiment. The operational controller compares these sensor inputs with the desired (commanded) attitude and commands the actuators (wheels or jets) to null any existing attitude errors.

The X-band RF interferometer derives pitch and roll attitude information from two sets of earth viewing horns on orthogonal base lines. Received signals are decoded digitally and routed to the ACS controller for closed-loop attitude control of the spacecraft.

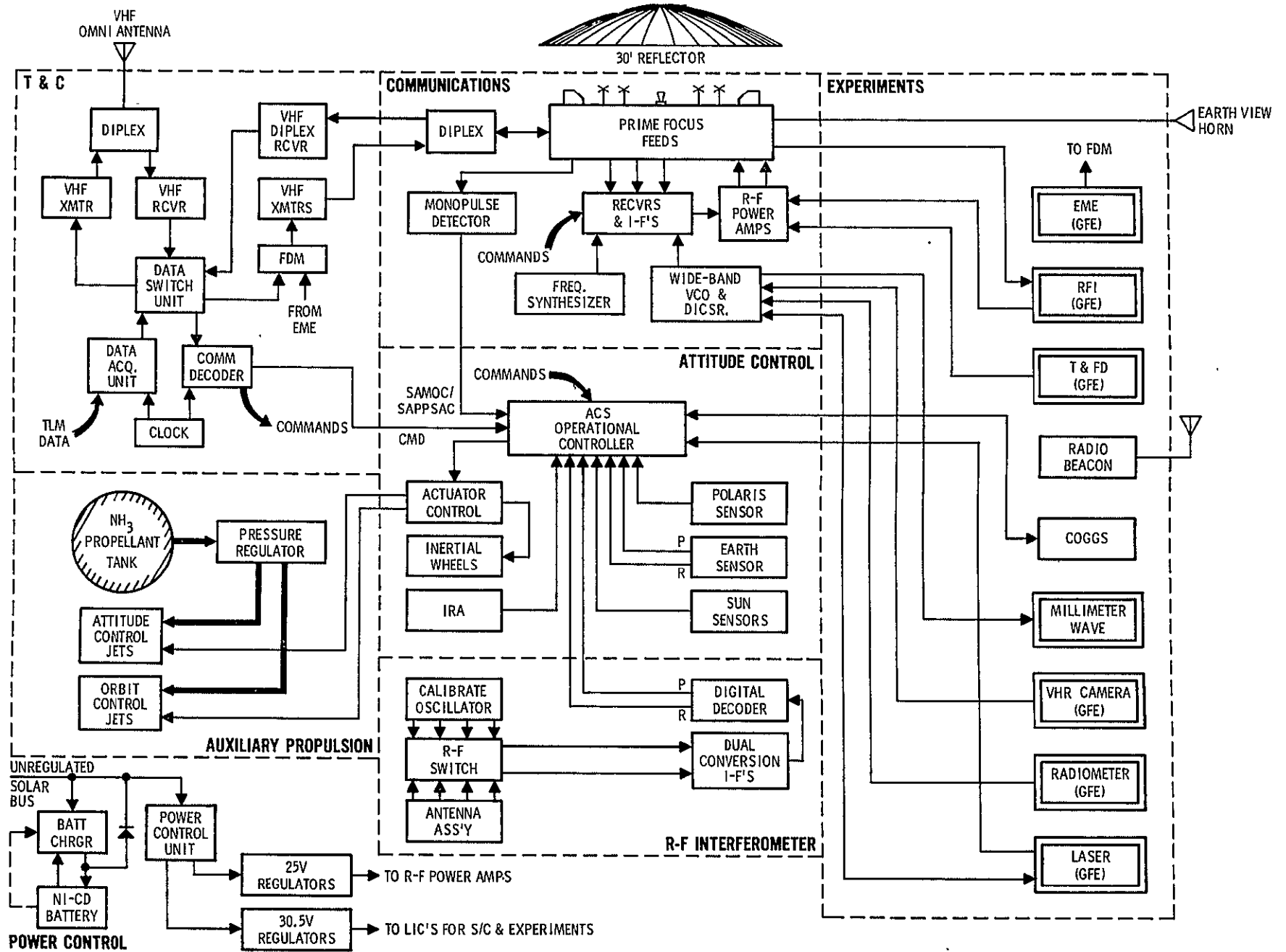


Figure 3.2-10. AT'S F&G Functional Block Diagram

The auxiliary propulsion subsystem controls the ammonia for the three-axis attitude thrusters and the N-S and E-W hot gas orbit control thrusters.

The T&C subsystem accepts telemetry inputs from all of the spacecraft subsystems, encoding and formatting them for transmission down the VHF RF link--through either of two omni directional whip antennas, or the single high gain earth--directed VHF antenna on the prime focus feed. The command receivers use the same VHF antennas, ground selectable by the choice of frequency, and can be switched to either command decoder, selectable by the choice of decoder address. Commands are routed to the various subsystems by means of the command addresses.

The power subsystem derives its power from two sources; the solar array panels, and nickel-cadmium batteries. Regulation is performed by series pre-regulator and multiple load interface circuits assigned to each load and each experiment. The RF power amplifiers are the exception where, for reasons of efficiency, a lower voltage pre-regulator supports these loads directly.

These operating subsystems are described in greater detail in the following sections of this report which is organized as a subsystem basis.

3.3

ATS-F EXPERIMENTS

Those experiments making extensive use of equipments provided as part of the basic spacecraft systems to demonstrate their required performance are classified as ATS-F Operational Experiments. In the following paragraphs, the experiment requirements imposed on the spacecraft equipments will be described, as will the Fairchild Hiller design approach in meeting the requirements of the subject experiment. The interface requirements of the GFE experiments, Radio Beacon, and COGGS experiments are also discussed.

3.3.1 INSTRUCTIONAL TELEVISION

3.3.1.1 Detailed Requirements

The Instructional Television (ITV) experiment imposes five basic requirements upon the ATS-F spacecraft. These requirements are:

- To transpond a 25 MHz Bandwidth FM TV signal from X-Band to UHF.
- Provide a solidstate 850 MHz UHF power amplifier with 80 watts RF output.
- Provide an ERP of 48 dbw at 850 MHz over a 3-degree field of view.
- Provide a two-way Special Data Link
- Provide an X-Band down link capable of monitoring ITV signal and having an ERP of 23.5 dbw over FOV,

The above itemized ITV requirements are depicted in Figure 3.3-1 for the special case of ITV to India. In addition to the above general requirements, the ATS-F transponder must meet the following detailed requirements:

- Repeater Bandwidth - The repeater 3 db bandwidth shall be no greater than 40 MHz.
- Gain Variation - The gain variation through the repeater will be less than plus or minus 0.5 db within the center 25 MHz of the repeater passband.
- Group Delay - Within center 25 MHz:
 - parabolic envelope delay less than 30 nanoseconds
 - linear envelope delay less than 15 nanoseconds
- AM-to-PM Conversion - Conversion through repeater not to exceed 6-degrees per decibel.
- Receiver G/T figure of merit of at least $-17 \text{ db}^{\circ} \text{K}$

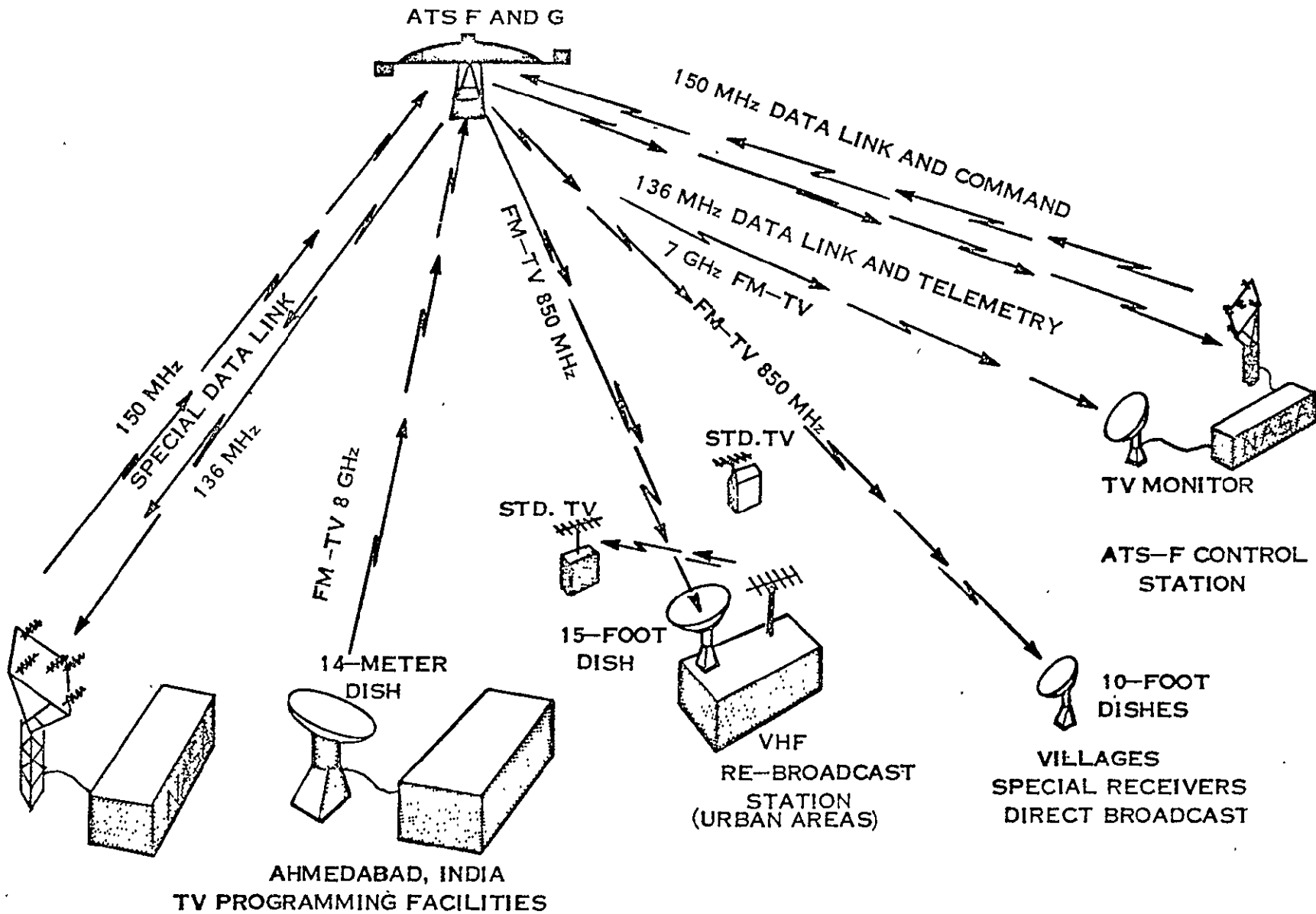


Figure 3.3-1. India Instructional Television

Approach and Performance Capability

The basic requirements for the ITV experiment have been reviewed and incorporated as an integral part of the ATS-F communication transponder and high-gain antenna feed design specifications.

The ATS-F communications subsystem includes an X-Band receiver which will meet the requirements of any of the communications experiments. The X-Band receiver has a noise figure (referenced to the preamplifier input) of better than 7 db and when combined with the gain of the earth coverage X-Band horn results in a G/T figure-of-merit ratio better than $-17\text{db}^{\circ}\text{K}$. The transponder has three selectable i-f amplifiers, each of which has selectable 40 MHz bandpass filters.

The output of each transponder i-f amplifier can feed two loads. Thus the same signal which is used to drive the 850 MHz up-converter will also drive one of the X-Band up-converters when the X-Band ITV monitor is being used.

A solidstate 850MHz power amplifier will be used to increase the UHF up-converter output power level to a value in excess of 80 watts. This signal will then provide the input to the special 850MHz feed to the high-gain antenna. In this manner an ERP of at least 48dbw will be developed over a 3-degree field of view which is centered on the axis of the 30-foot parabolic reflector.

A two-way Special Data Link (SDL) is available for use between the TV programming facilities and the ATS-F control station as shown in Figure 3.3-1. This link will utilize the ATS-F assigned command and telemetry frequencies. The data (normally 300 Hz to 2.7kHz voice) will be amplitude modulated on one of the command frequencies, on the ground, for transmission to the ATS-F. The command receivers will have special isolated outputs which will interface with a special multiplex. The special data frequency spectrum will fall below the command tone frequencies. Thus, there will be no interference between the two signals. The special data will be multiplexed along with the telemetry and the EME data for transmission over a single 136 MHz VHF PM link. The demodulated data will have a signal-to-noise ratio (SNR) in excess of 16 db on both up and down links under worst case operation. A SNR of only 13 db is required for a word intelligibility of 90 percent, and a SNR of only 4 db will provide a word intelligibility of about 70 percent. Thus the SDL is considered to possess adequate margin even under worst case operating conditions.

For ITV transmissions to India, a 625 line TV system will be used for programming. The carrier-to-noise density rateo (C η R) required to produce a CCIR quality picture is 90.8db -Hz. This value is based upon the following signal parameters and values.

f_{pp}/v_a (peak-to-peak deviation of the FM carrier due to composite baseband signal): 20MHz

f_{pp}/v (peak-to-peak deviation of the FM carrier due to the video baseband signal alone): 16 MHz

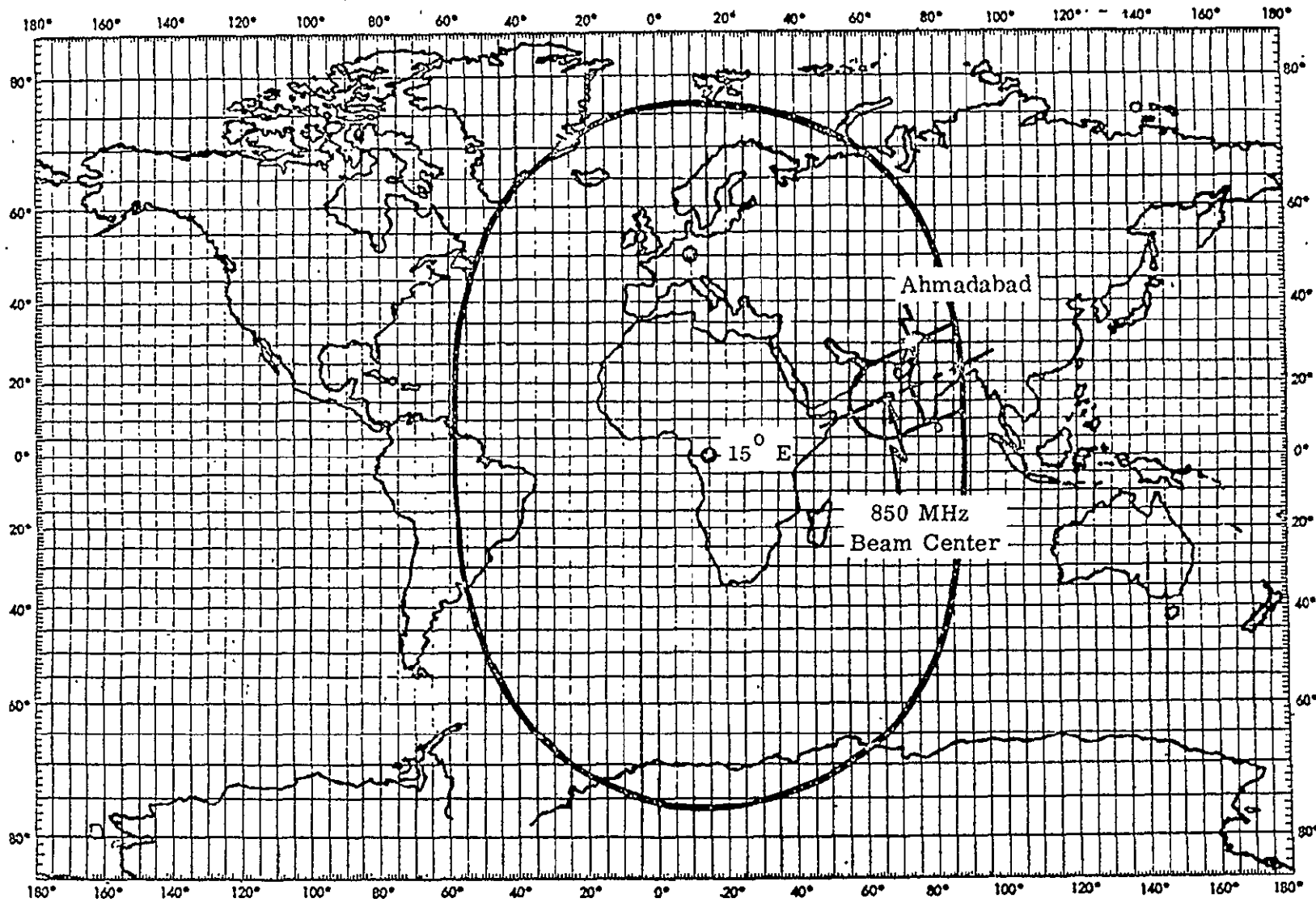
f_{pp}/a	(peak-to-peak deviation of the FM carrier due to the aural subcarriers located at 5.5 and 6MHz): 2MHz each
f_{pp}/as	(peak-to-peak deviation of the FM aural subcarriers by a 9 dbm test-tone): 400 kHz
B_v	(bandwidth associated with video signal): 5MHz
B_a	(bandwidth associated with sound signal): 15KHz
B_{rf}	(composite RF bandwidth using Carson's rule): 32MHz
$B_{rf/a}$	(aural subcarrier RF bandwidths centered at 5.5 and 6MHz): 430kHz

Using the above defined parameter values the demodulated SNR for video alone is found to be 29.7db for a carrier to noise power density ratio of 90.8 db-Hz. For the 625 line TV system the noise weighting factor due to preemphasis is 16.3db, and the conversion from rms to peak-to-peak signal is 9db. Therefore a SNR of 29.7 db at the output of a receiver discriminator will produce a peak-to-peak video signal (including sync) to a weighted rms noise ratio of 55b, as required by CCIR standards.

According to the link calculations provided by GSFC, the worst case ITV $C\eta R$ for the X-Band up link is 92 db-Hz for a G/T of $-17\text{db}/^\circ\text{K}$ (this value assumes a 40-foot ground antenna and a 2 kilowatt ground transmitter). The worst case $C\eta R$ for the 850MHz down link to a 15 foot ground antenna and 1000 degree receiver is also about 92 db-Hz. Thus the worst case over-all ratio is only 89 db-Hz or about 2db below CCIR quality.

The 850MHz ITV high-gain antenna will have its beam axis coaxial with the spacecraft Z-axis and the X-band monopulse beam axis. Therefore, the ITV signal can be received aboard the ATS-F via the monopulse high-gain sum channel. Since the dish gain at X-band is 34db greater than the X-band horn gain, its use would provide an essentially perfect ITV up-link.

Under normal ITV operations the ATS-F Z-axis will be directed to optimize the 850MHz antenna beam foot-print on the area to be covered. Figure 3.3-2 shows this foot-print covering India when the ATS-F is stationed at 15 degrees east longitude. From this figure it is seen that in order for the ATS-F to monopulse on the signal from Ahmadabad, the spacecraft Z-axis must move about 0.7 degrees north (note that the 850MHz beamwidth is 2.8 degrees). This reorientation of the Z-axis causes a loss of about 1db in the 850MHz antenna gain, in the direction of South India, but the quality of the overall link will improve by about 2db. It is possible to skew the 850MHz antenna beam axis with respect to the X-band beam by 0.7 degrees. This would allow a 1db improvement to be realized when using the X-band high gain antenna on the up-link from India when the ATS-F is located at 15 degrees east longitude. However, such a skewing of the beam axis is not recommended since the required angle is a function of the ATS-F location and the geographic location to which



850 MHz Antenna Beam Coverage
Of India For ITV

Figure 3.3-2. 850 MHz Antenna Beam Coverage of India for ITV

the 850MHz beam is being directed. The coaxial beam arrangement permits flexibility in positioning the ATS-F and also ensures good beam coverage to any new area which might be considered in the future.

3.3.2 POSITION LOCATION AND AIRCRAFT COMMUNICATION EQUIPMENT

3.3.2.1 Detailed Requirements

The Position Location and Aircraft Communication Equipment (PLACE) experiment imposes the following requirements upon the ATS-F spacecraft:

- To relay two RF links coherently through the spacecraft transponder in a multiple access mode; X-band to L-band and L-band to X-band
- To convert multiple input carriers to a single output carrier, FDM/PM
- Provide selection between high-gain L-band fan and pencil antenna beams
- Provide selectable premodulation filters
- Provide an ERP at L-band of 48dbw over a 1.5 degree conical field of view and 42dbw over a 1.5 by 7.5 degree rectangular field of view

The PLACE experiment operation is depicted in Figure 3.3-3. The function of the ATS-F is to provide multiple access operation between multiple ground stations and multiple aircraft. At the ATS-F, the composite signal consisting of FM signals from as many as ten ground stations is converted to a single phase modulated signal for retransmission to as many as 100 aircraft. On the reverse RF link a composite signal consisting of SSB signals from as many as 100 aircraft is converted to a single phase modulated signal for retransmission to the ground stations.

In addition to the above general requirements, the ATS-F transponder must meet the following detailed requirements for PLACE:

- Provide linear amplification of the multiple input signals in the IF amplifier prior to synchronously shifting the spectrum to baseband with a product demodulator. Amplification shall not produce significant intermodulation components.
- Repeater Bandwidth - The repeater 3db bandwidth shall be no greater than 12MHz as measured from the receiver input to the demodulator input.

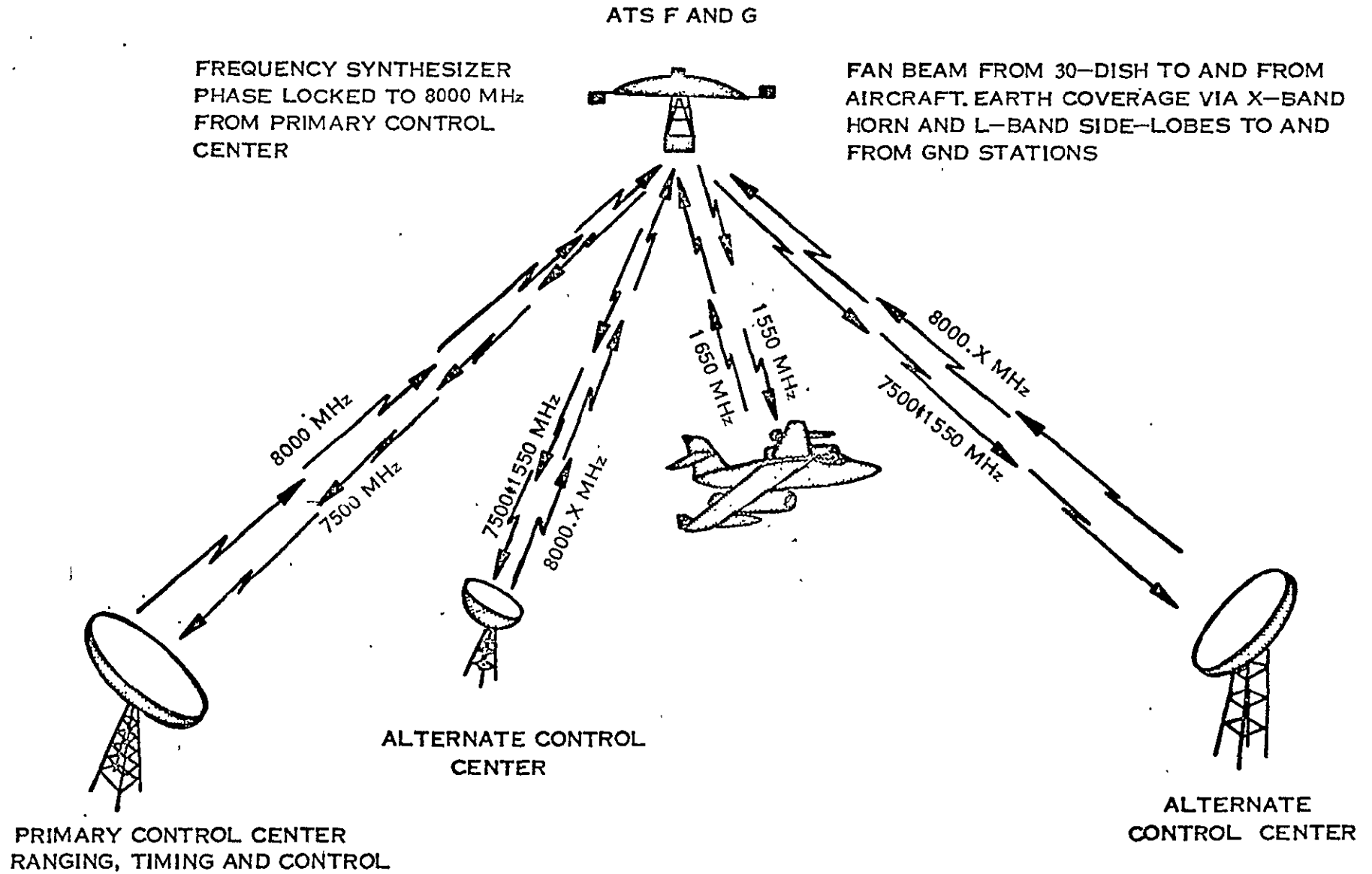


Figure 3.3-3. Place Experiment

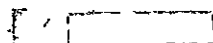
- Differential Time Delay - The differential time delay through the repeater shall not exceed 0.1 microseconds over the expected range of the input signal power levels.
- Baseband Bandwidth - Two baseband bandwidth shall be provided and shall be selectable by command. The bandwidths shall be 1.5kHz to 100kHz and 1.5kHz to 1MYz.
- Modulation Index - The modulation index of the transmitted signals (both links) shall be 1.0 ± 0.1 radians rms for an FM or SSB signal falling in the expected range of input signal power levels.
- Modulation Linearity - The phase modulation characteristics shall not deviate from a linear characteristic by more than ± 2.5 percent of the deviation for peak deviations of up to ± 3 radians.
- Modulation Response - The modulator and transmitter amplitude response shall not vary more than ± 0.5 db for modulation frequencies of from 1.5 Hz to 1 MHz.

3.3.2.2 Approach and Performance Capability

The detailed requirements for the PLACE experiment have been established by GSFC experimenters and have been adequately documented. These requirements have been tabulated above and have been reviewed for incorporation into the ATS-F Communication transponder and high-gain antenna feed design specifications.

Again as before the ground to ATS-F RF link signals are received via the standard gain X-band horn, which when combined with the receiver, provides a G/T of -17 db/ $^{\circ}$ K. PLACE utilizes the same selectable i-f amplifiers as mentioned before, each of which also has selectable 12 MHz bandpass filters in the main signal path of the amplifier.

The composite signal received either from ground stations or all the cooperating aircraft must be used to phase modulate the ATS-F transmitting signal with an rms modulation index of one radian. With a large number of aircraft channels being received simultaneously, it is not expected that individual output power control on each aircraft will be necessary in order to prevent large variations in the statistics of the composite signal. However, for a small number of aircraft signals it will be necessary to provide some control over the composite signals into the ATS-F phase modulator to ensure a nearly constant rms modulation index. Ideally then, it is desired to maintain the rms voltage level of the composite signal at the modulator input at a constant value, independent of the number of received carriers and their power levels. Consequently, AGC circuits will be included in the ATS-F i-f amplifiers to assist in maintaining a constant rms voltage level to the phase modulator.



The AGC loop for the PLACE experiment will include the synchronous or product demodulator and the selected lowpass premodulation filter. In this manner the effective i-f bandwidth in terms of signal and AGC filtering is reduced from 12MHz to either 1MHz or 100 kHz. The carrier-to-noise ratio at the AGC detector input is thus improved by 11db or 21db as compared to the AGC system which operated on the output of the 12 MHz filter. Thus the performance of the PLACE experiment will be greatly enhanced with this integrated transponder feature of selecting the AGC input bandwidth.

The imposed coherency requirement is met by utilizing a frequency synthesizer which can be phase locked to the carrier of the Primary Control Center.

In the case of the ground-satellite-aircraft link, the transmission frequency is 1550 MHz, and the specified ERP over the 1.0 x 7.5 degree field of view is 42 dbw. When the RF link is evaluated with this ERP, it is established that the received carrier to noise density ratio at the aircraft is 62 db-Hz. Using the aircraft receiver characteristics given on page 14 of the GSFC PLACE document (X-731-67-159), one concludes that 62 db-Hz will result in only 5.3 db in the 17 KHz FM voice predetection bandwidth. Since the threshold of the demodulator is given as 6 db, the specified ATS-F ERP of 42 dbw is about 0.7 db too low to meet the demodulator threshold. This evaluation assumes that ten ground stations are simultaneously transmitting voice signals through the ATS-F and hence that the L-Band ERP is shared by ten channels.

The required ERP of 42 dbw, which can be provided with a 20 watt L-Band transmitter, can support only about 7 X-Band voice channels. But a 25 watt transmitter is required to operate with the full complement of ten channels. The 40 watt solidstate L-Band power amplifier considered by FHC during most of Phase C can be supported by primary power with the PLACE experiment for 21 months. If the RF drive to this amplifier were lowered so that the RF output is only 20 watts, the required dc power drops by 40 watts and the PLACE experiment can be supported for a duration in excess of two years. After evaluating the above facts FHC decided to provide a solidstate L-Band power amplifier which is optimized for operation at 40 watts. A back-off to 20 watts, if desired, can of course be simply implemented. When it is realized that it is possible for the spacecraft battery to be utilized to achieve operation for the last three months and that the solar array degradation projection is conservative, the single 40 watt mode is the logical choice.

3.3.3 DATA RELAY SYSTEM

3.3.3.1 Detailed Requirements

The Data RELay System (DRS) experiment imposes the following requirements upon the ATS-F spacecraft:

- Relay two RF links through the ATS-F

- Provide steerable S-band antenna beams capable of tracking a low altitude satellite by maneuvering the ATS-F Z-axis
- Provide the capability of tracking two low altitude satellites with the S-band antenna beams, but only one beam must form part of an operational communication link
- Provide spacecraft fine pointing with an accuracy of 0.1 degrees and a slewing rate of at least 17.5 degrees in thirty minutes
- Earth coverage X-band antenna beam
- Capability of using either coherent or non-coherent signal relaying
- Selectable i-f noise bandwidths, 12 MHz and 40 MHz
- Relay emergency voice from AAP satellite

The above DRS requirements are partially depicted in Figure 3.3-4. In addition to the above general requirements, the ATS-F communications subsystem must meet the following detailed requirements:

- Repeater Bandwidth — The repeater shall have two selectable 3 db bandwidths, 12 MHz and 40 MHz.
- Repeater Frequency Response - The bandpass gain variation through the repeater shall be less than ± 0.5 db with respect to a 6 MHz signal frequency band centered in the 12 MHz bandpass, and with respect to a 20 MHz signal frequency band centered in the 40 MHz bandpass.
- Group Delay - The repeater group delay over a chord covering the specified signal spectrum within the bandpasses shall not exceed:

Linear Component:	0.3 Nanoseconds/MHz
Parabolic Component:	0.03 Nanoseconds/MHz ²
Peak-to-Peak Ripple:	8.0 Nanoseconds
- AM-to-PM Conversion - The AM-to-PM conversion through repeater shall not exceed 6 degrees per decibel.
- X-band G/T at least -20db/°K and ERP at least 24.5dbw, both over a 25 degree conical field of view.
- S-band G/T at least 7.8 db/°K and ERP at least 47.5dbW over a 1-degree field of view; G/T at least 2.5 db/°K and ERP at least 47.5 dbw over an angle of ± 7.5 degrees to both sides of the reflector axis and along the line traced by switching the beam centers.

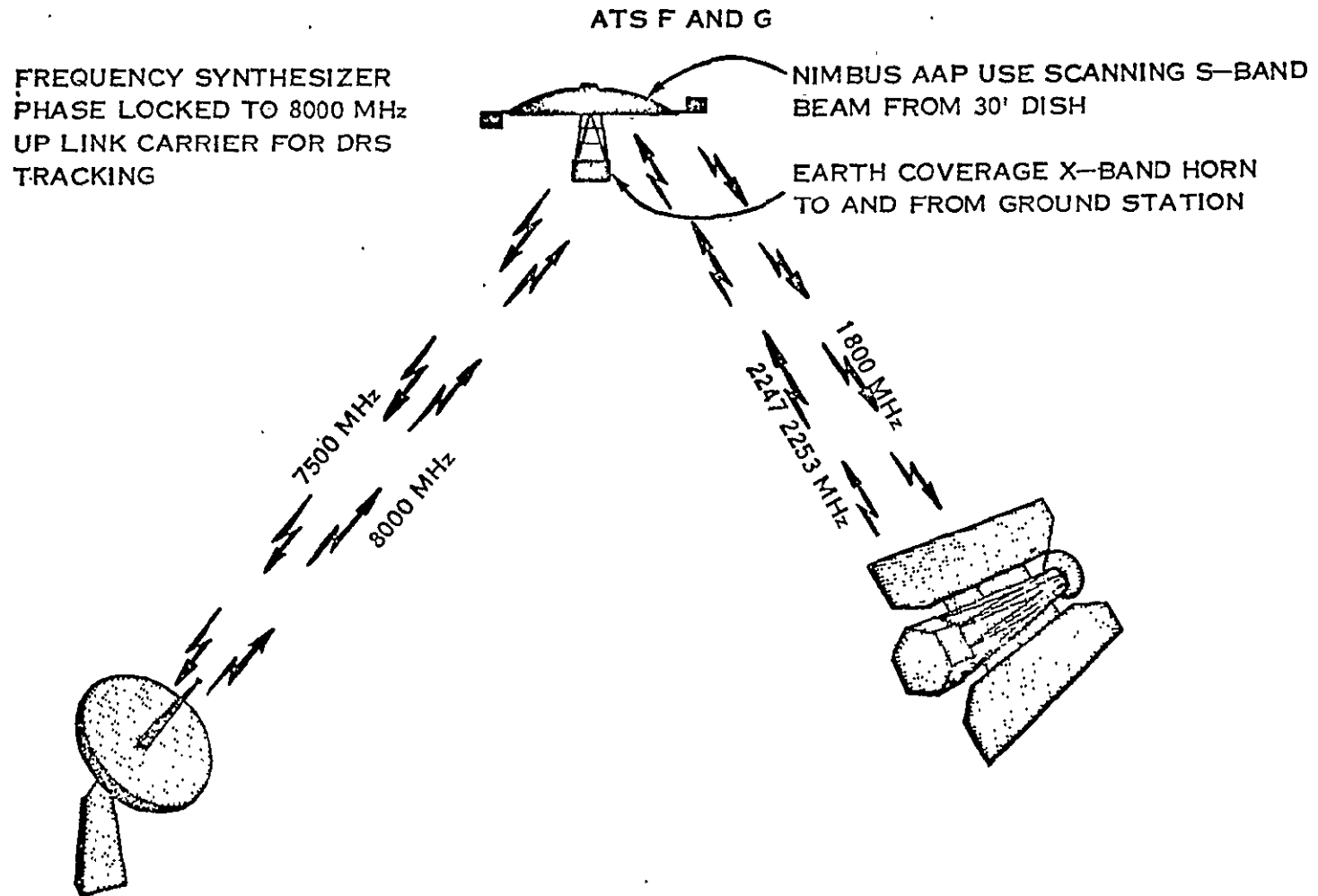


Figure 3.3-4. Nimbus/AAP Data Relay DRS

3.3.3.2 Approach and Performance Capability

After reviewing the requirements which DRS imposes upon the ATS-F spacecraft, it is seen that those requirements which differ mostly from the PLACE and ITV experiments are associated with the S-band antenna beam steering. The requirements imposed upon the design of the transponder have been reviewed and incorporated in the integrated transponder design specifications. As implied by the term "integrated transponder", certain requirements which are similar between the three communication experiments are fulfilled by the same basic units. Thus the same i-f amplifiers are used with all three experiments after selecting the required special features. Thus, when DRS is used for range and range rate tracking of low altitude satellites, the same 12 MHz bandpass filters used with PLACE are used. When television is relayed from the AAP satellite, the same 40 MHz bandpass filter used with ITV is used. Likewise, the transponder synthesizer will be phase-locked to receive X-band frequency during the DRS experiment as is done during PLACE.

The approach taken by FHC in meeting the requirements needed to track either a single low-altitude satellite or two low-altitude satellites led to the S-band antenna feed array shown in Figure 3.3-5. As shown in Figure 3.3-5, the feed elements form a crossed array with 16 elements along the X or roll axis and 16 elements along the Y or pitch axis. The four innermost elements also serve to produce, receive and transmit antenna beams along the spacecraft Z-axis for Z-axis tracking of a single low-altitude satellite.

Single satellite tracking can be accomplished by either closed loop monopulse tracking or open loop with computed pitch and roll commands based upon the ATS-F and low-altitude satellite ephemeris data. Before the actual low-altitude satellite transit occurs with open-loop tracking, the ground station must: (1) obtain suitably accurate orbit ephemeris data for the two satellites (low-altitude and ATS-F), (2) calculate the time-varying pitch and roll angles which the ATS-F must assume in order to point continuously at the low altitude satellite when it does transit, (3) determine coefficients for the approximating polynomials for these time-periodic angle signals, (4) transmit these coefficients to the ATS-F Digital Operational Controller, (5) Command the ATS-F to assume the initial values for the pitch and roll angles and, finally, (6) the ground station must give a start track signal at the appropriate time. When the S-band monopulse system is used, only items (5) and (6) of the above ground station requirements need be considered.

The crossed array of the S-band antenna feed elements is provided for the purpose of tracking two low-altitude satellites. One arm of the array will permit the S-band beam to be positioned in the North-South (N-S) direction, and the other arm will permit the beam to be positioned in the East-West (E-W) direction. Figure 3.3-6 will help to visualize two satellite tracking. Assume that Nimbus is at position 2 in its orbit trajectory and that AAP is at position 2 in its orbit trajectory. The ATS-F, Z-axis can then be shifted in the E-W direction until position 2 of the Nimbus path is covered by the N-S arm of the array; the AAP position 2 is then covered by the E-W array arm by moving the Z-axis in the N-S direction. Once the

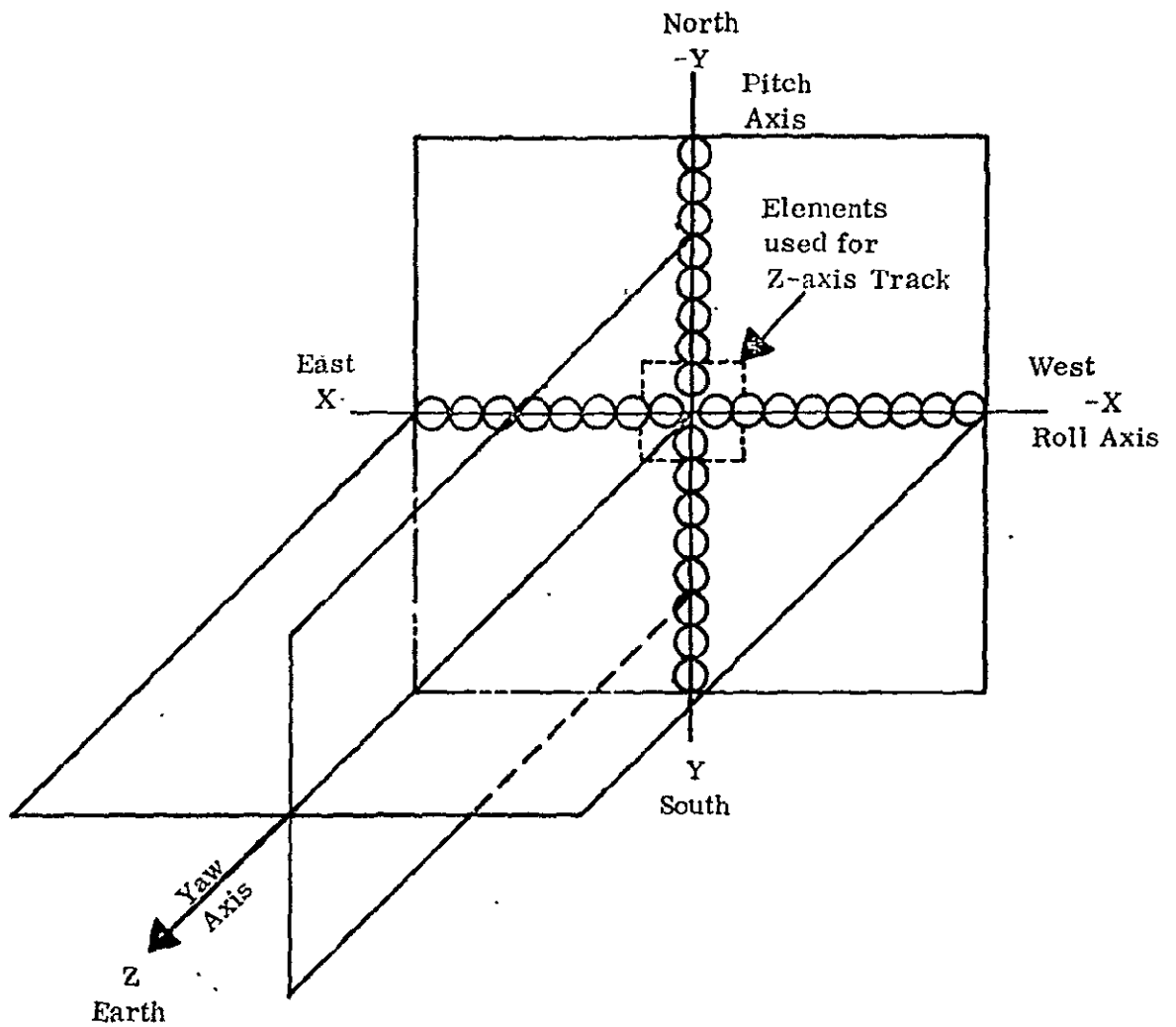


Figure 3.3-5. S-Band Antenna Feed Array Along With Defining Coordinate System of Beams

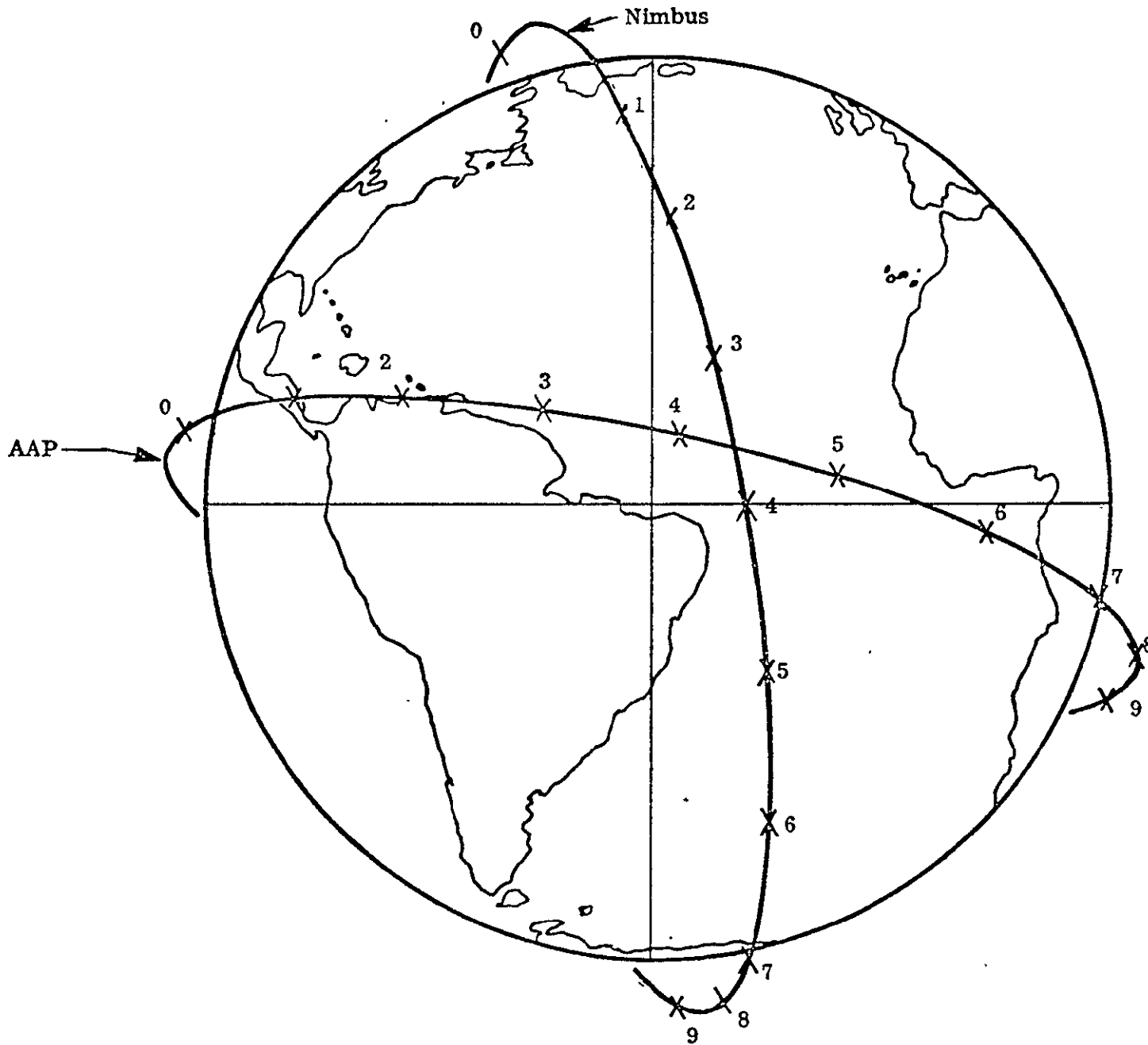


Figure 3.3-6. Two-Satellite Tracking (Nimbus/AAP)

two satellites are "acquired", the particular S-band feed which positions a beam over either satellite can be activated to establish an RF link. When once acquired the two satellites will be continuously tracked by sending commands to the ATS-F for incremented pitch (E-W) and roll (N-S) maneuvers, and for antenna beam switching.

Establishment of the necessary commands to perform a two satellite DRS tracking operation requires the use of a ground computer. Accurate orbit ephemeris data for the ATS-F and the two low-altitude satellites must be entered into the computer so that the positions of all three satellites are known as a function of time. The computer must calculate time-varying pitch and roll angles which the ATS-F must assume in order to point continuously at the low-altitude satellites. The pitch command will ensure that one low-altitude satellite is included in the Z-Y plane (which is defined by the ATS pitch and yaw axes, including N-S antenna feed array). The roll command will ensure that the other satellite is included in the Z-Y plane (which is defined by the ATS roll and yaw axes, including E-W antenna feed array). The angles from the spacecraft Z-axis (yaw) to each of the low-altitude satellites can then be computed, and a determination is made indicating which two antenna feed elements will illuminate the two satellites.

The initial pitch and roll commands must be sent to the ATS-F far enough in advance to allow the Z-axis to be properly positioned prior to the time the first low-altitude satellite comes in the field of view of the ATS. Precise timing must be established both to initiate the tracking operation and to provide the proper time intervals between subsequent commands.

The equations and computations required for two satellite tracking are not too different from those required for open-loop Z-axis tracking of a single satellite. In the case of two satellite tracking, two sets of computations must be performed, one set for each satellite. One set of computations includes a pitch command to position the ATS-F Z-Y plane to include one satellite plus a command to select the corresponding antenna beam. The other set of computations includes a roll command to position the ATS-F Z-X plane to include the second satellite, plus a command to select the corresponding antenna beam to cover the second satellite. Since the S-band antenna feed permits selection of only one feed out of the total 32 feeds of both arms (i. e. , there will be an active RF link between the ATS-F and only one of the satellites), a decision must be made as to which of the two computed feed select commands to transmit to the ATS-F.

It is assumed that the computer which develops the necessary commands for the ATS-F to track two satellites will not be available to the DRS experiment in real time. Therefore, the orbits of the two low-altitude satellites and the ATS-F must be predicted and the required commands and time intervals must be computed and stored in advance of the experiment performance.

A concept of the DRS Command operation configuration is given in Figure 3.3-7. Here a command storage and readout control unit is shown feeding commands to the encoder for transmission to the ATS-F. The commands are shown

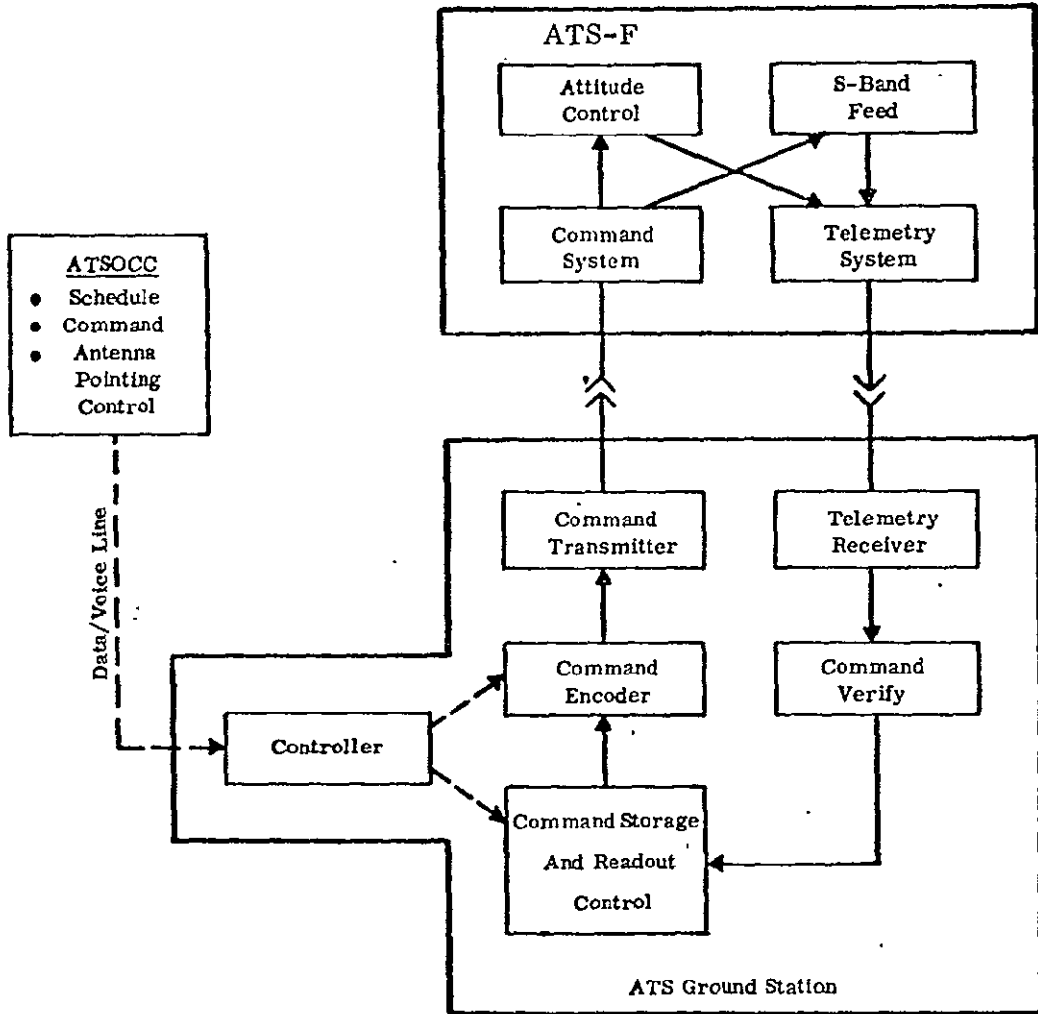


Figure 3.3-7. DRS Command Operation Configuration

as being prepared at ATSOCC and transmitted over a land line to the ATS ground station until scheduled for use by ATSOCC.

The Z-axis must traverse about 22 degrees to track a satellite across the face of the earth. Thus, if the pitch and roll commands were to occur at 0.1-degree increments, a total of 472 commands would be required, including 32 beam select commands. These commands must be properly spaced throughout the 45-minute transit time of a low-altitude satellite and require a minimum of three seconds spacing to permit command verification. A timing unit which can be programmed to control the command storage readout at the times determined by the large-scale computer, etc., is itself a special purpose computer. Thus, it appears that a desktop type computer could best fulfill the requirements of the command storage and readout unit.

3.3.4 SPACECRAFT ATTITUDE MANEUVERING OPTIMAL CONTROL/ SELF-ADAPTIVE PRECISION POINTING SPACECRAFT ATTITUDE CONTROL (SAMOC/SAPPSAC)

3.3.4.1 Requirements

The SAMOC/SAPPSAC experiment imposes two basic requirements upon the ATS-F spacecraft.

- Provision for ground control of the spacecraft attitude control jets and inertia wheels.
- Telemetry of attitude control data for transmission to the ground station.

A Functional Block Diagram illustrating the on-board equipment proposed for ground control of the jets and inertia wheels is shown in Figure 3.3-8. The approach shown is consistent with the following detailed requirements that have been identified as important to the experiment:

- Minimum pulse width of 50 milliseconds
- Pulse firing time uncertainty of 10 milliseconds
- Command rate of two/second
- A hold tone (interrupt) must be continuously provided during the performance of the experiment. Latching a jet in a firing mode is precluded
- Ten percent repeatability of impulse

Telemetry of attitude data is provided on the "main frame" of the PCM wavetrain. A sampling rate of one sample per three seconds is provided for pitch, roll, and yaw information from the Earth sensor and Polaris star tracker and (with ground computation) from the Interferometer.

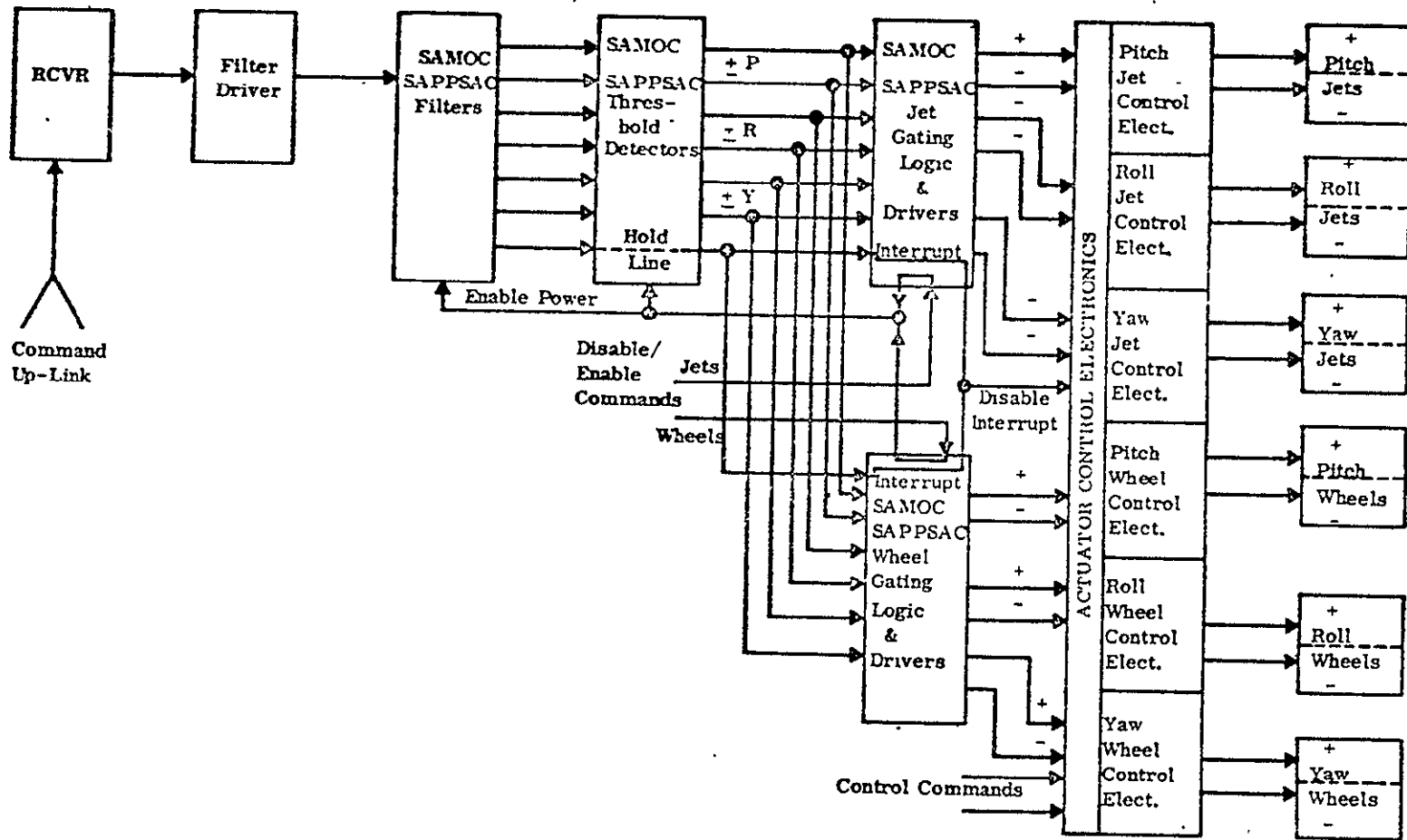


Figure 3.3-8. SAMOC/SAPPSAC Functional Block Diagram ATS-F On-Board Equipment

3.3.4.2

SAMOC/SAPPSAC Functional Performance

The requirements of the SAMOC/SAPPSAC experiment have been reviewed and incorporated into the design of the ATS-F Attitude Control System and Telemetry and Command System.

A signal-to-noise criterion has been established on the basis of the 10 millisecond firing time uncertainty. Utilizing a minimum pulse width of 50 msec, a worst case filter bandwidth (narrowest) of 60 Hz, and a requirement of less than 3 msec time delay uncertainty, a signal to noise ratio (SNR) of 14 dB has been established as the operating threshold required during performance of SAMOC/SAPPSAC. Listed below are the pitch, roll, and yaw SNR calculated for ATS-F operation with the omni-directional antennas (-3 dB gain, nominal).

	SNR (db)		
<u>Channel</u>	<u>Min.</u>	<u>Nom.</u>	<u>Max.</u>
Pitch	18.1	27.1	32.6
Roll	18.2	27.2	32.7
Yaw	18.1	27.1	32.6

In operation, the high gain (16 db, 25 degree) VHF antenna will be utilized, increasing the margin to a point where the contribution of error from the command system to the pulse firing time uncertainty is negligible.

The variation in pulse firing time due to the solenoid valve response and jet response are as follows. The valve contributes a pulse firing time uncertainty of approximately ± 1 millisecond and the jet less than ± 1 millisecond. Summing the uncertainties directly, results in an uncertainty with jets far less than 10 millisecond. The repeatability of the jet impulse is within four percent of nominal.

The command system utilized provides an inherent rate of two commands per second for discrete commands. In addition, the minimum pulse-width of fifty milliseconds is not limited in the spacecraft command system implementation. The command system (Figure 3.3-8) has implemented an interrupt that will disable the SAMOC/SAPPSAC mode upon interruption of the holding mode. Control can also be returned to the on-board system by using a discrete command.

Telemetry Data is provided as follows:

<u>Sensor</u>	<u>Parameter</u>	<u>Range</u>	<u>Accuracy</u>	<u>Resolution</u>
Earth Sensor	Roll Angle	$\pm 11.25^\circ$	$\pm 0.05^\circ$	$\pm 0.044^\circ$
Earth Sensor	Pitch Angle	$\pm 11.25^\circ$	$\pm 0.05^\circ$	$\pm 0.044^\circ$
Star Tracker	Yaw Angle	$\pm 3.5^\circ$	$\pm 0.05^\circ$	$\pm 0.0137^\circ$

Interferometer relative pitch count and roll count data will be available as 60 bits of serial data in the following format for the two ground station frequencies, f_1 and f_2 :

f_1 coarse roll data	5 bits
f_2 coarse roll data	5 bits
f_1 coarse pitch data	5 bits
f_2 coarse pitch data	5 bits
f_1 fine roll data	9 bits
f_2 fine roll data	9 bits
f_1 fine pitch data	9 bits
f_2 fine pitch data	9 bits
4 mode bits	

The coarse data is utilized to resolve ambiguity over the 35 degree range (nominal) of the interferometer. The fine data permits accurate measurement of the data within a 2.19 degree angular range consistent with the .03 degree accuracy of the interferometer.

3.3.4.3 SAMOC/SAPPSAC Operational Performance

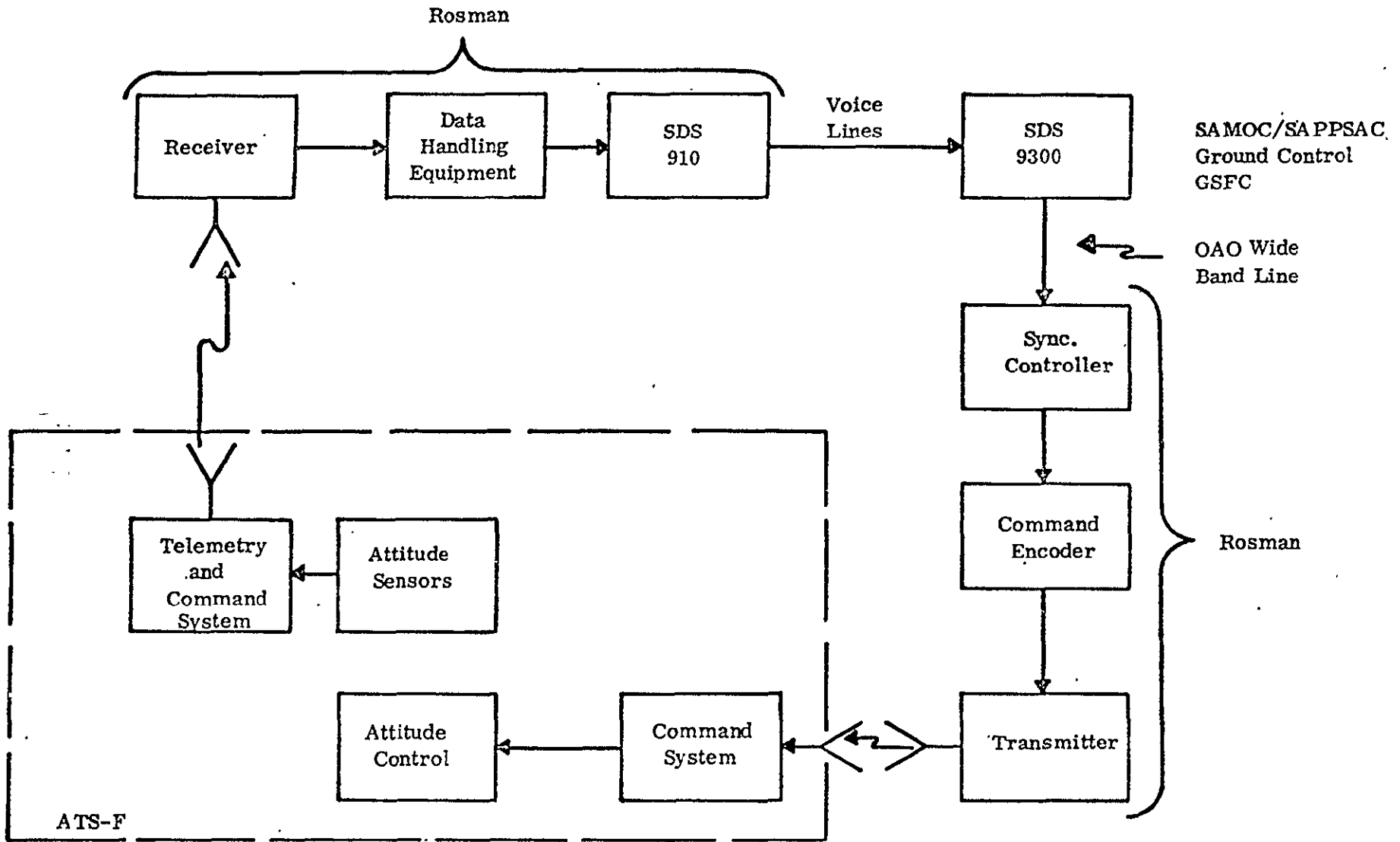
The operational configuration to be utilized for SAMOC/SAPPSAC is shown in Figure 3.3-9. The experiment will be performed under the operational cognizance of the ATS Operation Control Center. Facilities of the Goddard Space Flight Center and the ATS ground station located at Rosman are required to support the experiment.

Following is a description of the sequence of events required to place the spacecraft in the SAMOC/SAPPSAC mode of operation:

- The ground equipment is placed on-line, the holding tone is energized, and the SAMOC/SAPPSAC enable discrete command is sent.
- The attitude control subsystem is placed on ground control and the desired configuration of jets or wheels is selected.
- The adaptive control program selected is initiated. It is anticipated that the nominal test run time will be twenty minutes.
- During performance of SAMOC or SAPPSAC, loss of the hold tone will reset the command subsystem and place the attitude control subsystem under control of the onboard controller.

- The program can be terminated by discrete commands resetting the command subsystem and the attitude control subsystem.

The attitude data required by the experiment is available on the telemetry wavetrain. Interferometer use, would of course require support of an X-band ground transmitter.



FAIRCHILD HILLER

Figure 3.3-9. SAMOC/SAPPSAC Operational Configuration

Each GFE experiment requires what may be termed unique and general interfaces with the spacecraft. In the following paragraphs the particular requirements of each experiment selected for ATS-F and the Fairchild Hiller proposed system implementation will be discussed. Figure 3.3-10, the Experiment Subsystem Diagram, illustrates the electrical interfaces.

The ATS F&G spacecraft provides an environmentally controlled structure for the GFE experiments. The ATS F&G consists of an earth-viewing module (EVM), a 30-foot parabolic reflector, and a solar array assembly. The GFE experiments, except for the Environmental Measurements Experiments positioned on the hub, are mounted in the earth-viewing module. Emphasis has been placed on accommodating the experiment requirements, particularly towards ensuring that clear optical/RF fields of view are maintained.

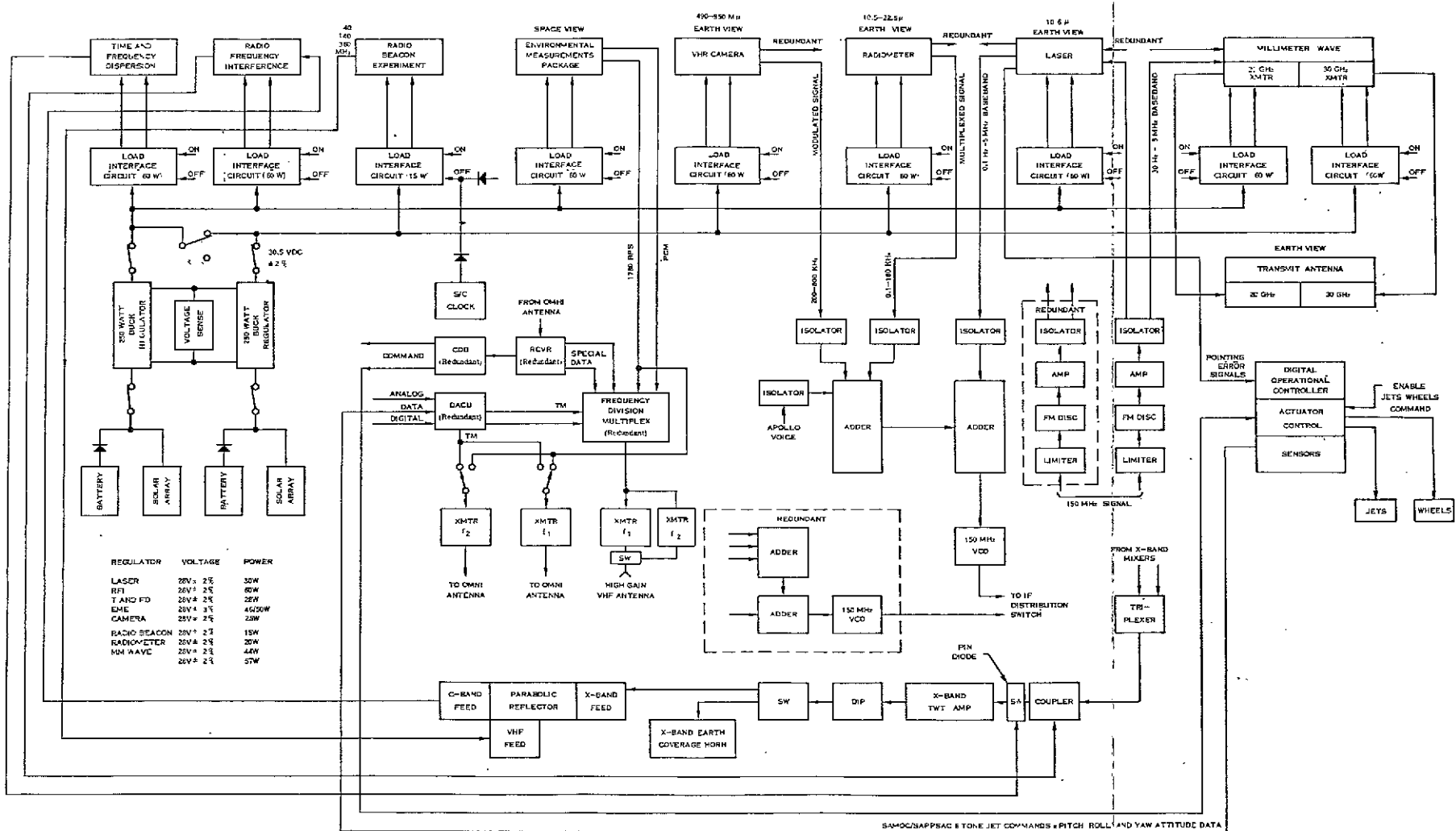
The following paragraphs describe the general characteristics of the support systems utilized by the experiments and summarize what can be termed as the capacity of each system dedicated to support of the GFE experiments. The systems to be discussed are the:

- Telemetry System
- Command System
- Power System
- Spacecraft Clock
- Attitude Control System
- Structural System
- Thermal Control System

The last section of 3.3 summarizes the special interfaces that have been provided to enable the GFE experiments to meet their mission objectives.

3.3.5.1 Telemetry System

The ATS F&G spacecraft provides a telemetry system with the capability of transmitting analog and digital data via a redundant PCM system to earth based ground stations. Analog information is converted to a nine-bit digital word, time multiplexed with the digital data, and transmitted at a bit rate of 388 bits per second. Sampling intervals of 1 sample per 2.97 second (1sp3s) and 1 sample per 47.55 second (1sp48s) are provided. Selected data sources requiring a higher rate can utilize a dwell mode provided for this purpose. The bit error rate on the telemetry channel will be less than 1×10^{-5} and less than 1×10^{-9} when the spacecraft is oriented in its



SA-MOC/NAPPSAC & ONE JET COMMANDS + PITCH, ROLL, AND YAW ATTITUDE DATA

Figure 3.3-10. Experiment Subsystem, Block Diagram

FOLDOUT FRAME 1

FOLDOUT FRAME 2

FOLDOUT FRAME 3

in-orbit operational attitude. It should be noted that no data storage is provided aboard the ATS F&G spacecraft.

3.3.5.1.1 Analog Data Inputs

Experiments requiring the transmission of analog data must meet the following requirements:

Voltage - Analog inputs range from 0-5.12 vdc.
The maximum allowable fault voltage is ± 25 volts.

Impedance - For an accuracy of three percent, the maximum data source impedance is 10K ohms, single-ended. For channels that require high accuracy (between 0.25 and one percent) the maximum data source impedance is 1K ohm and a differential drive is used.

A/D Conversion - The A to D converter digitizes analog data to a 9-bit accuracy.

Each analog telemetry channel is placed on redundant, isolated outputs within the experimenters unit. The redundant outputs are routed separately to the redundant telemetry systems. For single-ended lines, three or fewer channels utilize one return and four or more channels require two returns.

3.3.5.1.2 Digital Data Inputs

Experiments requiring transmission of digital data are required to be compatible with the following characteristics:

Voltage - Digital inputs range between -2 volts and +1.0 volt for a logic zero and +5.0 volts to +8.0 volts for a logic one. The maximum allowable fault voltage is ± 25 volts.

Impedance - The maximum data source impedance is 10K ohms.

Sample interval - The sample interval is 2.58 m sec/bit.

Multiple bit digital inputs are accepted in parallel. The telemetry system provides inhibit pulses where required by the experimenter.

Each digital channel is routed separately to the redundant ATS, PCM telemetry systems. Three or fewer digital bit channels utilize a single return. If four or more digital channels are required, two returns are utilized. The redundant, digital outputs are isolated within the experimenters unit.

3.3.5.1.3 Telemetry Capacity

Table 3.3-1 summarizes the telemetry requirements of the GFE experiments, COGGS, and Radio Beacon Experiment. The total as shown constitutes a significant portion of the total frame capacity (approximately 40 percent). Thirty analog words and six digital words will be implemented on the main frame (1sp3s) and six subcommutators will have analog inputs and one subcommutator will have half analog and half digital inputs.

Figure 3.3-2 displays the Frame Format proposed for ATS F&G. The concept of providing a "block" of data for GFE experiments provides maximum adaptability to changing telemetry requirements.

3.3.5.2 Command System

The ATS F&G Spacecraft command system provides the capability of controlling spacecraft functions from ground operations stations. The command system provides either discrete (relay) commands or digital word (magnitude) commands to users. A maximum command rate of two commands per second is available if ground verification, which is implemented as a feature of the system, is not utilized.

3.3.5.2.1 Discrete Command Output

Experiments requiring the utilization of discrete command are required to comply with the following characteristics:

Voltage - Discrete commands range from -0.5 to +0.5V for a logic one.

Pulse Duration - A pulse duration of 50 msec is provided.

Impedance - The source impedance is 1.2K ohms for a logic zero and less than 100 ohms for a logic one.

Discrete commands are routed to the experimenter from each of the redundant command systems. The command leads are single ended, unshielded lines with a limited number of returns. Three or fewer commands utilize one return; four or more commands two returns. The redundant command lines isolated against a failure (short) on one affecting the other.

3.3.5.2.2 Digital Word Commands

Experiments requiring the utilization of digital word (magnitude) commands are required to comply with the following characteristics:

Voltage - Magnitude commands range from -0.5 to +0.5V for a logic zero and +4.5 to +5.5V for a logic one.

Bit Rate - 128 bps

Table 3.3-1. Experiment Telemetry Requirements

EXPERIMENT	ANALOG		DIGITAL BITS	
	1SP3S	1SP48S	1SP3S	1SP48S
Laser	5	22	18	6
MMW	4	0	0	9
VHR Camera	3	12	0	9
Radio Beacon	0	6	0	6
Radiometer	3	12	0	9
EME	2	8	6	6
RFI	3	6	2	9
T&FD	3	6	2	9
COGGS	0	0	2	27
Experiment Spares	7	16	26	9
TOTALS	30	88	56	99

Clock - A 128 bps clock line will be provided to magnitude command users. Its voltage levels are:

0.0 \pm 0.5V for zero
+5.0 \pm 0.5V for one.

Execute - An execute line with the characteristics of a discrete command will be provided. The execute pulse is controlled by ground operation, allowing verification.

Magnitude commands will be routed to the experimenter from each of the redundant command systems. A single return will be provided for each serial command line, clock, and execute line. The redundant command lines shall be isolated against a failure (short) on one effecting the other.

3.3.5.2.3 Command Capacity

Table 3.3-2 summarizes the command requirements of the GFE experiment, COGGS, and the Radio Beacon Experiment. The totals shown reflect a liberal allocation consistent with experiment requirements. A total of 11 discrete commands and seven magnitude commands are allocated (including spares). The command system design and the philosophy of allocating a block of the available command resources to GFE experiments maximizes the systems adaptability to changing command requirements.

3.3.5.3 Power System

The ATS F&G spacecraft provides a power system that utilizes two solar cell arrays and two nickel-cadmium batteries as its primary power source. A regulated bus at 30.5 volts \pm 2 percent is supplied, as is an unregulated 28 to 45 volt bus for pulse loads.

Experiments are provided with dedicated load interface circuits (LIC) that operate off the 30.5 volt bus. The LIC is provided in two power ratings, 0 to 15 watts and 15 to 60 watts. The characteristics of the LIC's are shown below:

Voltage	27.44 to 28.56 volts
Current	0 to .55 amp dc (15w) 0 to 2.2 amp dc (60w)

Ripple - The ripple on the experiment bus is less than 10 mv to 100 KHz.

Conducted Noise Level - The conducted noise level is less than 10mv.

The LIC provides on-off redundant command control, a telemetry power monitor, and redundant power lines. Protection is provided to the experimenter in the form of input over-voltage protection, output under-voltage protection and current

Table 3.3-2. Experiment Command Requirements

EXPERIMENT	COMMAND	
	MAGNITUDE	DISCRETE
LASER	4	9
MMW	0	26
Radio Beacon	0	6
COGGS	0	8
VHR Camera	0	14
Radiometer	0	6
EME	2	24
RFI	0	6
T&FD	<u>1</u>	<u>10</u>
Spares	0	9
TOTAL	7	118

limiting. If a fault occurs, the LIC will automatically turn power off. The load interface circuit may be turned on by command once the condition has cleared itself. The protection limits are listed below:

Over-Voltage	36 volts
Under-Voltage	22 to 26 volts
Current Limit (15w)	0.55 to 1.0 amp
Current Limit (60w)	2.2 to 4.0 amp

The LIC is capable of accepting transient turn on conditions. The experimenter must, however, limit his effective input capacitance to less than 100 microfarads for the 15w, LIC and less than 250 microfarads for the 60w, LIC to ensure proper turn-on.

The experiment load interface circuit presents an effective load impedance of less than 0.1 ohm from 0 to 50 KHZ.

3.3.5.3.1 Power Requirements

Table 3.3-3 is a summary of the power requirements of the GFE experiments and Radio Beacon. The capacity of the power system is much greater than the power required by any single GFE experiment identified to date, having been sized by the communications experiments. The Environmental Measurements Experiment and Radio Beacon Experiment have contributed to the sizing of power system capacity because of their requirement to be on 24 hours a day. The power system is capable of providing sufficient power to support the experiment operating conditions identified to date.

3.3.5.4 Spacecraft Clock

The ATS-F/G Spacecraft provides a spacecraft clock with the capability of providing timing signals and a data time reference to experimenters.

3.3.5.4.1 Timing Signals

The basic clock operates with a 99.42 KHz fundamental from which binary submultiples can be made available. The following timing signals are currently brought out of the clock:

388 Hz

Six-Hour Pulse

The 388 Hz is the basic telemetry rate and the six hour pulse is provided as a safety turn-off of the Radio Beacon Experiment.



Table 3.3-3. GFE Experiment Power Requirements

<u>EXPERIMENT</u>	<u>POWER</u>
LASER	30 W
RFI	60 W
T & FD (Operating)	28 W
(Stand-by)	0.5 W
EME	46 W/ 53 W
CAMERA	25 W
RADIOMETER	20 W
RADIO BEACON	11 W
MILLIMETER WAVE	
20 GHz	44 W
30 GHz	57 W

The characteristics of the spacecraft clock are:

Voltage	0 to 5 volts
Timing Pulse Duration	50 msec
Timing Pulse Accuracy	<u>+0.5%</u>
Rise Time	Less than 125 microseconds
Fall Time	Less than 125 microseconds

3.3.5.5 Attitude Control Subsystem

The ATS Spacecraft attitude control subsystem provides three basic modes of spacecraft operation. The performance in each of these modes are available to experimenters is described in the following paragraphs.

The operational controller can be commanded into a pointing mode, permitting offset pointing in pitch and roll of up to ten (10) degrees off the local vertical. In the pointing mode the pitch, roll, and yaw error will be held to within +0.1 degree.

A low jitter mode of operation provides (as a design goal) high stabilization of the spacecraft. The jitter amplitude will be held to less than 0.003 degrees in 9 minutes and the jitter rate will be held to 0.0003 degrees per second.

Slewing can be performed in pitch and roll up to 10 degrees off the local vertical. The system is designed for a maximum rate of 1 degree/minute with an error of 0.5 degree (0.3 degree design goal).

As part of the spacecraft complement there are a number of sensors available for special use. Included in this classification are the X-band monopulse that is proposed for use with certain experiments (see Section 2.3.3 Operations), and the interferometer which, as a sensor, permits a greater closed loop offset pointing capability than the earth sensor.

3.3.5.6 Structural System

Figure 3.3-12 illustrates the ATS F&G mechanical configuration. The EME is mounted on the hub in a thermally uncontrolled environment. The remaining GFE experiments are located in the EVM.

The EVM is a cuboid structure consisting of three sections. The center section contains a majority of the basic housekeeping equipment provided as part of the Attitude Control System and Telemetry and Command System. The section on top of the EVM (towards the reflector) contains those equipments associated with the Communications System. The RFI and T & FD experiments, because of their interface with and functional dependence on the communications system, are also

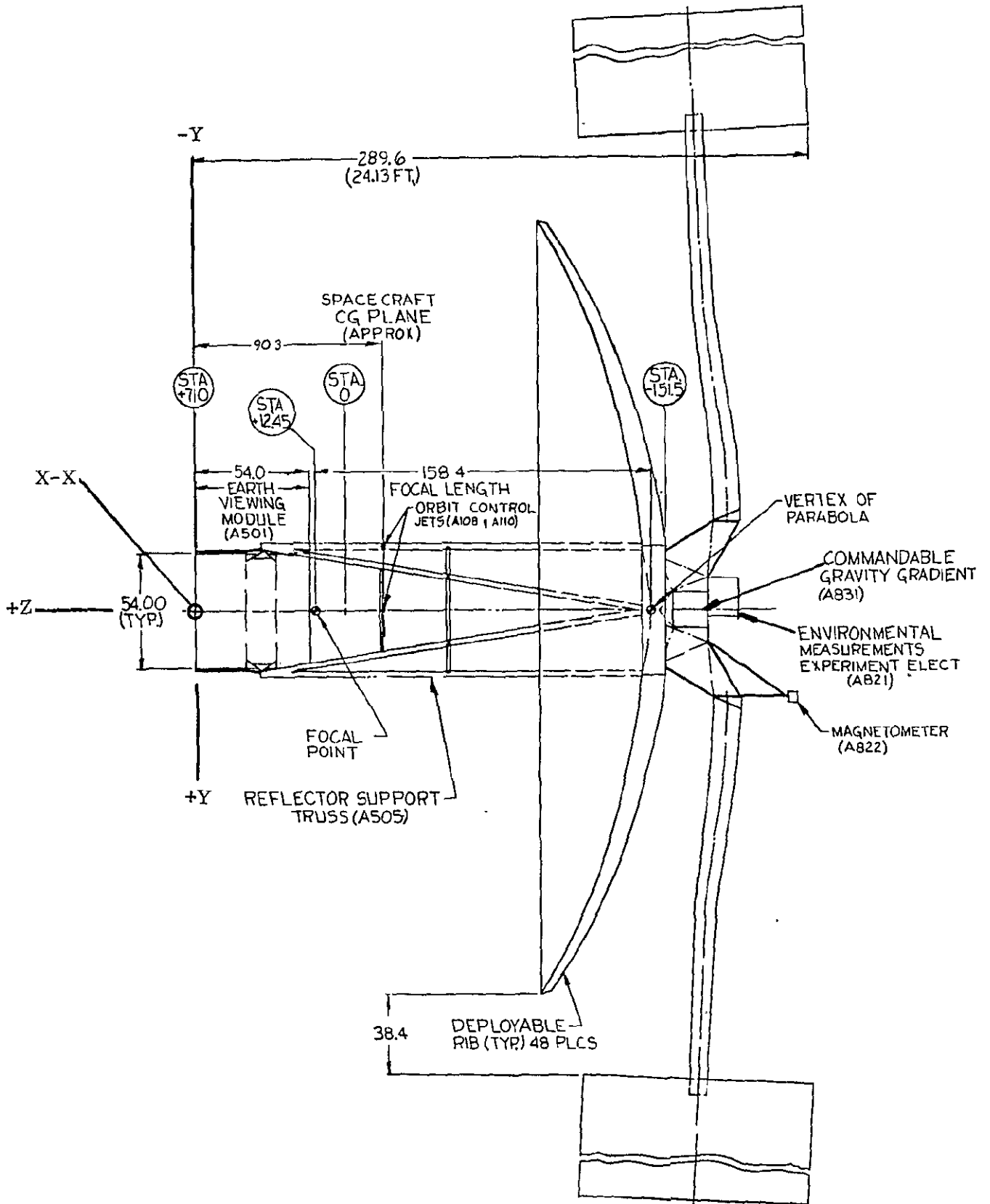


Figure 3.3-12. ATS-F & G Configuration

located in this section. The remaining four experiments require earth-view and therefore have been located in the lower section of the EVM. The EVM equipment configurations are shown in Figures 3.3-13 and 3.3-14. All sections of the EVM and the lower section of the EVM in particular, have been configured to provide the experimenter with maximum flexibility in both experiment size and shape. The present configuration allots approximately 1086 square inches of earth viewing surface to experiments, with approximately 526 square inches available for growth in the lower experiment module

The coordinate system proposed for utilization by experimenters in describing location requirements is shown in Figure 3.3-13.

- The station planes shall be utilized as the reference for describing mounting surfaces and functional parameters on the geometric centerline (Z-axis)
- Angular location of mounting surfaces shall be referenced to the -Y (north) axis looking towards earth in a counter-clockwise direction.
- Radial dimensions of mounting surfaces for functional parameters shall be referenced to the geometric centerline (Z-axis) of the spacecraft.

Access to EVM - mounted equipment will be from outboard of the structure and will be achieved by removing the spacecraft protective panels on the East and West facing sides. The access area for installation is limited to the panel area. The envelope necessary for test fixtures is specified and the experimenter specifies test fixture pick-up points on his experiment to ensure interface compatibility in the spacecraft.

Experiments are mounted to the structure providing a path for thermal conduction. Each experiment will be designed to support its own inertia between mounting supports and the interrelation between modules of an experiment (if required) is identified. The detailed mounting characteristics including mounting hole pattern, mounting hole size, thickness of the mounting surfaces, available mounting hardware clearances, and mounting surface description are identified (with tolerances) and considered in the spacecraft design.

Materials and finished used on experiments are required to have properties compatible with the ATS environment, particularly with the requirements imposed by the thermal control system interface. Wherever possible, nonmagnetic materials are recommended for use. Magnetic materials should be employed only where the electric or magnetic circuit properties are utilized. Materials should also meet the following requirements for weight loss and volatile condensable material:

Weight Loss	1% maximum
VCM	0.1% maximum

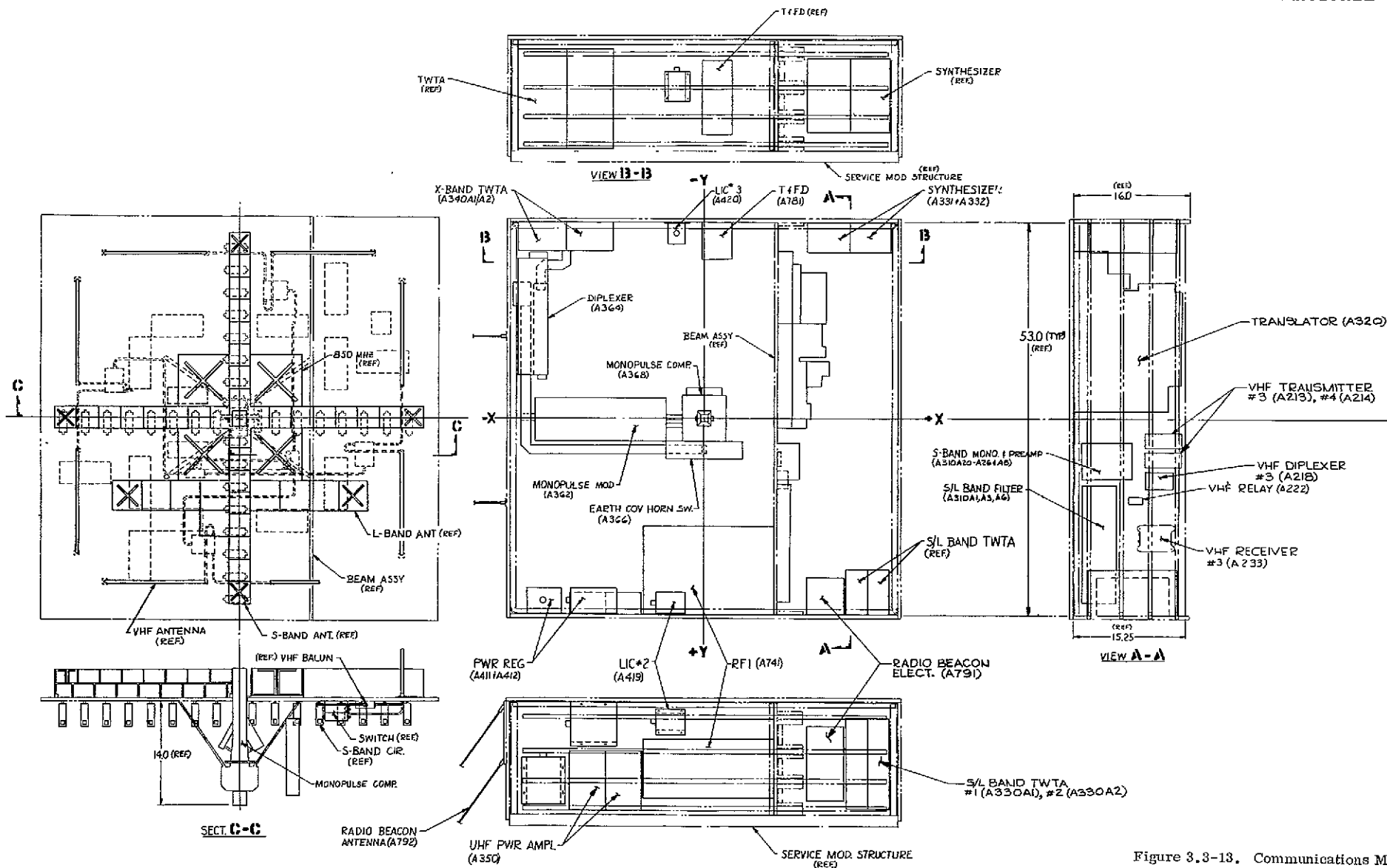


Figure 3.3-13. Communications Module Equipment Configuration

EXPLODED FRAME 2

EXPLODED FRAME

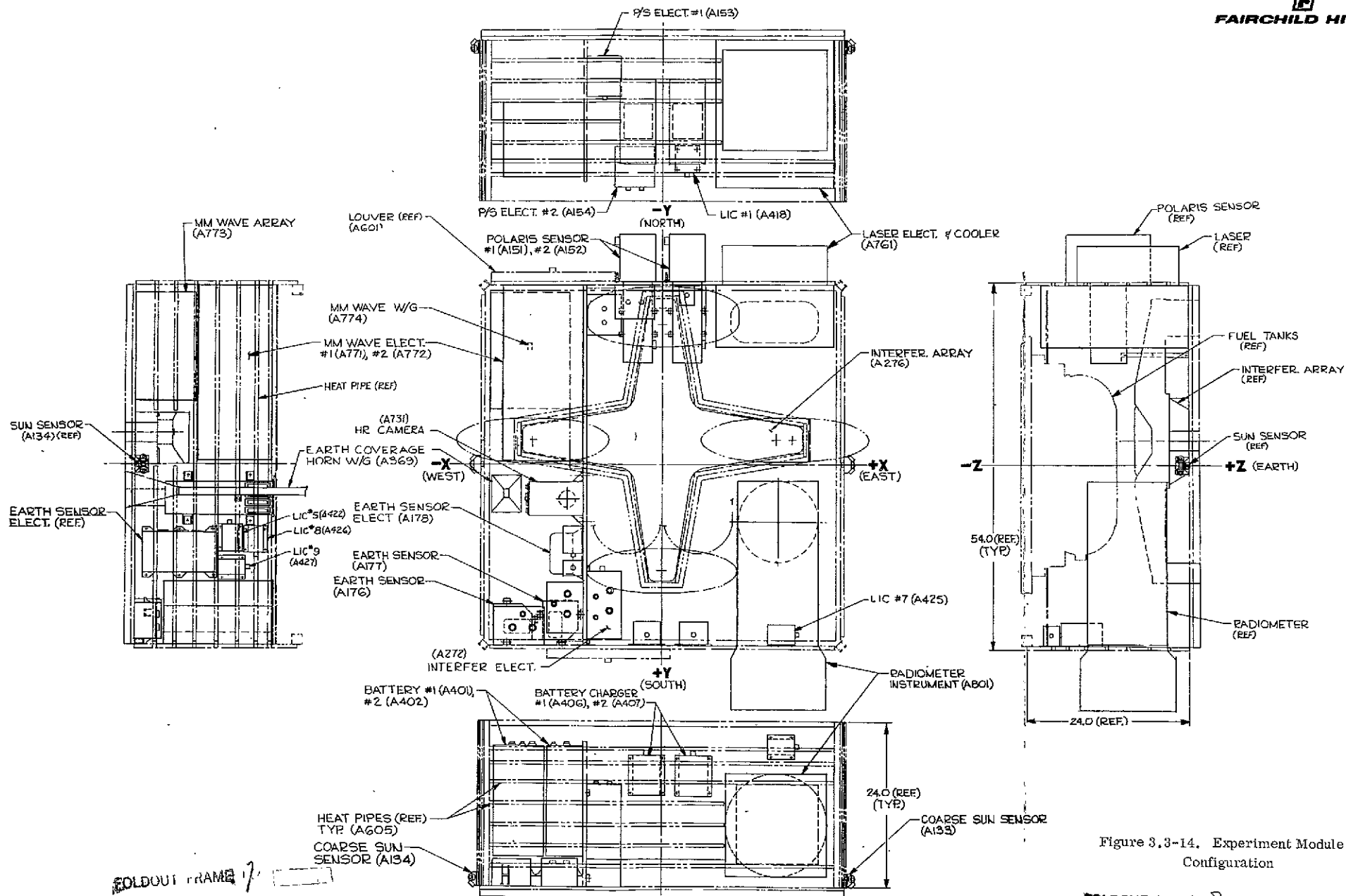


Figure 3.3-14. Experiment Module Configuration

An ATS-F/G mass properties control plan has been implemented. Table 3.3-4 is a summary of the weight and volume requirements identified for the GFE experiments.

The installation of experiments will be performed to detailed installation and handling procedures. The procedure will be written to ensure proper handling of the experiment in terms of unique requirements and to identify special procedures (e.g., torque levels on attaching hardware and alignment).

Alignment will be performed in all cases by controlling the component and structure mounting surface relationships.

The spacecraft contractor will align the experiment alignment reference to the spacecraft axis. The relationship between the experiment index and the internal component is the responsibility of the experimenter. For items requiring alignment to two axes, one alignment surface is required; for alignment to three axes, two alignment surfaces are required. Orientation requirements will be clearly marked on the experiment and on its interface control drawing.

Alignment pads will define the required parallel and perpendicular relationships. It is not planned to align experiments to better than 0.1 degree. It is recommended that experimenters position alignment pads to utilize maximum dimension of their component mounting surface. Experiment alignment surfaces that are controlled to the following limits are acceptable (ref: S-460-ATS-38).

Component Alignment Limits	Surface Finish	Pad Flatness	Max. Surface Slope	Pad Size or Span (Min.)
$\pm 0.5^\circ$	125 min.	0.001 in.	0.005 in/ft	1.0 in.
$\pm 0.1^\circ$	32 min.	0.0005 in.	0.0004 in/ft	1.0 in.

The alignment of experiments requiring ± 0.1 degree alignment will be checked optically and appropriate optical reference surfaces should be provided by the experimenter.

3.3.5.7 Thermal Control System

The ATS F&G thermal control system consists of thermal louvers, heat pipes, insulation, conductive mounting of heat dissipators, and thermal control coatings. Thermal control of the spacecraft is maintained during all orbital and operational conditions. The ATS thermal control system has been designed to reject a total of 446 watts. The component temperature, at any point on its surface, will be maintained between 5°C and 35°C . The component mounting baseplate will be maintained between 5°C and 35°C . Each of the EVM modules have been designed/optimized to accept fixed dissipation limits in accordance with identified operational configurations.

Table 3.3-4. Experiment Weight and Volume Summary

<u>EXPERIMENT</u>	<u>WEIGHT</u>	<u>VOLUME</u>
RFL-	30 lbs.	8" x 12" x 15"
LASER	40 lbs.	15" x 22" x 17"
VHR CAMERA	50 lbs.	21" x 8" x 5"
RADIOMETER	50 lbs.	12" x 12" x 24"
RADIO BEACON	11.7 lbs.	5" x 5" x 10"
MILLIMETER WAVE	85 lbs.	12" x 18" x 24"
EME	90 lbs.	18.5" x 14" x 14"
T & FD	12 lbs.	8" x 12" x 12"
MAGNETOMETER	1.5 lbs.	6" x 6" x 6"
COGGS	35.0 lbs.	12" x 18" x 18"
	<hr/>	
TOTAL	405.2 lbs.	

The average radiation environment of each component will be a temperature of $20^{\circ} \pm 10^{\circ}$ C and an emissivity of 0.8. The mounting surface of the structure will be flat to within $\pm .01$ in/ft.

The component dissipation of each experiment will be identified for each of its operating modes. The mounting surface characteristics shall minimize the thermal gradient across the mounting. Compliance with the following thermal interface characteristics by the experimenter is required:

- Dissipation rate of less than 3 watts/square inch, with a maximum utilization of the mounting surface as a conductive dissipating area.
- Emissivity of greater than 0.60
- Mounting surface flatness to within ± 0.01 in/ft.

The following characteristics will also have to be identified by the experimenter:

- The heat leak characteristics.
- The emittance and absorptivity for surfaces exposed to space
- Unusual/unique thermal characteristics.

To the maximum extent possible, heat dissipating components in an experiment should be located on the mounting surfaces.

3.3.5.8 Special Interfaces

The following paragraphs describe the special interfaces that have been provided for the GFE experiments.

3.3.5.8.1 Radio Frequency Interference Experiment

The RFI experiment utilizes a 6 GHz (C-band) feed, located on the spacecraft axis, provided as part of the complement of spacecraft equipment. The feed provides command selection of vertical, horizontal, or circular polarization. Characteristics of the proposed C-band feed are:

- | | | |
|---|------------------|--|
| ● | Frequency band | 5900 to 6400 MHz |
| ● | Polarization | Selectable:
Horizontal
Vertical
RH Circular |
| ● | Gain | 48 db minimum |
| ● | Output impedance | 50 ohms nominal |
| ● | VSWR | .4:1 maximum |

The downlink of the RFI experiment is implemented through a 10 db coupler inserted between the up-converters and power amplifiers of the communications transponder. The earth coverage horns is to be utilized as an antenna (16 db minimum gain, 25 degree conical beam width). The X-Band Traveling Wave Amplifier (TWTA), when in operation for the RFI experiment, will be utilized in a linear mode of operation, with the following characteristics:

- Frequency: 8GHz (nominal)
- Bandwidth: 500 MHz
- Maximum Input Level 7 dbm, peak for linear operation
- Dynamic Range: 40 db
- Input Impedance: 50 ohms

Scaling of the maximum input level at the input of the coupler will be implemented in the RFI experiment.

The RFI experiment waveguide interface with the ten db coupler (X-Band) and the C-Band feed located in the communications system make mounting of the unit in the upper communications system section of the EVM particularly attractive to minimize rf losses. Figure 3.3-13 illustrates the position of the RFI experiment in the communications module.

3.3.5.8.2 Laser Experiment

The Laser experiment will utilize equipment provided as part of the ATS-F/G communications system to modulate the X-band RF carrier with a 5 MHz bandwidth baseband signal. Listed below are the characteristics of the down-link, wide-band data interface:

Bandwidth	0.1 Hz to 5 MHz (\pm 1 db)
Impedance	75 ohms
Voltage	0 to 1.0 volt p-p
Stability	Better than 500 PPM (short term)
Spurious Response	- 20 db referenced to carrier

The Voltage Controlled Oscillator (VCO) proposed for use in the communications system transponder will operate at a center frequency of 150 MHz. The VCO's inherent linearity of ten percent over the proposed VCO maximum deviation of \pm 9 MHz permits a high quality microwave data down-link. An FM modulation index of 1.8 can be achieved, resulting in an unweighted signal to noise ratio of 52.4 db.

Baseband information, derived from the microwave X-band uplink, will be cross strapped to the Laser experiment. Listed below are the characteristics of that interface:

Bandwidth:	30 Hz to 5 MHz (± 1 db)
Impedance:	75 ohms
Voltage:	0 to 1 volt p-p

The discriminator proposed for use in the communications system transponder will operate at a center frequency of 150 MHz. The discriminator inherent linearity of one percent over the proposed maximum deviation of ± 9 MHz, result in a high quality microwave data up-link. An FM modulation index of 1.8 can be utilized, resulting in a signal to noise ratio of 68.5 db.

The Laser optical monopulse, utilized for locking up the optical beam, will be interfaced with the ACS system and utilized as an attitude sensor in conjunction with the digital operation controller and analog backup controller. When the Laser mirror is in the normal position, the outputs of the Laser monopulse are pitch and roll error signals. The required characteristics of the signal on this interface are:

Voltage	± 5 volts
Impedance	50 ohms
Frequency	Time varying dc
Scale Factor	50 volts/degree, linearity 5% to .05 degree, max 5.0 volt

The Laser is mounted on the earth viewing surface, facing the north facing side of the EVM. A clear field of view is provided for the ± 40 degree optical field of view in the equatorial plane and $+8$ degrees above and -8 degrees below the spacecraft Z-axis in the north-south direction. An elliptical view port of 7 x 10 inches is provided.

The Laser cooler faces north, along the $-Y$ spacecraft axis. The cooler field of view required of 45 degrees toward earth, 30° toward space, and $\pm 45^\circ$ East-West has been accommodated. Figure 3.3-14 shows the mounting position of the Laser.

3.3.5.8.3 Very High Resolution Camera

The Very High Resolution Camera video output contains 23.8 kHz baseband video information, modulated on an FM subcarrier. A bandwidth allocation of 500 kHz ± 300 KHz is provided on the wideband data interface of the communications transponder for the camera. Camera data is linearly added with Radiometer data (0.1 Hz to 180 kHz) and the resultant composite signal modulates the FM, 150 MHz Voltage Control Oscillator (VCO). The VCO output is then up converted to one of three X-band frequencies, amplified, and transmitted to the ground station.

The camera wide band data signal will have the following characteristics:

Voltage	1 V P-P
Frequency	200 KHz to 800 KHz
Impedance	75 ohms

The voltage level will be scaled in the transponder to provide the optimum input to the VCO, once the characteristics of the signal and voltage control oscillator modulation sensitivity are determined. The system as implemented can provide a potential signal to noise ratio of better than 50 db.

The high resolution (5000 lines) of the camera imposes a stringent requirement on the ATS-F, Attitude Control System (ACS) stability. A highly stable, earth oriented platform is required during the 8.75 minute scan of the camera field of view. As a design goal, a jitter amplitude of less than 0.003 degrees has been established in pitch and roll, corresponding to one line of camera frame resolution. As a design goal, a jitter rate of .0003 degrees/sec. has also been imposed.

Computer simulations have been performed, using the ACS control laws, to determine the performance capability of the ACS system. The results of one such simulation are shown below.

ϕ max	0.00193 degrees
θ max	0.00271 degrees
ψ max	0.00194 degrees
P max	0.00025 degrees/second
q max	0.00029 degrees/second
r max	0.00025 degrees/second

The low jitter mode of the ACS is selectable by a ground command supplied to initiate this mode. Upon initiating the low jitter mode, the ACS is designed to settle to the specified performance within five minutes. The digital operational controller, earth sensor, polaris sensor, and inertia wheels are utilized to achieve low jitter performance.

The Very High Resolution Camera is mounted on the earth viewing surface, with its viewing axis directed towards the earth disk. A clear field of view, larger (approximately 40 degrees) than the 20 degree cone angle required by the camera, is provided along the spacecraft Z-axis. A $2\frac{1}{2}$ inch diameter opening for the lens is provided. Figure 3.3-14 shows the mounting position of the VHR Camera.

3.3.5.8.4 Radiometer

The radiometer video output is a composite of digital and analog data that is to be constrained to a 0.1 to 180 KHz bandwidth. The radiometer data is linearly added with the VHR Camera data (200 kHz to 800 KHz bandwidth). The resultant signal is used to frequency a modulate 150 MHz voltage control oscillator (VCO). The VCO output is upconverted to one of three X-band frequencies, amplified, and transmitted to the ground station.

The Radiometer output will be transmitted to the communications system on two isolated lines with the following characteristics:

Voltage	1V p-p
Frequency	0.1 Hz to 180 kHz
Impedance	75 ohms

The voltage levels of the composite signal will be scaled in the transponder to provide the optimum input to the 150 MHz VCO. The system as implemented can provide a potential signal to noise ratio greater than 50 db on the 1 kHz analog channels and 24 db on the 24 kbps digital channel.

The Radiometer is mounted on the earth viewing surface on the south facing side of the earth viewing module. A clear field of view is provided for the twenty degree optical path. A twelve-inch diameter hole is provided for the Radiometer telescope. Figure 3.3-14 shows the mounting position of the Radiometer.

The Radiometer cooler faces south along the +Y spacecraft axis through a 15-inch access hole in the side of the EVM. A field of view of +45 degrees is required for the Radiometer cooler to provide the detector operating temperature. The solar array and 30-foot parabolic reflector limit the clear field of view to 28.2 degrees looking from the -Y axis towards the -Z axis (away from the earth). If the Radiometer cooler does require a clear field of view, it is proposed that the Radiometer cooler axis be offset (towards the earth viewing surface). This solution can be accomplished through design of the cooler cone and shield.

3.3.5.8.5 Millimeter Wave Experiment

Baseband information transmitted to ATS over the microwave X-band uplink, is cross strapped to the Millimeter Wave experiment for use in performing the communications experiments. Listed below are the characteristics of the wide-band data interface:

Bandwidth	30 Hz to 5 MHz
Impedance	75 ohms
Voltage	0 to 1 volt p-p

The discriminator proposed for use in the communications system operates at a center frequency of 150 MHz. The discriminator linearity of one percent over the maximum deviation of ± 9 MHz provides a high quality data up-link. An FM modulation index of 1.8 can be utilized, resulting in a signal to noise ratio of 68.5 db.

The Millimeter Wave Antenna Assembly is mounted on the earth viewing surface. A clear field of greater than 15 degrees is provided for the twelve by eighteen inch viewing area. Figure 3.3-14 shows the mounting position of the Millimeter Wave.

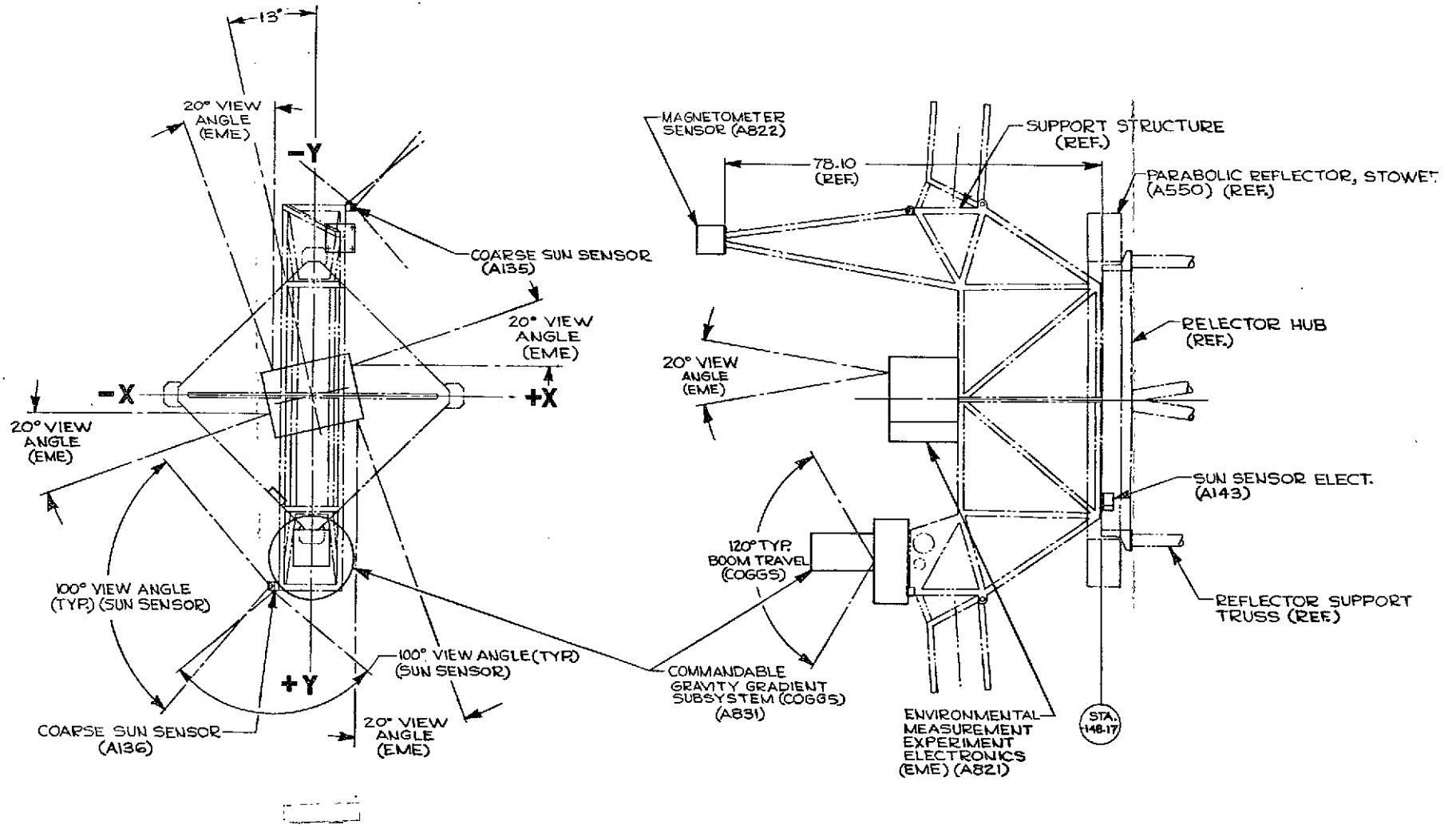
3.3.5.8.6 Environmental Measurements Experiment

The Environmental Measurements Experiment split phase PCM data output (1760 bits per second) is brought down from the hub on redundant lines to the ATS telemetry and command (T&C) system. Fairchild Hiller Corporation recommends that a voltage level of 5.0 volts be utilized and will provide an input impedance of 10K ohms. The T&C system provides two sets of redundant transmitter to which each of the lines is routed. In the event of any ATS attitude misorientation, the EME data can be placed on either of the transmitters, operating at frequencies of 136.23 and 137.11 MHz, feeding the VHF omni-directional array. For this configuration, a 0 dbw effective radiated power is achievable, resulting in a bit error probability of 1×10^{-5} .

In addition, Fairchild Hiller Corporation is proposing that a high gain (16 db) VHF antenna be included on the ATS-F spacecraft. Two additional, two watt transmitters are used to feed the high gain antenna. The EME data (at base-band) is keeping telemetry data. The 19 db increase in antenna gain, provides a 16.8 db worst case EME signal to noise ratio, with the proposed multiplex scheme. The 16 db, 17-degree beam width antenna will be utilized for in-orbit operations. The 16.8 db signal to noise ratio will result in a probability of bit error much less than 1×10^{-6} .

EME will be positioned to view along lines of magnetic field, perpendicular to lines of field, and outward away from the earth. The ATS-F spacecraft has the solar arrays positioned directly along the Y (North-South) axis. The EME will be positioned as shown in Figure 3.3-10 to provide the required 20 degree view angles. Listed below are some features of this configuration:

- It meets the field of views specified for the particle sensors selected for EME and provides flexibility for changes.
- It provides a fixed boom for mounting the Magnetometer remote from the spacecraft.
- The configuration shown provides sufficient room for the solar degradation experiment, solar cell panels.



FOLDOUT FRAME 1

Figure 3.3-15. EME Field of Views

FOLDOUT FRAME 2

3.3.5.8.7 Time and Frequency Dispersion

The T&FD experiment requires the transmission of calibrated, variable (1 to 10 nanosecond) keyed carrier pulses. The pulses will be transmitted at a selected pulse repetition rate. The selectable rates are 10, 20, 50 and 100 MHz.

The 7575 MHz r-f carrier will be keyed by the T&FD experiment. A diode modulator will be provided by the T&FD experimenter and will be inserted in the single path prior to the X-band Traveling Wave Tube Amplifier as shown in Figure 3.3-1. Drive level control will also be provided in the IF (6 db pad) to operate the TWTA in a semi-linear mode during T&FD operation. Listed below are the operating characteristics of the transponder:

Frequency	7575 MHz
On Power Level	> 5 dbw
Bandwidth	500 MHz (1 dB)
Frequency Stability	
< 250 msec	$< 1 \times 10^{-8}$
Long Term	$< 1 \times 10^{-6}$
Amplitude Stability	± 0.5 dB
Group Delay	(TBD)
AM/PM Conversion	< 35 degrees
Gain Slope	0.05 db/MHz
Reflections	< 32 dB below modulator output
Spurious	-30 dB below carrier

The modulator supplied by the experimenter shall supply the following performance characteristics:

Power on Level	-37 dBm
Pulse Shape	$\text{COS}^2 X$

The T&FD experiment interface with the pin diode modulator located in the communications module make positioning this experiment in this module attractive. Figure 3.3-7 illustrates the position of the T&FD experiment in the communications module.

SUMMARY OF SYSTEM CHARACTERISTICS

The intended purpose of this paragraph is to list the spacecraft system and subsystem characteristics by a series of summary tables. Detailed descriptions of the subsystems are given in the succeeding paragraphs. Table 3.4-1 presents some of the highlights of the ATS F&G Systems as proposed by Fairchild Hiller. Table 3.4-2 shows the electromagnetic communication bands used for the experiments and the spacecraft. An overall weight breakdown is given in Table 3.4-3. The RF reception and transmission characteristics established to meet the requirements of the ATS-F mission are defined in Table 3.4-4. Table 3.4-5 summarizes the Auxiliary Propulsion Subsystem requirements and characteristics. Table 3.4-6 lists the APS propellant weights. A summary of the Telemetry and Command requirements, by subsystem, is presented in Table 3.4-7. The telemetry functional parameters are highlighted in Table 3.4-8. Table 3.4-9 highlights the functional parameters of the command system that receives, decodes, and distributes discrete and data word commands to the spacecraft subsystems. Table 3.4-10 lists the Interferometer Subsystem characteristics. Figure 3.4-1 depicts the power loads required from the Electric Power Subsystem for the various spacecraft modes of operation.

Table 3.4-1. Overall System Characteristics

●	Orbit	Synchronous (22,235 st. mi) - Equatorial
●	Life (In-Spec Performance)	2 years or greater
●	Spacecraft Dimensions	
	Maximum Diameter	9 feet (folded for launch)
	Length	25.3 feet
	Span (Between Deployed Tips of Solar Paddles)	52 feet
	Earth Viewing Module	54 inch-cube
	Earth Viewing Surface	54 inch-square
●	Parabolic Antenna	30-foot diameter 100 MHz to 10 GHz f/d = 0.44 Stowed Dimensions, an amulus 6.5 feet OD x 5.5 feet ID x 1 foot high
●	Thermal Control	Heat pipes, Louvers, and Super Insulation Average Experiment Environment Temperature $20^{\circ} \pm 10^{\circ}$ C; 2 Mounting Surface Temperature $20^{\circ} \pm 15^{\circ}$ C.

Table 3.4-1. Overall System Characteristics (cont)

●	Solar Array	Two Semi-Cylindrical Panels with a total area of 208 sq. feet. 41,600 - 2 x 2 cm N on P Cells 400 watts (at end of two years)																		
●	Power Amplifiers	<table border="0" style="margin-left: 40px;"> <thead> <tr> <th colspan="3" style="text-align: center;"><u>Solid State</u></th> </tr> </thead> <tbody> <tr> <td>UHF</td> <td style="text-align: center;">-</td> <td>80 watts</td> </tr> <tr> <td>L-Band</td> <td style="text-align: center;">-</td> <td>40 watts</td> </tr> <tr> <td>S-Band</td> <td style="text-align: center;">-</td> <td>20 watts</td> </tr> <tr> <th colspan="3" style="text-align: center;"><u>Traveling Wave Tube</u></th> </tr> <tr> <td>X-Band</td> <td style="text-align: center;">-</td> <td>20 watts</td> </tr> </tbody> </table>	<u>Solid State</u>			UHF	-	80 watts	L-Band	-	40 watts	S-Band	-	20 watts	<u>Traveling Wave Tube</u>			X-Band	-	20 watts
<u>Solid State</u>																				
UHF	-	80 watts																		
L-Band	-	40 watts																		
S-Band	-	20 watts																		
<u>Traveling Wave Tube</u>																				
X-Band	-	20 watts																		
●	Repeater Operation	Coherent linear translation and/or modulation conversion (ϕ M) of up to 3 independent RF channels simultaneously. 5 MHz baseband VCO and discriminator																		
●	Attitude Control	Better than 0.1 degree in all 3 axes																		
●	Slewing Rate	To 1 degree/minute with max roll & pitch error 0.3-0.5 deg																		
●	Stabilization Jitter	0.003 degrees max excursion																		
●	Yaw Reference	Polaris Sensors																		
●	Pitch and Roll Reference	Earth Horizon Sensors																		
●	Alternate Station/Pointing/Tracking	Monopulse at VHF, S- and X-Bands, Laser, and Interferometer																		
●	Attitude Control Actuators	Momentum wheels and ammonia cold gas thrusters in all 3 axes																		
●	Station Keeping - Orbit Control	Ammonia hot gas thrusters V = 128 feet/second total capacity																		
●	Harness	Multi-Harness Construction appropriate for Modular EVM Design.																		
●	Telemetry Transmission (ERP)	20 dbw (High gain link) -3 dbw (omni-link)																		
●	Transmitter	2 watt FM/ ϕ M																		

Table 3.4-2. ATS F&G Spectrum Utilization

Function	Freq. Band	Nom. Freq. (MHz)	Ant. Gain Peak (dBi)	XMTR Power (Watts)	ERP (dBw)	G/T (dB/°K)
Radio Experiment Beacon	VHF	40	2.2	1.2	3.0	---
		140	7.0	0.48	3.8	---
		360	9.5	0.34	4.8	---
Telemetry (FDM) Command	VHF	136-137	17.8	2	20	---
		148-154	17.8	---	---	-18
Monopulse	VHF	150	17.8	---	---	-18
ITV	UHF	850	33.2	80	51.2	---
PLACE	L	1550	39.7	40	54.4	---
		1650	39.7	---	---	+8.7
DRSS	S	1800	41.5	20	52.2	---
		2250	43.8	---	---	+11.7
RFI	C	6300	52	---	---	+20
Spacecraft	X	7350, 7575, 7650	53.2	20	63.0	---
		8050, 8150, 8250	54.1	---	---	+19.1
Interferometer	X	8150, 8155	12	---	---	-28
mm Wave	K _u	20,000	27	4	33	---
	K _a	30,000	27	3.2	31	---
Laser	IR	28 10 ⁶ (10.5μ)	100	0.4	+96	---
			100	---	---	+63

Table 3.4-3. Summary of Weights

Subsystem and Components	Wt (lb)		Subsystem and Components	Wt (lb)	
Control System		312.2	Power		328.9
Attitude Sensors	44.0		Solar Array	174.8	
Controllers	39.0		Batteries	88.0	
Momentum Wheels	44.0		Electronics	66.0	
Inertial Sensors	18.0		Thermal Control		61.0
Actuator Control Electronics	10.0		Wiring Harness		102.0
Ammonia Resistojets	122.0		Telemetry and Command		63.6
Hardware	(56.2)		Communications		129.4
Fuel	(66.0)		Adapter and Separation System		59.4
Interferometer	34.6		Structure	39.4	
Parabolic Antenna		195.3	Separation System	10.0	
Reflector	140.0		Electronics	10.0	
Feed System	55.3		Spacecraft and Subsystem Weight		1648.8
Structure		397.1	Allowable Weight		2050.0
EVM	240.5		Margin for Growth and Experiments		401.2
Hub	56.2				
Reflector Support Truss	30.1				
Solar Panel Clamps	1.7				
Solar Array Deployment System	68.6				


 FAIRCHILD HILLER

Table 3.4-4. ATS-F Communication Requirements

MODE	USER	Nominal Frequency (MHz)	Bandwidth (MHz)	Polarization	Antenna Field of View (Degrees)	RECEIVER			TRANSMITTER		
						Peak Antenna Gain (dB)	Min G/T Over FOV (dB/°K)	G/T Peak (dB/°K)	Transmitter Output Power (Watts)	Min. ERP Over FOV (dBW)	ERP (Peak) (dBW)
30-Foot X-Band Receive	Laser	8250	40	Linear	0.3	50.0	+13.0	16	—	—	—
	MMW	8150	12								
	Monopulse	8050									
30-Foot X-Band Transmit	Laser	7650	40	Linear	0.3	50.0	—	—	20.0	57.0(1)	60(1)
	MMW	7575									
	Antenna Test	7350									
Horn X-Band Receive	DRSS, ITV	8250	40	Linear	>20	16.8	-20.0	-17	—	—	—
	Place, MMW	8150	12								
	Laser, ATS-R	8050									
Horn X-Band Transmit	DRSS, Beacon	7650	40	Linear	>20	16.0	—	—	20.0	25(1)	28(1)
	Place, Camera	7575									
	MMW, Laser	7350									
	Radiometer										
	ATS-R										
	RFI, T&FD	7500	500	Linear	>20	16			20.0		
30-Foot C-Band Receive	RFI, T&FD	6300	500	Horizontal	0.39	48.0	NA	NA	NA	NA	NA
				Vertical							
				RCP							
30-Foot S-Band Receive, Scan	DRSS	2250	12	RCP	13.2 (3)	40.5	7	—	—	—	—
			40								
30-Foot S-Band Transmit, on Axis	DRSS	1800	12	RCP	—	39.5	—	—	20.0	—	50.5
30-Foot S-Band Transmit, Scan	DRSS	1800	12	RCP	13.2 (3)	39.0	—	—	20.0	48	—
30-Foot S-Band Receive, on Axis	DRSS	2250	12	RCP	—	40.5	—	9.5	—	—	—
			40								
30-Foot L-Band Pencil Beam Receive	Place	1650	12	RCP	1.5	38.5	+ 2.5	5.5	—	—	—
30-Foot L-Band Pencil Beam Transmit	Place	1550	12	RCP	1.5	38.5	—	—	40.0	49.0	51
30-Foot L-Band Fan Beam Receive	Place	1650	12	RCP	1x7.5	31.5	- 5.0	- 2	—	—	—
30-Foot L-Band Fan Beam Transmit	Place	1550	12	RCP	1x7.5	31.5	—	—	40.0	42.0	45
30-Foot UHF, Transmit	ITV	850	40	RCP	3.0	33.0	—	—	80.0	48.0	51
30-Foot VHF, Receive (4)	Monopulse	150	6	Linear	>15	17	-20	- 18	—	—	—
30-Foot VHF, Receive (4)	Command	148.26	.03	Linear	>15	17	-20	- 18	—	—	—
		154.2									
30-Foot VHF, Transmit (4)	Telemetry	136.23	2	Linear	>15	17	—	—	2.0	17	20
	EME, SD	137.11									

(1) Single carrier operation

(2) Dual carrier operation

(3) This is a 13.2-degree plane including the Z-axis

(4) Established by FHC

Table 3.4-5. APS Mission Requirements

Item	Characteristic Velocity (ft/sec)	Impulse (Lb-Sec)		(Design S/C; T= 0.003 lb)
		Design S/C (2000 lbs.)	Max. Wt. S/C (2450 lbs)	
Initial Orbit Adjust	30	1875	2285	7.2 days
East-West Station Keeping (2 years)	14	870	1070	3.5 hrs (ea. month)
North-South Station Keeping (1 month)	14	870	1070	1.35 hrs. (ea. node every 12 hrs.)
East-West Station Repositioning (Transfer from 94° West to 15° East - 41.2 days)	60	3750	4570	7.2 days (each end)
Additional Orbit Maneuvers	10	635	850	---


 FAIRCHILD HILLER

Table 3.4-6. APS Propellant Weights

Item	Design S/C	Max. Wt. S/C
Orbit Control Propellant Wt (Lbs.) ($I_{SP} = 200$ sec.)	40	49
Attitude Control Propellant Wt (lbs) ($I_{SP} = 100$ sec.)	26	29
Total Propellant Wt. (Lbs.)	66	78

Table 3.4-7. Telemetry and Command Requirements

Telemetry

	<u>ISP3Sec</u>		<u>ISP48Sec</u>	
	<u>Analog</u>	<u>Dig. Bits</u>	<u>Analog</u>	<u>Dig. Bits</u>
Attitude Control	4	104	43	66
Telemetry & Command	3	72	0	30
Communications	0	13	5	94
Electrical Power	0	0	25	25
Structures	0	0	8	8
Experiments	<u>21</u>	<u>22</u>	<u>64</u>	<u>57</u>
Totals	28	211	145	280

Commands

	<u>Discrete</u>	<u>Non-Discrete</u>
Attitude Control	156	10
Telemetry & Command	56	3
Communications	8	1 (225 states)
Electrical Power	56	0
Structures	5	0
Experiments	<u>89</u>	<u>6</u>
Totals	370	20

Table 3.4-8. Telemetry Subsystem Parameters

Function	Characteristics
Frequencies	136.23 MHz, 137.11 MHz
Spacecraft Antennas	Near omnidirection mounted on solar panels. Directional via prime focus feed and parabolic reflector.
Modulation	PM on omni-associated transmitters, FM/PM or PM on prime focus feed-associated transmitters.
Formatting	Fixed format with dwell capability
Bit Rate	400 bps nominal
Word Length	9-bit
Minor Frame Length	Approximately 3 seconds
Subcommutation	16 words, 16 deep
Total Format Capacity	368 nine-bit words. Each word carries one digitized analog telemetry point of nine digital telemetry points.
Analog Channels	304
Digital Channels	513
Sync	First 3 words
Subframe Identification	Word 4
Calibration	Words 5-7
Command Verification	Words 8-11
Time Code Tag	Four words, once per minor frame
High Rate Telemetry, Special Data Mode	2000-bps EME data and voice bandwidth analog signal in the prime mode of operation are frequency division multiplexed along with the normal telemetry information onto the carrier of one of the two telemetry transmitters associated with the prime focus feed antenna (FM/PM). In a backup mode, either the EME or voice band analog data can modulate the prime focus feed-associated transmitter directly (PM), and either the EME or normal telemetry data can modulate the omni-associated transmitters directly (PM).
Technology	Optional qualified IC and MSI where weight, volume, power, and reliability indicate a need.
Ground Station/ATSOCC	Real-time link and/or VHF antenna, receivers, and DHE at ATSOCC desirable.

Table 3.4-9. Command Subsystem Parameters

Function	Characteristics
Modulation	FSK/AM/AM
Frequencies	148.26 MHz, 154.2 MHz
Spacecraft Antennas	Omnidirectional mounted on solar panels. Directional via prime focus feed and parabolic reflector.
Clock	128 Hz AM modulation of 0 to 1 tones
Command Word Length	64 bits
Bit Rate	128 bps
Command Word Format	Introductory 0's 27 bits (1-27) Sync Bit(s) 2 bits (28, 29) Spacecraft Address 8 bits (30-37) Data Word Address 6 bits (38-43) Command Address 9 bits (44-52) Trailing 0's 12 bits (53-64)
Command Discrete Addresses	512 max
Data Word Addresses	63 max
Verification	Telemetry 16 bits
Command Execution	Execute Tone
Digital Word Capabilities	9-bit word
Digital Word Execution	Data word is stepped to the selected subsystem as it is received by the command decoder. It is acted upon by the subsystem only upon receipt of an execute tone from the ground which is transferred to the same subsystem by the CDD.
Timed-tone Control	7 additional execute tones for SAMOC/SAPPSAC jets and wheels control.
Technology	Optional qualified IC & MSI technology where weight, power and volume savings and reliability increase is required.
TSOCC/Ground Station Data Link	Command link for real-time control of Timed-tone Execute tones.
Command Console	Similar to present OGO/ATS command console with addition of two octal thumb-wheels for data word address insertion and modification for SAMOC/SAPPSAC timed tone command capability.
Special Data Mode	AM modulation of the command carrier by voice bandwidth analog signals.

Table 3.4-10. RF Interferometer Subsystem Summary

Type of Receiver:	Dual conversion, dual channel Switched antenna elements
Input Frequency:	8.150 and 8.155 GHz
Noise Figure:	16 db
Vernier Baseline:	38.53" (26.6λ)
Coarse Baseline:	2.408" (1.66λ)
Configuration:	Crossed baselines with coarse element near end
Antenna Gain	+12 db
Angle Coverage	±12.5 degrees
Angle Accuracy (pitch, roll, yaw)	±0.03 degrees (3σ)
Angle Coverage - Degraded Accuracy	±17.5 degrees
Antenna Element:	Compensated horn
First IF/IF Bandwidth (BW)	150 MHz/30 MHz
Second IF/IF BW	(Dual) 32.5 MHz and 27.5 MHz/1 MHz
Output Frequency/BW	2 kHz/750 Hz
First LO Frequency	8.00 GHz
Second LO Frequency	122.5 and 122.502 MHz
Post-Filter SNR	+38 db at +76 dbw ground ERP
Vernier Clock Frequency:	1024 kHz
Coarse Clock Frequency:	1024 kHz
Counter Input Rate:	2 kHz
Vernier Averaging:	64 Samples
Telemetry Output	Digital 60 bits/3 sec (1 or 2 sta modes)
Weight	34.6 lbs
Power	30.3 watts

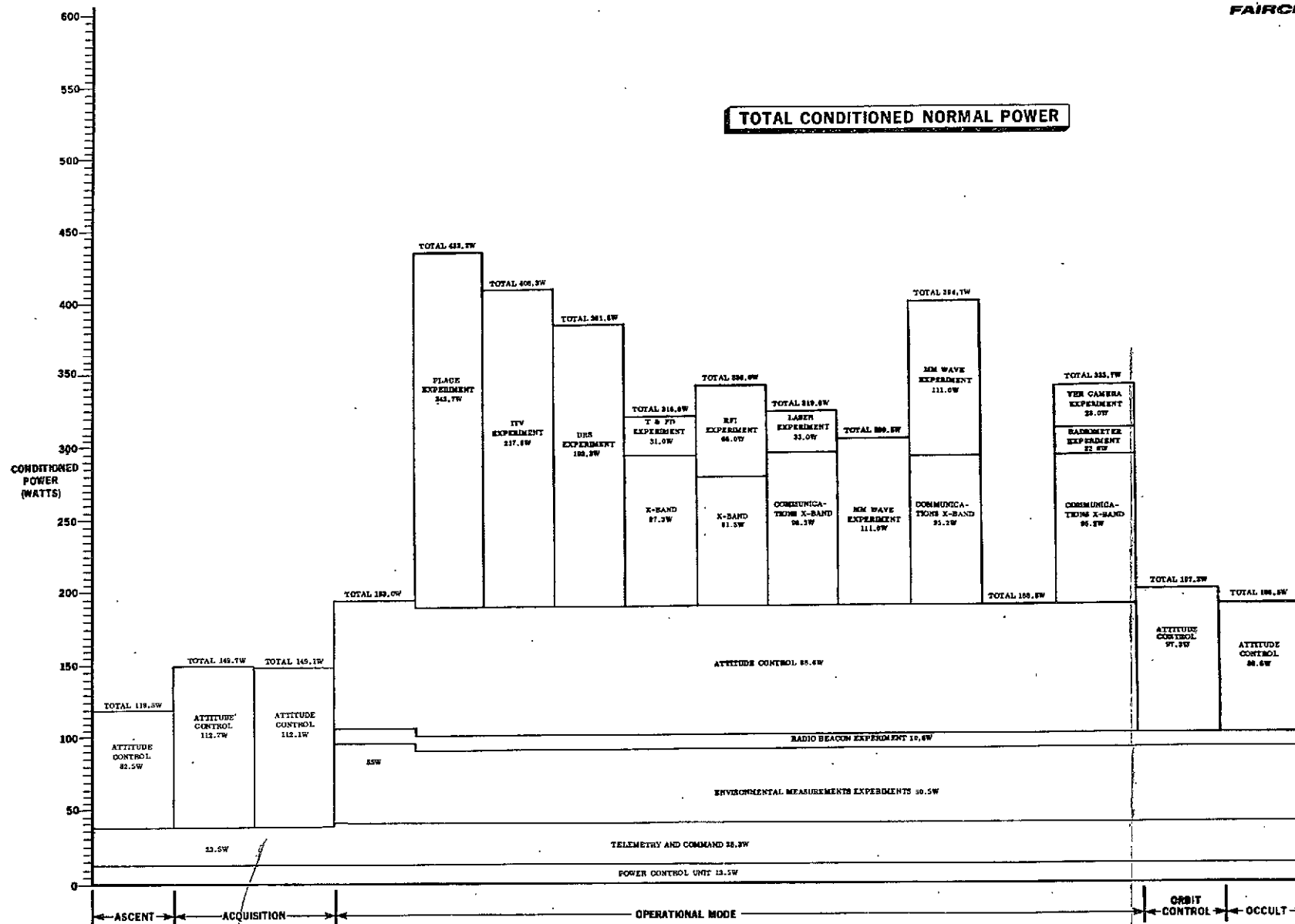


Figure 3.4-1. Total Conditioned Normal Power

FOLDOUT FRAME 2

FOLDOUT FRAME 3-97/3-98
2

3.5 MAJOR SYSTEM TRADE-OFFS

3.5.1 ONE VERSUS TWO EQUIPMENT MODULES

The initial month of Phase B was primarily concerned with a spacecraft configuration trade-off study.

A two-module "preferred" configuration was selected at the conclusion of the Phase A program in early 1967 and formed the basis for all subsequent work done both at GSFC and FHC until September 1968. During September 1968, a single-module inverted configuration was investigated and compared to the two-module approach. ATS-990-001, Single-Module versus Dual-Module Comparison Study Report for ATS F&G, 15 October 1968, presents the detailed results of the comparison between the two configurations. The two configurations were studied for both prospective launch vehicles, the SLV-3C/Centaur, and Titan IIC. Only those results associated with the Titan IIC are presented herein. The ground rules selected for this study are listed below:

- Both configurations shall fulfill the technical performance requirements of the GSFC Specification S-701-P-1 and subsequent documents.
- Both configurations shall incorporate the full complement of Category I experiments as defined at the briefing of 17 September 1968.
- The "preferred approach" shall be modified only to the extent necessary to conform to the latest GSFC defined requirements.
- The single-module inverted design shall avoid any subsystem design improvements that do not accrue directly from the configuration differences or that could be applied with equal benefits to the "preferred approach".
- Wherever possible in both configurations, the primary performance modules of each subsystem shall be designed to the same criteria so that differences will appear as penalties in weight, cost, and/or reliability.
- Both configurations shall utilize the SLV-3C/Atlas/Centaur/TE-364-4 and Titan IIC respective launch vehicles.
- Both configurations shall utilize the Goodyear petaloid reflector concept, preserving as much of the present design details as possible.
- Both configurations shall retain the preferred f/d ratio of 0.44.
- Both configurations shall allow for an equal earth-viewing surface area.

*It should be noted that both the one and two module configurations are compatible with the LMSC flex rib reflector selected after the trade-off study was concluded.

The three areas of comparison are cost, scheduling, and weight. The differences between the two configurations do not appear to exert a first order impact upon either the cost or scheduling of the program. The weight margin remains, however, an unqualified advantage of the single module inverted configuration. Table 3.5-1 illustrates the weights of major structural components are estimated during the trade-off study.

Fairchild Hiller has thus concluded that the single-module design should be selected for the ATS F&G Program.

Table 3.5-1. Weights of Major Structural Components (Oct. 1968)

COMPONENT	TWO MODULE	ONE MODULE
K Truss	130 lbs.	80 lbs.
EVM	95 lbs.	
AEM	147 lbs.	161 lbs.
Adapter	67 lbs.	43 lbs.
Total Struct. Wt.	439 lbs.	284 lbs.

3.5.2 LOCKHEED VERSUS GOODYEAR REFLECTOR

During the early part of Phase B/C of the program, FHC conducted, in conjunction with the assessment of the GSFC's Preferred Approach, an evaluation and trade-off study on available designs of large-aperture, deployable parabolic reflectors suitable for the general mission requirements.

This investigation was extended to include (in addition to the Petaline reflector concept of Goodyear Aerospace Corporation, originally intended by the Government to be used in this application) three more design concepts. These were the flexrib design of Lockheed Missiles and Space Company (LMSC), the PETA concept of General Dynamics (GD), and Fairchild Hiller Corporation's own Petaloid reflector design.

The Petaline concept of Goodyear Aerospace Corporation (GAC) consists of a reflector surface formed by semi-rigid petals, hinged to a central hub and joined to each other along radial hinge lines, permitting folding of the surface in petal fashion to form the launch configuration. The flexrib design (LMSC) comprises a dacron mesh reflector surface supported by radial ribs that are hinged to and stowed around a central hub. The PETA concept (GD) also has a surface formed by a mesh, but the mesh is supported by an expandable geodesic trusswork, hinged to fold into a compact launch configuration. The Petaloid design (FHC) is generally similar to that of the GAC Petaline, except for a different geometry of the petals that permit providing radial stiffening to the petals, which was found to be lacking in the Petaline concept.

The final results of the trade-off study were presented in detail in the Report on the Assessment of the Preferred Approach (FHC Document No. ATS-990-110), submitted to the Government under the present contract.

The results clearly indicate the superiority of the flexrib design for this application. This concept has shown properties equal to or in excess of those of the other three, with regard to all established criteria, except that it has an inherently low-torsional natural frequency. However, with the reflector designed to meet the 2 Hz minimum frequency requirement, it still weighs less than the other reflectors. Furthermore, since the critical design factor for the weight was the minimum natural frequency requirement, it was evident that if the latter could be lowered, the weight of the reflector would be reduced even more, while no weight savings could be realized in the other units.

As a result, Fairchild Hiller Corporation has selected the flexrib reflector design for the program, and will engage Lockheed Missiles and Space Company to design, fabricate, and qualify the ATS F&G Reflector Subsystem.

3.5.3 TITAN VERSUS ATLAS CENTAUR LAUNCH VEHICLES

One of the important factors which mold the design of a spacecraft is the launch vehicle. When a definite launch vehicle has been selected, this is a known design constraint and the spacecraft must be designed within this constraint. When more than one launch vehicle is under consideration, the question becomes more complex. While the spacecraft still must be designed to fit one launch vehicle, it additionally becomes important to select an approach which can be adapted to another launch vehicle with a minimum amount of design change.

The paramount constraint imposed by a launch vehicle is the limitation on the payload which can be placed in orbit. Next comes volumetric and environmental factors. Finally, guidance characteristics, which can affect system requirements such as injection error correction provisions.

The payload requirements and payload capabilities were computed for both the SLV-3C/Centaur and the Titan IIC. The result is that the SLV-3C/Centaur launch vehicle configuration has a payload deficit of 184 pounds whereas the Titan IIC has a payload margin of 323 pounds. Thus, a drastic 184-pound reduction would be required in the desired complement of experiments if the SLV-3C/Centaur launch vehicle were employed, together with the TE 364-4 apogee motor.

Alternatively, use of the Titan IIC provides additional payload capability adequate to accommodate still further experiments. The Titan IIC offers the following special advantages:

- It has a substantial payload margin (323 pounds for the single-module spacecraft);
- It is a well proven booster.
- It eliminates the requirements for a spacecraft attitude stabilization and control (spin) subsystem and auxiliary propulsion subsystem during the transfer orbit and during the synchronous orbit injection maneuver.

- It eliminates the need for correction of the synchronous orbit because of its superior orbit injection accuracy.
- It can inject the spacecraft in a desired, 3-axis stabilized attitude, thereby simplifying the acquisition maneuver required to achieve the nominal earth-referenced attitude.

3.5.4 CYLINDRICAL VERSUS FLAT SOLAR PANELS

During the early part of the Phase B/C program, the following five solar panel configurations were studied before selection of the semi-cylindrical approach:

- Flat panels (as used in the preferred approach)
- Folded semi-cylindrical panels
- Oriented Array
- Cruciform Array
- Semi-cylindrical with heat pipes

The criteria used for evaluation of the designs were size, cost, deployment consideration, reliability, weight, growth, ground handling, and spacecraft control.

The most important factors were weight and cost. As the array decreased in size, less folding and secondary support were required and it was possible to assign a higher reliability to the smaller array, with the exception of the oriented array. While the oriented array was attractive from the size standpoint, the reliability and development costs caused rejection of this concept.

The semi-cylindrical array provides power at almost a constant level, and there is no folding or rotation of the array itself. Array weight is heavier than the flat panel concept, but lower solar cell area requirements result in considerable cost savings, and total power system weight is no higher for equal power capabilities. The primary advantages and reasons for selecting the semi-cylindrical array are:

- Lower cost
- No hinge lines in the array panels
- No rotating shaft joints (only two simple hinge joints per side)
- Constant and smooth power output
- Ease of packaging
- Flexibility in area growth capability
- Does not cover EVM Thermal Control Louvers in the launch configuration.

3.5.5 CUBIC VERSUS CIRCULAR CROSS-SECTION FOR EVM

The EVM structural configuration was developed from a systems trade-off study comprised of normal good engineering parameters, such as: packaging, volume, load paths, thermal dissipation, weight and CG location, manufacturing cost and feasibility, accessibility, experiment viewing surface, particular system design requirements, and several geometric structural shapes.

Trade-off studies involving these same parameters are continuing but they are now on a subsystem level rather than on the overall EVM structural level.

The results of the first trade-off study directed the configuration concept toward a twelve-sided polygon 38 inches high and 78 inches across corners. This design consisted of a 48-inch diameter central cylinder, twelve bays separated by sheet metal webs, two toroidal-shaped shelves, and provisions for an apogee motor.

Continuing studies evolved an EVM with a smaller central cylinder and cone structure to enhance packaging and component positioning, installation of large size components, and simplified structural loadpaths. Both of these components used heat pipes in the horizontal shelves to distribute component dissipated heat around the EVM. The designs also were influenced by the requirement for a rotating prime focus feed assembly.

Disadvantages of the circular EVM were:

- Curved walls of bays made inefficient compartments for component packaging.
- Heat transfer to louver controlled North and South thermal dissipation surfaces was inefficient and extremely hard to predict, and resulted in large thermal gradients between components and the louver controlled surfaces.
- Components could not be effectively mounted directly to heat dissipating surfaces.

A change in the booster to the Titan IIC and continuing system trade-off studies have modified the initial structures to the present cubic shape. The main advantages of these modifications are ease and decreased cost of manufacturing, efficient component packaging, weight reduction, reduced blockage of the reflector, and improved thermal control.

These trade-off studies and their resulting system compromises have produced an EVM structural design that is efficient and compatible with all the considered system design parameters and yet is flexible to subsystem changes. Table 3.5-2 compared the best circular EVM to the cubic design.

Table 3.5-2. EVM Circular Versus Cubic Configuration Comparison

Parameters	EVM Configuration	
	Circular	Cubic
Internal Volume	92.0 ft. ³	91.1 ft. ³
Thermally Controlled Mounting Surface	67.4 ft. ²	76.7 ft. ²
North and South Viewing Surface Available for Louvers	26.5 ft. ²	36.4 ft. ²
Secondary Beam Blockage	28.3 ft. ²	20.2 ft. ²
Structural Weight of EVM	220. lbs.	219 lbs.
Thermal Control Subsystem Weight	53. lbs.	83 lbs.
Earth Viewing Surface	28.3 ft. ²	20.2 ft. ²
Thermal Gradients between Components and Louver Radiating Base Plate	≈ 20° - 35° Limited by Bulkheads	≈ 5° - 15° Better
Thermal Radiative Interchange Operational Temp. of Louver Base Plates with Component Temp. held constant	Lower	Higher
Component Packaging in EVM: Form Factor	Average	Best
Accessibility: For installation and integration of subsystems.		Much Better
For inspection during testing		Better
Subsystem Integration Dedicated Compartments which can be separated	No	Yes
Schedule impact	Longer	Minimum
Harnesses within subsystems	Limited	Maximized
Capability to install pre-assembled subsystems	No	Yes

3.5.6 TRADE-OFF STUDY OF FIXED VS. ROTATING S-BAND FEED

This discussion summarizes the findings made by FHC of a trade-off study aimed at eliminating the rotating feed assembly while fulfilling all program objectives and retaining most of the capability it provided for simultaneous communication coverage of two spacecraft in low earth orbit. Although the rotating feed assembly was "called out" in FHC's Final Approach and the requirement for simultaneous communication with two low orbiting satellites was implied, it was not until April 19, 1969, that the two satellite track became a firm requirement. Because preliminary estimates of the cost of the rotating assembly were substantial, FHC reevaluated the inherent need for the rotating mechanism and the possible substitution of Fixed S-Band feed arrangements. The arrangements considered were: 1) a cross array, and 2) a circular array.

It was decided that the minimum usable gain (38db) would be required for all configurations. The desire to minimize the number of feed elements in each type of array, and to maintain the desired minimum gain led to a design antenna angle coverage of 15° for the rotating feed, 15° for the cross feed, and 14° for the circular feed. The number of S-Band elements were 16, 32, and 48, respectively.

An "on-axis" beam is required at S-Band for Z-axis track of a single low orbiting satellite. For purposes of comparison, only NIMBUS/AAP was considered for the two satellite tracks. The Z-axis of the spacecraft was constrained to operate within 10.5° from the local vertical in order to stay within the constraints of the earth sensors for determining position. The Z-axis movement rate was constrained to remain less than 1°/minute.

A computer program was designed to permit a determination of the capabilities of various proposed feed approaches for simultaneous viewing and following two low orbiting satellites (NIMBUS/AAP). It was assumed that the ATS-F would be able to simultaneously track NIMBUS and AAP as long as they both were optically in view. The rotating feed, because of its 15° limited reach, can only track the two satellites 76% of the time. For the cross feed, the reach is limited by its 10.6° diagonal reach thereby tracking only 32% of the time. The circular feed had to be limited to a 14° reach to satisfy the minimum 38 db gain at the beam cross over point. Because of dynamic limitation, as well as a decrease in reach, the circular feed is able to track for 56% of the time. To put the two-satellite track requirement in proper perspective, two other DRS requirements (high gain steerable beam technology and Z-axis track of one satellite) were also compared. Each requirement was weighted equally. It was established that the only differences in performance occurred for the two-satellite track. However, since the two-satellite track requirements was one of three considered, the normalized total is a more representative figure of merit.

The cross feed was chosen as the best possible selection from among the three feed configurations. The fixed feed concept was chosen over the rotating feed because it was more cost-effective. The cross was chosen over the circular feed because it was about 25 pounds lighter in weight.

In addition, it is easier to implement hardware to perform a two satellite track with the cross-feed array than with any other array considered. The cross-feed configuration has the potential for having the two satellite track performed on board the ATS-F by the Digital Operations Controller.

Table 3.5-3 is a performance evaluation summary of the three considered feed systems.

Table 6.3-1. Performance Evaluation Based on Requirements

Requirement	Operational DRS	Rotating	Circular	Cross
High Gain Steerable Beam Technology	100	100	100	100
Z-Axis Track of One Satellite	100	100	100	100
Two Satellite Track	100	76	56	32
Total	300	276	256	232
Normalized Total	100%	92.0%	85.4%	78.3%

3.6

SYSTEM RELIABILITY

The reliability assessment of the FHC ATS System Design must be based on the results of not one, but several distinct analyses. A quantitative prediction assesses the probability of mission success. The Failure Mode, Effect, and Criticality Analysis reviews the design for failure characteristics of the system and provides an effective tool to assure that the system can operate effectively after the occurrence of a failure. The system is then reviewed to determine which elements are critical to mission success. These elements are examined to assure that adequate provisions for sufficient testing are made to minimize the risk to mission reliability. During Phase D these items will be closely monitored by Reliability Engineers to assure continued confidence in the areas of concern. FHC has instituted a part and materials assurance program during Phase B/C and will continue work in these areas during Phase D, in order to assure that the designed reliability is not degraded by the use of inadequate parts and materials for the mission requirements.

3.6.1

RELIABILITY PREDICTION

As with all space missions, reliability of the ATS F&G Spacecraft will be a paramount factor. The following discussion presents the mathematical models and predictions used to assess the probability that the FHC spacecraft will support the mission reliability goal of 0.85 as set forth in the ATS F&G Reliability Assurance Program Plan - RAPP. The probability of success computed for the FHC spacecraft is 0.73. When translated into terms of mission reliability it provides a success probability of 0.93.

The material that follows presents the overall system reliability aspects of the ATS F&G Spacecraft. An abbreviated mission analysis is included as an aid to the understanding of the reliability diagrams. The detailed analysis leading to this prediction is presented in Volume III, Book 2 of the proposal.

3.6.1.1

Mission Reliability

The reliability model for the ATS F&G spacecraft, designed to perform many individual missions for varying lengths of time, becomes quite complex and is a function of conditional probabilities.

The ATS F&G Reliability Assurance Program Plan defines three mission states as follows:

- State A - The state in which the only failures allowed are those which cause no performance degradation.
- State B - The state in which some performance degradation is allowed, but all mission goals can still be accomplished.

- State C - The state in which degradation is allowed to the extent that the bulk of the mission goals can still be accomplished on a restricted operation basis.

Additional information received from the ATS F&G Project Office, and listed in Table 3.6-1, further defines the required operating duty cycles for the various spacecraft experiments.

Table 3.6-1. Estimated Operating Times

Experiment	Run Time	Prime Mission Time	Number of runs
Camera	8.75 min/run	0-24 months	14,000
Radiometer	20 min/run	0-24 months	7,000
PLACE	5 hrs/run	0-24 months	200
TRUST (ITV)	4 hrs/run	0-24 months	400
EME	continuous	0-24 months	N/A
Radio Beacon	continuous	0-24 months	N/A
T&FD	4 hrs/run	0-6 months	50
RFI	4 hrs/run	0-6 months	50
LASER	6 hrs/run	0-24 months	300
MM Wave	2 hrs/run	0-12 months	150
DRS	1 hr/run	0-24 months	300
SAMOC/SAPPSAC	--	0 - 6 months	--

3.6.1.1.1 Reliability Diagrams

Reliability pictorial diagrams for the three mission states A, B, and C are presented in Figures 3.6-1 thru 3.6-3. The column at the left of the figure lists each spacecraft operational mode and total operating time, while the remaining columns identify the various spacecraft subsystems such as Electrical Power, Telemetry and Command, Attitude Control, etc. These subsystems are further divided into 48 Functional elements identified as R₁ thru R₄₈. The experiment operating times were computed using the data from Table 3.6-1 with the following exceptions.

- The Camera and Radiometer total times were rounded up to 2400 hours. Both times are considered to be the same because two camera runs are made for each radiometer run.

	PROBABILITY OF SUCCESS	ELECTRICAL POWER				EXPT LOAD INTERFACE	TELEMETRY AND COMMAND	SEPARATION AND DEPLOYMENT	ATTITUDE CONTROL												TRANSPONDER								PRIME FEED	FOCUS FEED	PARABOLIC REFLECTOR	STRUCTURE	THERMAL	CONTRACTOR FURNISHED EXPERIMENTS		GOVERNMENT FURNISHED EXPERIMENTS																	
		SOLAR ARRAY	BATTERY ASSEMBLY	2V REGULATOR	3V REGULATOR				TELEMETRY (TLM) & COMMAND	SEPARATION & DEPLOYMENT	AUXILIARY PROPULSION SYSTEM (APS)	TREKTA WHEELS & TACHMETER	SUN SENSORS	POLARIS SENSOR	INERTIAL REFERENCE	DIGITAL OPERATIONAL CONTROLLER (DOC)	ANALOG BACKUP CONTROLLER (ABC)	RF INTERFEROMETER	EARTH SENSOR	X-BAND MONOPULSE	S-BAND MONOPULSE	VHF MONOPULSE	IF	X-BAND RECEIVER	S-BAND RECEIVER	L-BAND RECEIVER	X-BAND TRANSMITTER	UHF TRANSMITTER						UHF BEACON	TRANSPONDER SUPPORT EQUIPMENT	DATA MODULATOR	L-BAND ARRAY	S-BAND ARRAY	C-BAND POLAR SWITCH	X & C - BAND FEED	EARTH COVERAGE HORN	VHF FEED	UHF FEED	REFLECTOR	STRUCTURE	THERMAL	RADIO BEACON	LOGS	ENVIRONMENTAL MEASUREMENTS EXPERIMENT	HIGH RESOLUTION CAMERA	RADIOMETER	LASER	TIME & FREQUENCY DISPERSION
		1	2	3	4	5	6	7	8	9	10	11	12	13	14	15	16	17	18	19	20	21	22	23	24	25	26	27	28	29	30	31	32	33	34	35	36	37	38	39	40	41	42	43	44	45	46	47	48				
COMMANDABLE GRAVITY GRADIENT (4400 HR)	0.9414																																																				
ENVIRONMENTAL MEASUREMENTS EXPERIMENT (17,520 HR)	0.897																																																				
HIGH RESOLUTION CAMERA (2400 HR)	0.938																																																				
RADIOMETER	0.938																																																				
LASER (1800 HR)	0.949																																																				
TIME AND FREQUENCY DISPERSION (200 HR)	0.985																																																				
RADIO FREQUENCY INTERFERENCE (200 HR)	0.995																																																				
MM WAVE, (300 HR)	0.993																																																				
OCCULT (150 HR)	0.998																																																				
STANDBY (9,440 HRI)	0.857																																																				

LEGEND:

- Represents components or subassemblies at the spacecraft level
- ◊ Represents components or subassemblies containing internal redundancy
- ▲ Represents components or subassemblies of the transponder used as part of the Attitude Control Subsystem. These contain internal redundancy
- ◻ Represents active redundancy
- ◻ (with 2 units) Represents standby redundancy where 2 are required and 1 is in standby
- ◻ (with 1 unit) Represents standby redundancy where 1 unit is required

These models are defined in lower level diagrams and are referred to as follows:

- ◊_{R8} Represents the Auxiliary Propulsion Subsystem
- ◻_{R19} Represents the VHF monopulse

Figure 3.6-1. Reliability Pictorial Diagram State A (Sheet 2 of 2)

FOLDOUT FRAME ?

3-111/3-112
FOLDOUT FRAME 2

	PROBABILITY OF SUCCESS	ELECTRICAL POWER				EXPT LOAD INTERFACE CIRCUIT	TELEMETRY (TLM) & COMMAND	SEPARATION AND DEPLOYMENT	ATTITUDE CONTROL												TRANSPONDER								PRIME FEED	FOCUS	PARABOLIC REFLECTOR	STRUCTURE	THERMAL	CONTRACTOR FURNISHED EXPERIMENTS	GOVERNMENT FURNISHED EXPERIMENTS																				
		SOLAR ARRAY		BATTERY ASSEMBLY					25V REGULATOR	31V REGULATOR	AUXILIARY PROPULSION SYSTEM (APS)	INERTIA WHEELS & TACHOMETER	SUN SENSORS	POLARIS SENSOR	LOS/LOS REFERENCE	DIGITAL OPERATIONAL CONTROLLER (DOC)	ANASOS BACKUP CONTROLLER (ABC)	RF INTERFEROMETER	EARTH SENSOR	X-BAND MONOPULSE	S-BAND MONOPULSE	VHF MONOPULSE	IF	X-BAND RECEIVER	S-BAND RECEIVER	L-BAND RECEIVER	X-BAND TRANSMITTER	US BAND TRANSMITTER	UHF TRANSMITTER	X-BAND BEACON						TRANSPONDER SUPPORT EQUIPMENT	DATA MODULATOR	L-BAND ARRAY	S-BAND ARRAY	C-BAND POLAR SWITCH	X & C - BAND FEED	EARTH COVERAGE HOEN	VHF FEED	UHF FEED	REFLECTOR	STRUCTURE	THERMAL	RADIO BEACON	CGGS	ENVIRONMENTAL MEASUREMENT	HIGH RESOLUTION CAMERA	RADIOMETER	LASER	TIME & FREQUENCY DISPERSION INTERFEROMETRY	MM WAVE
		1	2	3	4				5	6	7	8	9	10	11	12	13	14	15	16	17	18	19	20	21	22	23	24	25	26						27	28	29	30	31	32	33	34	35	36	37	38	39	40	41	42	43	44	45	46
SEPARATION AND DEPLOYMENT (12 HR.)	0.999																																																						
ACQUISITION (60 HR.)	0.999																																																						
ANTENNA SLEWING (30 HR.)	0.999																																																						
PLACE EXPERIMENT (1000 HR.)	0.984																																																						
INSTRUCTIONAL TELEVISION (ITV) EXPERIMENT (1500 HR.)	0.982																																																						
DATA RELAY SATELLITE (DRS) EXPERIMENT (300 HR.)	SINGLE SATELLITE (270 ORBITS)	0.993																																																					
	DOUBLE SATELLITE (30 ORBITS)	0.998																																																					
SAMOC/SAPPSAC EXPERIMENT (100 HR.)	0.999																																																						
RADIO BEACON (13,140 HR.)	0.814																																																						

LEGEND:

- Represents components or subassemblies at the spacecraft level
- Represents components or subassemblies containing internal redundancy
- Represents components or subassemblies of the transponder used as part of the Attitude Control Subsystem. These contain internal redundancy

- Represents active redundancy
- Represents standby redundancy where 2 are required and 1 is in standby
- Represents standby redundancy where 1 unit is required

These models are defined in lower level diagrams and are referred to as follows:

- Represents the Auxiliary Propulsion Subsystem
- Represents the VHF monopulse
- Represents ground computation required

Figure 3.6-3. Reliability Pictorial Diagram
State C (Sheet 1 of 2)

	PROBABILITY OF SUCCESS	ELECTRICAL POWER				EXPT LOAD INTERFACE	TELEMETRY AND COMMAND	SEPARATION AND DEPLOYMENT	ATTITUDE CONTROL										TRANSPONDER				PRIME FEED FOCUS		PARABOLIC REFLECTOR	STRUCTURE	HERMAL	CONTRACTOR FURNISHED EXPERIMENTS	GOVERNMENT FURNISHED EXPERIMENTS																				
		1 SOLAR ARRAY	2 BATTERY ASSEMBLY	3 ZEV REGULATOR	4 31V REGULATOR				5 EXP LOAD INTERFACE CIRCUIT	6 TELEMETRY (TUM) & COMMAND	7 SEPARATION & DEPLOYMENT	8 AUXILIARY PROPULSION SYSTEM (APS)	9 HEATER	10 INERTIAL SENSORS	11 POLARIS SENSOR	12 INERTIAL REFERENCE ASSEMBLY (IRA)	13 DIGITAL OPERATIONAL CONTROLLER (DOC)	14 ANALOG ATTITUDE CONTROLLER (AAC)	15 DC INTERFEROMETER	16 EARTH SENSOR	17 X-BAND MONOPULSE	18 S-BAND MONOPULSE	19 VHF MONOPULSE	20 IF	21 X-BAND RECEIVER		22 S-BAND RECEIVER	23 L-BAND RECEIVER	24 X-BAND TRANSMITTER	25 U-BAND TRANSMITTERS	26 UHF TRANSMITTER	27 X-BAND BEACON	28 TRANSPONDER SUPPORT EQUIPMENT	29 DATA MODULATOR	30 L-BAND ARRAY	31 S-BAND ARRAY	32 C-BAND POLAR SWITCH	33 X & C - BAND FEED	34 EARTH COVERAGE HORN	35 VHF FEED	36 UHF FEED	37 REFLECTOR	38 THERMAL	39 RADIO BEACON	40 COGS	42 HIGH RESOLUTION CAMERA	43 RADIONETER	44 LASER	45 TIME & FREQUENCY RADIO FREQUENCY INTERFERENCE
COMMANDABLE GRAVITY GRADIENT (4400 HRI)	0.947	•	•	•	•	•	•	•	•	•	•	•	•	•	•	•	•	•	•	•	•	•	•	•	•	•	•	•	•	•	•	•	•	•	•	•	•	•	•	•	•	•	•	•	•				
ENVIRONMENTAL MEASUREMENTS EXPERIMENT (7,520 HRI)	0.883	•	•	•	•	•	•	•	•	•	•	•	•	•	•	•	•	•	•	•	•	•	•	•	•	•	•	•	•	•	•	•	•	•	•	•	•	•	•	•	•	•	•	•	•	•	•		
HIGH RESOLUTION CAMERA (2400 HR [SIMULTANEOUS OPERATION])	0.970	•	•	•	•	•	•	•	•	•	•	•	•	•	•	•	•	•	•	•	•	•	•	•	•	•	•	•	•	•	•	•	•	•	•	•	•	•	•	•	•	•	•	•	•	•	•		
RADIONETER	0.970	•	•	•	•	•	•	•	•	•	•	•	•	•	•	•	•	•	•	•	•	•	•	•	•	•	•	•	•	•	•	•	•	•	•	•	•	•	•	•	•	•	•	•	•	•	•	•	
LASER (1600 HRI)	0.971	•	•	•	•	•	•	•	•	•	•	•	•	•	•	•	•	•	•	•	•	•	•	•	•	•	•	•	•	•	•	•	•	•	•	•	•	•	•	•	•	•	•	•	•	•	•	•	
TIME AND FREQUENCY DISPERSION (200 HRI)	0.997	•	•	•	•	•	•	•	•	•	•	•	•	•	•	•	•	•	•	•	•	•	•	•	•	•	•	•	•	•	•	•	•	•	•	•	•	•	•	•	•	•	•	•	•	•	•	•	
RADIO FREQUENCY INTERFERENCE (200 HRI)	0.998	•	•	•	•	•	•	•	•	•	•	•	•	•	•	•	•	•	•	•	•	•	•	•	•	•	•	•	•	•	•	•	•	•	•	•	•	•	•	•	•	•	•	•	•	•	•	•	
JMWAVE (300 HRI)	0.997	•	•	•	•	•	•	•	•	•	•	•	•	•	•	•	•	•	•	•	•	•	•	•	•	•	•	•	•	•	•	•	•	•	•	•	•	•	•	•	•	•	•	•	•	•	•	•	•
OCCULT (150 HRI)	0.999	•	•	•	•	•	•	•	•	•	•	•	•	•	•	•	•	•	•	•	•	•	•	•	•	•	•	•	•	•	•	•	•	•	•	•	•	•	•	•	•	•	•	•	•	•	•	•	•
STANDBY (9,440 HRI)	0.951	•	•	•	•	•	•	•	•	•	•	•	•	•	•	•	•	•	•	•	•	•	•	•	•	•	•	•	•	•	•	•	•	•	•	•	•	•	•	•	•	•	•	•	•	•	•	•	•

LEGEND:

- Represents components or subassemblies at the spacecraft level
- ◊ Represents components or subassemblies containing internal redundancy
- ▲ Represents components or subassemblies of the transponder used as part of the Attitude Control Subsystem. These contain internal redundancy.
- ⬆ Represents active redundancy
- ⬇ Represents standby redundancy where 2 are required and 1 is in standby
- ⬇ Represents standby redundancy where 1 unit is required
- These models are defined in lower level diagrams and are referred to as follows:
- ⬆_{APS} Represents the Auxiliary Propulsion Subsystem
- ⬆_{VHF} Represents the VHF monopulse
- - - Represents ground computation required

Figure 3.6-3. Reliability Pictorial Diagram State C (Sheet 2 of 2)

- The Radio Beacon is assumed to operate continuously for the first twelve months and at a 50% duty cycle thereafter for a total operating time of 13,140 hours.
- SAMOC/SAPPSAC operating time is not stated and a total of 100 hours is assumed.

3.6.1.2 Mission Analysis

The GSFC Reliability Assurance Program Plan for ATS F&G defines three states for the spacecraft as follows:

- State A - The state in which the only failures allowed are those which cause no performance degradation.
- State B - The state in which some performance degradation is allowed but all mission goals can still be accomplished.
- State C - The state in which degradation is allowed to the extent that the bulk of the mission goals can still be accomplished on a restricted operation basis.

An expansion of these states for purpose of the reliability analyses is presented in the following paragraphs.

3.6.1.2.1 State A

The state A definition translates at the spacecraft level to the following requirements:

- a. Precision pointing and control on demand for two years ($\pm .1^{\circ}$ pitch and roll, $\pm .2^{\circ}$ yaw)
- b. Ability to perform any compatible complement of experiments simultaneously, the only limitation being the available solar array power and the available battery power for peak loads.

Requirement (a) stipulates that backup equipment must have the capability of performing for two years, within specification. This eliminates the analog backup controller (ABC) as an operational backup for state A for the majority of mission modes since the ABC gives degraded pointing accuracy and control in the yaw axis. Similarly, jet-only control as a specification back-up for jet/wheel control can not be included as a state A backup because it is life-limited by propellant loading.

Requirement (b) translates into a requirement that two of the three 21-volt regulators be available for two years so that all the power available from the arrays can be conditioned for spacecraft use at all times.

3.6.1.2.2 State B

State B is defined in the RAPP as a state that allows degradation but still retains capability to perform all mission goals. One of the prime mission goals is to prove the feasibility of long life, precision pointing, 3-axis stability satellites. Thus, no degradation in pointing accuracy is allowed in this state.

Some degradation is permitted in the power subsystem by allowing two of the three 31-volt regulators to fail. In this mode, all experiments can be performed singly and the camera and radiation experiments can still be performed together. The EME experiment will still operate two years full time. The Radio Beacon Experiment will operate full time for one year and intermittently thereafter. The operation of other compatible experiments is now limited by the power available from a single 31-volt regulator.

3.6.1.2.3 State C

State C is defined in the RAPP as that state in which degradation is allowed while still allowing the bulk of the mission goals to be performed on a "restricted operation basis."

In this state, the pointing accuracy requirements have been relaxed to take the ABC into account. With the ABC, offset pointing is possible only through monopulse but with full specification accuracy in pitch and roll control. Local vertical pointing is possible using the earth sensor. Yaw control is degraded to approximately $\pm 1^\circ$ due to the apparent Polaris diurnal motion. Jet only control is allowed in state C as a life limited backup to jet/wheel control.

Within the Power Subsystem the batteries are allowed to fail to the extent that peak loads might no longer be accommodated and EME might have to be turned off during occult.

Another degradation allowed in state C is that the omni link is used for transmission of telemetry in the event of a failure in the reflector link. This allows EME data to degrade.

Also included in state C are situations which require on-line ground computation or heavy use of off-line ground computation.

3.6.1.3 System Reliability

The computation of the system reliability cannot be accomplished by merely taking the product of functional element reliabilities because of the complex configuration for the various mission requirements. The major area where this

complexity is a factor is in the Attitude Control Function, Elements R₁₂ through R₁₉. Refer to Figures 3.6-1 through 3.6-3.

System equations for states A, B, and C have been developed.

3.6.1.3.1 Effective Operating Time

Since some of the elements or configurations of elements are required to perform in an operational mode for periods of time less than two years, it was necessary to account for the time that the items are idle. It was assumed that the failure rate during the idle state is 10% of the active failure rate. For purposes of computation, the time was increased by 10% of the difference between 17,520 hours and the required operating time.

3.6.1.3.2 Assumptions

One assumption was made with respect to the Telemetry area. The Data Acquisition and Control Unit failure rate is computed strictly on part complexity without regard to failure modes and their effect on the mission. Since all of the telemetry data is not required for total mission success, an effective failure rate equal to one-third the computed value was established. Previous experience on other programs indicates that this is a reasonable assumption.

3.6.1.3 Probability of Success

The probability of success for the spacecraft has been computed for the two year mission. The program goal stated in the ATS F&G Reliability Assurance Program Plan, RAPP, requires one successful flight for two years and enough operating life on the remaining mission to adequately assess the various alternative subsystems and experiments being flown. The mission probability of success is determined by the probability expression $2R - R^2$. The values for spacecraft and mission probability of success are:

Mission State	ATS Failure Rates		MIL-HDBK-217A Failure Rates	
	Spacecraft	Mission	Spacecraft	Mission
A	0.67	0.89	0.63×10^{-8}	1.26×10^{-8}
B	0.67	0.89	0.73×10^{-8}	1.46×10^{-8}
C	0.73	0.93	0.52×10^{-6}	1.04×10^{-6}

3.6.2 FAILURE MODE, EFFECTS AND CRITICALITY ANALYSIS

3.6.2.1 System Analysis

Failure Mode, Effects and Criticality Analysis (FMECA) has been performed at the functional block level in each of the spacecraft subsystems. The systems level FMECA encompasses all failures causing major subsystem degradation

and shows how they effect the total spacecraft system.

In analyzing the system failure modes the following categories were used:

- Category I -- A failure which removes the ability to perform any one of the mission goals in the scheduled sequence (Critical failure)
- Category II -- Any failure which would be Category I except that redundant elements or functions are provided. Also included is any failure that has an extremely low probability of occurrence.
- Category III -- Failures which have no effect on any mission goal.

The subsystem FMECA used the above categories to define the criticality of a failure on the individual subsystem. It now becomes possible to take the detailed subsystem analyses and to "downgrade" the effects of a failure from the system viewpoint. For example, if a failure could critically degrade the Interferometer's performance, it would have no critical effect on the system. The Interferometer is used as a backup sensor to the Attitude Control and is not needed for mission success. This analysis has shown that there are no system level Category I failure modes.

3.6.2.2 Telemetry and Command Subsystem

The T&C Subsystem FMECA, performed on the subsystem functional block diagram as shown in Figure 3.6-4, exhibits no Category I failure modes. Of the 80 failure modes analyzed, 70 were Category II and 10 were Category III. The large number of Category II failure modes indicates the criticality of the command system. All the Category II failures would be Category I (mission critical) except for the redundant elements. The elements that do not appear on the functional diagram as being redundant, employ internal redundancy to eliminate their criticality.

The FMECA reflects several design changes. They include the addition of two transmitters and the Frequency Division Multiplexer (within the Data Switching Unit), which comprises the EME/Special Data Link Mode. The five Category I failures which existed in the March Reliability Interim Report (ATS-990-007) T&C FMEA were eliminated from the design by making provision for a redundant RF Assembly.

3.6.2.3 RF Interferometer Subsystem

The RF interferometer FMECA performed on the functional block diagram as shown in Figure 3.6-5 reveals 12 category I failures. These are summarized in the following tables.

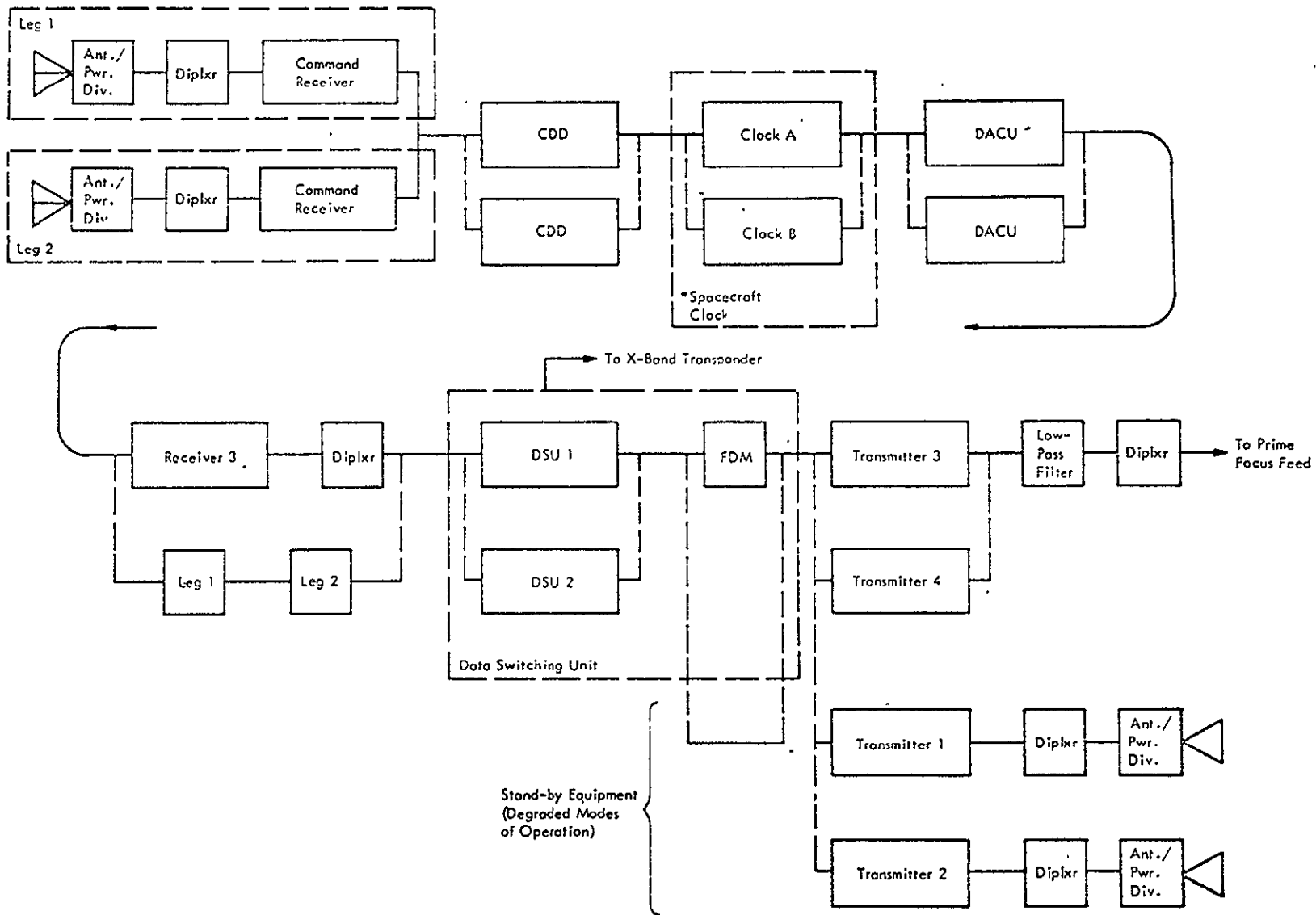


Figure 3.6-4. T & C Subsystem Reliability Diagram

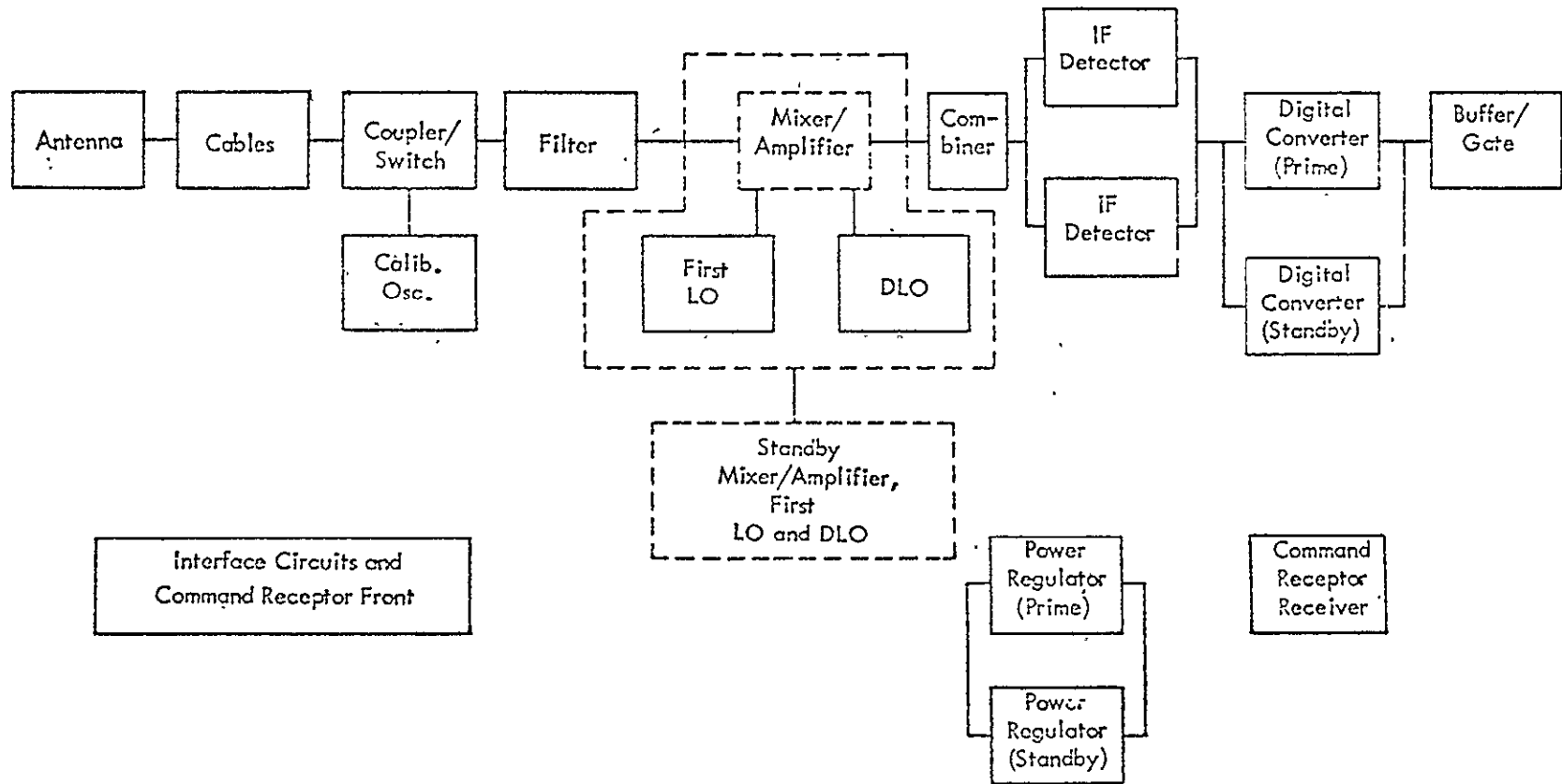


Figure 3.6-5. Simplified Reliability Diagram, RF Interferometer

All of the Category I failures are in simplex elements in the RF Interferometer, but all simplex failures are not Category I. Most of the simplex failures can be compensated for either in the spacecraft or on the ground.

In the spacecraft, the RF Interferometer is one of the alternate sensors. Therefore, the Category I failures do not cause loss of the spacecraft mission because the spacecraft can be controlled by other sensors, (i. e., sun sensors, Polaris sensors, IR horizon sensor and the monopulse systems). Some of these sensors, however, provide less accuracy or a smaller field of view.

The FMEA identified 55 cases of Category II failures and 53 cases of Category III failures.

3.6.2.4 Attitude Control and Auxiliary Propulsion Subsystems

The Attitude Control Subsystem FMECA was performed at the functional block level. In this analysis, 165 ACS/APS potential failure modes were analyzed. The failure modes were viewed in both the acquisition and operational control modes of the spacecraft. As shown in the following tabulation, the control mechanization has reduced the 165 failures at Category II (major) as Category III (minor) failure classifications. No Category I (Critical) failure modes exist.

MODE/SUBSYSTEM	FAILURE CATEGORY		
	I - Critical	II - Major	III - Minor
Acquisition Mode			
ACS	0	28	43
APS	0	8	9
Operational Mode			
ACS	0	32	28
APS	0	9	8

The single ACS/APS Category I failure mode which existed in the FMECA submitted in the March Reliability Interim Report (ATS-990-007), was the loss of attitude control due to a gross leak in the Plenum Tank. A backup tank has been added to supply ammonia to the jets if a failure occurs. This eliminates the single Category I failure mode from the subsystem.

The ACS/APS Subsystems are totally redundant in all modes of operation with the exception of Rate Nulling. Here, if there is an IRA failure, the Coarse and Fine Sun Sensors can be used to obtain information and the derived rate for the ground station to manually command the proper jets on. A summary of the existing primary and backup sensors, (for each axis), and controllers and torquers appear in Table 3.6-2.

Table 3. 6-2.Redundant Sensors/Controllers/Torques for ACS Modes

Page 1

MODE		SENSOR			CONTROLLER	TORQUER
		ROLL	PITCH	YAW		
RATE NULLING	PRIME	IRA	IRA	IRA	DOC #1 or DOC #2 or ABC or GND	APS #1/APS #2 or APS #1 or APS #2
	BACK-UP	CSS/FSS-DR	CSS/FSS-DR	CSS/FSS-DR	GND	SAME
SUN ACQ. (+x)	PRIME	IRA or DR	CSS/+xFSS	CSS/+xFSS	DOC #1 or DOC #2 or ABC or GND	SAME
	BACK-UP	SAME	SAME	+xFSS	GND	SAME
	BACK-UP	SAME	+xFSS	CSS/+xFSS	SAME	SAME
SUN ACQ. (-x)	PRIME	SAME	CSS/-xFSS	CSS/-xFSS	DOC #1 or DOC #2 or GND	SAME
	BACK-UP	SAME	SAME	-xFSS	GND	SAME
	BACK-UP	SAME	-xFSS	CSS/-xFSS	SAME	SAME
EARTH ACQ.	PRIME	IRA or DR/ES	+x or -x FSS/ES	+x or -x FSS	DOC #1 or DOC #2 or ABC (+xFSS) or GND	SAME
	BACK-UP	IRA or DR/VHF Mono	+x or -x FSS/VHF Mono	SAME	SAME	SAME
	BACK-UP	IRA or DR/Intf. (1 Sta)	+x or -x FSS/Intf (1 Sta)	SAME	SAME	SAME
POLARIS ACQ.	PRIME	ES	ES	IRA or DR/PS #1 or PS #2	SAME	SAME
	BACK-UP	VHF Mono	VHF Mono	SAME	GND or GND/DOC #1 or DOC #2 or ABC	SAME
	BACK-UP	Intf (1 Sta)	Intf (1 Sta)	SAME	GND or GND/DOC #1 or DOC #2	SAME
	BACK-UP	Intf (2 Sta)	Intf (2 Sta)	Intf (2 Sta)	SAME	SAME
ORBIT CONTROL	PRIME	ES	ES	PS #1 or PS #2	DOC #1 or DOC #2 or ABC or GND	APS #1 or APS #2 or APS #1/APS #2
	BACK-UP	Intf (1 Sta)	Intf (1 Sta)	SAME	DOC #1 or DOC #2 or GND	SAME
	BACK-UP	Intf (2 Sta)	Intf (2 Sta)	Intf (2 Sta)	GND or GND/DOC #1 or DOC #2	SAME
LEGEND		DR - Derived Rate		DOC - Digital Operational Controller	PS - Polaris Sensor	FSS - Fine Sun Sensor
		IRA - Inertial Reference Assembly		GND - Ground	ABC - Analog Backup Controller	Intf - Interferometer
		ES - Earth Sensor		CSS - Coarse Sun Sensor	Mono - Monopulse	APS - Auxiliary Propulsion Subsystem

Table 3. 6-2.Redundant Sensors/Controllers/Torques for ACS Modes (cont'd)

MODE		SENSOR			CONTROLLER	TORQUER
		ROLL	PITCH	YAW		
REF. ORIENT.	PRIME	ES	ES	PS #1 or PS #2	DOC #1 or DOC #2 or GND	APS #1/Wheels or APS #2/Wheels or APS #1 or APS #2 or APS #1/APS #2
	BACK-UP	Intf (1 Sta)	Intf (1 Sta)	SAME	SAME	SAME
	BACK-UP	Intf (2 Sta)	Intf (2 Sta)	Intf (2 Sta)	GND or GND/DOC #1 or DOC #2	SAME
LOCAL VERTICAL	BACK-UP	ES	ES	PS #1 or PS #2	ABC or DOC #1 or DOC #2 or GND	SAME - DOC/GND; APS #1 or APS #2 or APS #1/APS #2 - ABC
OFFSET POINTING (ANGLE OR GND COORD.)	PRIME	ES	ES	PS #1 or PS #2	DOC #1 or DOC #2	APS #1/Wheels or APS #2/Wheels or APS #1 or APS #2 or APS #1/APS #2
	BACK-UP	Intf (1 Sta)	Intf (1 Sta)	SAME	SAME	SAME
	BACK-UP	Intf (2 Sta)	Intf (2 Sta)	Intf (2 Sta)	GND or GND/DOC #1 or DOC #2	SAME
	BACK-UP	LASER	LASER	PS #1 or PS #2	GND/DOC #1 or DOC #2	SAME
STATION NULL POINTING	PRIME	VHF, S or X Band Mono	VHF, S or X Band Mono	PS #1 or PS #2	DOC #1 or DOC #2 or GND	SAME
	BACK-UP	SAME	SAME	SAME	ABC	APS #1 or APS #2 or APS #1/APS #2
	BACK-UP	Intf (1 Sta)	Intf (1 Sta)	SAME	DOC #1 or DOC #2 or GND	APS #1/Wheels or APS #2/Wheels or APS #1 or APS #2 or APS #1/APS #2
	BACK-UP	Intf (2 Sta)	Intf (2 Sta)	Intf (2 Sta)	GND or GND/DOC #1 or DOC #2	SAME
	BACK-UP	LASER	LASER	PS #1 or PS #2	DOC #1 or DOC #2 or GND	SAME
	BACK-UP	LASER	LASER	PS #1 or PS #2	ABC	APS #1 or APS #2 or APS #1/APS #2
SATELLITE TRACKING	PRIME	ES	ES	PS #1 or PS #2	DOC #1 or DOC #2 or GND	APS #1/Wheels or APS #2/Wheels or APS #1 or APS #2 or APS #1/APS #2
	BACK-UP	Intf (1 Sta)	Intf (1 Sta)	PS #1 or PS #2	GND or GND/DOC #1 or DOC #2	SAME
	BACK-UP	S-Band Mono	S-Band Mono	PS #1 or PS #2	DOC #1 or DOC #2 or ABC or GND	SAME - DOC/GND; APS #1 or APS #2 or APS #1/APS #2 - ABC
LOW JITTER	PRIME	ES	ES	PS #1 or PS #2	DOC #1 or DOC #2	APS #1/Wheels or APS #2/Wheels
	BACK-UP	Intf (1 Sta)	Intf (1 Sta)	PS #1 or PS #2	DOC #1 or DOC #2	SAME

FAIRCHILD HILLER

Table 3.6-2. Redundant Sensors/Controllers/Torques for ACS Modes (cont'd)

Page 3

MODE	SENSOR			CONTROLLER	TORQUER
	ROLL	PITCH	YAW		
ANTENNA PATTERNS PRIME	ES	ES	PS #1 or PS #2	DOC #1 or DOC #2 or GND	APS #1/Wheels or APS #2/Wheels or APS #1 or APS #2 or APS #1/APS #2
BACK-UP	Intf (1 Sta)	Intf (1 Sta)	SAME	GND	SAME
GRAVITY GRADIENT -PRIME	ES	ES	PS #1 or PS #2	DOC #1 or DOC #2 or GND	APS #1/Wheels or APS #2/Wheels
BACK-UP	Intf (1 Sta)	Intf (1 Sta)	SAME	SAME	SAME
BACK-UP	VHF, S or X Band Mono	VHF, S or X Band Mono	SAME	SAME	SAME
BACK-UP	Intf (2 Sta)	Intf (2 Sta)	Intf (2 Sta)	GND or GND/DOC #1 or DOC #2	SAME

3.6.2.5 Power Subsystem

The Power Subsystem FMECA was performed on the functional block diagram as it appears in Figure 3.6-6. Since the Power Subsystem is completely redundant, and no single failure can cause loss of power to the spacecraft, there are no critical, (Category I), failure modes. Of the 28 failure modes analyzed, 13 were grouped into Category II and 15 into Category III.

3.6.2.6 Structure Subsystem

Since the devices separation and deployment modes are "one slot" operation, maximum effort has been exerted to minimize the probability of any Category I failures occurring.

The FMECA points out four areas within the separation and deployment subsystems which are potentially Category I failures for the spacecraft. All of these relate to possible frictional hang-ups.

In all cases, space qualified designs and parts have been used to implement the separation and deployment motions. The designs are all such that there is a wide margin of spring forces acting on the bearing surfaces to overcome a wide range of anomalous frictional forces. Further, all frictional systems will be lubricated with space qualified lubricants.

The separation and deployment systems will be continually reviewed and every attempt will be made to improve the design in order to further reduce the probability of occurrence of these critical failures.

3.6.2.7 Reflector Subsystems

Since the reflector is critical to spacecraft success, maximum effort has been exerted to minimize the probability of any Category I failures occurring.

The FMECA disclosed five (5) failures which are potentially Category I. These are related to three different causes:

- Friction torques in bearing surfaces
- Mesh tearing on deployment
- Mesh reflective coating degradation

The action to minimize the probability of these failures is discussed in the following paragraphs.

The deployment designs are all such that there is a wide margin of spring forces acting on bearing surfaces to overcome a wide range of anomalous friction forces. Further, all frictional systems will be lubricated with space qualified lubricants in order to reduce friction torques to a minimum, thus further increasing the probability of success.

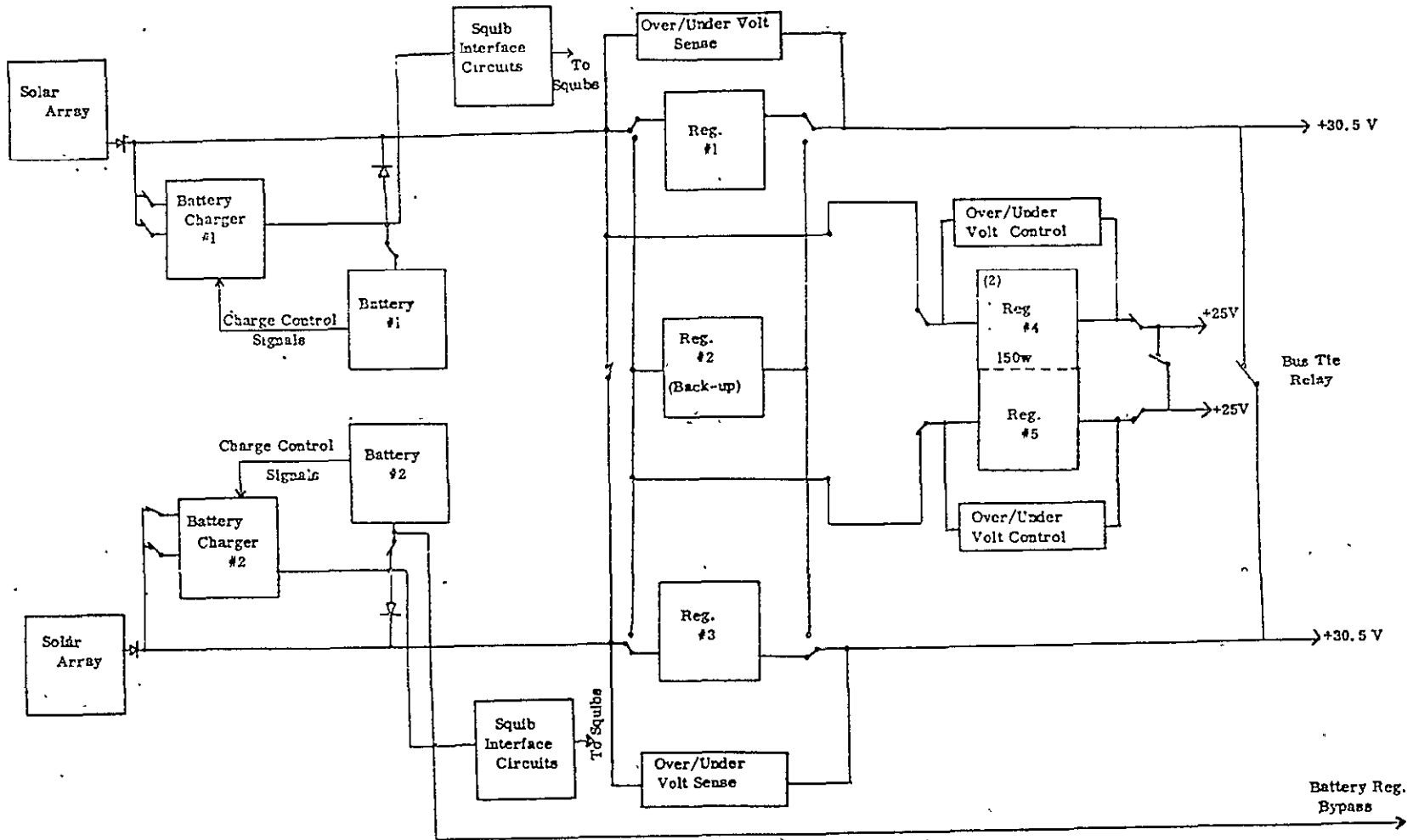


Figure 3.6-6. Power Subsystem Block Diagram

The mesh has been designed with a wide safety margin between deployment stresses and mesh strength. Proper packing of the mesh for storage is of the essence. The mesh packing procedures will be closely monitored to ensure that the reliability of the reflector will not be degraded.

The possible causes of degradation of the mesh reflective coating will be studied during Phase D and every attempt will be made to remove the causes or minimize their effects.

The reflector subsystem will be continually reviewed and every attempt will be made to improve the design in order to reduce the probability of occurrence of Category I failures.

Of the seven failure modes analyzed, there were six Category II, and one Category III.

3.6.2.8 Integrated Transponder and Feed Subsystems

An FMECA was performed on the Integrated Transponder and Feed Subsystems at the functional block level. There are two failure modes that could possibly be considered system critical in the Transponder and none in the Feed Subsystem. These failures are related to impedance changes in the X and S/L Band filters and are summarized in the attached FMECA worksheets. In both cases the probability of occurrence of a critical filter degradation is small and at worst, minor degradation to the X and S/L Band downlinks could occur.

This FMECA reflects several design changes that have reduced the number of Category I failures.

The addition of a parallel redundant TDA X-band pre-amplifier has been made after the completion of detailed reliability trade-off studies. The redundant pre-amplifier eliminates a Category I ITV, Place and DRS up-link degradation caused by a low pre-amp signal to noise ratio.

The rotating feed was eliminated and replaced by a fixed feed configuration. The major advantages of this change are:

- Two Category I failure modes are eliminated when the stepper motor and gear train are eliminated.
- A possible catastrophic failure resulting from the breaking of an RF cable is considerably less likely since the cables will not be flexed.
- By eliminating the electromechanical portion of the prime focus feed, the probability of a human induced failure is significantly reduced.

3.6.2.9 Thermal Control Subsystem

An FMECA was performed on the Thermal Control Subsystem to determine the effects of a critical failure on the spacecraft. It was assumed that 50% of all heat pipes failed and 10% of all louver blades seized in the worst case, i. e., open in the cold case and closed in the hot case. The results of this analysis indicates that reasonable, although not in-specification, thermal control can be maintained even if this assumed critical failure mode occurs. Thus, it is concluded that the failure of any single element will have a minor (Category III), effect on the system.

3.6.3 CRITICAL RELIABILITY AREAS

During Phase C, the various subsystem designs have been carefully reviewed with the objective of identifying items that are critical to the success of the spacecraft. The items are defined as critical because they are:

- Items that must operate one time such as deployment devices some of which are self destructing
- Items where testing is required to assure successful operation over extended periods
- New material usage.

This paragraph discusses these items, the area of concern, results of preliminary investigations, and what will be done in Phase D to provide assurance of successful mission accomplishment. The testing discussed will be implemented during the development, qualification, and acceptance test portions of the program.

3.6.3.1 Separation Nuts

The separation of the spacecraft from the adapter is accomplished by firing four redundant sets of separation nuts. These nuts are manufactured by Hi-Shear Corporation. A separation nut of the same size and with only superficial differences was qualified and used on the Lunar Surveyor Program. Preliminary investigation indicates that the critical parameters are the ability to actuate (without case fracture) at high temperatures when overcharged, and the ability to actuate at low temperature when undercharged. It is presently anticipated that during qualification testing of the nuts, sixteen samples will be randomly selected from the lot. Eight will be subjected to high temperature test and eight will be subjected to low temperature test. Investigation will continue to establish the exact charges and temperature conditions to be used.

3.6.3.2 Pyrotechnic Pin Pullers

All solar array deployment functions are initiated by releasing spring loaded pins through the action of a pyrotechnic pin puller.

The pin puller tentatively selected for ATS is manufactured by Horex Inc. and has been qualified for use in the SERT II program under similar application. A qualification test requirement similar to that for the separation nuts will be performed under simulated ATS pin side loads.

3.6.3.3 Solar Array Retention System

This system uses a design similar to one which was used on Nimbus. Five pins on either side of the solar array half cylinders act against springs in compression to hold the arrays in position as a cylinder. Upon release, the springs pull the pins to separate the array halves. Binding of this mechanism will prevent solar array deployment.

During development testing a pin joint and cable restraint mechanism will be tested under various temperature and loading to establish the maximum anticipated forces for the spacecraft temperature.

A sample restraint/release system will then be subjected to 300 cycles of operation under a condition equal to 1.5 times the maximum anticipated release loads.

Additional testing to be performed during the program is as follows:

- Ten release cycles under zero G conditions at anticipated loads using the Thermal Structural Model Solar Boom.
- Two cycles on the prototype spacecraft under anticipated loads.
- Two cycles on each flight spacecraft under anticipated loads.

3.6.3.4 Boom Deployment Mechanism

When the retention system is released, redundant springs at the boom knee joint act to deploy the booms. This motion is damped by redundant viscous dampers. Over-center latches lock the boom in a position to allow reflector deployment. The solar array halves rotate into their final position about a skew-hinge joint after release by a redundant pyrotechnic pin-puller. After reflector deployment, a second motion about the knee joint positions the boom in flight position.

The area of concern centers around friction in the joint bearings, and the ability of the viscous dampers to provide the proper damping rates.

The bearings to be used are identical to those used on the Apollo and Ranger programs. Investigations were conducted to establish the proper type and amount of lubricant to be used.

The viscous dampers are similar in concept and design to those successfully flown on the Nimbus Program and incorporated in the LES-7. Additionally, a similar type damper was used by FHC as part of a thermal vacuum test fixture for the RAE deployable boom. This damper was in the chamber and provided controlled damping rates during a 300 hour test. As part of the qualification test, the dampers will be subjected to 100 cycles of operation under ATS load conditions.

Engineering development tests will establish the maximum loading conditions to be seen by the skew hinge joint, the knee joint, and the viscous dampers. Each of the joints will be fabricated, and subjected to 300 cycles of motion under a condition equal to 1.5 times the maximum anticipated loads. Additional testing will be as follows:

- Ten deployments under zero G conditions at anticipated loads using the Thermal Structural Model Solar Boom
- Two cycles on the prototype spacecraft under anticipated loads
- Two cycles on each flight spacecraft under anticipated loads.

3.6.3.5 Separation System

Separation is accomplished by firing four sets of redundant separation bolts, thereby releasing four compressed springs, one at each attachment point. The stored energy in the springs impart an initial relative velocity of 3 feet per second between the spacecraft and the Titan III-C transtage. A track mounted to each corner of the spacecraft guides the separation. There are three areas of concern in this system,

- Proper separation velocities will be imparted
- A possible failure mode where all separation bolts fire but one spring malfunctions
- A possible failure mode where three bolts fire simultaneously and one is delayed. This may cause tipping of the spacecraft in the separation track.

The following tests will be performed using the Thermal Structural Models in a zero G simulation:

- Four separations with all bolts and springs installed. The bolts will be fired simultaneously and separation velocities measured.

- Four bolts and three springs will be installed. The missing spring will be a worst case simulation of a broken or malfunctioning spring. The bolts will be fired to determine whether sufficient separation velocities are imparted, or if the spacecraft will settle in a position that will allow the Titan transtage to back away effecting separation.

- Four bolts and four springs will be installed. Three bolts will be fired simultaneously and the fourth will be fired after a delay of several seconds. The information to be gained as a result of this test is the same as above.

Two normal separation tests will be performed on the prototype spacecraft. One separation test on each of the flight spacecrafts will also be performed.

3. 6. 3. 6 Graphite Fibre Reinforced Plastic (GFRP)

GFRP, the basic material of the reflector support truss, was selected for use on the ATS F&G because of its low temperature coefficient of expansion. Use of this material will minimize reflector defocusing due to thermally caused variations in truss length.

The material is a recent development and is relatively unproven in space applications. The following will be determined by test during Phase D:

- Reproduceability of design-critical parameters within manufacturing lots of truss tubes.

- Permanent temperature effects, if any, on design-critical parameters.

Early in the engineering phase of the program short tube sections will be manufactured to actual drawing requirements. These tube sections will be subjected to tests to determine their axial, bending, and buckling strengths. The samples will then be temperature cycled to the extremes that the truss will see prior to launch and the above parameters will again be measured. The results will determine if temperature testing prior to launch will degrade the reliability of the truss. The data from these tests will be correlated with the design values and design loads to determine, through statistical stress-strength techniques, the probability of meeting the design goal for the truss. Similarly, the data will be correlated with the expected launch loads to determine the probability of launch survival. This will serve to determine what action, if any, should be initiated to ensure that the probability of launch survival is commensurate with ATS requirements.

Subsequently, sample tube sections will be taken from the production lots for the qualification and flight trusses. The above tests will be repeated on these sample tubes to verify that the manufacturing processes have not deteriorated.

Additionally, tube acceptance prior to truss assembly will be contingent on verification by test that the bending modulus of each individual tube to be used meets the design requirement.

3.6.3.7 Flexure Pivots

The flexure pivots used to support the scanning mirror in the earth sensor design have been selected for use on the ATS F&G because they give the capability of performing the required scanning motion without restoring to frictional bearing motion.

Available data on the flexure pivots is insufficient to demonstrate compliance with the mission life requirement of 320 million cycles. Previous testing by the pivot manufacturer on six pivots showed no failures. However, only one pivot accumulated over 320 million cycles. The data is as follows:

<u>Cumulative Cycles</u>	<u>Failures</u>
3,097,440	0
8,575,200	0
8,758,080	0
36,760,640	0
53,816,400	0
4,689,932,256	0

To assure that the flexure pivots function properly for the ATS mission life, long term cycling under simulated load conditions and at ATS temperatures will be performed for one year on 20 flexure pivots. It is anticipated that these tests can be conducted at a cycling rate approximately four times greater than the actual mission conditions without invalidating the test results. Thus each of the flexure pivots may be run at higher load conditions to accumulate data on the safety margins in the ATS application.

3.6.3.8 Solid State Lamps

A lamp is required as a reference for the optical encoder in the earth sensor head. A solid state lamp was selected because solid state lamps do not "burn out" as do incandescents. They do, however, degrade in intensity. Limited life data is available as a result of tests performed for 2000 hours at higher current levels and temperatures than will be experienced on the ATS. Extrapolation of this data to a two year mission shows that, under these conditions, the intensity would not degrade below the minimum acceptable level of 50% in the ATS design. However, the actual behavior of the lamps throughout the ATS mission under earth sensor usage conditions is unknown. Life tests will be conducted on a sample of 20 lamps for a minimum of 12 months at current and temperature levels similar to, and higher than, the ATS application levels. In this way data on the degradation of intensity as a function of time, current level, and temperature will be obtained to verify the integrity of the lamps and to assure that acceptable intensity levels can be maintained.

3.6.3.9 Solid State S-Band, L-Band, and UHF Power Amplifiers

Amplifiers using solid state techniques have been selected for use on the ATS to minimize size and weight.

The transistors used in this application are at the state-of-the-art for transistor technology. A 2000 hour stability test will be conducted on one flight configured amplifier for each of the three designs to verify that the output power and frequency are sufficiently stable to successfully complete the ATS mission objectives. The tests will be conducted under thermal-vacuum conditions and the equipment will be cycled on/off in a 5 hour/1 hour ratio during the test to simulate expected ATS "on" cycling.

After cycling in thermal vacuum, the solid state power amplifiers will be continuously operated under ambient conditions as long as practicable to obtain life data and to gain confidence in the failure rate of the transistors.

3.6.3.10 PIN Diode Switches

PIN diode switches were selected in lieu of switching circulators for use in the S-Band feed array because they are less lossy and affect a great savings in weight. The PIN diode switch is a new technique with no spaceflight history. Two SP4T switches (one receive and one transmit) will be cycled through each switch position 10 times per hour for 500 operating hours each in thermal-vacuum (five hours on and one hour off). They will be switching the normal RF power that the devices will be switching on the spacecraft. The test will determine the long term low losses on the PIN switch under ATS operating conditions and under expected ATS "on" cycling.

3.6.3.11 Auxiliary Propulsion Subsystem (APS)

The critical areas within the APS have been identified as:

- Evaporator and heat exchangers
- Pressure regulator
- Valves
- Orbit Control Thrusters

3.6.3.11.1 Pressure Regulator/Evaporator and Heat Exchanger

The most stringent requirement for the heat exchanger and evaporator is during the rate nulling prior to acquisition. Under worst case conditions, the heat exchanger will be required to vaporize 1.5×10^{-3} pounds of ammonia per second for three to five minutes drawing the heat of vaporization from liquid ammonia in the tanks.

During the engineering phase of the program, tests will be conducted to optimize the heat exchanger design and ensure a wide safety margin over the ATS requirements.

Once the heat exchanger has been optimized, the test unit will be temperature cycled 25 times between the ATS extremes to determine if any incompatibilities exist resulting from differential expansion at the heat exchanger welds.

A pressure regulator assembly will be required in order to conduct the heat exchanger tests. As Table 3.6-3 indicates, there is only limited data on the pressure transducer of the regulator. Once the heat exchanger tests are complete, the pressure regulator unit will be cycled 5 million times at ATS pressures to gain more confidence in the ATS application of the entire regulator.

3.6.3.11.2 Valves

The attitude control, orbit control, and pressure regulator valves are used for controlling the expulsion of ammonia in the APS. They all can be considered functionally equivalent from a life standpoint since they have identical construction and differ only in their wattage rating. Table 3.6-3 shows experience accumulated on these valves. Fourteen valves exceeded the mission requirement level without failure - eight valves by a factor of 4 times and 6 valves by a factor of 40 times.

Each flight valve will be subjected to 10,000 cycles prior to acceptance. This will effectively be a screening test and will verify that the inherent reliability of the individual valve has not been degraded by manufacture.

The latching valves used to protect the APS from losing ammonia through leakage will experience a very small number of actuations. A very conservative number of the expected actuations including subsystem and system level pre-launch testing is 1000 cycles. During Phase C breadboard testing, two units have been cycled 20,000 cycles each without failure. This data combined with qualification testing and burn-in during acceptance testing which will be conducted in Phase D will provide the needed confidence.

During qualification, four latching valves will be subjected to 100,000 cycles each at varying conditions of liquid and vapor ammonia and at ATS temperature extremes to further qualify the latching valves for the ats mission. Further, each flight latching valve will be subjected to 10,000 cycles as part of its screening test.

3.6.3.11.3 Orbit Control Thrusters

Neither of the candidate orbit control thrusters can be considered fully qualified for ATS application. The TRW vortex thruster is still undergoing test and the AVCO resistojet thruster has seen much testing under lower thrust and power levels than in its ATS application.

Table 3.6-3. APS Component Life

APS Component	ATS F&G Mission Requirement (Cycles)	Test/Flight Experience			Source	
		No. Units	Cycles Per Unit			
			Ammonia Gas	Ammonia Liquid		
Attitude Control Valve	2×10^5	4	2×10^6	2×10^5	Valve Qualification	
Orbit Control Valve	1×10^3	2	2×10^3	2×10^3	ATS D Qual Unit	
Pressure Regulator Valve	5×10^5	2	2×10^3	2.9×10^4	ATS D Qual Unit	
		2	2×10^3	3×10	ATS D Flight	
		2	3×10^3	1×10^3	ATS D Flight	
		1	2×10^3	5×10^3	ATS E Functional	
		1	2×10^3	3×10^3	ATS E Functional	
		2	3×10^3	1×10^3	ATS E Functional	
		2	2×10^6	--	ATS F&G Developmental	
		2	2×10^7	--	Navy Research Laboratory	
		2	3×10^6	--	Navy Research Laboratory	
		26	--	1×10^5	Navy Research Laboratory	
		4	2×10^7	1×10^5	Navy Research Laboratory	
		Cumulative	52	1.38×10^8	3.83×10^6	
Latching Valve	1×10^3	2	2×10^4		ATS F&G Developmental	
Pressure Transducer	5×10^5 @ approximately 12% of full pressure range	1	2×10^6		Vendor Tests	
		-	3×10^6 @ full pressure range		Vendor Predicted Life	
Orbit Control Thruster	Less than 1000 hrs of hot time consisting of less than 20 temperature excursions	4	8000 (hrs) hot time consisting of 8000 temp. excursions at micropound thrust levels.			

The thrusters are such that two distinct thermal mechanisms could cause them to fail under normal operations. These are:

- Extended use (extended high temperature)
- Thermal shock (turn-on and turn-off temperature transients)

It is expected that the ATS orbit control thruster will see much less than a total of 1000 hours of hot operating time. This is expected to be a maximum of 20 cycles, during the two year mission. The longest cycle, 175 hours, is expected during the re-positioning maneuver.

As part of qualification, two thrusters will be subjected to continuous hot operation at 1.3 times the heater power dissipation to be used in flight. The thrust and specific impulse of the thrusters will be measured prior to and after this long term operation to verify the capability to perform without degradation.

The thrust and specific impulse will also be measured before and after 300 operating cycles with a minimum of 1000^oF between the hot and cold temperatures. The flow will be maintained during cooling to increase the cooling shock. These qualification tests will increase confidence in the ATS application of the thrusters.

3.6.4 ATS PARTS ASSURANCE PROGRAM

The ATS F&G Parts Assurance Program was established at the start of Phase B of the Program. Its main objective has been to assure that all parts to be used on the ATS F&G Spacecraft meet or exceed the stringent, high reliability requirements which are necessary to prevent spacecraft degradation and achieve all mission goals.

All parts which were selected during Phases B & C for use on the ATS F&G Spacecraft, have been compiled into a composite and detailed Preferred Parts List presented in Volume III Boox 2 of the proposal. Whenever possible, parts for this list were carefully selected from the ATS A-E Hi-Rel Preferred Parts List. Each part was evaluated to determine whether or not a part existed which was on the ATS A-E Preferred Parts List and which was suitable for accomplishing the job. If the part was not on the ATS A-E PPL, nor was there a suitable ATS A-E replacement, the needed part was then selected from other Hi-Rel space programs, preferred parts lists, whenever possible. These lists include the GSFC-PPL-10, MSFC-PPL, and Preferred Parts Lists from Hi-Rel, long-life spacecraft programs, including NIMBUS, IDCSP/A-COMSAT, and MARINER MARS 1969. In all cases, parts chosen from other Hi-Rel Spacecraft PPL's were evaluated to determine their suitability to the ATS F&G application. In addition to this evaluation, all parts used will be screened at ATS F&G levels on a 100% basis to eliminate infant mortality, and to insure that the parts are good. Lot qualification will be performed, as specified in the procurement specification, to insure that the lot from which the parts have

been selected has not been degraded due to new or faulty manufacturing processes and materials.

Because of the advanced state of technology of the ATS F&G spacecraft design, there are some parts that do not appear on the ATS A-E PPL and have not been used on other Hi-Rel spacecraft programs. These parts will require Qualification Testing before being used on the ATS Spacecraft.

The FHC Interim Reliability Report, ATS-990-007, dated 10 May 1969, included a Preliminary Preferred Parts List. This preliminary list included 138 parts that required qualification testing. The ATS A-E PPL was made available in May 1969. After thorough part application analysis, based on more detailed design definitions and review of the approved parts on the ATS A-E list, the number of non-qualified parts was reduced to 15. Part similarity reduces the number of tests to 12. Efforts to reduce this number further will continue during Phase D.

Also during Phase C, efforts have been made to standardize the types of parts to be used in the Program. For example, the low power Texas Instrument Integrated Circuit, SN54LXX series, will be used by all subcontractors instead of other functionally equivalent digital I. C. 's. Some of these Texas Instrument devices are on the ATS A-E PPL and the entire family has been qualified in-house by both Honeywell and Philco-Ford. Reduction of the number of different types of parts has been a major effort during Phase C and will continue to be an important task in Phase D of the Program.

Evaluations of all parts which are critical to the spacecraft design will be a major effort in Phase D. These evaluations will be detailed and will include physical inspection (both external and internal), and necessary environmental, electrical and reliability demonstration testing. Such evaluations will be made to increase our confidence in the part and to insure that the part can be used successfully on the spacecraft.

Parts which will be selected during Phase D of the ATS Program will undergo the same type of detailed analysis as did the parts on the present ATS F&G PPL. The reasons for selection of non-ATS A-E approved parts must include justification as to why approved parts cannot be used. All parts added to the ATS PPL in Phase D will be submitted to GSFC for approval prior to their inclusion on the ATS F&G Approved Parts List.

3.6.5 PREFERRED MATERIALS LIST

In active response to the provisions of Paragraph 3.22.2 of Contract NAS5-11609 between the NASA Goddard Space Flight Center (GSFC) and the Fairchild Hiller Corporation, Space and Electronics Systems Division (FHC), the ATS F&G Preferred Materials List has been prepared and submitted in Volume III Book 2 of the proposal. The listing is comprised of candidate materials which FHC and its three team subcontractors, (Honeywell, Inc., Philco Ford Corporation, and International Business Machines Corporation); anticipate using in the construction of the ATS F&G Spacecraft during the Phase D Program.

The Materials List is of a preliminary nature due to the status of the detail design at this point in time. It will be continually updated as the detail design progresses during Phase D, and shall be jointly reviewed with GSFC and subject to approval by the GSFC ATS Project Office.

SECTION IV

STRUCTURAL SUBSYSTEM

4.1 INTRODUCTION

The ATS F&G spacecraft, when in the orbiting configuration, will be considerably larger than most other spacecraft that have been placed in orbit. In addition, the functional requirements of the spacecraft dictate a high degree of precision in mechanical alignment and orientation. The spacecraft described herein is compact during launch and orbital injection, and structurally sound throughout the entire flight. It deploys the solar arrays and reflector very simply, and adapts ideally to all the mission and experiment requirements.

This section provides a detailed description of the Structural Subsystem, discusses briefly some aspects of the system design considerations. It also summarizes the structural dynamic and strength analyses conducted during phase B/C of the ATS F&G program. The spacecraft in the orbital configuration is shown in Figure 4.1-1. For the launch configuration, see Figure 4.1-2.

4.2 SYSTEM DESIGN CONSIDERATIONS

The configuration of the spacecraft Structural Subsystem is determined by many factors originating from mission requirements, other subsystems components functional or physical parameters, launch vehicle restraints, and experiment requirements. Furthermore, properties of materials used and fabrication methods influence the design, and the configuration should be selected to provide ease of equipment installation, integration, and test.

The 30 foot diameter reflector selected for installation on the ATS F&G spacecraft is designed by the Lockheed Missile and Space Company and is designated a Flex-Rib reflector. The design employs an $F/D = 0.44$ which with the reflector diameter, establishes the reflector/feed system spacing.

In the packaged configuration during launch, the reflector is stowed in a toroidal shaped container 58" ID x 78" OD x 12" high. This packaged configuration limits the structural hub size but has little affect on reflector support truss configuration. Reflector deployment characteristics affect design of the solar array deployment subsystem which must position the array to preclude interference between the solar array and the Reflector Subsystems. Mission dictated orientation of the spacecraft establishes new angles of the solar arrays and exercised a strong

influence in selection of the array configuration and in the positioning of the array to obtain a satisfactory compromise between array shadowing, minimum moments of inertia of the spacecraft, and star tracker and EME experiments field of view requirements.

The communications subsystem operational requirements for relative relative positional tolerance of prime focus feed assembly and reflector focal point influenced the choice of Graphite Fiber Reinforced Plastic (GFRP) composite material for the reflector support truss with focal point motion held to less than 0.040" for anticipated thermal deflections. A weight saving of 45 pounds is realized using GFRP in place of aluminum.

The Titan IIC launch vehicle, places packaging and weight limitations on the spacecraft, influences ground power and spacecraft/launch vehicle separation design, and establishes the strength design criteria for most of the spacecraft. Dynamic response of the spacecraft to launch vehicle induced vibratory and acceleration loads is a dominant consideration in design of all parts of the Structural Subsystem.

The ATS-F experiment compliment impose requirements on the structure in such areas as field and direction of view, initial alignment tolerances, and deviations due to thermal distortion, special cooling requirements, and mounting location influenced by experiments physical sizes and special operational requirements. The experiments, together with the interferometer, earth sensors, and prime focus feed assembly establish the EVM cross-sectional size and influenced selection of the square shape.

The EVM Thermal Control and Structural Subsystems interact to such a degree that, in reality, they can be considered as subassemblies of a larger structural assembly, the EVM. Each enhances the operation of the other. The square EVM with its north and south facing sides containing louver controlled heat dissipating areas, combined with heat pipe controlled surfaces for mounting equipment within the EVM, results in a spacecraft with very close temperature control.

The modular construction of the EVM provides an ideal structure for equipment installation, integration, and test.

The following paragraphs describe the Structural Subsystem in detail.

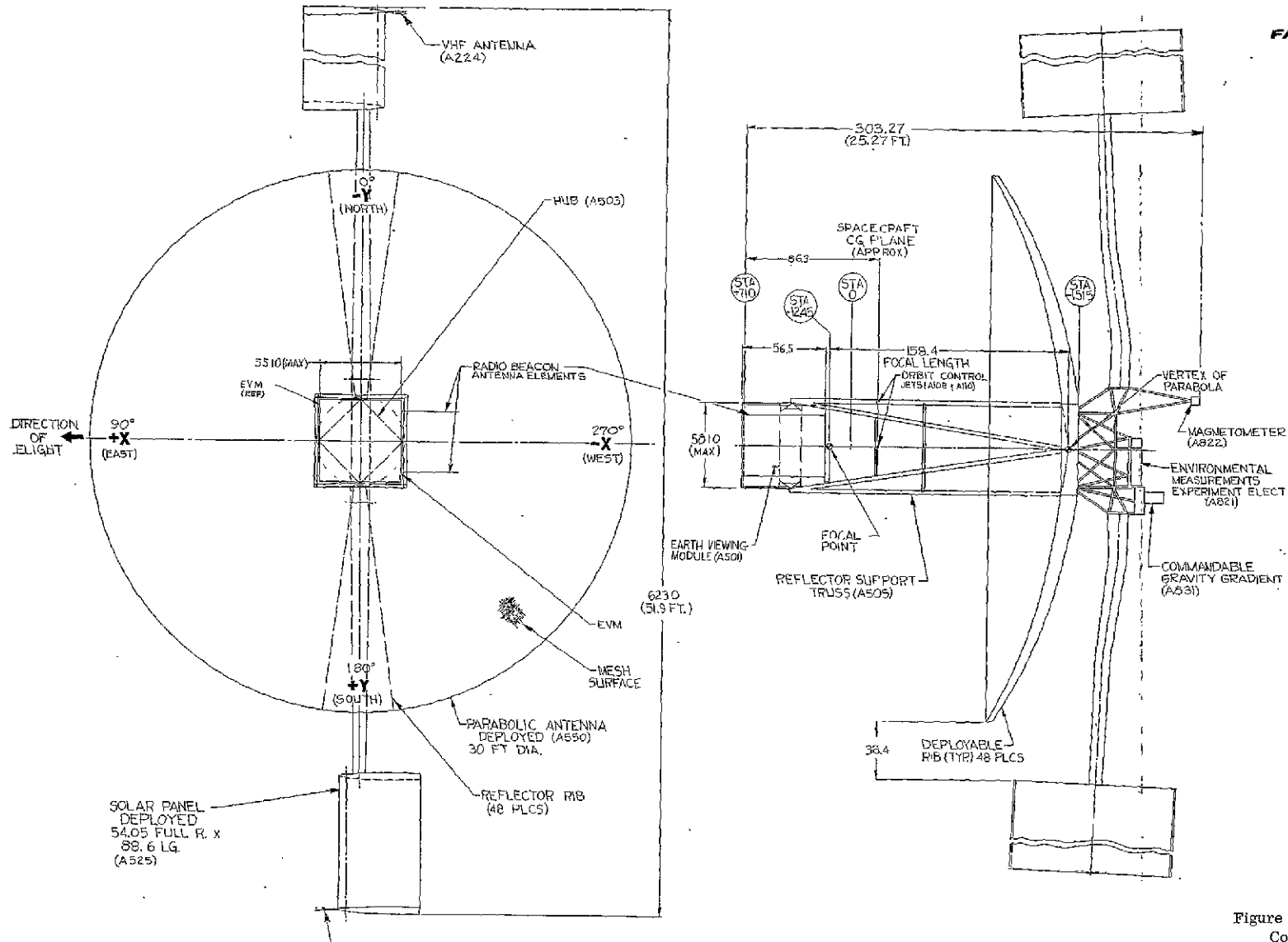
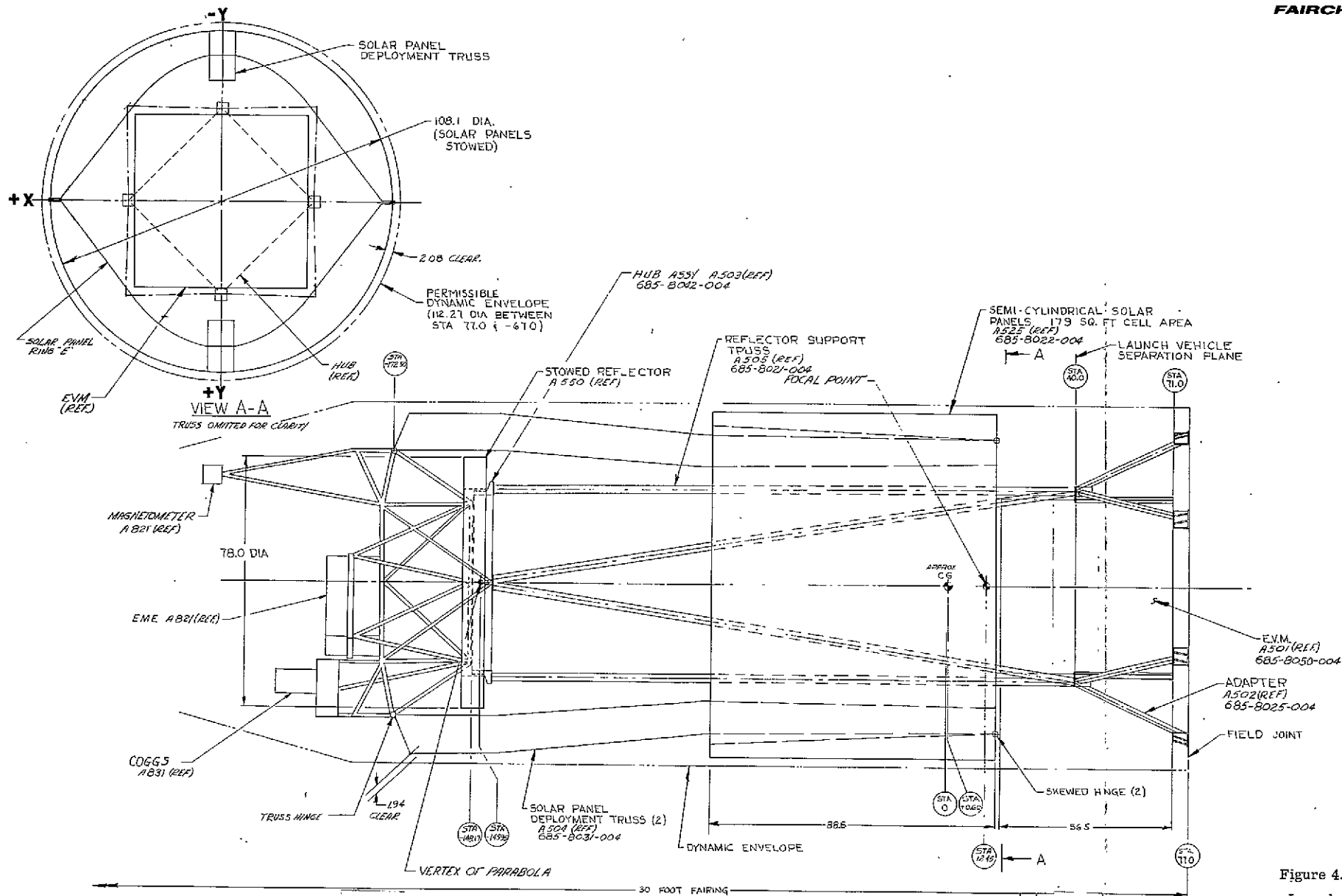


Figure 4.1-1. Orbital Configuration



FOLDOUT FRAME 1

FOLDOUT FRAME 2

Figure 4.1-2. Spacecraft Launch Configuration 4-5/4-6

4.3 STRUCTURAL SUBSYSTEM DETAIL DESCRIPTION

4.3.1 EVM

The EVM approximates a 54-inch cube consisting of three sections called modules. The lower section is designated the experiment module, the center section is designated the service module, and the upper section is designated the communications module.

The experiment module (EM) contains most of the experiments and all of the earth viewing system components. The service module (SM) contains the basic telemetry and command components, the central Power Subsystem components, and the attitude control components. The communications module (CM) contains the communications components and three experiments that are closely associated with the communications system. The volume usage is shown in Table 4.3-1.

The EVM structure includes interface fittings for supporting the EVM and the solar panels in the stowed configuration. The four EVM support fittings are attached at the corners of the service module. These fittings function as the mechanical tie between the EVM, the reflector truss, and the spacecraft adapter. They also provide handling points for the EVM alone. The mating surfaces of the EVM support fittings and the adapter separation fittings form the separation plane. The solar panel support fittings are located on the honeycomb panel that forms the top of the EVM (communications module).

Experiment Module Structure (Figure 4.3-1)

The experiment module (EM) structure consists of four corner posts, four frame angles, a honeycomb shelf and interferometer frame, an interferometer array mounting plate; four skin panels, and an interconnecting honeycomb panel beam.

The four corner posts are 24 inches long and are machined from aluminum alloy. The external projection of each post is machined to provide a track for the separation guidance rollers, and the upper surfaces of the posts provide holes for alignment to the service module. Stainless steel self-locking nuts are provided along the length of the corner posts for attaching the skin panels. The four frame angles are 0.075" x 0.75" x 0.062" aluminum alloy angles that are joined to the post flanges at the lower end of the corner posts, providing a surface to which the shelf and skin panels are attached.

The experiment shelf is a 54-inch square, 0.50-inch thick, honeycomb panel with 0.025" aluminum alloy face sheets and 3/16" x 0.0015" thick aluminum alloy cells. The central area and other local areas of the shelf are cut out for the interferometer array and other earth viewing components. The edge of the interferometer cutout (Figure 4.3-2) is reinforced by a welded aluminum alloy framework approximately 0.062" thick and 4.00 inches high. The shape of this framework is similar to a four-pointed star and at tow of the four points the frame-

Table 4.3-1. Area Volume of EVM

Volume	Communications Module	Service Module	Experiment Module	Total EVM
Available (Cubic Inches)	46,656	40,824	69,984	157,464
Occupied by Equipment (Cubic Inches)	7,497	12,389	35,919	55,805
% Used	16%	30%	51%	35%

NOTES:

△ DIMENSIONS APPLY IN BOTH AXES.

△ THE INTERFEROMETER ELECTRICAL AXES SHALL BE DETERMINED RELATIVE TO THE OPTICAL CUBE TO WITHIN 0.01 DEGREE AND ALIGNED TO THE SIC GEOMETRIC AXES TO WITHIN 0.1 DEGREES.

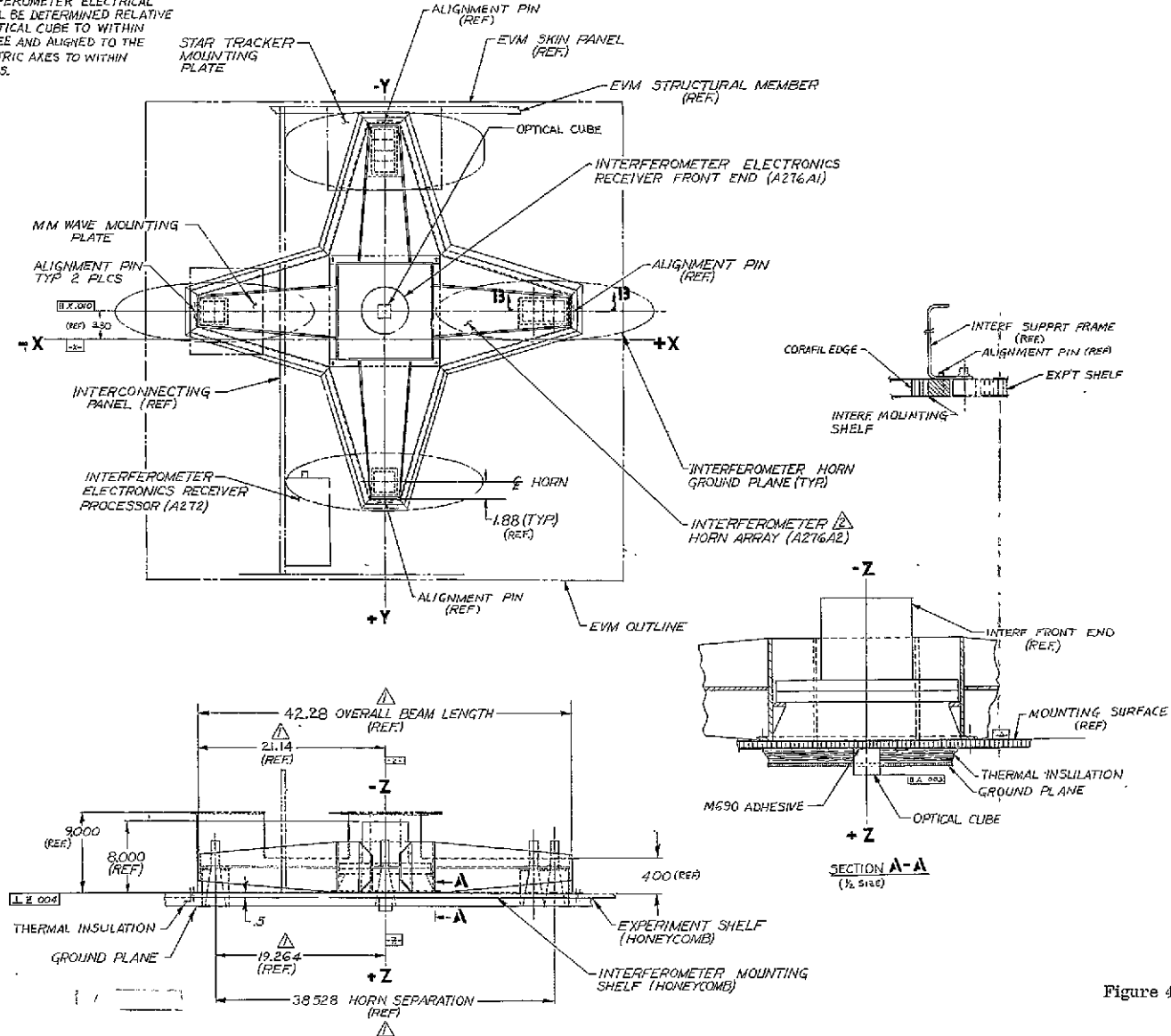


Figure 4.3-2. Interferometer

FOLDOUT FRAME 7

FOLDOUT FRAME 2

work is 9.0 inches high. The increased height in these two areas is designed to serve as support for module mounted components. The design permits the interferometer plate and the interferometer horn assembly to be removed as an assembly for calibration.

All edges of the honeycomb shelf are closed by filling with Corfil, then machined to present a smooth surface. Fiberglass blocks bonded into the honeycomb provide shelf attachment locations. The shelf attachment screws pick up the fastener nuts located on the frame angles and the welded frame. Component fastening is provided by potted inserts located within the honeycomb shelf.

The interferometer array mounting plate is constructed of the same material as the shelf, and forms a four-pointed star that attaches to the welded framework around the interferometer cutout.

The four skin panels (north, east, south, and west) are constructed of 0.55" thick x 24" x 51" aluminum honeycomb. The face sheets are 0.025" thick and the core is formed of 3/16" x 0.0015" cells. All skin panels have machined Corfil edges, and fiberglass blocks are located along their periphery for attachment to the corner posts and frame angles. The north and south panels contain 1/2" square heat pipes on 4" centers, by 49" long (except where interrupted by component viewing ports) and potted inserts for component attachment. The north and south panels are also provided with potted inserts for attaching the interconnecting panel, heat pipes, thermal control louvers, and thermal insulating blankets. The east and west panels provide inserts for the attachment of thermal insulating blankets.

The interconnecting honeycomb beam panel, which attaches to the shelf and to the north and south skin panels, is cut out to clear the interferometer frame. This panel is 0.55" thick x 21.50" x 53" and is fabricated with interior heat pipes, from the same materials, and in the same manner as the north and south skin panels. Attachment angles are provided as part of the beam assembly, and the upper edge of the beam panel is reinforced with a 0.062" x 0.75" x 0.75" aluminum alloy stiffening angle. The ends of the interconnecting panel heat pipes are normal to the panel, and are clamped to the north and south skin panels for a length of 4.0 inches. Each set of three thermally interconnected heat pipes in the north, south, and interior panels all lie in a plane parallel to the X-Y axes plane. Ground handling of the EM, when separated from the remainder of the EVM, is accomplished by placing a "picture frame" fixture around the outside of the EM at its interface to the service module (SM) and attaching the frame to the side skins and four corner posts. This frame provides the necessary rigidity to the EM structure that is required when equipment is installed.

Service Module Structure (Figure 4.3-3)

The service module (EM) structure forms a 14-inch by 54-inch square box. The basic structure consists of four upper 1.5" square, tubular frame members (each approximately 40 inches long) joined at their ends by four corner posts, and four identical lower tubular members joined by the same corner

posts. The posts separate the upper frame members from the lower frame members by approximately 14 inches. Opposite corners of the box frame are tied together by truss beams that are the full depth of the module.

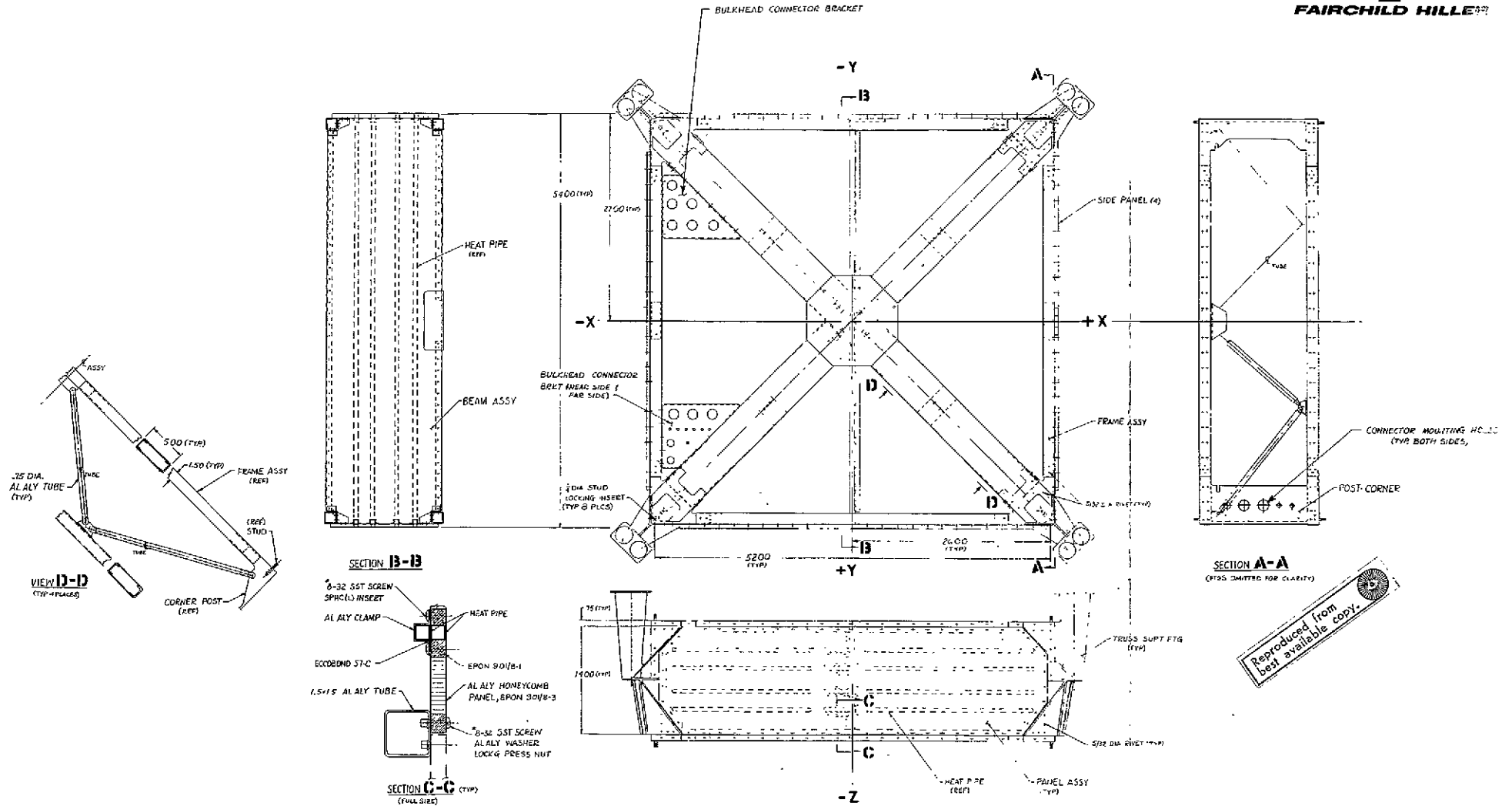
In addition to the four corner posts and the eight square tubular frame members; the service module structure comprises four reflector truss support fittings, four skin panels, an interconnecting panel, two truss type beams, gussets, brackets, and studs. All materials are aluminum alloy except for the studs, screws, and nuts, which are stainless steel. The four corner posts are 14 inches long and are machined from aluminum alloy to fit inside the mating four square tubular frame members. The two frame members at the top of each corner post are normal to each other, as are the two frame members at the bottom of each corner post. The posts are also machined to provide attachment of the truss type beams, which run diagonally across each square frame assembly. The truss beams are attached to the tops and bottoms of the corner posts by means of H-shaped gussets. The flanges of the corner posts are 0.062" thick, and locking press-nuts are provided for skin panel attachment. The posts also provide an attachment surface for the four reflector truss support fittings. The square frame members, the truss beam cap members, and the reflector truss support fittings are riveted to the corner posts. A flange is provided at each post for the truss beam diagonal members.

The four reflector truss support fittings are fabricated from aluminum alloy and are riveted to the corner posts. These fittings provide a mounting surface for the reflector truss at their upper surface, a mating surface for the adapter fittings at their lower surface, and attachment points for ground handling equipment. The adapter mating surface is the spacecraft separation plane. The fittings also form a continuation of the experiment module separation track.

The square tubular frame members are 0.040" x 1.5" square aluminum alloy tubing. These tubular members provide attachment locations for the skin panels by means of locking press-nuts installed on their outboard surfaces. A double row of nuts in each frame member provides attachment point for the communications and experiment module skin panels.

The four skin panels (north, east, south, and west) are fabricated of 0.55" thick x 14" x 51.5" aluminum honeycomb. The face sheets are 0.025" thick and the core is formed of 3/16" x 0.0015" cells. All skin panels have machined Corfil edges. Fiberglass blocks are located along their periphery for attachment to the corner posts and frame members.

The north and south skin panels contain 1/2" square x 47" long heat pipes, and potted inserts for component attachment. The north and south panels are also provided with potted inserts for attaching the interconnecting beam heat pipes, the thermal control louvers, and the thermal insulating blankets. The east and west skin panels provide for the attachment of the thermal insulating blankets only.



Reproduced from
best available copy.

FOLDOUT FRAME 1

FOLDOUT FRAME 2

4-15/4-16

The interconnecting panel is 0.55" thick x 15.25" x 53", is located on the Y-Y axis, and is fabricated from the same materials and in the same manner as the north and south skin panels. It differs from them in that it attaches to the truss type beams and the north and south skin panels. Attachment angles are provided as part of the beam assembly, and the edges of the panel are reinforced with two 0.062" x 0.75" x 0.75" stiffening angles. The ends of the interconnecting panel heat pipes are normal to the panel, and are clamped to the north and south skin panels for a length of 4.00 inches.

The truss type beams that run diagonally across the upper and lower module frames consists of 0.050" x 1.50" x 5.00" rectangular aluminum alloy cap members (upper and lower) and 0.75" diameter x 0.035" wall-thickness tubes acting as truss diagonal members. These diagonals are bolted at each end to the cap members to allow removal. The two truss beams are joined at the center of the module by gussets riveted to the cap members. Each of the beams is tied to the interconnecting panel by machined fittings.

Eight stainless steel studs are located at the corner posts on 52.0 inch centers. These studs provide a tension tie between the three modules, and are threaded to receive stainless steel self-locking nuts installed at assembly of the three modules.

Communications Module Structure (Figure 4.3.4)

The communications module (CM) structure consists of four corner posts, four frame angles, a honeycomb shelf, four skin panels, an interconnecting honeycomb panel, and an RFI shield that completely covers the module cavity at the communications module/service module interface.

The four corner posts, each 15.25" long, are 0.062" x 0.75" x 0.75", angles machined from aluminum alloy. The lower surfaces of these posts are provided with holes for attachment to the service module. Stainless steel self-locking nuts are provided along the length of the corner posts for attaching the skin panels.

The communications shelf is a 54-inch square, 0.55 inch thick honeycomb panel with 0.025" aluminum alloy face sheets and 3/16" x 0.0015" thick aluminum alloy cells. The shelf is attached to the four frame angles and to the interconnecting panel by stainless steel screws. Where holes in the shelf are required by the antenna elements, the edges are filled with Corfil and machined smooth. Potted inserts are provided in the shelf for mounting all communications equipment and supporting members. Fiberglass blocks are located along the edges of the panel for attachment, and all edges are filled with Corfil and machined.

The four skin panels (north, east, south, and west) are fabricated of 0.55" thick x 16" x 53" aluminum honeycomb. The face sheets are 0.025" thick, and the core is formed of 3/16" x 0.0015" cells.

All skin panels have machined Corfil edges and fiberglass blocks, which are located along their periphery for attachment to the corner posts and frame angles. The north and south panels contain 1/2" square x 49" long heat pipes and potted inserts for attaching the interconnecting panel heat pipes, the thermal control louvers, and the thermal insulating blankets. The east and west panels provide for the attachment of thermal insulating blankets and the Radio Beacon Antenna. The interconnecting honeycomb contains heat pipes spaced in the same manner as the service and experiment modules. The handling provisions for the communication module (CM) alone are similar to those for the experiment module.

4.3.2 REFLECTOR SUPPORT TRUSS

The reflector support truss shown in Figure 4.3-5 consists of eight 2 1/2" diameter tubes with 0.040" wall thickness, symmetrically arranged in a circular A-frame configuration to form the frustrum of a cone. The lower ends of the tubes terminate in four machined fittings that attach to the EVM structure. The upper ends of the tubes terminate in four fittings that attach to the structural hub assembly. The tubes are stabilized at their mid-points by a series of eight 1" diameter tubes connected from the mid-point of each tube to the mid-point of the adjacent tube.

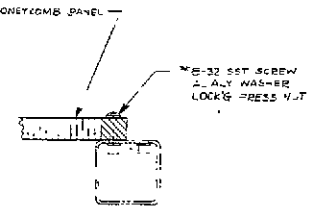
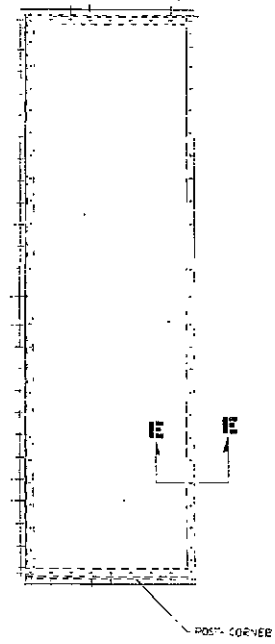
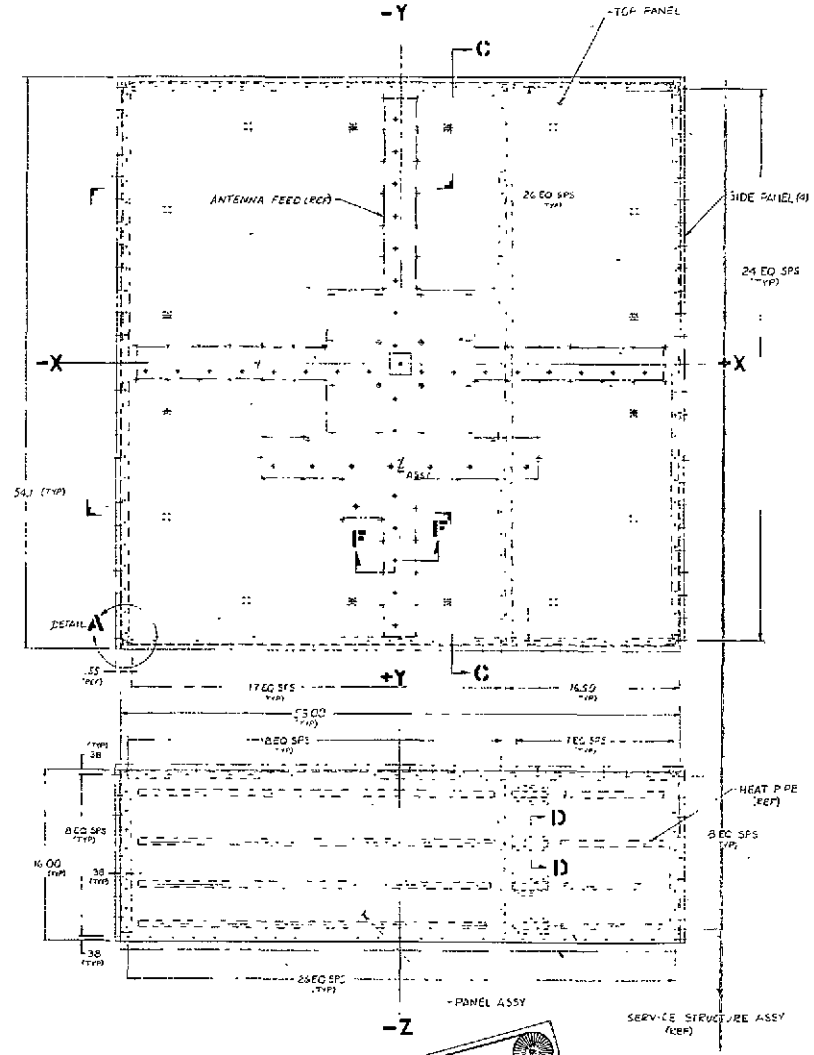
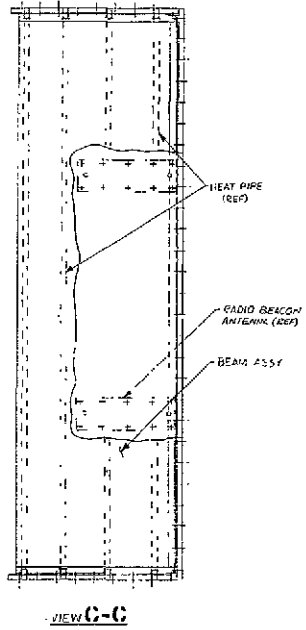
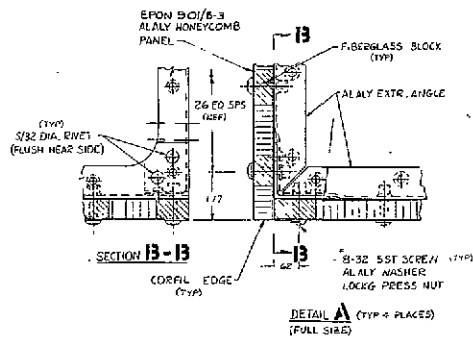
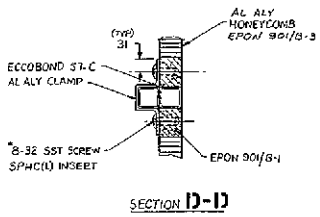
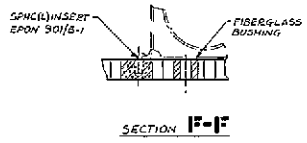
The four fittings that attach to the EVM structure lie on an 84" diameter circle with the center line of the fittings on axes that are at 45° to the spacecraft X and Y axes. The four fittings that attach to the hub are on a 58" diameter circle with the center line of the fittings lying on the spacecraft X and Y axes. The total height of the truss is 169.9 inches.

In addition to the stabilization members connecting the midpoints, there are two non-structural members bridging between four of the truss members. These members are 1.5" diameter tubes and support the orbit control nozzles of the attitude control subsystem. The members are located to position the orbit control jet nozzles' thrust lines through the center of gravity of the deployed spacecraft and pointing along the X and Y axes.

The fittings attaching the truss to the hub assembly consist of 1/8" plates with two sections of tubing located at the skew angles to receive the two truss members that terminate at each fitting. The truss members are permanently attached to the fittings by mechanical fasteners or by bonding. The method of attachment will be selected and proven by test in Phase D.

The fittings attaching the support truss to the EVM are machined fittings with integral brackets that pick up the truss members with method of attachment to be determined as above described.

The stabilization members consist of 1.5" diameter tubes with fittings bonded to each end. Each fitting is a half saddle with flanges, and straddles the main truss member. The fitting on each end mates with the fitting on the adjacent tube, and is attached through the flanges. There are no holes drilled through



Reproduced from
best available copy.

Figure 4.3-4. Structure Assembly -
Communications Module
4-19/4-20

EXPLODED FRAME ?

EXPLODED FRAME 2

NOTES
1. FINAL DIMENSION TO BE DETERMINED LATER

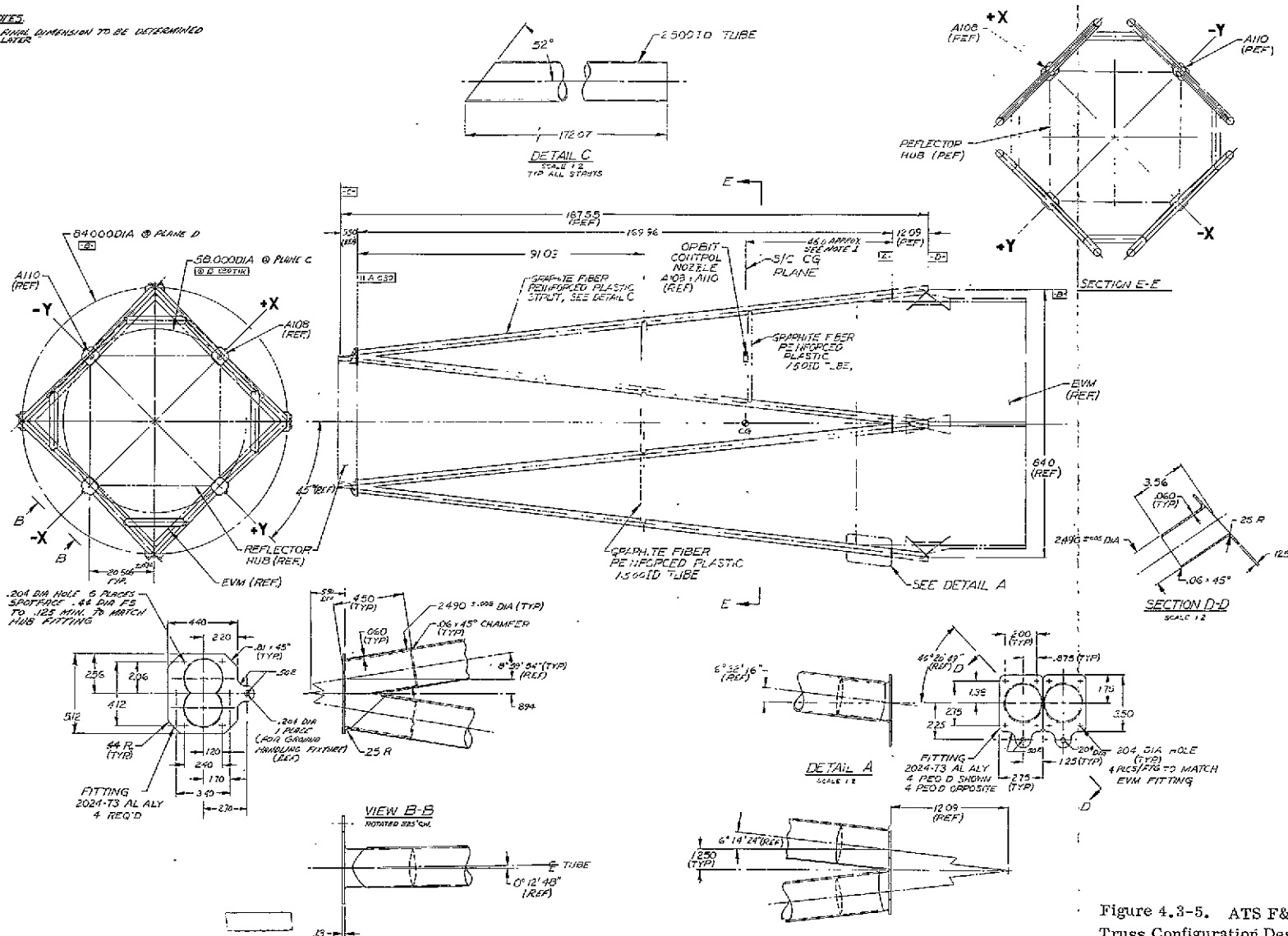


Figure 4.3-5. ATS F&G Reflector Support Truss Configuration Design Layout

the truss members for attaching the stabilizing members. The geometric configuration of the truss members prevents any movement of the stabilizing members with relation to the main truss members.

Similar fittings and fastening methods are used for the tubes supporting the orbit control nozzles.

The material selected for the reflector support truss is Graphite Fiber Reinforced Plastic (GFRP). The tubes are formed of longitudinal layers of the graphite yarn with a layer of glass filament wound around the tube O.D. and bonded integrally to enhance the tube circumferential strength and stiffness. GFRP was selected primarily because of its weight savings as compared to aluminum (45 lbs.). GFRP exhibits little or no distortion when heated or cooled (coefficient of thermal expansion range, $+0.2 \times 10^{-6}$ to -0.4×10^{-6}) thereby minimizing alignment problems between the parabolic reflector and its feed caused by the thermal cycling encountered throughout the ATS mission. Since the GFRP requires additional material in the area of joints and fasteners, thermal stresses induced within and at the interface between the aluminum and GFRP components of the joint have been considered in the design; these stresses are well within the design allowables of all materials so used.

The fittings attaching the reflector support truss to the hub are fabricated from 6061 aluminum. This material was selected primarily for its good welding characteristics and its light weight. The difference in coefficients of thermal expansion of GFRP and aluminum has been considered in the joint design and results in acceptable stress levels in the joint components. The material selected for the fittings attaching the reflector support truss to the EVM is 6061 aluminum.

The fittings at the ends of the stabilization members are made of fiberglass reinforced plastic, selected because of its ease of fabrication and light weight.

4.3.3 STRUCTURAL HUB

The structural hub is shown in Figure 4.3-6. The basic structure is a box 41 inches square and 6 inches deep. The outside frame of the hub is constructed of upper and lower cap angles connected by a sheet metal web, forming a 6" deep channel section around the periphery. The top and bottom of the box are open. The four side beams terminate in four machined fittings, which serve as the attachment for the reflector support truss and for the flex-rib antenna. This design effectively reduces the effect of hub thermal excursions on reflector pointing to an insignificant value. The centroidal axes of the beams intersect at four points coincident with the centerlines of the reflector support truss tubes, thus eliminating any eccentricity at these joints.

The use of the bridging truss structure above the hub to support the solar array support boom hinges and the EME and COGGS experiment packages allows these loads to be introduced into the hub structure in close proximity to the reflector support truss, thus resulting in a minimum weight hub design.

Four hoisting lugs are provided on the upper surface of the hub for handling the hub or the complete spacecraft. These lugs are to be removed prior to launch of the spacecraft.

The material used for all webs, caps, and fittings of the hub structure is 2024 aluminum.

4.3.4 SOLAR ARRAY PANELS

The solar array is shown in Figure 4.3-7. The stowed array forms a cylinder 107.8 inches in diameter and 88.6 inches long, with solar cells on the convex surface only. The array consists of two identical semi-cylinders which stow to form a complete cylinder having a surface area of 208.3 square feet. The semi-cylinder structure is an open gridwork consisting of five semi-cylindrical rings, or formers, spaced along the 88.6 inch dimension. Running transverse to these rings is a channel member at each edge and four Z-sections spaced at 36° intervals. This open framework is supported at its centerline on a tapering open truss beam which serves as a "spine" for the solar array. When attached to the deployment boom, this "spine" is a continuation of the deployment boom.

The depth of the four upper rings is approximately four inches. The bottom ring of each array varies in depth from two and one half inches at one end, increasing to 17.5 inches at its midpoint, then decreasing to approximately four inches at the other end. This lower ring supports the EVM launch support fitting. The vertical load reaction from the launch support fitting is absorbed by a diagonal brace running from the lower ring to the ring above.

The array framework of each semi-cylinder results in a grid with 20 openings of 22 x 34 inches each (Figure 4.3-7). The solar cells are mounted on an aluminum honeycomb panel substrate 0.125" thick with 0.005" face sheets. The modules are attached to the array framework by mechanical fasteners that provide a simple means of replacing damaged modules without requiring removal of the entire solar array panel. There are ten modules on each semi-cylindrical panel, with each module covering two of the openings in the framework grid.

4.3.5 SOLAR ARRAY PANEL SUPPORTING BOOMS (Figure 4.3-8)

The solar array supporting boom is a tubular box truss approximately 185 inches long. It is attached to the boom support structure at the hub by a simple hinge, which allows the boom to fold downward to support the solar array in the stowed position.

The truss is constructed of 1" square tubing welded to form a tapering box section 12" square at the hub end and 8" square where it attaches to the solar panel. The four chords of the truss section are 1" square tubing with 0.065" wall thickness. The diagonal truss members are 1" square tubing with 0.035" wall thickness. The diagonal members of opposite sides of the truss are staggered with respect to each other in order to minimize thermal distortions caused by shadowing.

NOTES:
1. HUB ASSEMBLY DESIGNED FOR ADDITION
OF 485-8068-001 SUPPORT STRUCTURE
FOR STRUCTURAL INTEGRITY.

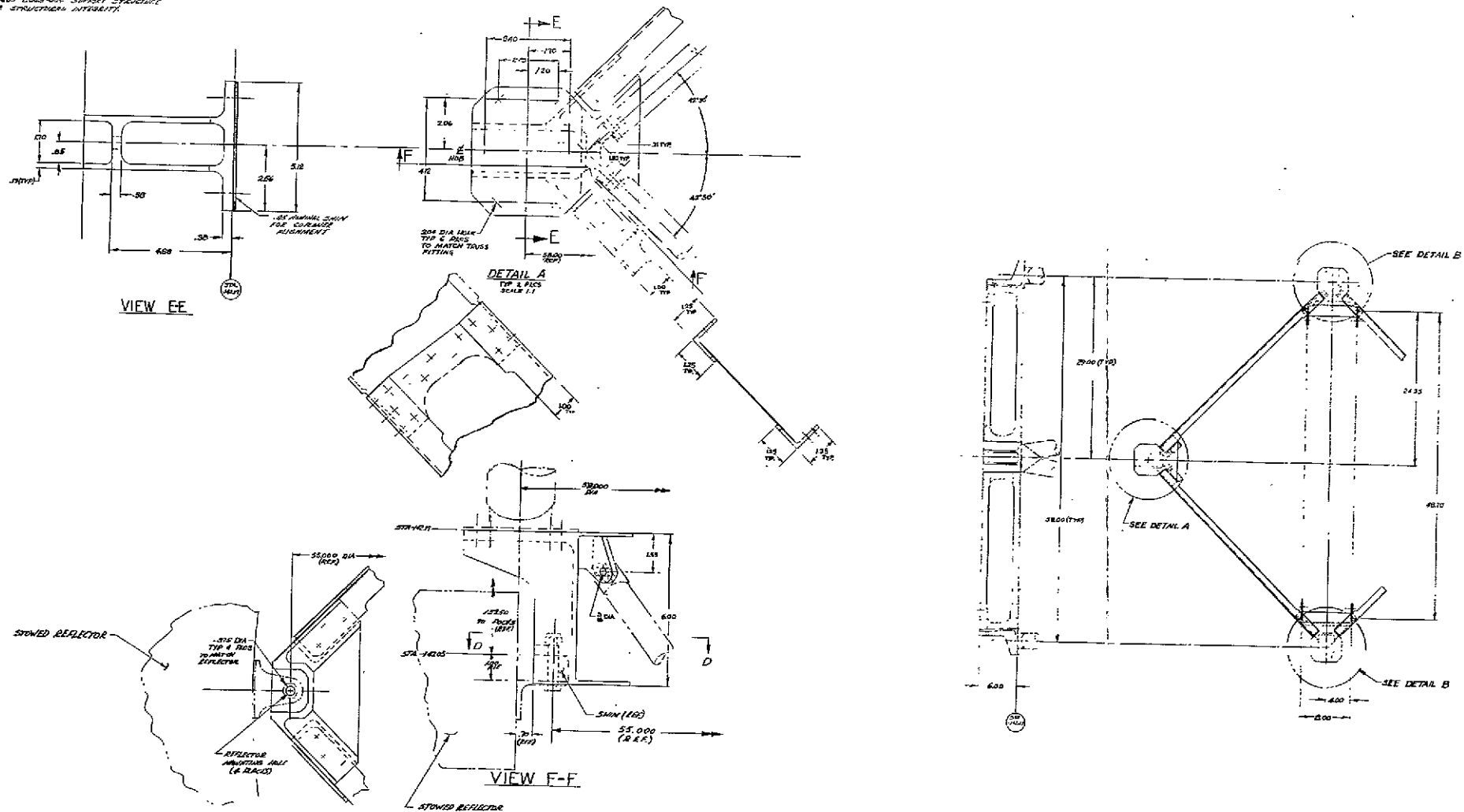


Figure 4.3-6. Hub Assembly (Sheet 1 of 2)

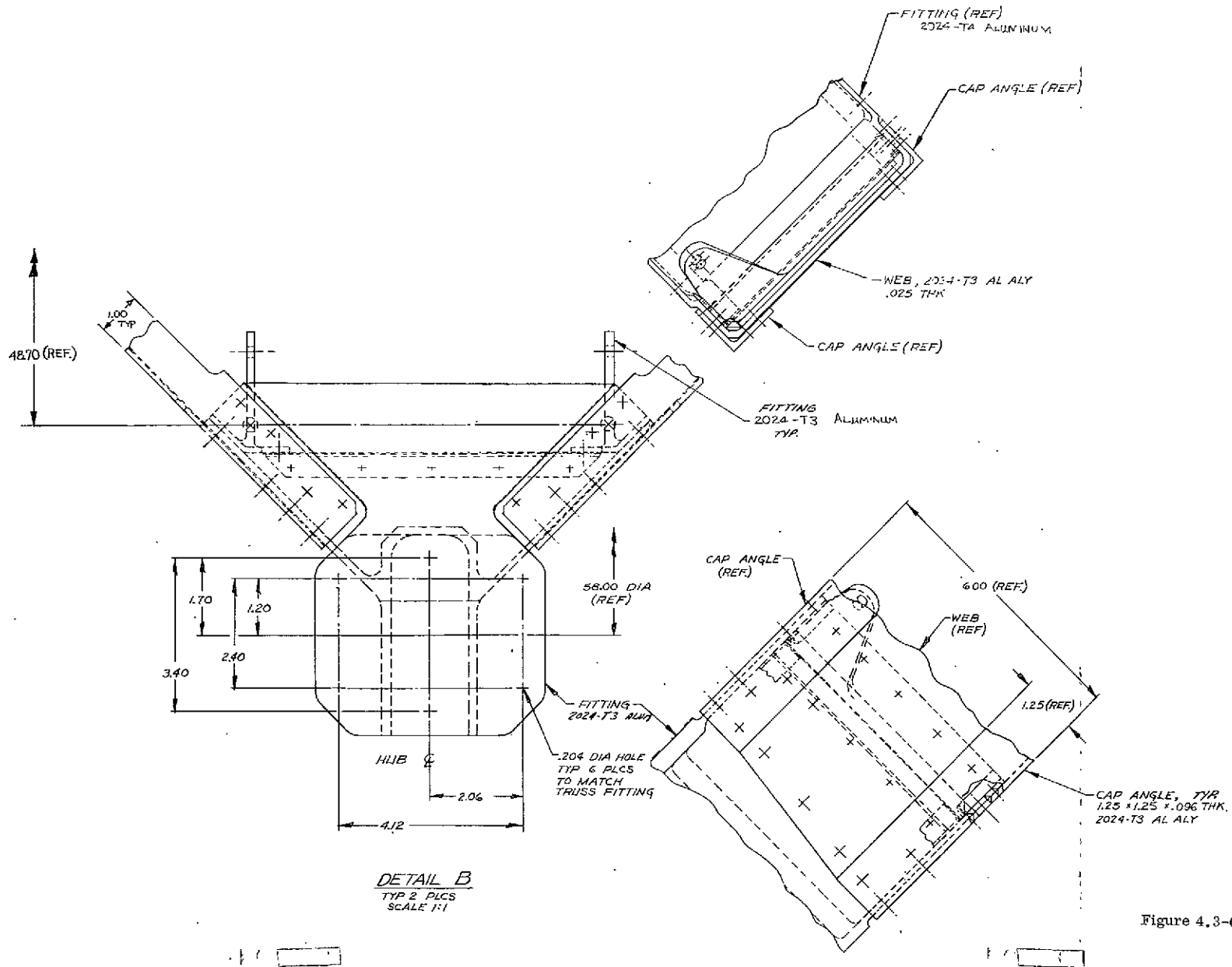
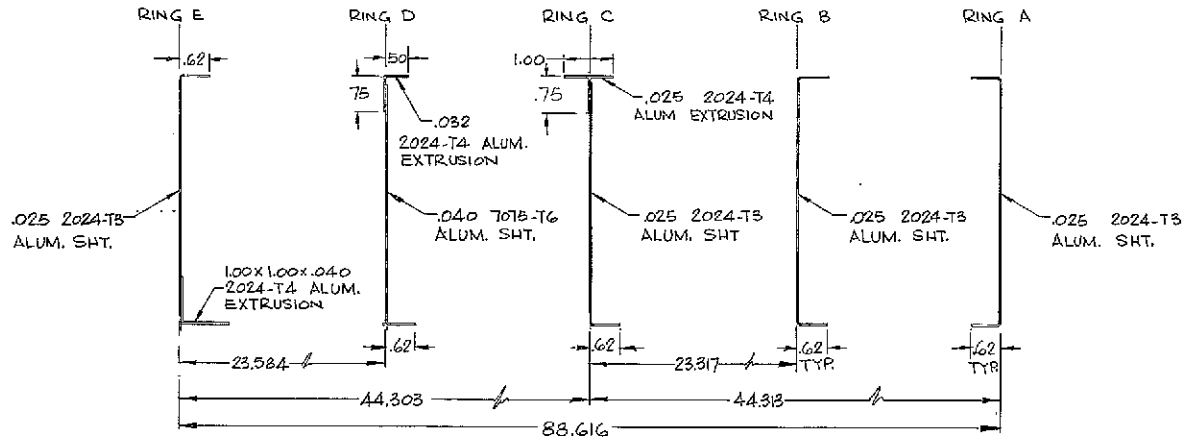
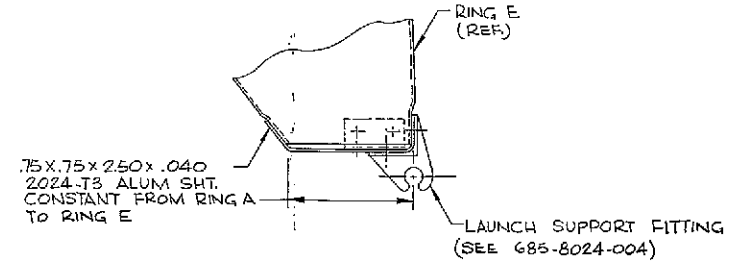


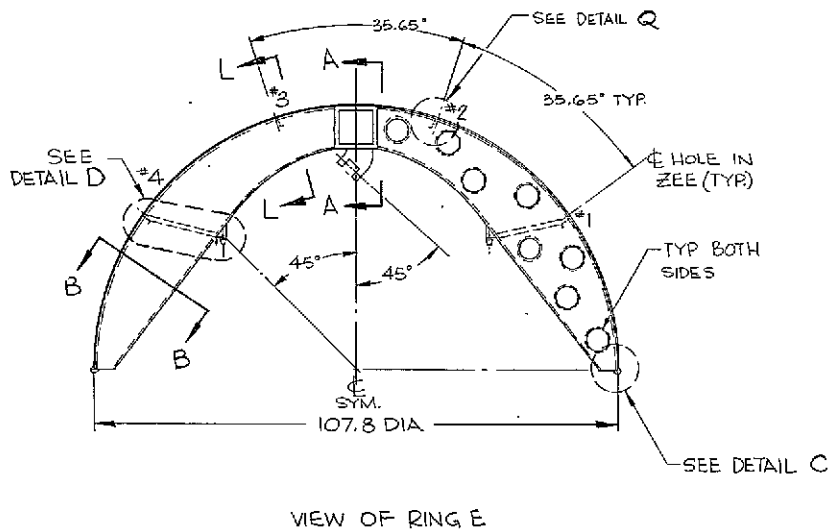
Figure 4.3-6. Hub Assembly (Sheet 2 of 2)



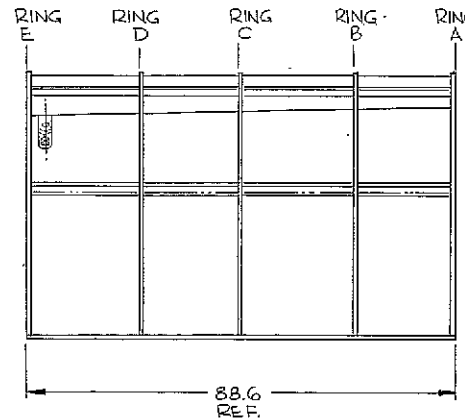
SECTION B-B
NO SCALE
ROTATED 50° C.W.



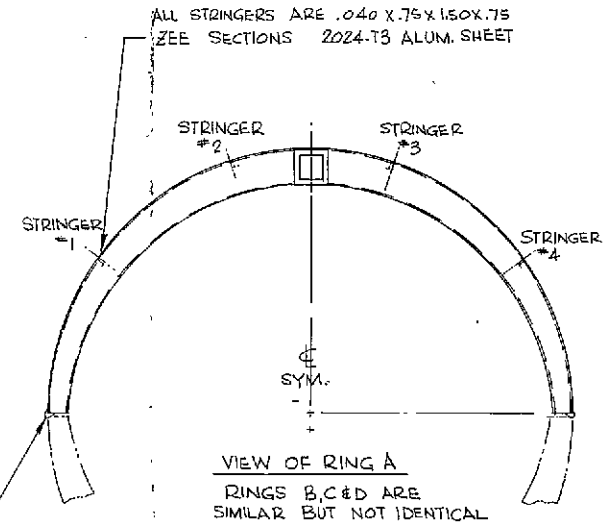
DETAIL C
SCALE = 1/4



VIEW OF RING E



LAUNCH LATCH POINT



VIEW OF RING A
RINGS B,C & D ARE SIMILAR BUT NOT IDENTICAL

Figure 4.3-7. Solar Array
(Sheet 1 of 3)

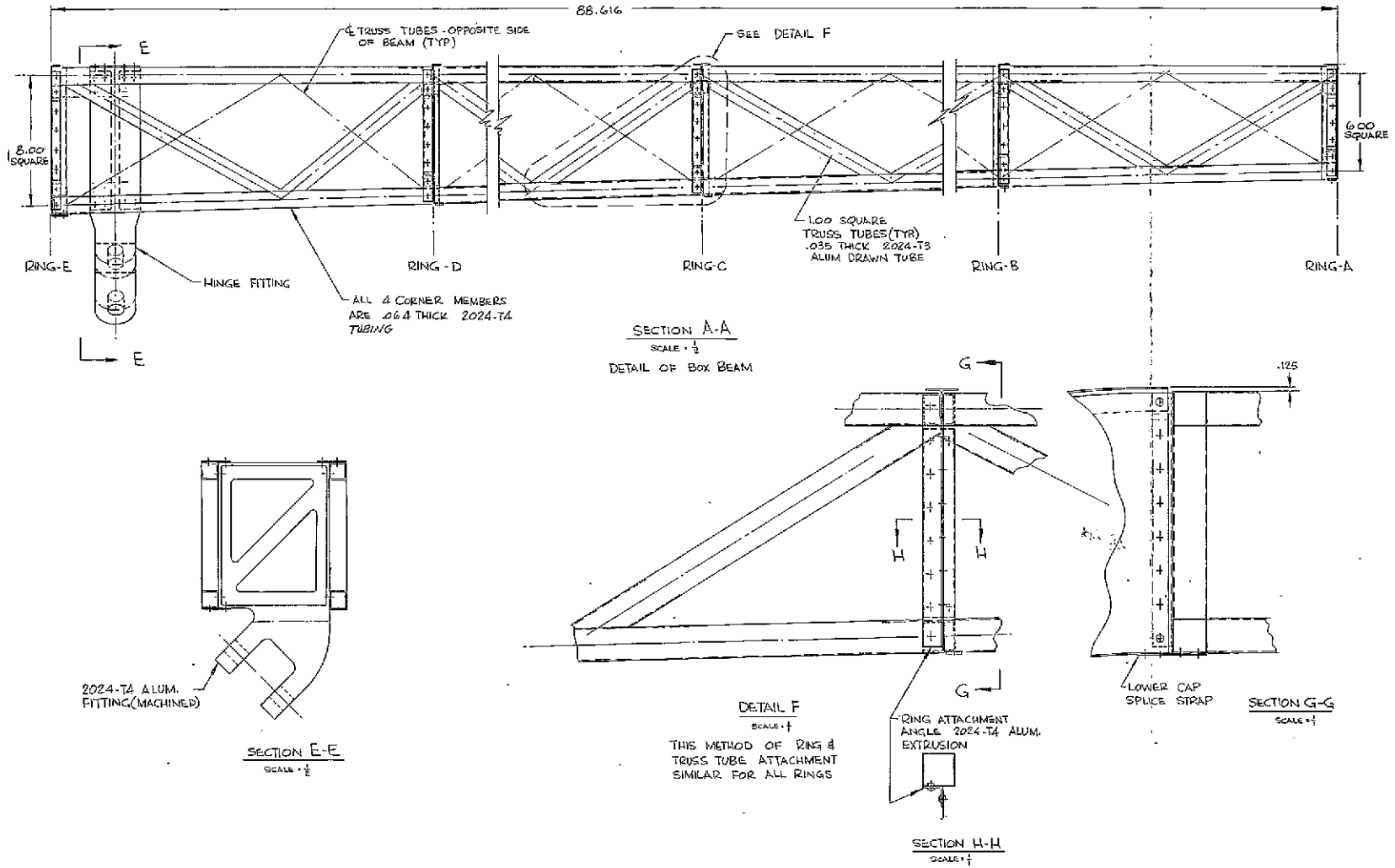
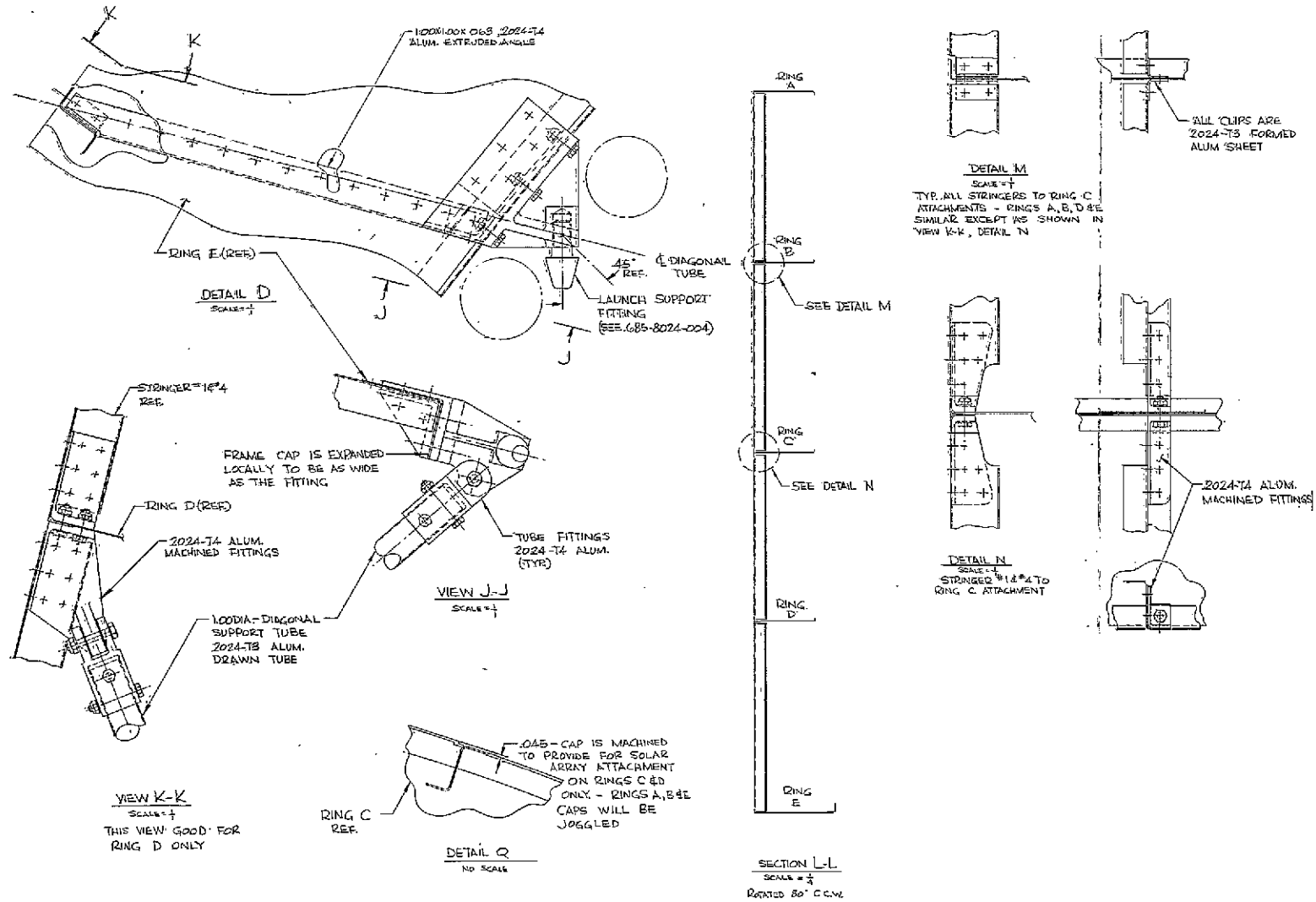


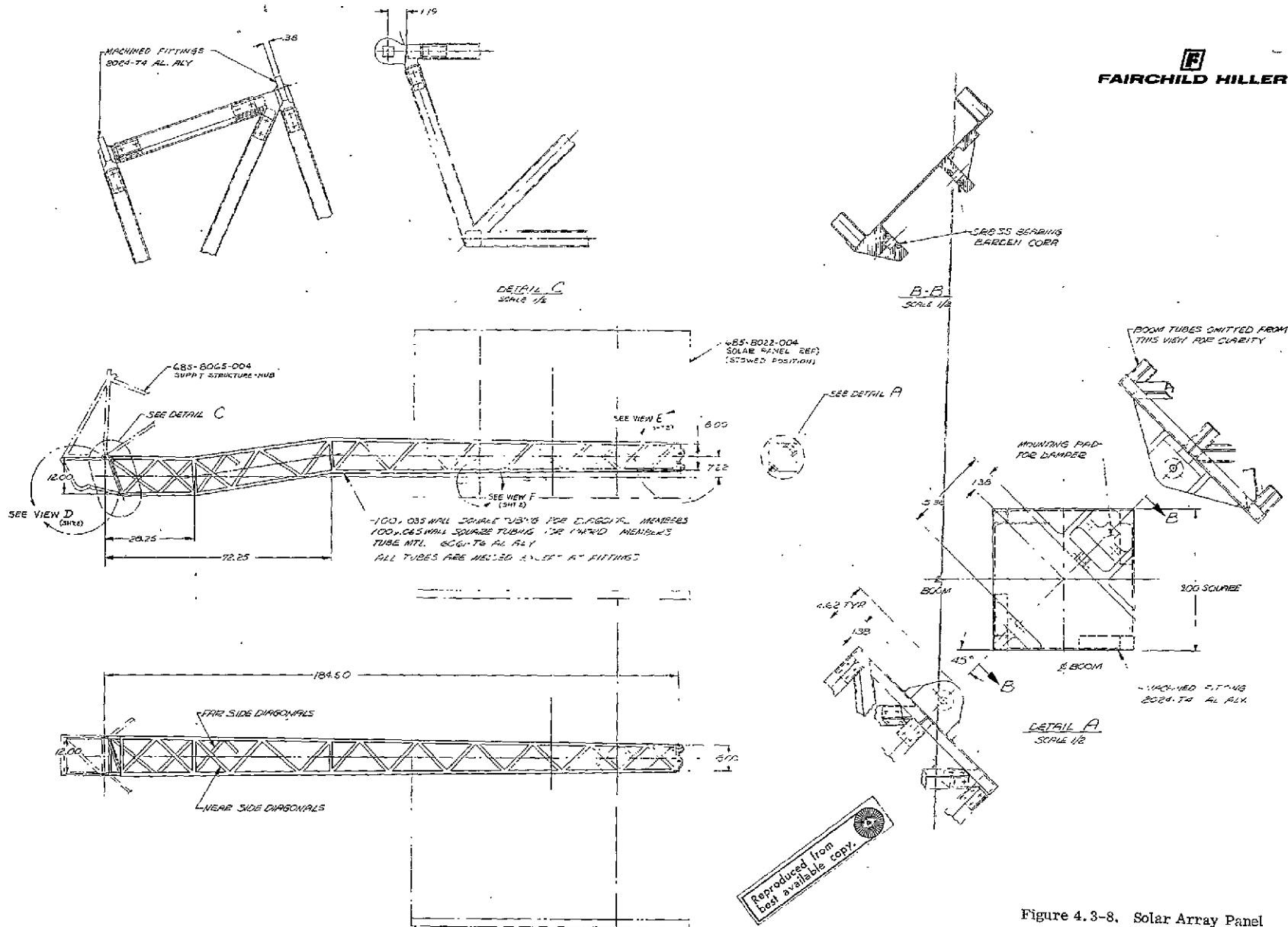
Figure 4.3-7. Solar Array
(Sheet 2 of 3)



FOLDOUT FRAME 1

FOLDOUT FRAME 2 4-33/4-34

Figure 4.3-7. Solar Array
 (Sheet 3 of 3)



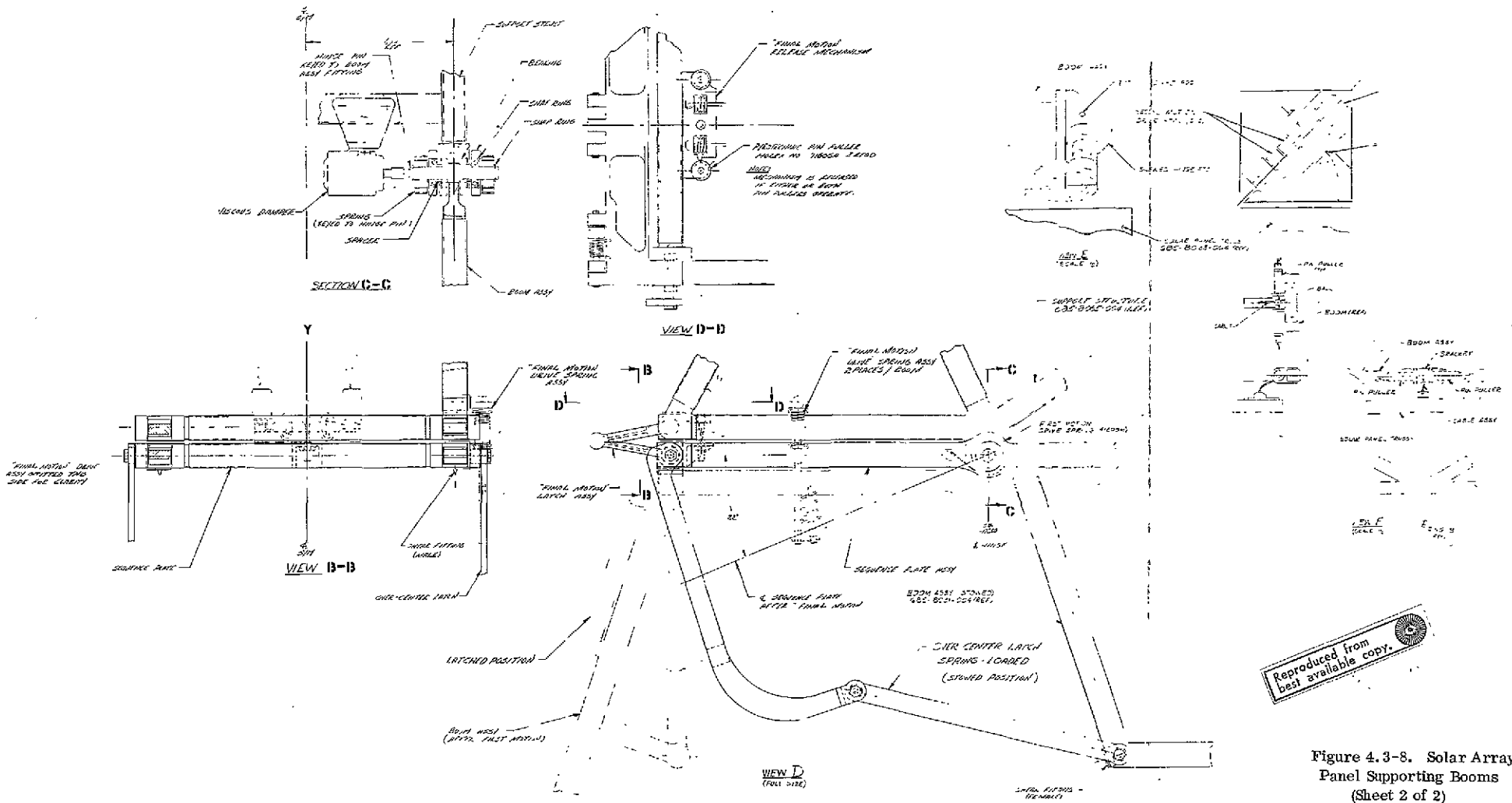
Reproduced from
best available copy.

Figure 4.3-8. Solar Array Panel Supporting Booms (Sheet 1 of 2)

FOLDOUT FRAME 2

4-35/4-36

FOLDOUT FRAME 2



Reproduced from best available copy.

Figure 4.3-8. Solar Array Panel Supporting Booms (Sheet 2 of 2)

FOLDOUT FRAME 7

FOLDOUT FRAME 2

The solar panel is attached to the boom by a 45° skewed hinge that permits the panel to rotate through 180°. During this rotation of the panel, a rotation of 90° about the longitudinal axis of the boom is produced.

4.3.6 ADAPTER, SPACECRAFT/LAUNCH VEHICLE (Figure 4.3-9)

4.3.6.1 Configuration Details and Materials

4.3.6.1.1 Struts

The adapter struts are fabricated from 6061-T6 aluminum alloy tubing, 2.0 inches in diameter, with a wall thickness of 0.058 inches. Clamp attachments to the struts are provided for the separation electrical harness connecting the Titan III C squib firing circuit to the separation system explosive nuts.

4.3.6.1.2 Separation Fittings

These fittings are machined from 6061-T6 aluminum alloy and incorporate one-inch diameter space approved roller bearings, which provide separation alignment control when the spacecraft is released from the adapter. (Mating tracks are described in paragraph 4.3.1 and 4.5.1). Integral with the fitting is the pretempered stainless steel separation spring, a 2024-T3 aluminum alloy cylindrical spring retainer, a Delrin bushing that provides the sliding surface for the spring retainer, and a stainless steel threaded spring stop that contains the spring and retainer after separation. The retaining stud is inserted into the adapter fitting and screws into one pyrotechnically released nut on the reflector support truss fitting. A second pyrotechnically released nut is installed to retain the stud at the opposite end. The adapter fitting is designed with a shoulder that nests within a matching socket provided in the reflector support truss fitting.

TITAN Interface fittings - These fittings mate the adapter to the Titan III C, and are machined from 6061-T6 aluminum alloy. A single bolt tension tie and two shear pins are provided at each of the eight locations.

4.3.6.2 Subsystem Component Interfaces & Layouts

The adapter, consisting of four V-truss elements as described above, contains the separation springs, spacecraft retaining studs and release nuts, and separation pyrotechnic devices. The adapter, on one V-element, has a plate for mounting a squib interface box that houses those relays, relay drivers, and load dividing resistors that belong to the Titan III C power system side of the spacecraft/adapter separation subsystem. Clamps are provided to attach the wiring to the adapter tubes for all wires routed along the adapters. These include not only wiring interconnecting the separation subsystem components, but also the ground power wires from the Titan transtage to the spacecraft. A fly-away disconnect on one adapter leg at the spacecraft interface transfers Titan III C signals to the spacecraft and vice versa for spacecraft initiated backup separation commands. Similarly, on another adapter/spacecraft interface, Titan IIC ground power is routed to the spacecraft.

There is also an attachment point on a leg of one adapter truss, to which the separation event instrumentation switch lanyard is fastened.

4.3.7 FABRICATION AND ACCESSIBILITY EVALUATION

The jig and fixture requirements to fabricate this type of EVM structure have been built before and present no problem. All fabrication processes required for the EVM structural parts, such as joggling of extruded shapes, sheet metal forming required in flat webs and skins, honeycomb bonding, heat pipe forming, louver fabrication, welding, and application of thermal insulating blankets and thermal control coatings are within the hardware capability of the Fairchild Hiller Corporation. Hardware representing these processes, except heat pipe fabrication, have been delivered on RAE, Nimbus, SERT II, Pegasus, OAO, and OGO-E. The development of heat pipes is now in process and the corner design details required in the ATS design have been accomplished and tested.

Accessibility to all system components and experiments after mating of the three structural submodules is accomplished by removal of the EVM east and west side panels. Accessibility to most components mounted in the EVM is good, but there are a few components that will be difficult to reach. Removal of the smaller components can be accomplished from the east or west sides of the EVM. Removal of the largest components will require separation of the affected modules. Accessibility to the experiment packages is good.

4.3.8 EVM VENTING

The venting area required for the EVM is four square inches to ensure a pressure differential that will not exceed 1 psi.

Ascent venting will occur through the EVM structure around the components that protrude through the skin and at the interfaces of the basic structural components. A 0.010" clearance between the skin panels and these components will provide the required venting area. Air venting through the structure that is covered by thermal blankets is provided by bleeding through the blankets at the stand-off locations. Venting of the thermal blankets is accomplished by cutting scallops in the blanket edges, allowing air trapped between insulation layers to flow to the edges, then out to space at the stand-off locations.

4.4 EQUIPMENT LOCATION

4.4.1 SUBSYSTEM COMPONENT LAYOUT (Figures 4.4-1, -2, -3, -4)

The majority of the system components are located in the service and communications modules, separating them from the experiments in order to allow alteration or changes of experiments without major impact on the system packaging.

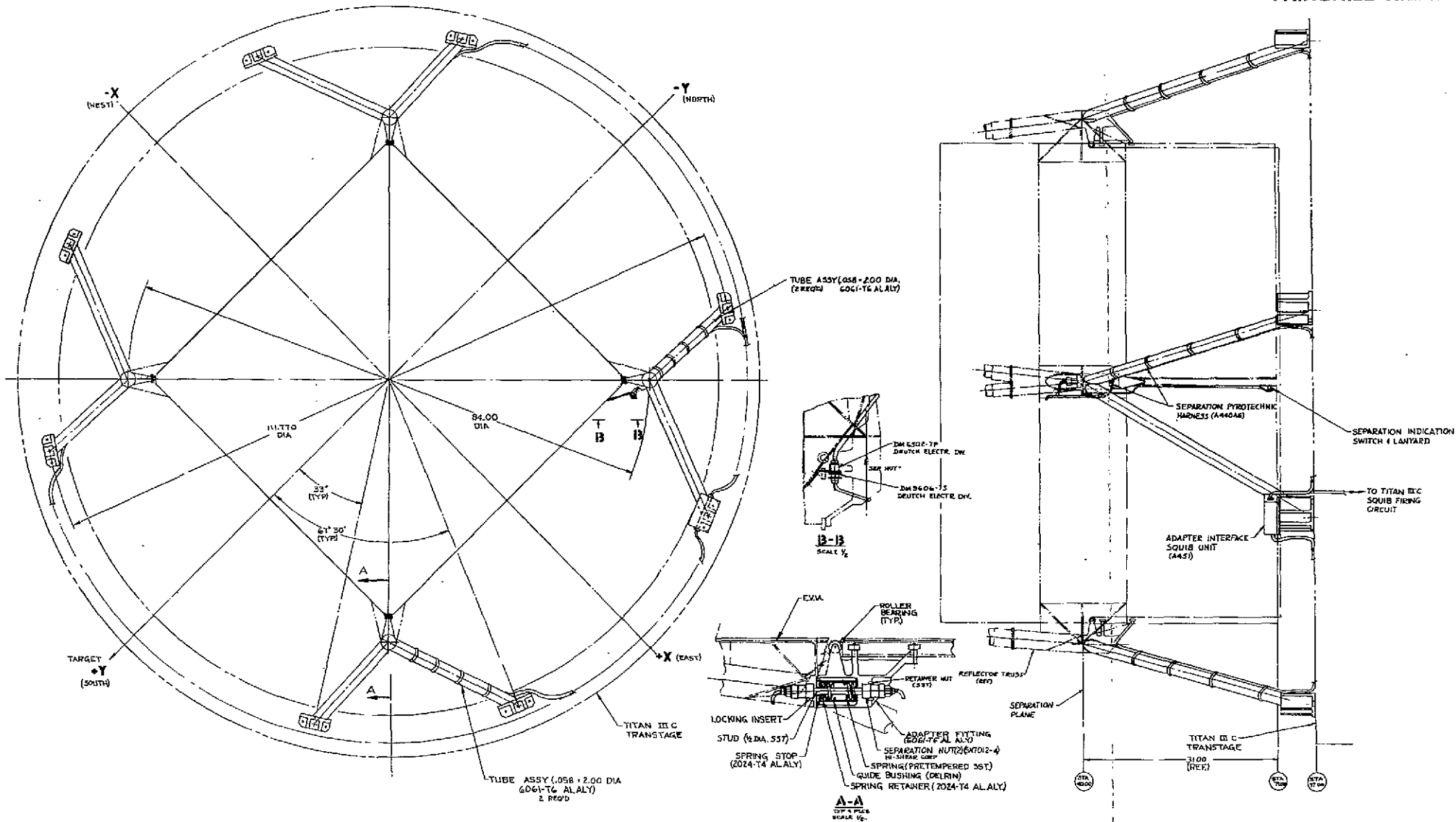


Figure 4.3-9. ATS F&G Adapter- Configuration Layout (FH 685-8025-004).

4-41/4-42

EOLDOUT FRAME 1

EOLDOUT FRAME 2

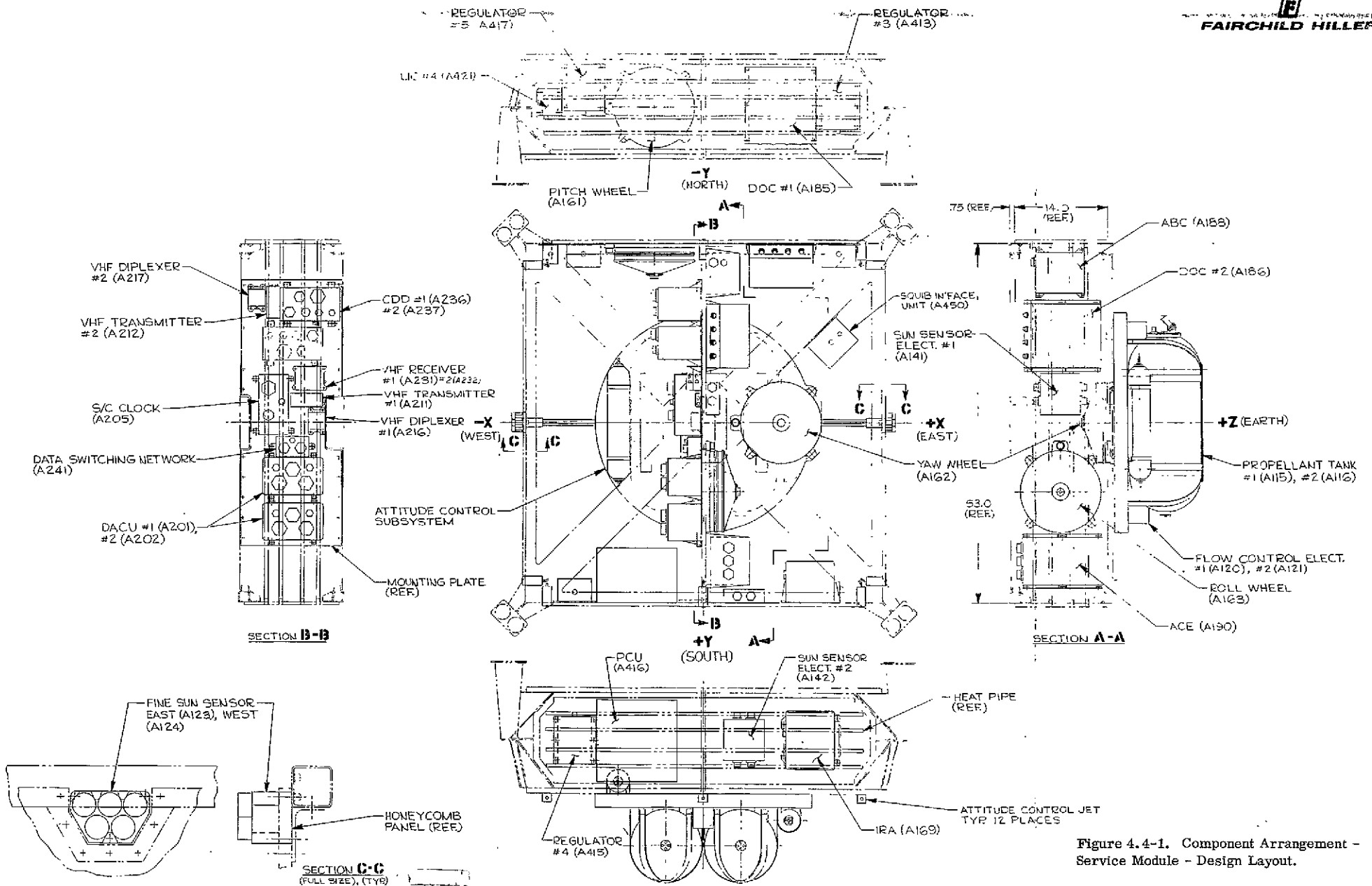


Figure 4.4-1. Component Arrangement - Service Module - Design Layout.

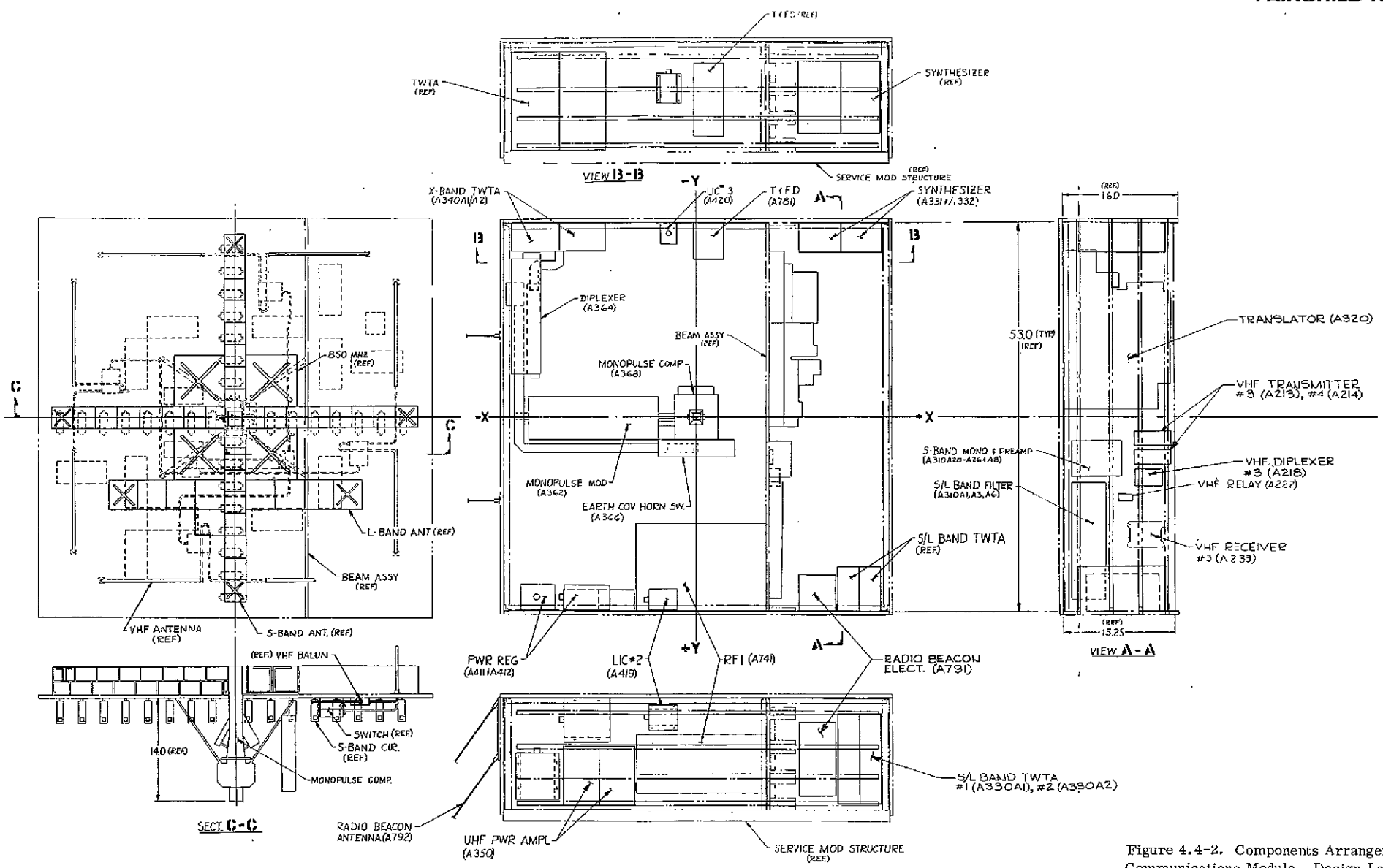


Figure 4.4-2. Components Arrangement - Communications Module - Design Layout

SOLDOUT FRAME 1

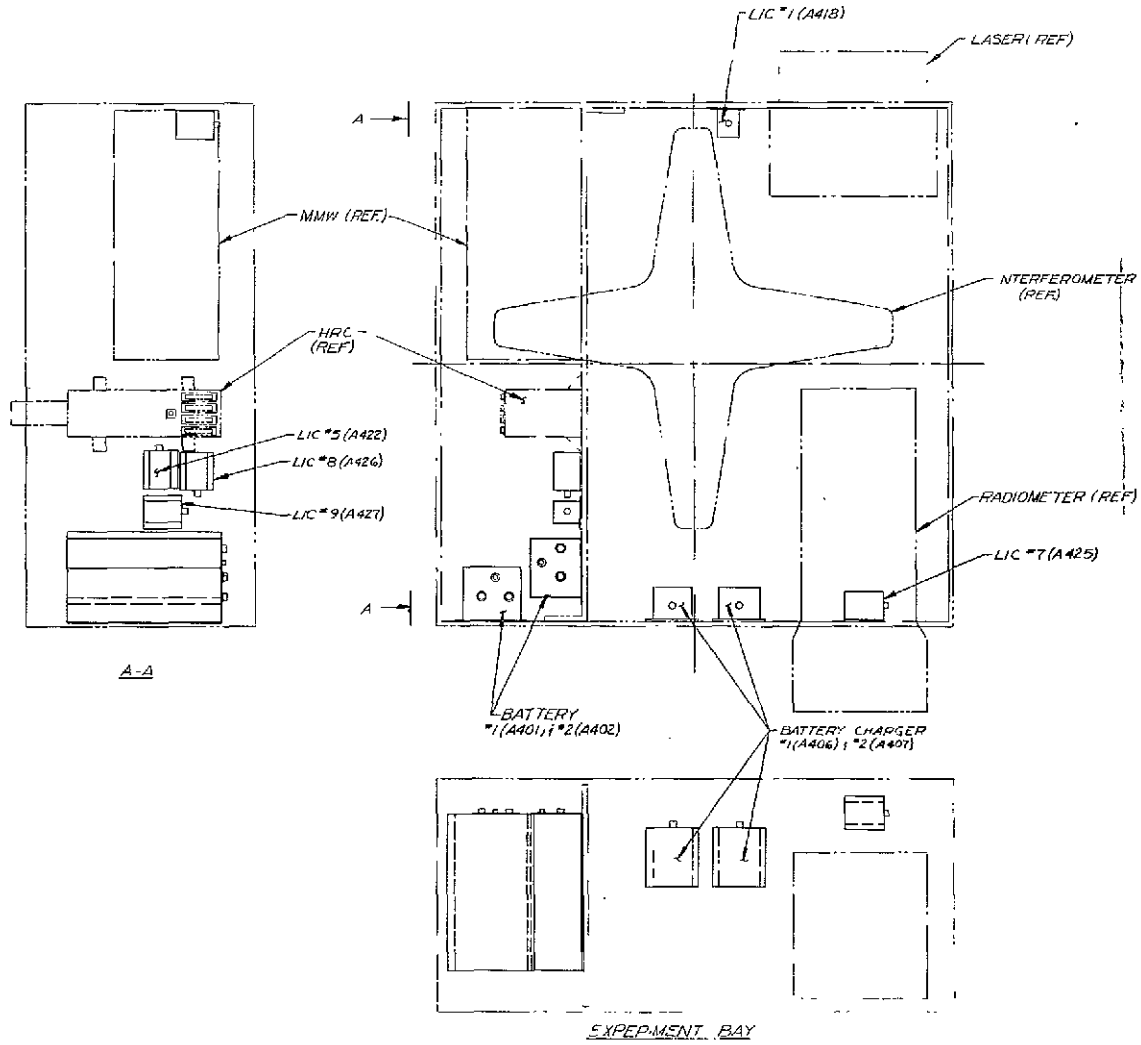
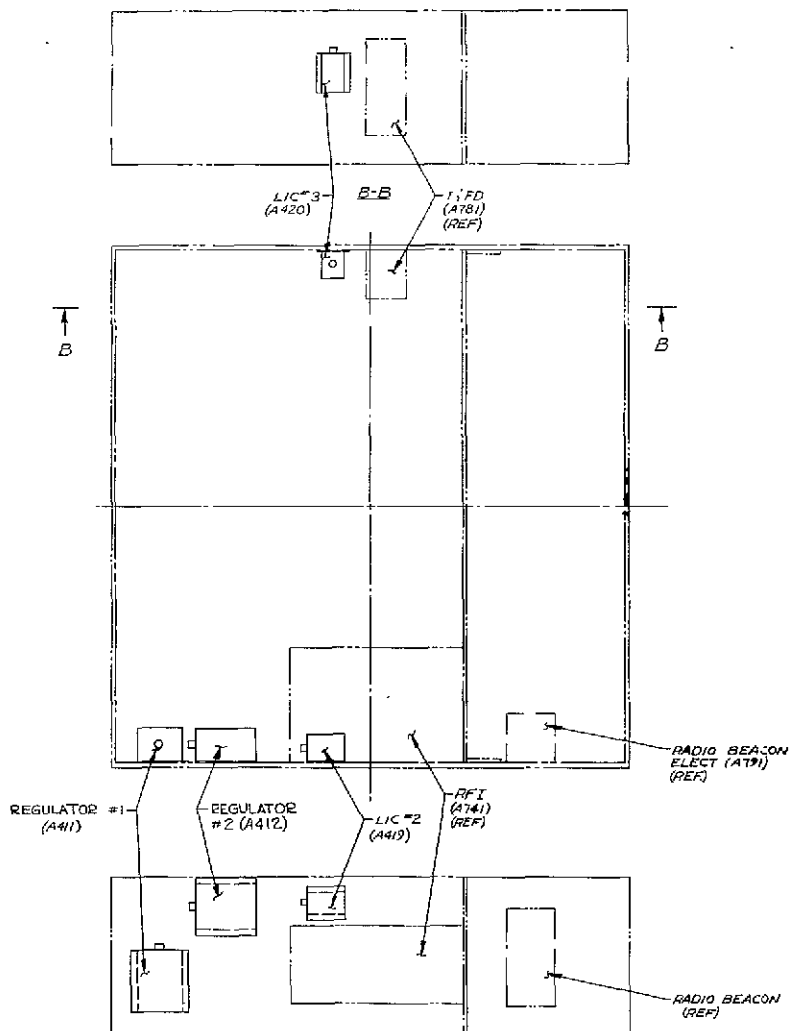
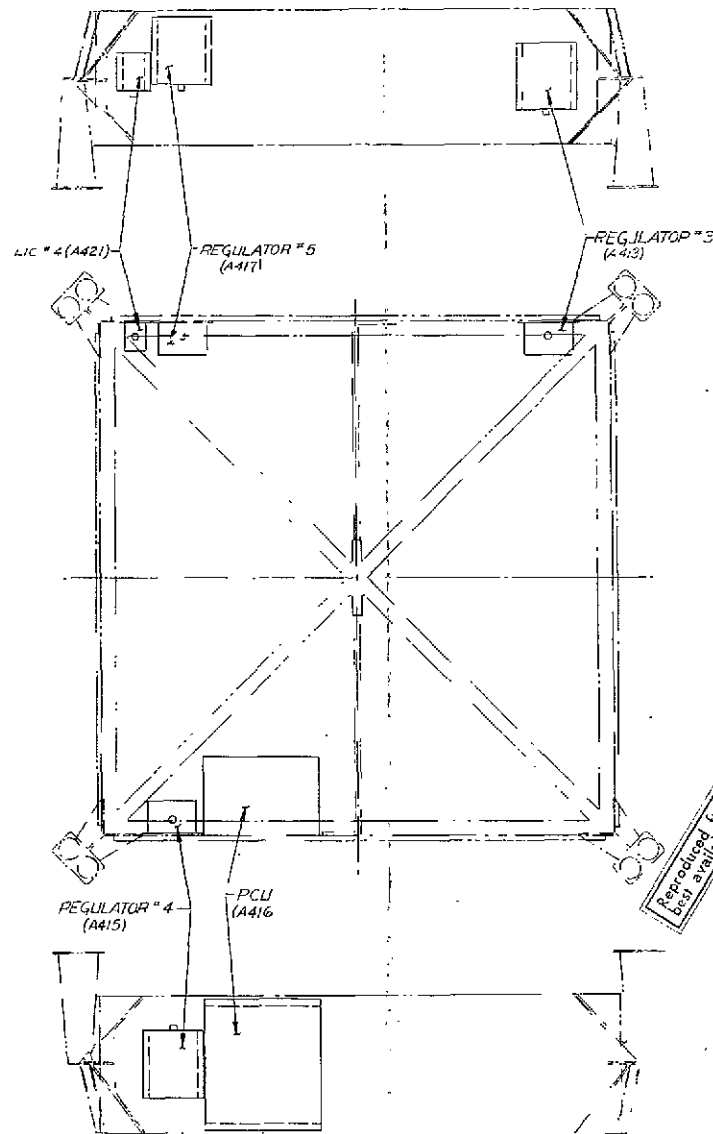


Figure 4.4-3. ATS F&G Power Subsystem Installation Design Layout (Sheet 1 of 2)

4-47/4-48



COMMUNICATIONS MODULE



SERVICE MODULE

Figure 4.4-3. ATS F&G Power Subsystem Installation Design Layout (Sheet 2 of 2)

FOLDOUT FRAME 1

FOLDOUT FRAME 2

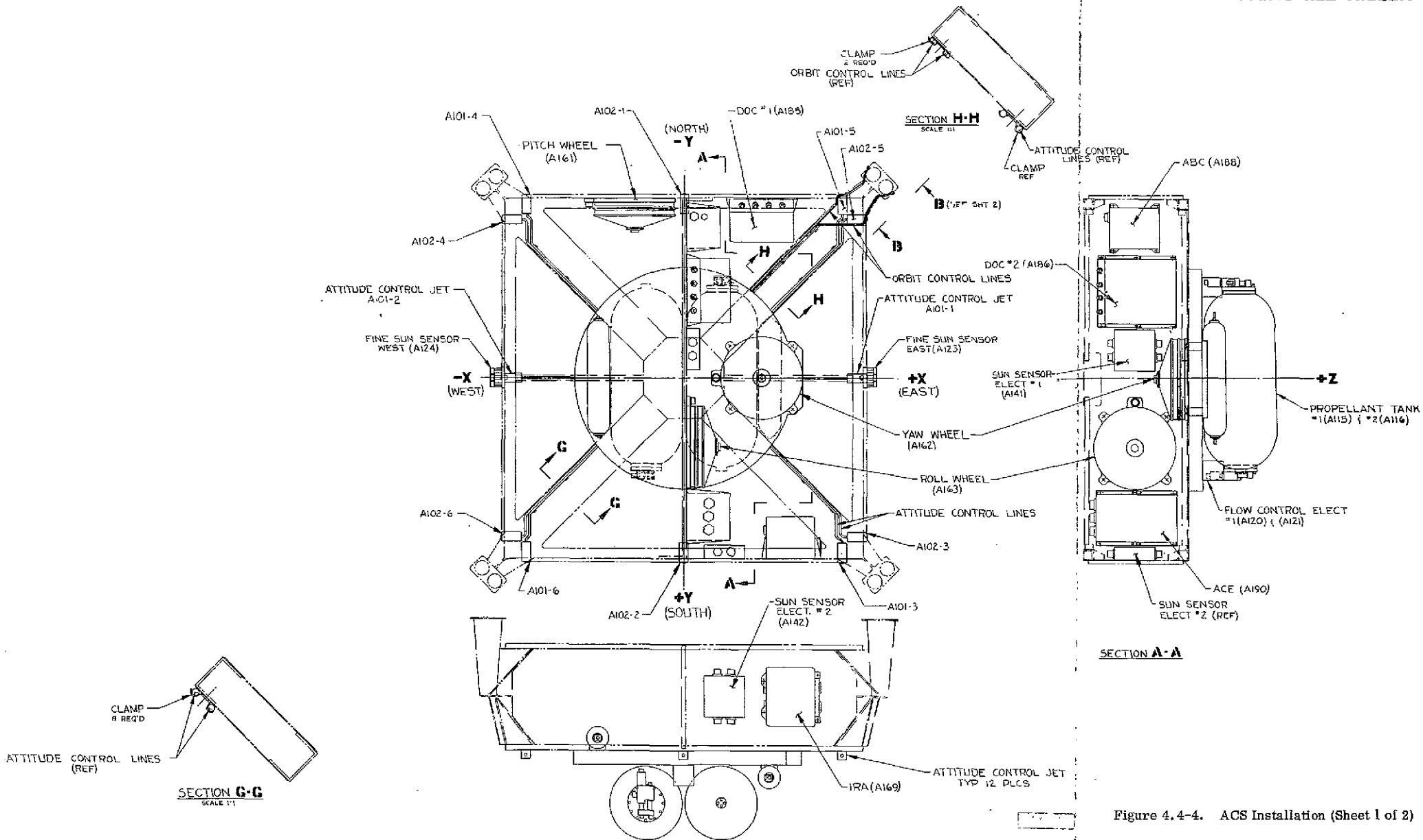
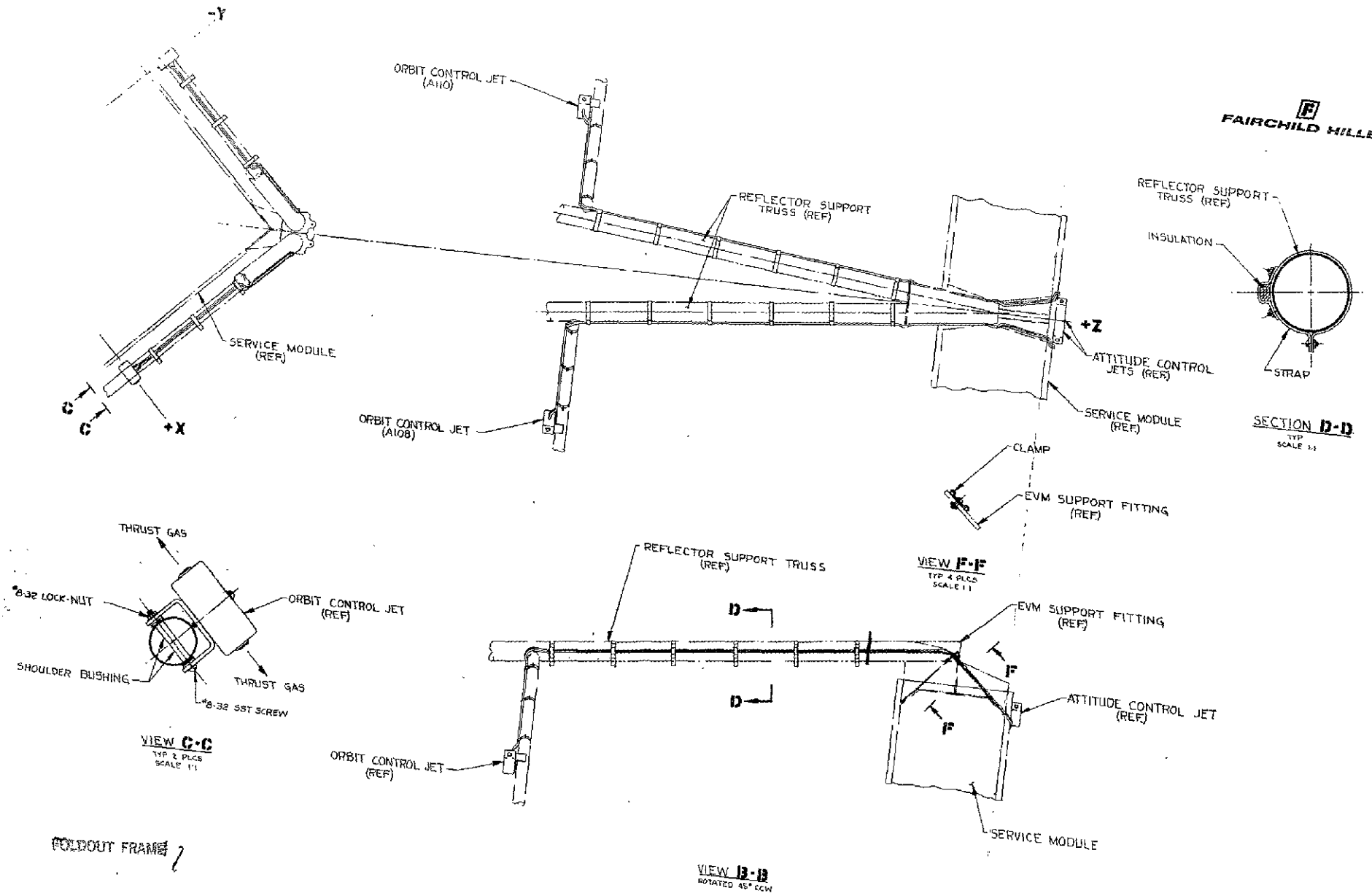


Figure 4.4-4. ACS Installation (Sheet 1 of 2)

FOLDOUT FRAME 1

FOLDOUT FRAME 2



FOLDOUT FRAME 2

Figure 4.4-4. ACS Installation (Sheet 2 of 2)

4-53/4-54

FOLDOUT FRAME 2

The auxiliary propulsion system (APS) consists of ammonia storage tanks, altitude control and orbit control jets, valves, interconnecting piping, and associated components and mounting plates. The APS is assembled as an integral unit in a clean room and essentially sealed. It is never opened thereafter, thus insuring that the system remains uncontaminated. For these reasons, the APS installation in the EVM is designed to be accomplished without disconnecting any of the lines.

The communications subsystem is mounted within the CM together with related experiments (RFI, T&FD, Radio Beacon). The only exception is the earth coverage horn which is mounted in the EM and connected to the communication subsystem in the CM by a wave guide that passes through the SM. The prime focus feed assembly radiating elements are installed on the outside surface of the communications CM module face that views the parabolic reflector and interconnected to the interior of the EVM by local coaxial feed-throughs. The basic structural surface and super insulation covering provides the necessary ground planes for the radiating elements (other than the cavity backed elements which do not require external ground planes).

Concentrating all communications equipment in the CM permits total installation and testing with subsequent EVM assembly to be accomplished without having to disconnect any of the intersystem wiring.

All system components have been located with consideration for thermal requirements, mass balance, harness routing, and accessibility requirements. Electrical connections between the three modules is provided by bulkhead connectors at module interfaces, or, in some cases, by extended harnesses between modules.

The north and south skin panels provide mounting surfaces for the components that have the highest thermal dissipation requirements. These components are the UHF power amplifiers, S/L-band power amplifiers, X-Band power amplifiers, inertial reference assembly, and the analog back-up controller (ABC). Components with lower thermal dissipation requirements have been located on the north to south transverse beam assembly. These components include such items as the digital operational controller (DOC), command decoders, clock and duplexers.

All of these components have been located to present a thermally balanced design, based on the component dissipations and their operational modes. Components are mounted in a manner to span across as many heat pipes as possible.

Accessibility for component removal, bolt pattern compatibility with heat pipes, and electrical connection with the harness have also been considered in the component locations. Accessibility with the east and west skins removed is good for all components except the Polaris sensors and their electronics packages, the actuator control electronics, and the ABC.

The interferometer places a special requirement on the structure in that a ground plane must be provided which exhibits flatness tolerance of less than $\lambda/16$ in a critical area around each horn. This desired critical area is illustrated by the dotted ellipses in Figure 4.4-5; acceptable area is roughly bounded by dimensions 60% of those shown. The ground plane is formed by a honeycomb core sandwich panel, 0.125 inches thick with 0.005 inch aluminum face sheets. The panel covers the entire earth viewing surface of the EVM, contains viewing ports as required by earth viewing sensors, and acts as a retaining surface for thermal control super insulation which is placed in the one inch deep cavity formed by the ground plane and the structural surface.

4.4.2 EXPERIMENT LAYOUTS (Figure 4.4-5)

All experiments except the Radio beacon, RFI, and T&FD located in the EVM are mounted on the honeycomb skin panels of the experiment module. The experiments have been located on these panels with the same design considerations as those used to mount the spacecraft system components. Additional factors considered were their alignment requirements and their isolation separation from vibration and shock loads that will be transmitted through the adapter to the EVM support fittings. These experiments have also been located in accordance with their thermal dissipation requirements and represent a thermally balanced design.

The radiometer, laser, and millimeter wave experiments have been located on the north and south skin panels. Spacecraft system components mounted in the experiment module include the batteries and their chargers, the interferometer array and electronics unit, earth sensors, and the Polaris sensors. These components are located in this module due to their size or earth viewing requirements.

The interferometer array and the earth sensors are mounted on the honeycomb plate that is attached to the interferometer support frame structure.

The Auxiliary Propulsion System is mounted on the lower surface of the service module above the interferometer array. This location of the propulsion system allows it to be bench assembled and installed as an integral system, and makes maximum use of the available module volume. All valves, jets (including orbit control jets located on the reflector support truss) fill, purge, and interconnecting lines remain intact during installation.

4.4.3 HUB MOUNTED EQUIPMENT

The equipment installed on the structural hub includes the EME and COGGS experiments, and two coarse sun sensors with associated electronics package (Figure 4.4-6). Electrical harnesses for this equipment, solar array deployment harnesses, and solar array power collection harnesses are also routed through the hub structure.

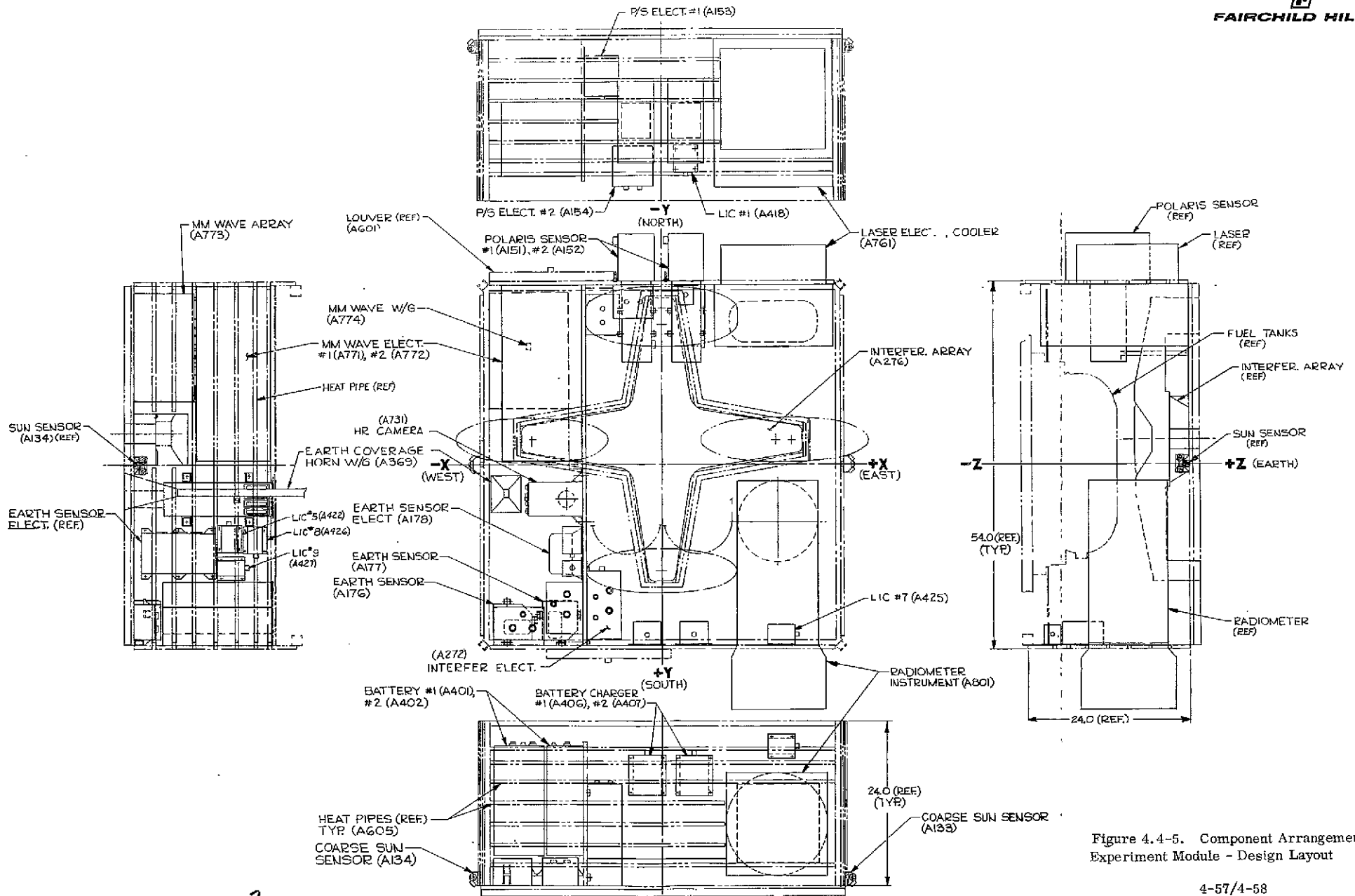


Figure 4.4-5. Component Arrangement - Experiment Module - Design Layout

4-57/4-58

FOLDOUT FRAME 7

FOLDOUT FRAME 2

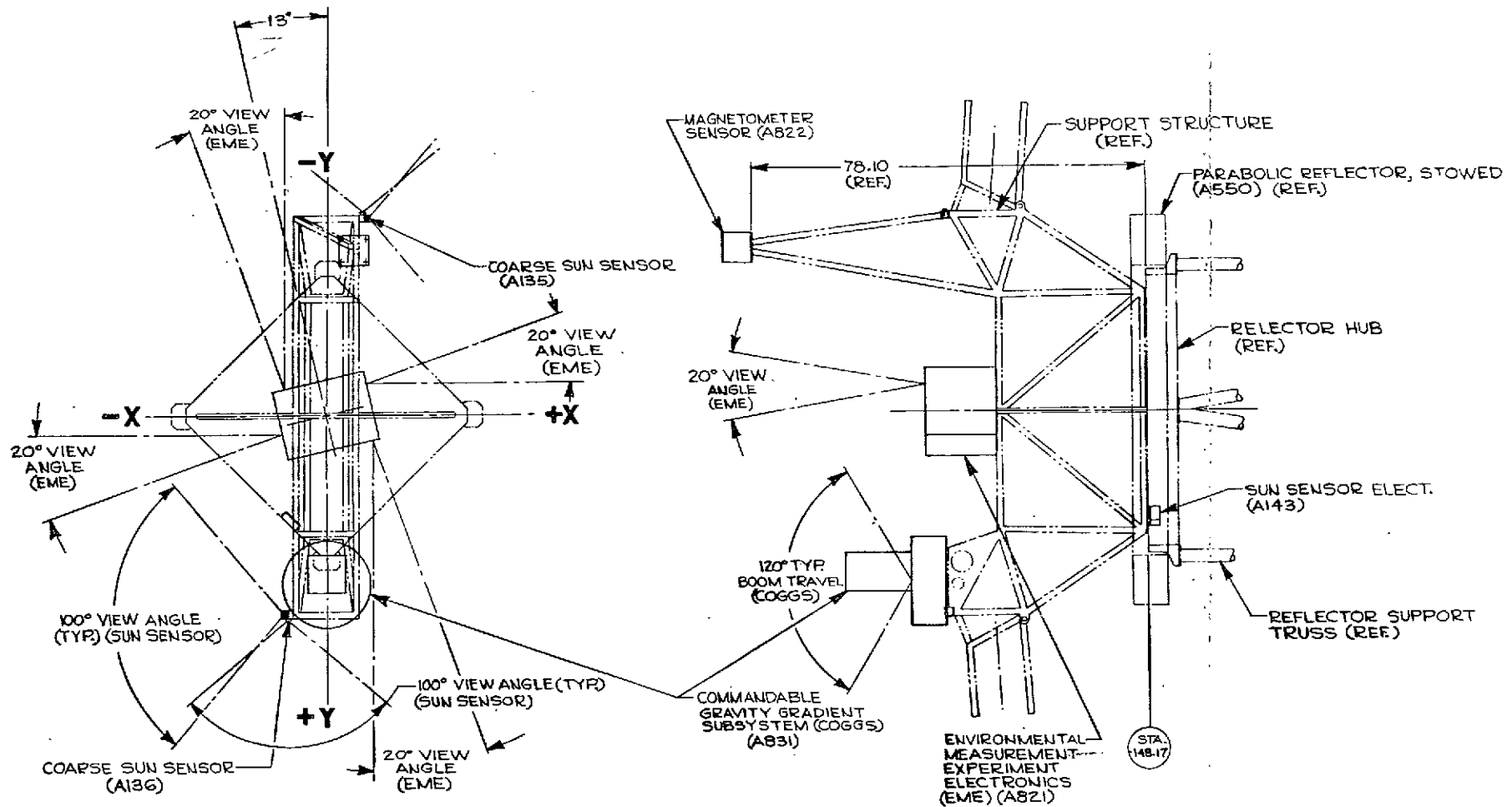


Figure 4.4-6 Hub Equipment Layout
(Proposed Configuration-Small EME)

FOLDOUT FRAME 1

FOLDOUT FRAME 2

Those components requiring special alignment are located within $\pm 0.007''$ of true position, and with an angular tolerance of ± 0.1 degree.

Alignment within these tolerances will be attained by using special close tolerance jigs and fixtures for assembly of the basic structure and drilling of attachment fastener holes in the structure. If the required tolerance is not attained for a special installation, shims will be employed at the attachment points. Thermal conduction between component base and structure will be insured by using thermal conducting grease for very thin gaps. If major shimming is required, a special tapered shim covering the entire mounting interface will be used. The philosophy of using shims and hard mounting for alignment rather than mechanically adjustable mountings insures that, once established, the alignment will not change.

The third alignment provision to be applied to those system components where such is applicable, is the use of correction signals that are determined at installation and stored in the DOC.

The most critical system component to be aligned is the interferometer array, which requires an angular mechanical alignment of 0.1 degree. This array is aligned relative to an optical cube, representing the spacecraft axis, that is mounted on the array mounting plate. The alignment of the interferometer array electrical axis will be optically measured relative to the cube to within 0.01 of a degree. All other components requiring critical alignment are provided with optical mirrors, and are aligned relative to the array (spacecraft axis) by using the optical cube as a reference.

4.4.4 ALIGNMENT PROVISIONS

Three methods of alignment have been provided in the EVM for all components.

Those components that do not require accurate alignment are located within normal good manufacturing tolerances. These components are located within $\pm 0.014''$ of true position with an angular tolerance of ± 0.5 degree.

4.5 SPACECRAFT/ADAPTER SEPARATION SUBSYSTEM

4.5.1 CONFIGURATION DESCRIPTION

The adapter is attached to the fittings at the corners of the service module by 0.5 inch diameter studs with pyrotechnically released nuts on each end. The space qualified explosive nuts selected for this application are Hi Shear No. SN 7012-4.

The basic configuration of the adapter/spacecraft and the separation plane places the pyrotechnic release devices in close proximity to the hard structure of the EVM. Analytical determination of the shock magnitude at any given point within a complex structure, such as the EVM, is extremely difficult. In the

final analysis, the structure must be instrumented and the magnitudes of the shock determined at the various locations by test. If this system exhibits unacceptable shock levels at the various component locations in the EVM, sufficient time remains in the overall program to initiate a recovery plan to reduce shock to an acceptable level. Prior to initiating such a program, however, efforts will be made to modify the EVM structural design to reduce the shock to an acceptable level using the space qualified fracturing nut design approach.

The mechanical structural separation system consists of the adapter separation fittings, the reflector truss fittings, studs with separation nuts on each end, separation spring, spring retainers, guide bushings, spring stops, and nut and stud retainers. The electrical initiation characteristics of the nut squibs are:

- 1 amp @ 1 watt --- no fire
- 5 amps ---- all fire

The separation fittings are aluminum alloy members machined to form a shoulder and socket arrangement, and are designed to take all shear and compressive loads. The stud and explosive nuts accept only tensile loads in this arrangement. The stud fits within a stainless steel separation spring, which is protected and retained by an aluminum cylindrical "piston" that strikes against a Delrin guide bushing. The stroke of the spring and piston is limited by a stop that is screwed into the adapter separation fitting.

The release electrical system is designed to fire, and thus release, the nuts on both ends of the studs. To prevent the stud from floating away, a low strength retaining pin affixes the stud to the spacecraft fitting. Strength of the retainer is very much less than the separation spring force available and does not constitute a danger to separation.

The separation event mechanical motion consists of spring forces acting throughout the first 3 inches of travel during which time a relative separation velocity of 3 ft/second is attained. This is followed by a non-powered but guided glide of the EVM out of the adapter as the rollers on the adapter move along the corner tracks of the EVM. The design, in this manner, establishes a relative separation velocity between spacecraft and adapter/launch vehicle with a minimum of relative rotational disturbances. Tip-off rates are constrained within 0.05 degree/second.

Upon release of the four retaining studs, the spacecraft is forced away from the adapter along the spacecraft/launch vehicle centerline by the four balanced separation springs. Two of the three guide rollers on each adapter V-truss are so oriented as to react at the truss any tip-off motions components lying in the plane of the V-truss. The third roller transmits separation force inboard radial reactions to the EVM for reaction by similar forces introduced by the separation spring located diametrically opposite.

In the unlikely event that a double failure occurs in the separation subsystem and one stud is not released, the shape of the guide rail tracks will retain the guide rollers within the track even though some tip-off motion and misalignment of spacecraft/launch vehicle centerlines will occur because of separation spring forces. Subsequent release of the stud through backup commands will permit the delayed application of the restrained separation spring force. If this force is insufficient to achieve separation (as monitored by spacecraft telemetry), the Titan transtage retro rocket can be fired to effect complete separation. The reaction of the separation system to this malfunction will be determined by test on the Thermal/Structural Model.

4.5.2 ELECTRICAL SUBSYSTEM

The electrical subsystem for initiating spacecraft/adaptor separation is shown schematically in Figure 4.5-1.

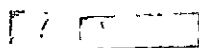
The electrical system employs redundancy throughout to ensure simultaneous initiation of the release pyrotechnics at the four hold-down studs, located at the spacecraft/adaptor interface.

Each of the four studs has a frangible nut at each end. Release of either nut will permit the joint to separate. Redundant squibs are used on each nut, with each squib on a separate firing circuit and battery. The nuts on the adapter side of the interface receive power from the Titan transtage batteries through a squib interface box located on one of the four adapter V-truss legs. The nuts on the spacecraft side of the interface are powered by the spacecraft batteries, with their operation controlled by a squib interface box located in the EVM. This design requires at least two series failures to occur to prevent release of all four retaining studs.

The primary circuit enabling signal and primary firing signal are supplied by a timed command from the Titan transtage. Back-up commands for enabling and firing are available through the spacecraft command subsystem. Commands are directed from either source to both squib interface boxes through a fly-away connector at one of the spacecraft/adaptor interfaces. Circuit disabling provision is made in both squib interfaces boxes. The disable function in the adapter-mounted squib interface box must be activated by a second timed signal from the Titan if such is required. If this disabling function is not required, it will be deleted.

Separation subsystem wiring is divided into two major harnesses: one is located within the EVM except for the leads to the four pyrotechnically actuated nuts on the spacecraft side of the separation plane; the second harness interconnects the four pyrotechnically actuated nuts on the adapter side of the separation plane, the squib interface circuit box mounted on one adapter leg, and the leads to the Titan transtage power and command systems.

The adapter harness is routed along the legs of the adapter V-trusses and to the transtage station 77 circumferential ring.



The two harnesses are interconnected at one corner of the EVM through a fly-away connector that is disengaged during spacecraft/transstage separation. Only command and separation electrical-system signals (enable, disable, and firing) and one telemetry signal are conducted across this connector.

The status of the enabling circuits is monitored by spacecraft telemetry.

4.5.3 INSTRUMENTATION

Spacecraft/adaptor separation is confirmed by spacecraft telemetry. A switch, located on the EVM at one of the spacecraft/adaptor interface joints, is activated by a 30-inch long lanyard attached to the adaptor. The length of the lanyard was selected to delay activation of separation confirmation until the spacecraft has cleared the adaptor structure.

4.6 SOLAR ARRAY DEPLOYMENT SUBSYSTEM

4.6.1 LAUNCH LOCK AT THE RELEASE MECHANISM

The two semi-cylindrical solar array panels are locked together at their edges to form a cylinder when in the launch configuration. The interconnection consists of two shear ties and five latches along each intersection line (Figures 4.6-1 and 4.6-2). The latch employs a yoke similar to a clevis fitting, a lug that mates inside the yoke, and a round pin to hold the lug and yoke together. The lug has a hole to receive the pin and a slot in one side of the lug hole that is smaller than the pin diameter.

The five pins along each intersection between array panels are fastened together, in line, by a stainless steel solar panel release restraint tension cable, which holds the pins in position against the forces exerted by individual retraction springs on each pin. Release of the cable tension permits the pins to be retracted along the pin centerline a distance sufficient to remove the pin from the lug hole, leaving only the smaller tension cable in the lug hole. The cable diameter is small enough to easily pass through the slot in the lug, effecting complete disengagement of the latch. The slot in the lug hole is oriented so that normal deployment motion of the solar array panels causes the cable to pass through the lug hole slot without dragging on the lug.

This method of fastening the two semi-cylindrical solar array panels together was used in the Fairchild Hiller Nimbus Bi-Fold Solar Array design, and has been successfully qualified. The system has also been flight proven on all Nimbus vehicles that have been orbited. The proven reliability of operation strongly influenced its selection. The system is low in weight and highly redundant, since each spring acts to release all pins in the pin/cable chain between itself and the cable release restraint mechanism.

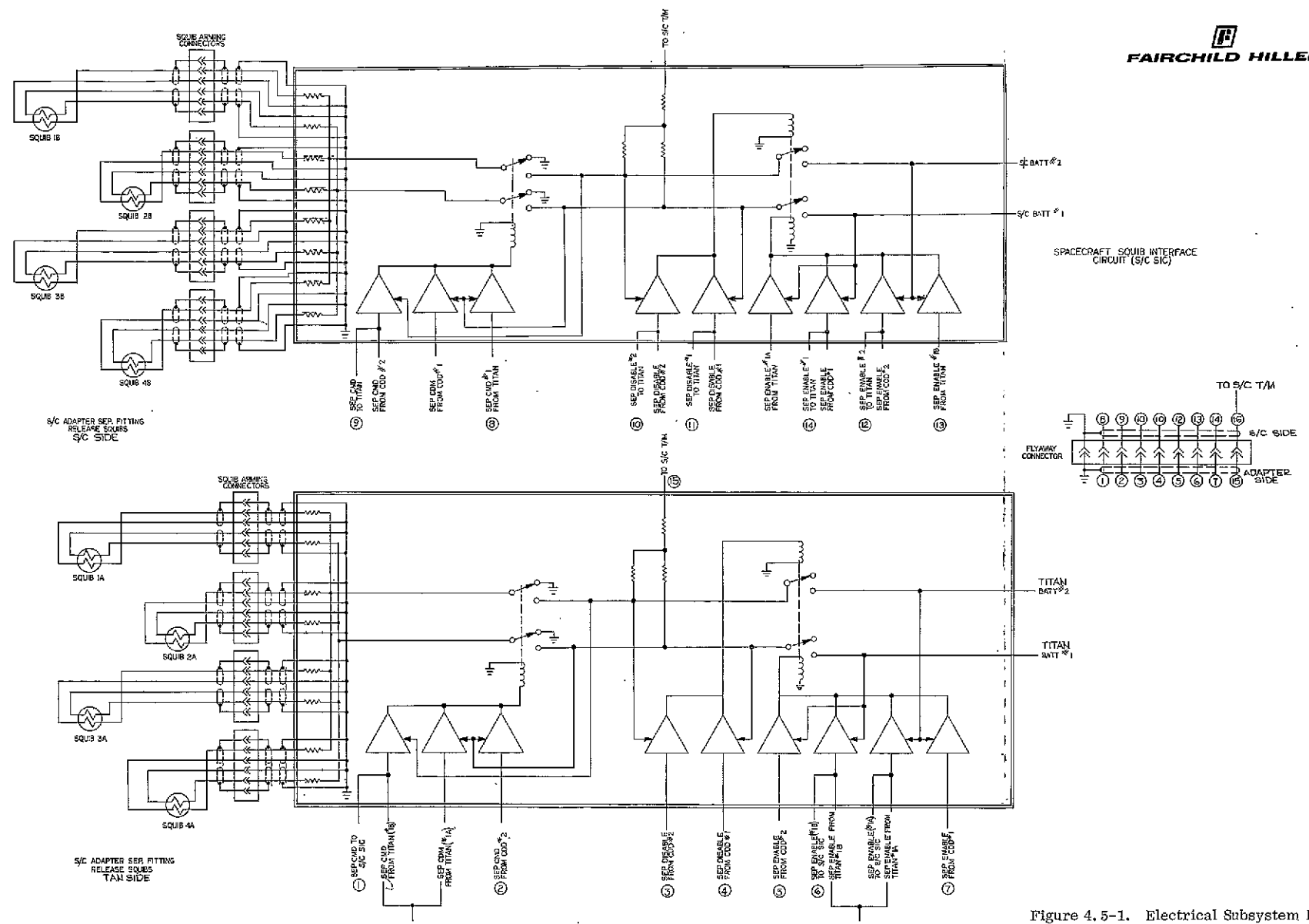
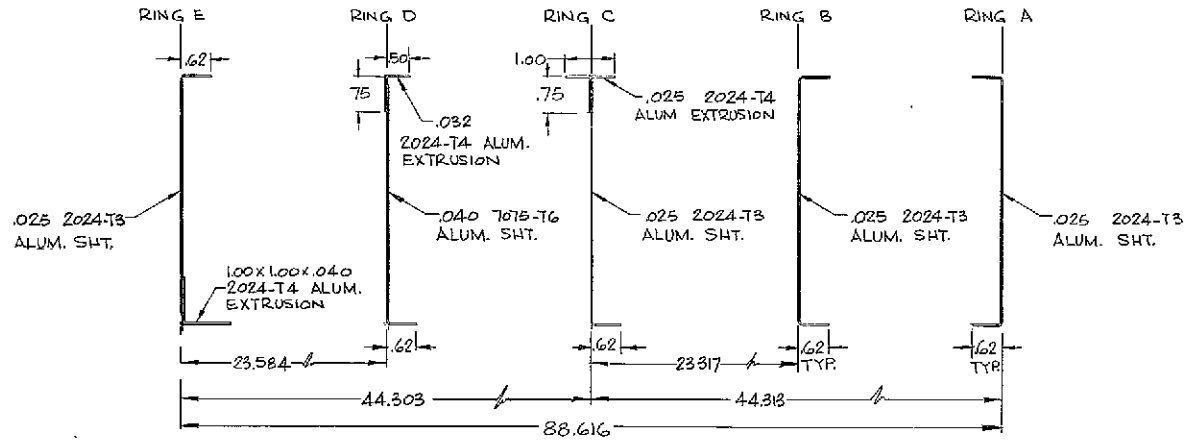


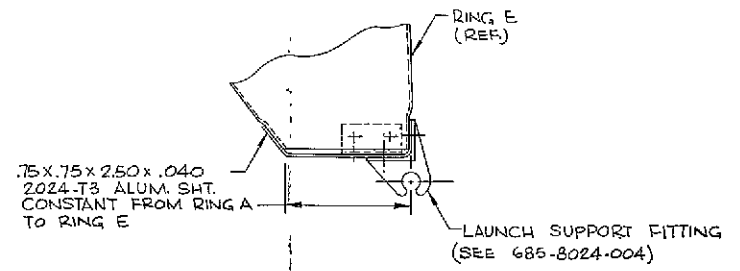
Figure 4.5-1. Electrical Subsystem For Initiating Spacecraft/Adapter Separation Schematic

FOLDOUT FRAME 2

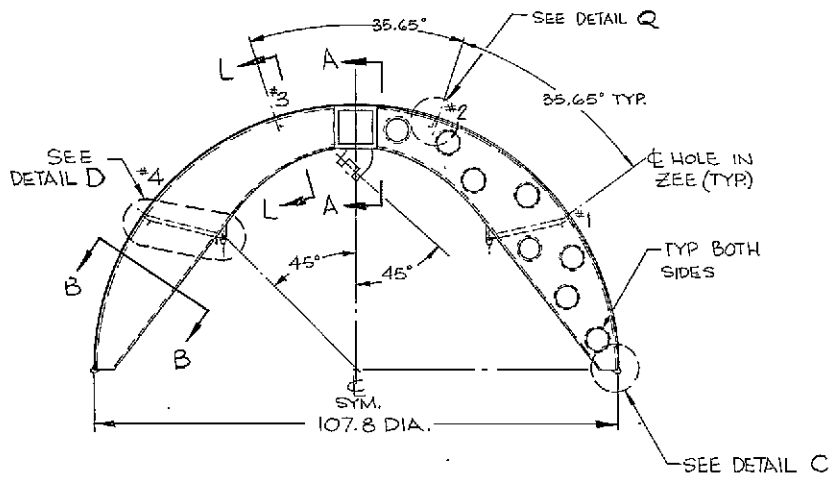
FOLDOUT FRAME 2



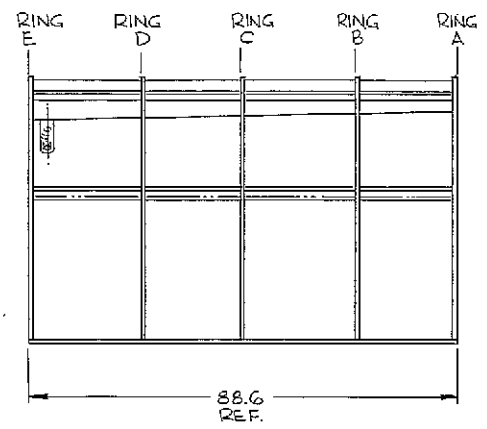
SECTION B-B
NO SCALE
ROTATED 90° C.W.



DETAIL C
SCALE = 1/4



VIEW OF RING E



LAUNCH LATCH POINT

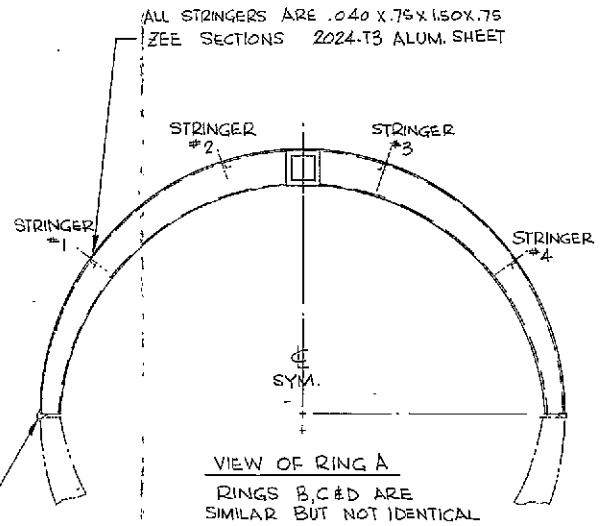


Figure 4.6-1. Cylindrical Solar Panel (Sheet 1 of 3)

FOLDOUT FRAME ?

FOLDOUT FRAME 2

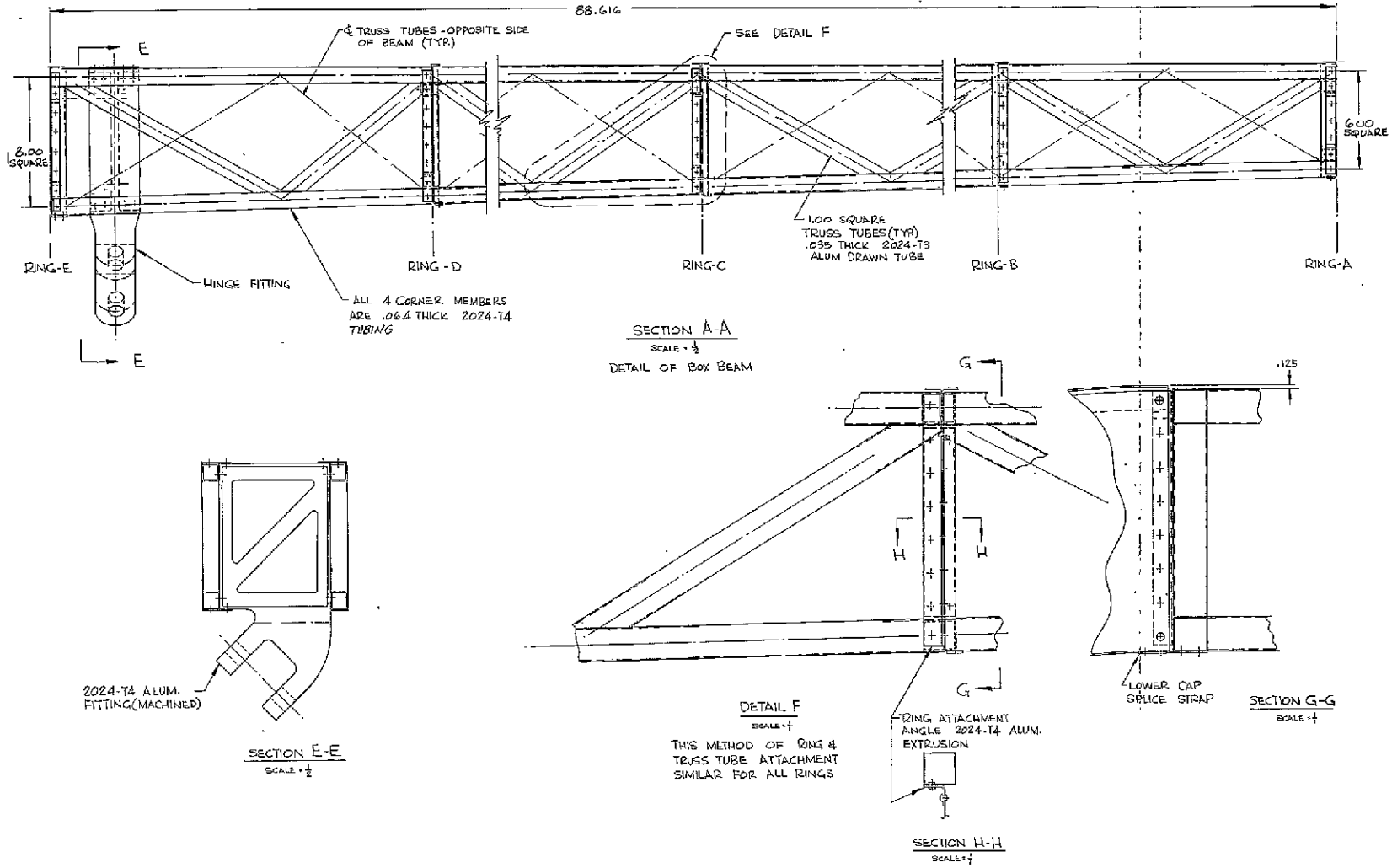


Figure 4.6-1. Cylindrical Solar Panel
 (Sheet 2 of 3)

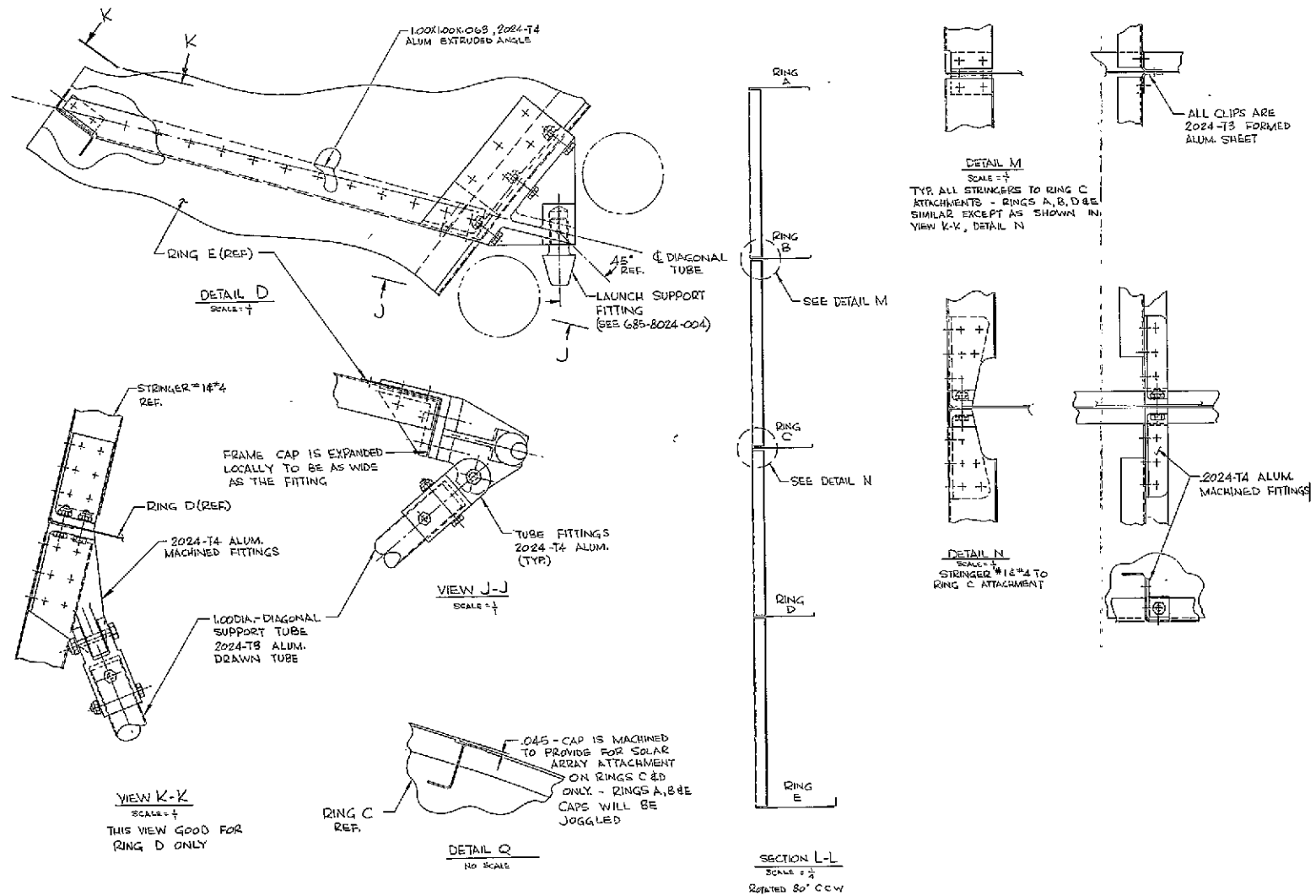


Figure 4.6-1. Cylindrical Solar Panel (Sheet 3 of 3)

PODOUT FRAME 7

FOLDOUT FRAME 2

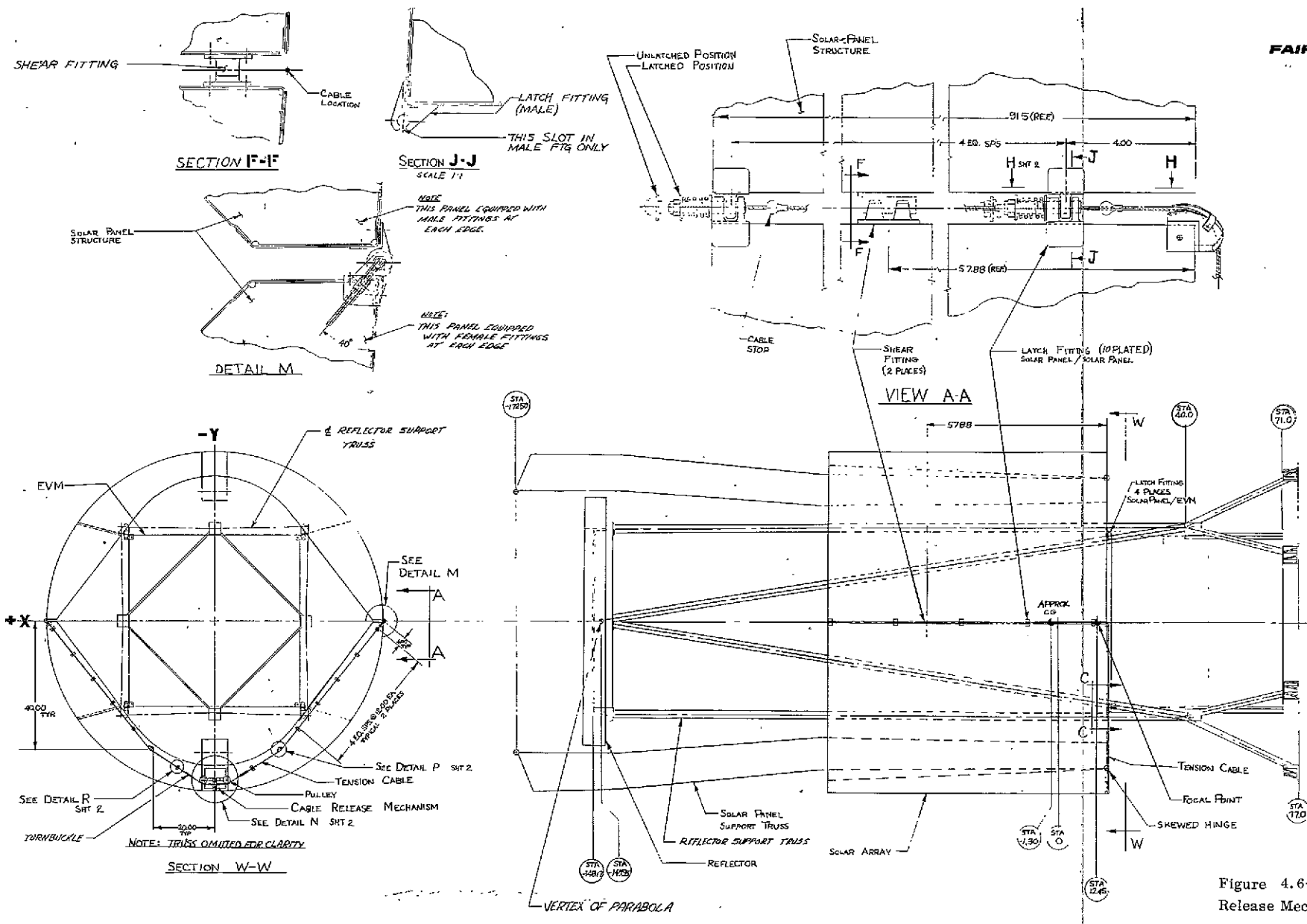


Figure 4.6-2. Solar Array Release Mechanism (Sheet 1 of 2)

FOLDOUT FRAME 1

FOLDOUT FRAME 2

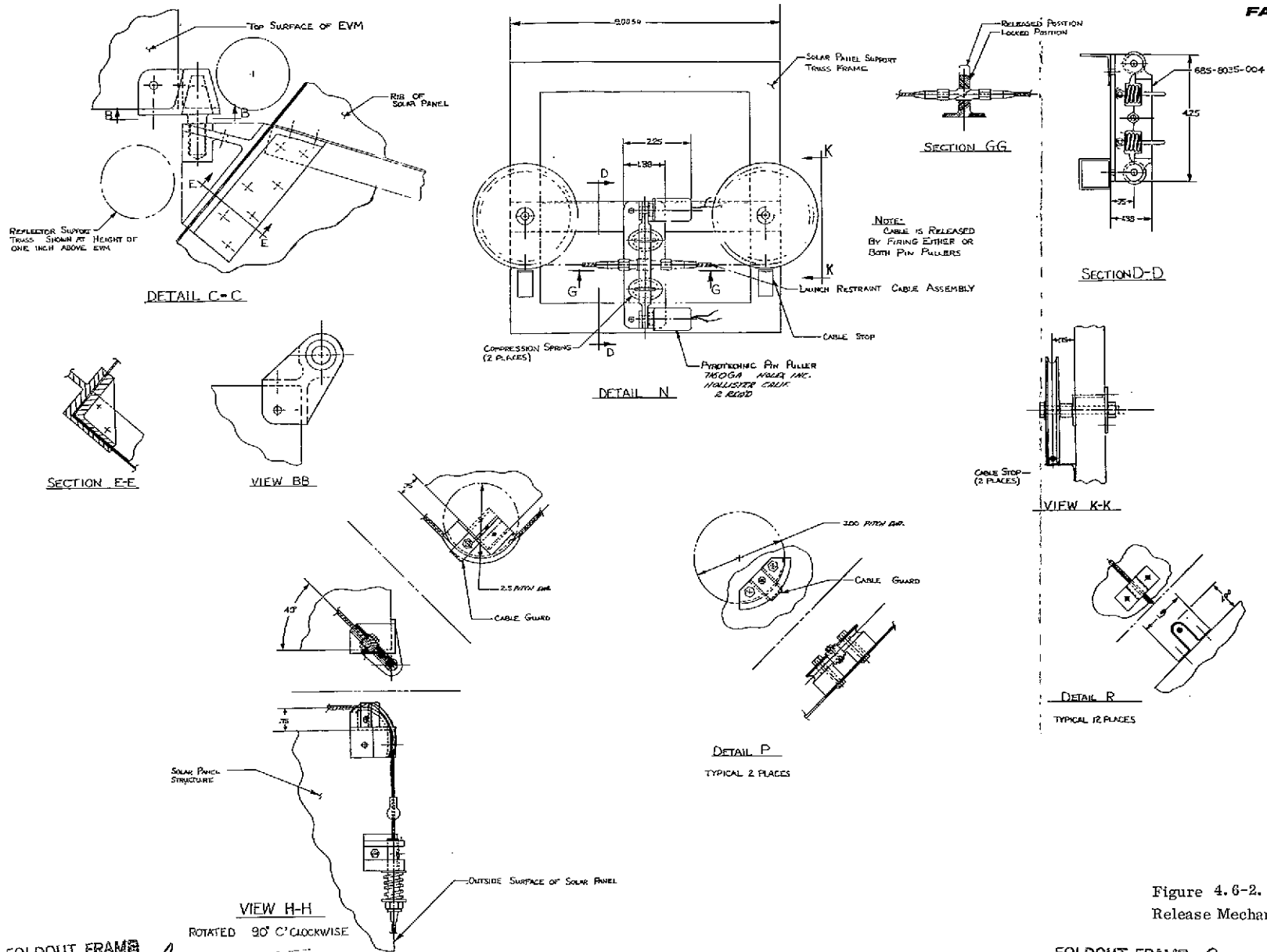


Figure 4.6-2. Solar Array Release Mechanism (Sheet 2 of 2)

The solar array panels, when in the latched, full-cylinder launch configuration, are supported at four approximately equally spaced points near the corners of the EVM top cover. The support points are located symmetrically about the array support boom attachment plane (Section WW of Figure 4.6-1). At each point, a plug mounted on the array fits into a tapered socket mounted on the EVM (View CC of Figure 4.6-1).

The plug is firmly seated in the socket by inducing axial loads along the centerlines of the four plugs with the two solar array semicylindrical panels locked together at their interface. The magnitude of the axial loads is changed by varying the position of the plug which is threaded into a fitting attached to the array panel. By releasing the two solar array panels from each other, the plugs are free to exit from the sockets. This design permits all plug loads in the X and Z directions to be reacted by the socket. Plug loads that are parallel to the plug centerline (Y direction) and directed toward the EVM are also reacted. Loads in the opposite direction are transferred around the solar array ring (located in the plane of the plugs) to the opposite side of the array.

The tension cables from the two lines of the panel latches are routed along one panel ring (nearest to the EVM) to a cable release mechanism. The cables are fastened together by a fitting as shown in Detail N and Sections GG and WW of Figure 4.6-1.

The two mating cables release end fittings join together in such a manner that, by constraining their centerlines to be coincident, the fittings cannot separate. The constraint is accomplished by two mating bars with a hole centered in their intersecting face plane to clamp the fittings together. One bar (base bar) is mounted on the top of the EVM; the second (floating) bar is retained to the base bar by two space-qualified, dual redundantly fired pin pullers, located one at each end of the mated bar assembly.

The floating bar is restrained to the base bar by two pivoted wire "U" bolts. The bars are forced apart, upon actuation of either or both of the pin pullers, by compression springs located around the "U" bolts, and also by the ramp design of the tension cable fitting mating surfaces, which try to force the fitting centerlines apart when cable tension is applied.

Only one launch restraint/release system is required to secure the solar arrays during launch. Very high reliability of release system performance is obtained by using redundant springs, releases, pin pullers, and by employing driving forces from several parts of the system to accomplish release motion of any given element within the total launch restraint system. Turnbuckles provide adjustment for cable tensions. Other dimensions that are critical (such as cable-release/clamping-bar fit) are assured by careful control of detail part tolerances. Solid lubricants are used on surfaces requiring low friction coefficients, such as the pin pullers of the cable release system. Molybdenum disulphide has been selected, with type of application to be determined. If deployment testing indicates any tendency for the

plug to wedge into the socket, an additional spring can be added to force the plug out of the socket.

The solar panel release system is so designed that all parts are retained upon release activation, and no contamination particles are released.

All members of the solar array framework are constructed of 2024 aluminum, except for the studs that mate with the EVM launch support fittings. Type 304 stainless steel was selected for these studs because its good bearing strength eliminates brinelling of the mating surfaces.

The fittings along the edge of the solar panel are 2024 aluminum, while the springs, latch pins, and cable are stainless steel.

The face sheets of the module sandwich are .005" thick, 5052-H39 aluminum, and the honeycomb core is 3/16 - 5052 - .0007 (aluminum). The sandwich edging members are 2024 - T3 aluminum. The module substrates are assembled using EPON 901/B3 adhesive.

4.6.2 DEPLOYMENT ACTUATION AND LOCKING MECHANISM

LMSC states that the 30 foot diameter reflector, during deployment, may oscillate above the tangent line at the back (convex) side of the reflector hub as much as 5.7° .

It is desirable to position the solar array booms such that the reflector, during deployment, will not impact the booms, even in a boom deployment failure mode. The design accomplishes this objective, provided the first boom hub hinge joint motion is completed. Assuming that only the first motion is accomplished, the reflector can be deployed and a degraded Power Subsystem mission may be attained.

The order of deployment is established to prevent the T&C antenna (located on both outboard edges of the deployed solar array panels) from being blocked after reflector deployment and prior to solar panel/boom hinge deployment. The deployment of the solar array takes place in three discrete steps, (Figure 4.6-3).

Upon release of the solar panel restraint system, the solar panel boom rotates upward about the inboard (hub) hinge until it reaches its full open position. At this point, the solar panel boom extends upward at an angle of 18° above the horizontal to ensure clearance between solar panel and the deploying reflector. The solar array panels then rotate about the skewed hinge to their fully extended open position. At this point, the reflector is deployed. (This motion may be performed with reflector deployed).

After reflector deployment, a pyrotechnic release at the hub hinge is actuated which allows the boom to rotate downward through an angle of 22° , coming

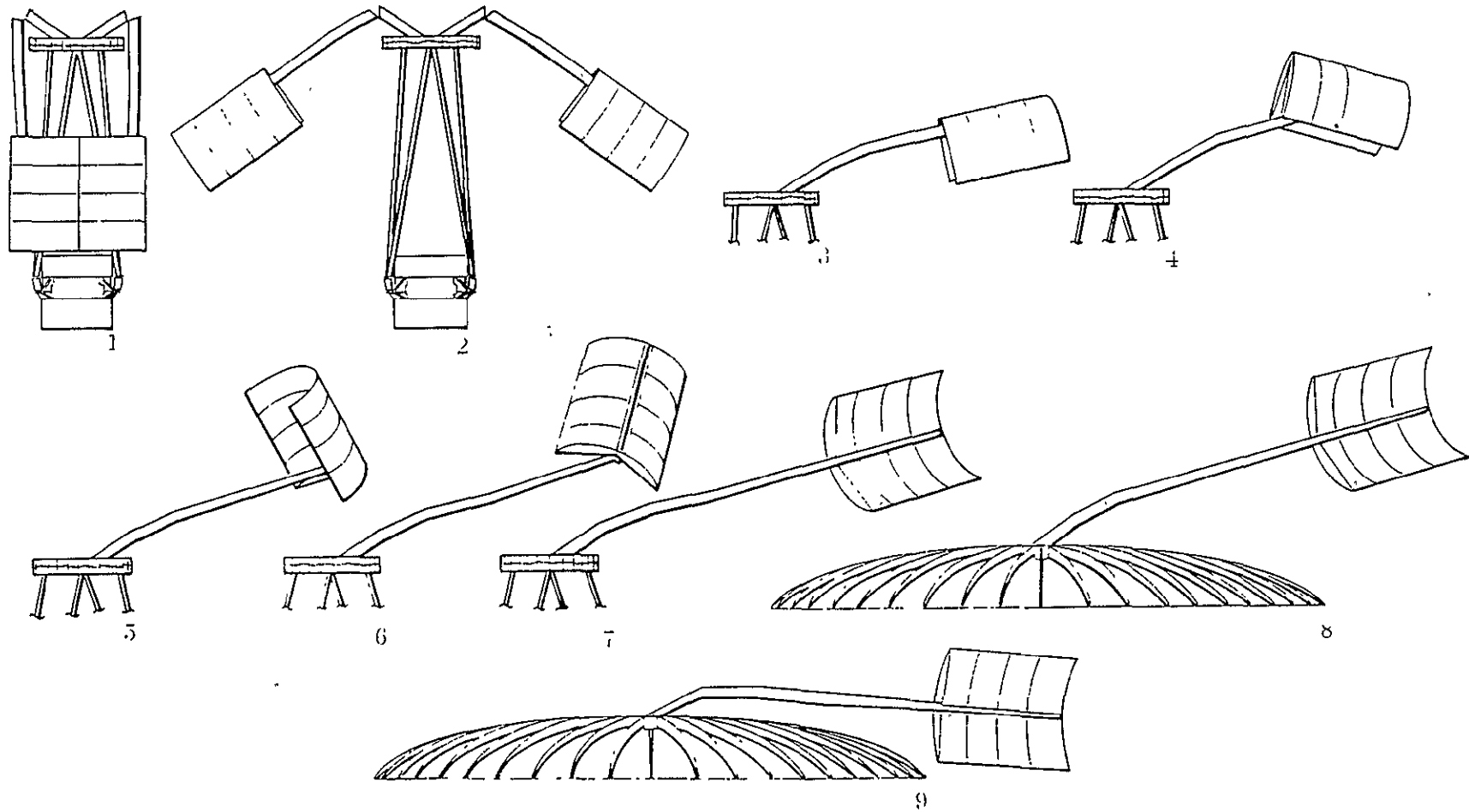


Figure 4.6-3. Solar Panel Deployment Sequenced

to rest at a position of 4° down. This third motion is utilized to lower the CG of the deployed spacecraft and to prevent shadowing of the solar panels by the deployed reflector.

When deployed, the two solar panel semicylinders are oriented, one facing east and one facing west, with the cylinder element oriented parallel to the YZ plane and approximately parallel to the XY axis. Motions of the solar array boom lie in the YZ plane.

The limiting position of the deployed solar arrays along the +Z axis is defined by the required unobstructed view angle of the Polaris Star Tracker; i. e., the array shall not violate the space below a line that extends from the star tracker sensor in the YZ plane and 30° upwards from the horizontal. Also, the inboard rim of the array must be positioned outboard of the reflector a distance sufficient to prevent shadowing by the reflector of active solar cell area. The power for deployment is furnished by springs incorporated into the hinge fittings. The time of deployment is less than 30 seconds for the rotation about the skewed hinge, and approximately 10 seconds for the final rotation about the hub hinge.

4.6.2.1 Locks and Releases

The hinge system at the hub is shown on Figures 4.6-4 and 4.3-8. It consists of a pair of spring-loaded hinges at the lower two boom chords, and a pair of overcenter latches located at the upper chords.

The hinge pin is keyed to the male portion of each hinge, and rotates in ball bearings pressed into the female portion of the hinge. The hinge pin protrudes through both sides of each hinge and is keyed to flat wire torsion springs, which furnish the power for deployment. This design was selected in preference to the ordinary coiled wire torsion spring because it is more compact and reduces the bending moments imposed on the hinge pin by the springs. It also allows the use of four redundant springs at each hinge joint without significantly increasing the length of the hinge pin.

The spring-loaded over-center latches are attached to the two upper boom chords, (Figure 4.6-4). These latches close as the boom rotates upward, and securely latch the boom when it reaches a position 18° above the horizontal. The latch elements are spring loaded at their central pivot. This spring, due to latch geometry, causes the latch to exert a strong force near the end of lock-up that acts to force the joint into the fully deployed position.

The skewed hinge at the outboard end of the boom is shown in Figure 4.3-8. The male fitting is a part of the solar panel boom, and the female fitting is integral with the solar panel structural "spine". A continuous hinge pin is used, and is keyed to the male portion of the hinge. The female portion of the hinge incorporates ball bearings for reduced friction. The spring selected for use at the skewed hinge is a pair of conventional wire torsion springs. The design of the fittings

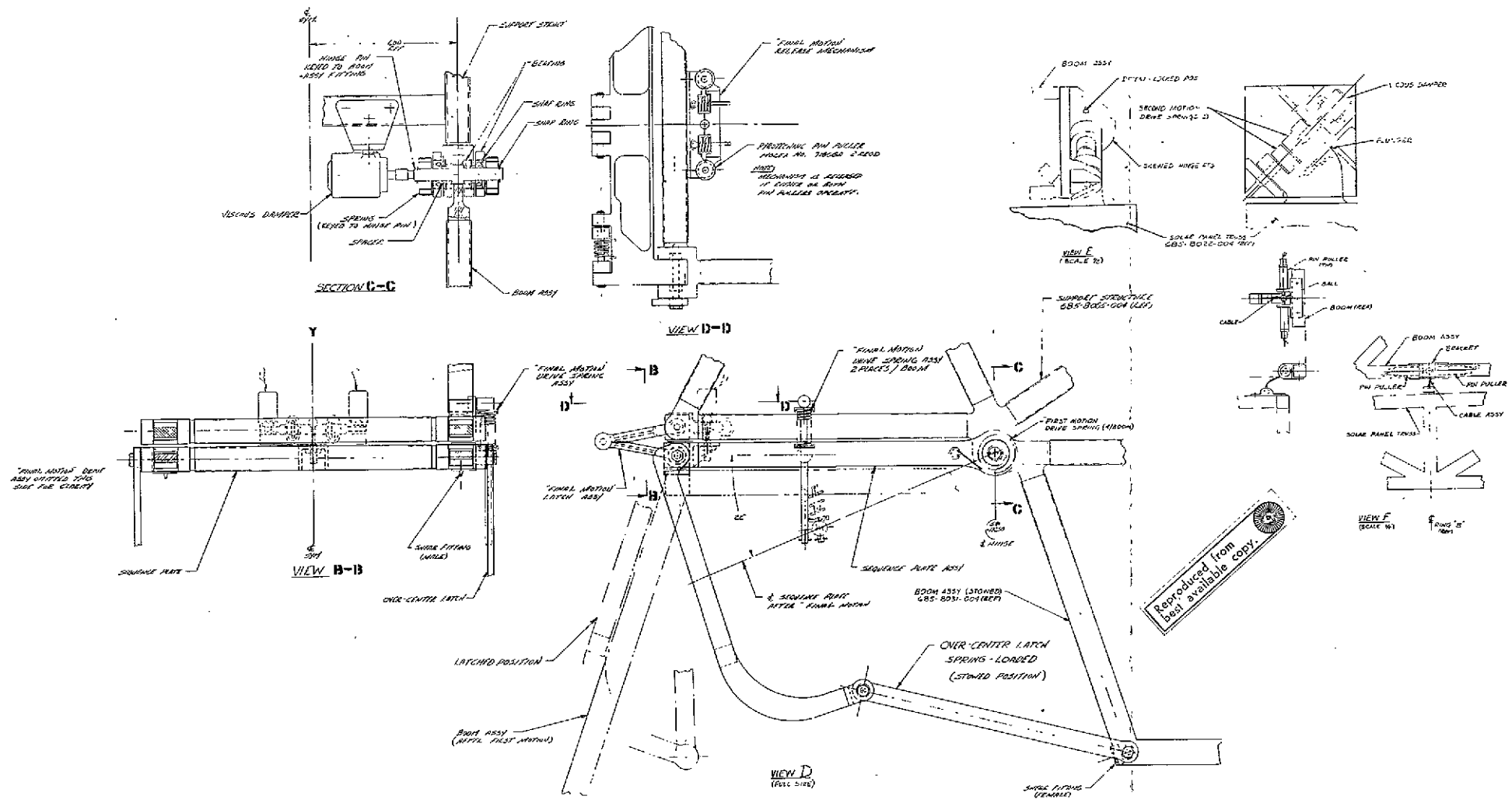


Figure 4.6-4. Hinge Lock Configuration
4-81/4-82

FOLDOUT FRAME 1

FOLDOUT FRAME 2

lends itself better to this type of spring than to the flat wire springs used at the hub hinge.

In the present design, the skewed hinge itself is not locked when in the undeployed position, but the solar array panel is loosely attached to the boom at the end furthest away from the skewed hinge. For deployment, the panel is released from the boom by two pyrotechnic actuated pin pullers equipped with dual squibs for redundancy. A spring-loaded pin engages a detent to retain the panel in the deployed position.

Both the hub hinges and the skewed hinge are equipped with viscous dampers of similar design. The type tentatively selected is the SESCO 1025-950. A similar space approved unit is now being used on the LES-7 program. This unit is a viscous damper type that is rate sensitive; therefore, the damper restraining force is available to overcome joint friction or other deployment restraining forces. The design does not lend itself to ganged release of the launch locks, other than the solar panel release from the EVM.

4.6.2.2 Materials

The material used in the boom structure is 6061 aluminum tubing, selected primarily because of its good welding characteristics.

The machined fittings are 2024 aluminum and are attached to the boom by mechanical fasteners.

The hinge pins are type 302 stainless steel, and the ball bearings are type 440C stainless steel with dry film lubricant.

The springs used in the boom deployment system are made of AS35 stainless steel.

The arms used in the over center lock mechanism are 2024 aluminum with stainless steel pins and bearings.

4.6.3 ELECTRICAL SYSTEM

The electrical system for initiating firing of the various pyrotechnic actuated release mechanism to accomplish solar array and reflector deployment is shown in Figure 4.6-5. Correct sequencing of several operations is necessary to prevent physical interference between the solar array subsystems and reflector during their deployment, and to prevent T&C subsystem antenna blockage with the systems partially deployed. The design uses specific commands for each operation rather than automatic sequencing, so that ground verification and control is maintained throughout deployment.

The sequence for deployment is:

1. Release solar panel launch locks x
2. Solar panel booms rotate about knee joint
3. Knee joint locks engage at end of joint travel o
4. Release solar panel/boom launch locks x
5. Solar panels rotate 180° about skewed hinge
6. Solar panels lock at end of rotation o
7. Release 30-ft. diameter reflector x
8. Verify reflector release o
9. Release knee joint sequencing plate lock x
10. Solar Panel Booms rotate 22° at knee joint toward reflector
11. Knee joint locks in final position o

NOTE: x = Command Signal
o = Telemetry Verification Signal

The above actions apply to both solar array panel and boom assemblies, and telemetry verification is for each lock on both solar array booms.

The electrical system employed to control solar array and reflector deployment uses "Enabling" and "Disabling" latching relays and momentary contact "Firing" relays. Relay drivers are used to amplify the various commands. "Firing" relay drivers receive power only when the "Enabling" relays are engaged. Completely redundant Command, Enabling, and Firing circuits, including power from separate spacecraft batteries, is used for high reliability. Redundant bridgewire squibs are used for each pyrotechnic device, and two pyrotechnic devices are used for each release mechanism. This approach ensures that at least two failures must occur to prevent any release system from operating. Both sides of redundant firing circuits are actuated simultaneously, but backup (redundant) commands are transmitted only if the first command does not produce the desired result.

4.6.4 INSTRUMENTATION AND POWER WIRING

The solar array panel electrical power is collected by a wiring network and brought to an electrical connector adjacent to the panel/boom hinge. The power harness is routed along the boom and, with suitable strain relief, across the rotating joints. Extreme care is taken to ensure that the harness does not adversely affect joint motion or interfere with the action of the joint locks and launch lock releases. Similarly, harness strain relief is selected to prevent chafing, or extensive cold working due to launch vibration and joint deployment motion.

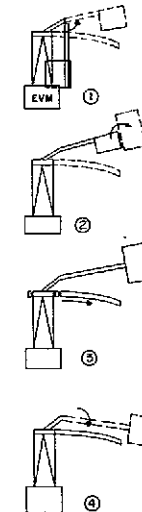
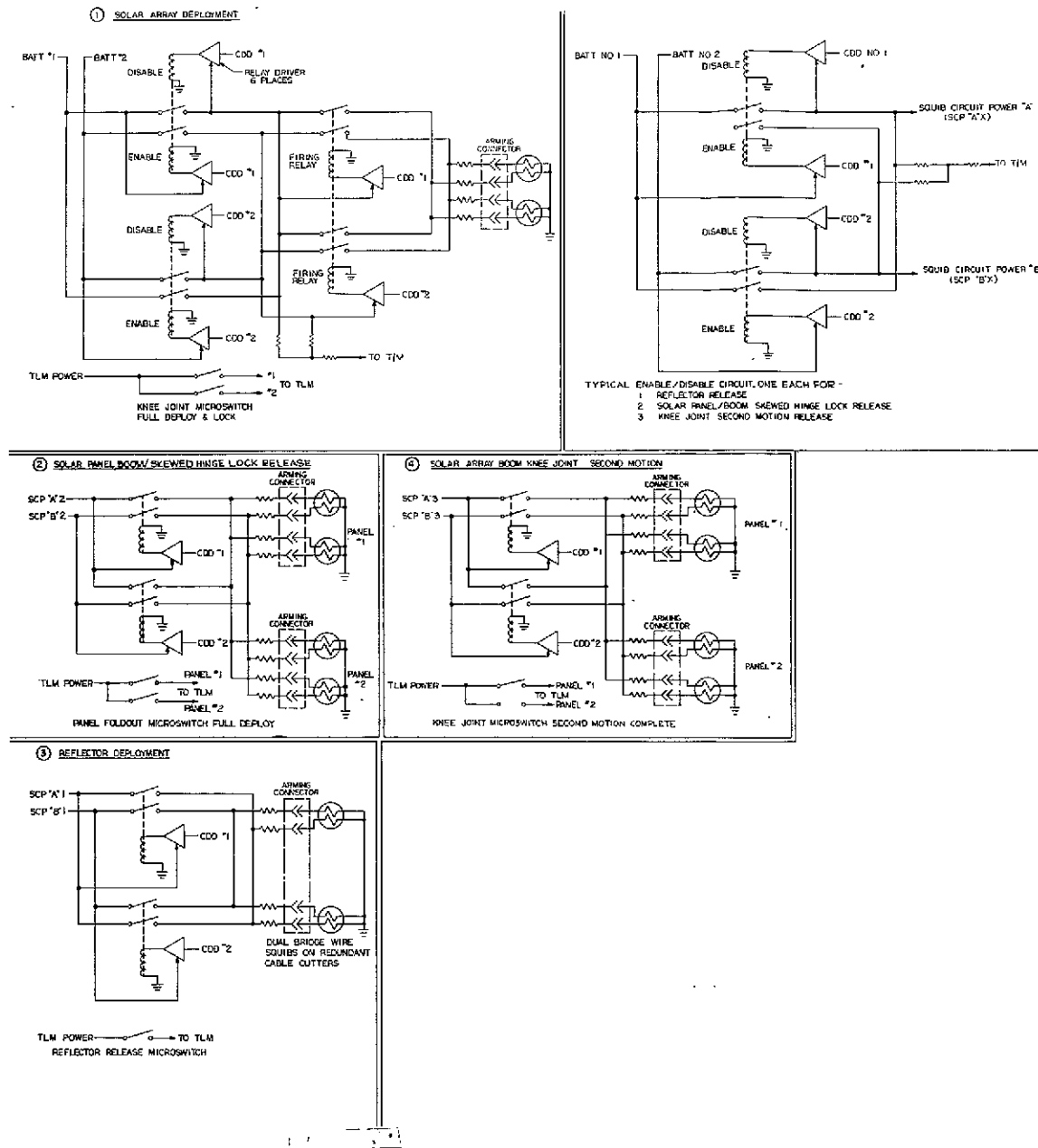


Figure 4.6-5. Pyrotechnic Electrical System

FOLDOUT FRAME 1

4-85/4-86
FOLDOUT FRAME 2

4.7 MATERIALS

The materials used in the Structural Subsystem are defined in the preceding descriptive paragraphs of the various structural components and on the drawings of the structure presented herein.

4.7.1 METALLICS

The primary materials selection criteria for the EVM, other than functionality, are proven performance in space and an established FHC processing capability. Highly toxic materials have not been used. All metals used in the Structural Subsystem have a history of successful space application. Standard approved finishes of metallic parts are used throughout.

4.7.2 NON-METALLICS

Outgassing of materials, including volatile condensable material (VCM) that could contaminate optical surfaces, must be considered in material selection. FHC has elected to use the knowledge obtained on the NASA ATM program as a guide to selection of structural non-metallic materials; the results of the ATM materials program is reported in NASA document 50M02442, "ATM Materials Control for Contamination Due to Outgassing".

4.8 DYNAMIC ANALYSIS

Presented herein is a summary of the results of the dynamic analyses performed during phases B and C. The complete analyses are presented in the following documents:

- ATS-990-040 - Structural Dynamic Analysis for
ATS F&G
- ATS-990-041 - Additional Studies of the Solar Array
Boom.

The ATS F&G spacecraft has been designed to withstand the dynamic environments associated with the launch phase, transition from launch to orbital phase, and during the orbital phase.

A tabular summary of the dynamic characteristics of the spacecraft during the launch and orbital phases are presented below.

For the launch phase, design goal fundamental frequencies have been established so as to minimize the environmental levels throughout the spacecraft, and preclude any adverse effects on the spacecraft/launch vehicle system. These values, considering the spacecraft and launch vehicle transtage to be cantilevered at Station 132, are as follows:

Lateral	6.0 Hz
Torsional	4.0 Hz
Longitudinal	25.0 Hz

To ascertain the compliance to these values a coupled, spacecraft/transtage, dynamic analysis need be performed. In lieu of such an effort, which was prohibitive from a schedule viewpoint during Phase C, the reference station was changed to the launch vehicle interface, Station 77. The spacecraft fundamental frequencies referenced to the launch vehicle interface have been computed to be:

Lateral	8.0 Hz
Torsional	11.3 Hz
Longitudinal	44.3 Hz

It is expected that the compliance of the launch vehicle transtage will not cause the spacecraft frequencies to fall below the minimum specified values.

The dynamic environmental levels throughout the spacecraft are also dependent upon a coupled spacecraft/launch vehicle analysis. Again, in lieu of such an analysis, an approximation was required. Quasi-steady load factors were assumed, and the results of structural analysis utilizing these factors are presented in ATS-990-026 Revision A, Structural Analysis for ATS F&G.

Approximations, within 10% of the lateral and torsional spacecraft fundamental frequencies can be made by considering only the reflector truss flexibility. Longitudinally the spacecraft fundamental frequency can be approximated by only considering the adapter flexibility.

In order to reduce the vibratory levels to which the hub and EVM mounted experiments and components will be subjected during the launch phase, the component mounting surfaces have been designed to be frequency separated from both the overall spacecraft characteristics and the components themselves.

The separation of the spacecraft from the launch vehicle is achieved when the 31 inches of EVM below the separation plane clears the confines of the adapter. This is accomplished in 0.91 seconds with a relative separation velocity of 3 ft. per second. The maximum spacecraft acceleration achieved during separation is .734 g.

The deployment of the solar array subsystem is accomplished using a spring damper driven, 3 stage system. The first 2 stages, consisting of large angular rotations, 108° and 180° respectively, have been investigated. The third stage, however, consisting of a much smaller rotation, 22.0° , and correspondingly lesser significance, has not been investigated and is not expected to be a defining condition for any portion of the spacecraft. The first stage deployment occurs in 13.5 seconds, with a final angular velocity of 0.133 rad/sec and a

maximum panel acceleration of 2.3 g. The second stage deploys in 22.5 seconds with a final velocity of 0.099 rad/sec and imparts a 0.77 g acceleration to the panel.

The deployment of the Lockheed flex rib antenna has only been preliminarily investigated. The results of the preliminary analyses, however, do not indicate any problems associated with the deployment. Limited information on the dynamics of the antenna deployment is the reason for the preliminary status.

4.9 STRUCTURAL ANALYSIS

Presented within is a summary of the results of the structural analyses performed during phases B and C. The complete analyses are presented in the following documents:

- ATS-990-026, Structural Analysis for ATS F&G
- ATS-990-042, Additional Structural Investigations
- ATS-990-041, Additional Studies of the Solar Array Boom

The loads environments to which the spacecraft has been analytically subjected consist of the following:

- Launch vehicle induced loads
- Thermal loads
- Spacecraft functional loads (solar array and reflector deployments)

Presented in Table 4.9-1 is a summary of the structural criteria to which the spacecraft has been designed.

The launch vehicle induced loads consisted of analytically subjecting a 2500 lb spacecraft to quasisteady environments consisting of load factors inclusive of both dynamic and sustained accelerations. The shear, bending moments, and axial loads resulting from these environments are presented in Figure 4.9-1.

The 5 major components of the structural subsystem, (i.e., the hub, reflector support truss, solar array, EVM, and adapter) along with their design conditions are illustrated in Figure 4.9-2 and discussed separately herein.

- Hub - The structural design of the hub was dictated by the loads attributed to the deployment of the solar arrays and the inertia of the hub mounted components during the launch phase.

Table 4.9-1. Structural Criteria And Compliance

<u>REQUIREMENT</u>			<u>COMPLIANCE</u>
<u>Launch</u>	<u>Strength</u>	9.0g + 3.9g 3.9g + 3.9g	Positive Margin on all Analyses
	<u>Frequency</u>	Acoustic (142 Overall SPL) 6.0Hz (Lateral Bending) 25.0Hz (Longitudinal) 4.0Hz (Torsional)	Solar Panel Design 8.0Hz, 16.1Hz 44.3Hz 10.3Hz
<u>Separation</u>	<u>Velocity</u>	3 Ft./Sec. Between Spacecraft and Transtage	Spring System Develops 3 Ft./Sec. With a Stroke Length of 3 Inches
<u>Orbit</u>	<u>Strength</u>	Deployment of Solar Array Subsystem and Parabolic Reflector	Positive Margin on all Analyses for Both Deployments
	<u>Dynamic Response</u>	At or Below 1.0Hz The Dynamic Amplification Shall be 1.2	Establishment of Minimum Frequency of 2.5Hz 2.5Hz (Solar Array Bending) 3.0Hz (Solar Array Bending) 5.2Hz (Reflector Truss Torsion) 8.3Hz (Reflector Truss Bending)

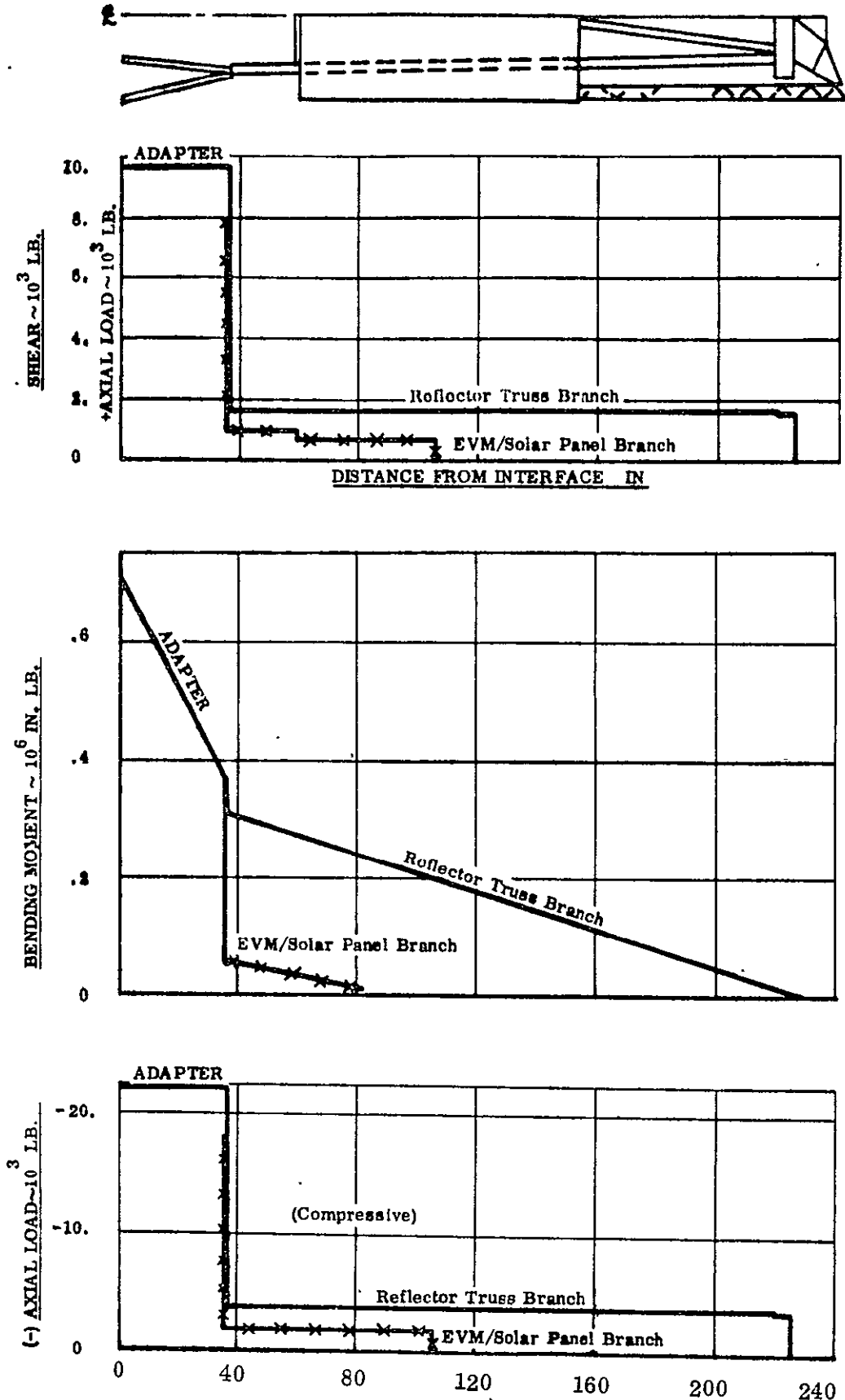


Figure 4.9-1. Shear/Bending Moment Diagrams

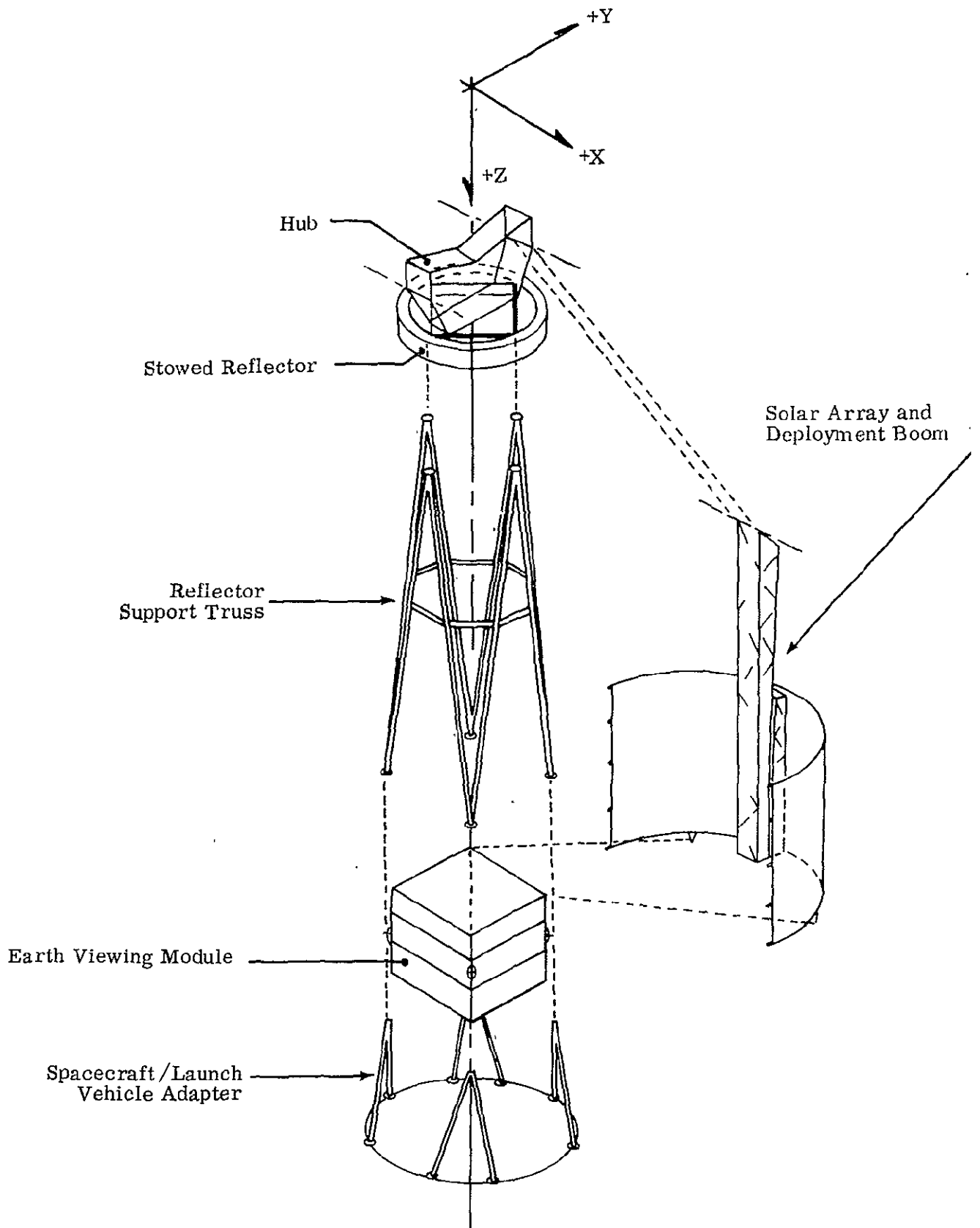


Figure 4.9-2. Components of Structural Subsystem

- Reflector Support Truss - Associated with the relative newness of the GFRP material the philosophy of maintaining a 50% strength margin of safety, in conjunction with the GFRP material, has been adopted. The critical design condition is the column stability of the tubular members when subjected to the quasisteady launch environment.
- Solar Array - The solar array subsystem consists of two components, the deployment booms, and the semi-cylindrical solar panels. The design condition for the deployment boom is the loading associated with the deployment of the solar arrays. The solar panel structure is designed by launch loads and the deployment loads. The loads induced into the solar array booms due to thermal environments have been investigated and shown to be of a tolerable level. Also investigated was the deployment under thermal environment.
- EVM - The basic EVM structure is design critical for loads imposed upon it during the launch phase. Two aspects of the EVM were investigated, the primary structure which functions integrally with the adapter as an overall load path, and secondly the honeycomb panels which must withstand the loads produced by the inertia of the packages mounted to these surfaces.
- Adapter - The tubular members of the adapter are Euler-column critical for the application of the launch quasisteady load factors.

SECTION V

THERMAL CONTROL SUBSYSTEM

5.1 THERMAL SUBSYSTEM FOR EVM

The thermal control subsystem must maintain all internal mounting plate temperatures within a 30° C temperature excursion, and must prevent temperature changes which degrade alignment accuracy of spacecraft subsystems. Simultaneously, while maintaining internal mounting plate temperatures within a 30° C temperature excursion and in accordance with GSFC requirements, the average component environmental radiation surface temperature of 10° to 30° C must be maintained.

This section describes the thermal control system which meets all these requirements. To accomplish this, the system includes the use of superinsulation, thermal louvers, heat pipes, passive coatings, a unique cubical spacecraft configuration which lends itself to radiative cooling, and the judicious placement of heat-dissipating components within the structure. The design incorporates a significant degree of redundancy (e.g., 10% of the thermal louver blades and 50% of the heat pipes can fail and still produce acceptable temperatures), conservatism (maximum coating degradation has been assumed, as well as worst-case solar conditions and a "cold" condition below the analytical minimum), practicality (e.g., the heat pipe configurations are all in parallel planes, so that the system can be tested in a 1-g field), and adaptability to emergency conditions (e.g., large thermal time constants). The system uses hardware elements with which Fairchild Hiller has experience and familiarity, and provides complete temperature control for the spacecraft during ground testing, pre-launch, ascent, and orbital phases.

The EVM, or earth viewing module, pictured in Figure 5.1-1, has six sides. One of the prime reasons for selecting this shape was because of its adaptability to a relatively simple efficient thermal control system. Four of these sides have considerable exposure to the sun and hence are covered with superinsulation. The two remaining sides, facing north and south, are honeycomb panel containing 17 square feet of active thermal louver arrays, and it is these thermal louvers, coupled with the low α/ϵ thermal coated panels, which provide the radiative path from the EVM to space. Embedded in the north/south panels are heat pipes which effect a uniform temperature distribution over the surfaces, and within the EVM is a transverse beam carrying heat pipes which provide a heat-sharing path between the north and south faces. High-dissipative components are mounted on the interiors of the north/south faces directly over one or more heat pipes.

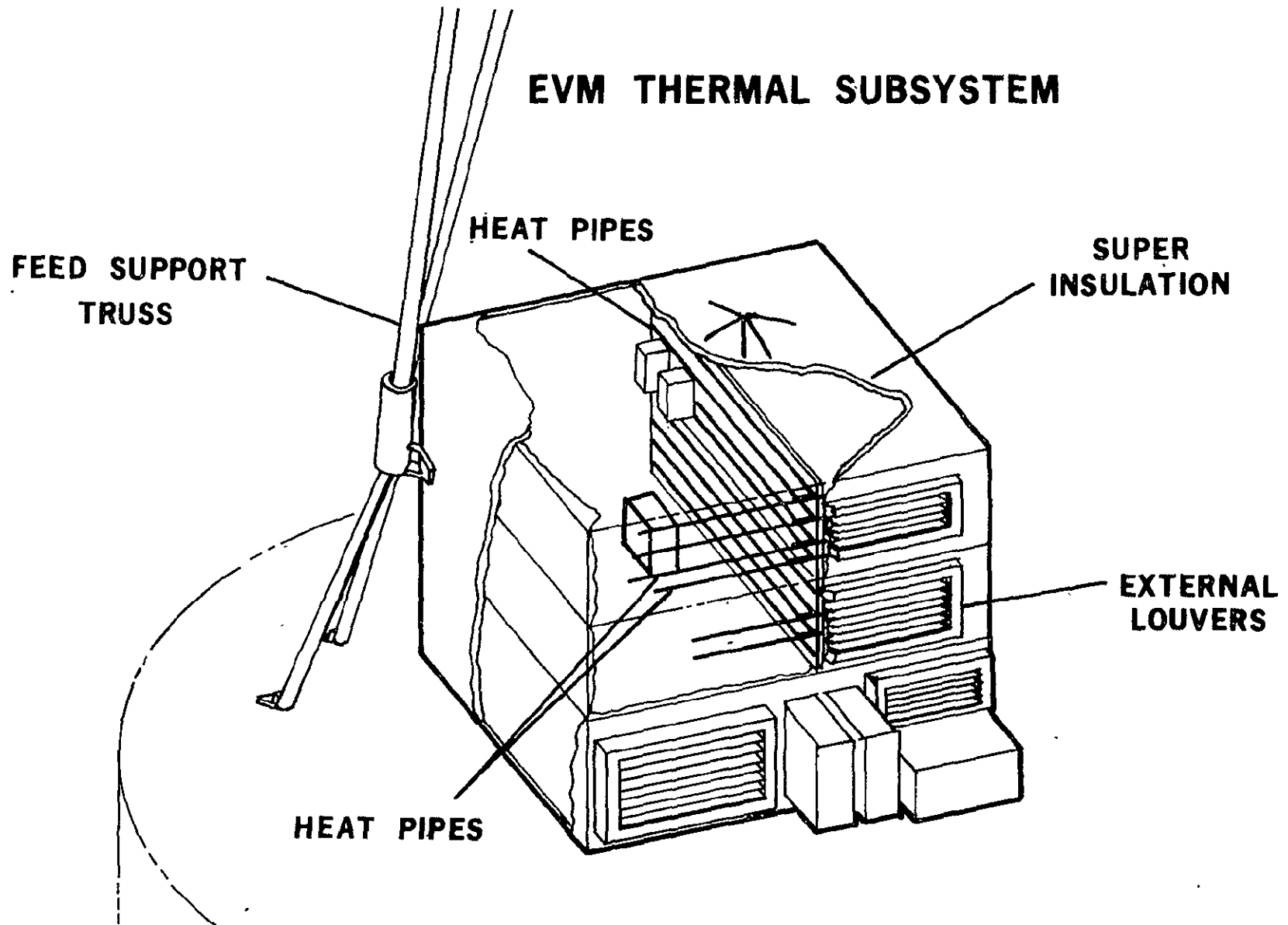


Figure 5.1-1. Earth Viewing Module

Within this combination of thermal control mounting component surface, temperature limits of $20 \pm 10^{\circ}\text{C}$ (50°F to 86°F) are maintained for all orbital conditions and operating modes. Detailed temperature maps, which are the result of a 140-node computer program, are given in Section 3.2.4, Vol 1B Thermal Control Subsystem.

The hardware elements of the thermal control subsystem are well within the state-of-the-art and Fairchild Hiller's realm of experience. Fairchild has provided NASA with thermal louvers for OAO, Pegasus, and Nimbus D; thermal insulation blankets for Nimbus, OGO, and OSO; and thermal control coatings for Pegasus and SERT. Heat pipes of the proposed design have been under test for some time in Fairchild's heat pipe laboratory.

In order to minimize wide swings of solar radiation, the four faces of the EVM which face the sun are covered with a blanket of 30 layers of aluminized mylar superinsulation. The insulation reduces the dependence on thermal coatings to a minimum, and assures that radiant heat transfer to space will take place primarily through the uninsulated north and south faces.

The north and south faces are honeycomb panels which house several sets of thermal louvers. These louvers, plus the thermal coatings on the surfaces, provide the radiative paths which permit the spacecraft components to stay within their required temperature limits despite the wide power excursions. The louvers provide a variable thermal resistance which is a function of temperature.

In order to use the louvers most efficiently, it is necessary to distribute internal heat loads to the louver areas, and to maintain as uniform an internal EVM temperature as possible. This is done by (a) mounting the bulk of the electronic components directly to the interior surfaces of the honeycomb, and embedding heat pipes within the honeycomb panels to distribute heat loads over the entire faces, and (b) providing north to south heat pipes which provide a positive thermal path to allow heat sharing between the faces.

On the exterior surface of the louvered skins a low α , high ϵ thermal coating will be applied. The low α is desirable to minimize solar input when the north-south faces are not parallel to the sun. A large ϵ is required to maximize heat rejection to space, i.e., minimize the louver area. The recommended technique is an optical solar reflector, vapor deposited silver on 8 mil thick fused silica.

The following paragraphs present a brief treatment of these four elements of the EVM thermal control subsystem, i.e., thermal louvers, heat pipes, thermal coatings, and multilayer insulation.

5.1.1 THERMAL LOUVERS

At a given point in its mission profile the various spacecraft components will be subjected to different degrees of heating caused by solar thermal radiation and internal power dissipation. The parameters which, in most cases, control the spacecraft heat rates are the solar absorptance factor (α) and the emittance factor (ϵ). The solar absorptance determines how much solar thermal radiation the spacecraft will absorb and the emittance regulates the amount of thermal energy radiated to space. The ratio α/ϵ controls the spacecraft's equilibrium temperature.

If the changes in internal power dissipation or external heat flux are severe, it is not possible to maintain the internal component temperatures within the allowable design temperature limits unless the α/ϵ ratio can be varied. A very popular and reliable method which effectively gives a variable α/ϵ ratio is through the use of thermal louvers (Figure 5.1-2). When the louver blades are open, the effective α/ϵ ratio is low (low α , high ϵ) and when the blades are closed the effective α/ϵ ratio is high (low α , low ϵ). In effect, the louvers act as a "thermal valve" to regulate the flow of heat out of the spacecraft. This property, when properly utilized, provides an additional thermal design tool in that louvers reduce the dependence of the spacecraft on the value of optical coatings which have a tendency to degrade from their nominal values during a long-term mission.

Thermal louvers, as designed and manufacturing by FHC (approximately 1.4 lbs/ft²) consist of a rigid, light weight polished aluminum frame which contains low-friction pivots for the louver blades. The blades are thin, highly polished, specular finish aluminum and are actuated by bimetallic sensors which are located in a housing thermally insulated from outside influences. The bimetallic sensors expand and cause the louver blades to open, thus allowing more heat to be radiated to space. The opening and closing temperatures of the blades are regulated by adjusting the bimetallic sensors. It should be noted that the louver blades are independently actuated (one bimetallic sensor per pair of louver blades) providing a redundant system. The typical louver has 10 or more pairs of blades so that in case of failure of one actuator, the overall system degradation is small. These louvers have been employed on many spacecraft and have proven to be a reliable temperature control system. At FHC, louvers have been used on the highly successful Pegasus spacecraft, and on the attitude control system for Nimbus D. For the NASA/GRUMMAN Orbiting Astronomical Observatory (OAO) Program (Spacecraft II, III, and IV), FHC has designed and produced over 40 thermal louvers.

Thermal louvers recommended for ATS F&G Spacecraft are shown on Figure 5.1-3. They are mounted directly to the north and south facing honeycomb panels. The north face contains 5 assemblies for a total active area of 8.5 square feet; the south face contains 4 assemblies for a total active area of 8.5 square feet.

5.1.2 HEAT PIPES

Heat pipes exhibit a very high heat transport capability while maintaining near isothermal conditions along their length; they are utilized to achieve thermal equalization of the north and south louvered baseplates. The ATS heat pipes are oriented parallel to the earth viewing face and at the same level in all three panels (north, south, and transverse). The heat pipes in each panel are independent and interconnected at the juncture of the transverse beam with the north and south panels by thermal conduction only.

To provide a good thermal conduction path, the pipes within the transverse panel have a 90° mitered bend at their ends and extend approximately four inches parallel to the North and South faces to which they are coupled mechanically with a high conductive epoxy. A cutaway view of a typical 90° miter bend is shown in Figure 5.1-4. Figure 5.1-5 shows the array of heat pipes used for temperature control on a model parabolic dish which was fabricated during a study program for the Goddard Space Flight Center.

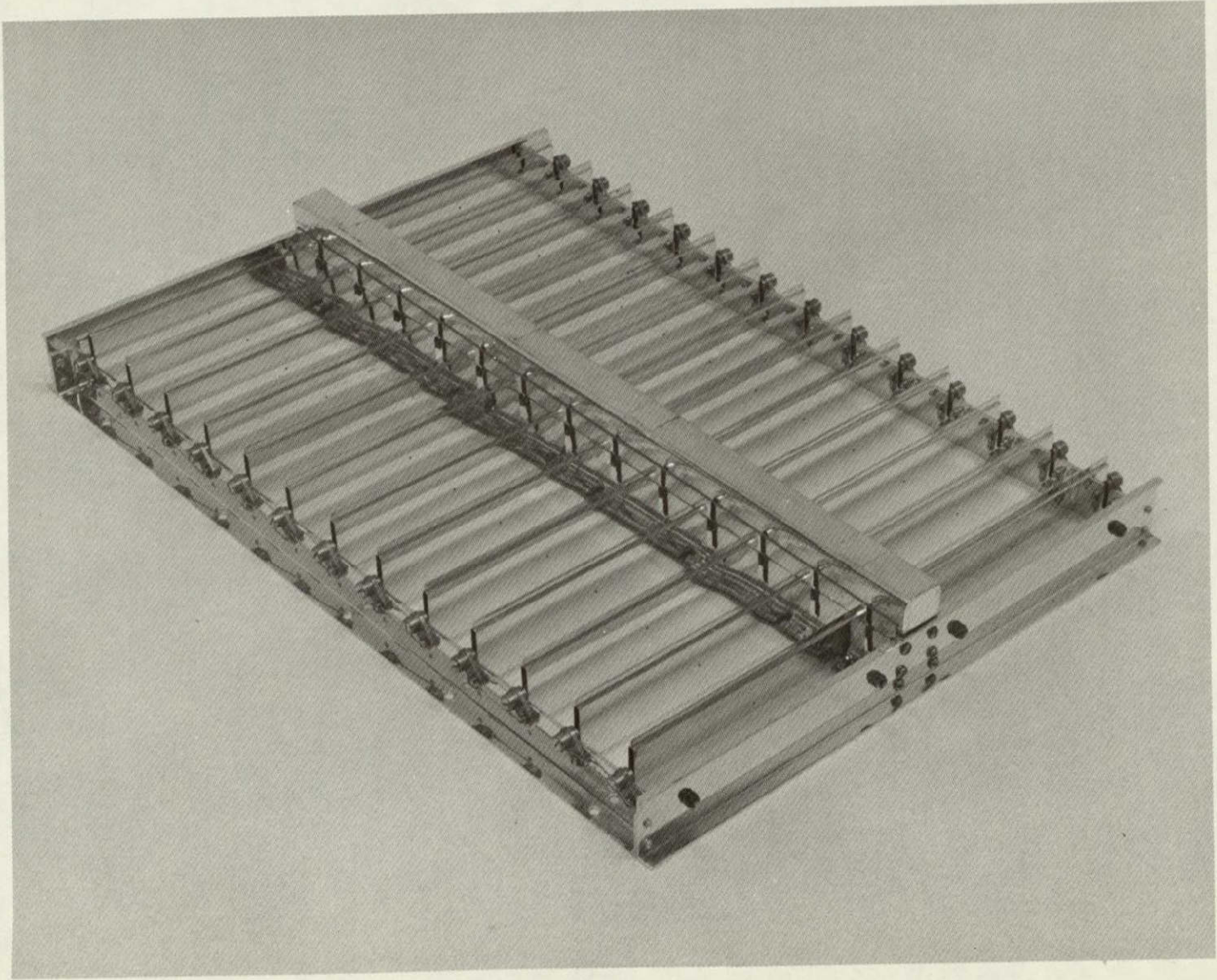


Figure 5.1-2. Thermal Louvers


FAIRCHILD HILLER

1
202

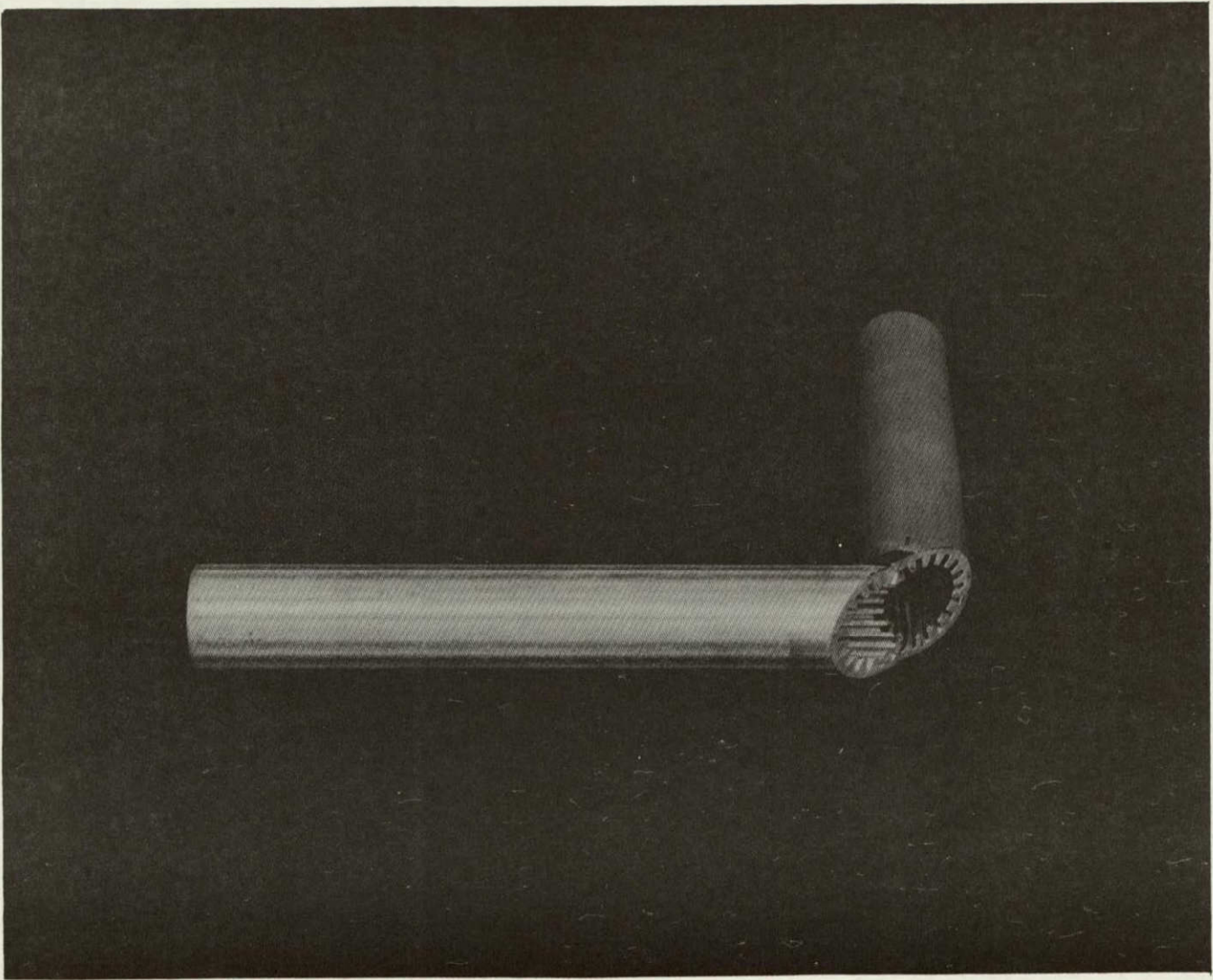


Figure 5.1-4. Typical Heat Pipe 90° Miter Bend

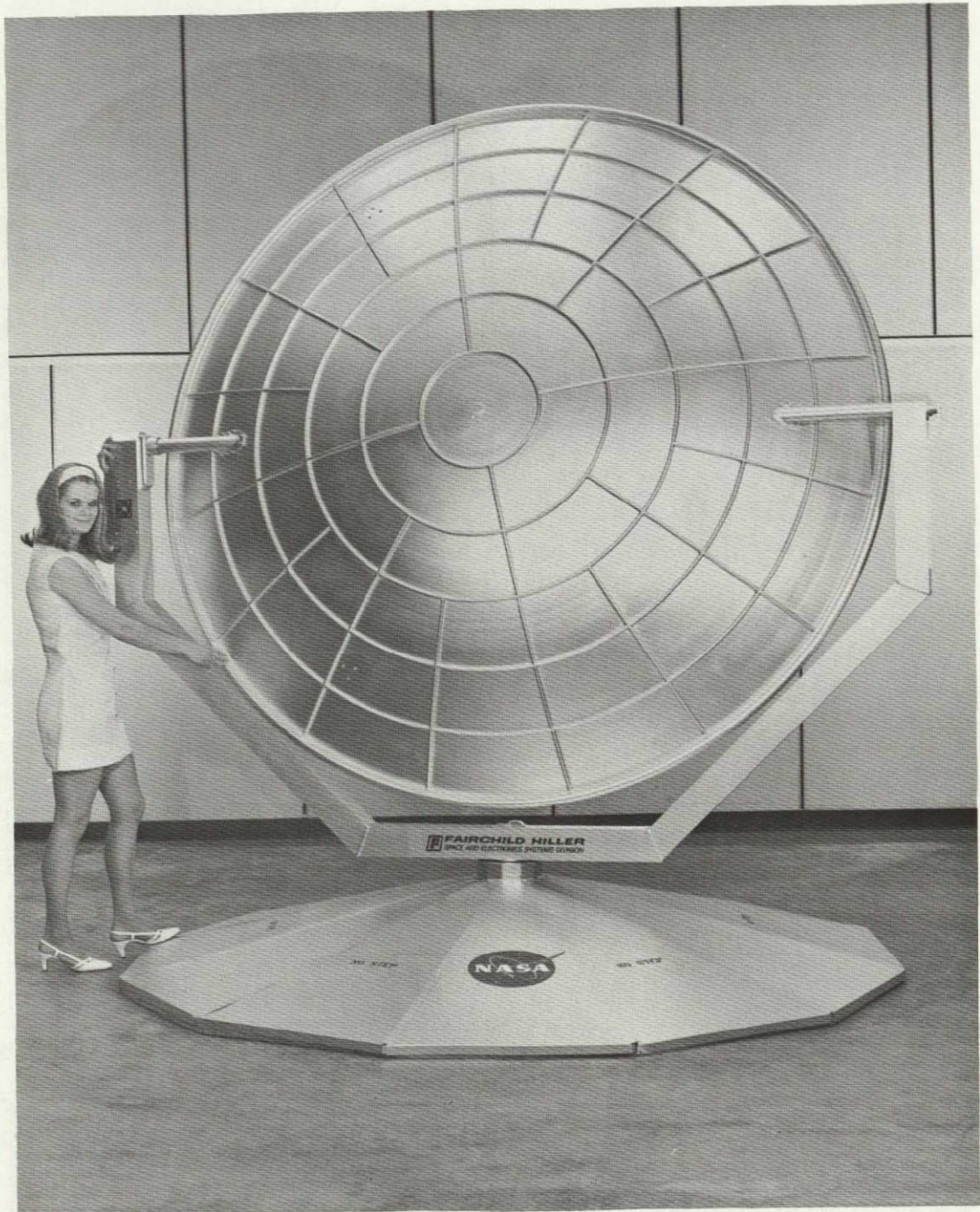


Figure 5.1-5. Parabolic Dish Model for Millimeter Wave Communications Satellite

The basic heat pipe consists of a closed tube, a wick, and a working fluid. Heat is transported by the utilization of change of phase and mass transfer. This is accomplished by evaporation of the working fluid in the heat source region, vapor flow to and condensation at the heat sink region, followed by return of the liquid phase working fluid through the wick structure to the heat source region.

The working fluid selection is based on the thermophysical properties, chemical stability, and compatibility with the container tube and wick materials. All of these parameters are important. The final selection is generally a compromise between the necessary and desirable conditions. Based on the selection process discussed in more detail in Volume 1B of the proposal acetone is chosen as the optimum working fluid for the ATS F&G application.

Aluminum has been chosen as the containing material because it is light in weight, easily obtained as an extrusion in any cross-section, and has the necessary weldability and formability for fabrication and assembly of the heat pipes. Internal longitudinal grooves are provided to function as channels for condensate return.

One potential disadvantage of grooved heat pipes without a screen wick is that in the presence of a gravitation field, the grooves of an optimum design for space application may not be capable of supporting the same amount of fluid as a pipe with wicks in an inclined position. Since it is invariably necessary to test a heat pipe in a 1-G environment, modifications on the optimum design may be implemented to greatly reduce the gravitational effects without any reduction in the performance under space conditions. The addition of a fine mesh screen covering the rectangular grooves will not only aid the operation of the heat pipe in the slightly tilted position, but will increase the maximum heat transport capability.

It has been shown analytically that the plain grooved heat pipe will meet the requirements of ATS F&G with a considerable growth potential. The performance of many such heat pipes have been verified during horizontal testing in the Heat Pipe Development Laboratory (Figure 5.1-6).

Because of the uncertainty of the heat pipe position (slightly tilted) during ground testing, FHC is proposing to add a fine mesh screen to the grooved pipe. The use of a square heat pipe cross-section instead of the round is also recommended. Not only will the transport capability increase for the same width (0.50 in), but more important, the contact area and thermal conductance between heat pipe and honeycomb face sheets is greatly increased. Structurally, the square cross-section is stiffer and the pipe walls will not distort because of the operating pressure which is at approximately 4 psia.

5.1.3 THERMAL COATINGS

Solar reflector coatings ($\alpha_s/\epsilon \ll 1$) must be employed when the amount of solar energy input to the spacecraft surface must be minimized while as much thermal energy as possible is concurrently emitted. Thermal analyses of the ATS F&G spacecraft have shown the desirability of covering the external surfaces of the north and south panels behind the louvers with such a coating.

300

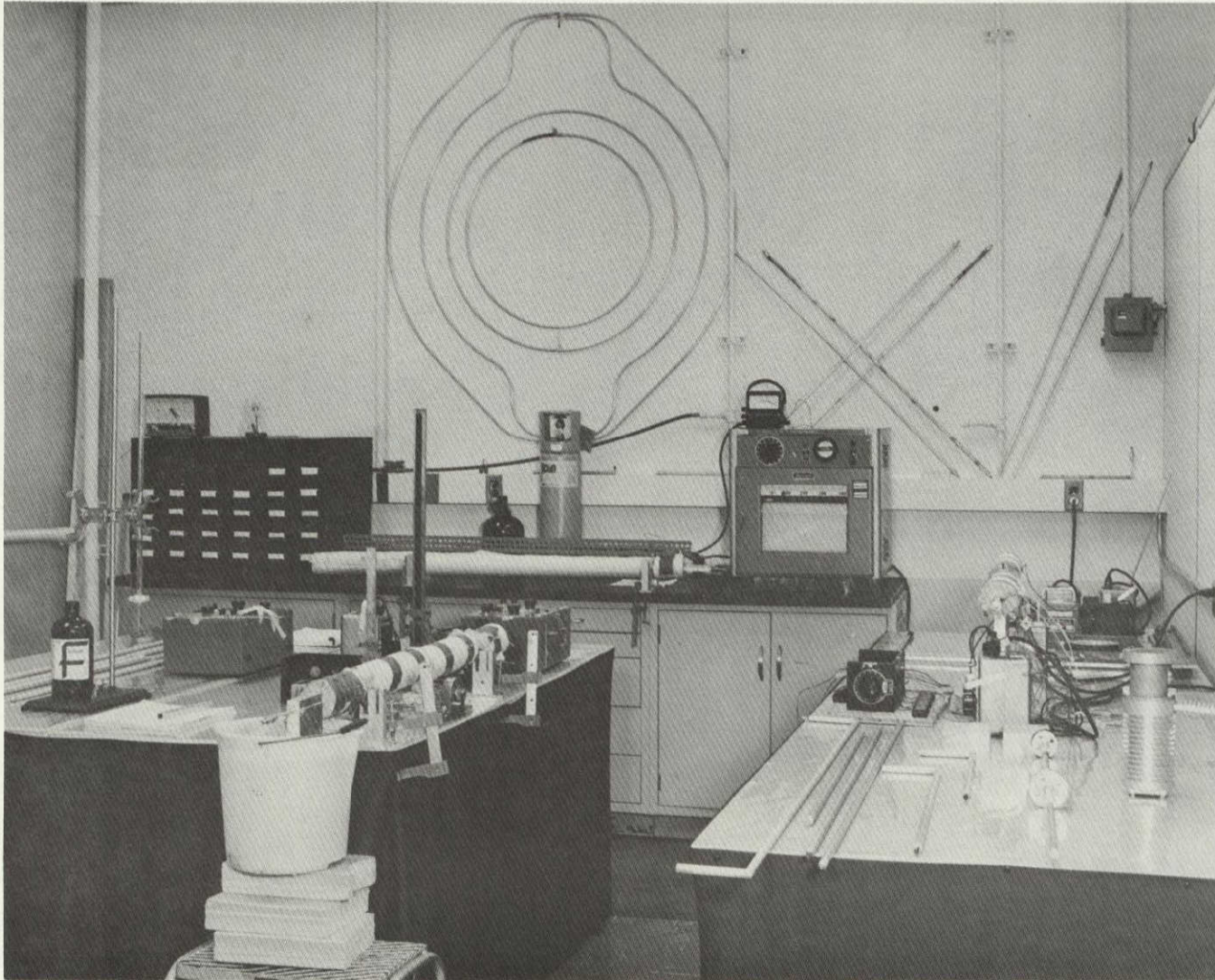


Figure 5.1-6. Heat Pipe Development Laboratory

The low α_s is desirable to minimize solar input when the sun strikes the north-south faces obliquely. A high ϵ is required to maximize heat rejection to space, thereby minimizing the louver area.

In selecting a solar reflector coating, both initial values of α_s and ϵ any changes in these values during a mission lifetime are very important. Most solar reflectors are subject to optical and/or physical degradation in the space environment, while others may be difficult to handle, apply, or maintain in the ground environment.

For long life missions in the range of 2 to 5 years, degradation of the α_s can be large for all white paints. In Volume 1B of the proposal, the results of an extensive coatings investigation are presented and the use of a second surface mirror coating system is recommended. Such a coating is vapor deposited silver on 8 mil thick fused silica called an Optical Solar Reflector (OSR). This coating exhibits little or no degradation in the space environment. It has been flown on Lunar Orbiter and OSO spacecrafts and has been extensively tested in the laboratory. The present design is predicated upon the use of OSR.

A secondary choice is the less costly series emittance coating system of silver-teflon. The series emittance thermal control coating consists of a transparent (to the solar spectrum) dielectric film over a highly reflecting metallic substrate. The reflectance of the metal primarily controls the solar absorptance; the thickness of the transparent film governs the emittance. This coating system has certain advantages over the OSR; however, it is still in the development stages. Detailed information on the above coating systems is provided in Volume 1B of the proposal.

5.1.4 MULTILAYER INSULATION

The ATS F&G Earth Viewing Module (EVM) will be thermally controlled through the use of thermal louvers. These louvers effect a change in the α/ϵ ratio of the radiating areas used to reject the EVM heat dissipation. In order to make full use of the temperature control derived by the use of thermal louvers, all heat rejected should pass through the louvers. In practical applications, the requirement can only be approach through the use of insulation systems.

The most efficient and reliable thermal insulation concept yet found for spacecraft applications is the multilayer system. This insulation represents at least an order of magnitude reduction in thermal conductivity over all other insulating systems, and is the most efficient insulation on a weight to thermal resistance basis. These multilayer insulations are composed of a large number of very thin layers of material having a high infrared reflectance separated by either continuous or discontinuous layers of a very low conductance material, or by physically deforming the reflective layers so as to provide effective separation of adjacent layers with a minimum of contact conductance. The reflective layers are usually a very thin (1/4 mil) film of plastic such as Mylar or Kapton supporting a vacuum-deposited layer of aluminum, silver or gold. A variety of spacer materials such as silk or nylon netting foam and organic or glass fibers have been used for both aerospace and commercial application. Integral spacers have been developed by such methods as crinkling or dimpling the metalized films, or by bonding small areas of fibers to one surface of the reflective sheet.

The advantages of using this multilayer insulation on the EVM are summarized in the following list:

1. Minimizes uncontrolled heat rejection
2. Reduces the solar flux input
3. Reduces the antenna reflected solar flux input
4. Minimum degradation due to space environment
5. Provides large thermal time constant during occult or bit acquisition, and in case of misalignment
6. EVM temperature gradients reduced
7. Most efficient insulation on a weight to thermal resistance basis.

These advantages are obvious except perhaps for items 4 and 6. Multilayer insulation does not degrade in space; however, the outer surface coatings used on the space viewing layer or cover may degrade during the lifetime of the spacecraft. At present, it is proposed to use a Kapton cover sheet with vapor deposited aluminum on the inside surface. This outer cover for the multilayer insulation is presently being used by Fairchild Hiller on the Nimbus D altitude control section. Little or no degradation of Kapton is expected; however, even with significant changes in the optical properties, the effect on the EVM temperature is negligible. Reduced EVM temperature gradients (Item 6) is brought about by essentially enclosing the EVM in an insulated box resulting in all the insulated outer structural surfaces being much closer to the internal temperature.

5.2 SOLAR ARRAYS

The solar arrays consist of two semi-cylindrical paddles, each of which has replaceable slats to which the solar cells are mounted. The primary thermal objectives concern minimization of the operating temperature of the cells and determination of the temperature profile during orbit.

The solar cell temperature is a function of the thermal properties of all external surfaces and the effective thermal paths between the cells and these surfaces. The external surfaces can be subdivided into five areas:

1. The cell cover glass - with respect to thermal emittance and the portions of solar energy reflected and absorbed
2. The front cell surface - with respect to the solar energy absorbed from that which the cover glass is transmitted
3. The exposed inter-cell wiring
4. The interstitial area between cells and
5. The anti-sun surface of the honeycomb substrate

There is very little that can be done thermally with the limited choice of candidate cells and cover glasses. The selection of an optimum cover glass which reflects a maximum of solar energy is well defined and thermally fixed. The optimum cover glass reflects a maximum of solar energy which the cell is not able to utilize, and transmits that portion of the solar spectrum which the cell can use, with minimum absorptance loss.

Past trade-off studies concerning the modification of the exposed inter-cell wiring and interstitial area between cells to reduce temperature (for increased efficiency) have shown very definite increases in fabrication complexity, cost, and system weight. Thus, efforts to optimize, with respect to cell temperature, this relatively small area of the sunlit surface, has been somewhat futile. Therefore, the average effective thermal properties of the complete front surface have been fixed to be $\alpha = 0.70$ and $\epsilon = 0.85$.

The only area left for thermal control is the rear surface of the paddles. It is desirable for the space viewing side of the honeycomb substrate to have a high emissivity maximizing heat rejection to space and to have a low absorptivity, minimizing the effect of solar irradiation when the sun views the bottom of the substrate. To obtain these properties, it was decided to coat this surface with Thermatrol, a white paint having an $\epsilon = 0.85$ and an $\alpha = 0.20$ which was conservatively estimated to degrade to $\alpha = 0.40$.

The second area of thermal study of the solar array was to determine the temperature profile during orbit. Having concluded selection of coatings in the preceding study, this was readily accomplished using a multinode mathematical mode. A complete discussion of this analysis is presented in Volume 1B of the proposal. The results of the analysis were used by the Spacecraft Power group to satisfactorily verify the array design.

5.3 REFLECTOR SUPPORT TRUSS

Dependence on a refined truss temperature control system alone to prevent misalignment between the feed and the reflector is not practical. Hence, the truss is to be constructed of a material having a negligible thermal expansion coefficient and is protected by a passive coating using aluminized kapton with the kapton facing out. The kapton will not degrade in the space environment and eliminates high temperature extremes.

Three possible temperature conditions have been identified which could lead to errors in the feed position. These temperature conditions are:

- Orbital changes in average truss temperature
- Temperature gradients across a tube
- Temperature differences between tubes

The average truss temperature is determined by the environment, the thermal control coatings and the thermal capacitance. Changes in the average temperature result in a movement of the feed along the z-axis. Temperature gradients across a tube may be caused by the sun lighting one side of a tube. This gradient varies as a function of the sun angle to the tube axis with the maximum gradient occurring

when the sun is normal to the axis. The temperature difference between truss tubes is caused by the shadow of the hub, the EVM and other tubes. Different temperature distributions occur during the orbit, thus requiring a complete orbit analysis for this effect.

Analysis has shown that in the absence of super insulation large temperature variations will occur on the truss tubes during orbit, and cause unacceptable errors in the feed position if the support truss is made of aluminum, titanium, or beryllium. Since the coefficient of thermal expansion for these materials is quite high, a search was initiated to find a more suitable tube material. Graphite fiber reinforced plastic (GFRP) was chosen since it satisfied all structural requirements and has a low coefficient of thermal expansion requirement. Whereas the use of this material does not improve the orbital temperature swings, the extremely low coefficient of thermal expansion eliminates feed errors.

Should the lower temperature extreme prove to be detrimental, it may be increased by stripping the kapton with polished aluminum or employing a stripped pattern of black paint and polished aluminum. Additional details related to the feed support design and transient analysis are given in Volume 1B of the proposal.

5.4 REFLECTOR HUB COMPONENTS

There are two experiments, EME and COGGS, located on the hub-bridge truss which require temperature control. These experiments will be thermally isolated from the spacecraft and will be temperature controlled by passive means.

As an example which illustrates how these experiments will be thermally controlled, consider the EME experiment. The experiment is to be supplied by GSFC and ultimately the responsibility for thermal control is theirs. The subject thermal analysis is presented by way of illustration using size, weight, and dissipation values supplied by Goddard.

The components are contained in a box 18.5 in x 14 in x 14 in and weight 90 lbs. Since the hub and the hub-bridge truss are open structures, the EME will receive solar radiation during most of the orbit. Using this flux input together with an internal power dissipation of 46 watts, the temperature profile of the EME was calculated for a surface coating having optical properties of $\alpha = 0.2$ and $\epsilon = 0.26$, which may be obtained from second surface mirrors.

The result of the calculation shows that for a constant 46 watt dissipation, temperature control will be maintained between 42° and 75°F. The lower curve corresponding to no dissipation may be used to predict the initial temperature at start-up. Thus, depending on the position during orbit, the temperature when the component is activated could be as low as -45°F. It is anticipated that this lower limit will not present a problem; should this not be the case, the lower limit can be increased by changing the thermal-optical properties of the exterior coating at the expense of elevating the upper temperature bound only slightly.

5.5 GROUND COOLING SYSTEM

5.5.1 LABORATORY

An auxiliary forced air cooling system is recommended to maintain acceptable surface temperatures during laboratory testing. The system consists of a set of integrated "tee" shaped air ducts that are mounted to an auxiliary structure which rolls on wheels. When the auxiliary system is in the operation position, a set of ducts press against both the North and South faces of the EVM using a compressible protective gasket as a seal. During these tests, the thermal louvers will not be attached to the EVM faces. By forcing air across the North and South skins, high convective heat transfer coefficients can be obtained which are equivalent or superior to the effective radiation coefficients realized in space.

5.5.2 PRE-LAUNCH CHECKOUT TESTING

No auxiliary cooling system will be required during pre-launch testing which occurs on the launch pad when the spacecraft is positioned on the launch vehicle. Transient thermal analysis has shown that natural convection in the air conditioned shroud will be sufficient to maintain acceptable surface temperatures for the short duration checkout tests periods. Additional details and transient curves are included in Volume 1B of the proposal.

SECTION VI

TRANSPONDER SUBSYSTEM

6.1 INTRODUCTION

The transponder subsystem of the ATS F&G satellite provides the basic interface between the experiments in the satellite and ground terminals. In many instances, the transponder is itself a part of the experiment. To accommodate the wide variety of experiments in the satellite, an exceptionally versatile and flexible transponder has been developed. In addition, Philco-Ford Corporation, Fairchild-Hiller's team subcontractor, as a result of in-house programs, has developed several "state of the art" components to help achieve minimum weight and cost with maximum reliability. In total, the transponder described in the following volume represents a unique and exceptionally efficient solution to the requirements of the ATS F&G satellite.

The functions to be performed by the transponder subsystem may be grouped into two broad categories. First, the transponder must receive signals from ground terminals, airborne terminals, and other spacecraft. The ATS F&G transponder processes these signals and either retransmits them at different frequencies or routes them to experiments and other subsystems on board the satellite. Second, the transponder must accept data generated within the satellite and prepare it for transmission to ground terminals.

The transponder is housed in the top separable section of the EVM along with the related Radio Beacon, RFI and T&FD experiments. With the composite Feed subsystem being integral with the top cover this allows the entire Communication Subsystem to be assembled and tested separately but in parallel with the rest of the ATS F&G, thus saving much program time. In addition, this grouping will provide improved isolation from undesirable interference products.

The most meaningful way to characterize the overall transponder performance is to include the antenna parameters which were summarized in the Parabolic Antenna Feed Volume so that G/T and ERP estimates may be made. A summary of these performance estimates is given in Table 6.1-1. Values of ERP and G/T are given in the table for the various frequency bands for antenna beam peaks and as minimum values over a defined field of view. The field of view minimum values set a worst case limit on the expected system performance. Many other system parameters such as frequency response, phase linearity, group delay, frequency stability, spurious levels, and time delay are of interest in an overall description of the transponder performance. In general, these parameters are delineated in the Transponder Subsystem Specification and will not be discussed in detail here. Certain parameters of interest are discussed in the transponder subassembly descriptions which follow. A description of the overall transponder breadboarding and a discussion of the test results are given in a separate breadboard summary volume.

Table 6.1-1. Communication Subsystem Performance Summary

	X-BAND		S-BAND	L-BAND		UHF (850 MHz)	VHF (150 MHz)
	HORN	DISH		FAN	PENCIL		
RECEIVE							
Receiver Noise Figure (dB)*	7.2	7.2	4.1	5.6	5.6	-	12.0
System Noise Temp (°K)(1)	1525	1525	746	1045	1045	-	4590
Antenna Gain (dB) (3)							
Peak	18.0	50.9	40.4**	33.4	39.0	-	16.5
Min (over field of view)	15.0 (20°)	47.9 (0.3°)	36.6 (13°)	29.7 (1°x7.5°)	36.0 (1°)	-	13.5 (16°)
G/T (dB/°K) (2)							
Peak	-13.8	19.1	11.7	3.2	8.8	-	-20.1
Min	-16.8	16.1	7.9	-0.5	5.8	-	-23.1
TRANSMIT							
Transponder output power* (dBW)	+12.5	+12.5	+12.8	15.6	15.6	18.6	-
Antenna Gain (dB) (3)							
Peak	17.2	50.5	39.5**	33.4	39.0	33.0	-
Min (over field of view)	14.2 (20°)	47.5 (0.3°)	36.4 (13°)	29.7 (1x7.5°)	36.0 (1°)	30.0 (3°)	-
ERP (dBW)							
Peak	29.7	63.0	52.3	49.0	54.6	51.6	-
Min	26.7	60.0	49.2	45.3	51.6	48.6	-

* Including Transponder line and diplexer losses

** On-axis gain

$${}^{(1)}T_S = 290(L)(NF)$$

where L = feed line loss
 NF = receiver noise figure
 Antenna noise temperature = 290°K
 T_S = system noise temperature

$${}^{(2)}G/T \text{ (dB)} = 10 \log (\text{Antenna gain}) - 10 \log T_S$$

{}^{(3)}Gain figures include antenna subsystem feed losses

NOTE: C-Band (6.3 GHz) antenna gain is 49.3 dB peak, including antenna subsystem feed losses. Field of view (3 dB) is 0.4 degrees.

6.2 TRANSPONDER CONFIGURATION

The following subsections describe the major transponder assemblies and their functions. A block diagram of the proposed transponder is shown in Figure 6.2-1. The transponder consists of four major assemblies: the receiver, the IF amplifier, the transmitter, and the frequency synthesizer. Supporting the major assemblies are the RF input-output circuitry, wideband data unit, monopulse detector, transponder command distributor and dc-dc converters.

6.2.1 RECEIVER

The receiver assembly includes preamplifiers, monopulse modulators, mixers, and appropriate filters and interconnecting circuitry. The preamplifiers and mixers are discussed in the following paragraphs. The monopulse circuitry is discussed in Paragraph 6.2.6 and the filters and interconnecting circuitry in 6.2.5.

The preamplifiers are provided at X-, S-, and L-band to achieve maximum transponder signal-to-noise ratio. The X-band and S-band preamplifiers are tunnel diode types with a noise figure of 7 dB and 3.7 dB respectively. L-band preamplifiers use transistors with a noise figure of 4.5 dB. The gain of the preamplifier is approximately 15 dB. Redundancy is employed to increase reliability. A triplexer is used to separate and combine the three X-band channels and also for image suppression. Filtering has been selected rather than hybrids in order to decrease the RF losses. Interdigital filters will be used for this application. Five mixers are included in the receiver to down convert the received signal frequencies to the intermediate frequency. The mixers used on ATS are of the balanced type with diodes and circuitry appropriate for the frequency of operation. Three operate at X-band (8025, 8150, and 8250 MHz), and one at L-band (1650 MHz), and one at S-band (2250 MHz).

6.2.2 IF AMPLIFIER

The IF amplifier consists of an IF input switch matrix, three identical IF amplifiers and an IF output switch matrix. To achieve high reliability with maximum flexibility, IF switching is provided to interconnect the various circuits. The input switch matrix allows any down-converter to be connected to any IF amplifier. The output switch matrix allows any IF amplifier to be connected to any up-converter or the monopulse detector. Further, the wideband data unit can be connected to any up-converter. The IF amplifier is a cascade of high gain, wide bandwidth amplifier stages. The use of wideband stages ensures that the IF amplifier frequency response (both amplitude and delay) is determined only by the bandpass filter. A greatly simplified block diagram of the IF amplifier is shown in Figure 6.2-2. The amplifier includes a high accuracy AGC, selectable bandwidths, and provides signal processing for either signal translation modes or multiple access modes. Special functions have been included to provide the proper signal interfaces for experiments such as, monopulse wideband laser and millimeter wave, and Apollo emergency voice among others.

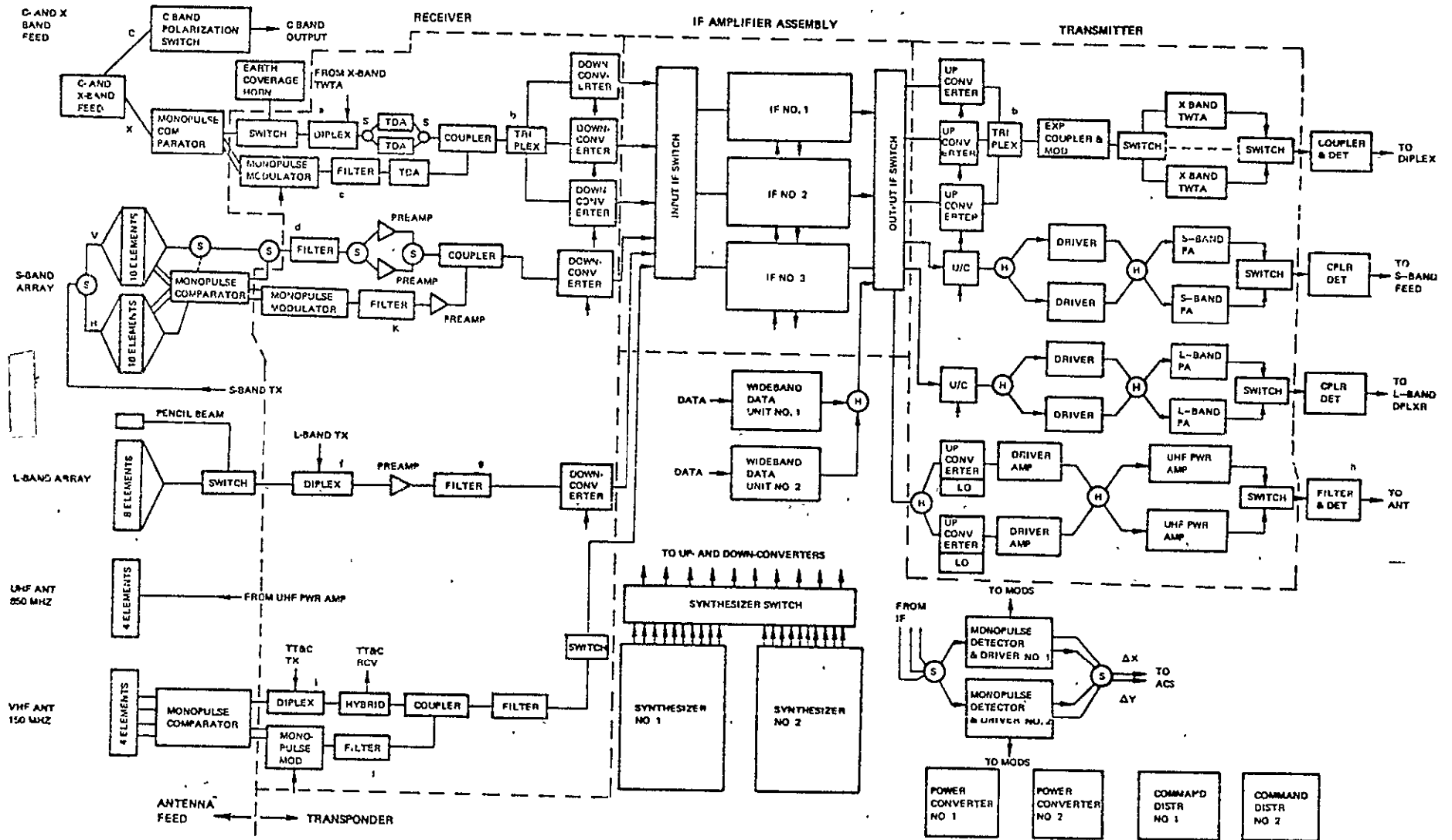


Figure 6.2-1. ATS-F Communication Subsystem Block Diagram

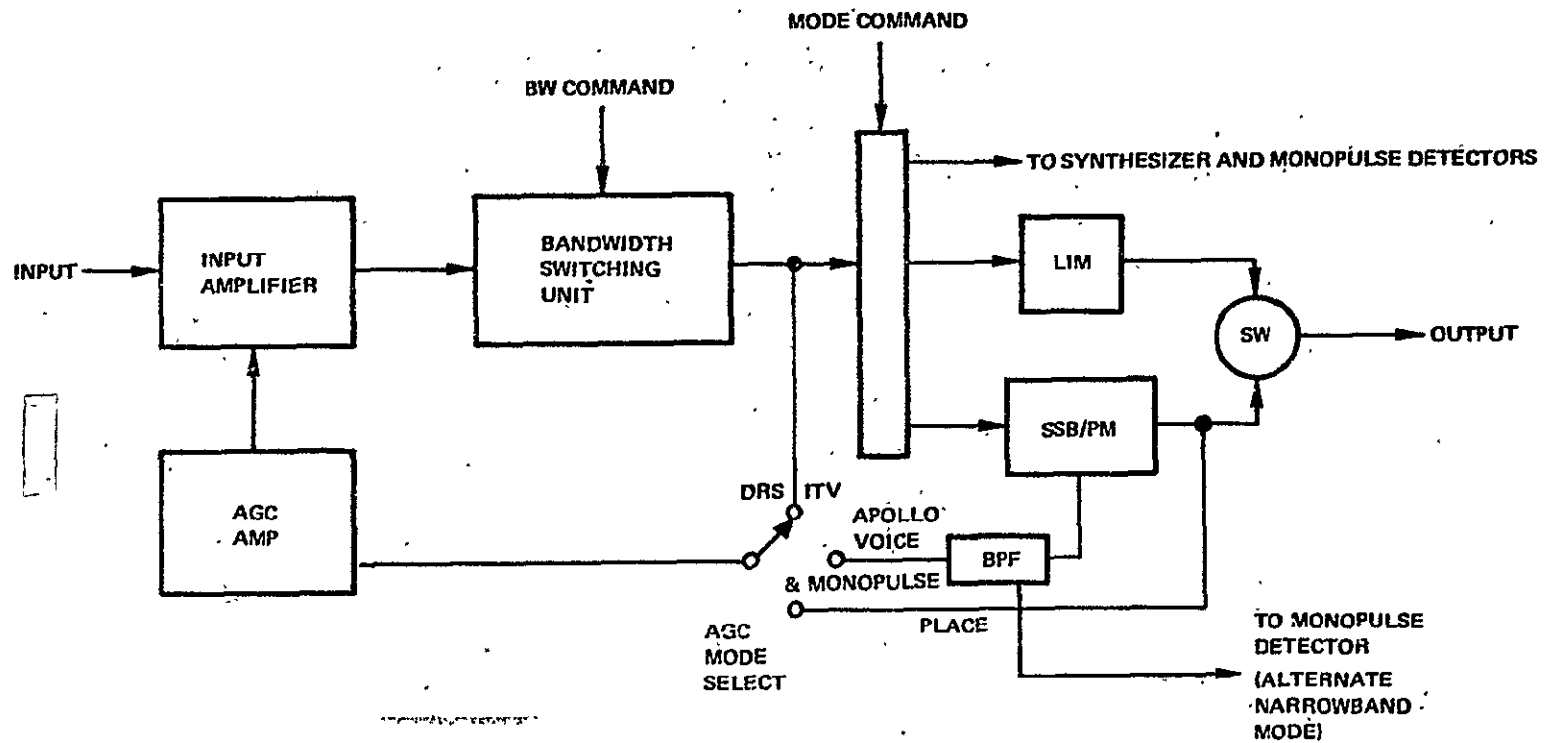


Figure 6.2-2. Simplified IF Amplifier Block Diagram

6.2.3 SYNTHESIZER

The synthesizer used direct synthesis from a single frequency standard. The simplified block diagram shown in Figure 6.2-3 does not show all the multiplication details which are covered in Section 2. The figure shows the signal flow for the coherent repeater operation mode. The 8150 MHz signal is chosen as an example receive frequency and 1550 as an example transmit frequency. Since the 8000 MHz local oscillator is derived by direct multiplication and division of a 100 MHz master VCO, all the synthesizer outputs are coherent to the VCO. Once the VCO is locked to a received frequency all other frequencies derived from the VCO by combinations of multiplication and division are also coherent to the received signal. The 150 MHz IF signal is mixed up to 1550 MHz, amplified and transmitted and is coherent to the received 8150 MHz signal. When it is desired to have the synthesizer operate independently of the received frequency, a highly accurate reference oscillator is substituted in place of the IF signal in the phase detector, and the synthesizer locks to the reference oscillator. High reliability is achieved by having a standby synthesizer.

6.2.4 TRANSMITTERS

Six up-converters are provided to convert the intermediate frequency signals to the output frequencies. Balanced type mixers are employed. In the case of the three X-band up-converters, about +5 dBm of output is needed. This would require as much as 100 mW of local oscillator power for a conventional mixer. This is overcome by using a parametric up-converter with a 25% LO to RF efficiency with local oscillator power of +11 dBm. The X-band power amplifier consists of two traveling-wave tube amplifiers (TWTA's) in a switched standby redundant configuration. The amplifier selected consists of a Hughes 240H TWT and a Hughes power supply. The TWTA provides 20 W output power at 7.2 GHz with 40 dB gain. The S- and L-band power amplifiers are solid state amplifiers capable of 20 watts and 40 watts output respectively. Except for tuning and number of stages, the amplifiers are identical. The UHF amplifier is used in the ITV experiment to transmit the television signal. The basic requirement is 80 W of output power at 850 MHz. A transistor amplifier was selected. The signal is 40 MHz wide and frequency modulated so it can be handled by a Class C amplifier.

6.2.5 INPUT-OUTPUT CIRCUITRY

The input-output circuitry consists primarily of the diplexers. The diplexing filters contribute to the noise figure of the receiver and the transmitter losses. Consequently, waveguide techniques are used which minimize the losses.

6.2.6 MONOPULSE TRACKING OPERATION

The ATS-F includes three monopulse tracking systems. One at VHF (150 MHz), one at S-band (2250 MHz) and one at X-band (8 GHz). This gives the system the capability of coarse and fine pointing. The error signals are routed directly to the attitude control system, making the satellite self-controlled. Although the hardware for the three frequencies differ, they perform the same system function.

6.2.7 WIDEBAND DATA UNIT

The wideband data unit is consolidated interface for sending several types of information from the spacecraft to the ground. The information handled is laser video, radiometer, high resolution camera and Apollo emergency voice.

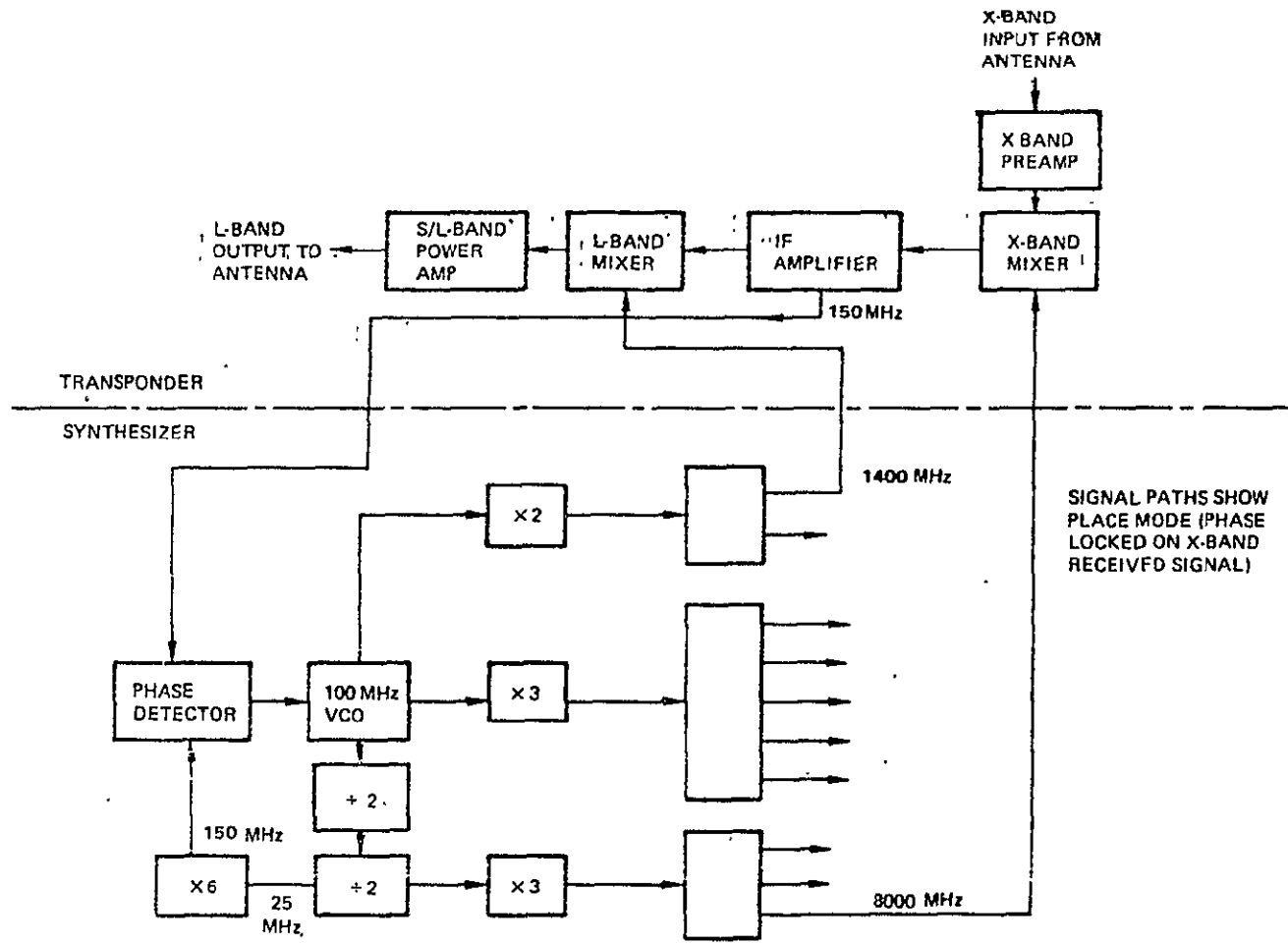


Figure 6.2-3. Simplified Synthesizer Block Diagram

6.3 RF RECEIVE SECTION

The receive portion of the integrated transponder contains all preselector filters and diplexers, preamplifiers, and down-converter mixers (transmit filters and up-converters are also included in this section for convenience). These components for each of the transponder frequency bands are discussed in the following paragraphs.

6.3.1 DIPLEXERS AND FILTERS

The filters required in the various signal paths through the transponder are shown cross-hatched on the block diagram of Figure 6.3.1. The circled numbers on the diagram identify the various components for clarity in the following discussion.

The design approach taken on all transmit and receive filtering is that all interfering signals at the input of the microwave preamplifiers should be at least 10 dB below the thermal noise level (kTB) for in-band spurious and low band spurious signals. It is assumed that out-of-band spurious signals which may be generated by the individual transmitters will be at least 60 dB below the maximum output power for that transmitter.

These criteria were used to calculate the filter design data which is summarized in Table 6.3-1. Each filter identified in this table was analyzed in detail to determine the optimum tradeoff between construction type (waveguide or interdigital) insertion loss, bandwidth, number of poles and required rejection. The filter design is necessarily preliminary in character but is sufficient to indicate that filter/diplexer/triplexer performance requirements are nominal and will not present a problem in the final design of the integrated transponder.

6.3.2 RF PREAMPLIFIERS

Preamplification prior to down conversion is used at X-band, S-band, and L-Band in order to obtain minimum noise figures. Tunnel diode amplifiers are used at X-band and S-band, while transistor preamplifiers are used at L-band. Redundant preamplifiers are included in the sum channels of the X- and S-band monopulse feeds, while single nonredundant amplifiers are used in the error channels. Link calculations show that sufficient power is available at VHF (150 MHz) so that preamplification is not necessary prior to amplification at the IF frequency.

6.3.2.1 X-Band Preamplifiers

The X-band tunnel diode amplifier is a Philco-Ford proven design for space applications. The measured noise figure of the amplifier is 5.5 dB, the gain per stage is 15 dB over a 800 MHz bandwidth, and weighs 0.33 lb per stage.

Considerable work has been done on X-band tunnel diode amplifiers at Philco-Ford which has resulted in several improvements in amplifier design that are not generally available in commercial units. Philco-Ford has designed, for space application, a TDA which has both good performance as an amplifier and controlled limiting characteristics. The TDA is capable of operating over a wide frequency band as required by the ATS-F application. A typical frequency response curve for the amplifier is shown in Figure 6.3-2.

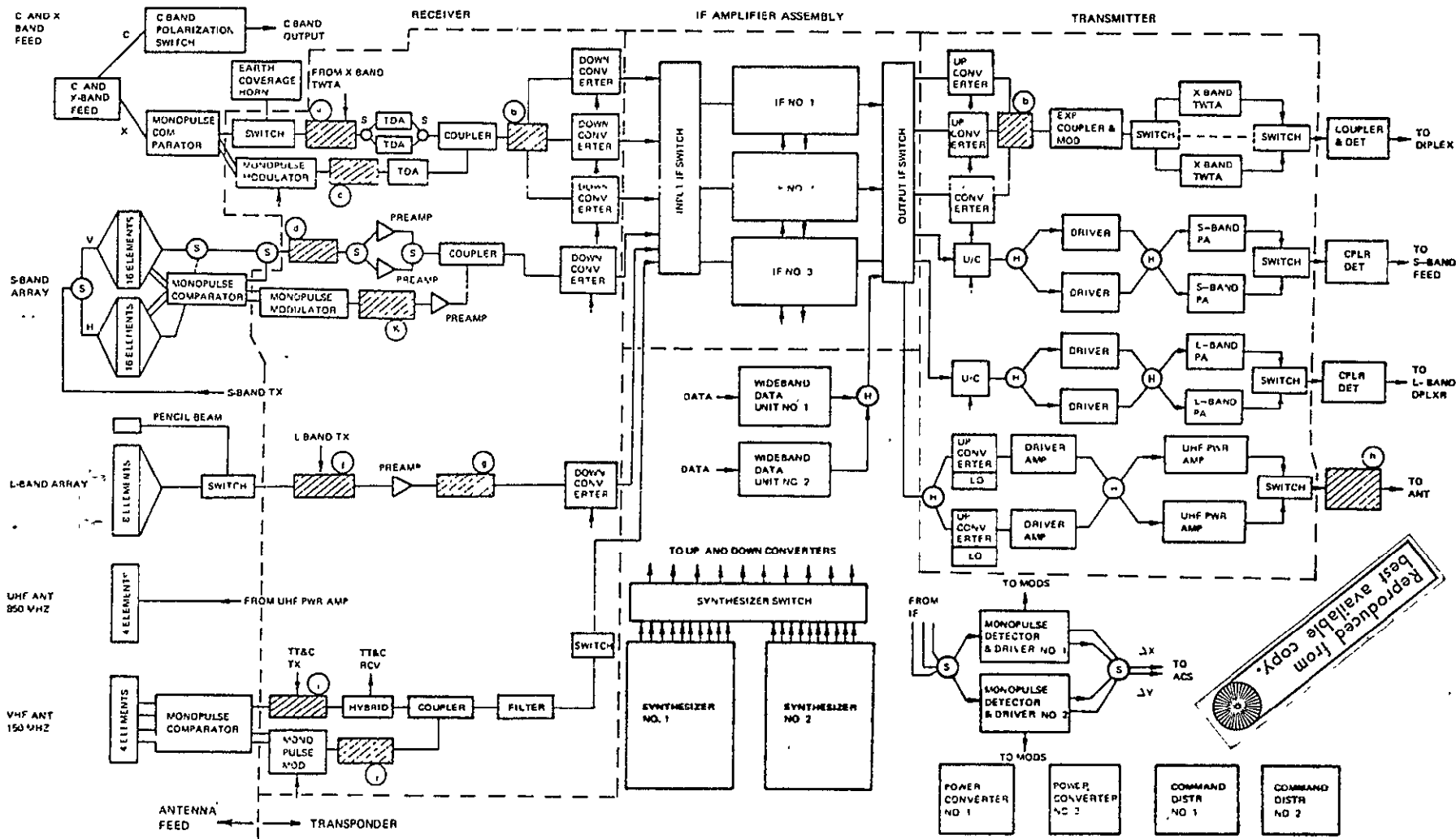


Figure 6.3-1. Transponder Diplexers and Filters

Reproduced from
 best available copy.

Table 6.3-1. Microwave Filter Summary

Component	Description	No. Sect	Fo GHz	Ins. Loss (db)	Rejection		Ripple BW (GHz)	3 dB Bandwidth (MHz)
					F (GHz)	L (db)		
(a) X-Band Transmit/Receiver Diplexer	Rcvr WG Filters	11	8.150	0.232	7.600	137	414.4	275
	Xmit WG Filter	8	7.400	0.210	8.000	76	522.3	425
(b) X-Band Triplexer	Rcvr Interdigital	5+5	8.250	2.0	8.15	30		76
	Rcvr Interdigital	5+5	8.150	2.0	8.25&8.025	30		76
	Rcvr Interdigital	3	8.025	1.0	8.15	20		52
	Trans Interdigital	5+5	7.650	2.0	7.575	20		66
	Trans Interdigital	5+5	7.575	2.0	7.65&7.35	20		52
(c) X-Band Error Channel Filter								
(d) S-Band Rcv Filter	22 in. of WR-284 waveguide near cutoff	NA	2.250	0.18	1.800	130		50
(e) L-Band Trans/Rcv Diplexer	Interdigital Rcvr	9	1.650	1.45	1.550	141	49.44	
	BPF Coaxial Cavity Bandstop Xmit	10	1.550	0.20	1.650	81		
(f) L-Band Rcv. Filter	Interdigital WB		1.650	0.03	2.225	30		600
(g) UHF Xmit Filter	Interdigital BPF	5	0.850	0.159	0.450	88	180.34	
(h) VHF Diplexer	Helical Resonant BPF	5	0.151	0.850	0.850	148	22.79	
(i) VHF Mplse Filter	Helical Resonant BPF							

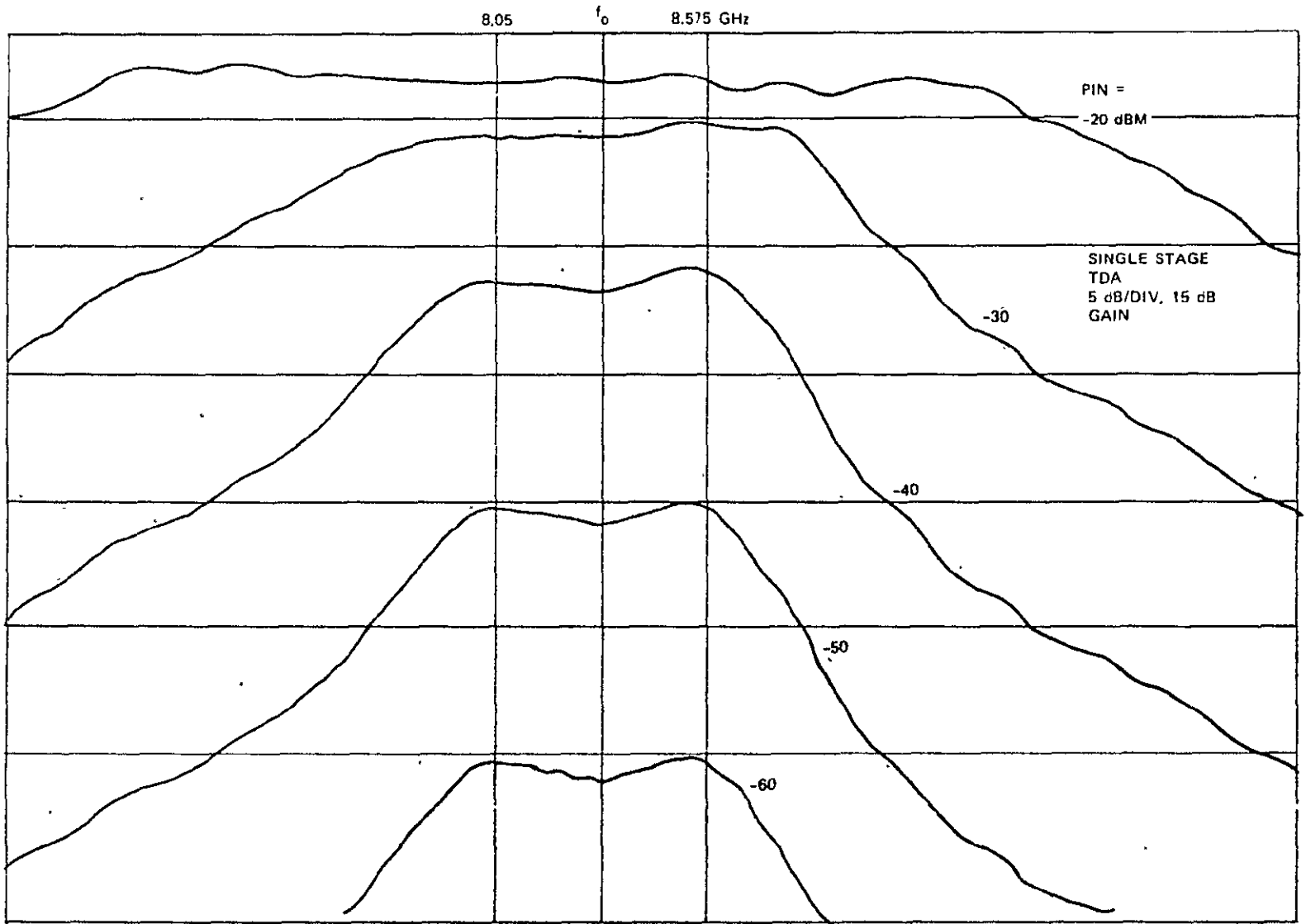


Figure 6.3-2. Typical TDA Frequency Response

Considerable attention has been devoted to the reliability aspects of the TDA design in order to obtain the maximum possible life. The diodes used in the amplifier have been subjected to extensive reliability and life testing by the vendors, and Philco-Ford plans to conduct its own testing of both the diodes and the completed TDA's.

6.3.2.2 S- and L-Band Preamplifiers

Two types of preamplifier could be used at L- and S-bands. One would be the tunnel diode amplifier, the other would be the transistor amplifier.

A survey was made of current microwave transistor types which would be suitable for the input stage of a RF preamplifier at L-band and S-band. The study showed that transistors were available having 4.0 dB noise figure and 9 dB gain at 2 GHz.

Presently available commercial amplifiers are able to attain a 5.0 dB noise figure at 2.25 GHz and a 4.5 dB noise figure at 1.6 GHz. "State-of-the Art" TDA's at S-band can achieve 3.7 dB noise figure. The reliability figures are similar for the two types, while the size and weight of the TDA is about twice that of a transistor amplifier. The disadvantage of the transistor amplifier is that it will not allow signal feedthrough with a bias failure, while a TDA will lose the normal gain plus about 1 dB. A transistor amplifier is less temperature sensitive than the TDA amplifier and its gain is adjustable in 5 dB increments by adding stages; the minimum TDA increment is about 15 dB.

The present G/T requirements at S-band will require a two stage TDA to achieve a noise figure compatible with the system antenna gain. At L-band however, the advantages of the transistor preamp outweigh the advantages of the TDA and the transistor is recommended for L-band.

6.3.3 DOWN-CONVERTER MIXERS

6.3.3.1 X-Band Mixers

The X-band front end will use separate mixers in each of the three X-band channels for down conversion to the 150 MHz IF frequency. Each mixer will use doubly-balanced Schottky diodes. The conversion loss for each mixer with isolators is about 8 dB, making the total system noise figure at the preamp input approximately 6.8 dB. Where necessary, isolators are used to insure the mixer will have a flat frequency response over the required range.

6.3.3.2 S-Band and L-Band Mixers

A doubly-balanced Schottky diode mixer will be used to convert the S-band and L-band signals to the 150 MHz frequency. The conversion loss with isolator will be about 8 dB, and the reciprocal isolation between signal and local oscillator ports is about 20 dB. The required LO power is nominally +3 dBm. A commercially available unit such as the Aertech 2017 or similar will be used.

Frequency Range	7.3 to 7.7 GHz
Power Output	20 W min.
Gain	43 dB min.
Phase Linearity	±2.0 degrees/10 MHz
AM/PM Conversion	6.0 degrees/dB
Spurious Responses	60 dB below carrier
Noise Figure	30 dB. max.
VSWR (input)	1.4:1
Power Consumption	80 watts
Amplitude Response	±0.5 dB (saturated)

6.3-4 S- AND L-BAND POWER AMPLIFIER

During the Phase C study, numerous tradeoffs were conducted comparing a TWTA vs solid-state amplifiers for the S- and L-Band power amplifiers. The reduced cost and weight associated with the solid-state amplifiers led to the use of two transistor amplifiers (one for S-, and one for L-) rather than a single dual mode TWTA.

A block diagram of the proposed configuration for each of the amplifiers is shown in Figure 6.3-3. The S-band amplifier uses four RCA TA7205 transistors in parallel to produce 20-W output power at 1800 MHz. The output stage is preceded by five single transistor stages which provide more than 30 dB gain and raise the S-Band and up-converter output level to that required to drive the output stage. The L-band amplifier uses eight parallel-combined RCA TA7205 stages to produce 40-W output power at 1550 MHz. The output stage is driven by two similar stages in parallel, preceded by four single transistor drive stages.

The transistor amplifiers for both S-band and L-band are connected in a standby redundant configuration to provide high reliability. The desired amplifier is selected at the output port by means of a latching ferrite circulator switch. Block diagrams of the redundancy switching for the solid state amplifiers are shown in Figure 6.3.4. The redundant TWTA configuration is also shown for comparison. Table 6.3-2 shows performance trade-offs for solid state vs TWT.

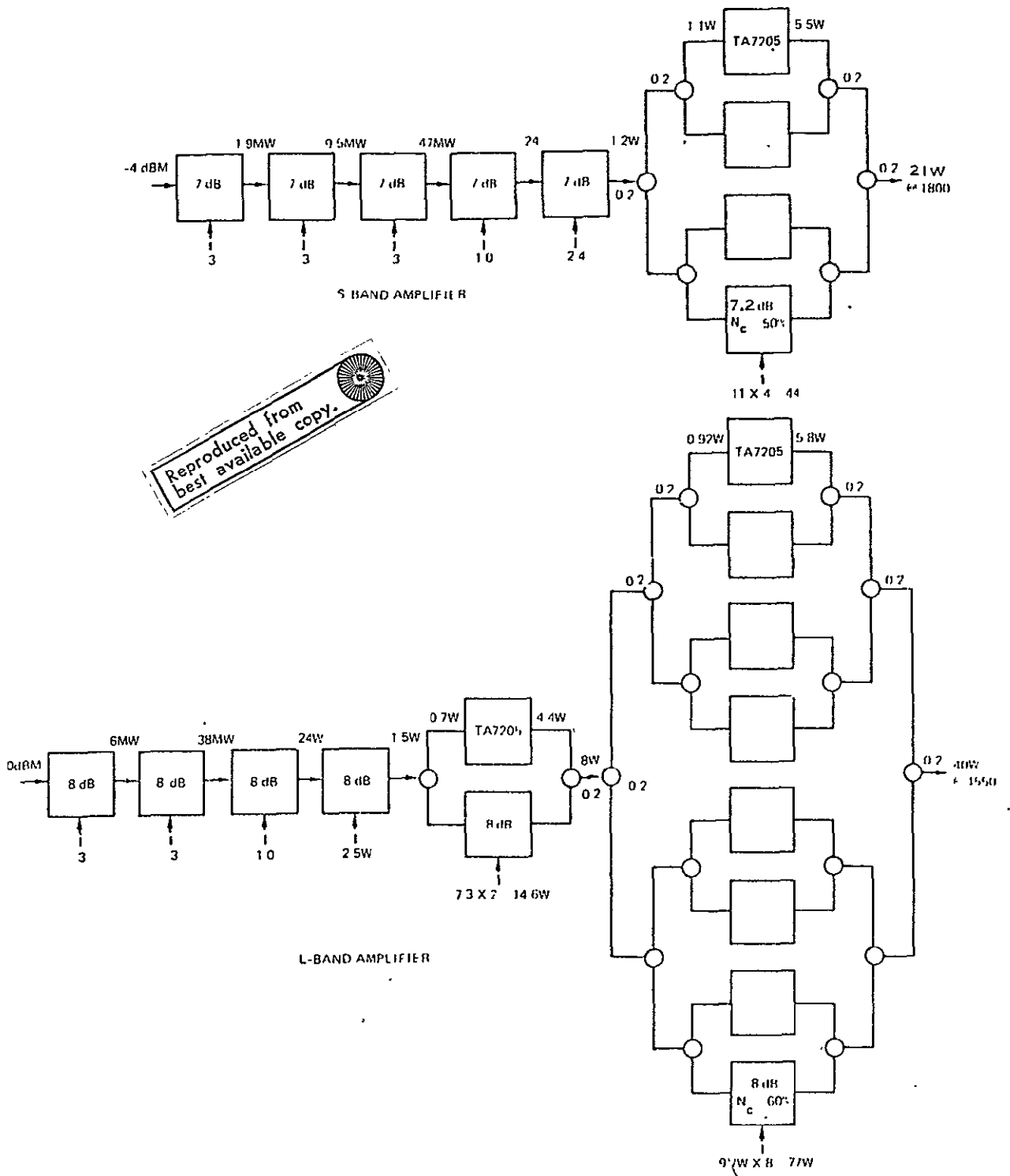
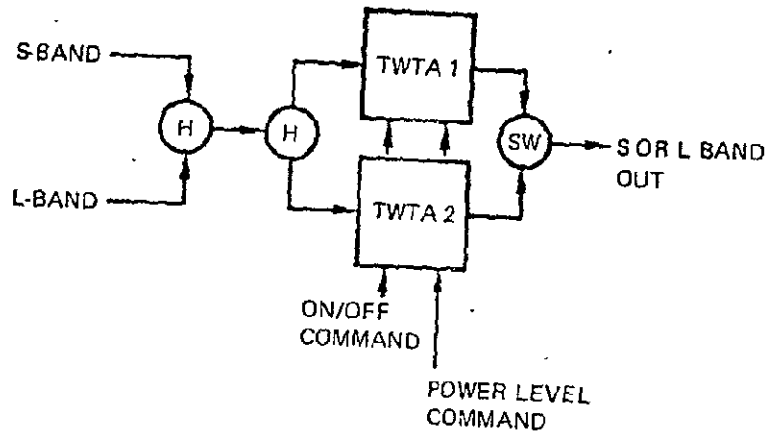
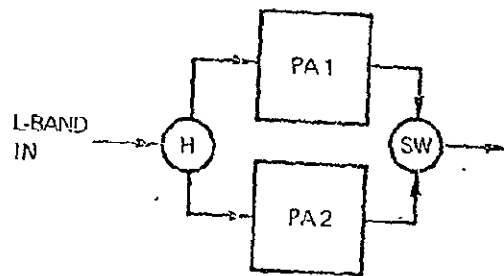
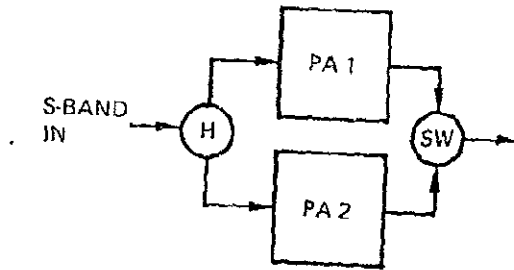


Figure 6.3-3. Solid State S- and L-Band Power Amplifier Configurations



(a) TWTA Redundancy Configuration



(b) Solid State Power Amplifier Redundancy Configuration

Figure 6.3-4. S- and L-Band Power Amplifier Redundancy Configurations

Table 6.2-3. Comparison of TWTA and Solid State S- And L-Band Power Amplifiers

	TWTA	Solid State
Configuration	Single S-/L-band TWTA, 2-mode power supply standby redundant	Separate S- and L-band amplifiers standby redundant
Efficiency	26%	30 - 40%
Weight	21 lbs	8 lbs
Reliability	0.991	0.9998
Relative Cost	1.0	0.3

6.3.5 UHF TRANSMITTER

The UHF transmitter provides 80 W RF output power at 850 MHz for the ITV experiment. Solid state and tube approaches to generating this power were examined, and the solid state approach was chosen on the basis of the superior dc to RF efficiency obtainable and the increased reliability compared to tube approaches.

A block diagram of the recommended UHF transmitter configuration is shown in Figure 6.3-5. It consists of redundant driver amplifiers driven from a hybrid power splitter, followed by redundant power amplifiers.

The driver amplifiers and power amplifiers are connected by a hybrid coupler. This arrangement provides maximum reliability by allowing each driver amplifier to drive either power amplifier. The output of the power amplifier is connected to the UHF antenna through a coaxial switch.

A block diagram of the power amplifier stage is shown in Figure 6.3-6. It uses eight 2N5595 transistors combined in parallel using seven hybrid combiners on the input and output. This stage is driven by four 2N5595's in parallel which are combined with three hybrids, and this stage is in turn driven by a single 2N5595. An alternative transistor choice for the power stages is the RCA TA7205. The performance obtainable is approximately the same, but the coaxial transistor package is mechanically more difficult to integrate into a final amplifier package.

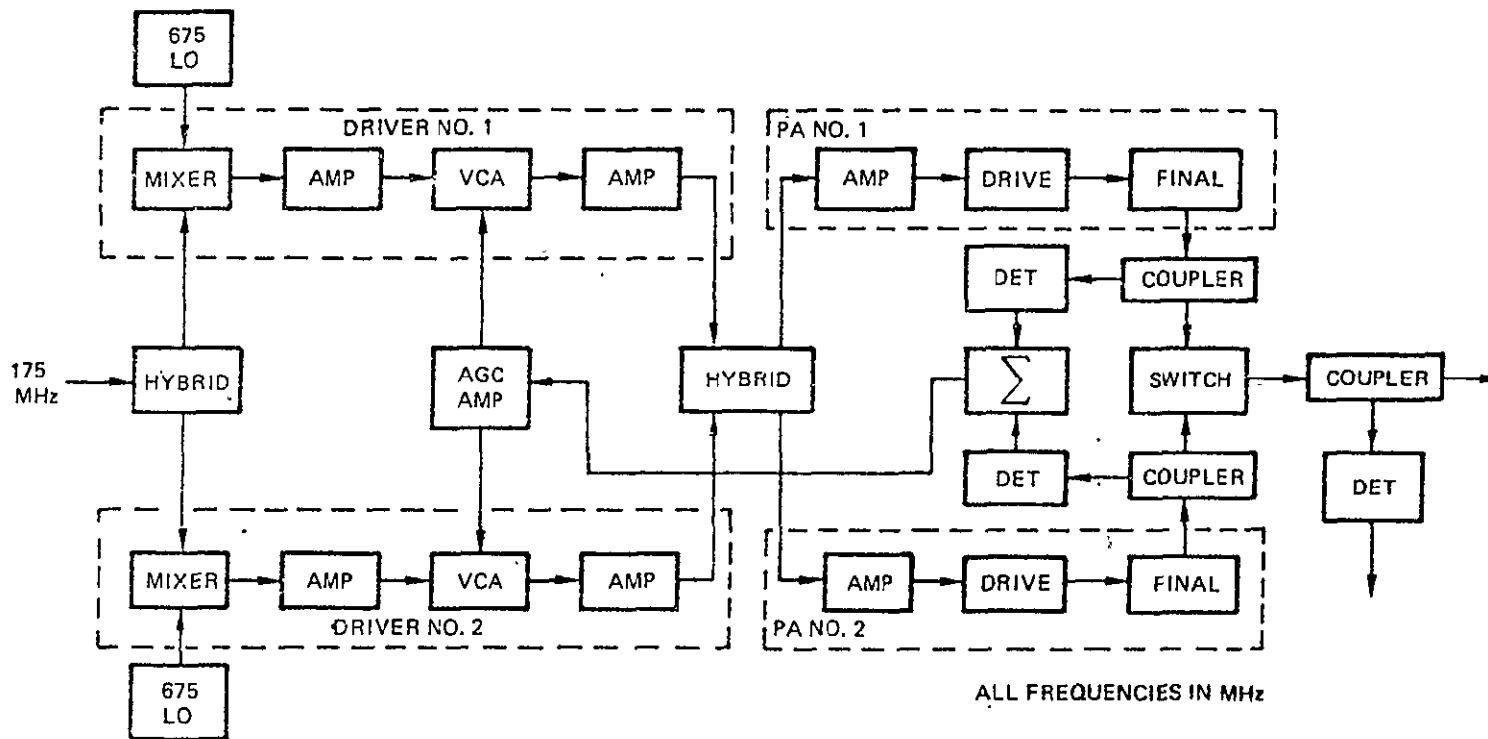


Figure 6.3-5. Proposed UHF Transmitter Configuration

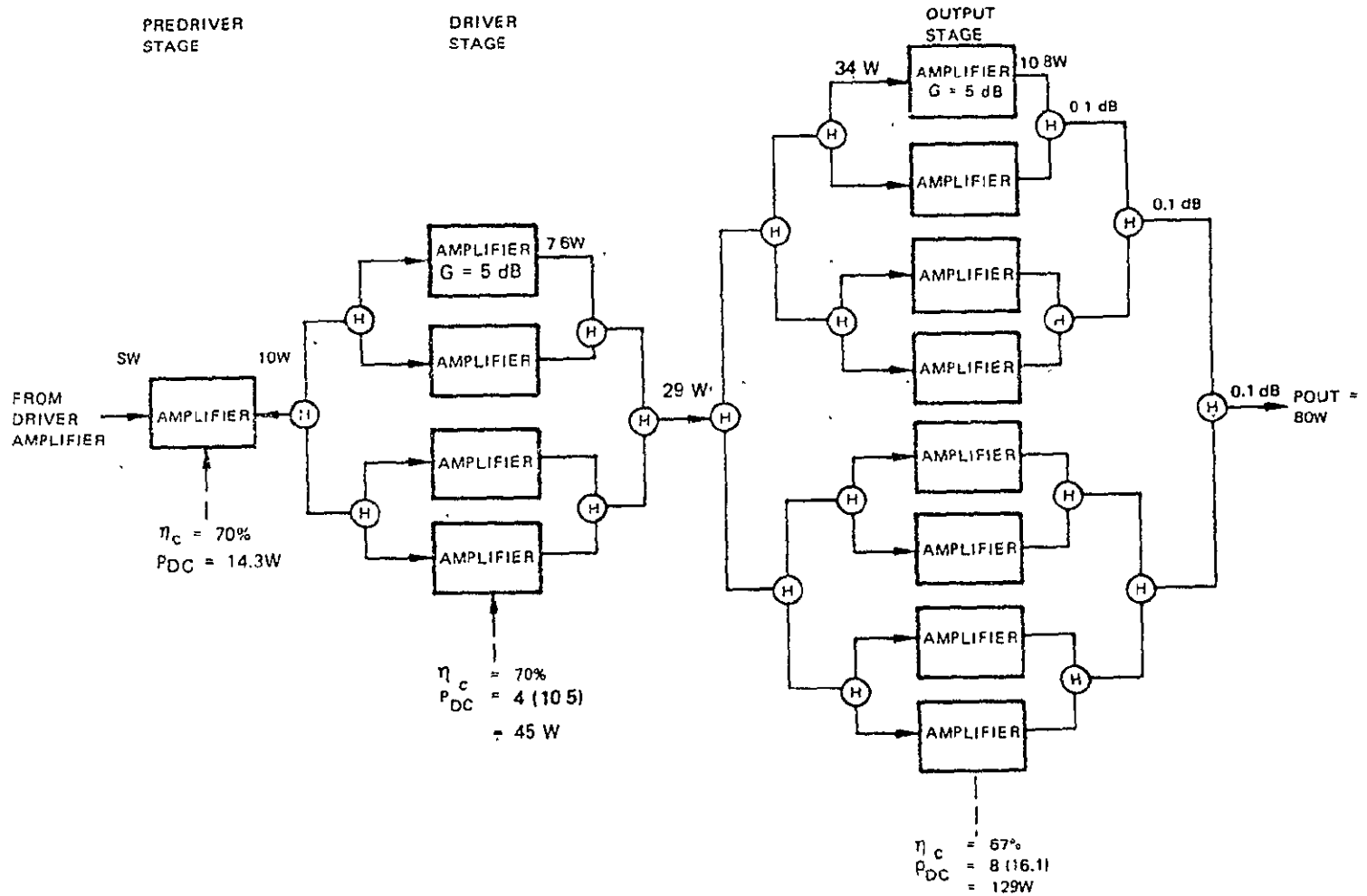


Figure 6.3-6. UHF Power Amplifier Configuration

6.3.6 TRACKING BEACON

In order to allow closed-loop antenna pointing by ground tracking stations, it is desirable to provide an X-band CW beacon signal. The beacon signal will be offset approximately 10 MHz above the upper corner of the signal band, or 30 MHz above the nominal center frequency of the channel in use. The beacon power requirement is 1 W ERP, which is 29 dB below the signal power at the X-band TWTA output.

The beacon signal is provided by a separate 90 MHz crystal oscillator and doubler. The 180 MHz doubler output is connected to the output power combiners of each of the three IF amplifiers and up-converted to X-band along with the IF signal. The power level of the input signal to the TWTA is -20 dBm (23 dB below input signal power); therefore, the output power required from the oscillator/doubler is very small. Since the beacon signal is not generated by the synthesizer, the beacon frequency can easily be changed by changing the oscillator frequency.

6.3.7 RFI AND T&FD EXPERIMENT

Provision is made in the X-band signal path of the transponder transmitter section for the Radio Frequency Interference (RFI) experiment and the Time and Frequency Dispersion (T&FD) experiment. A block diagram of the proposed configuration is shown in Figure 6.3-7. Signals from both experiments are coupled into the X-band signal path between the up-converter triplexer and the TWTA redundancy switch. The X-band RF signal from the RFI experiment is fed into the transponder TWTA through a 10 dB directional coupler.

The pulse information from the T&FD experiment is modulated onto the X-band carrier by a diode amplitude modulator which follows the RFI coupler. The modulator consists of a 3 dB directional coupler with microwave diodes connected at both load ports in the coupled line with quarter-wave lines. When no modulating voltage is applied, both coupler loads are shorted by the open diodes so that no power is dissipated, and the input signal to the coupler passes through without attenuation. When the modulating pulse is applied to the diodes, an open circuit appears at the load ports, allowing power to be dissipated, and the insertion loss of the coupler becomes 3 dB. The resulting waveform at the coupler output will be 50% amplitude modulated with the T&FD pulse information.

The drive power to the TWTA must be reduced so that it is operating in the linear region before amplitude modulation will pass through the TWTA. This is accomplished by switching in a 6-dB attenuator in the IF amplifier, which reduces the drive power to the TWTA by 6 dB and allows semi-linear operation.

6.4 IF AMPLIFIER

6.4.1 IF DISTRIBUTION NETWORKS

The IF distribution networks are switching matrices which allow any down-converter to be connected to any IF amplifier, and any IF amplifier to be connected to any up-converter. As many as three channels can be handled simultaneously.

The IF distribution switch is implemented by the use of single-pole single-throw latching relays. These relays are connected to achieve the multipole multi-throw functions required by the system. The input switching matrix is shown in Figure 6.4-1 and the output switching matrix is shown in Figure 6.4-2.

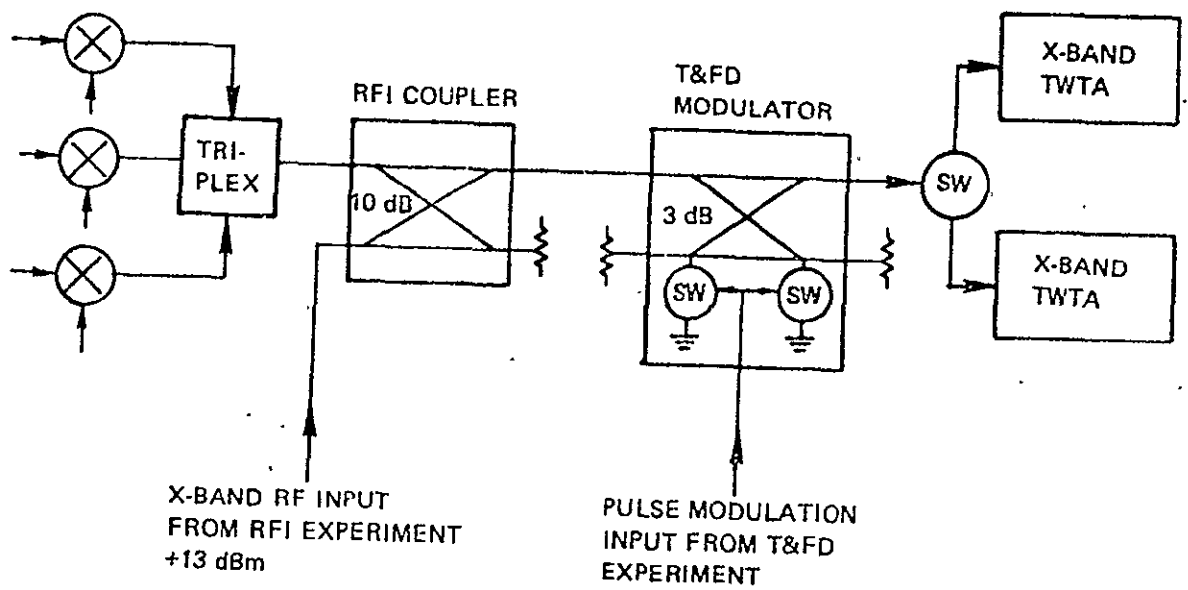


Figure 6.3-7. RFI and T&FD Experiment Interface

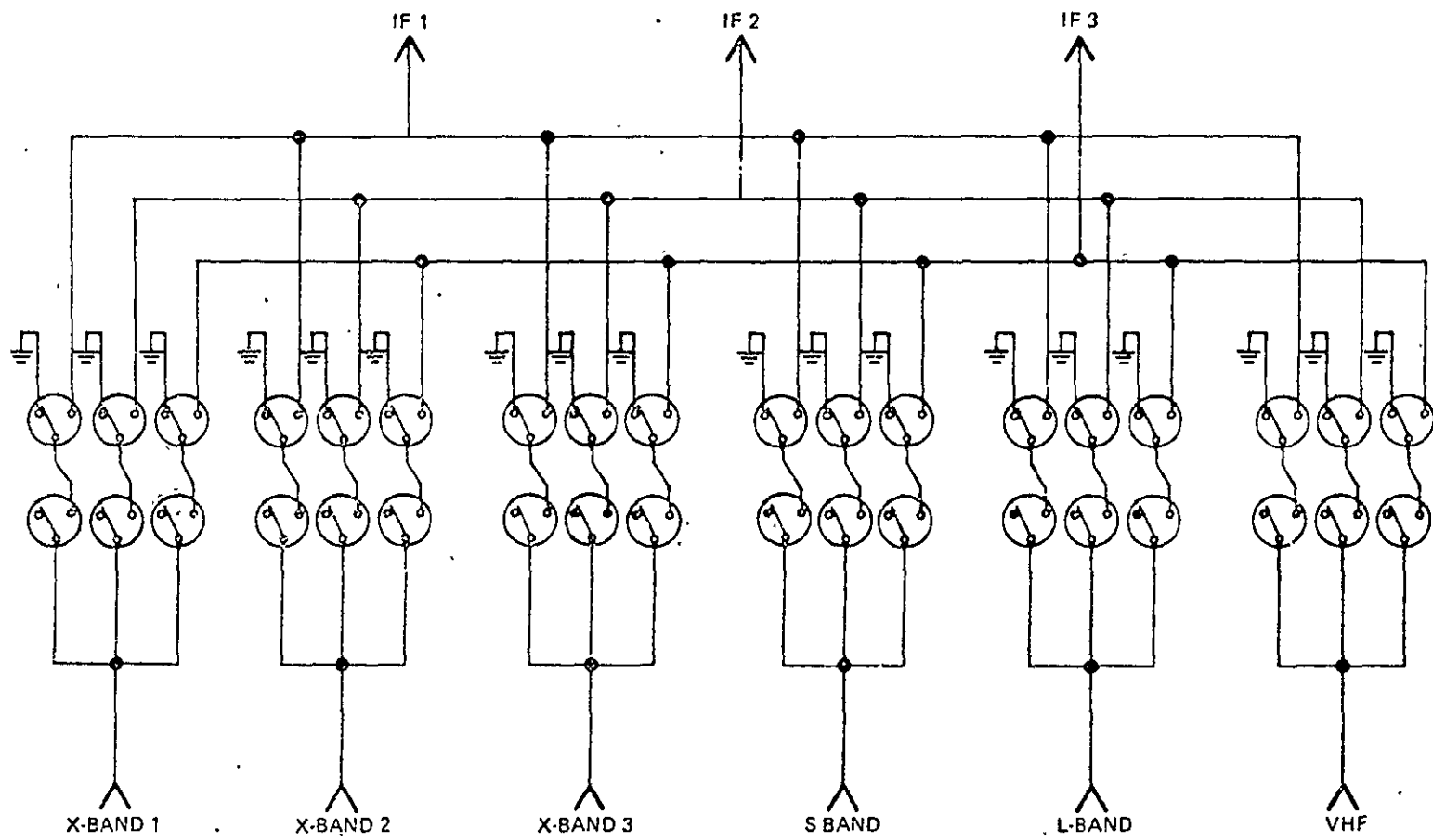


Figure 6.4-1. Input IF Switching Matrix

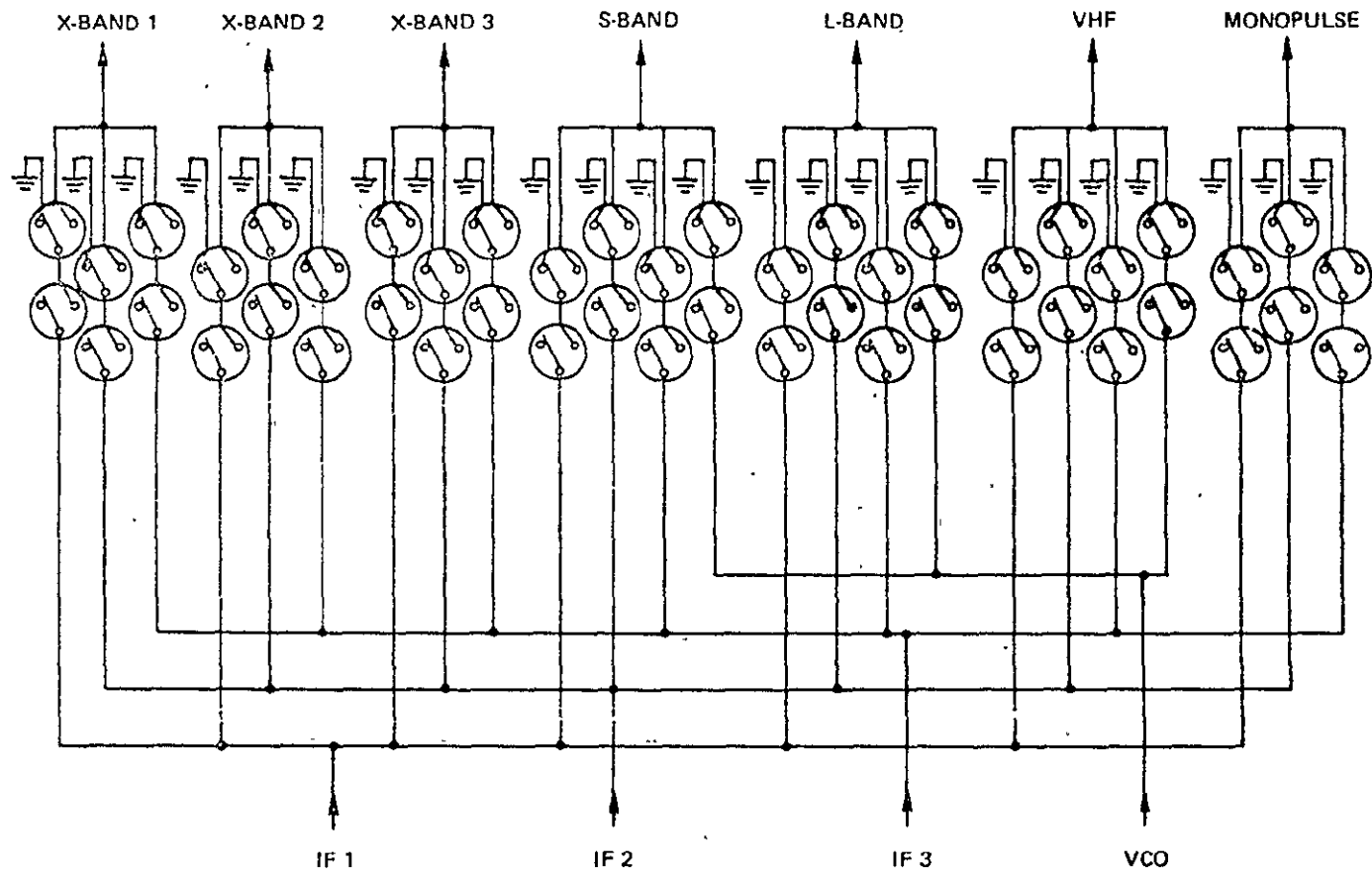


Figure 6.4-2. Output IF Switching Matrix

The switch matrix is constructed by mounting the required relays on a printed circuit board assembly and interconnecting them with miniature semi-rigid coaxial cables or striplines. All relay cases are connected to chassis ground and the interconnecting lines are arranged for maximum isolation between channels.

6.4.2 IF AMPLIFIER

A block diagram of the proposed IF amplifier design is shown in Figure 6.4.3 and its operation is discussed in the following paragraphs. The breadboard IF amplifier work which was done during the phase B/C study differs from the proposed design in some respects due to changes in system requirements and philosophy, and is discussed later.

The IF amplifier is basically a high gain, wideband, AGC-controlled amplifier with two switchable filters to adjust the RF bandwidth as desired, followed by two selectable output signal paths depending on the experiment mode being used. Details of the configuration and operation are given below. Refer to Figure 6.4-3 in tracing the various signal paths through the amplifier.

6.4.2.1 RF Bandwidth Selection

The bandwidth of the IF amplifier is determined by one of two bandpass filters. The input IF signal is amplified and then split into two paths by a power splitter. One path contains the 40 MHz filter, the other the 12 MHz filter. Switches in series with the filters allow selection of one of the two paths. The 40 MHz filter is followed by a 5 dB attenuator so that the noise power at the output of the two paths will be equal under negative signal-to-noise ratio conditions.

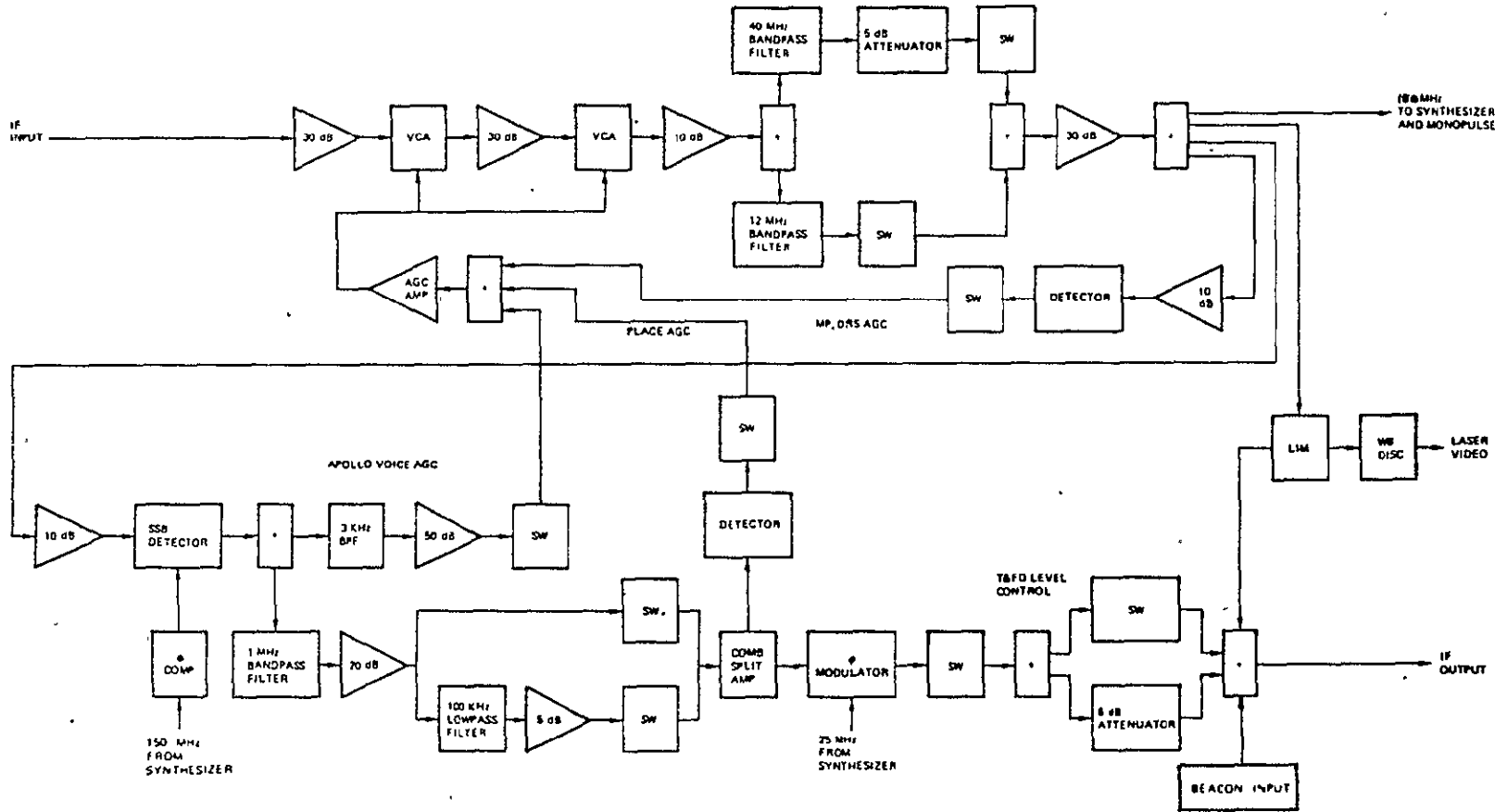
6.4.2.2 Output Signal Processing

Following bandwidth selection the IF signal is amplified and split into four paths. The first is a linear output path to the frequency synthesizer and monopulse detectors. The signal to the synthesizer serves as a reference for the phase lock loop in the coherent mode. The second path goes through a limiter and then to the IF output, and is used for wideband FM translation modes such as DRS. A signal is also split off the limiter to drive the wideband discriminator which demodulates laser video signals. In the fourth path, the signal is routed to a single sideband detector and the resulting baseband output signal is filtered and used to remodulate an internally generated carrier; this path is used for SSB to PM conversion in the PLACE mode and generates the coherent AGC voltage for the Apollo emergency voice mode.

6.4.2.3 Single Sideband Detector and Baseband Filters

The single sideband detector is a balanced ring modulator which translates the amplitude modulated 150 MHz input signal to baseband. The 150 MHz input reference signal to the detector is derived from the synthesizer.

In order to maximize the baseband signal-to-noise ratio when conducting the PLACE experiment with a small number of stations (one airplane, for example), provision is made to select either 1 MHz or 100 kHz postdetection bandwidths by switching a 100 kHz low-pass filter in or out of the signal path.



Revised 9/11/69

Figure 6.4-3. Proposed IF Amplifier Block Diagram

6.4.2.4 Phase Modulator

The phase modulator configuration selected consists of a 25 MHz modulator followed by a X6 multiplier. Consideration was given to several combinations of center frequencies and multiplication ratios that are capable of generating the required 150 MHz carrier modulated at 3 radians peak index. A frequency of 25 MHz appears to be a good compromise in terms of linearity, bandwidth, and complexity of the circuitry required.

6.4.2.5 Wideband Discriminator

A wideband discriminator is provided at the output of the limiter in order to demodulate uplink signals to provide an input at baseband to the laser and millimeter wave experiments. A delay line discriminator is proposed for this application as it is simple to implement and is capable of providing extremely wide bandwidths with reasonably good linearity.

6.4.2.6 Output Level Control

The required carrier for the TWTA for the T&FD experiment is produced in the IF amplifier at 150 MHz then up-converted to X-band. This is done by turning on the 25 MHz input to the PLACE phase modulator with no baseband modulation input. The output power level of the carrier from the IF amplifier is reduced from its normal level to back the TWTA off from saturation by switching in a 6 dB attenuator immediately following the phase modulator.

6.4.2.7 AGC Operation

Recent studies of the expected received signal levels for the various experiment modes have resulted in some additions to the AGC circuitry shown in the Phase B report. In certain cases, the IF signal-to-noise ratio in the 12- and 40-MHz bandwidths is negative, making it necessary to use somewhat more complicated AGC methods than the simple loop originally proposed.

There are three different selectable AGC modes in the presently proposed IF amplifier. The first is a predetection AGC which is required for the wideband translation modes such as DRS. The output signal of the 12- or 40-MHz filters is the reference for the AGC loop in this mode. The second mode is used with PLACE and includes the SSB detection and baseband filtering in the loop. This mode is analyzed in more detail below. The third mode is used with the Apollo emergency voice signal and provides coherent AGC which allows the phase-modulated Apollo signal to be detected in the synthesizer with an equivalent 6 kHz noise bandwidth. This mode is also used for the narrow band monopulse. Here the AGC detector also recovers the monopulse error signal. The coherent AGC keeps the synthesizer's loop gain constant for negative signal-to-noise ratios so that it can remain locked to the Apollo signal for received signal levels as low as -130 dBm. The synthesizer's reference signal must be taken from a linear rather than a limited IF output to take advantage of the coherent AGC.

6.4.2.8 Effect of Received Signal Levels on AGC Design

A summary of the expected signal levels at the transponder input for the various experiment modes is given in Table 6.4-1. The figures are taken from the most recently available GSFC Experimenter's specifications for the Communication Subsystem.

Table 6.4-1. Expected Received Signal Levels

Mode	Band	Antenna	Received Signal (Isotropic)		Transponder Input Signal ⁽¹⁾	
			Max	Min	Max	Min
Coherent Receive	X	Horn Dish	-90 dBm	-105 dBm	-73 dBm -40 dBm	-88 dBm -55 dBm
PLACE	X to L L to X	Horn	-75 dBm	-100 dBm	-58 dBm	-83 dBm
		Fan	-120 dBm	-140 dBm	-88 dBm	-108 dBm
		Pencil			-82 dBm	-102 dBm
DRS	X to S S to X X to X	Horn	-75 dBm	-100 dBm	-58 dBm	-83 dBm
		Array	-125 dBm	-145 dBm	-86 dBm	-106 dBm
		Horn	-75 dBm	-100 dBm	-58 dBm	-83 dBm
Apollo Voice	S	Array	TBD	-157 dBm	TBD	-118 dBm
ITV	X to UHF	Horn Dish	-75 dBm	-100 dBm	-58 dBm -25 dBm	-83 dBm -50 dBm
MM, Laser, ATS-R	X to X	Horn	-75 dBm	-100 dBm	-58 dBm	-83 dBm
Special Beacon	STOX	Array	TBD	-167 dBm	TBD	-128 dBm

Notes:

(1) Assumes the following nominal antenna gains:

X-band horn	17 dB
X-band dish	50 dB
S-band array	39 dB
L-band fan	32 dB
L-band pencil	38 dB

The previously proposed IF system had an average detector sampling the IF output before the SSB detector. The loop was adjusted so that the IF output level was held at 0 dBm. If the signal-to-noise ratio is high, the detector responds almost totally to signal. The signal level at the output of the IF will remain at 0 dBm as the input signal changes. As the signal-to-noise ratio decreases, the noise at the output of the IF plays a more dominant role in determining the AGC level. The AGC maintains a total output of 0 dBm signal plus noise so that as the signal-to-noise ratio decreases the power of the signal component decreases. At negative signal-to-noise ratios the noise tends to determine the AGC level so that the IF is acting as a fixed gain amplifier.

After detection and filtering the resulting signal has large variations in power level even though the signal-to-noise ratio is relatively large. This phenomenon is shown graphically in Figure 6.4-4. Curve "A" shows the output level of the signal component when pre-detection AGC is used. Curve "b" is the output level of signal plus noise (total output) for the same conditions. The analysis assumed the standardized output levels, a 0.1 MHz low pass filter following the SSB detector, and PLACE L-band receive conditions. It should be noted that no matter how much gain is put after the AGC loop an 11 dB variation in output level will occur.

If instead of detecting the AGC signal at the IF output the AGC is taken after the 0.1 MHz low pass filter, a different situation results. Assuming 12 dB of fixed gain is placed after the SSB detector to equalize the power levels, the post detection AGC will act to maintain constant power (signal plus noise) at the output of the low pass filter. At this point the signal-to-noise ratio is higher so that the signal maintains control of the IF gain. Curve "c" on Figure 6.4-4 shows the signal component of filter output as a function of received signal level, while curve "d" is the total (signal plus noise) output from the filter. Note that the received signal levels and noise figures are the same for both cases, only the AGC sampling point is changed.

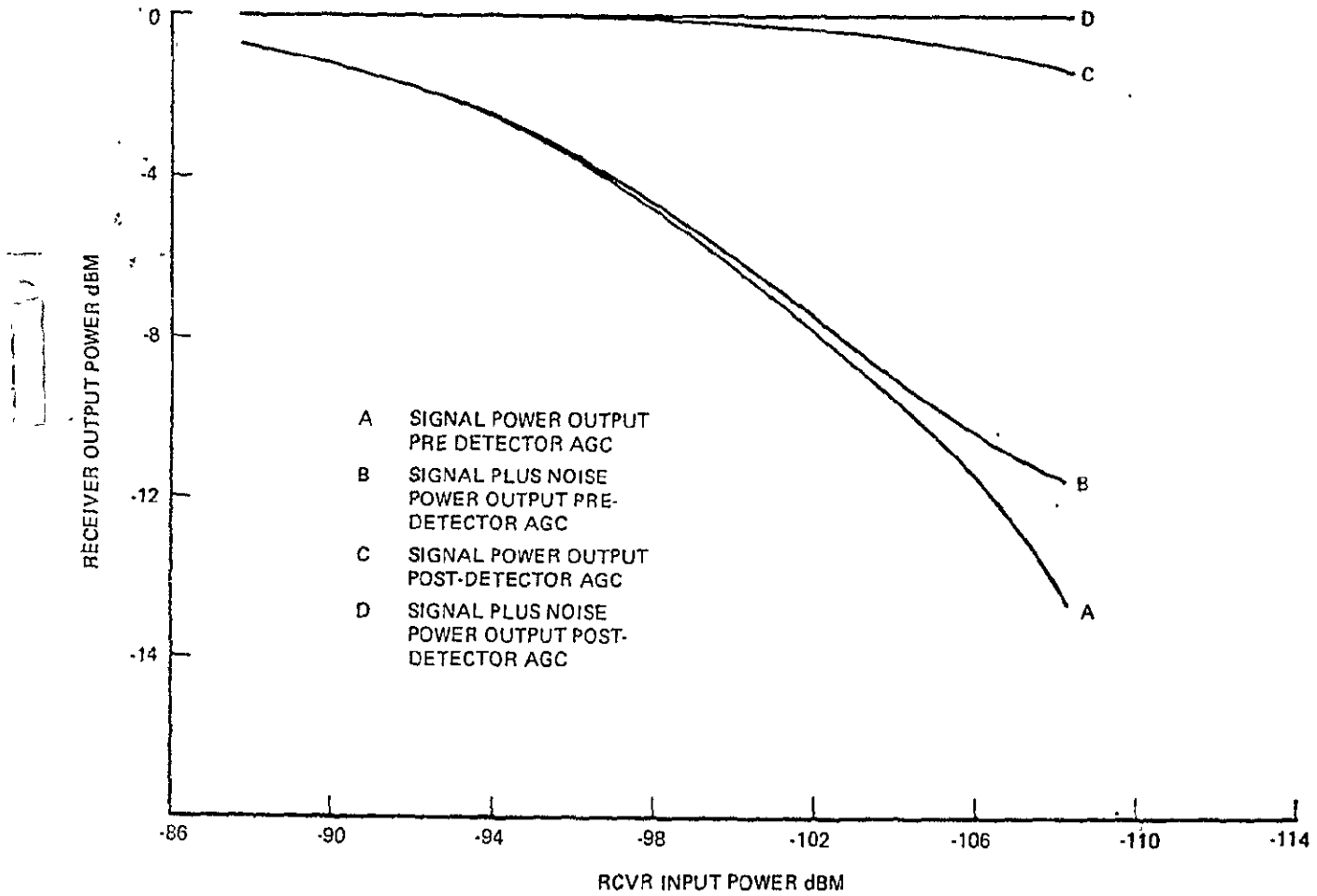


Figure 6.4-4. IF Signal Output Power With Predetection and Post-detection AGC

6.5 FREQUENCY SYNTHESIZER

6.5.1 RECOMMENDED CONFIGURATION

The generation of the majority of the local oscillator frequencies for the transponder occurs within the frequency synthesizer. The various frequencies are derived from a common master oscillator by a series of multiplication chains. The master oscillator may be phase-locked to the receive signal for coherent operation or phase-locked to an internal crystal oscillator for non-coherent operation.

The performance requirements that have been established for the synthesizer are summarized in Table 6.5-1.

A block diagram of the recommended synthesizer configuration is shown in Figure 6.5-1.

6.5.2 CIRCUIT OPERATION

A 100 MHz VCXO is the master oscillator for the synthesizer. The VCXO output is amplified to a level sufficient to drive the multiplier chains, the output frequencies of which are integral multiples of 100 MHz. All other output frequencies are multiples of either 25 or 50 MHz. A small amount of 100 MHz power is coupled from the 100 MHz power amplifier through two divide-by-two circuits to produce 25 MHz, which is then multiplied by six to produce 150 MHz. This 150 MHz signal is used as the phase reference for comparison with the receiver IF frequency of 150 MHz. The difference in phase of these two signals is fed back to the VCXO as an error voltage, thus completing a phase-lock loop.

Seven of the desired output frequencies (1400, 1500, 2100, 7200, 7500, 8000, and 8100 MHz) are obtained by direct multiplication of the basic 100 MHz signal. Three frequencies (1650, 7425, 7875) are generated by multiplying the 25 MHz signal.

The low order multiplier (x2, x3) are of the transistor or varactor type, while the higher order multipliers (x5 and above) are step recovery diode types.

Most of the filters are of the tubular type. The X-band output filters are interdigital and those below 200 MHz are of conventional lumped element design.

The synthesizer power consumption is minimized in the ITV mode where the maximum spacecraft dc power limit is being approached by turning off the 25 MHz power amplifier which drive the multiplier chains. This reduces the dc power required from a maximum of 26 W to 11 W and leaves one X-band transmit and one X-band receive frequency operating.

6.5.3 PHASE LOCK LOOP CONFIGURATION

A block diagram of the recommended phase lock loop configuration is shown in Figure 6.5-2. It was selected out of four alternative configurations with varying degrees of acquisition range because of its simplicity (a discussion of the alternatives is given in the phase B report).

A possible problem with this configuration is that of maintaining the VCXO quiescent frequency within the capture range of the phase-lock loop. The capture range or maximum frequency offset at the receiver input which can be reduced to zero by

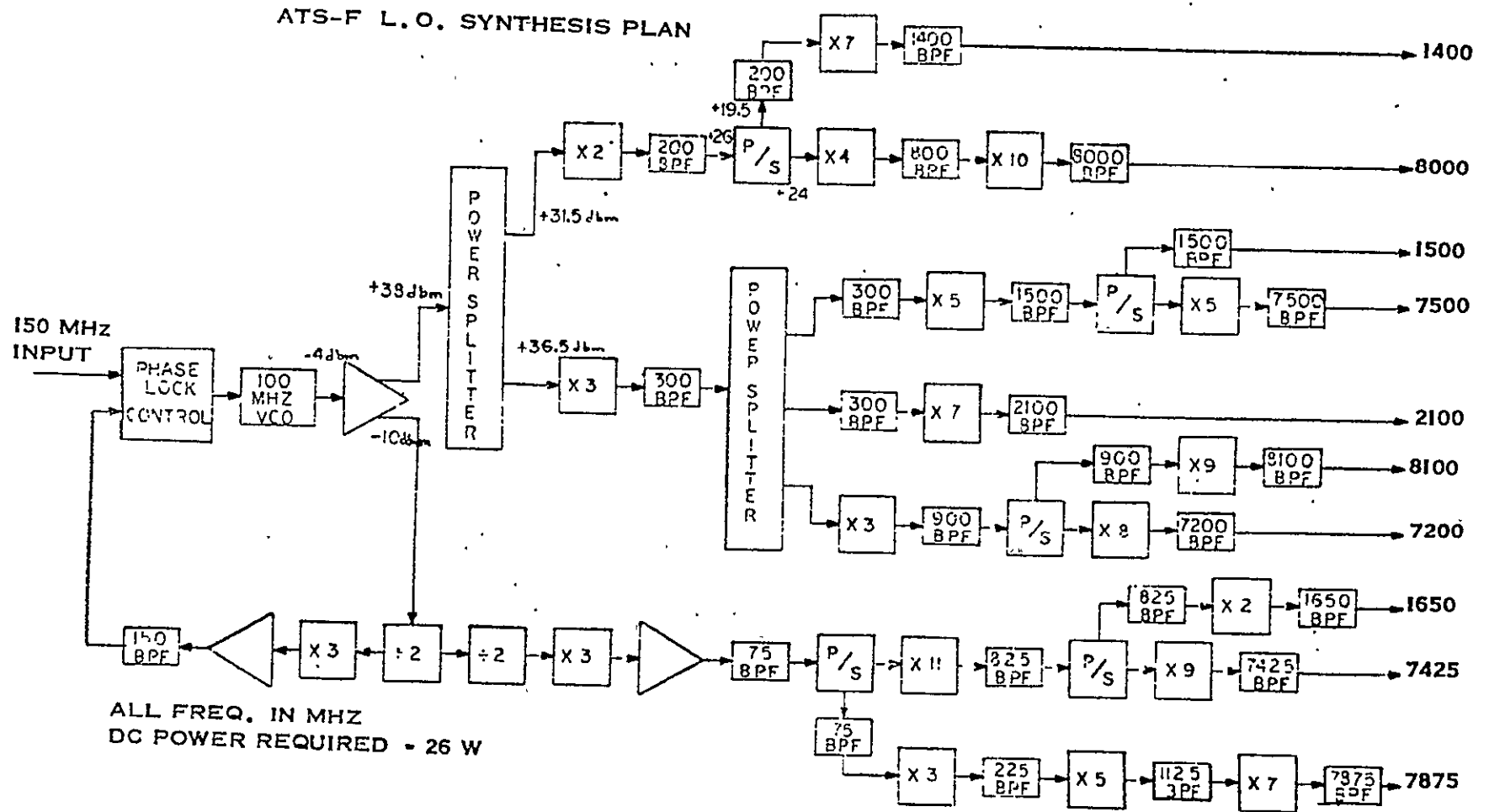


Figure 6.5-1. Frequency Synthesizer Configuration

pull-in action is approximately 50 kHz. This is fixed by the loop bandwidth and pull-in time. The 50 kHz at X-band is equivalent to 650 Hz at the VCXO with a center frequency of 100 MHz. If the VCXO should drift more than 650 Hz in its nominal quiescent (nonlocked) frequency, then the loop would be unable to acquire. Ground station stability is several orders of magnitude better in stability than the VCXO and should not affect offset. The degree of stability required is of the order of 3 parts in 10^6 which may be somewhat difficult for a VCXO.

The degree of stability which can be obtained in the VCXO is being investigated. If it turns out that this specification is difficult to meet with a practical design, a simple sweep will be incorporated in the loop to insure that no acquisition problems will be encountered.

TABLE 6.5-1

FREQUENCY SYNTHESIZER PERFORMANCE REQUIREMENTS

Phase Lock Loop Performance:

Noise Bandwidth (single sided)	500 Hz $\pm 10\%$ nominal (1500 Hz max)
Minimum Capture Range	± 50 kHz at X-Band
Static Phase Error	2° RMS
Dynamic Phase Error	10° RMS
Acquisition Time	1 min (maximum)
VCXO Drift (open loop)	3 parts in 10^6 (maximum)

RF Input Requirements: 150 MHz IF at 220 mv signal + noise
 Minimum signal/noise (IF BW = 40 MHz) = +1 dB

RF Output Requirements:

	<u>Down</u> <u>Conversion</u>	<u>Up</u> <u>Conversion</u>
Level	+3 dBm	+13 dBm
Spurious	-100 dBm	-60 dBm

DC Power Required

11 W ITV Mode
 26 W all other modes

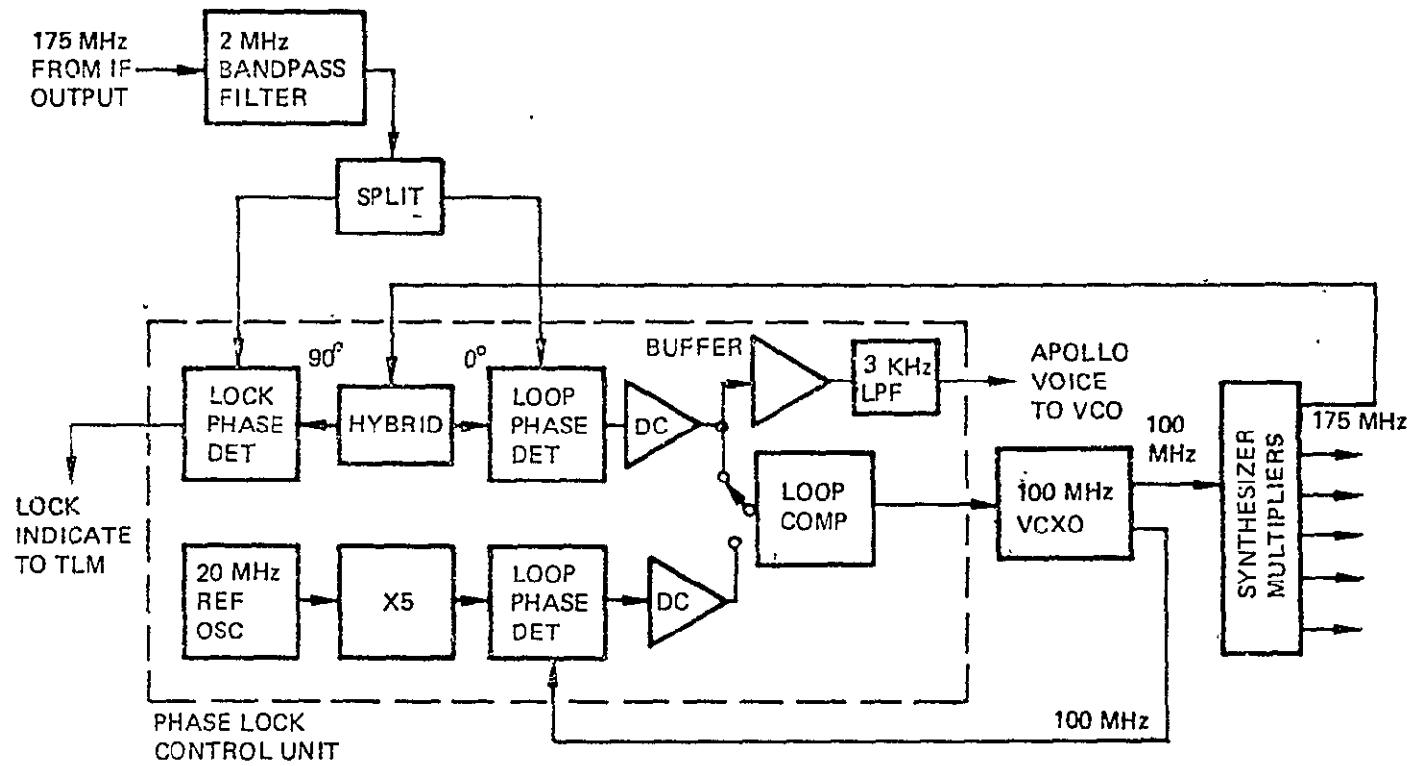


Figure 6.5.2. Synthesizer Phase-Lock Loop Configuration

6.5.4 REFERENCE OSCILLATOR

When the synthesizer is not being operated in the coherent mode, it is phase locked to an internal 100 MHz reference signal. This signal is generated by a highly stable crystal-controlled 20 MHz oscillator followed by a x5 multiplier.

The performance characteristics of the reference oscillator are summarized below:

Initial frequency tolerance @ 25°C:	±10 ppm
Long term stability:	±3 ppm in 3 months
Short term stability:	1×10^{-8} parts per second (0.25 second averaging period)

The technique of phase locking the VCXO to a 100 MHz reference signal rather than switching the VCXO out and switching in the 100 MHz oscillator was chosen for the proposed synthesizer design because it provides better filtering of harmonics of the 20 MHz oscillator sidebands. The phase-lock-loop acts like a very narrowband filter and furnishes the necessary sideband rejection without requiring additional 100 MHz bandpass filters.

6.5.5 SYNTHESIZER REDUNDANCY SWITCHING

Each frequency synthesizer has 10 different frequency outputs. Each up- and down-converter must be able to be switched from one synthesizer to the other to obtain the desired redundancy. At the relatively high frequencies involved, this switching is best done with ferrite circulator switches. Where power margins permit, it is desirable to eliminate the switches entirely and connect both synthesizers to the up- or down-converter through a hybrid combiner; this method has the highest reliability but incurs a 3 dB power penalty due to loss in the hybrid load.

Consideration was given to switching at lower frequencies within the synthesizer chains but this has the disadvantage of reducing the reliability by making some multipliers common to both chains and nonredundant.

The recommended monopulse system configuration is similar to the one discussed in the Phase B report and the GSFC preferred approach. It consists of VHF, S-band, and X-band monopulse receivers, and utilizes the transponder IF amplifiers and a common detection circuit for all three bands.

6.6.1 RECOMMENDED CONFIGURATION

A block diagram of the recommended monopulse receiving system is shown in Figure 6.6-1.

The receivers each use quadrature horns and hybrid combiners in producing three information channels: elevation error, azimuth error, and sum. Sequenced phase shifting is applied to the error channels and then combined with the sum channel both in phase and 180° out of phase. The resultant amplitude signal contains the sense and magnitude of the error. This AM modulated signal is then converted to the 150 MHz frequency and synchronously detected.

Spacecraft commands determine which receiver output is selected for further processing. Provision is also made in each receiver for switching into the sum channel, thus allowing the antennas to be used for other experiments when the monopulse function is not being used.

6.6.2 RF MONOPULSE MODULATORS

The monopulse modulation approach is that recommended by the preferred approach. Block diagrams of the VHF, S-band, X-band modulators are given in Figures 6.6-2 and 6.6-3, respectively. The operation of both devices is nearly identical. In both cases the input azimuth error and elevation error waveforms are combined in hybrid couplers. At VHF these couplers are 90° stripline hybrids. At X-band and S-band they are 180° waveguide or coaxial hybrids. In both cases the two combined signals pass through phase shifters. At X-band and S-band the phase shifters are ferrites, while at VHF they are diodes coupled in and out of the circuit by 90° stripline couplers. After passing through the phase shifters, the signals are recombined in a coupler (waveguide or coaxial at S-band and X-band, stripline at UHF). By proper sequencing of the phase shifters, the required plus and minus elevation and azimuth error signals are generated.

6.6.3 MONOPULSE DETECTOR

A block diagram of the monopulse detector circuitry is shown in Figure 6.6-4.

In normal operation, a wideband mode is used in which the 150 MHz signal from the transponder's down-converter is amplified in the 40 MHz or 12 MHz bandwidth (depending upon signal bandwidth). The IF AGC is in the "pre-detection mode." The signal from the IF is further amplified to a level of +6 dBm and detected in a linear amplitude detector contained in the monopulse detector. After detection the signal is switched into the synchronous demodulator.

A narrow band mode can be provided in which the synthesizer is phase locked to the received signal; the place SSB detector is used as a coherent detector to recover the monopulse information and develops the IF AGC voltage. The detected monopulse signal is filtered by a 3 kHz low-pass filter giving the system an equivalent

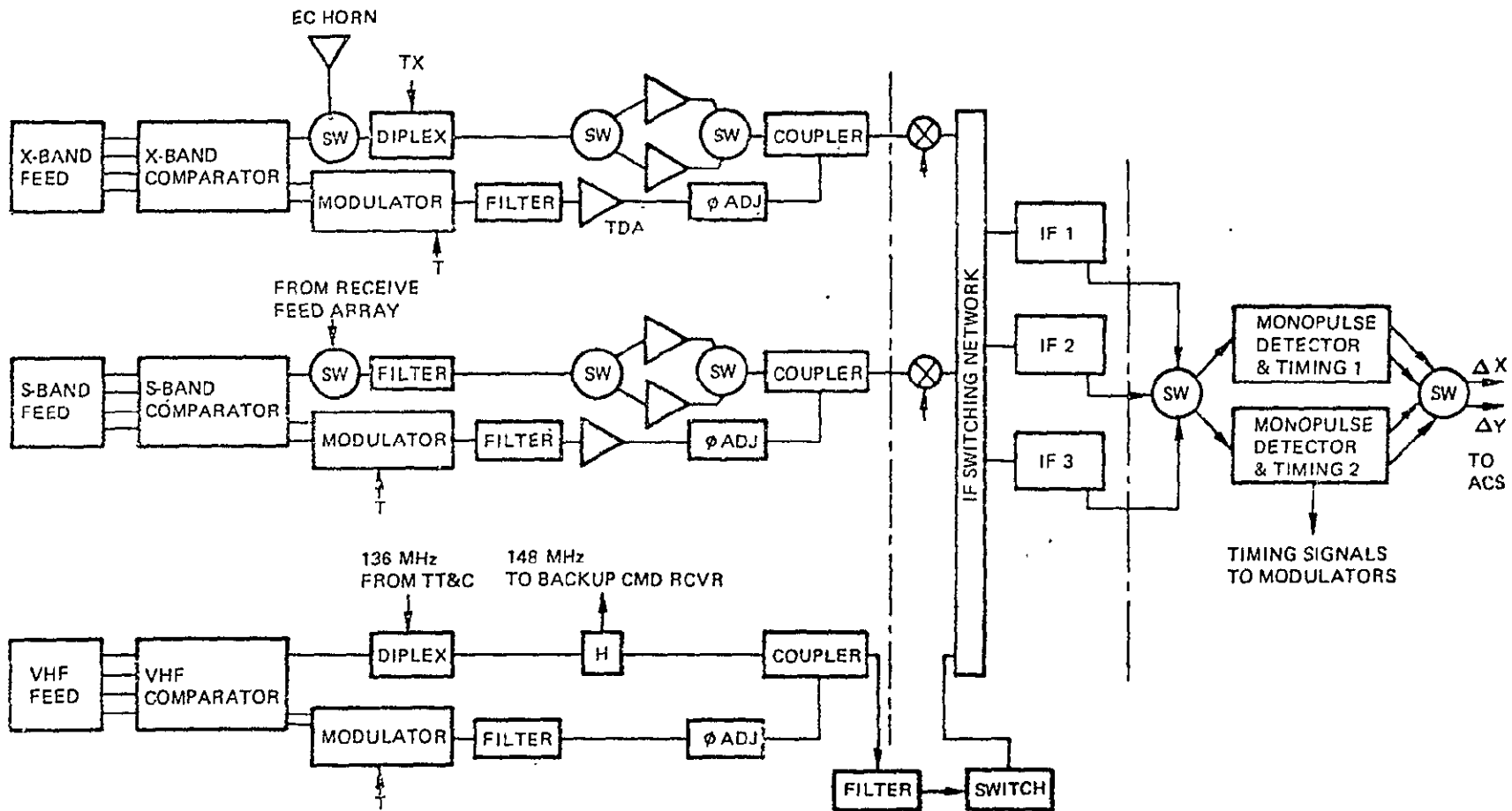


Figure 6.6-1. Monopulse Receive Portions of Transponder

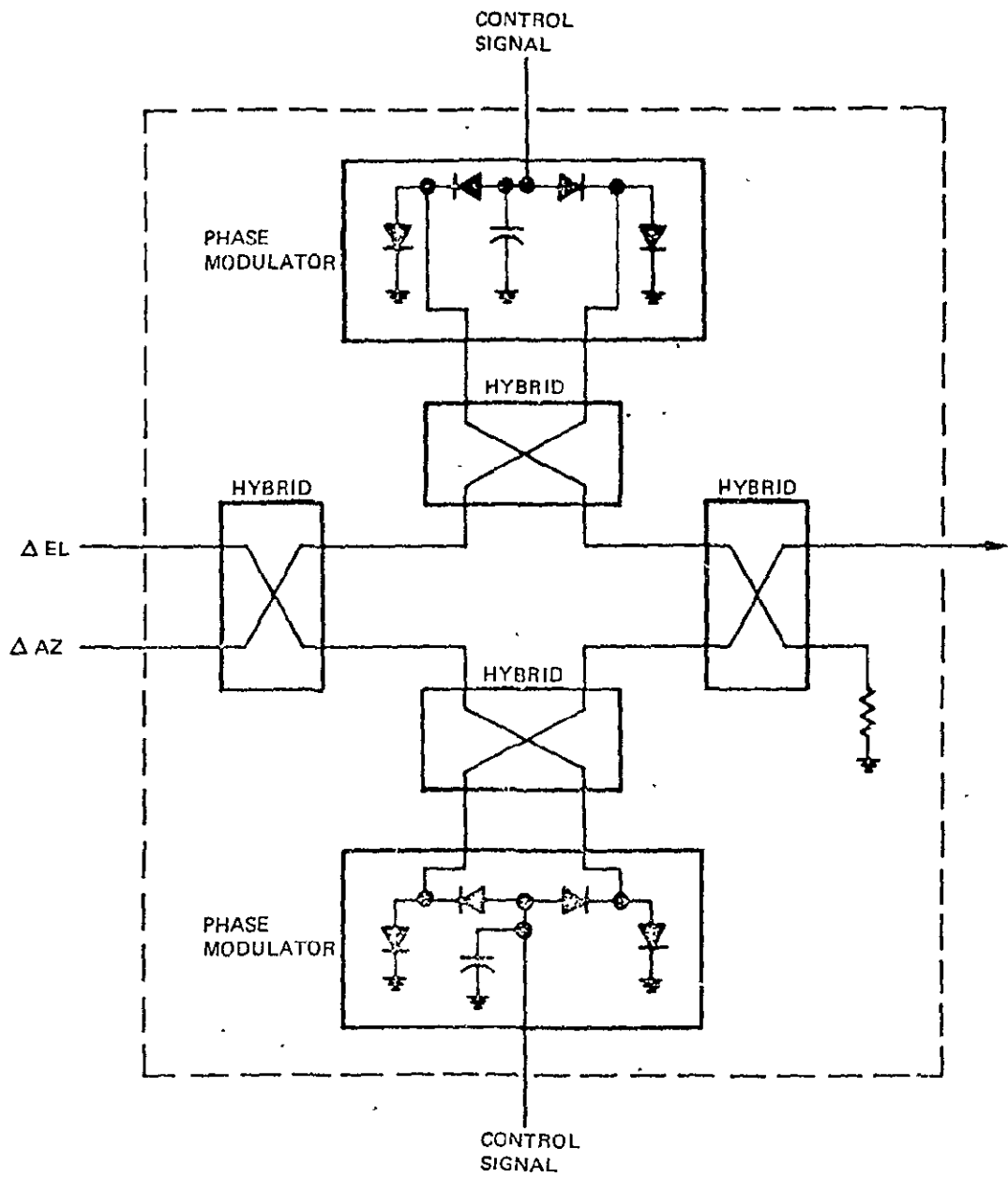


Figure 6.6-2. UHF Monopulse Modulator

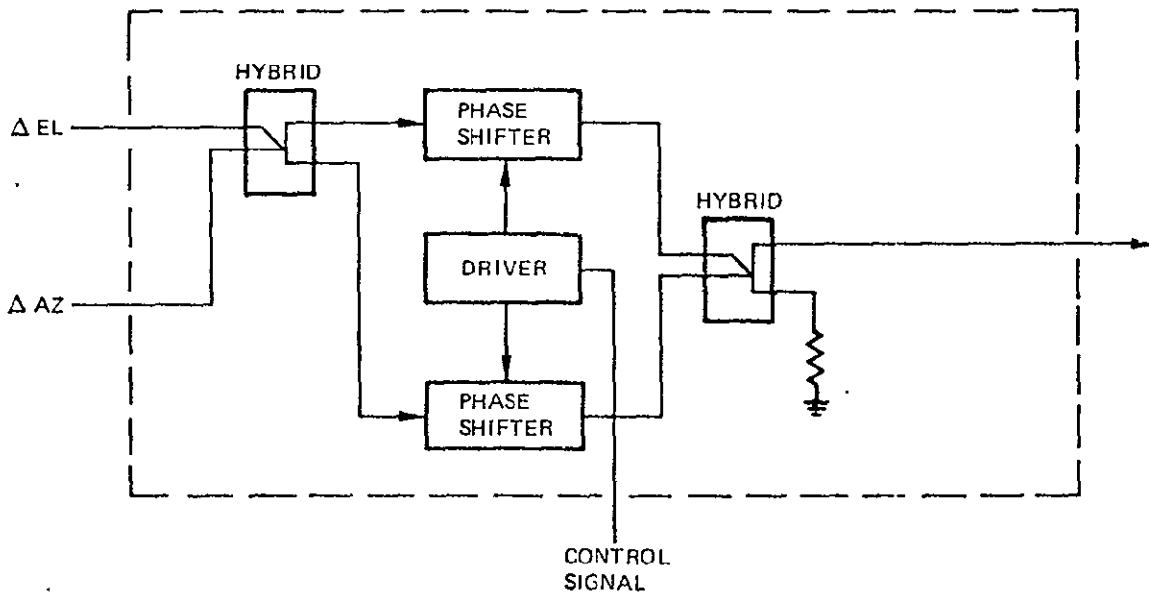


Figure 6.6-3. S-Band and X-Band Monopulse Modulators

7

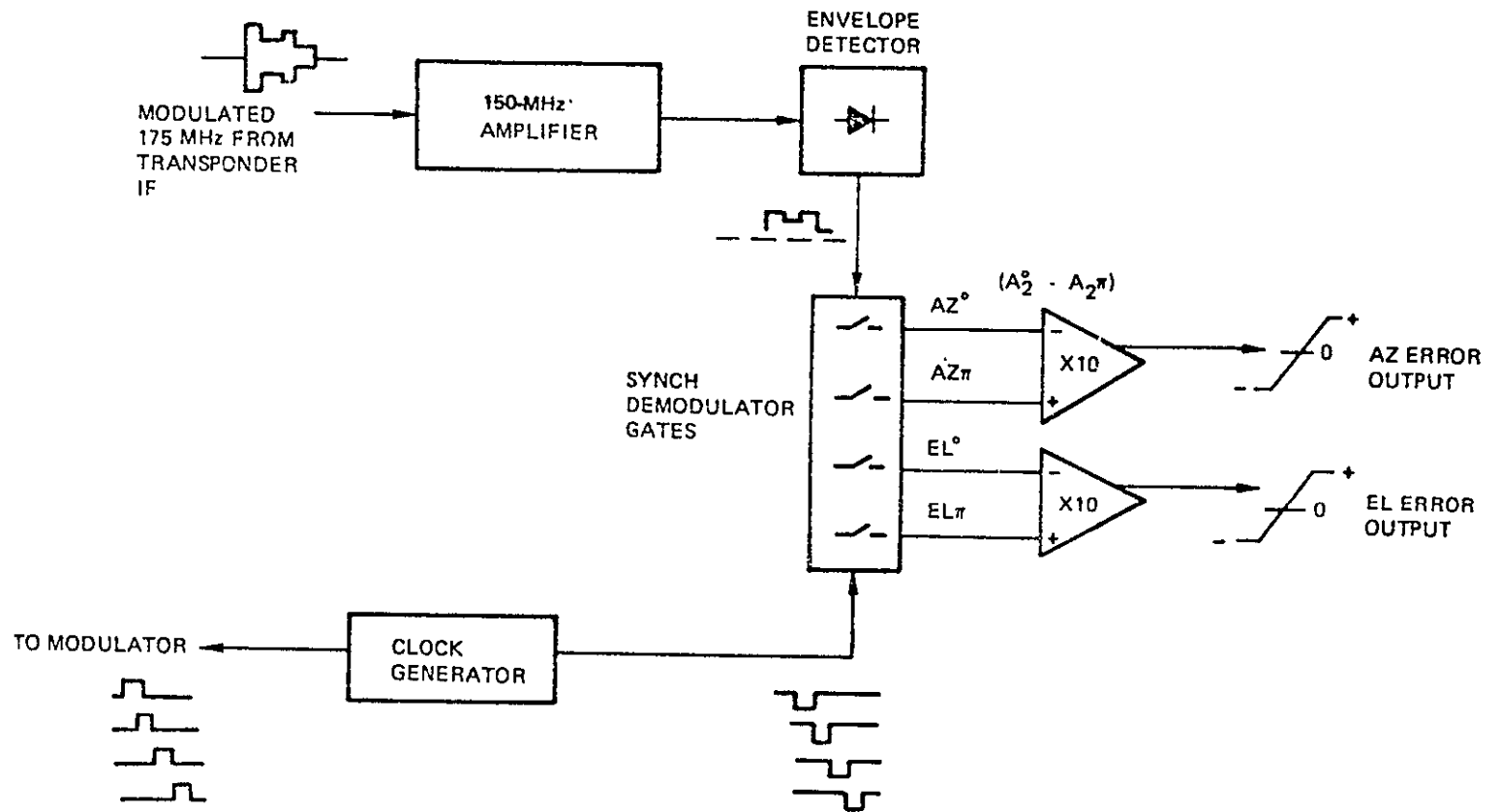


Figure 6.6-4. Monopulse Demodulator

bandwidth of 6 kHz suitable for tracking extremely low level signal. After amplification the signal is switched into the synchronous demodulator (by passing the linear detector). In the synchronous demodulator, the dc error signal is sequentially sampled by four FET sample-and-hold circuits. The outputs of the azimuth sum and difference channels are connected to the sum and difference inputs of two operational amplifiers. The operational amplifiers provide the ± 5 volt dc error output signals to the spacecraft attitude control system.

6.7 WIDEBAND DATA LINK

The wideband data unit consists of the voltage-controlled oscillators which provide information-modulated subcarriers to be transmitted to the ground from various experiments, along with miscellaneous buffer amplifiers, baseband filters, and summing networks.

6.7.1 SYSTEM CONFIGURATION

The block diagram of the recommended VCO configuration for the wideband data unit is shown in Figure 6.7-1. The various baseband inputs from the Laser, radiometer, high-resolution camera, and Apollo voice circuit are combined in a linear summing circuit and applied to the modulation input of the voltage-controlled oscillator. Buffer amplifiers supply isolation between the input signals and the VCO, and baseband filters limit the input signals to the specified frequency range.

Since the laser baseband spectrum overlaps that of the Radiometer and HR camera, the laser cannot be operated simultaneously with the other experiments. In the case of the Apollo voice signal, simultaneous operation with the radiometer and HR camera is possible if the baseband input signal (300 Hz to 3 kHz) is modulated on a subcarrier which lies in the 200 Hz to 5 MHz region before being applied to the 150 MHz VCO. This configuration has been assumed for the baseline system. The intermediate VCO could be eliminated and the baseband signal used to directly modulate the 150 MHz VCO if simultaneous operation with the radiometer and HR camera is not necessary.

System reliability is achieved by including a standby redundant wideband data unit. The input lines from each experiment are connected to both units and the 150 MHz VCO outputs are summed in a hybrid combined to a single line which is connected to the up-converter IF distribution switch.

6.7.2 VOLTAGE CONTROLLED OSCILLATORS

A block diagram of the proposed voltage-controlled oscillator circuit is shown in Figure 6.7-2.

The configuration is similar to that used on ATS-E. It consists of two high-frequency VCO's, one at 275 MHz and one at 425 MHz, whose outputs are subtracted from one another in a mixer and amplified to provide the desired 150 MHz output signal.

Similar designs are used for both the 275 MHz oscillator and the 425 MHz oscillator. The modulation input is applied to both oscillators but causes positive deviation in one case and negative deviation in the other. Any nonlinearities in modulation sensitivity tend to be common to both oscillators and are cancelled out. Drifts in the center frequency of the VCO output also tend to cancel because of the subtraction process. The maximum modulation frequency is less than 2% of the center frequency of the oscillators so linear deviation is reasonably easy to obtain.

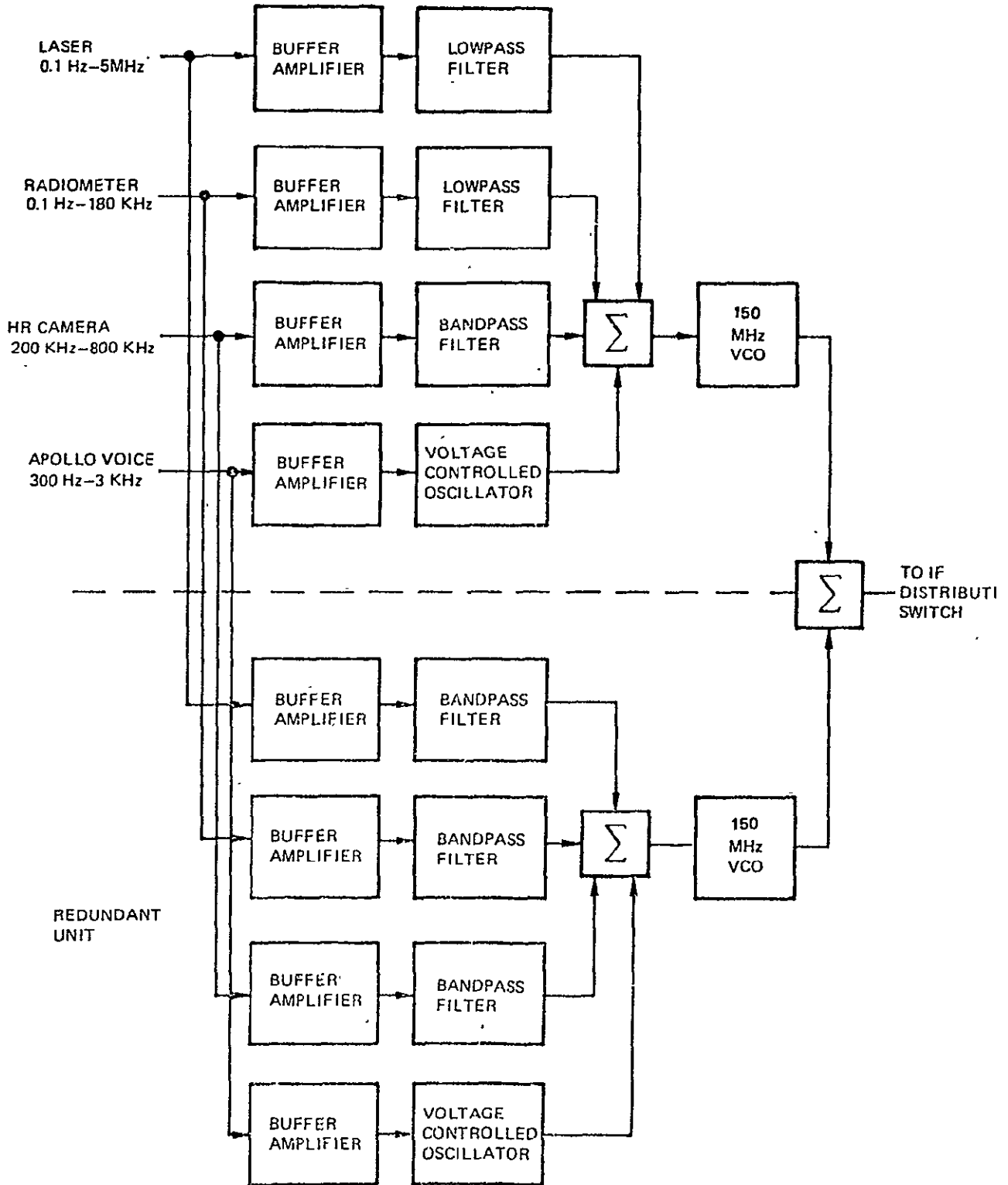


Figure 6.7-1. Proposed Wideband Data Unit

One area which requires further study is the requirement for 0.1 Hz baseband frequency response. The existing ATS-E design is capable of operation to 10 Hz and would have to be modified in order to accommodate the 0.1 Hz requirement. It will be necessary to verify that the short-term stability of the oscillators is sufficiently good to insure that thermal or random frequency excursions in a 10-sec averaging time are at least an order of magnitude less than the desired baseband frequency response stability. Circuit implementation details will also have to be examined. These areas are presently under study.

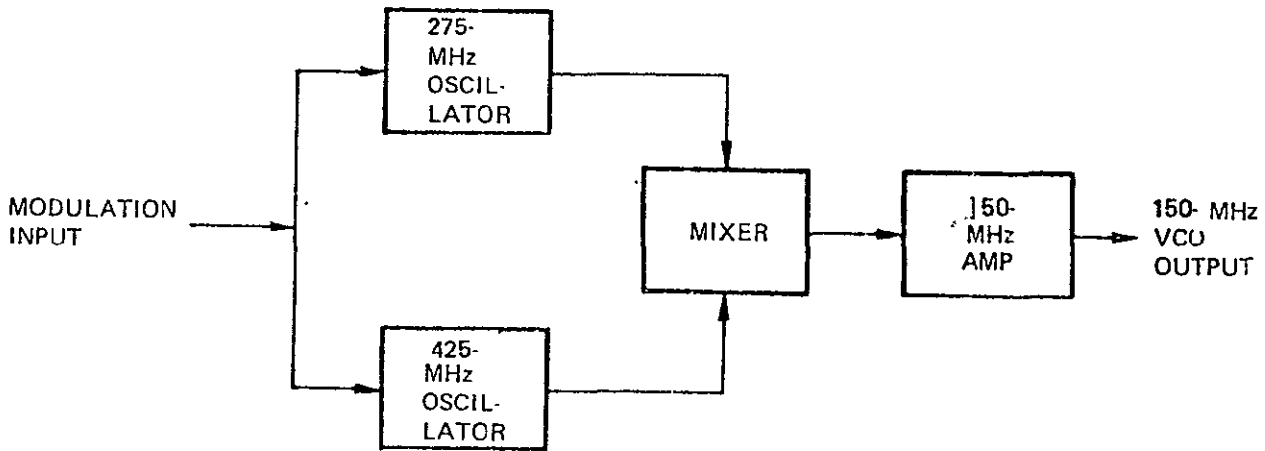


Figure 6.7-2. 150 MHz Voltage Controlled Oscillator Block Diagram

6.8 COMMAND, TELEMETRY AND POWER SUBSYSTEMS

6.8.1 COMMAND, TELEMETRY AND POWER

The Telemetry and Command (T&C) portions of the radio transponder contain a serial input command distributor with memory, and telemetry signal conditioning circuits.

Most of the command interface equipment is located in an assembly called the transponder command distributor (TCD). The remainder is distributed around at various points of use. The telemetry interface circuits are not so readily visible, because they are not concentrated in one place, but distributed at the data sources.

6.8.1.1 Interface with Spacecraft Command Decoder

The transponder receives a nine-bit serial data word, its associated clock and execute lines, and eight discrete commands. All commands come from the spacecraft command decoder and distributor (CDD) which is standby redundant. The serial data word and four of the discrete commands go to the transponder command distributor (TCD), which is also standby redundant. The remaining four discrete commands go to the transponder power supply which is in turn standby redundant.

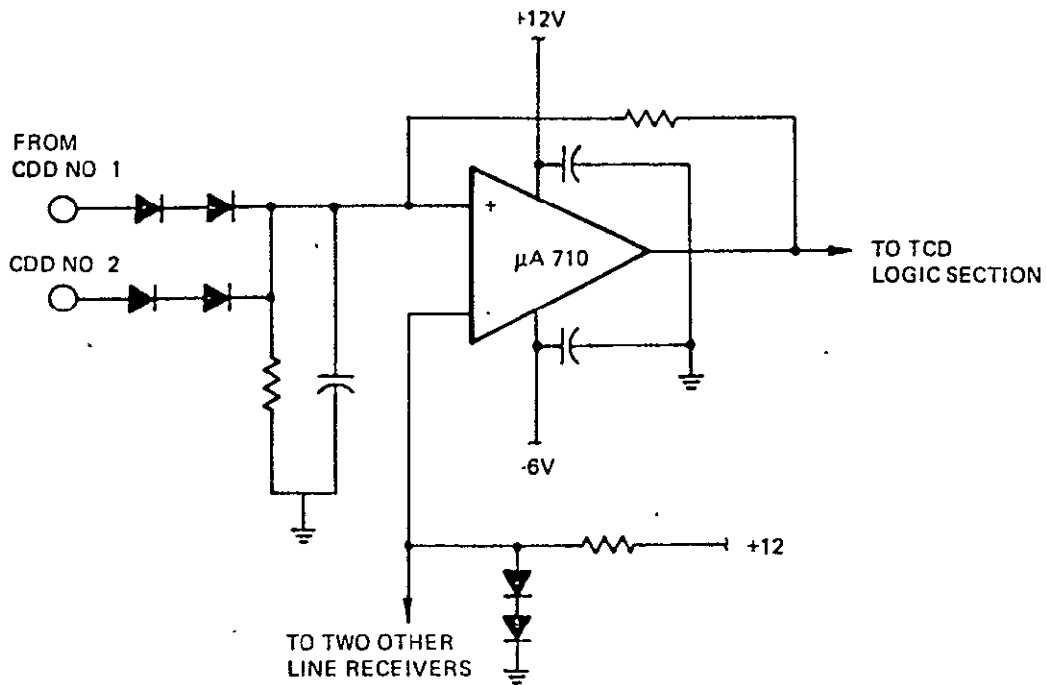
The high degree of redundancy complicates the interconnections. Each discrete command requires two wires, one from each CDD. The data word can come from two places, and goes to two places, so each of the four signals involved requires eight wires. So far, only signal or "hot leads" have been mentioned. The transponder power supplies must have a return to each CDD. The TCD, because of the large number of signal wires, must supply two returns to each CDD. Table 6.8-1 summarizes these connections.

A circuit diagram of the input interface circuit used in the transponder command decoder is shown in Figure 6.8-1(a). Series-redundant OR diodes combine the lines from the two CDD's. The Fairchild uA710 makes an excellent high-noise-immunity line receiver. A small amount of positive feedback introduces some hysteresis to further increase the noise immunity. It also ensures that the output will have rise and fall times better than 1 ms. The input rise time of 1 ms is a ramp by comparison. To prevent a race condition between data and clock transitions, the clock waveform is delayed in the CDD by one-half the clock period.

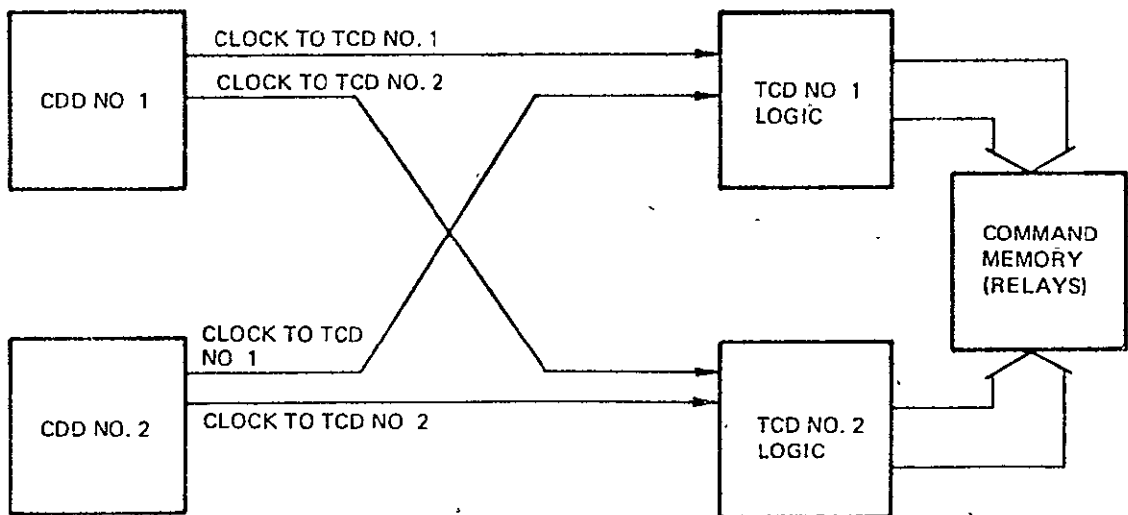
The cross-strapping interconnection between the two spacecraft command decoders and the transponder command decoders is shown in Figure 6.8-1(b).

Table 6.8-1. Summary of Connections

<u>Signal</u>	<u>Wires</u>
1. Gated clock from CCD No. 1 for TCD No. 1	1
2. Gated clock from CCD No. 2 for TCD No. 1	1
3. Gated data from CDD No. 1 for TCD No. 1	1
4. Gated data from CDD No. 2 for TCD No. 1	1
5. Execute pulse from CCD No. 1 for TCD No. 1	1
6. Execute pulse from CCD No. 2 for TCD No. 1	1
7. Gated clock from CDD No. 1 for TCD No. 2	1
8. Gated clock from CDD No. 2 for TCD No. 2	1
9. Gated data from CDD No. 1 for TCD No. 2	1
10. Gated data from CDD No. 2 for TCD No. 2	1
11. Execute pulse from CC No. 1 for TCD No. 2	1
12. Execute pulse from CC No. 2 for TCD No. 2	1
13. Discrete cmd TCD No. 1 ON from CDD No. 1	1
14. Discrete cmd TCD No. 1 ON from CDD No. 2	1
15. Discrete cmd TCD No. 1 OFF from CDD No. 1	1
16. Discrete cmd TCD No. 1 OFF from CDD No. 2	1
17. Discrete cmd TCD No. 2 ON from CDD No. 1	1
18. Discrete cmd TCD No. 2 ON from CDD No. 2	1
19. Discrete cmd TCD No. 2 OFF from CDD No. 1	1
20. Discrete cmd TCD No. 2 OFF from CDD No. 2	1
21. and 22. Returns to CDD No. 1 from TCD	2
23. and 24. Returns to CDD No. 2 from TCD	<u>2</u>
TOTAL COMMAND WIRES INTO TCD	24
25. Discrete Command PS No. 1 ON from CDD No. 1	1
26. Discrete Command PS No. 1 ON from CDD No. 2	1
27. Discrete Command PS No. 1 OFF from CDD No. 1	1
28. Discrete Command PS No. 1 OFF from CDD No. 2	1
29. Discrete Command PS No. 2 ON from CDD No. 1	1
30. Discrete Command PS No. 2 ON from CDD No. 2	1
31. Discrete Command PS No. 2 OFF from CDD No. 1	1
32. Discrete Command PS No. 2 OFF from CDD No. 2	1
33. Return to CDD No. 1 from PS	1
34. Return to CDD No. 2 from PS	<u>1</u>
TOTAL COMMAND WIRES TO PS	10
TOTAL WIRES ACROSS INTERFACE	34



(a) Non-discrete Command Input Interface Circuit



(b) Command Decoder Cross-strapping

Figure 6.8-1. Command Interface Details

6.8.1.2 Transponder Command Distributor (TCD) Configuration

A simplified block diagram of the proposed transponder command distributor is shown in Figure 6.8-2.

The TCD receives in serial data form all the commands required to operate the transponder, except for the four power supplies mentioned above. The data word contains nine bits, so the TCD could generate as many as 512 distinct stages; however, not all are needed. The output of the TCD to the transponder is embodied in latching-relay contact closures. The entire TCD except for these relays is duplicated for reliability.

There are several reasons for including a separate command distributor in the transponder. The transponder requires many discrete commands; so many, in fact, that the ability of the CDD to handle its other assignments would be jeopardized if it were required to provide discrete transponder commands. A "dedicated" command distributor allows the CDD/transponder interface to be frozen before the TCD/transponder interfaces have become clear. Specialized circuitry to meet peculiar transponder needs can be used. Interface problems will appear earlier in the schedule, at transponder integration, rather than at spacecraft integration.

6.8.1.3 Command Distributor Operation

Data is shifted into the shift register nine bits at a time from the CDD most significant bit first, just as it is transmitted up from ground control. The decode and matrix circuits work full-time, even while the register is being shifted. No relay can change state, however, until the execute command arrives to strobe the relay drivers. The execute command (a pulse) is normally sent after the re-transmitted (telemetered) command has been verified by the operator. This may take several seconds, or it may begin on the next clock pulse (finger on button already). If an error is detected, it is assumed that a new data word will be shifted in before the execute is sent. There is no lockout in the TCD to prevent overlap of shift and execute functions; it is assumed that the necessary separation is taken care of on the ground. This applies also to all sequences of commands. Some command sequences are likely to damage the transponder; the necessary sequencing is assumed to have occurred on the ground.

The TCD decodes the data word to the intended relay-driven enable stages, and then the execute command completes the circuit, so to speak. There are actually two sets of commands in the eight bits after the first one (No. 9 as numbered in the diagram): S-band feed instructions, and transponder instructions. The state of shift register stage No. 9 is used to steer the execute command to one group or the other. Each nine-bit combination is unique, of course, so only the selected relay state completes an AND when the execute comes in. The maximum possible number of relays changing state on any command is 8, and then only if all 8 bits of the S-band receive feed group are different than they were previously. It is more likely that only one relay will change state on any given command. If a multibit command contains repeats in some of the bit positions, as is likely, the relay drivers give out the selected drive pulses, but relay movement only occurs in those cases where the relay state does not match the drive pulse. This is also true of any single-bit command if the command is repeated.

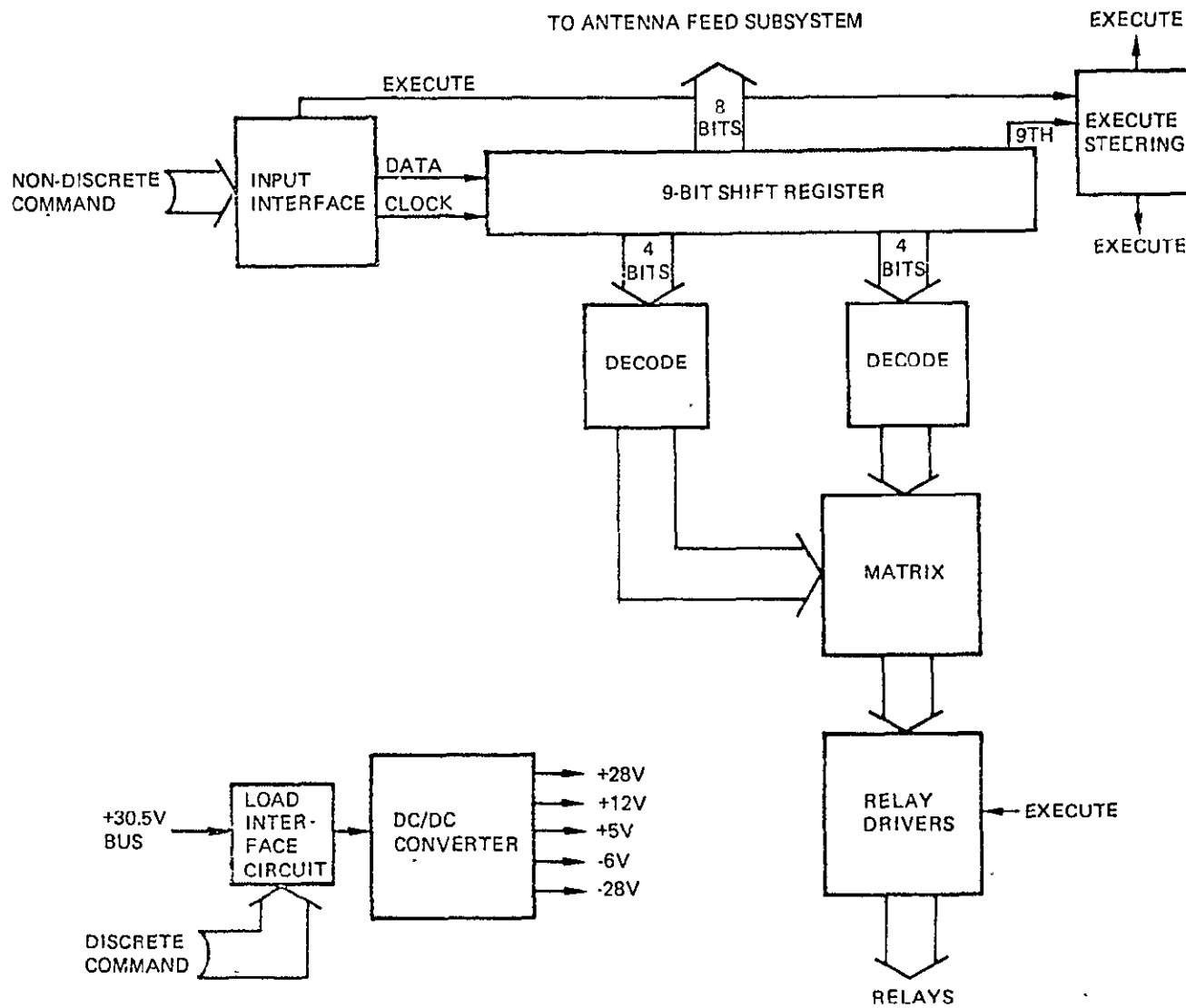


Figure 6.8-2. Transponder Command Distributor Block Diagram

6.8.1.5 IF Distribution Switching

The IF distribution switches require two relays in series in the RF path to achieve the desired isolation at 150 MHz. Each section of the IF distribution switching is organized as a one-pole four position switch, so a total of 8 relays are required for each section.

Latching relays will be used in the IF distribution matrix. These relays will be driven from the TCD with the circuit shown in Figure 6.8-3. This circuit selects one of four outputs from the decode matrix states.

Telemetry readout is provided by the circuit shown in Figure 6.8-4. Two gates are used at each output to provide the required isolation and interface conditions.

2.6.1.6 Relay Drivers

A schematic of the proposed relay driver circuit is shown in Figure 6.8-5. Essentially, it consists of two energy storage capacitors, C1 and C2, and two switches, Q6 and Q7. The capacitors are oppositely charged so that current of either polarity can be supplied to the relay coil between the "coil" and "ground" terminals. In operation, all transistors are normally off. The "strobe" line is low (near zero volts) and the other inputs (pins 2 through 5) may be high or low, although they would usually be high (+3.6V).

A total of 125 relay drivers are required for each TCD, or a total of 250 per satellite. The large number of drivers required poses a size and weight problem if they are assembled from discrete purchased parts. These circuits will therefore be fabricated using thick-film hybrid construction.

With the use of thick-film hybrid construction, the entire driver circuit can be specified, procured, and installed as a single component. The benefits are reduce size and weight, and reduced cost through reduced documentation and efficient mass production methods.

6.8.1.8 Telemetry Interfaces

Insofar as possible, only digital information is telemetered out of the transponder. Most parameters of interest can be easily transformed in a two-state (ON or OFF) signal. Power levels, for example, are monitored as above or below a nominal value. Almost all the parameters of link performance can be measured on the ground. The exception is AGC voltage from the IF. Since there are three IFs, there are three of these analog telemetry points.

All the telemetry points in the transponder are conditioned to standard levels and brought out to the data acquisition and control unit (DACU). All multiplexing, etc., is accomplished in the DACU. Since the entire telemetry subsystem, including the DACU, is standby redundant, each telemetry monitor point has two outputs.

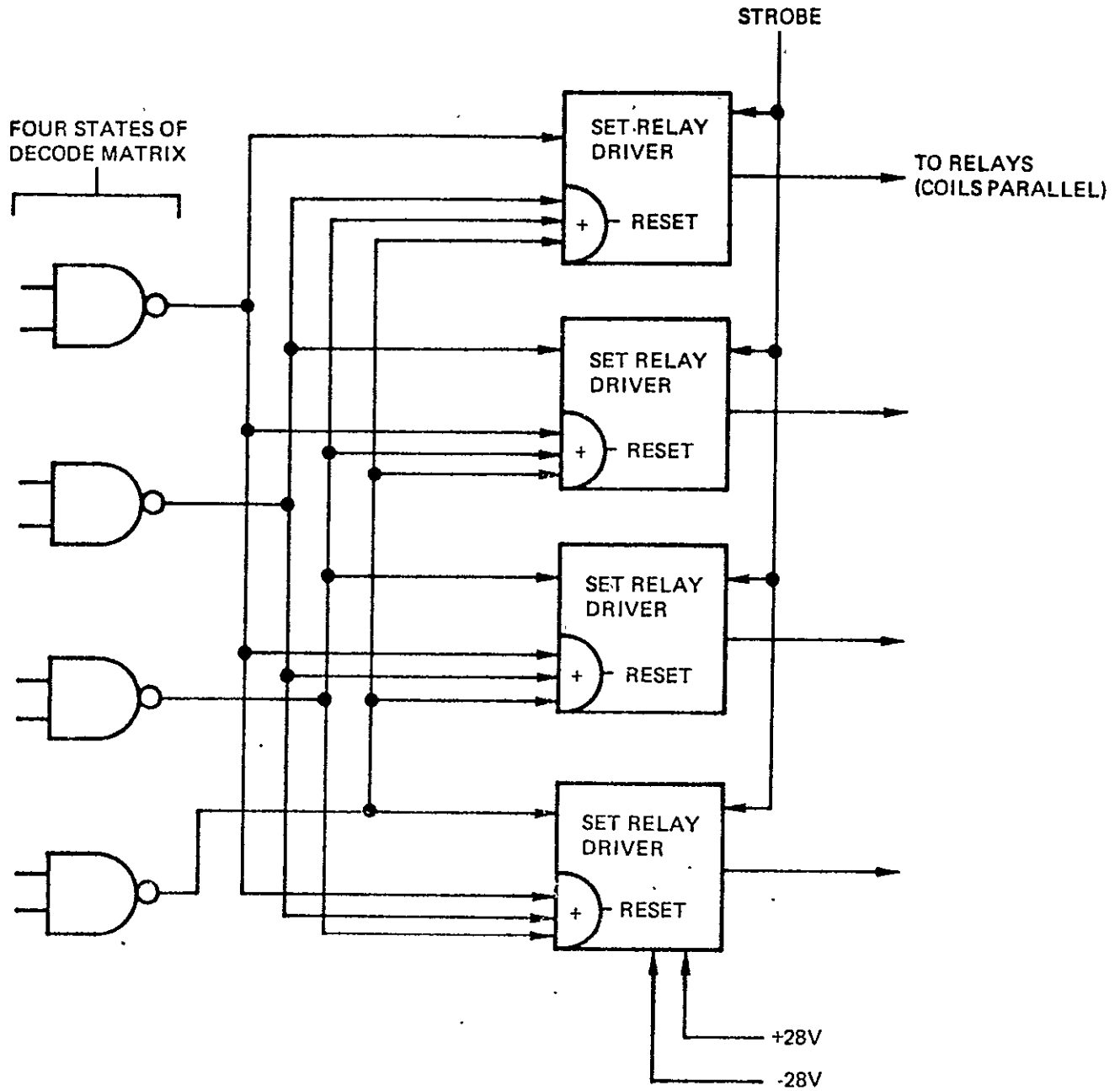


Figure 6.8-3. Select-One-of-Four Command Distributor Switching Circuit

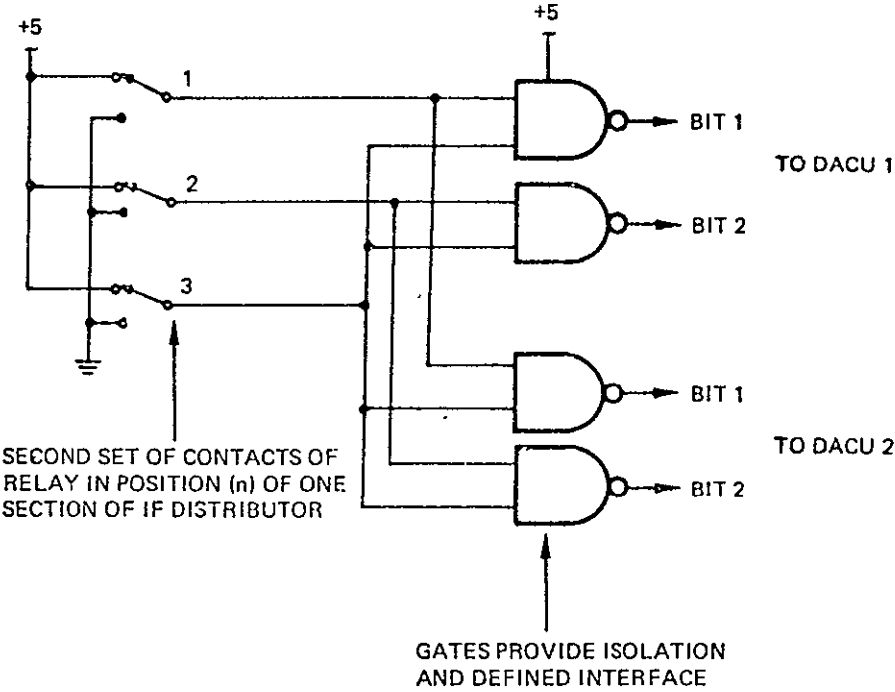


Figure 6.8-4. Telemetry Interface With Select-One-of-Four Circuit

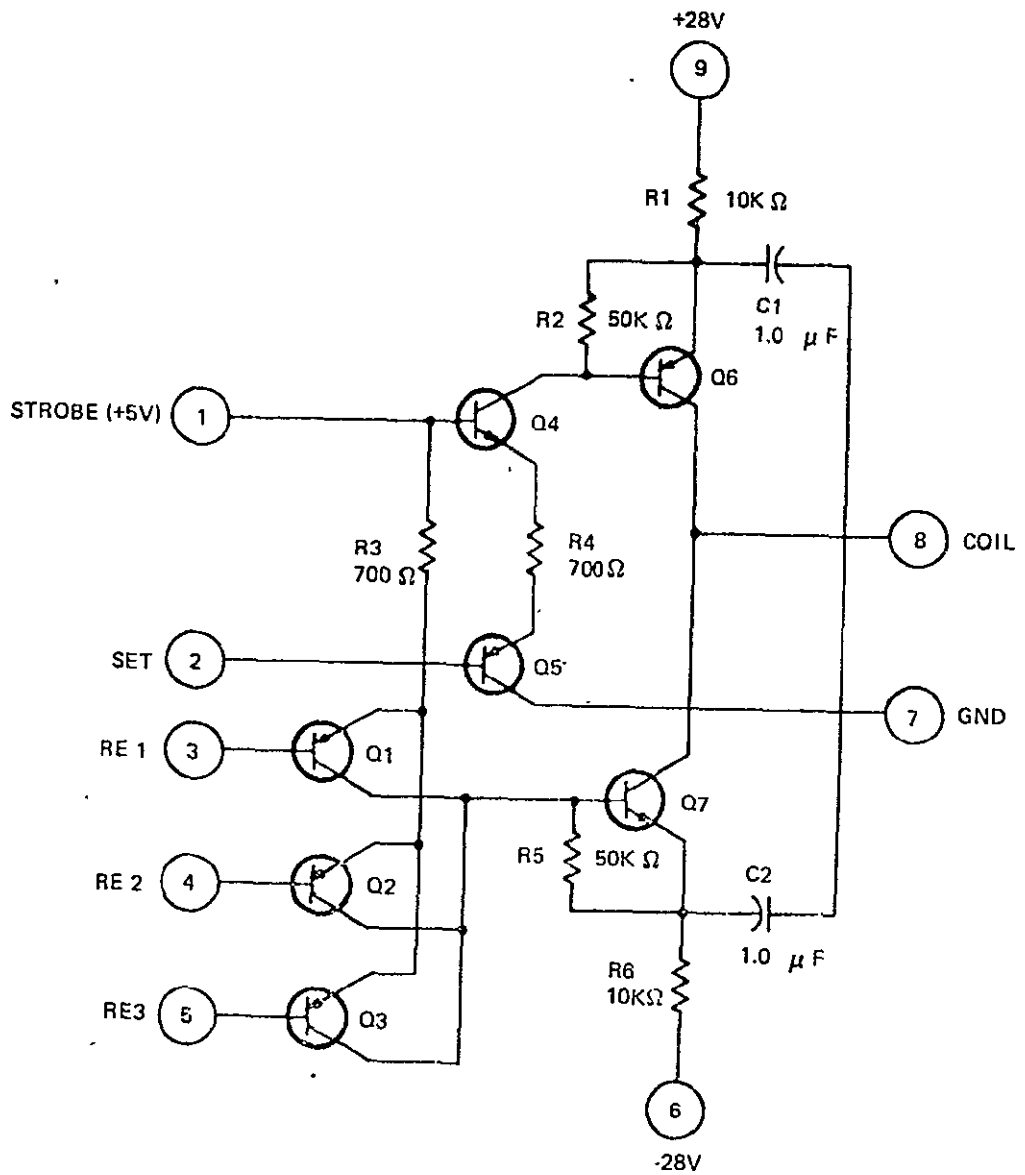


Figure 6.8-5. Relay Driver Schematic

A generalized block diagram of the telemetry interface for digital signals is given in Figure 6.8-6. Relay contacts will be used wherever practical. In some cases, however, monitor points will require transistor switches. The switches will be very simple in cases where small threshold variations with temperature or supply voltages are not critical. Slightly more accuracy and complexity may be required in the case of RF power monitors ($\pm 10\%$) and bi-level temperature monitors.

A block diagram of the telemetry interface for analog signals is given in Figure 6.8-7. The only such point presently proposed is the IF amplifier AGC voltage, which indicates relative received signal level. The operational amplifier shown in the diagram samples the drive voltage to the voltage-controlled attenuator in the IF amplifier AGC loop. Resistive isolation is used between the transponder and each DACU unit.

6.8.1.8 Command and Telemetry Lists

A summary of the Communication Subsystem command and telemetry requirements are given in Section 3.4.

6.8.2 POWER SUBSYSTEM INTERFACE

The eight discrete commands to the transponder all turn power supplies on or off. There are four supplies, in two pairs. They operate off the +30.5 volt bus system, which is itself redundant. The #1 unit of each pair operates off the #1 bus, and the backup unit operates off the #2 bus. Between each power supply and its bus is a Fairchild-Hiller-designed load interface circuit (LIC). The LIC provides ON and OFF control by pulse commands, provides line filtering and dc regulation, and will latch off for overvoltage, undervoltage, or overcurrent. A block diagram of the interface between the transponder and power subsystem is shown in Figure 6.8-8.

It should be noted that the transponder power supply carries only the low power portions of the subsystem. There are eight power amplifiers in standby redundant pairs that operate off a dedicated +25 volt bus system. Again, the No. 1 unit of each pair is tied to the No. 1 bus, while the No. 2 unit is tied to the No. 2 bus. The X-band power amplifiers are traveling-wave tube amplifiers with their own DC/DC converters. The TWT's require very tight control of their operating voltages, so their power supplies are usually supplied with switching mode preregulators. Turn-on and turn-off of these units will be effected by controlling this preregulator. When off, a few parts at the input of the TWTA are still on-line, but the probability of a failure here is considered slight in the mission lifetime.

The UHF and S/L-band power amplifiers pose special problems of power interfacing. They require high power (up to 200 W) at 25 V, and do not require any other voltage. Any kind of converter or regulator to make this voltage is intolerably inefficient unless it is the only one between this load and the solar array, therefore this is the approach proposed. The converter (actually two of them for redundancy) is located in the PCU and supplies only (is "dedicated" to) the transponder power amplifiers. The 25 V bus system exists as a requirement of the UHF S- and L-band power amplifiers. The TWTA's are operated off it as a convenience.

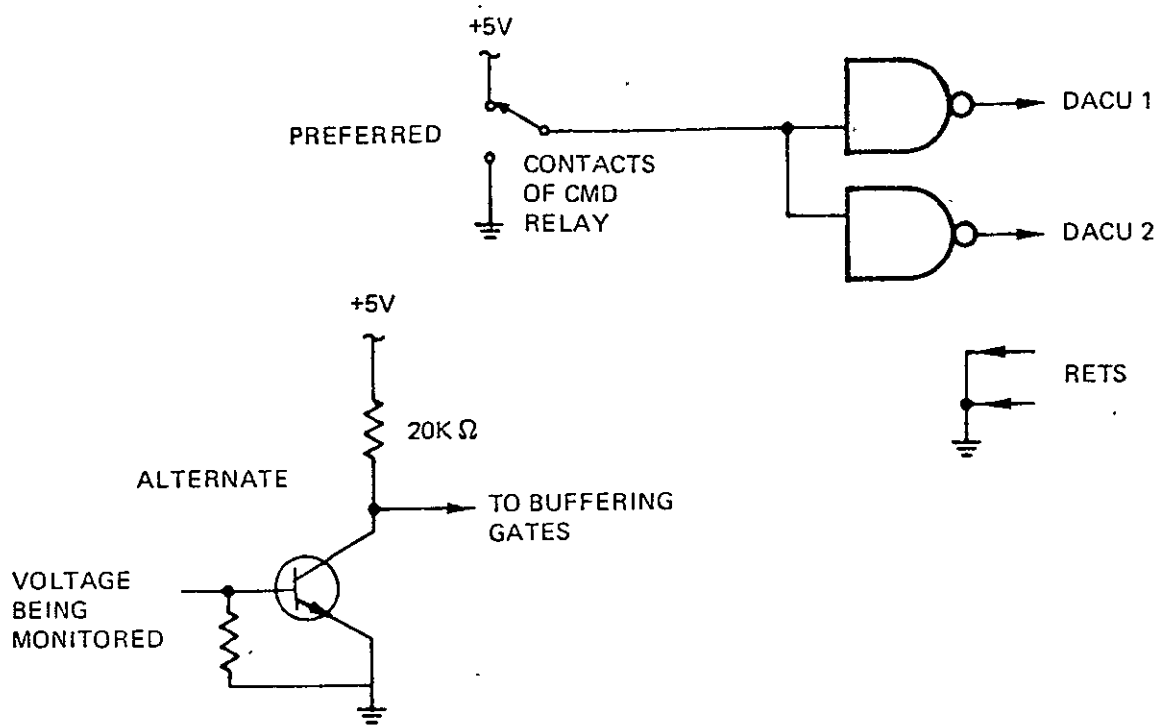


Figure 6.8-6. Typical Digital Telemetry Interface

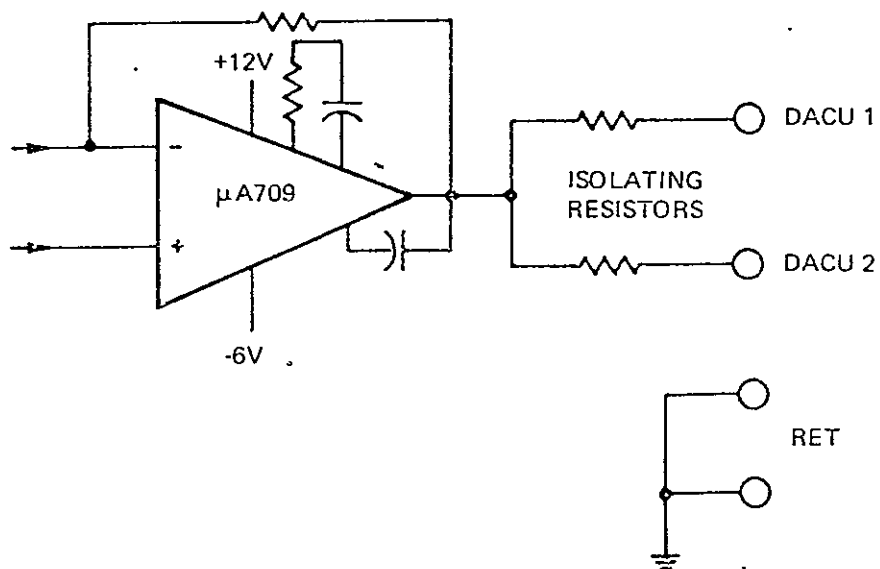


Figure 6.8-7. Typical Analog Telemetry Interface

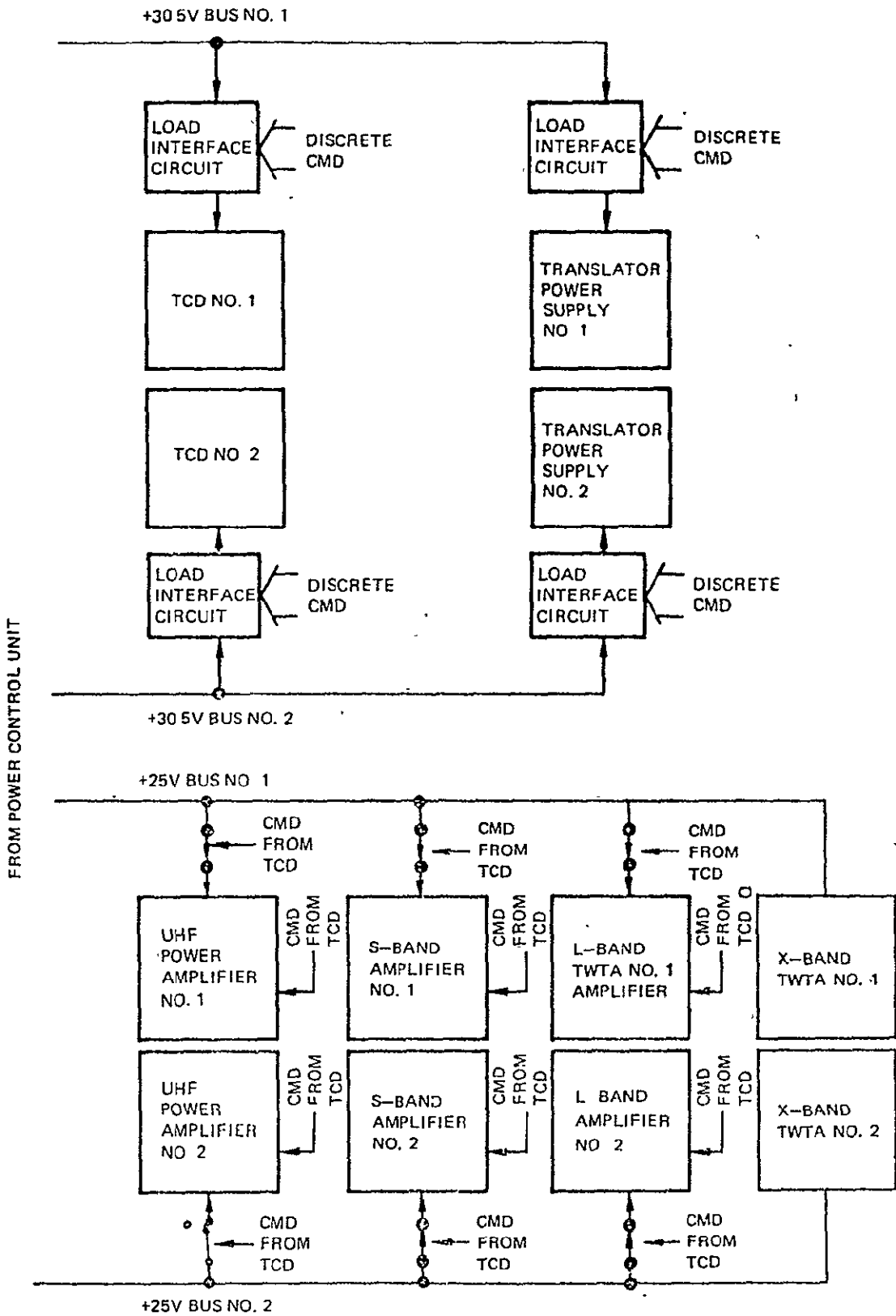


Figure 6.8-8. Transponder Prime Power Interface

6.8.2.1 Transponder Power Supplies

The transponder power supply carries all the transponder but the TCD's and power amplifiers. There are two reasons for its existence: (1) to provide the multiple voltages required, and (2) to provide ground isolation. Regulation is not required. The LIC provides 28 V $\pm 2\%$, so the supply is basically a simple DC/DC converter with no additional regulation capability of its own.

To prevent failure propagation, each supply must be short-proof. Repeated application of overloads on any or all outputs must not damage it. Philco-Ford has developed a magamp overcurrent detection circuit for another program which is sufficiently reliable and compact that each supply output lead will be so monitored. The circuit is kept very simple by using the DC/DC converter chopper as the excitation source. The outputs of these monitors will be combined and introduced into the LIC to latch off if any output line becomes overloaded. The transponder goes off the air, of course, and the ground control personnel must locate the fault by turning off the suspected unit and commanding the power supply on again. This method of operation has the advantages of simplicity and reliability without sacrificing flexibility.

If the fault turns out to be in the power supply itself, then the standby unit may be commanded on-line. Automatic load transfer is effected by diode OR'ing the outputs of the two supplies together.

PHYSICAL DESCRIPTION

6.9 This section discusses the Mechanical Design aspects of the transponder subsystem, including physical layout, component design, size, weight, and thermal requirements.

6.9.1 LAYOUT

The physical arrangement of the overall communications subsystem is shown in Figure 6.9.1. The EVM design is such that a modularized system can be used simplifying the overall mechanical and electrical integration problems. The EVM consists of three basic building blocks. The upper box will house the transponder and prime focus feed, and is detachable from the remainder of the EVM. The transponder and antenna feeds will be incorporated into this box, tested as a single unit and then integrated with the rest of the EVM. The top cover is removable and allows parallel integration of the transponder and feeds as shown in Figure 6.9.2.

Figure 6.9-3 shows the general layout of the transponder within the box. The bottom of the box will be covered with an RF shield to eliminate RFI problems at spacecraft integration. The earth viewing horn protrudes through the shield as shown and is located on the earth-viewing face of the EVM.

A more detailed layout of the transponder is shown in Figure 6.3-4. The arrangement of the various components was determined by optimizing thermal load distribution and minimizing harness lengths and RF losses as discussed in Section 3.2.

6.9-2 COMPONENTS AND ASSEMBLIES

The transponder subsystem is divided into the eight major assemblies listed below:

Translator	Synthesizer
S/L band filters	UHF transmitters
S/L band power amplifiers	X-band power amplifiers
S-band monopulse	X-band switching and diplexing

The majority of the transponder circuitry is located in the translator assembly and arranged so as to minimize RF cabling and harness lengths. Thermal control considerations determined the placement of the various power amplifiers.

A variety of packaging techniques are used in the transponder in order to obtain maximum performance and reliability, minimum size and weight, and lowest cost. These include printed circuit modules, T-frame modules, thick film logic circuits, stripline microwave assemblies, and machined microwave and waveguide assemblies.

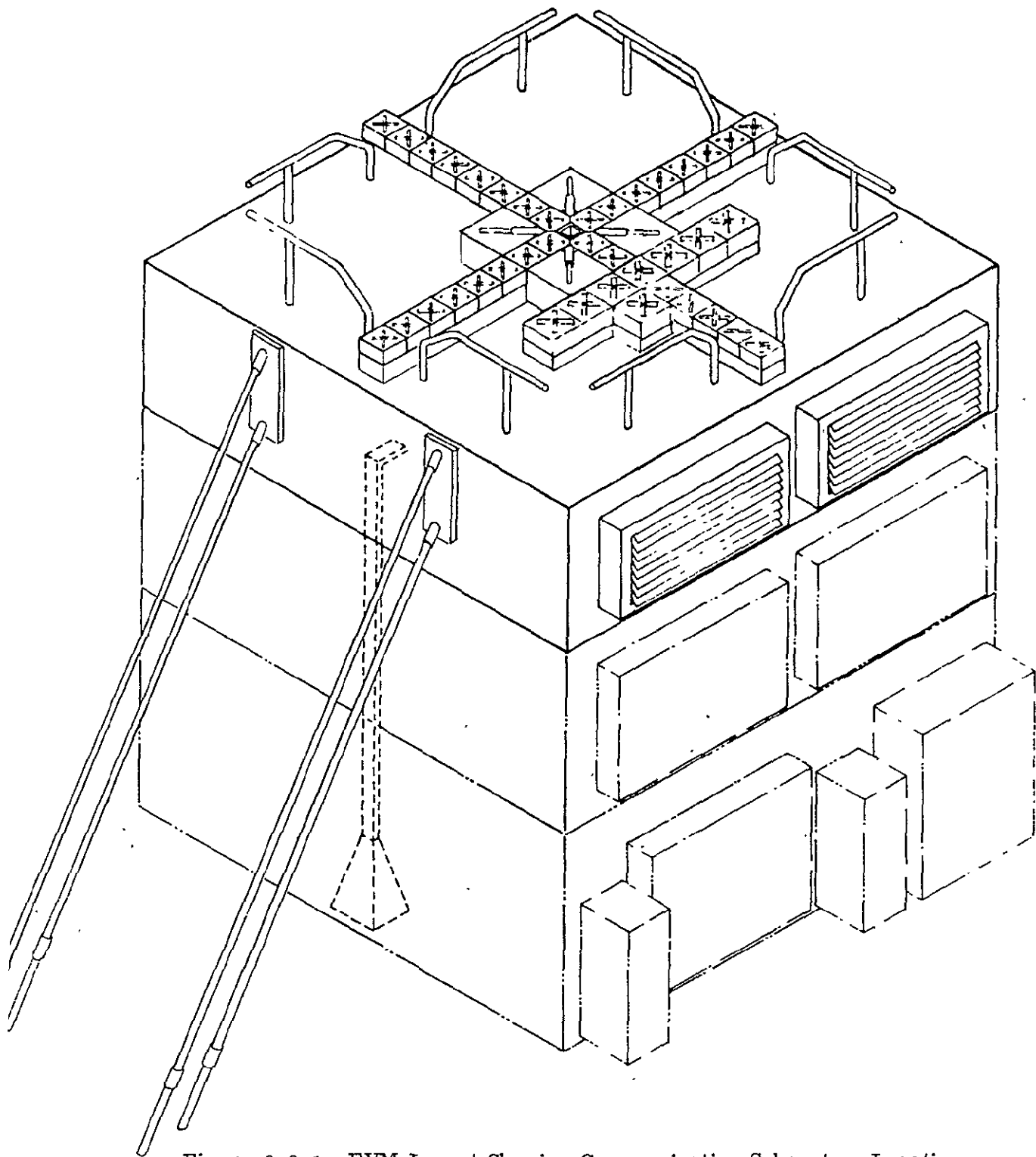


Figure 6.9-1. EVM Layout Showing Communication Subsystem Location

Revised 9/11/69

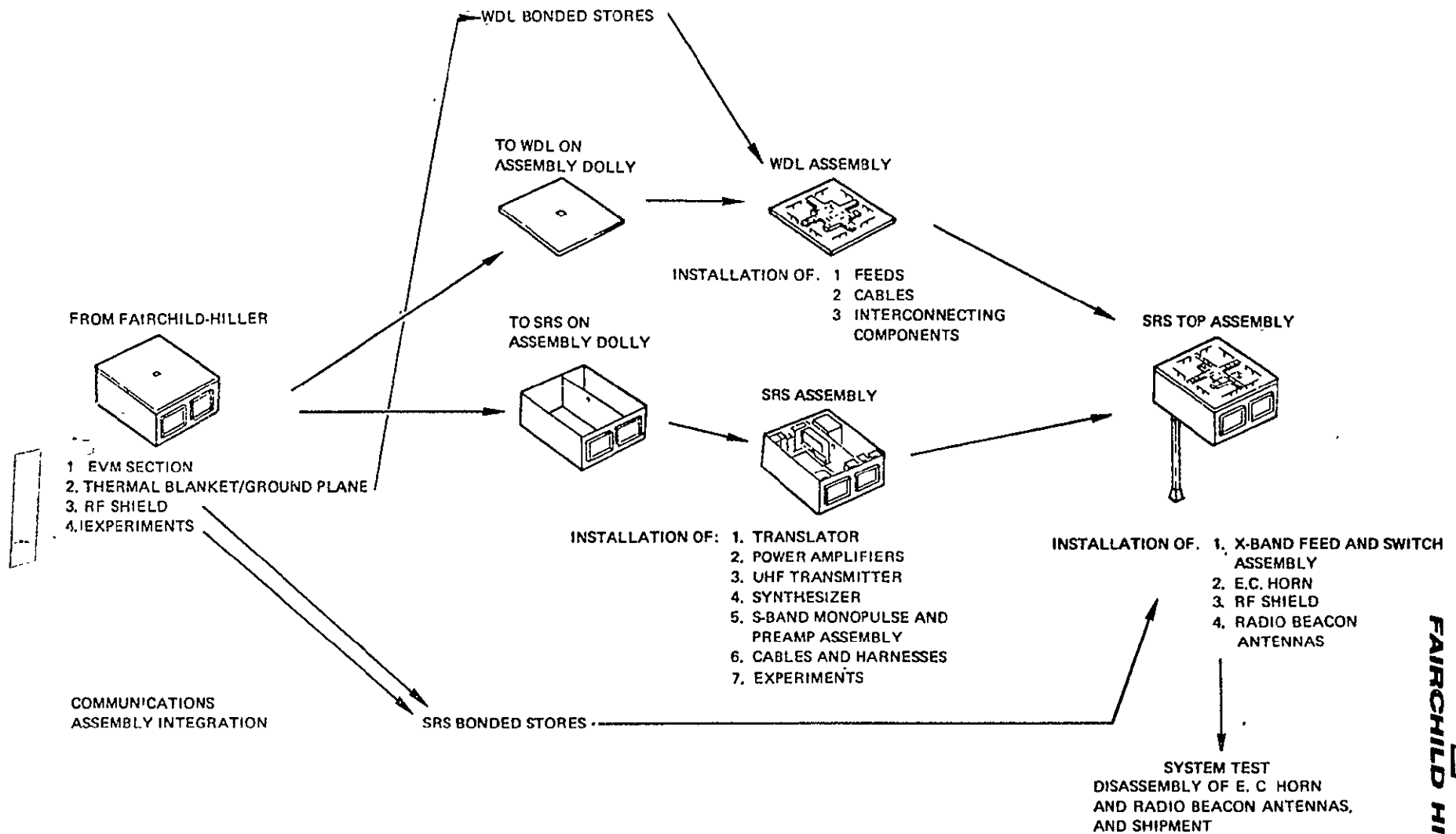


Figure 6.9-2. Transponder and Feed Integration

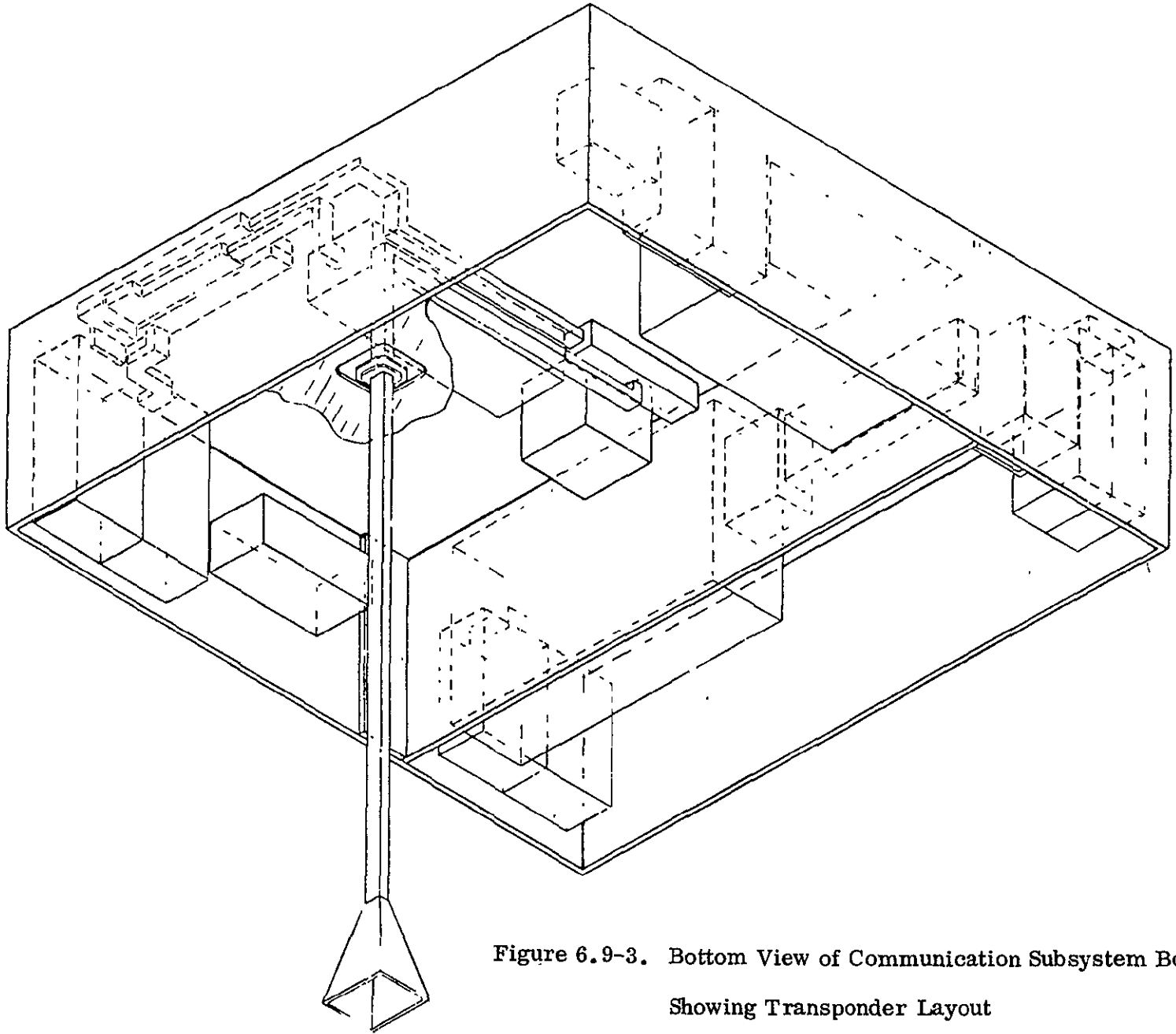


Figure 6.9-3. Bottom View of Communication Subsystem Box
Showing Transponder Layout

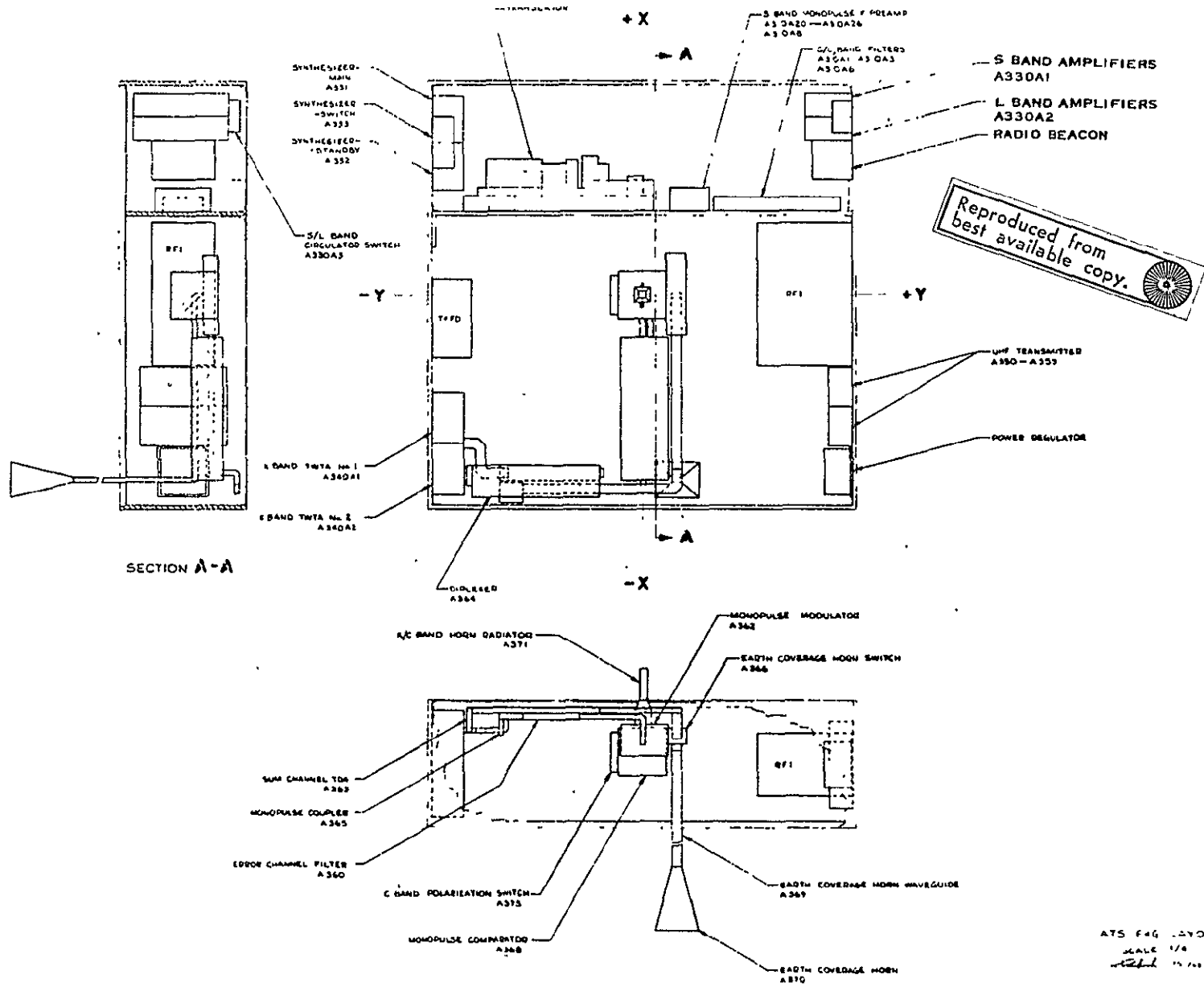


Figure 6.9-4. Transponder Layout

ATS F46 LAYOUT
 SCALE 1/4
 12/53

The printed circuit module consists of an etched printed circuit upon which the components have been soldered and a shielding enclosure. The majority of the components are mounted parallel to the board. Only where short lead length is dictated between two components will the components be mounted vertical to the board. All component interconnections are made opposite to the component side of the board. On the component side of the board, a groundplane will be used. Where thermal requirements dictate, high heat dissipating components will be mounted on the metal portion of the module and wired into the printed circuit board.

Use will also be made of T-Frame construction methods for RF modules where appropriate. In this construction method, the electrical components are bonded to a plated aluminum frame which contains dividers to separate dc and RF wiring and to provide interstage shielding. The frame also contains the feedthrough terminals and mechanical parts required for mounting the module.

A combination of cordwood and thick film construction will be used for the low frequency analog, digital, and command circuitry. In the command decoder, in particular, the large number of identical relay driver circuits required makes it desirable to use thick film construction from both a weight and cost point of view.

A modular packaging approach has been used for the transponder. Each module represents a functional portion of the total circuits and may be tested separately. All modules are secured to the chassis with threaded devices so that there is no dependence upon the soldered joints for mechanical security. The module interconnections and their decoupling networks are conformal coated for environmental protection. Upon completion of the module interconnections and coating, a cover is fastened down over the base opening which provides complete RFI shielding of the system along with adding to the mechanical strength of the system.

6.9.3 WEIGHT ALLOCATION

Table 6.9-1 summarizes the weight and size of the various transponder components.

6.9.4 POWER CONSIDERATIONS

Heat loads are handled in four areas of the communications section of the EVM. These areas are the north and south walls which have heat pipes and louvers, the intercostal which is both a structural member and a heat pipe interconnection for the north and south walls, and the EVM cover that supports the antenna feed elements. Table 6.9-2 shows the heat loads imposed in these areas by the transponder during the required experiment modes. The EVM cover is the interface for both heat leaks and solar radiation input through the feed elements. The heat leak condition is estimated at 12W, and the maximum input is 23W. Table 6.9-3 shows the component power dissipation for the various experiment modes.

This thermal design requires the high heat dissipation units, namely the power amplifiers and the synthesizer, be located on the north and south walls of the EVM, behind louvers. Placement was also influenced by the various experiment modes, so that heat loads would be minimized for the louvers.

The low power units are mounted on the east and west faces where there is no thermal problem.

Table 6.9-1. EVM Heat Loads (Watts)

EXPERIMENT MODE	NORTH WALL	HEAT PIPE INTERCOSTAL	SOUTH WALL	EVM COVER
DRSS	86.0	13.05	60.0	12.05
PLACE	86.0	11.05	120.00	5.25
X-Band Monopulse	26.0	8.8	0.0	3.3
S-Band Monopulse	26.0	9.8	0.0	0.5
VHF Monopulse	0.0	5.6	0.0	0.0
ITV	71.0	8.8	120.00	2.05
VHR Camera & Radiometer, MM Wave	86.0	6.3	0.0	1.8
Laser	86.0	8.3	0.0	2.05
T&FD	86.0	8.3	0.0	1.8
RFI	60.0	1.5	0.0	1.8

The power amplifiers and the synthesizers are packaged with redundancy units and switches on a common chassis. This permits partial heat dissipation through the chassis of the non-operating unit.

Assemblies are finished to meet the thermal requirement of surface emittance of greater than 0.80. Surface absorptance values are based upon requirements derived from empirical data.

Table 6.9-2. Transponder Component Size And Weight

A NUMBER	COMPONENT	SIZE (INCHES)	WEIGHT (LB)	TOTAL WEIGHT
Translators				
A320A5	IF Amplifier No. 1	10.00X5.00X2.00	1.90	1.90
A320A6	IF Amplifier No. 2	10.00X5.00X2.00	1.90	1.90
A320A7	IF Amplifier No. 3	10.00X5.00X2.00	1.90	1.90
A320A4	X-Band Down-Conv.	4.50X3.25X2.00	1.37	4.11
A320A2	S-Band Down-Conv.	5.00X4.50X1.00	1.57	1.57
A320A1	L-Band Down-Conv.	6.00X4.50X1.00	1.75	1.75
A320A16	S-Band Up-Conv.	4.50X6.00X1.50	1.87	1.87
A320A17	L-Band Up-Conv.	4.50X6.00X1.50	2.12	2.12
A320A8	X-Band Up-Conv.	5.00X4.50X2.00	1.82	5.46
A310A19	X-Band Exp Mod & Coup.	4.00X2.00X.63	0.20	0.40
A320A11	Up-Converter IF Dist.	7.00X4.00X3.00	0.90	0.90
A320A12	Down-Converter IF Dist.	6.00X4.00X3.00	0.70	0.70
A320A14	Wideband Data Unit No. 1	5.00X3.00X1.50	0.50	0.50
A320A15	Wideband Data Unit No. 2	5.00X3.00X1.50	0.50	0.50
A322	X-Band Beacon	3.00X3.00X2.00	0.50	0.50
A321A1	Power Converter No. 1	5.00X5.00X2.00	2.00	2.00
A321A2	Power Converter No. 2	5.00X5.00X2.00	2.00	2.00
A367A1	X-Band Down-Conv. Tri.	8.00X1.00X.50	0.25	0.25
A367A2	X-Band Up-Conv. Tri.	8.00X1.00X.50	0.25	0.25
A341A1	TCD Logic No. 1	3.00X5.50X5.75	3.50	3.50
A341A2	TCD Logic No. 2	3.00X5.50X5.75	3.50	3.50
A341A3	TCD Output Interf	5.00X2.00X4.00	1.50	1.50
A320A9	Monop. Det/Drv'r No. 1	1.75X9.00X2.00	0.90	0.90
A320A10	Monop. Det/Drv'r No. 2	1.75X9.00X2.00	0.90	0.90
A372	VHF Coupler	5.60X2.00X.38	0.20	0.20
A373	VHF RECV HYBRID	3.00X3.00X.50	0.31	0.31
A376	VHF Sum Ch. Filter	4.00X.25X.25	0.20	0.20
A377	VHF XMIT DIPLEXER	3.00X2.00X1.00	0.35	0.35

Table 6.9-2. Transponder Component Size And Weight (Cont'd)

A NUMBER	COMPONENT	SIZE (INCHES)	WEIGHT (LB)	TOTAL WEIGHT
A380	VHF Error Ch. Filter	4.00X.25X.25	0.20	0.20
A374	VHF Monop. Mod.	8.00X6.00X.50	0.80	0.80
				<u>42.94</u>
L BAND FILTERS				
A310A1	L BAND RECV FILTER	10.00X2.00X1.00	1.70	1.70
A310A3	L BAND PREAMP/FILTER	3.00X2.00X.50	0.50	0.50
				<u>2.20</u>
S/L BAND AMPLIFIERS				
A330A1	S BAND AMPLIFIERS	3.25X13.00X2.00	2.68	2.68
A330A2	L BAND AMPLIFIERS	6.50X13.00X2.00	5.36	5.36
A330A18	S BAND XMIT HYBRIDS	1.00X1.00X1.00	0.15	0.30
A330A19	S BAND DRIVER AMPL.	.50X2.00X6.00	0.70	1.40
A330A20	L BAND XMIT HYBRIDS	1.00X1.00X1.00	0.15	0.30
A330A21	L BAND DRIVER AMPL.	.50X2.00X6.00	0.70	1.40
A330A3	Circulator Switches	2.50X2.00X1.50	0.50	1.00
				<u>12.44</u>
S-Band Monopulse and Preamp Assembly				
A310A8	MONOPULSE SEL. SW.	7.00X3.00X1.00	0.50	0.50
A310A20	Sum Channel Preamp	3.00X2.00X.50	0.50	1.00
A310A21	Sum Channel Filter	3.00X2.00X.25	0.25	0.25
A310A22	Error Channel Preamp	3.00X2.00X.50	0.50	0.50
A310A23	Error Channel Filter	3.00X2.00X.25	0.25	0.25
A310A24	Monop. Mod.	7.00X5.00X1.00	3.00	3.00
A310A25	Coupler	2.00X2.00X.50	0.15	0.15
A310A26	Horiz. and Vert Comb Sw.	3.00X3.00X.50	0.31	0.31
				<u>5.96</u>

Table 6.9-2. Transponder Component Size And Weight (Cont'd)

A NUMBER	COMPONENT	SIZE (INCHES)	WEIGHT (LB)	TOTAL WEIGHT
Synthesizer				
A331	Synthesizer - Main	6.00X4.00X10.00	8.00	8.00
A332	Synthesizer - Standby	6.00X4.00X10.00	8.00	8.00
A333	Synthesizer Switch	6.50X1.63X3.75	1.63	1.63
				<u>17.63</u>
UHF Transmitter				
A352	Up-Converters	1.00X1.00X.50	0.10	0.20
A351	Driver Amplifiers	3.00X5.00X1.00	0.30	0.60
A350	Power Amplifiers	5.00X8.00X3.00	3.80	7.60
A353	Coaxial Relay	2.00X2.00X2.00	1.50	1.50
A354	Filter/Detector	1.00X1.00X3.00	0.30	0.30
A355	Local Oscillators	2.00X3.00X1.00	0.70	1.40
				<u>11.60</u>
X-Band Power Amplifier				
A340A1	X-Band TWTA No. 1	13.50X6.50X4.00	10.00	10.00
A340A2	X-Band TWTA No. 2	13.50X6.50X4.00	10.00	10.00
A340A3	Circulator Switches	4.00X3.50X2.00	1.75	1.75
				<u>21.75</u>
X-Band Switching & Diplexing Assembly				
A371	X/C-Band Horn Radiator*	1.85X1.85X6.00	2.50	2.50
A368	Monopulse Comparator*	6.00X6.00X6.00	2.20	2.20
A362	Monopulse Modulator	18.00X6.00X4.00	2.20	2.20
A366	Earth Coverage Horn Sw*	10.50X2.40X2.00	2.50	2.50

* Feed Items

Table 6.9-2. Transponder Component Size And Weight (Cont'd)

A NUMBER	COMPONENT	SIZE (INCHES)	WEIGHT (LB)	TOTAL WEIGHT
A364	FILTER	8.00X4.00X.63	0.50	0.50
A360	Error Channel Filter	7.00X1.25X.63	0.40	0.40
A365	Monopulse Coupler	2.00X1.00X.50	0.20	0.20
A361	Error Channel TDA	3.00X2.50X.70	0.30	0.30
A363	Sum Channel TDA	3.00X2.50X.70	0.30	0.30
A373	C-Band Pol. Switch*	1.00X4.00X5.00	1.50	1.50
A375	Coupler Detector	4.00X2.00X.63	0.20	0.20
A379	Sw/Dipl. Waveguide	1.25X.63X 9.00	0.22	0.22
A381	Pwr Amp/Dipl Waveguide	1.25X.63X14.00	0.34	0.34
A383	Mod/Filter Waveguide	1.25X.63X14.00	0.34	0.34
A384	Comp/Mod. Waveguide	1.25X.63X6.00	0.17	0.34
			Subtotal	<u>14.38</u>
			Total	<u>128.90</u>
Cables and Harnesses				6.50
(For connections to feeds, between transponder components, and experiments)				
Attachment Hardware				
(Screws, washers, cable clamps, brackets, etc)				<u>3.75</u>
Transponder Weight with Integration Hardware				<u>139.15</u>

* Feed Items

Table 6.9-3. Communications S/S Thermal Dissipation

MODE	1	2	3	4	5	6	7A	7B	8	9	10	11A	11B	12	13	14	15	16	17	18	19	20	21	
	A361, A363 X-Band Error and Sum Channel Preamps	A310 A8 S-Band Preamps	A310 A3 L-Band Preamp	A373, A382 VHF Sum and Error Channel Preamps	A320 A5, A320 A6, A320 A7 IF Amplifiers	A340 X-Band Power Amplifier	A330 S/L-Band Power Amplifier S-Mode	A330 S/L-Band Power Amplifier L-Mode	A330 UHF Power Amplifier	A320 Monopulse Detector and Driver	A321 Power Converters 1 and 2	A331 Synthesizer - ITV Mode	A331 Synthesizer - All other modes	A322 Beacon (X-Band)	A320 Wideband Data Units	A341 Transponder Command Distributor	A362 X-Band Monopulse Modulator	A310A24 S-Band Monopulse Modulator	A374 VHF Monopulse Modulator	A310 A9, A310 A10, A310 A11 S-Band Switch Array	RF Losses S-Band Array	RF Losses X-Band Switch	RF Losses L-Band Switch	TOTAL FOR MODE (WATTS)
DRSS	0.25	0.25			5.0	60.0	60.0				5.8		26.0	TBS	0.50	1.5				6.0	4.0	1.8		171.10
PLACE	0.25		0.25		5.0	60.0		120.0			4.3		26.0	TBS		1.5							5.0	222.30
X-Band Monopulse	0.50				2.5					0.50	4.3		26.0			1.5	1.0					1.8		38.10
S-Band Monopulse	0.50				2.5					0.50	4.3		26.0			1.5		1.0						36.30
VHF Monopulse				3.0	2.5					0.50	0.30					1.5			0.50					5.60
ITV ¹	0.25				5.0	60.0			120.0		2.3	11.0		TBS		1.5						1.8		201.85
VHR Camera Radiometer MM Wave						60.0					1.3		26.0	TBS	0.50	1.5						1.8		94.10
Laser	0.25				2.5	60.0					4.3		26.0	TBS		1.5						1.8		96.35
T&FD					2.5	60.0					4.3		26.0			1.5						1.8		96.1
RFI						60.0										1.5						1.8		63.3

¹ With X Band Video Monitor

SECTION VII

PRIME FOCUS FEEDS

7.1 INTRODUCTION

The proposed design provides all of the required capabilities of the ATS F&G satellite and a number of additional capabilities with a relatively high degree of radiation efficiency and minimal interaction between feed elements. These capabilities are listed below:

- a. VHF - The basic requirement for a high gain telemetry transmitting and receiving capability have been expanded to provide a wide-angle, attitude-sensing monopulse capability.
- b. UHF - The UHF transmission capability for the ITV experiment has been placed "on axis" so that the X-band monopulse may automatically orient the satellite for coverage of the receiving area.
- c. L-Band - The transmission and reception functions for the PLACE experiment employ two separate, selectable beams: a fan beam and a symmetrical (pencil) beam.
- d. S-Band - The transmission and reception functions for the DRSS experiment use multiple symmetrical beams that cover up to 7.5 degrees in two orthogonal planes of scan. This will provide the two satellite tracking capability required without the use of relatively lossy and unreliable rotating mechanisms. A monopulse system for single satellite tracking is also provided.
- e. C-Band - Reception for the RFI experiment using a symmetrical, on-axis beam with two orthogonal linear and circular polarization modes is provided in a system integral with the X-band feed.
- f. X-Band - Tracking, transmission and reception using monopulse technique.

The X-band earth coverage horn provides the primary communications link between the earth and the ATS F&G satellite by illuminating the entire earth's disc. In addition, the horn is used as a reference antenna to measure the gain of the parabolic antenna.

The proposed design has evolved from an extensive Phase B and C study effort and from experience gained on previous multi-frequency antenna feed projects.

7.2 SUMMARY DESCRIPTION

The composite feed concept, designed to satisfy the ATS F&G requirements, is shown in Figure 7.2-1 and the simplified RF schematic in Figure 7.2-2. The composite feed is an integral part of the top cover of the Communication Subsystem section of the earth viewing module (EVM) for simplicity of assembly and test, and the shortest possible RF cable lengths. The earth coverage X-band horn is located in the bottom cover of the EVM. Its waveguide connection to the transponder subsystem is provided with quick disconnects for easy assembly.

The antenna feed includes all of the RF components required between the transponder output and the RF radiated signal. Hence, the RF switches, monopulse comparators, etc., are a part of the antenna feeds. For ease of integration, all of these components are mounted to the top cover of the EVM, which then forms the ground plane for the composite feed. (The transponder is mounted inside of the EVM so that the two subsystems can be assembled separately and easily integrated).

As seen from Figure 7.2-1, there is a great deal of commonality between radiating elements. To satisfy the circular polarization requirement, cavity-backed crossed-dipole elements are proposed for UHF, L- and S-band feeds. These elements provide simple and reliable operation at the frequencies and the bandwidths required by ITV, PLACE, and DRSS experiments. Considerable experience with crossed-dipole and monopulse elements has been gained by Philco-Ford on previous multifrequency antenna projects.

The proposed X- and C-band feed is a common radiator using a multimode concept. The VHF elements are simple $\lambda/4$ loops (stubs) which make up four dipoles arranged as shown. Each feed subsystem is described briefly in the following paragraphs.

7.2.1 X-BAND FEED AND EARTH VIEWING HORN

The X-band feed consists of a center-mounted multimode horn, a comparator, and the RF switch required for interfacing with the earth coverage horn. The radiating aperture is reduced in cross section and is dielectric-loaded to support the necessary modes and to shape the primary radiation pattern.

The horn is excited from a conventional four-port comparator through a four-port rectangular-to-square transition. All modes needed for monopulse operation are thus generated within the horn structure and in combination produce sum and difference primary patterns.

An RF switch is placed in the sum channel output from the comparator. This switch provides the following capabilities:

- Reception from the dish while transmitting on the earth coverage horn
- Simultaneous transmission and reception from either the dish or horn.



FAIRCHILD HILLER

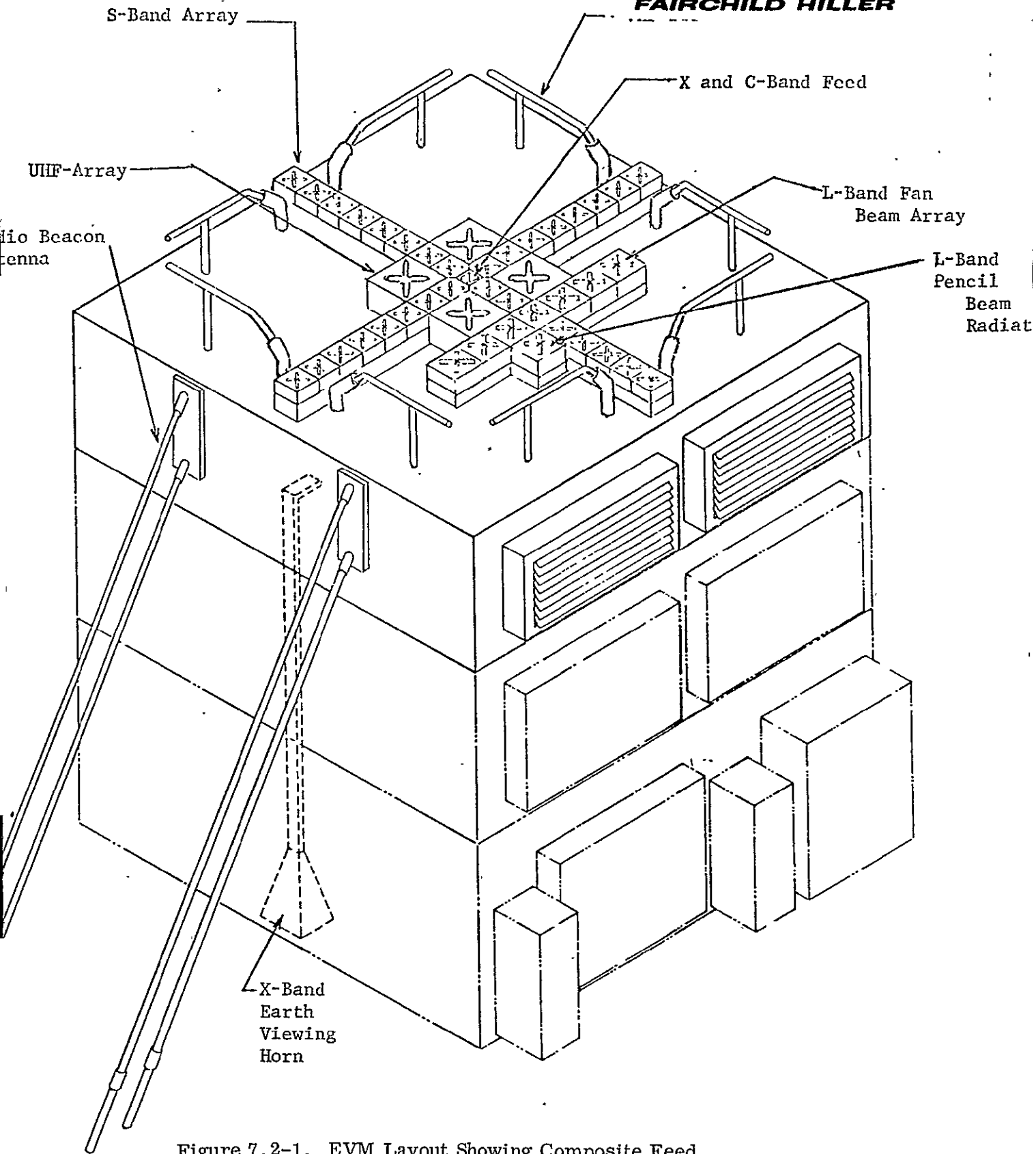


Figure 7.2-1. EVM Layout Showing Composite Feed

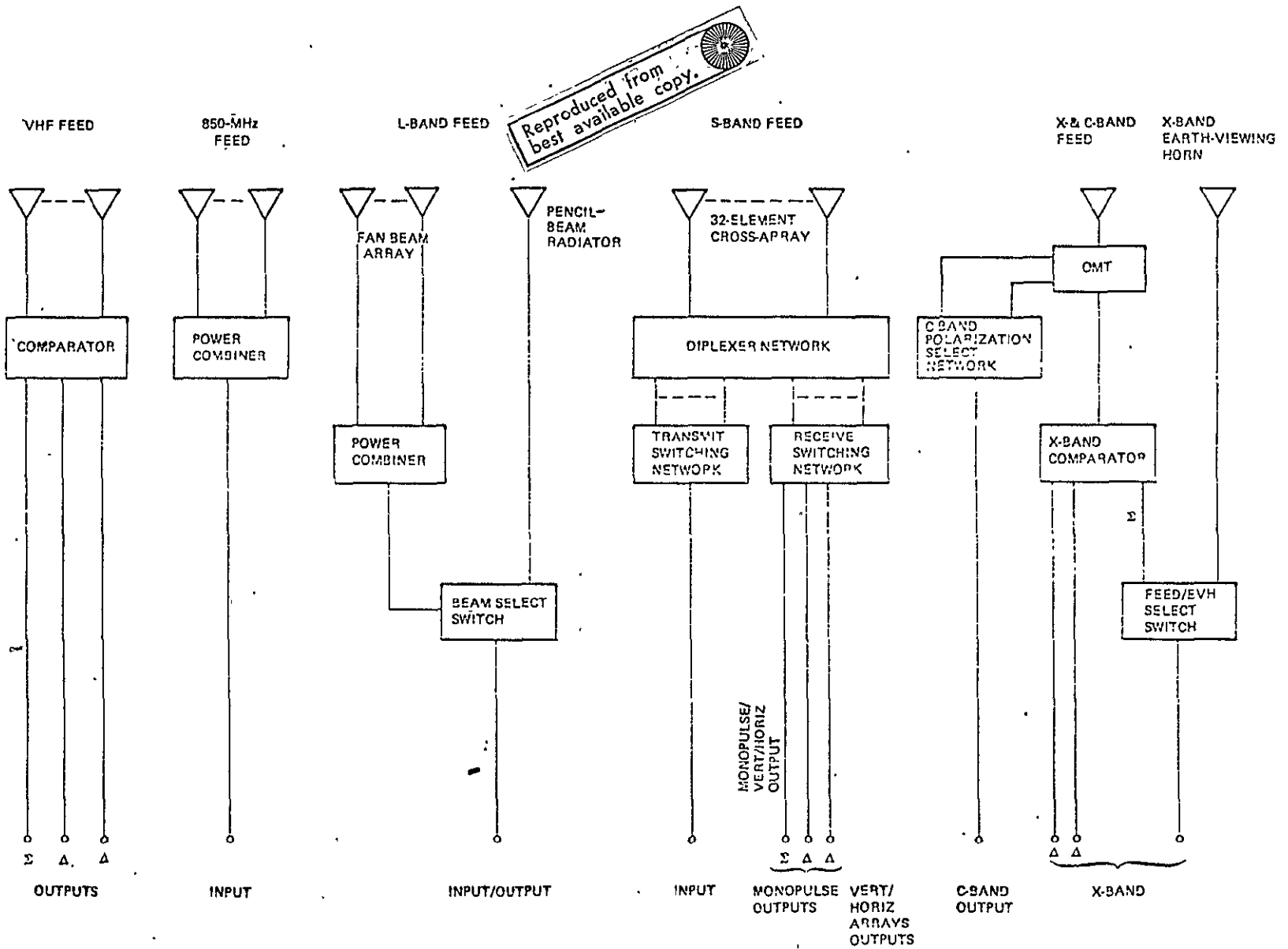


Figure 7.2-2. Antenna Feed, RF Schematic

The earth coverage horn is a simple pyramidal horn placed at the bottom of the EVM. This horn provides coverage of a 20° cone angle.

7.2.2 C-BAND FEED

The C-band feed makes use of a unique design, in which the X-band multi-mode horn is shared at C-band. This permits the C-band beam to be coincident with the X-band sum channel beam, easing operational problems for the RFI & TFD experiment.

At C-band, the feed is excited through the shunt ports located on opposite walls of the horn. The horn is thus excited with two orthogonal (TE_{10} and TE_{01}) modes. Polarization selection from two orthogonal linear and one circular mode is obtained through a network consisting of two phase shifters and a quadrature hybrid. Remote polarization selection capability is obtained using voltage controlled, solid-state phase shifters.

7.2.3 S-BAND FEED

The S-band feed is composed of 32 cavity-backed turnstile elements, mounted in a cross-array coincident with the feed axis. This approach is selected over the single rotating array proposed in Phase A to decrease cost and complexity. Additional advantage of the cross-array is that the four innermost elements form a monopulse feed having a diamond configuration, which can be used for single satellite tracking.

Each of the 32 turnstile elements is connected to a diplexer. Separate transmit and receive switching networks enable a remote selection of feed element(s), providing an independent-feed phase center for generating 32 secondary beams for the communications coverage in two orthogonal planes out to $+7.5^{\circ}$ from antenna system axis.

The switching is accomplished with a specially-designed single-pole, four-throw PIN-diode switch. A single-pole, four-throw switch replaces three single-pole, double-throw switches (either ferrite- or PIN-diodes) that would normally be required. A significant reduction in both weight and RF losses is achieved. PIN-diodes are also used to switch the four innermost elements through a comparator network, for generating an on-axis beam (sum channel) and two orthogonal error channel beams for monopulse operation.

7.2.4 L-BAND FEED

The L-band feed is made up of seven cavity-backed, crossed-dipole elements, mounted in a line-array to form the fan beam, and a separate element to form the pencil beam. The array consists of two groups of three elements and a seventh element, which is shared with the S-band array. These elements are excited in equal phase but with varied amplitudes through a power-dividing network mounted on the back of the array.

The feed-array illuminates the reflector with an elliptical primary pattern, producing a normal amplitude and constant phase characteristics in one plane, while in the orthogonal plane, only a portion of the reflector is illuminated with a constant phase energy. Asymmetric reflector illumination generates a fan-shaped secondary beam having an approximate half-power beamwidth of $7.5^{\circ} \times 1.1^{\circ}$. Due

to feed displacement from the composite feed axis, the secondary beam is squinted approximately 3° off the antenna axis. The beam steering is accomplished by tilting the spacecraft.

In addition to the fan beam described above, a symmetrical pencil beam is generated using a separate, single-cavity-backed, crossed-dipole element. A separate element is used to minimize the switching losses. A ferrite switch enables the selection of the desired L-band beam.

7.2.5 UHF FEED

The UHF feed consists of four cavity-mounted crossed-dipole radiators, forming an on-axis array. The size of the S-band cross-array requires that the cavities be reduced in size to allow closer element spacing to obtain proper reflector illumination. The four elements are fed through a simple power divider.

7.2.6 VHF FEED

The VHF feed consists of eight $\lambda/4$ loops (stubs), making up four dipoles mounted at the ends of the S-band array. The dipoles are connected to a comparator network, generating a circularity-polarized sum and two orthogonal, linearly-polarized error patterns. The feed illuminates the 30-ft reflector, generating a secondary beam in the 136-150 MHz frequency range with sufficient gain to provide a special data link. This feed is also used for tracking and for transmitting certain telemetry data to ground.

7.2.7 RF DESIGN

This section discusses the RF design of each feed subsystem. Although each feed subsystem is independent of the others, the proximity of the elements and the spacing constraints imposed by adjacent feed required several iterations in the configuration. The present design has eliminated these problems and the bread-board test data has demonstrated the ability to achieve the proposed gains and other performance parameters.

7.2.8 X-BAND FEED

The X-band feed consists of a multimode horn, a waveguide comparator and an RF switch that selects either the 30-ft dish or the earth coverage horn. These devices are discussed in the following paragraphs:

Several design approaches (multi-mode spiral, conventional four-horn feed, coaxial cavity feed) were considered as candidates for X-band feed. Each of these approaches was evaluated on the basis of its RF performance as well as size, weight and complexity.

A conclusion was reached that the multi-mode radiator provided the best approach offering a compact package mounted on the axis of the parabolic reflector and satisfying both the X-band and the C-band requirements. The design is not intended to provide the performance (i. e., suppressed sidelobes, equal E- and H-plane patterns) usually associated with low-noise antenna systems. Rather, the design provides a simple, reliable, compact approach capable of covering two widely separated frequency bands.

The feed consists of a square multimode horn as shown in Figure 7.2-3. X-band operation is obtained by exciting the square horn from a conventional four-port comparator through a four-port transition. The sum channel pattern is produced by exciting the TE_{10} mode, while $TE_{11} + TM_{11}$ modes produce the E-plane difference pattern and TE_{20} mode produces the H-plane difference pattern. The mode configuration within the horn structure is shown in Figure 7.2-4.

The linear polarization requirement simplifies the design since the TE_{11} and the TM_{11} modes, required to produce the E-plane difference pattern, propagate with a common velocity. The only remaining requirement is to match the four individual waveguides into a common horn.

The radiating aperture is reduced in size and then dielectric-loaded to support the previously mentioned modes. The reduction is mainly for the control of the primary radiation pattern, since the oversized horn results in too large an aperture and hence too much directivity yielding poor illumination efficiency. In addition to primary pattern shaping, the reduced X-band aperture enables a closer spacing of the inner-most S-band elements as discussed in later paragraph.

The monopulse comparator used with the multimode horn is a standard waveguide type using 4 hybrids. The hybrids are arranged as shown in Figure 7.2-5. The error channels are developed at ports A and B and the sum channel at port C. These outputs are then sent to the monopulse modulator located in the transponder subsystem.

The sum channel output requires an RF switch since the X-band feed, when coupled with the earth viewing horn, must provide transmit and receive functions in several modes. The most demanding requirement is to provide an ITV experiment mode whereby the earth-coverage horn is used as a transmitting antenna and the parabolic antenna as a receiving antenna. Furthermore, at least 40 dB isolation is required between the two antennas so that the higher gain parabolic antenna is decoupled from the transmitter.

Several solid state (ferrite) switch configurations were considered for this application. A two-junction switch can be arranged to provide three different X-band modes (i. e., transmit and receive on earth-coverage horn, transmit and receive on parabolic antenna, and transmit on earth-coverage horn-receive on parabolic antenna). The two-junction switch cannot, however, provide the necessary 40 dB isolation.

The proposed X-band antenna select switch, made up of three switchable junctions, is shown in Figure 7.2-6. The circuit will satisfy the stated requirements of simultaneous transmission/reception modes with necessary isolation between the transmitter and the parabolic antenna. The transmitter and the earth-viewing horn are connected to the same junction to provide highest ERP from the low-gain antenna. The insertion loss between the transmitter terminal and the parabolic antenna terminal (all three junctions) is estimated to be 0.8 dB.

The switchable circular junctions will be built into a single structure. The ferrite disks will be magnetized by coil utilizing a single yoke requiring very low power consumption (estimated at 210 mW per coil).

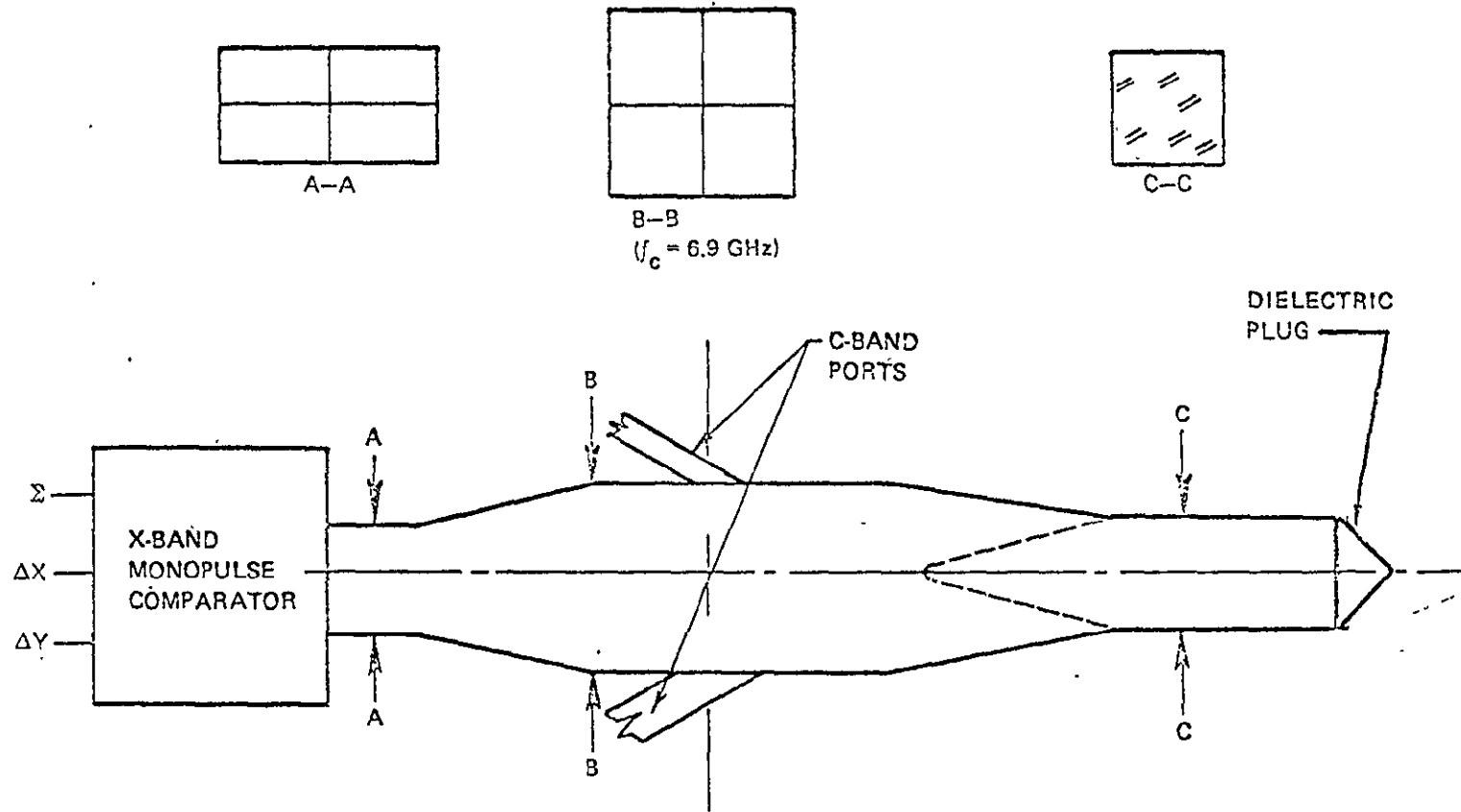
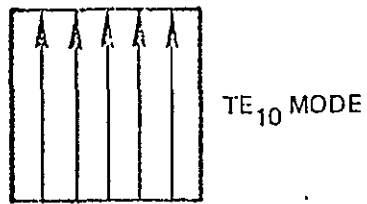
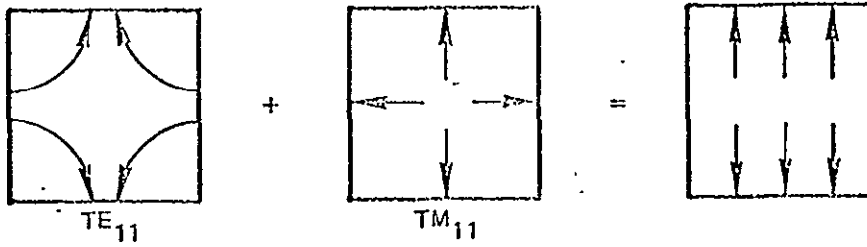


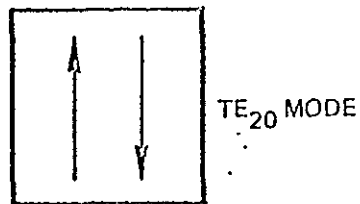
Figure 7.2-3. X- & C-Band Multimode Waveguide Feed



a) SUM CHANNEL



b) E-PLANE DIFFERENCE



c) H-PLANE DIFFERENCE

Figure 7.2-4. X-Band Horn Module Configuration

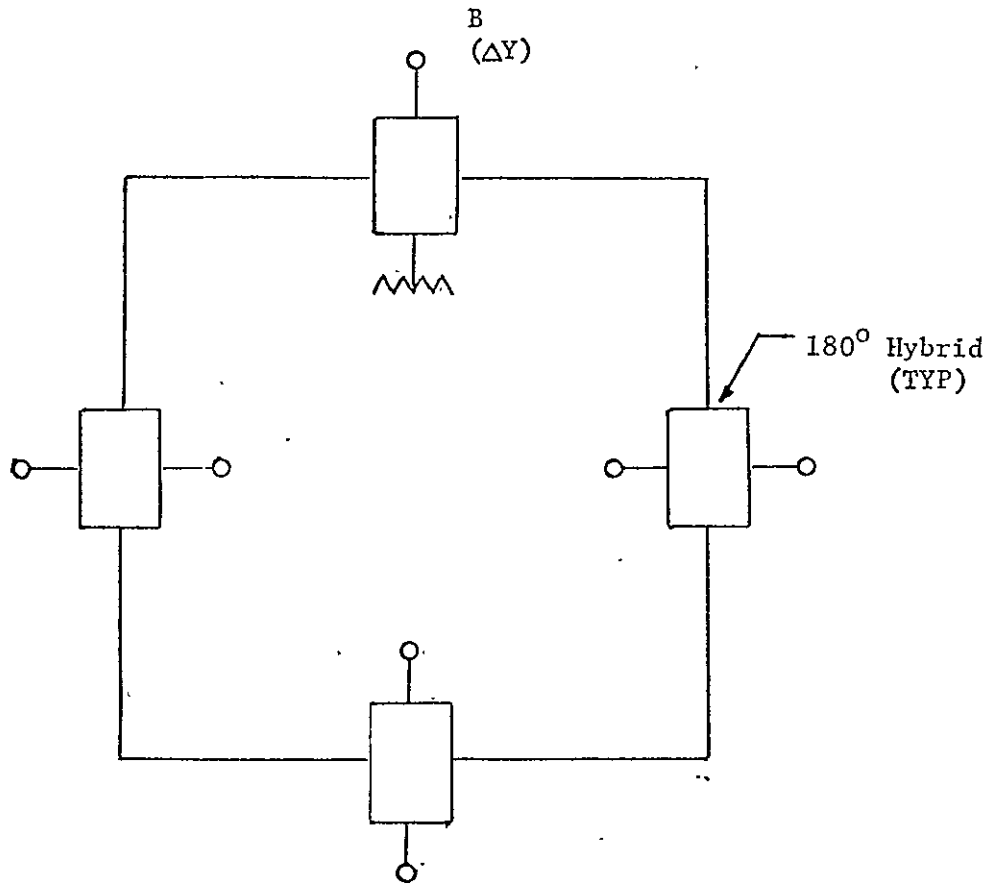
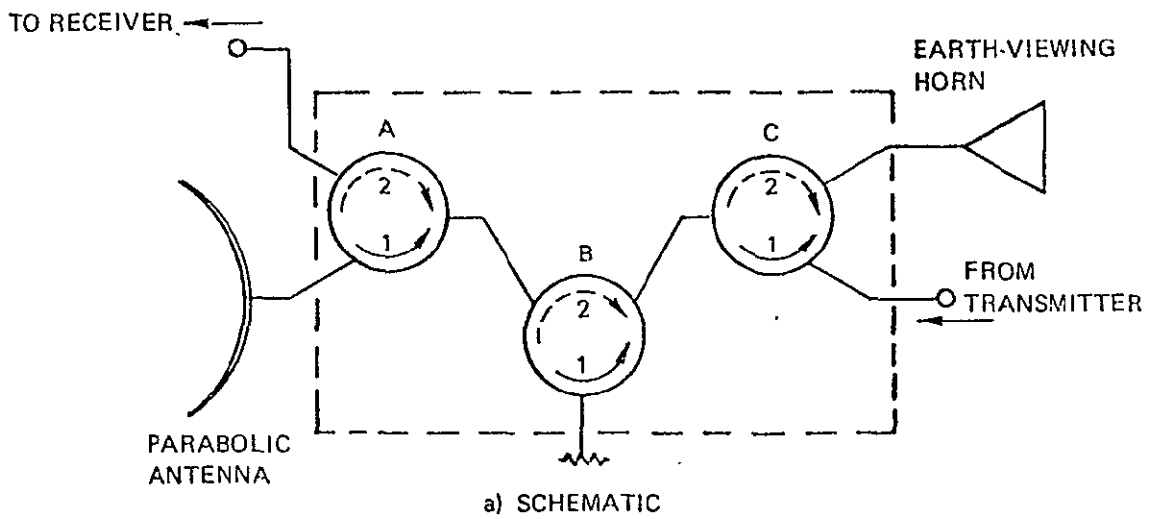


Figure 7.2-5. X-Band Monopulse Comparator



SIMULTANEOUS MODES		JUNCTION POSITIONS		
TRANSMIT	RECEIVE	JUNCTION A	JUNCTION B	JUNCTION C
HORN	DISH	2	2	1
DISH	DISH	2	1	2
HORN	HORN	1	1	1

b) SWITCHING MODES

Figure 7.2-6. X-Band Antenna Switching Circuit

7.2.9

C-BAND FEED

The C-band feed consists of the feed element, which is shared with the X-band element, and the switch necessary to select the desired polarization. These items are discussed below.

The reflector illumination at C-band is obtained by exciting the multimode horn described previously. Referring to Figure 7.2.4, the two orthogonal (TE_{10} and TE_{01}) modes are excited through shunt ports located on opposite walls. Since the four square X-band waveguide openings are adjusted to cutoff at 6.9 GHz, this interface acts as a shorting plate for C-band frequencies, forcing the energy to propagate along the horn axis. The combination of structures consisting of two orthogonally-positioned coupling slots and the four square X-band waveguide openings, thus form a built-in diplexer separating the two frequency bands.

The methods of exciting the multimode horn at C-band frequency have been verified using full-scale breadboard models. The initial concept was to excite the horn using the balanced four-port method, however, this method resulted in greatest feed complexity. Simplified methods of excitation were, therefore, attempted and the most successful approach proved to be one of exciting the horn from opposite walls through orthogonally-placed coupling slots with the input guides tilted toward the back of the horn. In addition each coupling slot incorporates longitudinal fins which short out the orthogonal mode.

The C-band primary illumination pattern is very similar to the X-band pattern. The similarity is due to the rather small frequency separation (approximately 17%) between the C-band and the X-band transmit band.

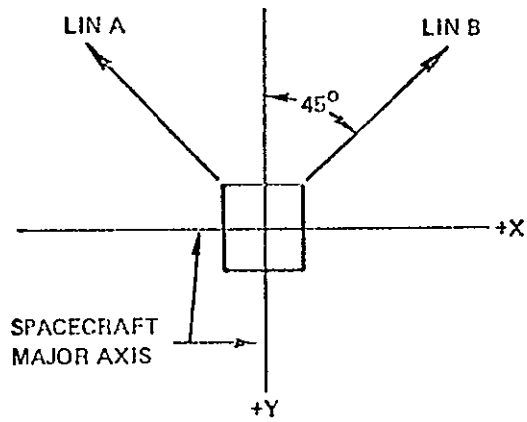
Remote polarization selection will be accomplished through a simple circuit consisting of two phase shifters and a quadrature hybrid shown in Figure 7.2-7. With both phase shifters set at 0 degrees, the signals from vertical and horizontal ports will combine through the hybrid, providing circular polarization mode. With phase shifter A placed in 90 degree position, the vertical and the horizontal inputs will add in phase generating a linear polarization vector oriented at 45 degrees to the two input ports. Setting phase shifter B in 90 degree position will generate the orthogonal linear polarization vector.

The phase shifters of the circuit can be built in several variations such as nonlatching twin-slab ferrite shifter, a latching ferrite shifter, or a diode shifter. The prime considerations are size and compactness. It is, therefore, anticipated that the entire circuit will be built in stripline. The insertion loss of the circuit is expected to be below 1 dB.

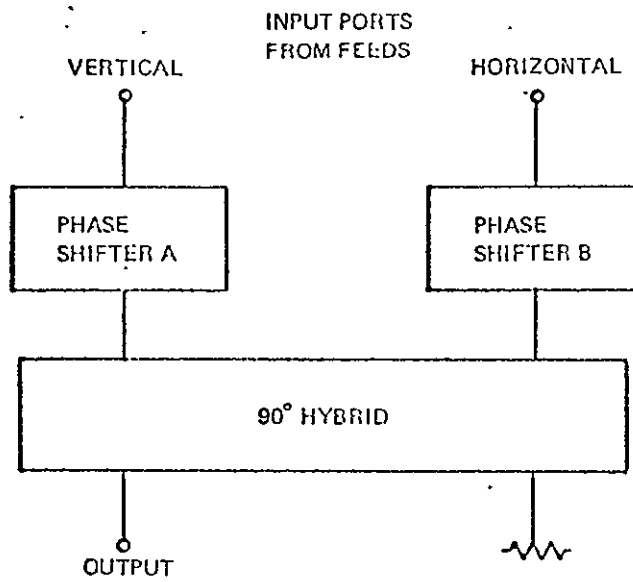
7.2.10

S-BAND FEED

The S-band Feed consists of 32 cavity-backed turnstile radiators arranged in a cross array. The scanning mode operation is obtained by selecting one of the radiating elements thru a feed distribution matrix. The on-axis mode (monopulse) operation is obtained by connecting the four center-most radiating elements to a monopulse comparator and to a power divider.



a) POLARIZATION ORIENTATION



b) RF SCHEMATIC

FEED POLARIZATION	PHASE SHIFTER A SETTING	PHASE SHIFTER B SETTING
CP	0°	0°
LIN A	90°	0°
LIN B	0°	90°

c) SWITCHING LOGIC

Figure 7.2-7. C-Band Polarization Control Network

7.2.10.1 Radiating Elements

Assuming the use of a linear array, it was established that 16 separate beams are needed in the plane of scan to provide reasonable cross-over level between adjacent beam positions and to provide about $\pm 7.5^\circ$ of scan. Therefore, a considerable amount of analysis was performed to select a proper feed element that would provide best reflector illumination. In view of the circular polarization requirement, the radiating element choice was narrowed to the three arrangements shown in Figure 7.2-8.

The double-row, cavity-backed spiral array, with four elements being excited simultaneously, provides highly tapered illumination. This minimizes spill-over and improves secondary pattern sidelobes for off-axis beam positions; however, this arrangement results in low overall antenna efficiency and maximum feed complexity.

The single-row spiral array provides a more uniform illumination in plane orthogonal to the plane of scan while in the plane of scan, the amplitude taper is obtained by exciting two elements at a time. This arrangement results in good reflector illumination and the necessary amplitude taper in the plane of scan. However, the feed is still complicated by the switching scheme that must provide double element excitation.

To reduce the feed complexity, especially the weight of the switching unit, single element excitation was considered next. Two feeds, one consisting of cavity-backed spiral elements and the other made up of helical elements, were analyzed. The analyses were performed at the center of the receive frequency band, because the higher frequency (narrower beamwidth) was expected to have greater performance degradation for off-axis (scanned) beam cases. The calculated cases did not include the feed support blockage effect.

The primary element patterns used in the analysis indicated that the helical element provides substantially higher amplitude taper (-15 dB edge directed illumination versus -6.5 dB for a spiral) which, in turn, is expected to produce broader secondary beam and hence higher cross-over level between the beams at the expense of antenna efficiency.

The computed secondary results indicate a rather small difference between the performance of two feeds, as seen from Figures 7.2-9 and 7.2.10. It should be noted that the absolute gain provided by the antenna for the worst condition (i. e., gain at crossover point between Beams 7 and 8) is the single most meaningful measure of its performance. Although the helical element (higher amplitude taper) case indicates less off-axis scan loss referred to the first beam peak, the absolute gain at the worst point is within 0.5 dB, with the helical element feed being slightly better. A comparison of feeds analyzed is shown in Table 7.2-1.

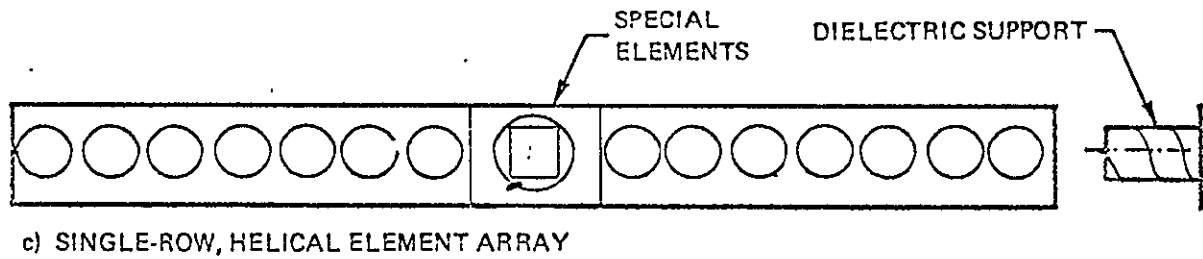
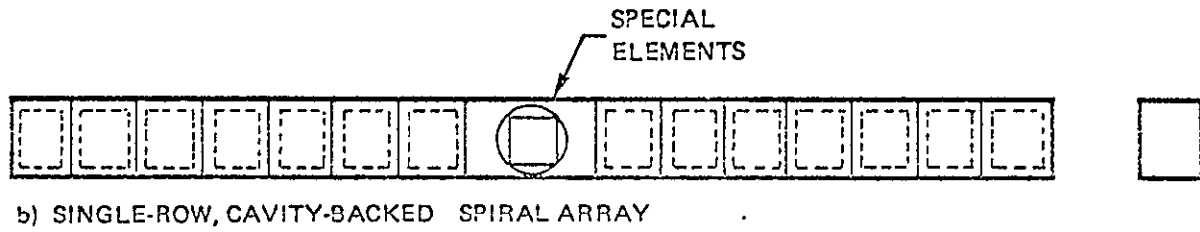
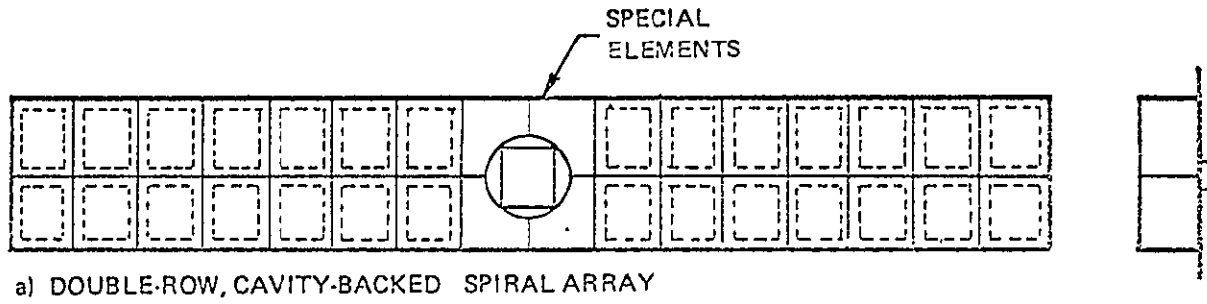


Figure 7.2-8. S-Band Feed Element Arrangements

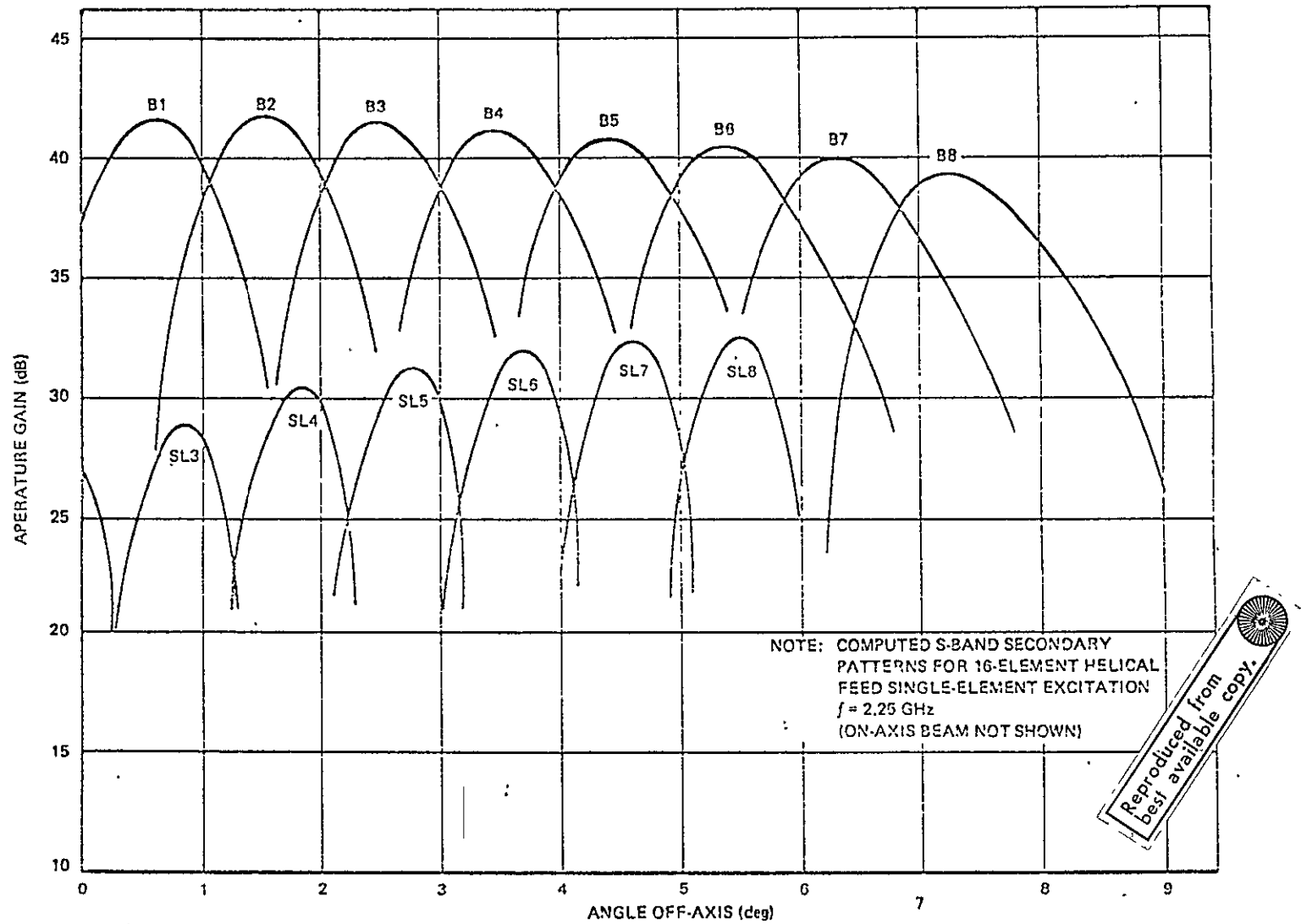


Figure 7.2-9. Calculated Secondary Patterns for Single Helical Element Excitation

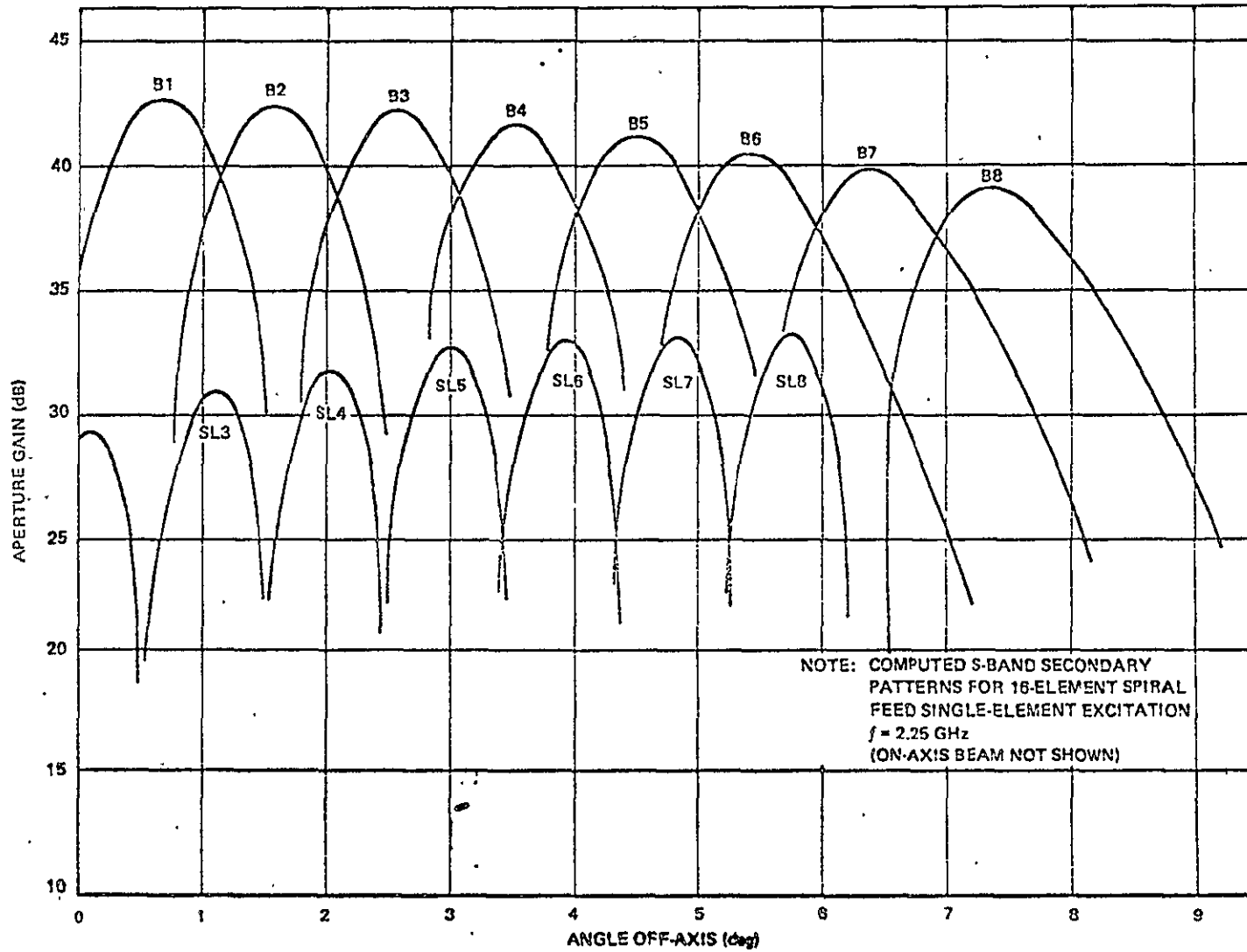


Figure 7.2-10. Calculated Secondary Patterns for Single Spiral Element Excitation

Another noteworthy consideration is the scanning performance provided by axially displacing the offset feed elements behind the focal plane. Computations were made to check a potential scanning performance improvement by displacing the feed elements axially so that feed phase center loci form a parabolic curve with a focal length of $f/2$ tangent to the focal plane.* The results indicated that improvement consisted of about 1.0 dB lower sidelobe for the last beam position. Therefore, it was concluded that for several beamwidths of scan, the improvement was too small to justify additional feed complexity.

Table 7.2-1. S-Band Feed Performance Comparison

$f = 2.25$ GHz

Feed Configuration	Illumination Taper (dB)	Crossover Level Between Beams (dB)*	Illumination x Spillover Efficiency (%)	Gain at Worst Beam Position (dB)**
Double-row, cavity-backed spiral array (four-element excitation)	30	-2.04	58.3	—
Single-row, cavity-backed spiral array (two-element excitation)	30†	-2.04	69.1	—
Single-row, cavity-backed spiral array (single-element excitation)	-9.5	-3.10	73.9	37.3
Single-row helix array (single-element excitation)	-18.5	-2.2	67.0	37.8

* in plane of scan

** crossover between Beams 7 and 8

* J. Ruze, "Lateral-Feed Displacement in a Paraboloid," IEE Trans., Volume AP-13, September 1965, p.661.

Based on the above analysis an S-band feed array, made up of helical elements, was breadboarded on 1/3 scale model set-up. The breadboard results disclosed unsatisfactory antenna performance due to interaction between neighboring feed elements. The interaction narrowed the secondary patterns and degraded the axial ratio.

In view of the measured interaction with helical S-band elements, a decision was made to use flush-mounted elements such as cavity-backed crossed dipoles. These elements provide advantages of less interaction, better control over cross-polarized radiation, and increased mechanical strength and reliability.

Additional analysis and breadboard measurements were made to determine a best compromise between the scanning performance and the feed complexity. The most elaborate scheme consists of single-, double-, single-element excitation, which provides scanning performance with a minimum crossover loss by generating twice as many beams. Multiple-element excitation is considered to be feasible using the diode switch matrix described in the next sub-section, although the switching matrix power consumption, the command network, and other requirements would increase the S-band feed complexity.

The previously discussed considerations formed a basis for selecting a flush-mounted element S-band feed using single-element excitation as a baseline design. The performance degradation, primarily high sidelobe levels, is believed to be offset by the feed simplicity.

The S-band monopulse operation at the receive band and the on-axis beam at the transmit band are obtained by exciting the four innermost feed elements. To obtain favorable sum channel illumination, the four innermost feed element cavities are "chamfered" to allow closer element spacing. The chamfered elements were first breadboarded at full scale to ensure that the impedance was not severely degraded by the reduced cavity size.

7.2.10.2 S-Band Feed Distribution Network

Selection of one of the 32 elements for transmission and reception requires a rather complicated switching matrix imposing significant weight and RF losses. A detail study of alternate switching techniques has been conducted during the Phase B and C study. This effort has included analysis, component development and testing, and the problems of implementing the control of the switches, thereby minimizing weight and losses and maximizing reliability. A summary of basic configurations is shown in Table 7.2-2. (This comparison includes the diplexing elements in addition to the switches).

Table 7.2-2. S-Band Switch Matrix Configuration Summary

Parameter	SP2T		SP4T PIN	SP8T PIN	SP4T-WB PIN
	Ferrite	PIN			
Insertion Loss	1.8 dB	1.5 dB	1.05 dB	1.30 dB	1.7 dB
Weight	48 lb	46 lb	28 lb	26 lb	6.5 lb
Isolation	24-26	30-35	30-35	30-35	30-35
Holding Power	2 W	4 W	3 W	3 W	3 W
Bandwidth	±200 MHz	±80 MHz	±80 MHz	±80 MHz	±250 MHz

As seen from the table, PIN-diodes in the single-pole, two-throw configuration provide negligible advantage over the ferrite switch. However, the single-pole, four-throw and the single-pole, eight-throw switches reduce the insertion loss by as much as 0.8 dB, and the weight by nearly 20 pounds. The slight increase in insertion loss of the single-pole, eight-throw switch over the single-pole, four-throw switch is offset by the decreased weight and integration problem. Therefore, the choice between these two approaches is not clean-cut. The single-pole, four-throw switch has been selected because of its decreased manufacturing problems.

The significant decrease in weight of the wideband switch matrix is due to the elimination of the circulators. This approach is extremely attractive, but insufficient data is available to date to evaluate this device.

The resultant proposed distribution network shown in Figure 7.2-11 utilizes separate transmit and receive matrices, making use of a single-pole, four-throw switch specially developed for this application. The switch provides a significant weight reduction while decreasing RF losses.

Selection of the monopulse system on receive and an on-axis transmit beam requires the use of a single-pole, three-throw switch which selects either the horizontal array, the vertical array, or the on-axis beam. Single-pole, single-throw switches are used with the center four elements to connect them to the monopulse comparator and to the power divider. The command that turns on the eight SPST switches also removes the ON-bias from the rest of the switches so they are all open.

The PIN-diode SP4T switch is shown in Figure 7.2-12. Extensive development effort was first expended on a single-pole, two-throw switch to produce minimum loss at the S-band frequencies. The SP4T switch is based on the results obtained from SP2T switch.

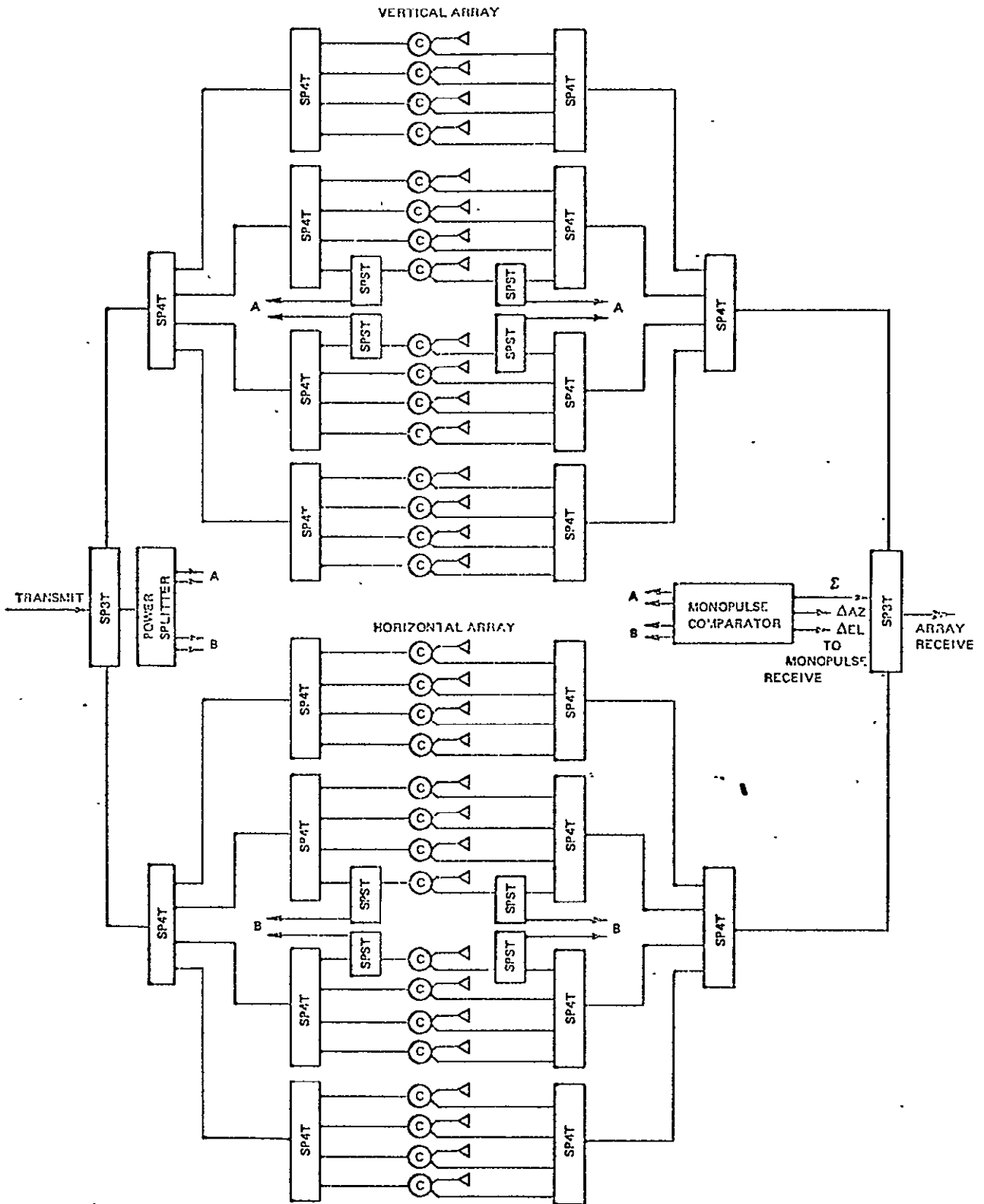


Figure 7.2-11. Recommended S-Band Feed Distribution Network Using SP4T Pin-Diode Switches

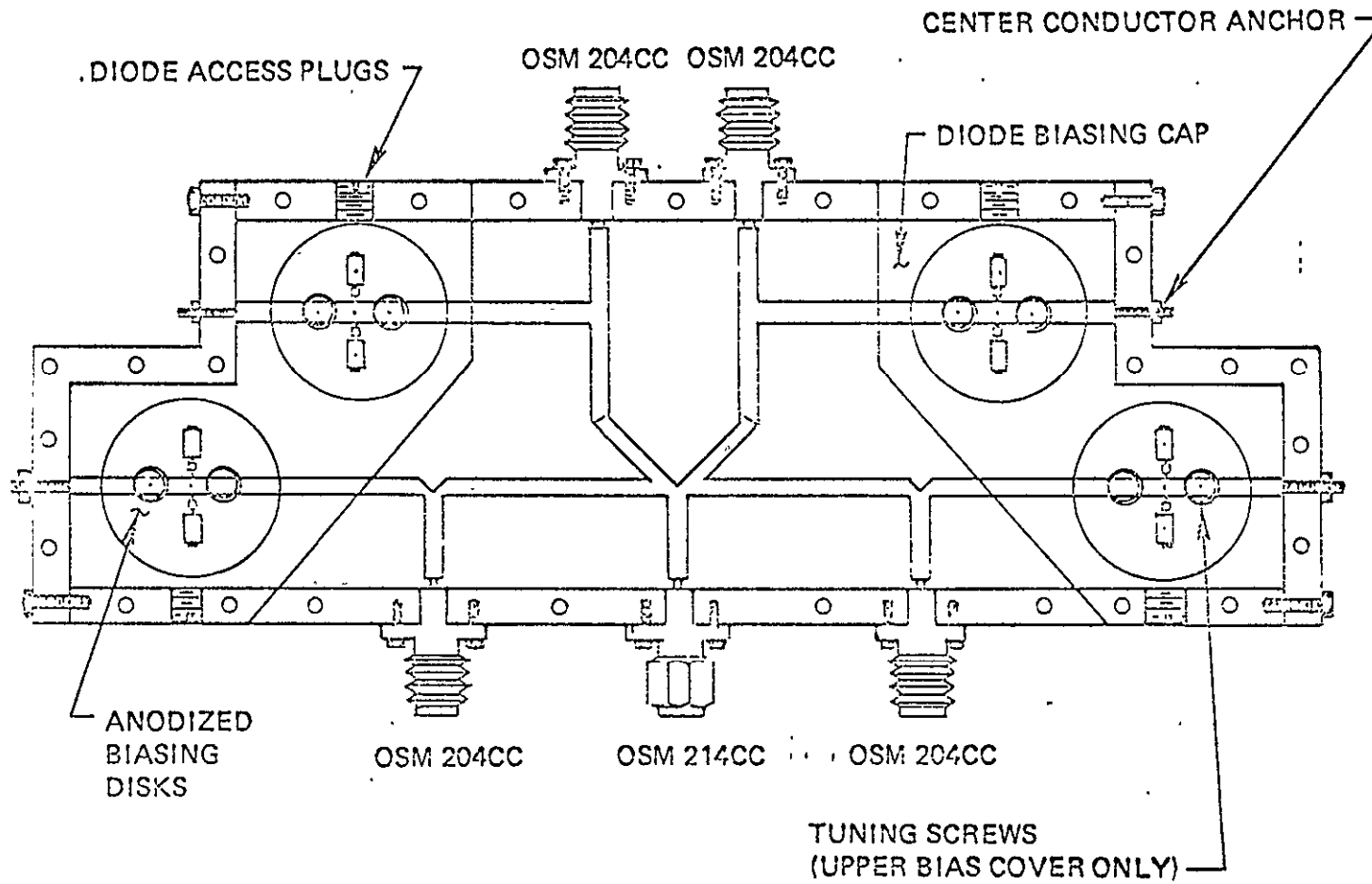


Figure 7.2-12. S-Band SP4T Pin-Diode Switch

The RF schematic of the developed switch is shown in Figure 7.2-13. As in the single-pole, two-throw switch, the diodes are located $1/4\lambda$ from the junction. If the diodes are forward biased, the low impedance is reflected as an open circuit at the junction, and the port is properly terminated. If the diode is reverse biased, it appears as an open and is reflected back to the junction as a low impedance with a high VSWR. If two sets of diodes are forward biased, the power is divided between the two ports with some power reflected due to impedance mismatch.

The control of the switching matrix is exercised by ground command. These commands are decoded in the transponder command decoder and sent to the S-band switch matrix as a five-bit parallel command.

For the baseline system, command inputs to the transmit and receive switch matrices are ganged, except for the monopulse mode where transmit power goes from one input to the four center elements, while receive goes from the four center elements to four inputs on the monopulse comparator.

From a dc point of view, the two matrix trees are paralleled, or overlaid, with four PIN diodes at each switch point. Since spreading resistors are already included to operate two diodes in parallel, four (or more) may be driven in parallel by merely increasing the setting of the current regulator.

Figure 7.2-14 is a schematic of the RF switch paths through the two matrix trees to the 32-fixed circulators that feed the antennas. The PIN switches have been numbered in arbitrary order for later reference. Note the four (ganged) single-pole switches (85, 86, 87, 88) which pick up the four inputs for the monopulse comparator. These are ganged with 89, 90, 91, 92 and 93 to pick up the TX on-axis beam. When Tx path 1, 3, 11 is selected, Rx path 43, 75, 83 is on also, and so forth. This is the normal mode of operation. To conserve power, only the PIN diodes in the selected paths are on; all others are biased off.

Any one of the 32 elements is selected by a single five-bit command. The most significant bit controls the first tier (switches 1, 2), the next two bits control the second tier, and the last two bits control the third tier of switches. In the second and third tiers, the one-of-four groups are ganged; for example, 3 and 7 are enabled together. The one that comes on depends on whether 1 or 2 is on. Similarly, 11, 15, 10, 23, 27, 31, 35 and 39 are enabled together. (To simplify these examples, the receive-side switches that are also picked up are not called out). The actual hardware savings achieved are not as great as the ganging might imply because the relays have only two sets of contacts, and the relay drivers can only drive two relays each.

When monopulse operation is desired, a separate command is sent that causes the power splitter and the monopulse comparator to be connected to the central antenna elements. This command also disconnects the ON-bias (-5V) from the TX and RX trees so that all of those switches are open.

Figure 7.2-15 is a schematic of the antenna feed network from the control point of view. The diagram illustrated is for command 00111 to select the eighth feed element. If the mode of operation is non-monopulse, only six PIN switches are on. In the monopulse mode, nine PIN switches are on. At 100 mA per PIN and bias voltage of -5 volts the power dissipated in the non-monopulse mode is about 3.0 W. In the monopulse mode the dissipated power is about 4.5 W.

SCHEMATIC DIAGRAM OF S-BAND SP4T PIN-DIODE SWITCH
 (PORTS A, B, C, & D RF OUTPUT PORTS; V_s = DC STEERING BIAS)

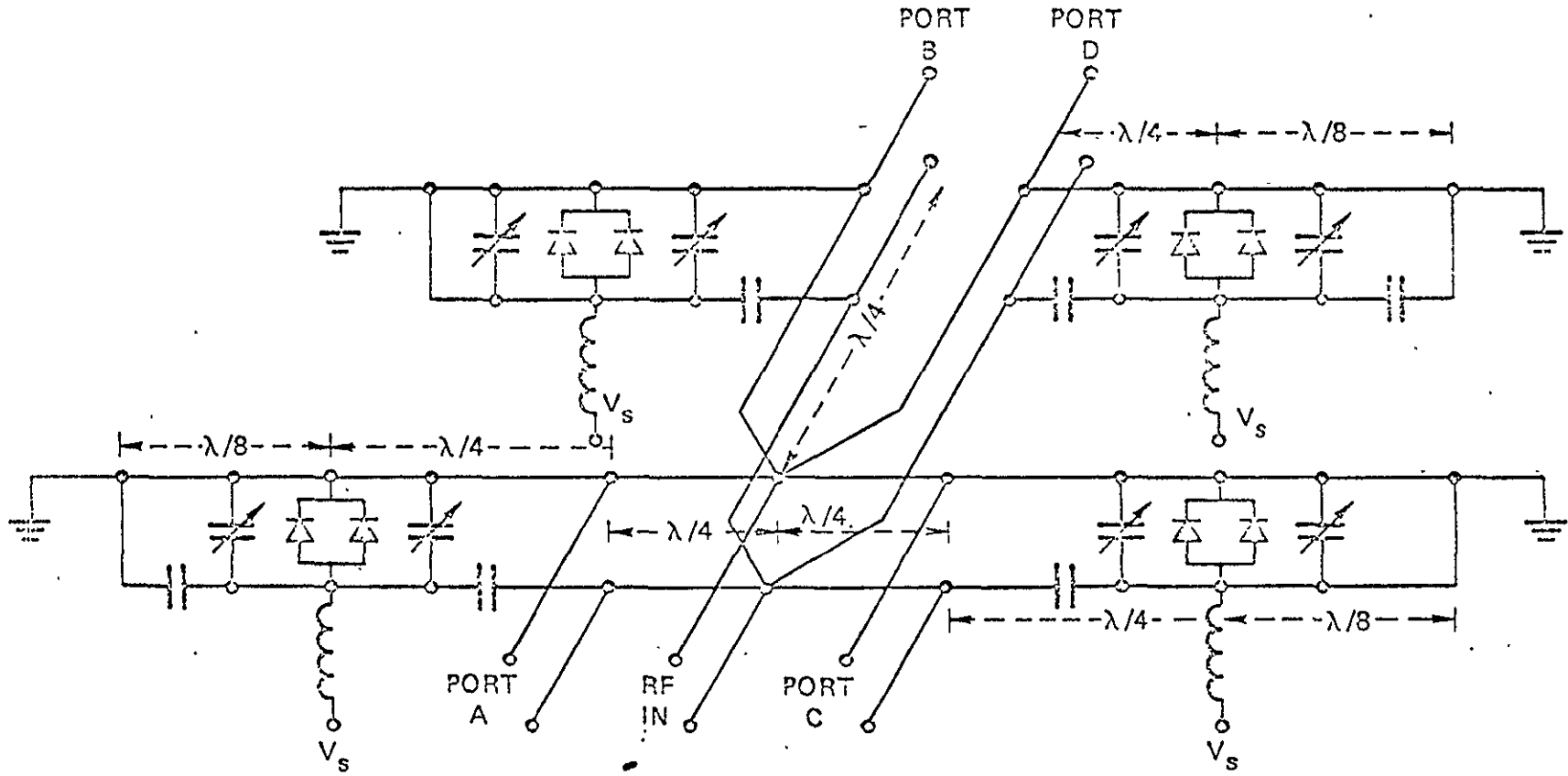


Figure 7.2-13. Schematic Diagram of S-Band SP4T PIN-Diode Switch

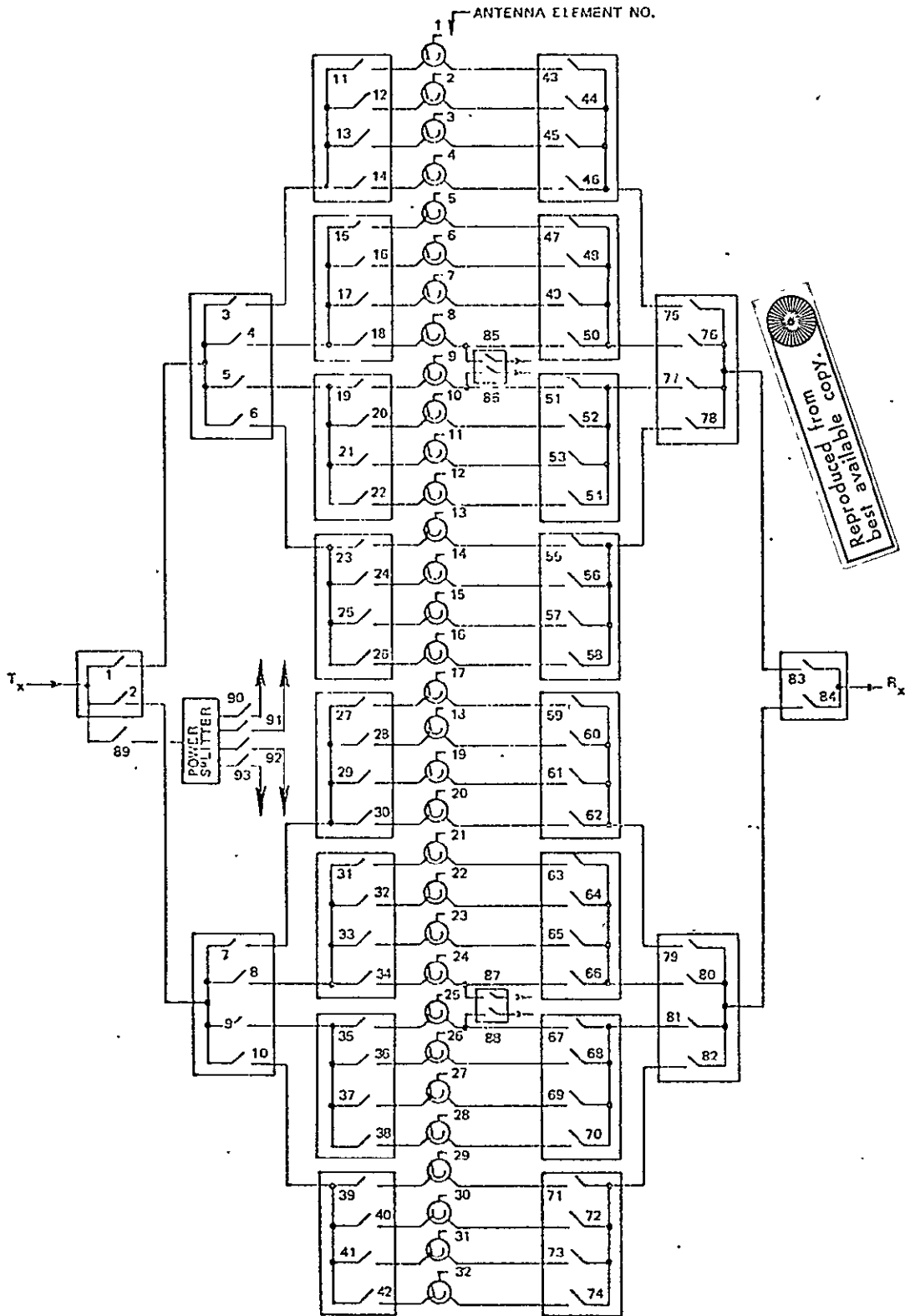


Figure 7.2-14. S-Band Antenna Feed Network RF Path Configuration

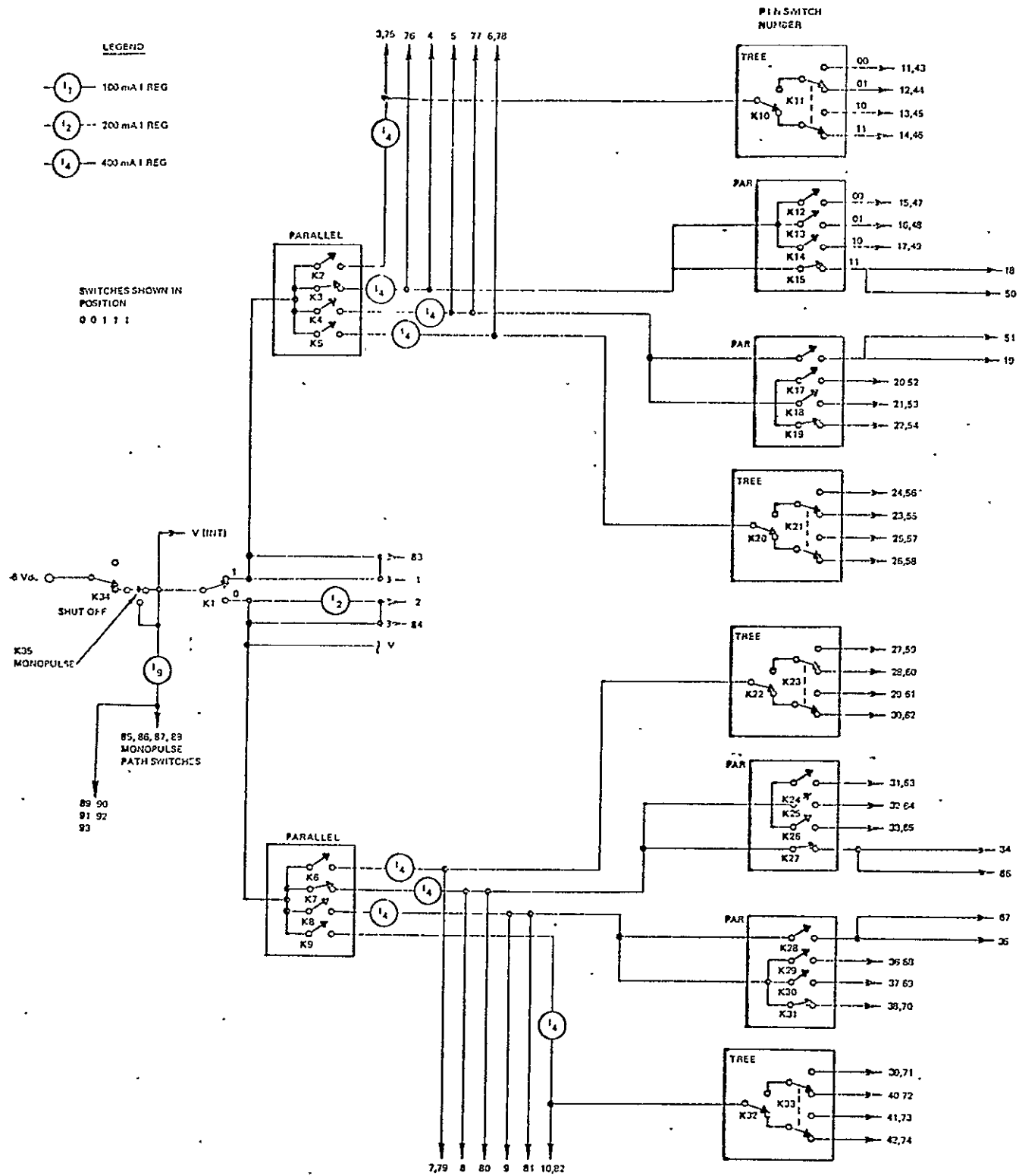


Figure 7.2-15. S-Band Antenna Feed Network, Control Side

The PIN diodes are necessarily grounded to the chassis. Isolation for dc is feasible, of course, but the control scheme proposed offers isolated relay contacts for telemetry, and the bias supplies involved are dedicated.

A shutdown relay is included in the bias supply line to reduce standby power when the S-band array is not in use, and to remove the load from the line in the event of a catastrophic failure. Control for this relay is simply another two-state (on/off) command from the TCD.

The total network contains 88 PIN switches (176 diodes), 35 relays, 34 relay drivers, 11 current regulators and 7 IC flatpacks.

7.2.11 L-BAND FEED

The L-Band Feed consists of an array of radiating elements which are used to form the fan beam, a separate element used to form a higher gain pencil beam, and an RF switch for selecting one or the other. These items are discussed in the following paragraphs.

To generate an elliptical beam having a half-power beam width of $7.5^\circ \times 1.5^\circ$, the reflector must be illuminated by a feed producing a wide primary pattern in one plane and a narrow pattern in the orthogonal plane. In one plane the entire reflector is thus illuminated with a constant phase energy, while in the orthogonal plane only a portion of the reflector is illuminated with the same phase.

Two design approaches were considered appropriate for the L-band feed. These were sharing a number of adjacent S-band radiators, or providing a separate line array feed. The S-band feed, using broadband radiators, is capable of operation at L-band; however, a major disadvantage of this approach stems from diplexing requirements. Since the common array would be required to perform separate functions, each radiating element would have to be diplexed separately. The diplexers would, therefore, offset a potential weight saving realized by sharing the S-band elements. This consideration favors a separate feed array. The presence of the vertical S-band array causes the separate L-band feed array to be split. As an alternate one element must be shared by both arrays. Analysis indicated that a split array could provide desirable reflector illumination if the array elements were fed with varied amplitudes. However, the breadboard results disclosed that amplitude tapering did not provide sufficient control.

The proposed L-band feed design approach utilizes a separate continuous 7-element L-band feed array offset from the feed center. The offset feed placement results in a secondary beam squint of approximately 3° in one plane. This beam offset will result in less spacecraft tilting than would be required with an on-axis L-band beam.

Flush-mounted cavity-backed crossed dipoles have been selected as feed elements. The configuration is expected to cause minimum interaction with other feed elements. The center element is shared by both the L-band and the S-band frequencies using a diplexing arrangement shown in Figure 7.2-16.

The generation of symmetrical (pencil) beam will be accomplished by exciting a separate L-band element. Use of a separate element, rather than selection of element(s) from the fan beam array, is justified by switching network simplification. If one or more elements were to be selected from the fan beam array, two switches would be needed, thus doubling the losses.

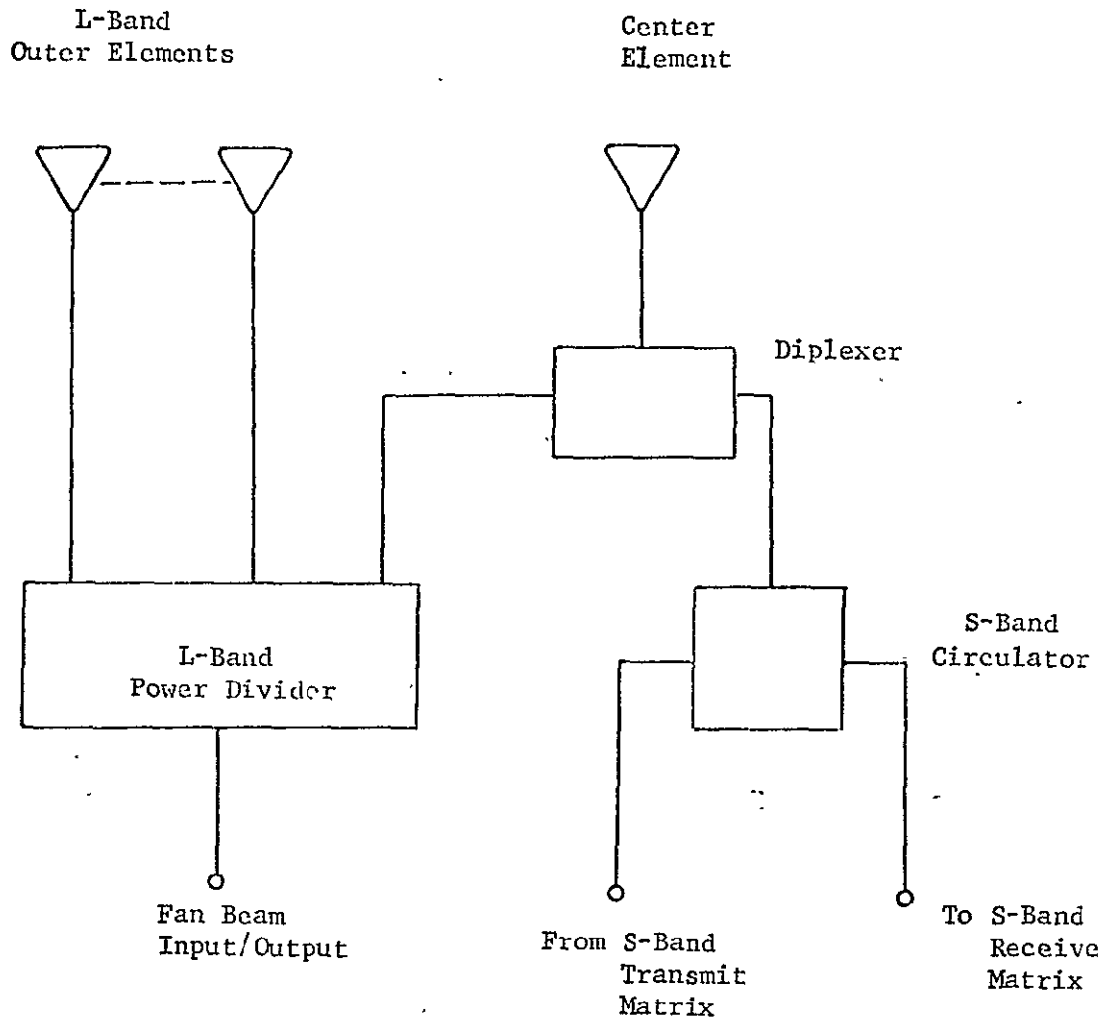


Figure 7.2-16. Feed Network for Common L and S Band Radiating Element

The proposed switch arrangement, shown in Figure 7.2-17, consists of a four-port, double-junction ferrite switch performing both the beam selection and the diplexing functions. The switch will use off-the-shelf types of circulator switches, which will provide about 20 dB of isolation between transmit and receive channels.

7.2.12 UHF FEED

Two UHF feed concepts for providing a circularly-polarized on-axis beam were analyzed. The first concept consists of four monopoles positioned between the S-band arrays as shown in Figure 7.2-18. The monopoles are fed in phase progression, forming a turnstile antenna. A scale model of this feed was built and primary patterns were measured. The patterns indicated approximately -12 dB amplitude edge taper, and the measured axial ratio was less than 1 dB.

Secondary breadboard measurements indicated that this feed approach produced an asymmetric pattern. The asymmetry was found to be caused by the L-band array acting as a ground plane and hence modifying the low-directivity UHF primary pattern.

The proposed UHF feed is made up of four separate, cavity-backed, crossed dipole elements. The normal 0.5λ cavity size results in too large a spacing between the elements because of S-band cross array. The large element spacing (in excess of 0.7λ) generates too directive primary pattern illuminating a portion of reflector with out-of-phase energy producing a broad secondary beam at the expense of overall antenna efficiency.

To overcome this problem, the UHF cavities have been reduced to 0.4λ in size. This cavity size, which has been verified with breadboard tests, reduces the element-to-element spacing to approximately 0.6λ resulting in more favorable reflector illumination. Breadboard tests have indicated that a 3 degree secondary beam and sufficient gain is achieved with this feed arrangement.

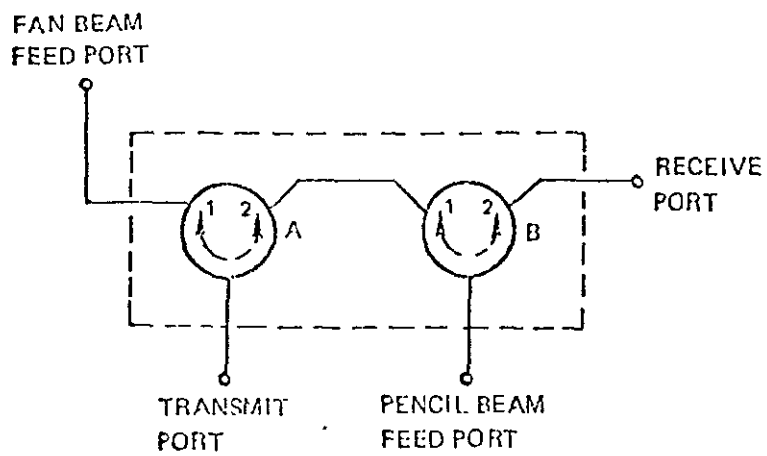
The four elements are fed through a power divider. This device will be built in stripline resulting in a more compact and lightweight package.

7.2.13 VHF FEED

The VHF feed design is based on the following considerations:

- a. Selection of elements with small dimensions or having configurations which minimize interaction with the other feeds.
- b. Choice between a single on-axis beam and a feed with monopulse capability.

The monopulse capability is highly desirable, since the previously planned 450 MHz monopulse feed has been deleted to accommodate the on-axis 850 MHz feed. The low frequency ($\lambda = 87$ in) operation of this feed, causes its dimensions to be large. Elements employing cavities, such as slots or spirals, would require substantial depth, leading to interference with the existing equipment located inside the EVM. Elements protruding above the EVM cause added blockage and interference with the radiation characteristics of the other feeds. Consequently, it is desirable that the radiating elements be small so that a minimum scattering cross-section is presented to the other feeds.



a) RF SCHEMATIC

L-BAND MODE		SWITCH FUNCTION POSITIONS	
TRANSMIT	RECEIVE	JUNCTION A	JUNCTION B
FAN BEAM	FAN BEAM	1	1
PENCIL BEAM	PENCIL BEAM	2	2

b) SWITCHING POSITION

Figure 7.2-17. L-Band Feed Switch Network

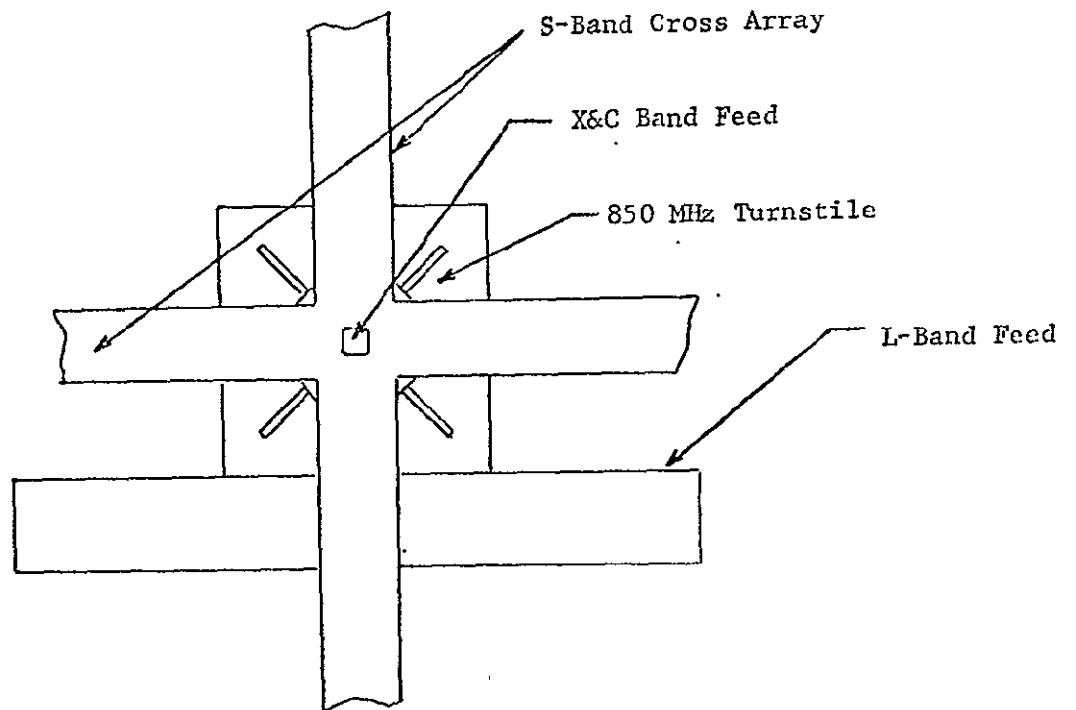


Figure 7.2-18. On-Axis Turnstile 850 MHz Feed

The proposed VHF tracking feed is shown schematically in Figure 2.6-1. The radiating elements are sleeved monopoles bent outward from the S-band array in order to minimize interaction with other elements. This configuration is based on scale model study which considered illumination characteristics, impedance and interaction with other feed elements.

As seen from Figure 7.2-19, the four loop (stub) pairs are combined through their individual baluns forming four dipoles in a diamond configuration. For generating the sum channel pattern, the elements are combined to produce circular polarization. The two error channel patterns, whose tracking axes are coincident with the X- and S-band tracking feed axes, are orthogonally, linearly polarized, indicating that only circularly polarized signals can be tracked at VHF with this feed. The tracking pattern polarization is not expected to cause a problem, since all known VHF ground antennas are circularly polarized.

7.2.14 X-BAND EARTH-VIEWING HORN

The X-band earth-viewing horn must cover a frequency range of 7.35 to 8.25 GHz providing a maximum gain over 20° field of view. Two earth-viewing horn designs have been considered for meeting the stated requirements.

The first design considered a lens-corrected conical (TE_{11} mode) horn. A major advantage offered by this design is compactness. Since the lens is used to correct the phase error across the horn aperture, the structure results in length-to-width ratio of only 1.3:1. Computed gain, as a function of its aperture size, is shown in Figure 7.2-20. The figure indicates a horn of approximately 5.5 inch diameter would provide an optimum gain over 20° FOV.

The lens-corrected conical horn has been built and flight qualified by Philco-Ford for the IDCSP/A Communications Satellite. It consists of a 5.5-in diameter conical feed horn and a 45° flat reflector for directing the beam normal to the spacecraft spin axis. The artificial dielectric lens is fabricated as a foam supported three-dimensional, metallic obstacle array. The entire antenna weighs 0.75 lb. This design approach offers an attractive choice from the standpoint of size, weight and performance. The disadvantage of this design stems from its relatively high cost due to the sophisticated design and the fabrication methods.

The second design approach consists of pyramidal horn with optimum dimensions. The term optimum refers to a horn with aperture dimensions that have been chosen to provide a maximum gain for a given axial length. The electrical design and calibration of the pyramidal horn is rather straightforward¹, although the mechanical design requires effort to satisfy weight, thermal, structural, and other requirements.

The computed performance for the two designs (including the X-band subsystem losses for medium gain mode) is summarized in Table 7.2-3. As seen from the table, the lens-corrected conical horn offers a significant performance advantage.

¹William T. Slayton "Design and Calibration of Microwave Antenna Gain Standards," NRL Report 4433, Washington D. C., 1954

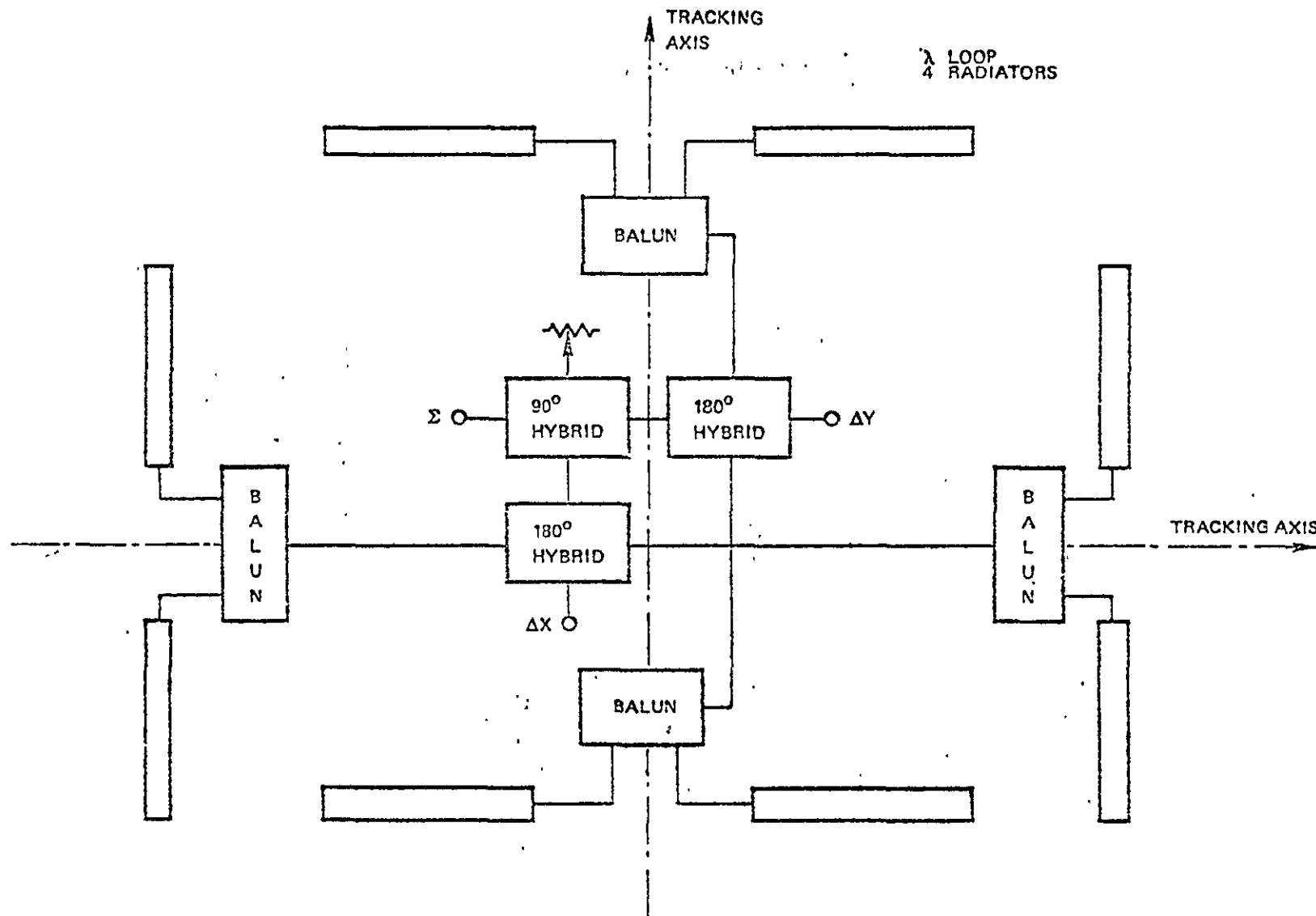


Figure 7.2-19. VHF Tracking Feed

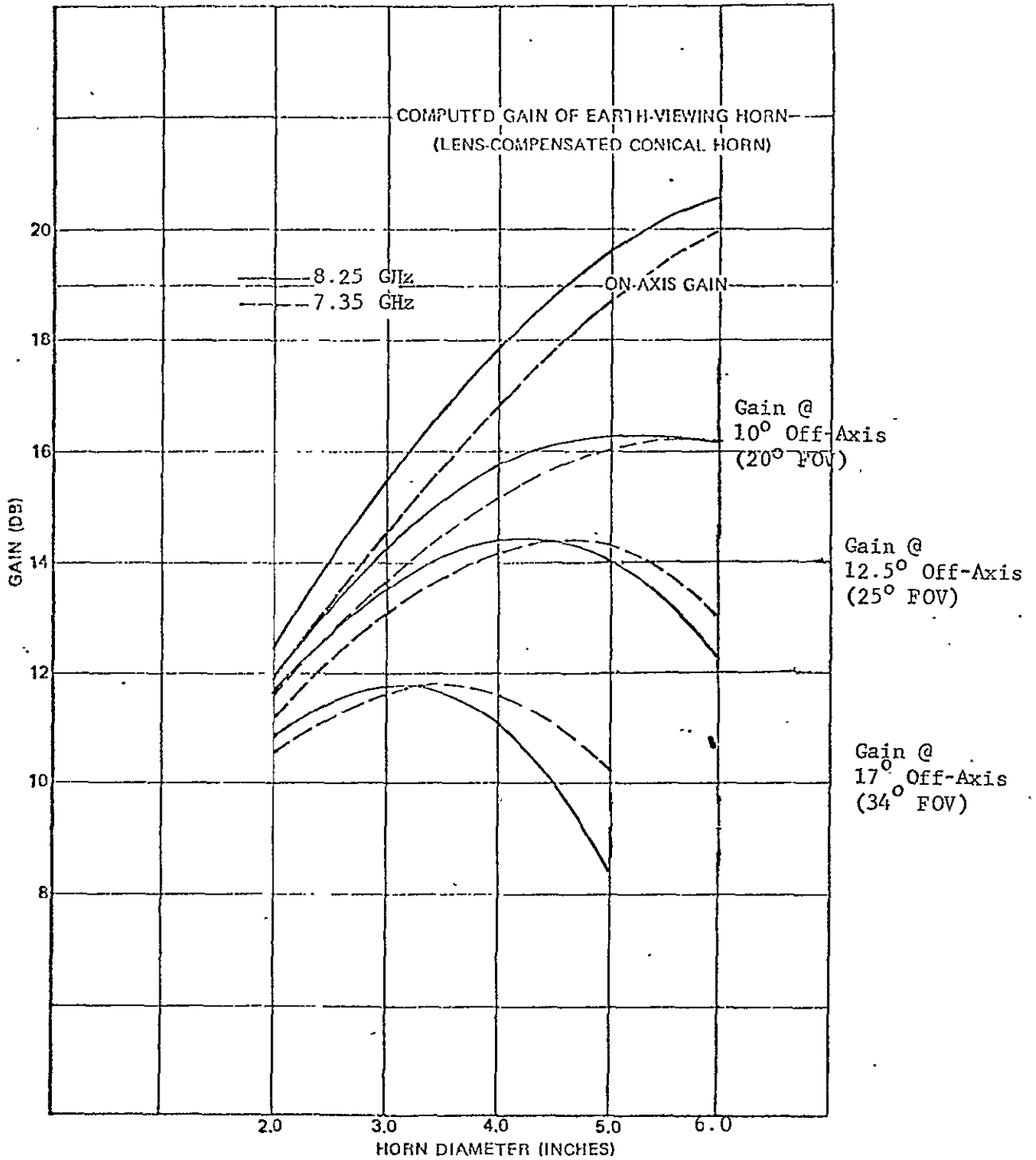


Figure 7.2-20. Lens-Compensated Horn Gain

Table 7.2-3. Estimated X-Band Horn Performance Parameters

PARAMETER	TRANSMIT BAND		RECEIVE BAND	
	Pyramidal Horn	Lens-Corrected Conical Horn	Pyramidal Horn	Lens-Corrected Conical Horn
On-axis Aperture Gain (dB)	16.5	19.5	17.5	20.3
Aperture Gain over 20° FOV (dB)	14.0	16.1	14.5	16.3
Network Losses (dB):				
Horn	0.05	0.15	0.05	0.15
Switch	0.3	0.3	0.8	0.8
Waveguide	0.15	0.15	0.15	0.15
Total Loss (dB)	0.5	0.6	1.0	1.1
On-Axis Gain at input terminals (dB)	16.0	18.9	16.5	19.2
Gain over 20° FOV at input terminals (dB)	13.5	15.5	13.5	15.2

Since the pyramidal horn gains are consistent with the communication sub-system requirements and because of simplicity, the pyramidal horn is the present choice for the X-band earth-viewing antenna. The estimated pyramidal horn aperture dimension is 4.25 in. x 5.25 in. and an axial length of 8 in.

7.2.15 EXPECTED PERFORMANCE SUMMARY

The composite feed design, discussed in previous sub-sections, has been verified by analysis and by 1/3 scale model breadboard measurements. The analysis employed Philco-Ford computer program SECPAT-6710, which is designed to calculate secondary patterns and related efficiencies of a circular aperture. Theoretical primary patterns or patterns obtained from similar feed designs were used during the analysis phase. The feed losses were estimated using data obtained on switches, cables and components, as summarized in Table 7.2-4.

The 1/3 scale model breadboard effort included both the primary and the secondary measurements. Patterns, gain, axial ratios and other parameters were recorded. The breadboard effort enabled an accurate prediction of expected antenna performance by simulating radiation characteristics that include EVM and the support-truss blockage and scattering. In most cases, good agreement was obtained between the computed and the measured results.

Based on the computed and the measured results, the required and the expected RF characteristics for the ATS F&G 30-foot parabolic antenna are summarized in Table 7.2-5. As seen from the table, the RF requirements are satisfied for all frequency bands.

Table 7.2-4. Itemized Composite Feed Component Losses (dB)

Component	VHF 150 MHz	UHF 850 MHz	L-Band 1.6 GHz		S-Band			C-Band 6.1 GHz	X-Band	
			Fan Beam	Pencil Beam	Scanning Beams		Monopulse 2.25 GHz (1)		7.3 GHz	8.1 GHz
					1.8 GHz	2.25 GHz				
Radiating Element	0.15	0.1	0.1	0.1	0.15	0.15	0.15	0.15	0.15	0.15
Comparator	0.4	-	-	-	-	-	0.4	-	0.15	0.15
Power Combiner	-	0.3	0.3	-	-	-	-	-	-	-
Switch	-	-	0.5	0.5	0.7	0.7	0.25	-	0.8	0.8
Diplexer (Circulator)	-	-	-	-	0.3	0.35	0.35	-	-	-
Cable or Waveguide	0.25	0.1	0.1	0.1	0.75	0.5	0.25	0.45	0.1	0.1
Polarization Network	-	-	-	-	-	-	-	0.6	-	-
Total Dissipative Losses	0.8	0.5	1.0	0.7	1.90	1.7	1.4	1.2	1.2	1.2
Mismatch Loss	0.5	0.2	0.3	0.3	0.5	0.5	0.5	0.2	0.2	0.2
Total Feed Loss	1.3	0.7	1.3	1.0	2.4	2.2	1.9	1.4	1.4	1.4

(1) The on-axis transmit (1.8 GHz) mode losses are same as the receive mode losses

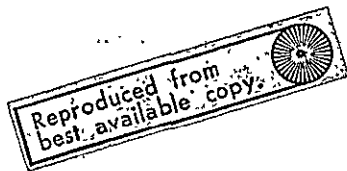


Table 7.2-5. Predicted Vs. Required RF Characteristics
For
ATS F&G 30-Ft Parabolic Antenna

Experiment	Function	Frequency (MHz)	Antenna FOV (Degrees)	Required ERP (dBw) or G/T (dB/°K)		Predicted ⁽¹⁾ Antenna Gain (dB)		RF Power (dBW) or Receive System Temp. (°K)	Predicted ERP (dBW) or G/T (dB/°K)	
				Peak of Beam	FOV	Peak of Beam	FOV		Peak of Beam	FOV
ITV	XMT	850	3.0 ⁽²⁾	51	48	33.0	30.0	18.6	51.6	48.6
DRSS	XMT	1800	13.2	50.5	48	39.5 ⁽³⁾	36.4	12.8	52.3	49.2
	RCV	2250	13.2	+9.5	+7	40.4 ⁽⁴⁾	36.6	746	+11.7	+7.9
PLACE (Fan Beam)	XMT	1550	7.5x1.0	-	42	33.4	29.7	15.6	49.0	45.3
	RCV	1650	7.5x1.0	-2	-	33.4	29.7	1045	+3.2	-0.5
PLACE (Pencil Beam)	XMT	1550	1.1 ⁽²⁾	51	-	39.0	36.0	15.6	54.6	51.6
	RCV	1650	1.1 ⁽²⁾	+5.5	-	39.0	36.0	1045	+8.8	+5.8
Monopulse	XMT	7350 7575 7650	0.3 ⁽²⁾	60	-	50.5 ⁽⁵⁾	47.5	12.5	63.0	60.0
	RCV	8025 8150 8250	0.26 ⁽²⁾	+16	-	50.9 ⁽⁵⁾	47.9	1496	+19.1	+16.1
	RCV	6300	0.4 ⁽²⁾	-	-	49.3 ⁽⁵⁾	46.3	-	-	-
RFI	XMT	136	-	-	-	15.0	12.0	-	-	-
VHF	RCV	150	16.0 ⁽²⁾	-	-	16.5	13.5	4590	-20.1	-23.1

(1) Gain at antenna subsystem input terminals (includes feed losses listed in Table 5.9-1)

(2) Half Power Beam width

(3) On-axis transmit beam

(4) On-axis sum channel beam

(5) Gain estimate includes degradation due to flight reflector surface inaccuracy
(1.1 dB at 8.0 GHz, 1.0 dB at 7.3 GHz and 0.7 dB at 6.3 GHz)

7.3 MECHANICAL DESIGN/INTEGRATION

This section discusses the mechanical design aspects of the Prime Focus Feed Subsystem, including layout, component design and size, weight, and thermal requirements.

7.3.1 LAYOUT

The physical arrangement of the overall Prime Focus Feed Subsystem is shown in Figure 1-1. The EVM is designed so that a modularized system can be used, simplifying mechanical and electrical integration problems. The EVM consists of three boxes, with the upper box housing the transponder and antenna feeds. These units will be assembled into the flight version of this box and will be tested as a single unit. The top cover is removable and allows parallel integration of the transponder and feeds as shown in Figure 7.3-1.

The detailed antenna feed assembly layout is shown in Figures 7.3-2, 7.3-3 and 7.3-4. To maintain the maximum structural integrity of the feed assembly, the cavity elements are mounted directly to a honeycomb EVM cover. This design avoids the need for large holes or slots cut through the cover. Only small individual clearance holes are required for passing each interconnecting line.

The physical layout or interrelationship among the various feed elements was determined by the electrical results obtained from testing a 1/3-scale model composite feed; however, the design will satisfy the structural environmental and the weight requirements.

The composite feed bears a fixed relationship to the prime (z) axis of the EVM. An adjustment capability is provided at the junction of the truss and parabolic reflector hub to properly relate the feeds and the reflector. To properly locate the feed phase center at the focal plane of the reflector, axial adjustment will be provided at the junction of each truss leg and the reflector hub. Up to ± 0.75 inch of adjustment will be provided by shims at each mounting point to accurately align the focal plane and focal axis of the reflector with respect to the feeds. The RF beam collimation will be accomplished by shimming one or more truss legs, thereby laterally shifting the feed phase center with respect to reflector axis.

7.3.2 COMPONENT DESIGN

The composite feed component mechanical design is influenced by optimum electrical performance, environmental conditions, minimum weight, low cost fabrication and high reliability. Considering the factors listed above, the mechanical design and the fabrication methods of major composite feed components are described in following paragraphs:

- a. Radiating Elements The combined X- and C-band feed is a thin metal wall square horn whose 2-in. square aperture is located flush with all other cavities. At X-band frequencies the horn is excited from a comparator network consisting of waveguide hybrids. At C-band, the horn is excited through two shunt coupling slots located on the opposing walls. Outside the coupling slots, waveguide-to-coaxial transitions are used to transform the line into coax and to connect the two lines to a polarization control unit.

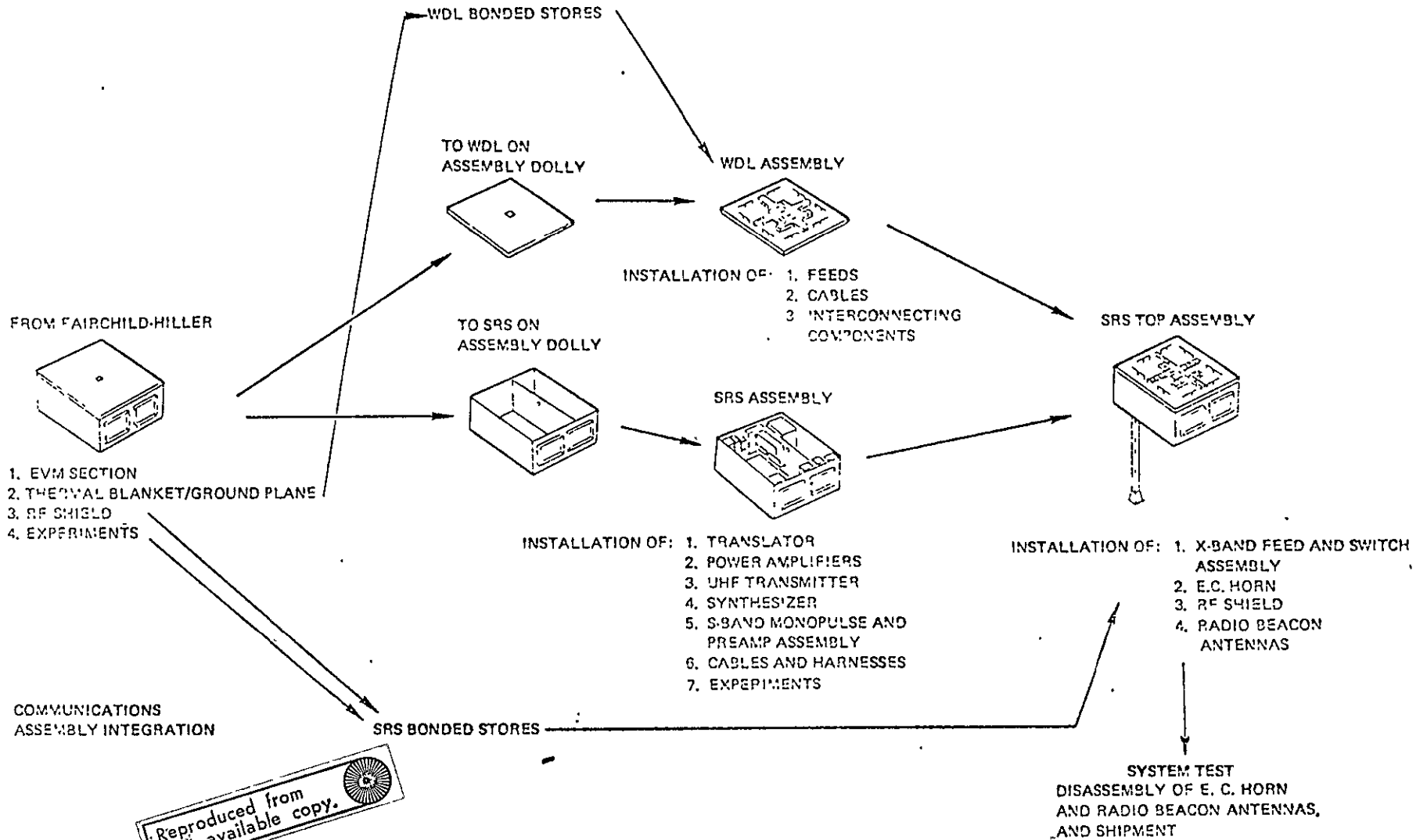


Figure 7.3-1. Transponder and Feed Integration

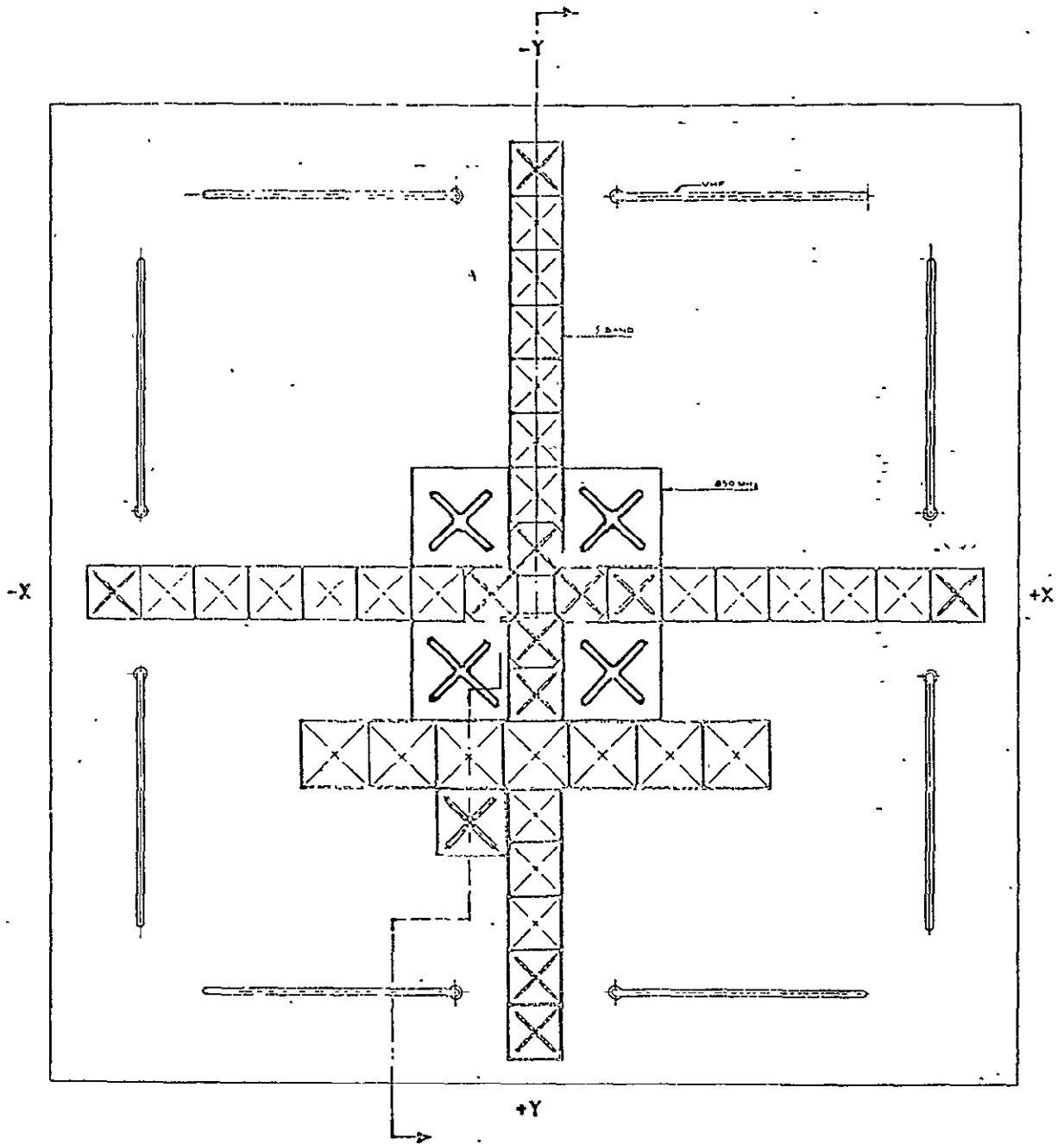
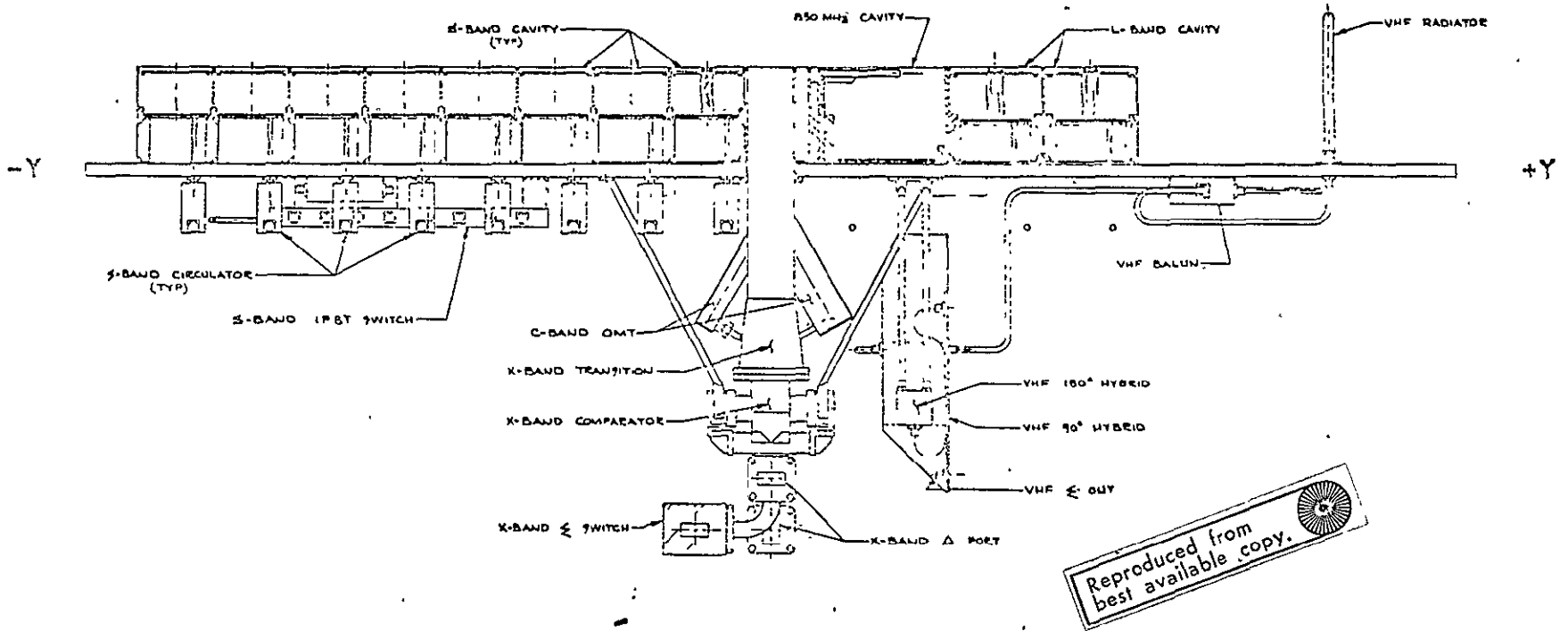


Figure 7.3-2. Composite Feed Assembly (Plan View)



Reproduced from
best available copy.

Figure 7.3-3. Composite Feed Assembly (Side View)

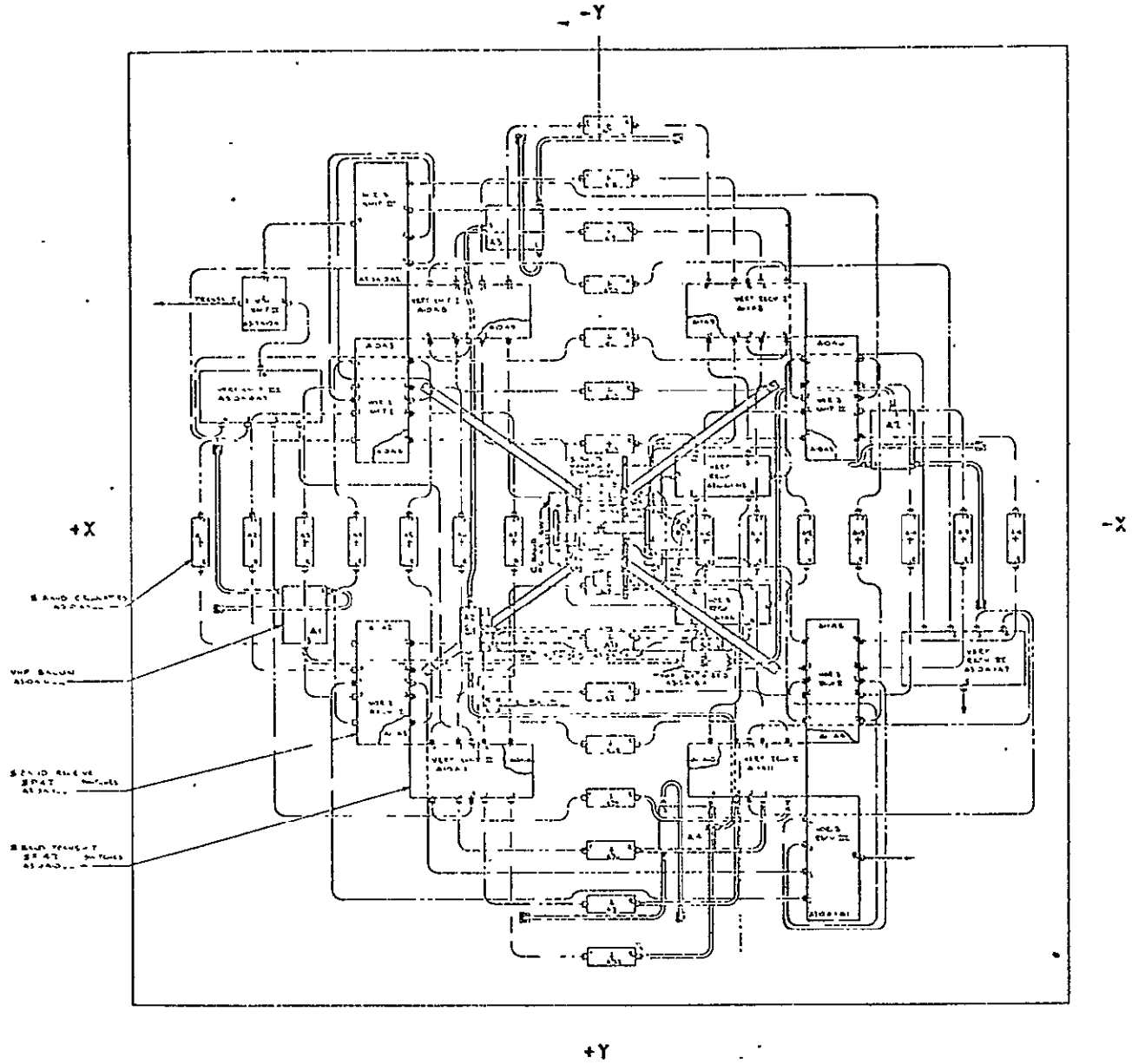


Figure 7.3-4. Composite Feed Assembly (Bottom View)

Reproduced from
best available copy.

a. Radiating Elements (Continued)

The S-band cross-array is made up of 31 cavity-backed crossed-dipole elements. Each cavity will be 3.0 x 3.0 x 1.5 in. deep. The total length of the array is 50 in. The crossed-dipole elements will be fabricated using printed circuit techniques. This method ensures identical electrical performance of each element, low-cost fabrication, lightweight construction, and adherence to the spacecraft environmental requirements.

The S-band elements will be mounted into their aluminum alloy cavities and will be supported on an inside lip or ridge. The coaxial balun and the stripline polarization hybrid will also mount to the EVM side of the cavity array.

The design, fabrication, and assembly techniques of each L-band element is identical to the S-band elements except for size. Each L-band cavity is 3.75 in. x 3.75 in. x 1.85 in. A detailed crossed-dipole subassembly is shown in Figure 7.3-5.

The UHF cavities are 5.5 in. x 5.5 in. x 3.5 in., clustered around the center of the S-band arrays. A crossed-dipole radiator is mounted in each cavity. The power combining network for the UHF feed is made of stripline (tri-plate) and mounted beneath the elements.

The VHF elements, shown in Figure 7.3-6 are quarter-wave loops (stubs) making up 4 dipoles mounted along the major feed axis. A lightweight metal tube will be used in its fabrication. The elements will be adequately supported with dielectric posts.

- b. Cavity Housing. The aluminum alloy cavity housing is machined using the numerical controlled process. All radii are 0.25 in. maximum so that standard 0.50 in. diameter end mill cutting tool can be used during the machining phase. Inner and outer walls are approximately 0.03 in. thick, reinforced by extra material for structural strength. The total cavity housing weight has been calculated to be about 5.5 lb. The cavity housing will have a surface finish dictated by spacecraft thermal requirements.

In order to locate all cavities in the focal plane, the S-band array will be elevated above the ground plane. The S-band diplexers (ferrite circulators) and the switching matrices will be mounted below the EVM cover (inside of the EVM). This location provides a better thermal control for the solid state components.

- c. Earth Viewing Horn. The X-band earth viewing horn mounts on the opposite end of the EVM as viewed from the composite feed assembly. This horn will be a pyramidal horn fabricated of thin wall aluminum alloy. The radiating aperture dimensions will be 5 1/2 x 4 1/2 in. The surface finish will be in accordance with thermal requirements.

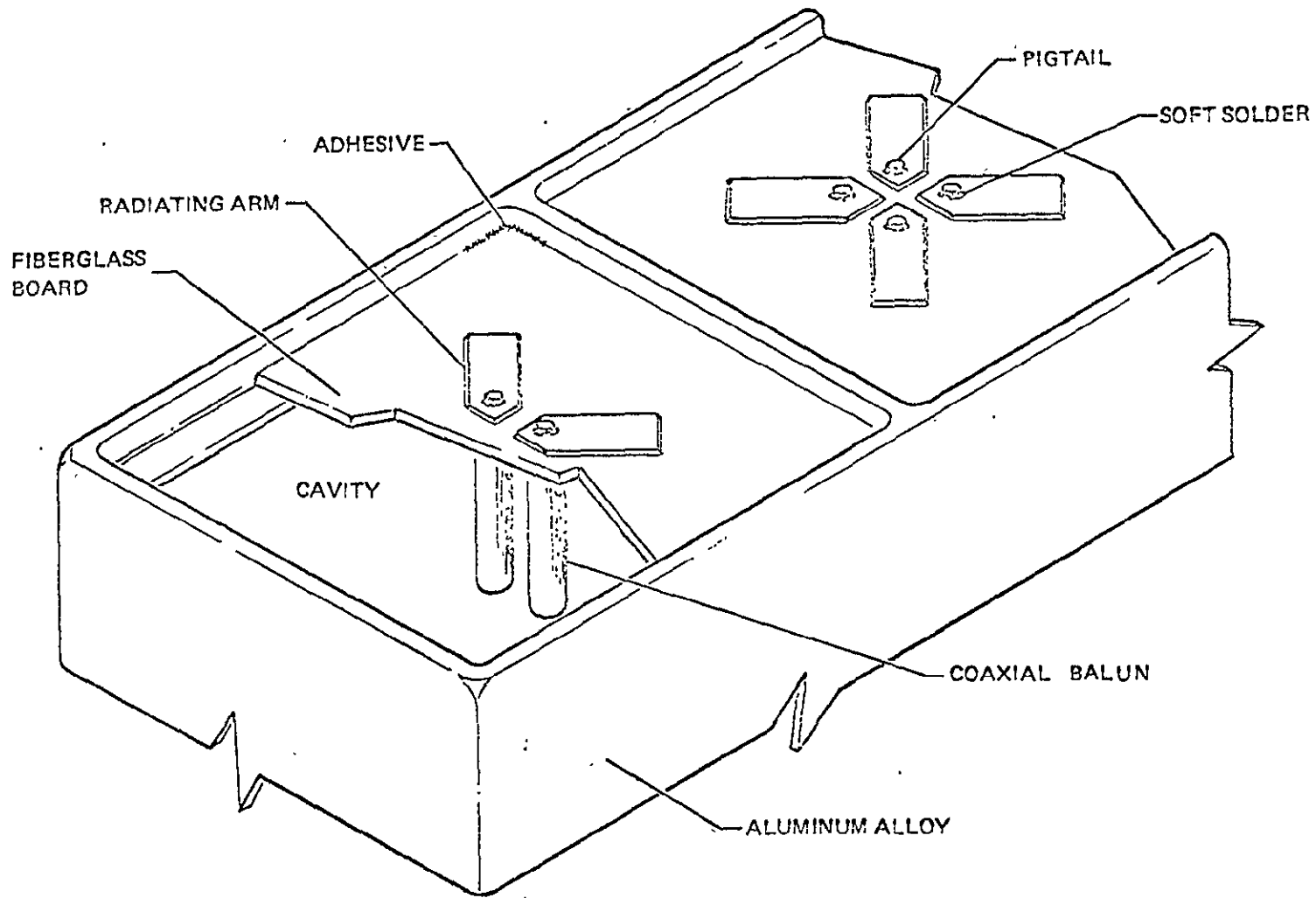


Figure 7-3-5. Crossed-Dipole Design Detail (Typical for S- and L-Band)

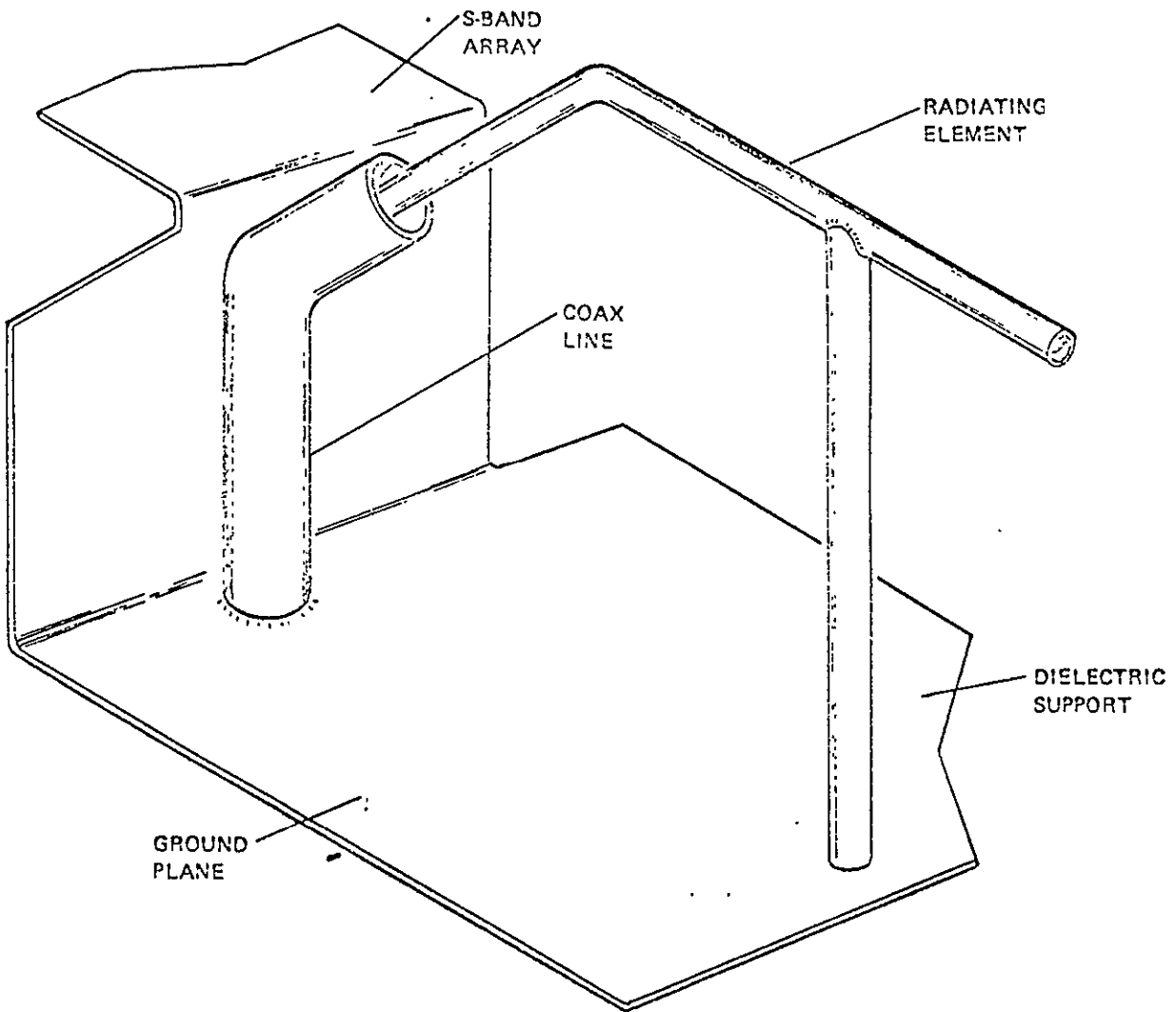


Figure 7.3-6. VHF Element

c. Earth Viewing Horn (Continued)

The earth viewing horn connects with a waveguide run leading through the EVM compartment to the X-band antenna select switch located next to the composite feed. The waveguide run will be disconnected when integrated with the EVM.

- d. Composite Feed Interconnections. The X-band feed and earth viewing horn are interconnected with WR112 waveguide. Waveguide walls and the flanges are machined in specified areas to save weight. Sufficient material will be left to ensure structural strength.

All other interconnections between the radiating elements, strip-line networks, polarization control units, and hybrids will utilize semirigid coaxial cable and OSM miniature coaxial connectors. Cable clamps will be used to support the cable to ensure feed integrity during launch and transportation.

7.3.3 WEIGHT ALLOCATION

The estimated Composite Feed weight is given in Table 7.3-1. All major components are itemized showing both the size and the weight. The cable weight estimate is based on lengths obtained from feed layout. Miscellaneous items (fasteners, clamps, etc.) are estimated on the basis of medium density packaging.

Table 7.3-1. Composite Feed Weight Estimate

A Number	Description	Size (in.)	Unit Weight (lb)	Total Weight
<u>Feeds and Switches</u>				
A310A7	S-Band Elements	3.00 x 3.00 x 1.50	0.15	4.65
A310A9	S-Band Fixed Circulators	2.50 x 2.00 x 1.50	0.50	16.00
A310A10	S-Band Xmit PIN Sw. *	7.00 x 3.00 x 1.00	0.50	5.50
A310A11	S-Band Recv. PIN Sw. *	7.00 x 3.00 x 1.00	0.50	5.50
A310A4	L-Band Beam Sel. Sw.	1.50 x 1.50 x 1.25	1.50	1.50
A310A5	L-Band Elements	3.75 x 3.75 x 1.85	0.30	2.40
A310A15	850 MHz Antennas	5.50 x 5.50 x 3.50	0.65	2.60
A310A14	VHF Elements	22.00 x 7.0 R	0.12	0.96
A310A16	VHF Baluns	2.00 x 4.00 x 0.50	0.22	1.28
A310A17	VHF 90° Hybrids	14.00 x 2.00 x 0.50	0.22	0.22
A310A18	VHF 180° Hybrid	2.00 x 4.00 x 0.50	0.85	1.70
A310A2	L-Band Power, Combiner	28.00 x 4.50 x 0.13	3.00	3.00
A370	Earth Coverage Horn	4.50 x 5.50 x 8.00	0.75	0.75
A369	Earth Coverage Horn			
	Waveguide	1.25 x 0.63 x 56.00	1.40	1.40
A310A13	850 MHz Power Combiner	12.00 x 12.00 x 0.13	2.00	2.00
<u>Cables</u>				
(RF and DC Cables and Connectors)				5.29
<u>Mounting Hardware, Feed</u>				
(Screws, Washers, Housing, Cable Clamps, etc.)				6.52
				66.10
*These values are for the SP4T Configuration.				

SECTION VIII

PARABOLIC REFLECTOR

8.1 GENERAL DESCRIPTION

The parabolic reflector subsystem will be designed and built by FHC subcontractor, Lockheed Missiles and Space Company (LMSC), Sunnyvale, California. The reflector will have a diameter of 30 feet, and a focal distance to diameter ratio (f/D) of 0.44. It will be designed to be operated at frequencies from 100 MHz to 10 GHz. The rf characteristics of the reflector will be such that, operating in conjunction with the Composite Feed Subsystem of the spacecraft as an antenna system, the overall antenna gain (on-axis) at a frequency of 8 GHz is a minimum of 50 dB under the worst case orbit position. The gain loss contribution of the reflector itself to the total antenna system losses is expected to be less than 2 dB, under nominal orbit conditions at an operating frequency of 8 GHz. Criteria considered of primary importance in the design of this subsystem will be minimum size and weight, mechanical reliability, and ability to maintain rf gain characteristics with minimum degradation under continued exposure to space environment and potential space environmental variations.

The reflector assembly (shown in Figure 8.1-1) is a skin-stressed, rigid-ring base, flexible radial beam paraboloid. It consists of 48 flexible rib assemblies supporting a copper coated dacron mesh rf reflector surface, and a ring-shaped hub assembly. The hub assembly contains rib mounting, storage and deployment assemblies, and the antenna/spacecraft mounting interface. The reflective fabric is attached to the inner edge of each rib to produce the paraboloidal reflector surface. The ribs are attached to the hub through hinges that permit pivoting the ribs from their normal, radial position by 90 degrees to a tangential position relative to the hub. For stowing the reflector, the ribs are wrapped around the hub, and the fabric is folded in radial lines between the ribs and wrapped on the hub between the rib spirals.

In the stowed configuration, the reflector package will have approximate inside and outside diameters of 58 and 78 inches respectively, and a height of approximately 12 inches. The design weight goal of the reflector assembly is 140 pounds; the maximum is 150 pounds. A series of doors is closed over the outer periphery of this ring shaped container and secured by a circumferential retaining cable. Deployment of the reflector is initiated by a pyrotechnically actuated cable cutter. Upon release of the cable, the springloaded doors open, and the elastic energy stored in the bent ribs will cause the ribs to unwrap from the hub and straighten out to their unstrained condition. Wire coil torsion springs incorporated in the rib hinges ensure that each rib will rotate on its hinge into a radial position, where it will latch

and remain radial with respect to the hub. The cable remains attached to the doors to avoid interference with other components of the spacecraft. The only power required from the spacecraft system is that required to actuate the pyrotechnic device.

The reflector is designed in such a manner that the ribs exert a slight elastic force upon the mesh which maintains the latter in taut condition at all times during orbit. The ribs are thereby preloaded in a cantilever mode, always in the same direction. This preloading enables establishing the rib position with great precision while providing the required clearances in the rib hinges, which would otherwise become a problem in the zero-g environment. The magnitude of the elastic interaction between the ribs and the mesh built into the reflector by design also has a significant effect on the magnitude and nature of deformations of the reflecting surface caused by the varying thermal environments to which the reflector is exposed during orbit. Therefore, this property is used as a design tool to minimize the reflector surface deflections in general, and to restrict the maximum deformations and the resultant minimum antenna performance to those orbit positions where it will have the least significant impact on the overall spacecraft system operation.

Thermal distortions of the reflector surface under varying solar exposures will be minimized through application of passive thermal controls to the various reflector components. This will be accomplished through application of adhesive tape faced with vacuum-deposited aluminum and overcoated with silicon monoxide or other secondary coatings, and thermal insulation blankets.

Threaded holes will be provided on the reflector hub for attaching the eyebolts of the lifting sling used in the ground handling operations. A safety belt will be secured around the periphery of the reflector hub during ground handling, to ensure against accidental opening of the retaining doors.

Several specific design selections were made by Fairchild Hiller Corporation based on trade-off studies and engineering evaluations conducted during the preliminary design phase. These consist of the following:

- A fixed, non-rotating hub design was selected instead of the originally proposed design which featured a freely rotating hub. The chosen design is the simpler, lighter, and more reliable.
- The reflector mounting tabs will be located in the central plane of symmetry of the reflector hub, to minimize the interfacing problem resulting from differential thermal expansions between the reflector hub and the mounting structure.
- The torsional natural frequency of the reflector will be approximately 1.5 Hz. This will result in a more optimized reflector design and a weight reduction of 10 pounds, compared to the originally considered 2 Hz design.

A number of potential problem areas related to the reflector design were investigated by FHC, namely:

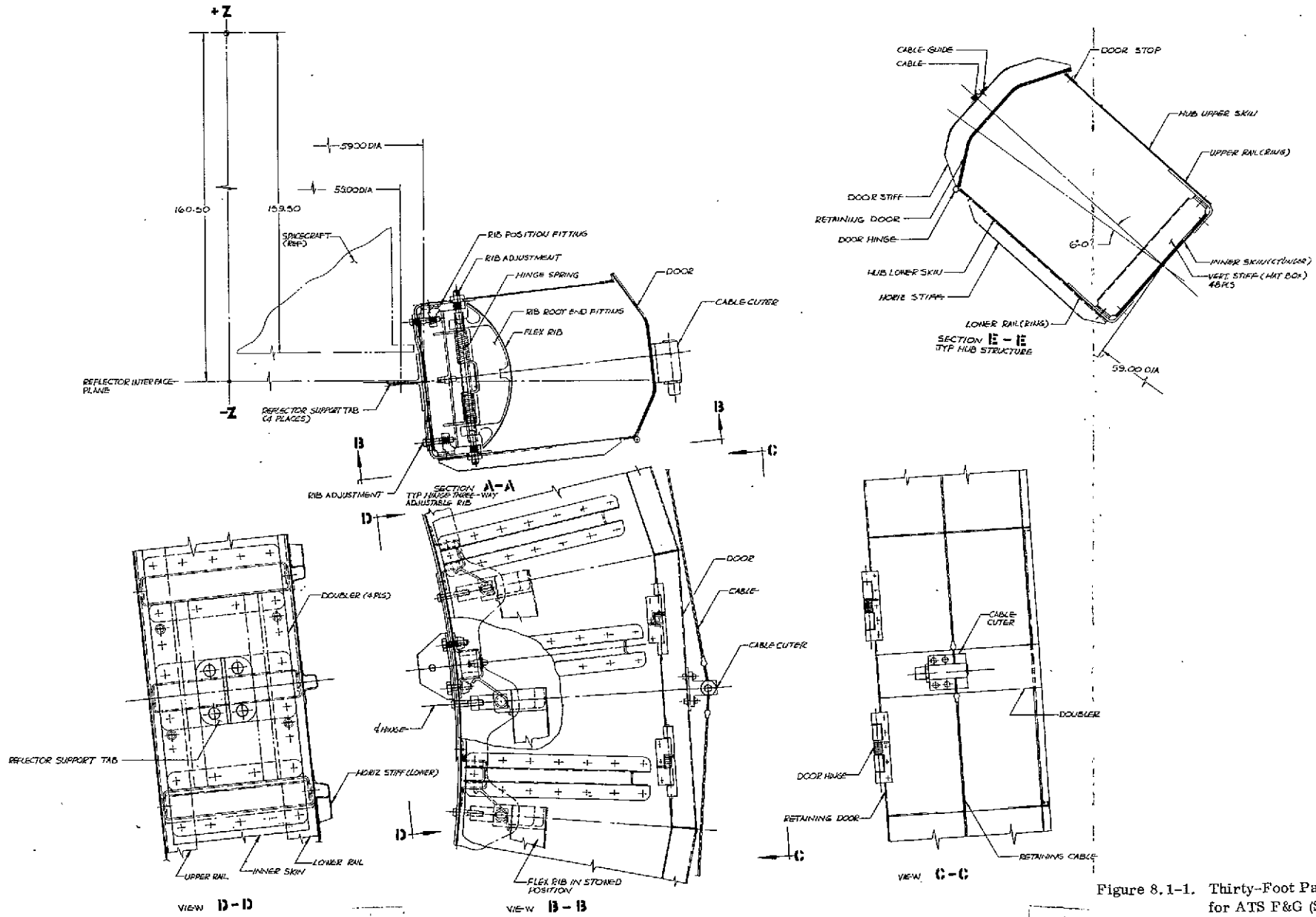
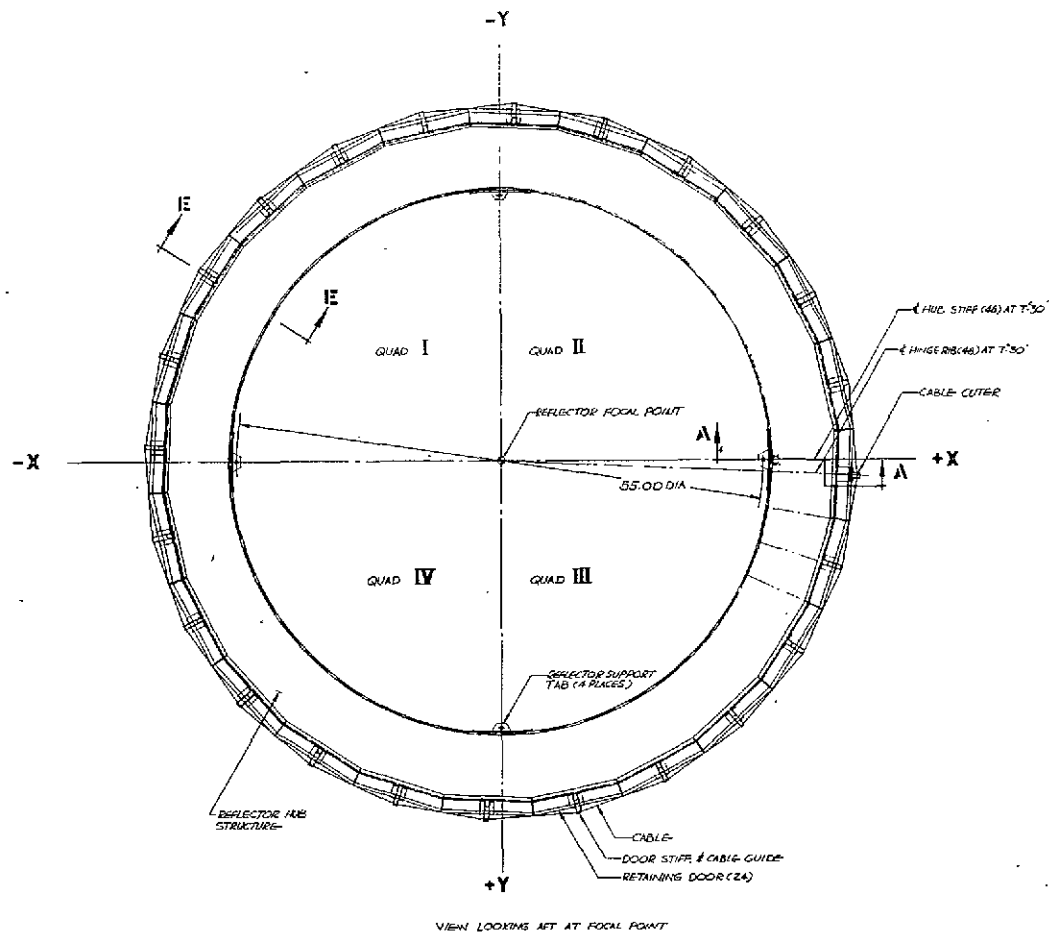


Figure 8.1-1. Thirty-Foot Parabolic Reflector for ATS F&G (Sheet 1 of 4)

FOLDOUT FRAME 1

8-3/8-4
 FOLDOUT FRAME 2



REFLECTOR STOWED POSITION

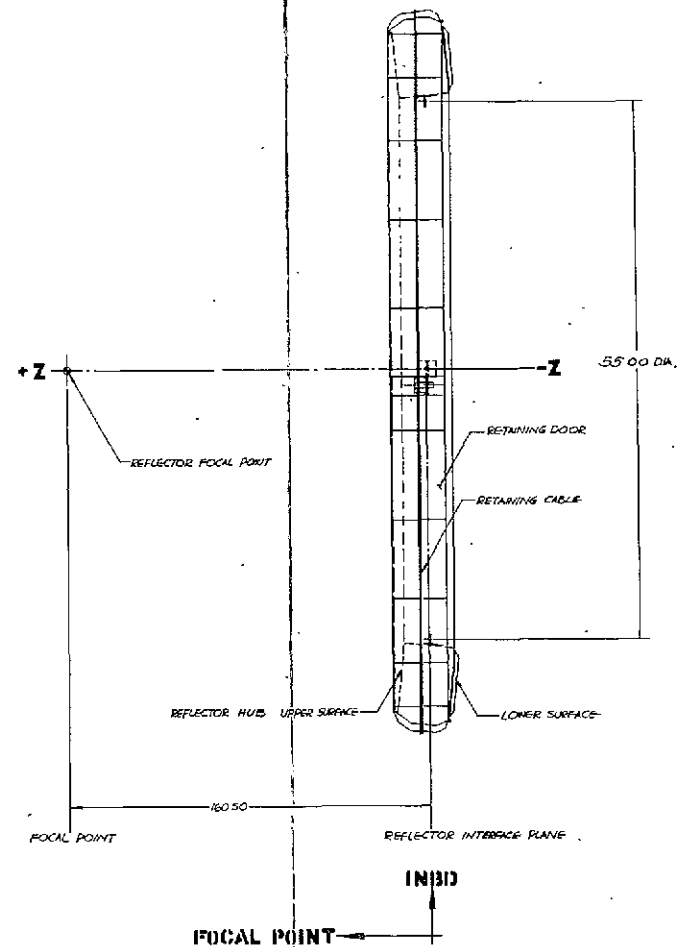
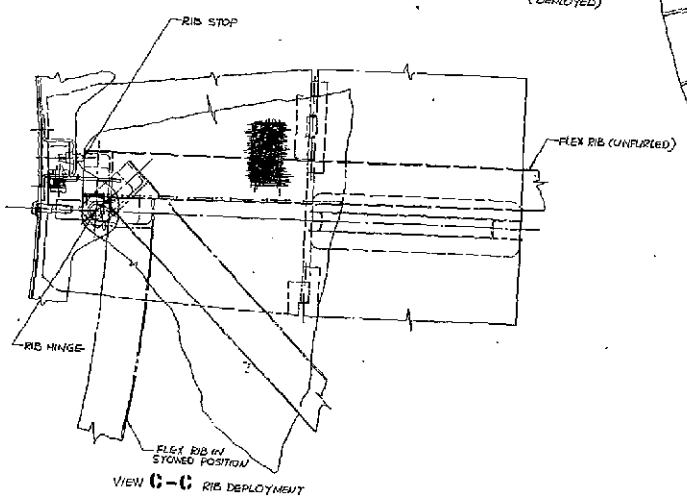
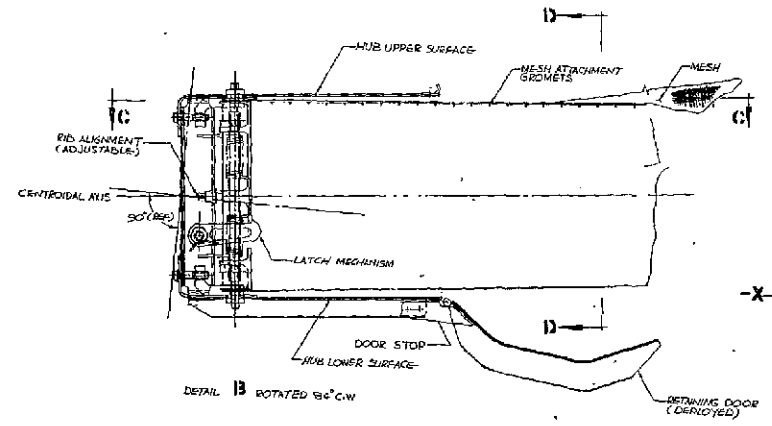
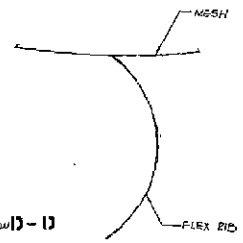
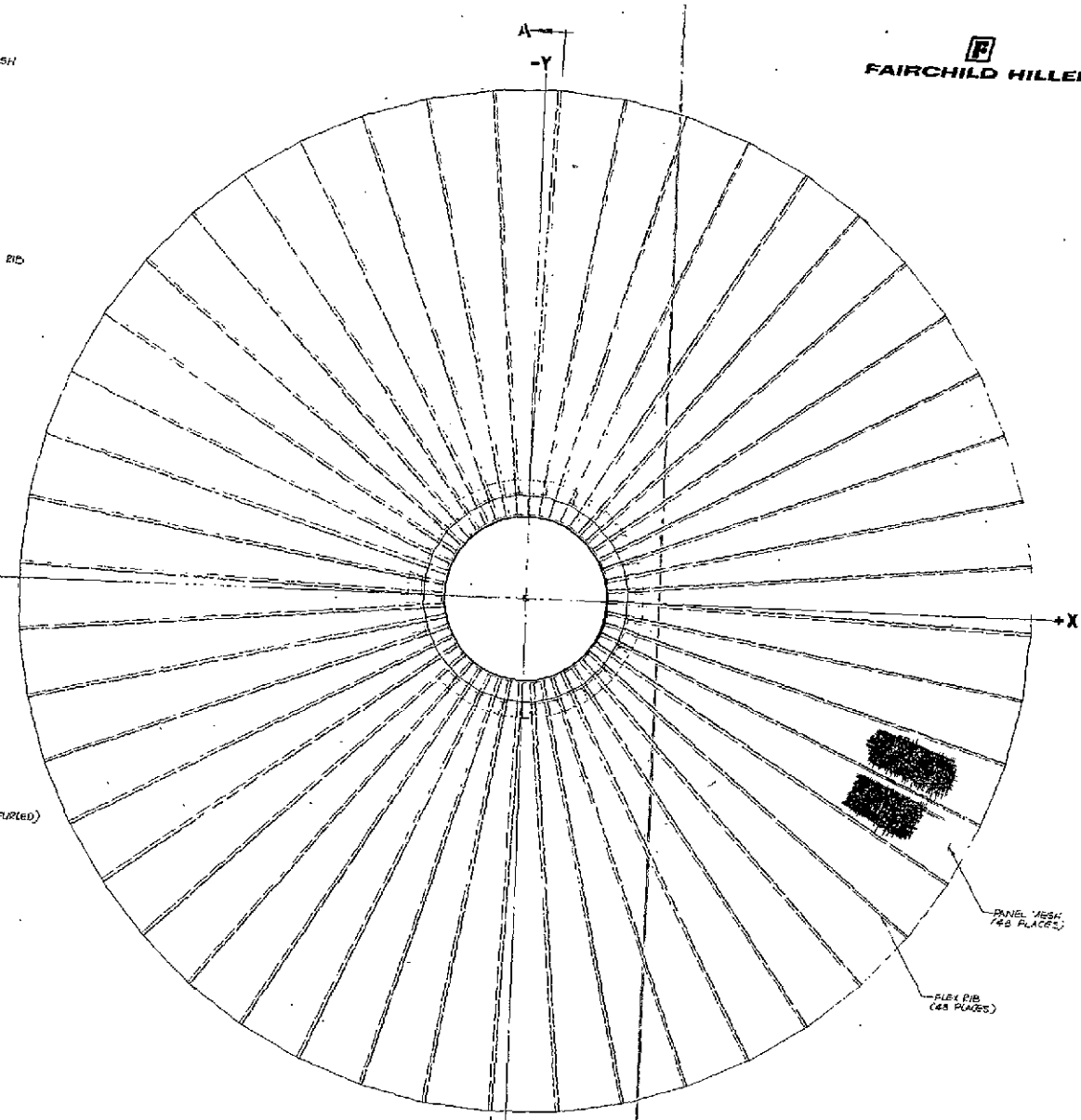


Figure 8.1-1. Thirty-Foot Parabolic Reflector for ATS F&G (Sheet 2 of 4)



FOLDOUT FRAME 1



VIEW LOOKING AFT AT FOCAL POINT
REFLECTOR UNFURLED

Figure 8.1-1. Thirty-Foot Parabolic Reflector for ATS F&G (Sheet 3 of 4)

FOLDOUT FRAME 2 ^{8-7/8-8}

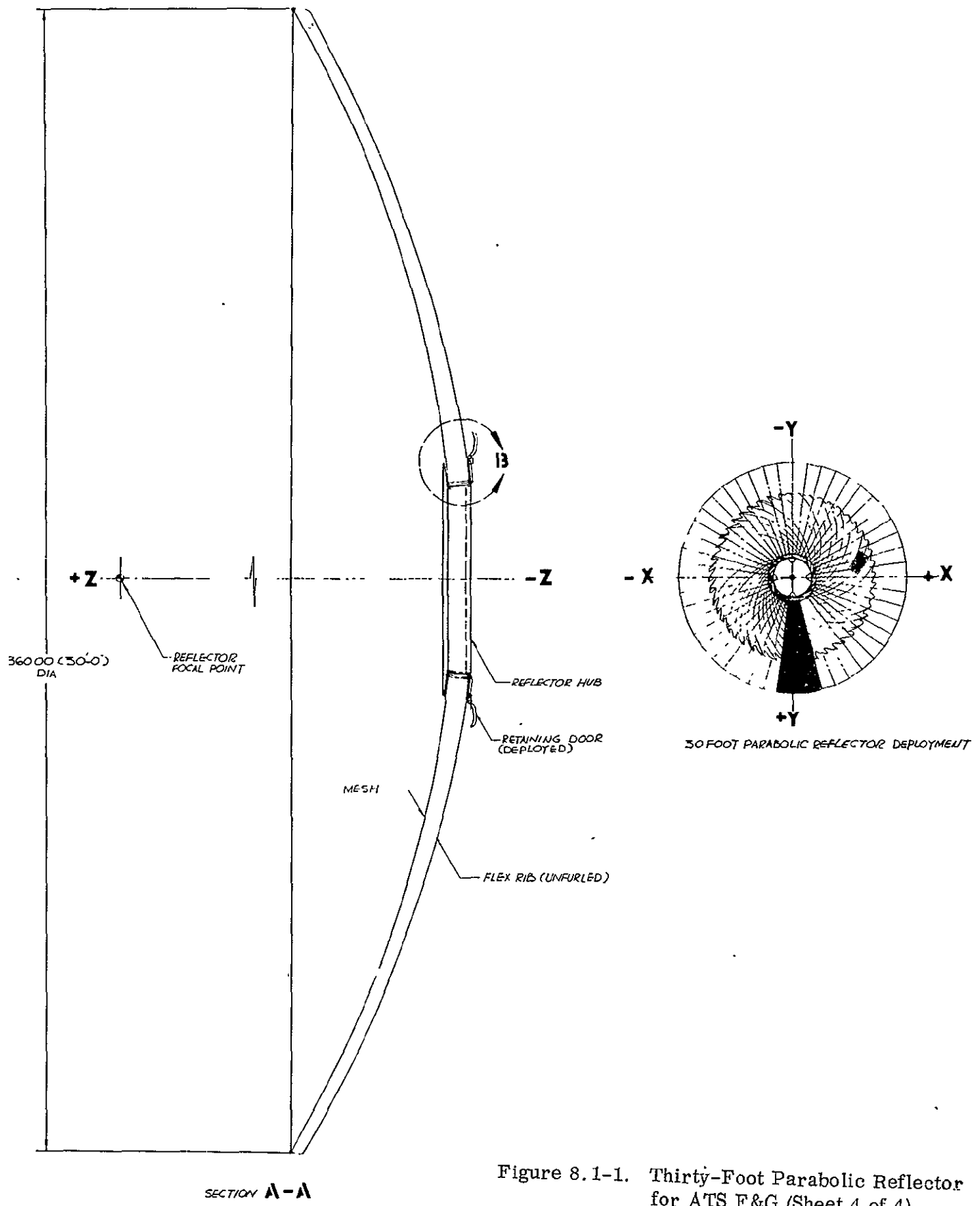


Figure 8.1-1. Thirty-Foot Parabolic Reflector for ATS F&G (Sheet 4 of 4)

- The possible adverse effects of the propellants considered for use in the APS on the mesh material. Independent investigative efforts of FHC, LSMC, and the Government (GSFC) all lead to the conclusions that ammonia does not effect the mesh whereas hydrazine will rapidly attack it. FHC will use an ammonia system for the APS.
- The reflectivity of the mesh at the low end of the required operating frequency range. An analysis performed by FHC showed that the thickness of copper coating used on the mesh is more than adequate to handle frequencies down to 100 MHz. Testing is now being performed to corroborate the analytical results.

The RF performance verification tests will be performed with the reflector in a free condition, without the originally proposed contour support fixture.

A method for in-orbit measurement of the reflector contour has been developed by FHC and is offered as an option to NASA/GSFC. The method involves a rotating panoramic facsimile camera viewing targets placed onto the reflector surface.

8.2 PHYSICAL DESCRIPTION

The parabolic reflector subsystem will consist of three major subassemblies, namely the hub, the rib and the reflective surface assemblies.

8.2.1 HUB ASSEMBLY

The hub structure is basically a ring with a channel cross-section, made of sheet metal and formed-sheet hat section stiffeners. The open side of the channel is around the outer periphery of the hub, allowing the ribs to be folded radially into the hub. Closure and rib stowage retaining is provided by a series of spring-loaded doors spaced around the outer periphery of the hub. These doors are restrained in the closed position by a cable wrapped around the hub's outer periphery that passes through redundant cable cutters mounted to one of the doors.

The inner periphery, or base, of the hub is fabricated from two corner angles, tied together by a shear web which is stiffened by formed-sheet hat sections. The forward and after hub surface plates which form the channel shaped section, are attached to the corner angles at approximately right angles to the shear web. The forward hub surface is parabolic in shape and forms a continuation of the antenna reflective surface. Formed-sheet hat sections are spot welded radially to the after hub surface plate to add strength and rigidity. The closure doors are of formed sheet stiffened by hat sections, and are hinged around the outer periphery of the after hub surface plate, spring-loaded to the open position. A formed-sheet angle which is spot welded around the outer periphery of the forward hub surface plate, provides structural stiffness and a door closure stop.

A series of rib position fittings (the hub half of a rib hinge) are spaced on 48 equal radial centers around the inner peripheral corner angles. These position fittings are mounted in pairs, one against the forward and one against the after hub surface plates. Adjustment stubs are threaded through the fittings

and protrude through radially slotted holes in the surface plates. A lock nut is provided at the outside of the surface plates on the adjustment stubs to lock the stubs and fittings in place. A captive adjustment screw protrudes through the inner periphery of the hub into the base of each position fitting allowing individual adjustment of each fitting in the radial direction. An adjustable stop is mounted in the hat section adjacent to each rib root, which provides circumferential rib tip positioning adjustment. These adjustments permit minimization of the effects of manufacturing tolerance buildup by allowing post assembly adjustment of rib length, mounting angle and fore-aft alignments.

The ribs are spring loaded to their open position by torsional coil springs located on the rib hinge pins. A rib latch is mounted to the hub near each rib hinge attachment point. These pawl-type latches are spring-loaded, and are adjustable in the radial direction by means of their cam/pivot mounting.

The pyrotechnic cable cutters are fully space qualified units that have been used by LMSC on earlier reflector designs. One or two cutters will be provided, depending on the results of the deployment reliability analysis. The squibs have dual bridge wire actuators which will be fired simultaneously by redundant power sources in the spacecraft.

Clips will be attached to each door to locate and maintain the position of the cable under the launch ascent environmental conditions, and retain the cable to the stowage canister doors after deployment. A minimum weight tensioning device will be provided for adjusting the cable length upon reflector stowage.

The mechanical reflector-to-spacecraft interface will consist of four mounting provisions spaced radially on 90-degree centers around the inner surface of the ring-shaped hub. The lugs will extend radially inward from the center of the hub and provide mounting holes on a diameter of 55.0 inches. The design of the mechanical mounting interface will consider the effects of differential thermal expansion between the reflector hub and the supporting structure.

Two microswitch type indicators will be provided to indicate completion of the reflector deployment process. These indicators will be located at the rib hinges, and will be actuated by the ribs themselves as they attain their fully deployed position.

Interface connectors for the electric power to the cable cutters and for the deployment indicator signals will be mounted on the reflector hub. Their location will be coordinated with FHC/SESD to ensure compatibility with the spacecraft harness routing. Electric power and signals will be routed through separate, isolated connectors.

All hub structure will be fabricated from magnesium sheet. The rib position fittings will be cast magnesium and will have stainless steel inserts to provide strength in the threaded holes for the hinge adjusting stubs and the block mounting adjustment screws. The hinge latches will be magnesium. The adjusting stubs (hinge pivots) will be fabricated from titanium. The door restraining cable will be fabricated from 0.062 diameter stranded twisted stainless steel wire. The cable tensioning device will be made from stainless steel.

Basic thermal control of the hub assembly will be provided by a multilayer insulation system consisting of twenty layers of 0.25-mil thick crinkled aluminized mylar. These radiation shields will be aluminized on one side only and therefore will not require a spacer material between the layers to reduce conductivity.

The shields will be stacked in layers of ten to form a blanket module held together with a teflon button and pin retainer assembly. Two such blankets will be fabricated to form the required 20 layer thickness. Each complete 10-layer blanket will be divided into four segments to facilitate the installation operation.

The first blanket will be held in place by the fasteners bonded to the hub skin. The second 10-layer blanket will be installed so that the butt joints of the first blanket are overlapped to reduce the effects of a direct heat leak through the joints. The second blanket will be held in place by parachute type dacron ribbons strapped over the insulation shields and fastened to the nylon snaps. The joint of the mating panels will be controlled and held together by velcro tabs which can adjust the gap between the sections. A dacron retainer net will be installed on the top and bottom of each 10-layer segment to prevent accidental damaging of the thermal shields during handling and installation.

In addition to the 20-layer thick insulation blanket, a 0.5 inch thick layer of fiberglass batting encapsulated in a dacron net will be installed between the support ribs on one skin of the hub. The purpose is to provide a smooth surface to lay the insulation blankets over and improve its thermal performance.

A flexible, reflective (metalized-surface mylar film) shade will be mounted between ribs at the outer peripheral edge of the hub, to prevent the interior surface of the hub from being exposed to solar radiation.

8.2.2 RIB ASSEMBLY

The ribs will be thin flexible members, with parabolic shaped inner edges, tapered both in width and thickness. Transverse to the parabolically curved principal axis, the ribs will be formed into an arch, with a decreasing radius of curvature from root-to-tip. Riveted to the root of each rib will be a rib root fitting (the rib half of the rib hinge) for mounting the rib to the hub. Each rib will have holes drilled along its length near the inner (concave) surface to provide for attachment of the mesh reflective surface to the ribs.

The ribs, nominally 179.85 inches long, will be cut from 0.080 inch thick, 7178-T6 aluminum alloy sheet that has been chemical mill tapered over three-fifths of its length to a thickness of 0.030 inch. The width of the ribs will be approximately 7 inches at the root tapering to approximately 4 inches at the tip. The camber radius will be approximately 4.0 to 4.5 inches. The final values of these dimensions will be determined by the design analysis.

The rib root end fittings will have a curved surface matching the inside radius of the root of the rib. Extending from the back side of this mounting surface or flange will be two bearing tabs, bored to accept a tubular hinge pin. The tabs will be joined together and to the rib mounting flange by a web, which runs between the edges of the rib. This web will contain a cut-out to form the catch for the rib latch.

The rib root end fittings will be cast from magnesium and the hinge pins will be fabricated from thin-wall titanium tubing. The pins will be secured to the root end fittings with steel spring pins.

Thermal control provisions will be provided for the ribs by selectively covering them with 0.0005-inch thick, adhesive backed mylar tape that has a vapor deposited aluminum coating, and white Dow Thermatril paint, to provide the desired α/ϵ ratio.

8.2.3 REFLECTIVE SURFACE ASSEMBLY

The parabolic-shaped rf reflective surface assembly is fabricated from 48 tapered mesh segments, bonded together to form the desired parabolic shape. The joints coincide with rib locations on the deployed antenna. Attachment to the ribs is made by stitching with nonmetallic thread through the holes spaced along the inner edge of each rib. To avoid excessive deformation of the mesh due to sewing them to the ribs, a narrow strip of fabric is sewed to the mesh along the rib-line. The two sides of the strip are then bent up to flank the rib, and are stitched to the rib.

The reflective mesh is made of a copper-coated dacron cloth, woven with about 32 single strands per inch in one direction and 24 double strands per inch in the normal direction. The copper is protected against mechanical handling and environmental degradation with a thin overcoat of silicone sealant, which also increases the thermal emissivity. The mesh has a rectangular weave as shown in Figure 8.2-1. The warp yarns (twisted pairs) will be nearly radial from the center of the hub. The filling yarns (single) will be circumferential.

8.3 PROPERTIES AND CHARACTERISTICS

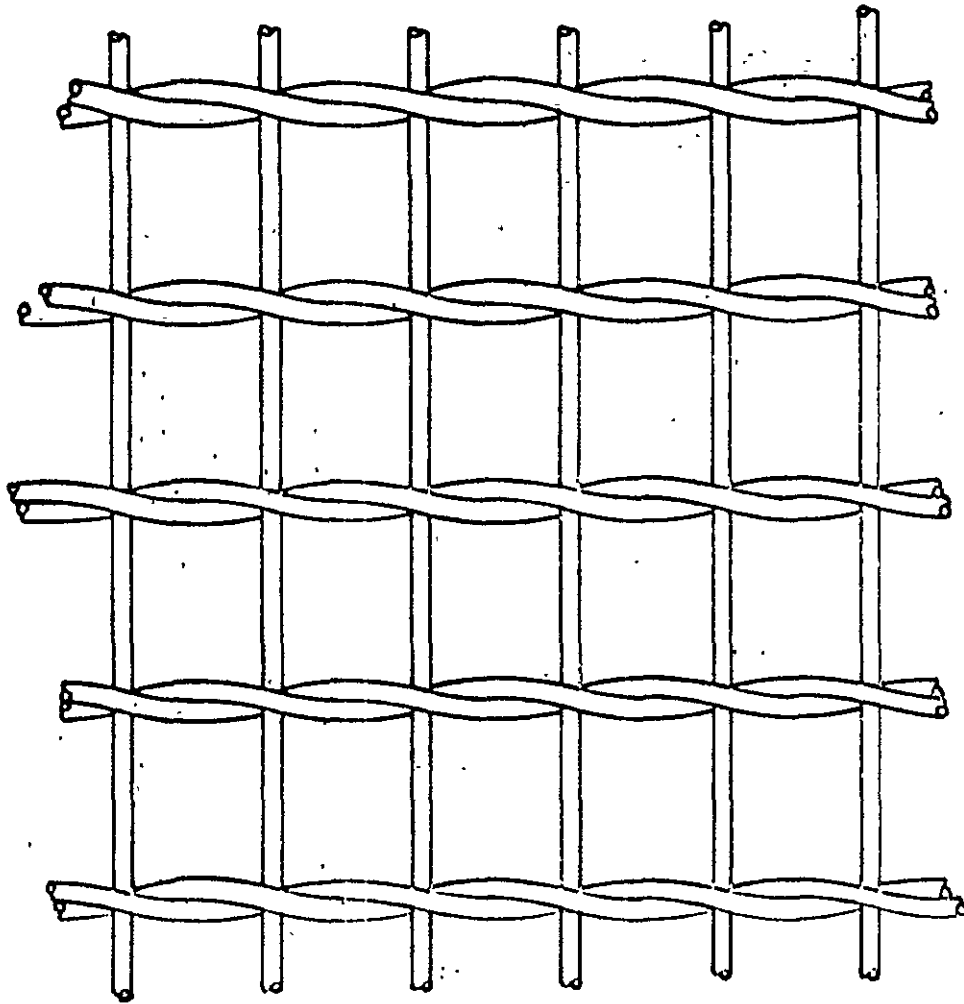
8.3.1 GENERAL

The deployed reflector will have an outside diameter of 30 feet and a nominal focal length of 158.4 inches. The depth of the cup, measured from the rib tips to the theoretical apex will be approximately 51 inches.

The reflector is not a true circular paraboloid, but an approximation of the same by the parabolic cylindrical sections formed by the mesh panels spanning adjacent ribs. The chosen design of 48 ribs approximates the true paraboloid within 0.025 inches rms error when not subjected to thermal distortions. This is the error associated with the "perfect flex-rib" configuration which will actually never occur in orbit; that configuration exists only if the reflector is in a truly isothermal environment and even then only at one particular temperature. In orbit, the surface will undergo a constant change as the sun angle changes around the spacecraft.

The reflector will be assembled and adjusted in such a manner that the ribs will place the mesh under slight tension. Appropriate selection of this tensional loading between the mesh and the ribs will ensure that the deviations of the surface from the theoretical paraboloid under the orbital thermal environments remain a minimum.

Warp (End) Yarns



Filling (Pick) Yarns

Leno (Doup) Weave

Figure 8.2-1. 25X Scale Travis Marquisette No. 635
(Multifilament Yarns Shown as Monofilament)

The thermally caused surface movements of the reflector during the changing environments can best be illustrated using simple isothermal conditions. As the reflector temperature decreases, the ribs will shrink radially inward, reducing the spacing between the attachment points of the mesh on adjacent ribs. The circumferential fibers of the mesh spanning this distance will also contract under the reduced temperature; however, their length will be reduced less than the change in the spacing since the mesh has a lower thermal coefficient of expansion than the ribs. Consequently, the spring strength of the preloaded ribs will move the reflector surface to a more open-cup position. The converse will be true when the reflector temperature increases, and the reflector cup will move to a more closed position. In the actual orbital thermal environments, this effect is even further accentuated because a decrease in rib temperature is generally associated with an increase in the surrounding mesh temperature, causing an even more pronounced cup opening tendency. This is due to the fact that the two surfaces are approximately perpendicular to each other. As the position of the sun changes relative to the rib surface to produce a lower incidence angle causing a reduction of the rib temperature, it will simultaneously have a greater incidence angle with the mesh, causing the mesh temperature to increase.

When sufficient mesh tension is provided at manufacturing temperature, the larger value of rib shrinkage over mesh shrinkage at orbital temperatures will not allow the mesh surface to relax from a taut condition at any time, with the exception of the period of extreme variations during emergence from the eclipse. This period is considerably less than 1 hour.

In most orbit positions the individual ribs are subjected to varying incidence angles of solar radiation. Thus, the ribs will generally be at varying temperatures and rib deflections will vary around the periphery of the reflector. However, the relatively low lateral stiffness of the ribs will permit equalization of the circumferential mesh tension from rib-to-rib, regardless of the local vertical or radial rib deflections. This ability will ensure minimum local distortions of the reflector surface.

The initial tension is built into the unit by fabricating the mesh assembly undersize and pitching the ribs at the same outward, away from the mesh. The required optimum value of initial mesh tension will be attained by employing accurate fabrication and alignment techniques.

The rib position adjustments at the rib hinges enable changing the mesh tension values within a reasonable range, in case that such a change be required. These adjustments, which permit changing the axial and radial position of the rib roots as well as the pitch angle of the ribs independently, will be calibrated. Therefore, any re-adjustment of the mesh tension after the initial assembly and adjustment will be accomplishable directly, without requiring additional measurements to be performed. A simple tool will be provided that will permit performing the adjustments with the required degree of accuracy.

8.3.2

MATERIAL PROPERTIES

The ribs will be made from 7178-T6 aluminum alloy. The coefficient of thermal expansion of this material is 12.0×10^{-6} inches per inch per degrees F, and its minimum allowable yield stress in tension is 72,000 pounds per square inches.

The coefficient of thermal expansion of the magnesium alloys used in the hub assembly is approximately 15.0×10^{-6} inches per inch per degree F.

The mesh material has been subjected to material and physical properties tests by LSMC, at high and low temperatures as well as in hard vacuum including exposure to actual and simulated solar radiation environments.

The physical and thermal properties of the dacron yarn as well as its resistance to abrasion, fatigue, and deterioration by heat, light, and chemicals make dacron a desirable material for use in the reflector mesh. The high extent of recovery from low stresses (deformations) and the low moisture sensitivity of dacron contribute to the good wrinkle resistance (shape retention) of the fabric. Vacuum stability and compatibility with the processing required for the copper coating are mandatory characteristics that are satisfied by dacron.

Weighing only about 0.017 pound per square foot, the mesh material has good flexibility and strength and is practically free from creasing degradation. Radio frequency tests at 16 GHz have proven this metalized cloth to be as reflective as solid sheet metal.

Mechanical properties of the mesh are shown in Table 8.3-1 and Figure 8.3-1. The modules of elasticity units are pounds-per-yarn-per unit strain. The unit of pounds per yarn was selected because it presents the most useful data (the double twisted yarns are counted as one yarn). Yield strength is based on 1 percent permanent offset and was found by cycling the specimen at increasing tensile loads until a set of 0.010 in/in was observed; units are pounds per yarn. Ultimate strength is the maximum load reached during a test; units again are pounds-per-yarn.

Table 8.3-1. Mechanical Properties of Mesh Material

Item	Cu - SI-Dacron			
	Warp Yarns (Double, Twisted)		Filling Yarns (Single)	
	Room Temp.	-320°F	Room Temp.	-320°F
Modulus of Elasticity lb per $\frac{\text{in.}}{\text{in.}}$ / Yarn	13.59	40.5	10.18	27.9
Yield Strength (1% e)	0.264	1.452	0.186	0.828
Ultimate Strength lb/Yarn	1.16	2.168	0.631	1.062

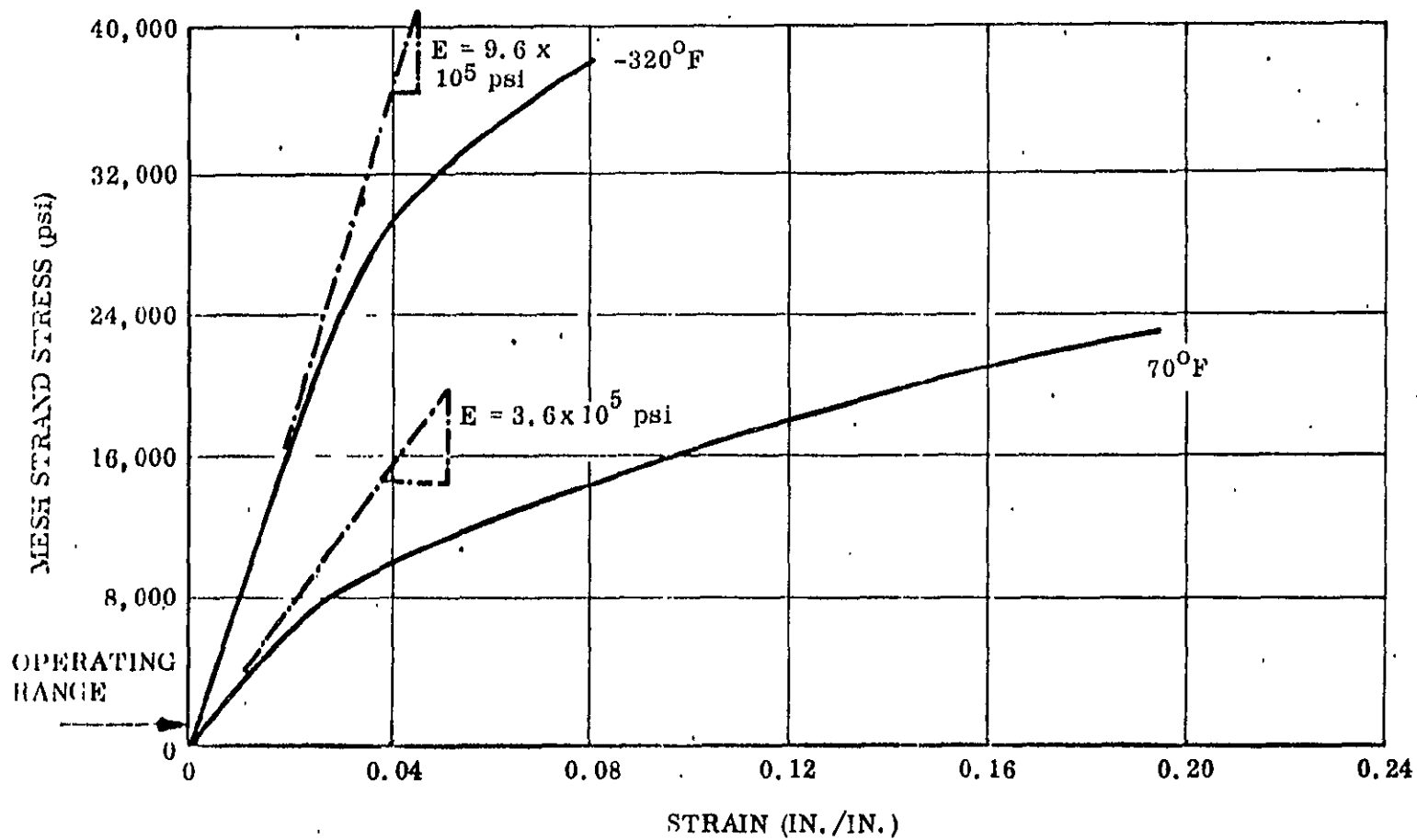


Figure 8.3-1. Mesh Stress--Strain Curve

The coefficients of thermal expansion are shown in Figure 8.3-2. The positive coefficient of the twisted (double) warp yarn is a result of the partial straightening of each twist on temperature reduction. This latter feature will ensure little or no stress in the mesh surface radial direction.

Values of mesh transmittance relative to solar radiation are shown as a function of incidence angle in Table 8.3-2.

Table 8.3-2. Transmittance of Mesh vs. Incidence Angle

<u>Incidence Angle</u>	<u>Transmittance (%)</u>
0	75
10	74.5
20	73.1
25	73.1
35	71.8
50	68.1
60	59.9
70	41.2
80	13.2
90	0

The optical surface properties of the mesh material are:

$$\text{Solar absorptance } (\alpha_s) = 0.20$$

$$\text{Infrared emittance } (\epsilon) = 0.35$$

The α/ϵ value of the mesh due to the weave characteristics is less, since the solar energy is absorbed to a factor proportional to the yarn diameter and the energy radiated to space is a function of the circumference (π times the diameter). The exact factor is slightly less than π due to weave of the mesh where energy is exchanged between strands; i. e., the entire circumference does not radiate to space. A practical value α/ϵ used for thermal analysis is 0.287. Tests to date indicate that the α/ϵ ratio degrades asymptotically towards 0.213 after approximately 6 months of service. The lower value of α/ϵ ratio is therefore used as a bandwidth limit for thermal predictions.

The substrate of the mesh consists of dacron strands (5-15 mils in diameter) from which the sizing has been removed. The strands are coated with the desired micron thickness of copper by a proprietary electroless process. After the plated mesh is rinsed and dried, it is coated with a dimethyl siloxane compound (Dow Corning 92-009 Dispersion Coating). A double-strand cross-section is shown in Figure 8.3-3 at 200-fold magnification. This particular specimen was coated by brush. Other possible methods of application include dipping and spraying. The coating varies in thickness from about one mil to about one micron, but its external continuity is evident. The thickness variation is due to the asymmetrical shape of the strands and the surface irregularities of the fibers. The copper coating is better discernable in Figure 8.3-4, a 1000-fold magnification of the plated, uncoated strand.

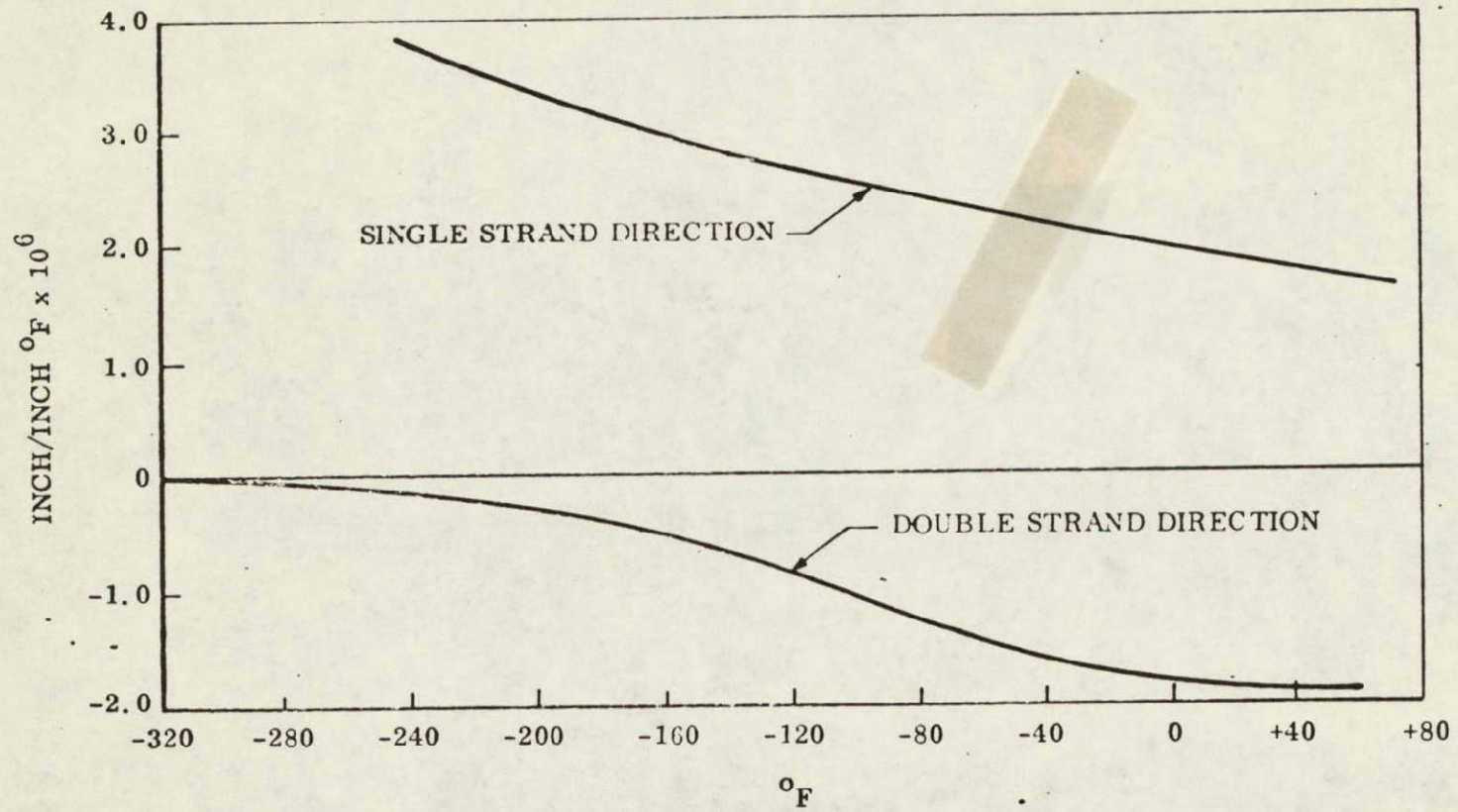


Figure 8.3-2. Mesh Coefficient of Thermal Expansion

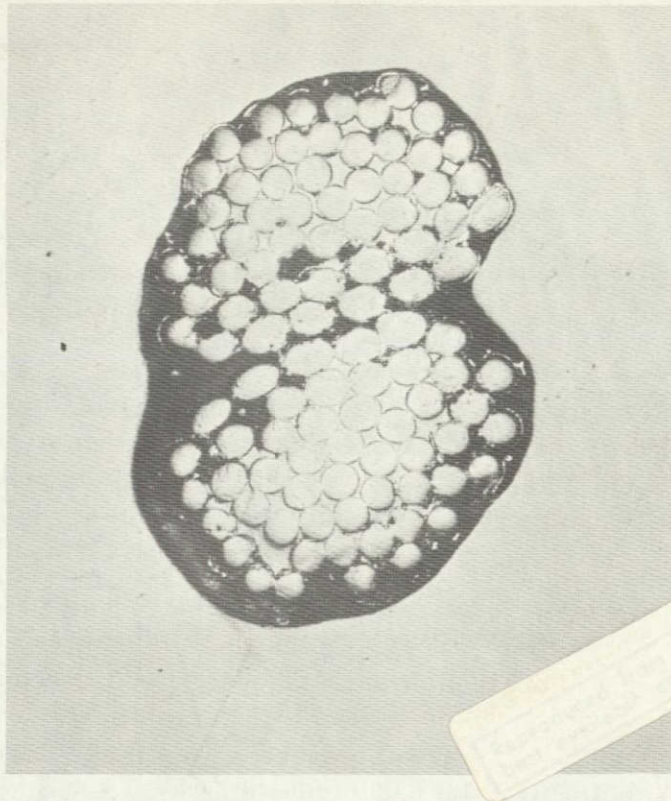


Figure 8.3-3. Coated Stand (200X)

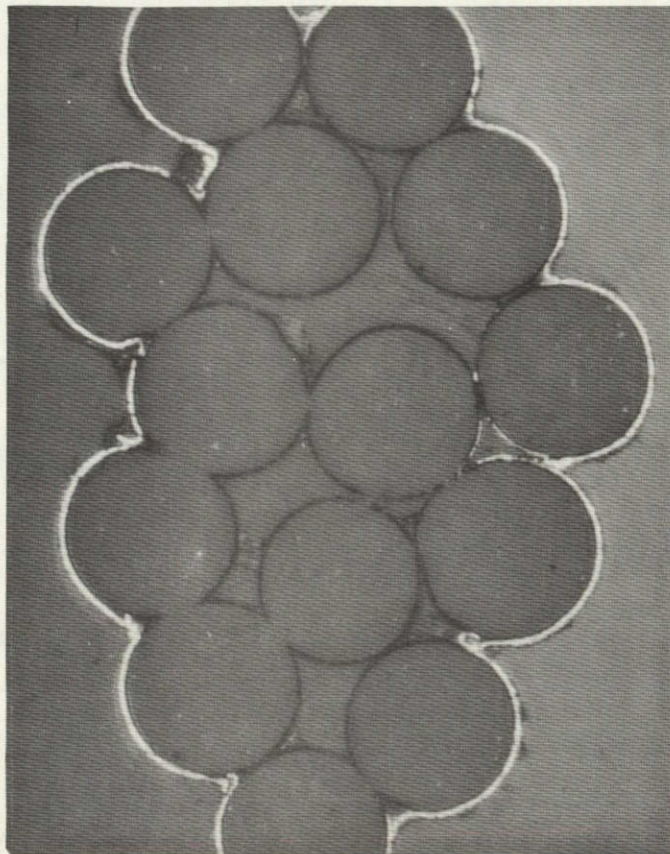


Figure 8.3-4. Uncoated Stand (1000X)

8.3.3 MASS PROPERTIES

8.3.3.1 Weight

The maximum weight of the Reflector subsystem will not exceed 150 pounds. The following is a listing of the present estimate of the maximum weight and the weight allocations to the individual components.

Reflector Weight Budget

Hub Components	<u>lb.</u>	
Rib hinges	5.5	
Hinge pins and bearings	1.6	
Hinge adjustor blocks	3.2	
Adjustor hardware	2.7	
Structure	16.8	
Hinge latches	1.6	
Doors and door hinges	<u>4.2</u>	<u>35.6</u>
 Hub Operating Components		
Door fastening cable and cutter	1.8	
Hub attachment	6.2	
Electrical harness	<u>0.8</u>	<u>8.8</u>
 Ribs		
Aluminum tapered ribs	86.0	
Thermal control surface	<u>3.8</u>	<u>89.8</u>
Hub thermal control surface	3.8	
Parabolic contour mesh	<u>12.0</u>	<u>15.8</u>
Reflector total weight		150.0

A concentrated effort will be made to minimize the weight of the reflector as much as possible by tradeoff and optimization studies during the final design process. The design goal will be a total reflector weight of 140 pounds.

8.3.3.2 Centers of Gravity and Moments of Inertia

In the deployed configuration, the reflector center of gravity will lie within 0.1 inch of the reflector design axis and will be approximately 15 inches from the parabola vertex along the reflector axis toward the focal point. The center of mass of any rib and panel segment will lie at approximately 86 inches radially out from the reflector axis. The mass moment of inertia of the reflector about the reflector axis will be between 200 and 300 slug-ft².

In the stowed configuration, the cg of the reflector, will lie within 0.1 inch from the hub axis and its mass moments of inertia will be between 30 to 40 slug-ft².

8.3.4 STRUCTURAL CHARACTERISTICS

In the orbital configuration, the loads due to spacecraft control system perturbations will be small, inducing very low stresses in the reflector structure.

The critical loads and stresses for the reflector will occur during the impact of rib roots on the hub at the completion of the deployment phase. These loads and stresses have been calculated for the preliminary design presented to ensure that all critical stresses are within material allowables. The present design has been found to be sufficient to withstand the calculated stresses.

The loads encountered by the stowed reflector during ground handling, qualification testing, and launch conditions will not be critical, since the ribs and mesh are fully supported and totally restrained by their tightly wrapped condition in the hub annulus. The hub structure itself is inherently compact and stiff for any possible inertia loads in the stowed condition. Extensive previous test experience shows that no mesh chaffing or degradation occurs during launch type vibration of the wrapped ribs and mesh elements stowed in the hub, because no significant relative motion can occur in this tightly confined state. The stresses induced by worst case qualification testing of the stowed reflector will be determined for the final design and used to ensure the integrity of the stowed reflector for qualification testing.

In the stowed condition, the ribs are wrapped circumferentially, overlapping the hub. The ribs will flatten from their unloaded semilenticular cross-section shape as they wrap around the hub. The rib considered for this design is 7 inches deep at the hub end with a 4.3-inch radius of curvature. Fully flattened stress is therefore close to

$$F = \frac{10^7 \times 0.025}{(2 \times 4.3)} = 29,000 \text{ psi}$$

Since the stowing wrap is in the direction that reduces this stress level, it may be treated as a maximum.

8.3.15 DYNAMIC CHARACTERISTICS

The optimal natural frequency in torsion of this size of reflector is at 1.5 Hz. Attempting to lower the frequency below this value tends to jeopardize one-g testability, while an increased requirement will rapidly add weight to the system. The frequencies in the other modes, will be approximately 7 cps for pitch and roll, and 9 cps for axial vibrations.

The modal shape of each rib for these excitations is the first cantilever vertical bending mode with torsion essentially restrained by the mesh. The deployed reflector has good damping characteristics. Observation of self-damped oscillations in similar previous reflectors shows that the oscillation amplitude decays by one-half on each successive cycle.

The natural frequencies of the stowed package will be quite high and should be of no concern. These frequencies and associated modal shapes will be calculated as a check on the design for launch environment integrity. No problem is expected in this regard since the stowed package is inherently stiff and compact.

The deployment torque transmitted to the structural supports will be approximately 5700 ft-lbs.

8.3.6 THERMAL CHARACTERISTICS

Prior to launch, the reflector assembly will be exposed to normal earth ambient conditions. On the launch pad and during ascent and orbital injection, the assembly environmental temperatures will range from 0°C to 50°C. This environment will cause no operational problems for the reflector. Actual expected temperature levels during launch, inside the aerodynamically heated shroud, and during the transfer orbit prior to deployment will be determined during the design phase of the program, and, if necessary, thermal control provisions will be provided to maintain acceptable temperature levels of the deployment mechanism.

The major portion of rf gain losses of the reflector is contributed by thermal deflections. In order to reduce these deflections, sophisticated thermal control measures are applied to the structural parts of the reflector, namely to the hub, and the ribs themselves (Reference paragraphs 8.2.1 and 8.2.2).

As a result of the foregoing, the temperature fluctuations of the various reflector components were predicted to be as follows:

hub: -20 to +60 degrees C

ribs: -160 to +0 degrees C

mesh: -200 to +35 degrees C

8.3.7 POTENTIAL PROBLEM AREAS

LMSC's considerable experience with flex-rib antenna design for space environment minimizes anticipated potential problem areas. During Phase B/C of the ATS F&G Program, a number of potential problem areas were investigated and resolved.

The reflectivity of the mesh at the low end of the intended operating frequency range (100 MHz) has been investigated. An analysis performed by FHC showed that the mesh reflectivity will not be effected adversely until the thickness of the copper layer is reduced to the 10^{-2} to 10^{-4} micron range. This is several orders of magnitudes below the normally used coating thickness which ranges from 0.5 to 1.5 microns. In addition, LMSC can increase the coating thickness if required up to 5 to 6 microns without affecting their design. A test program has been undertaken to corroborate the above mentioned analysis.

Exposure of the mesh material to various liquids and gasses that could exist in the ambient environments has been investigated.

It has been established that ammonia, used as the propellant is the Auxiliary Propulsion System of the spacecraft and will not have any adverse effects on the mesh properties.

Sulfide type gasses, which could exist in terrestrial environment, may cause in very high concentrations some degradation of the mesh reflectivity. Further testing will be conducted during the design phase of the program to establish the effects of exposure to concentration levels that will actually exist in the ambient environments to which the reflector will be exposed. In addition, provisions will be made to afford maximum protection of the reflector against unanticipated environments. This will be accomplished by providing a sealed enclosure for storage and transport of the reflector. After receipt of the unit at FHC, it will only be exposed to controlled environments during all spacecraft assembly and test operations, including shipment to the launch site and launch preparations.

Results of tests that were recently performed by NASA/GSFC indicated certain degradations in physical properties of the mesh under exposure to ultra violet radiation. Prior reports from LMSC indicated no adverse effects on mesh performance under long time exposure to solar radiation environments. A test program will be conducted during the design phase to resolve the apparent discrepancy between these reported test results.

Furthermore, additional tests will be performed to determine the effects of nuclear radiation and thermal cycling upon the mesh, as well as those of flexing and other mechanical stress conditions to which the mesh may be exposed.

8.4 PERFORMANCE

The detailed performance of the reflector presented below has been derived from preliminary simplified analyses, similar to those described in the next section. These analyses were based on a set of design variable that satisfied the basic structural, dynamic, deployment and weight requirements. The selection of the values of these variables has, however, not been based on a full design optimization process. Furthermore, these analyses were made prior to incorporation of some of the most recent design improvements. Consequently, the performance values presented below are an indication of the nature and the ranges of the expected reflector performance, and are used to demonstrate that the reflector design will meet the stipulated performance requirements. This design will be used in the program as the departure point for further optimization in accordance with the design procedure described in Paragraph 8.5.

The performance data presented are those determined for a reflector design consisting of a 48-rib surface with each semilenticular shaped rib 7 inches high at the hub and 4 inches high at the tip and a camber radius of 4.3 inches. The rib material is 7178-T6 aluminum alloy, 0.080 inch thick, chemically-milled to the desired section. The mesh pre-tension chosen was 0.060 inch chord shortness shortness between each rib tip-to-tip. The rib pre-set chosen was 0.30 inch vertical dimension at the rib tips in the cup opening direction, i.e. the direction of increasing focal length. The chosen rib thermal control was 90 percent aluminum thermal control tape and 10 percent white paint, and a 6-months or more degraded value of $\alpha/\epsilon = 1.070$ was used for the thermal calculations. The surface mesh properties were assessed at $\alpha/\epsilon = 0.273$.

8.4.1 DEPLOYMENT AND ONE-G TESTABILITY

The calculated peak value of the deployment torques transmitted to the support structure is 5,700 in-lbs. The opening time span in vacuum will be approximately 1.5 seconds. Damping in the structure will provide a rate of decay of the post deployment oscillatory motions of approximately 2:1 between successive cycles, which corresponds to a damping ratio of nearly 0.1.

The maximum clearance envelope required for the reflector on the convex side to insure interference - free deployment will not exceed a cone which has its apex at the center of the top surface of the reflector hub structure and is at a distance of 18 inches above the same reference surface at a diameter of 30 feet.

The reflector will be capable of deployment in the terrestrial, one-g environment in all three major orientations, namely cup up, cup down and with the reflector axis oriented horizontally.

The effects of the standard terrestrial environments upon the reflector contour were predicted as follows:

- In a 75 degrees F ambient temperature, the reflector surface will deflect inward, in the cup closing direction by an amount of approximately 0.1 inches measured at the outside diameter, relative to the perfect flexrib configuration (i. e. that with no thermal deflection effects).
- The effects of gravity will be the following surface deflections, as measured at the rib-tips.
 - a. In the cup down or cup up orientations, 0.070 inches, uniform at all rib-tips, in the cup closing or opening directions, respectively.
 - b. In the axis horizontal orientation 0.040 inches at the top and bottom ribs, with the surface deflecting inward at the top and outward at the bottom vertically oriented ribs.

The reflector will meet the specified RF performance requirements after six deployments, and meet all other requirements after a total of fifteen deployments.

8.4.2 THERMAL EFFECTS AND SURFACE DEVIATIONS

The thermal environment during orbit consists of solar and earth radiations to the spacecraft and reflector, and radiation from them to space.

Shadowing from the earth occurs for a period of approximately one hour, at equinoctial orbits, i. e., when $\beta =$ angle between sun and earth's orbit plane = 0, and for gradually decreasing lesser time periods until the solar angle reaches a value of approximately 9 degrees, after which no more earth shadowing takes place. The total time of the spacecraft in earth's shadow is approximately 110 hours per year, or 1.25 percent of the mission time; and shadowing always occurs at the relatively least important time of the day namely, around local midnight at the satellite sub-point.

Shadowing of the reflector from various parts of the spacecraft, (EVM, trusses, solar panels, etc.), occurs throughout the orbit as a function of the spacecraft's orientation relative to the sun.

The typical temperature history of the hub, the ribs and the mesh panels are presented in Figures 8.4-1 through 8.4-3. Figure 8.4-4 shows the maximum cross-wise temperature gradients in the various ribs for the entire normal orbit ($\beta = 0$).

Table 8.4-1 presents a summary of the temperature ranges and extremes for the various reflector components.

Table 8.4-1. Reflector Component Temperatures During Orbit

Component	Item	Temp, Degrees F.
Ribs	Range of mean temperatures (entire orbit):	-260 to +35
	Typical minimum difference, hottest to coldest mean temperatures (hours 0 and 12)	80
	Typical maximum difference, hottest to coldest mean temp's (hours 6 and 18)	300
	Maximum lengthwise gradient	200
	Maximum cross-wise gradient	3.5
Mesh Panels	Range of mean temperatures (entire orbit):	-395 to +95
	Typical minimum difference, hottest to coldest mean temperatures (hours 0 and 12)	0
	Typical maximum difference, hottest to coldest mean temperatures (hours 6 and 18)	140
Hub	Range of hub temperature (entire orbit):	-5 to +140
	Max. axial temperature gradients, end surface to end surface (any one radial location):	10
	Max. lateral temperature gradients on either end surface	75

The focal point shift of the "best-fit" true paraboloid defined by the reflector surface will not exceed, in any orbit positions, ± 0.13 inches in the axial direction and a radius of 0.05 inches in the lateral plane (perpendicular to the reflector axis), relative to the best fit focal point location of the perfect flex-rib.

The deviations of the actual reflector surface from the theoretical paraboloid in a direction normal to the surface are presented for orbit hours 4 and 11 in Figure 8.4-5 and 8.4-6. Figure 8.4-7 denotes the numbering system used for identifying rib and mesh points.

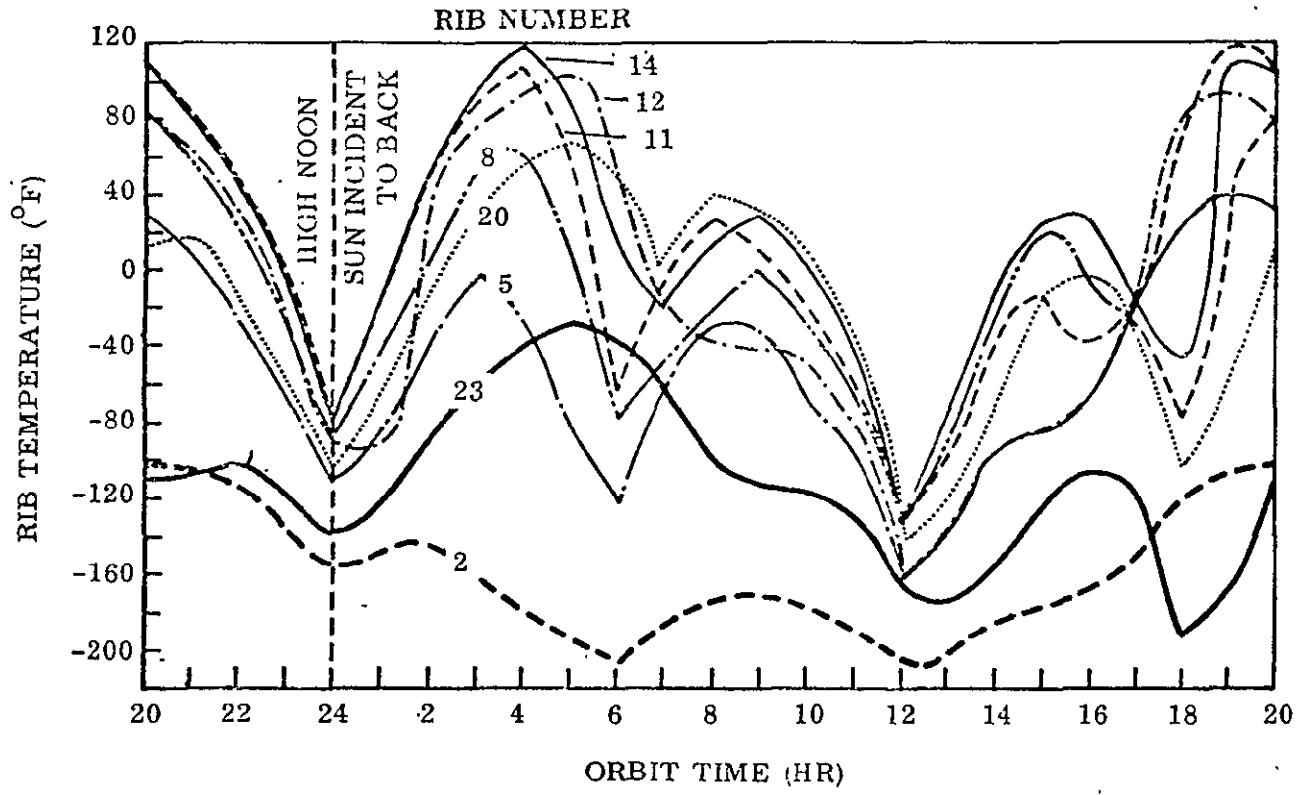


Figure 8.4-1. Temperature History of Ribs

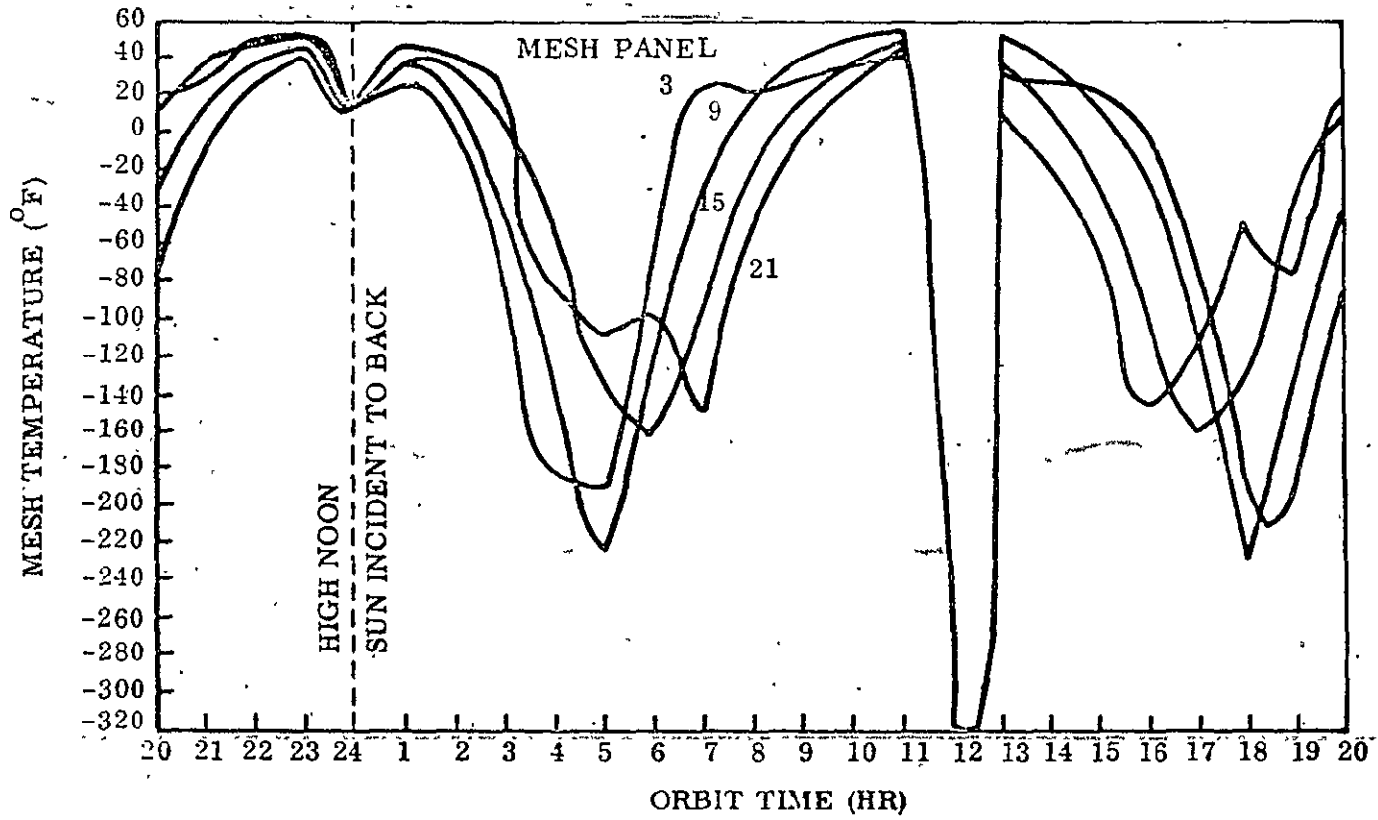


Figure 8.4-2. Temperature History of Mesh Panels

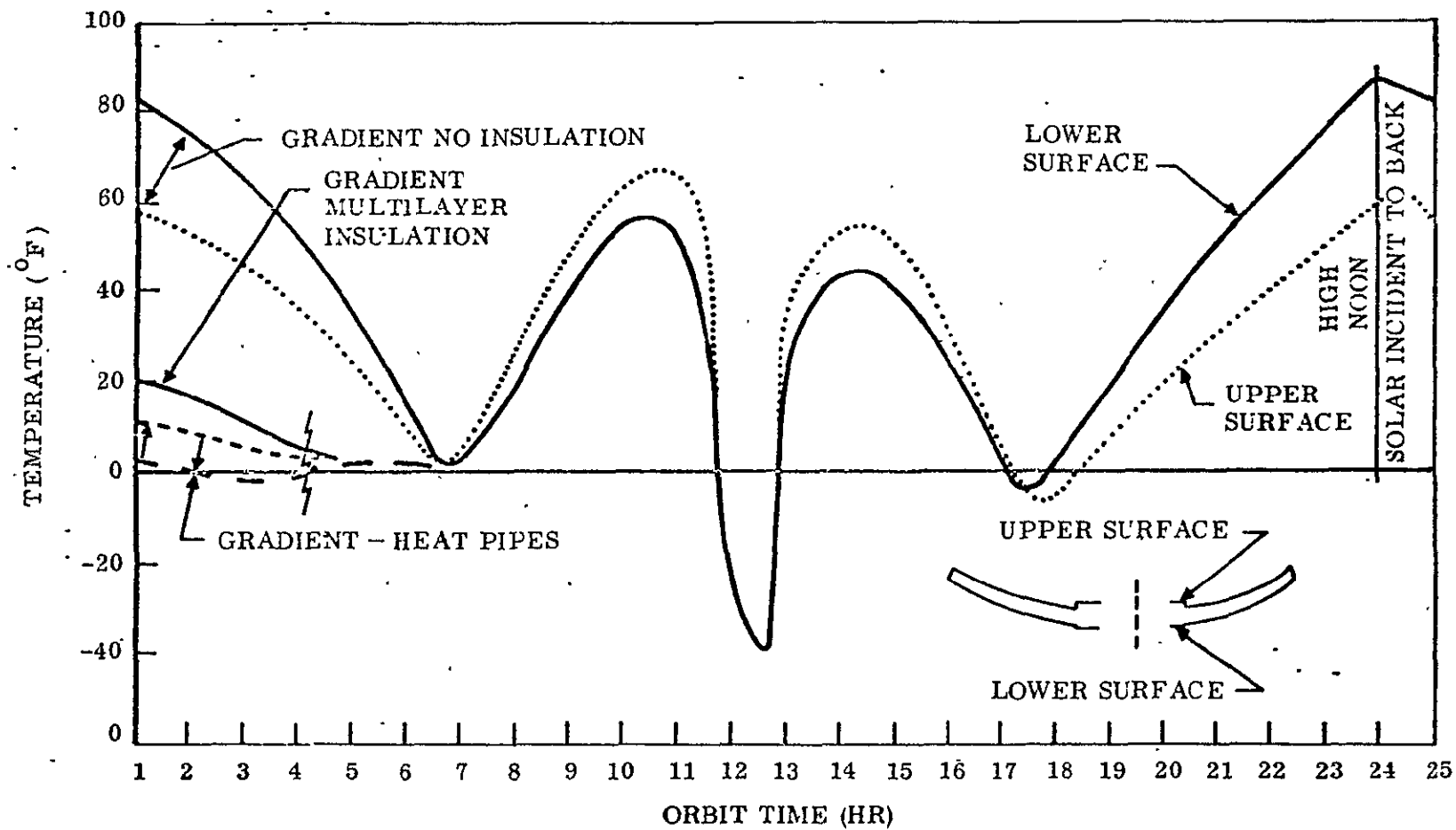


Figure 8.4-3. Hub-Surface Temperature Histories

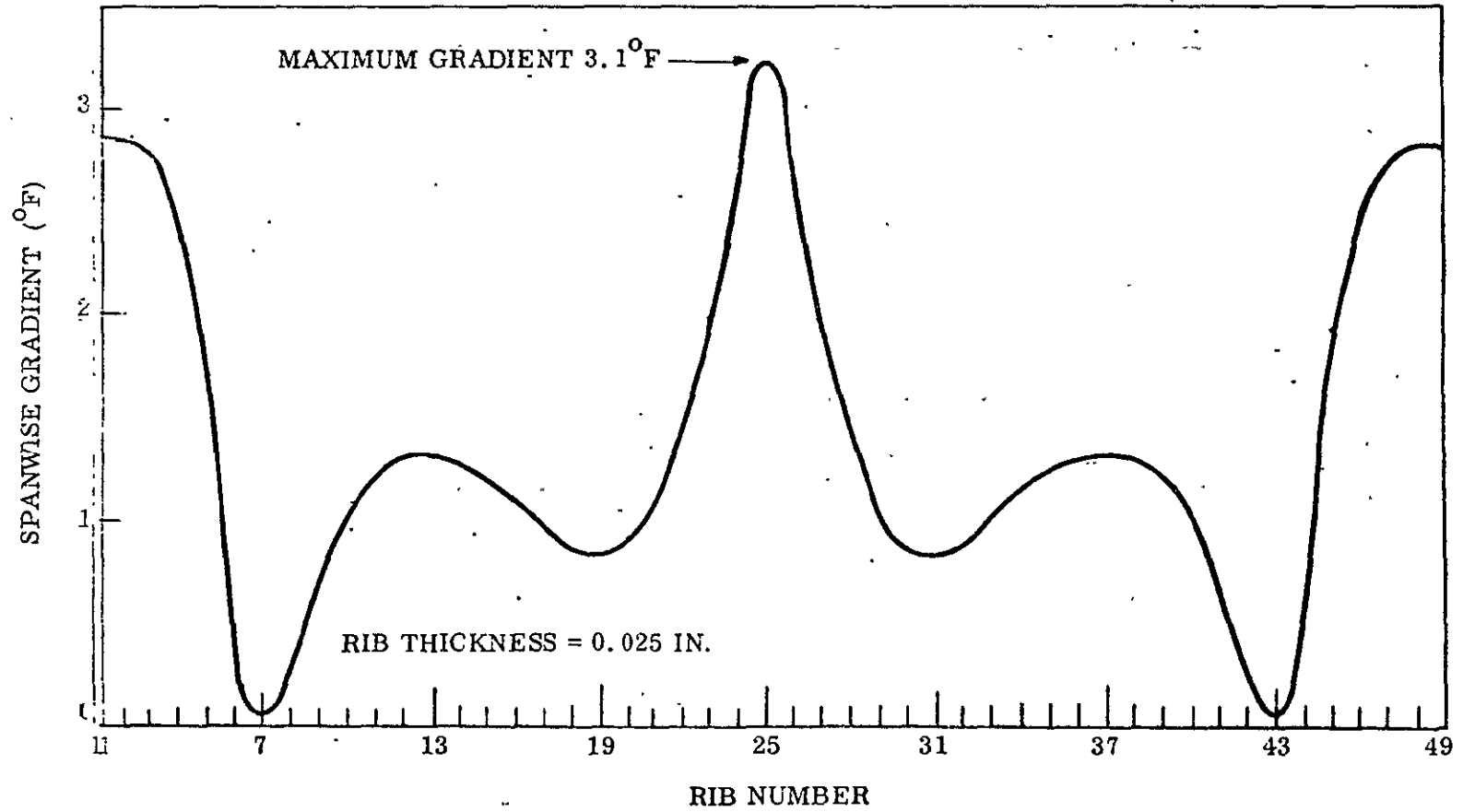
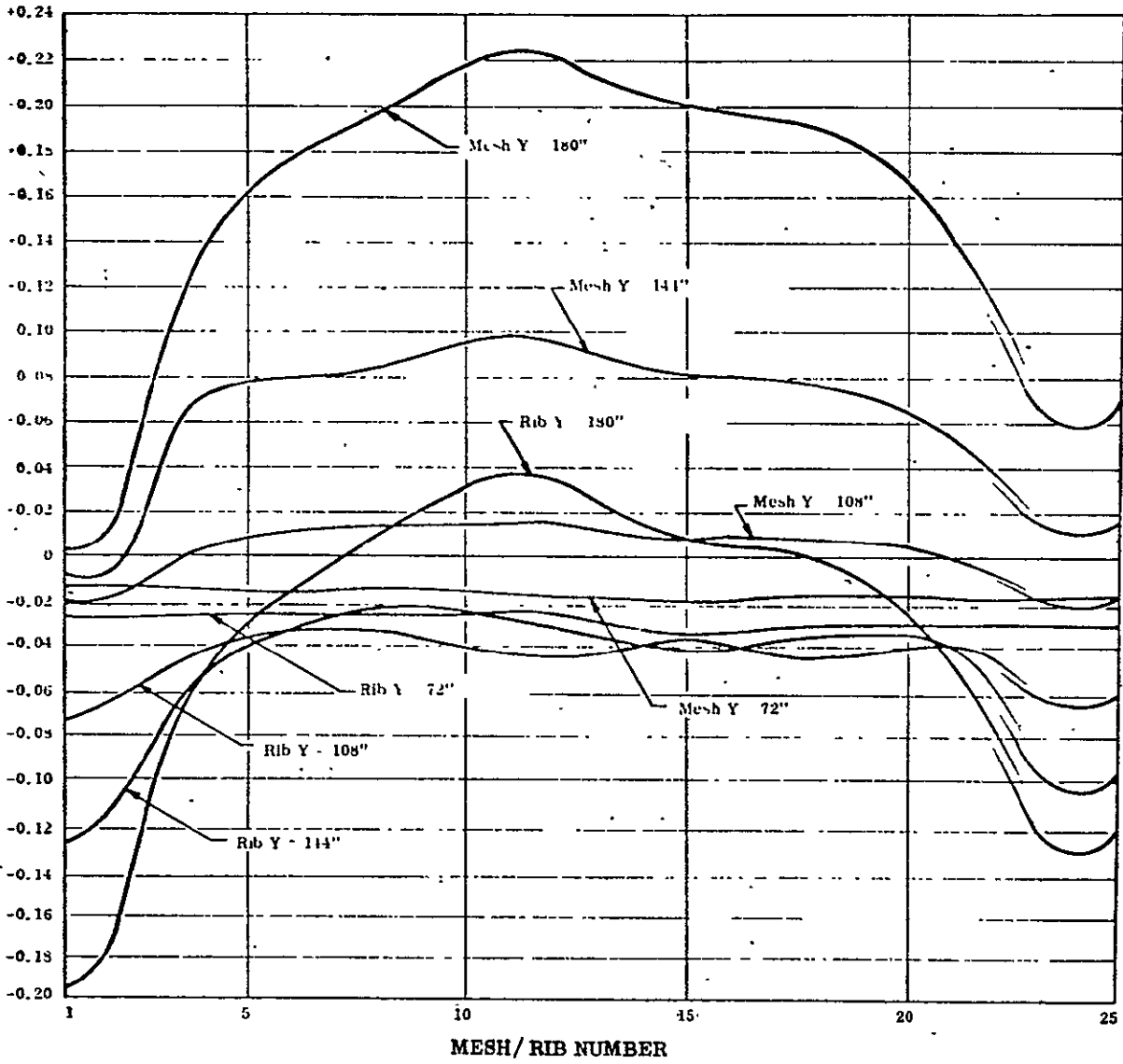
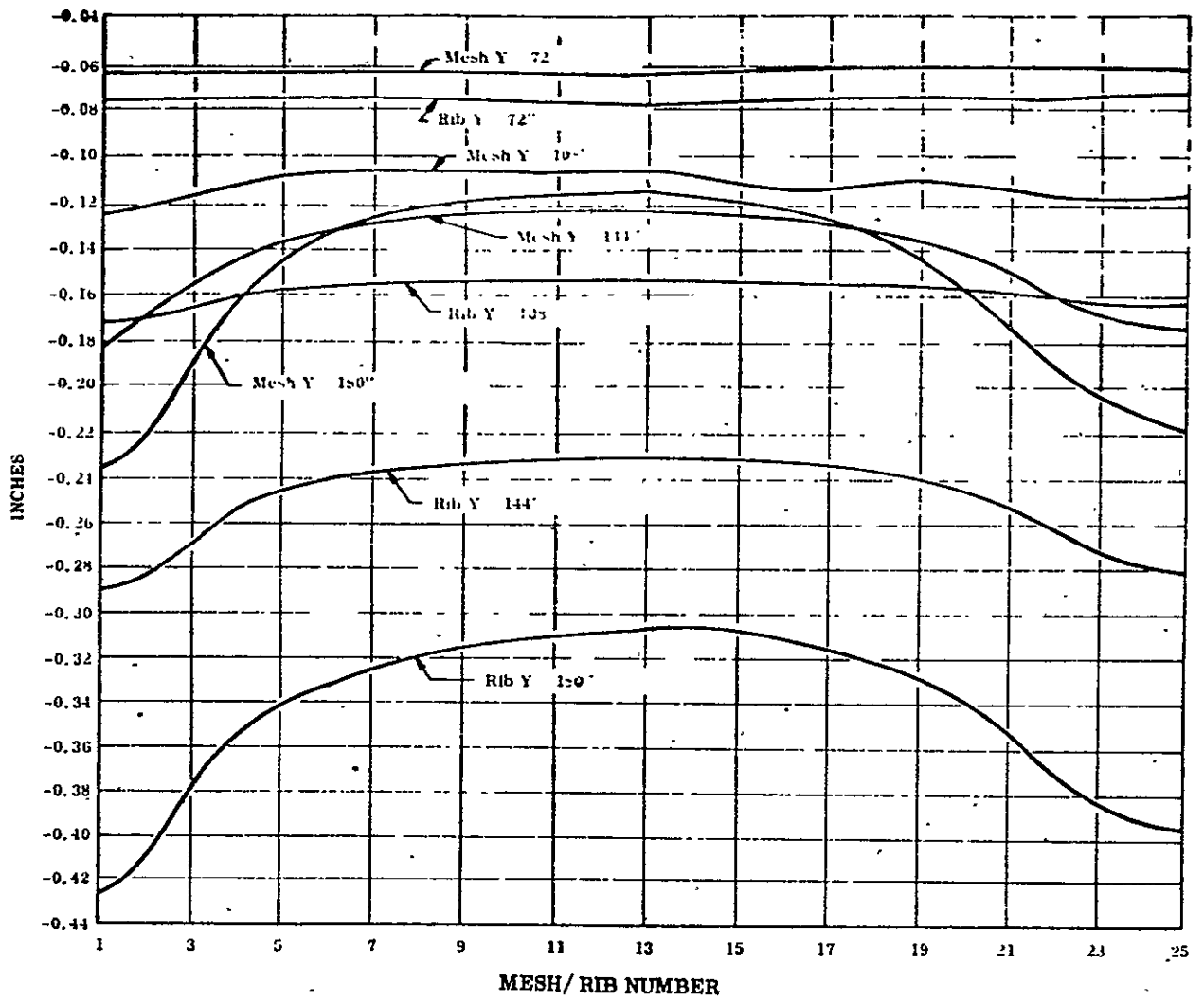


Figure 8.4-4. Maximum Spanwise Temperature Gradients



Reproduced from
 best available copy.

Figure 8.4-5. Surface Deviation from Theoretical Paraboloid at Orbit Time Hour 4



Reproduced from
best available copy.

Figure 8.4-6. Surface Deviation from Theoretical Paraboloid at Orbit Time Hour 11

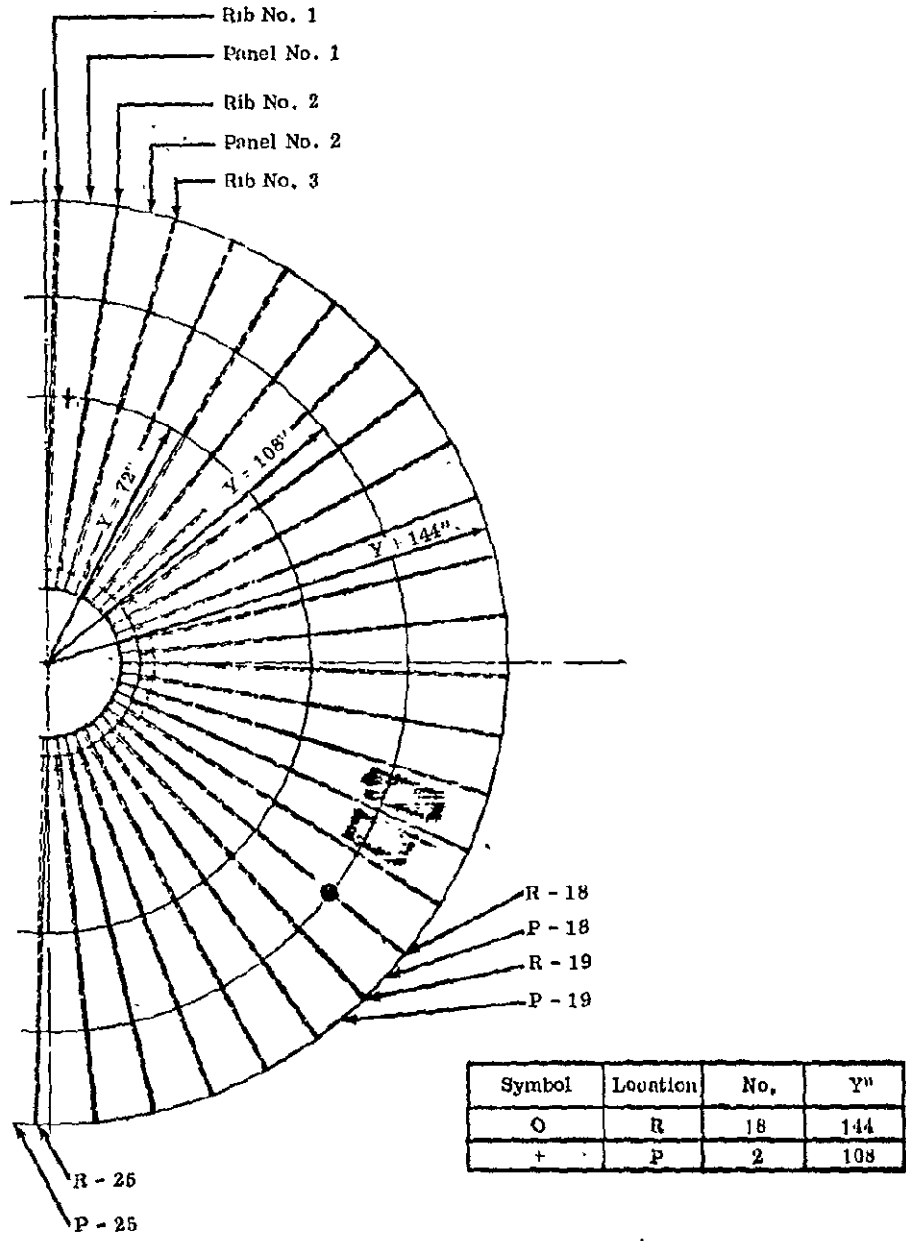


Figure 8.4-7. Numbering System of Ribs and Mesh Points

It should be noted that the maximum surface excursion at orbital hour 4 (Figure 8.4-5) from the basic paraboloid surface is 0.228 inch above contour for the center line of one surface mesh panel at the tip. The maximum rib tip excursion at this time is 0.198 inch below contour. The maximum rib tip excursion and the maximum mesh excursion do not occur in the same panel, as can be seen in the figure. With the chosen values of pre-tension and pre-set used, the worst condition shows the rib tips to be 0.426 inch below basic parabolic surface contour at orbital hour 11 (Figure 8.4-6).

Figure 8.4-8 shows the orbital history of surface rms condition of the selected design, for the equinox (maximum umbra) i.e. $\beta = 0^\circ$, and solstice, i.e. $\beta = 23.5^\circ$, conditions. The average rms value for a full 24-hour orbit is 0.049 inch. Peak rms value for period of orbital hour 13 to 14 varies from 0.101 to 0.072 inch.

The minimum rms value is 0.032 inch. This value lies above the minimum rms value of 0.025 inch corresponding to mesh flatness alone and indicates that additional optimization of design could lower the average orbital surface rms value. However, this may simultaneously result in an increase of the maximum rms, for example at hour 11.

Conversely, by modifying the chosen pre-tension and pre-set towards lower values, the maximum excursion from basic paraboloid may be reduced, for example at hour 13. However, it should be remembered that higher values of surface rms will be obtained during orbital hours 1 to 8 and 17 to 24, with a resultant higher average value of surface rms during the total 24-hour orbit.

The greatest excursion of the chosen design occurs for a short period only during a relatively unimportant orbital hour period, namely around 1 AM local time at the satellite subpoint, while a relatively even, low value of rms occurs over the more useful long period from hour 17 through hour 8 which is 5 AM to 8 PM local time at the satellite sub-point. Therefore it was decided to show this design, as it possesses near conformancy over the longest period of time.

Adjustments of the relative values of these excursions can be easily made to suit the desired requirements, by merely changing the values of the rib pre-set and/or the mesh pre-tension.

8.4.3 RF PERFORMANCE

The rf performance of the reflector was determined at two orbit positions, namely those corresponding to orbit hours 11 and 4. Orbit hour 0 is defined as the time when the spacecraft is on the far side of the earth, as viewed from the sun. The reason for this choice was based on LMSC's prior experience which indicated that for a normal choice of ΔV and ΔL_g values, hour 11, which is just prior to the spacecraft entering the earth shadow, is generally representative of a near maximum gain degradation—excepting those conditions that are affected by earth umbra, while hour 4 has a performance that is near the orbital average.

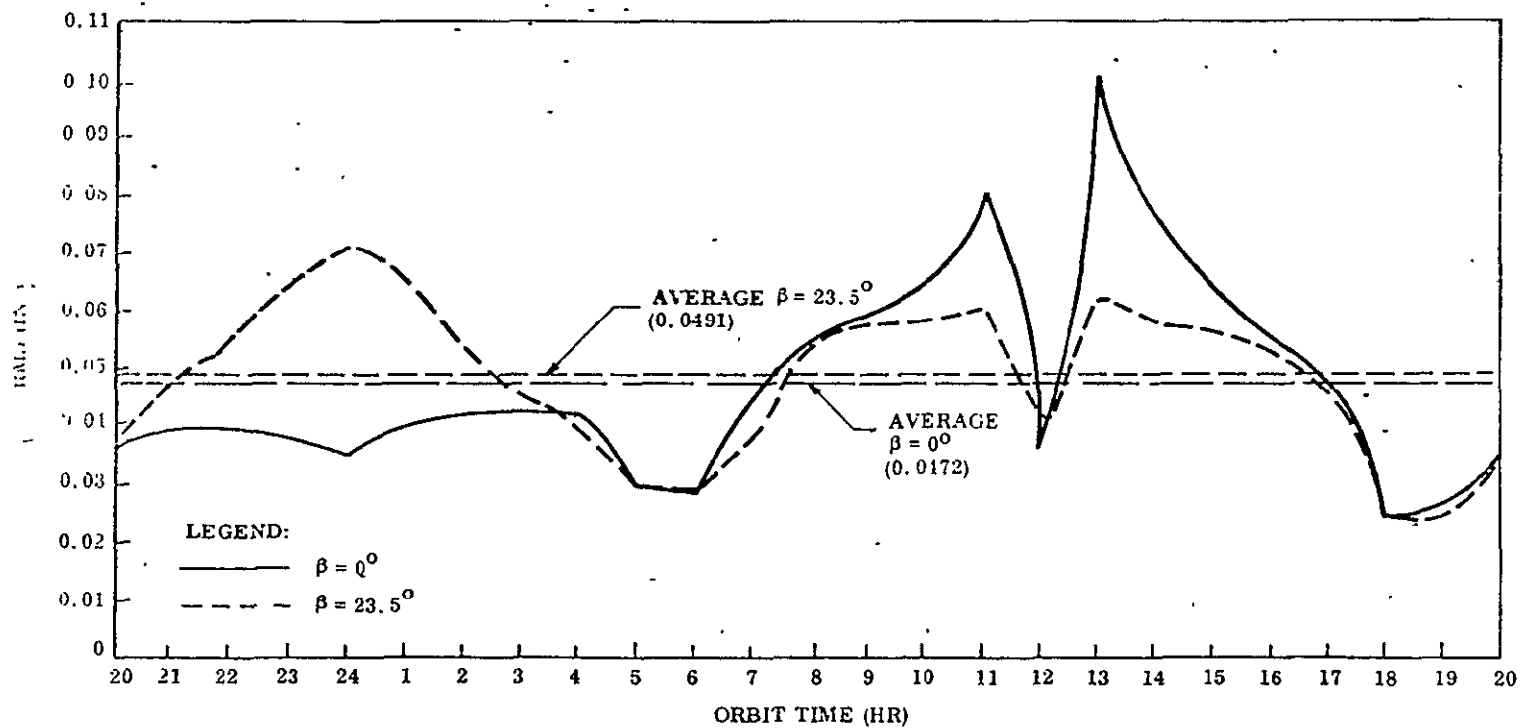


Figure 8.4-8. RMS vs. Orbit Time

The On-axis gain was determined for these two orbital cases for an operating frequency of 8 GHz, with an ideal $(\cos^{2.5})$ feed providing an illumination edge taper of approximately -10 dB and without blockage losses. The gain was found to be 55.4 dB for the orbital average case (hour 4) and 55.0 dB for the maximum loss case excluding umbra conditions (hour 11).

These losses include the following approximate individual loss contributions.

Flats effect (perfect flexrib)	0.3 dB
Manufacturing Tolerance effects	0.1 dB
Deployment repeatability effects	0.1 dB
Hole in the center of the reflector	0.5 dB
Effects of the illumination taper	1.0 dB
Thermal effects, hour 4	0.1 dB
Thermal effects, hour 11	0.5 dB
Total reflector losses, hour 4	2.1 dB
Total reflector losses, hour 11	2.5 dB

The theoretical gain of a true paraboloidal surface of this size, at the same frequency is 57.5 dB.

The minimum on-axis gain of the reflector at the earth's shadow will be approximately 1 dB below that at hour 11, or 54 dB.

8.4.4 RELIABILITY

The reliability for reflector deployment will be in excess of 0.9999.

The predicted reliability for operation during a five year period with a performance degradation not exceeding 1 dB is 0.99.

8.5 DESIGN PROCEDURE

8.5.1 GENERAL DESIGN APPROACH

Exposure of the reflector to the varying thermal environments will cause the hub structure and ribs to deform from their initial position. To minimize the excursions of the actual flexrib surface from that of the theoretical paraboloid, the mesh is assembled onto the ribs so that an adequate initial tension load is applied, preventing the mesh from going slack under any anticipated mission environments.

This is accomplished by fabricating the mesh panels under-size and simultaneously pitching the ribs slightly outward, at their attachment points to the hub (away from the reflector surface). The measure of mesh panel shortening, called pre-tension (ΔL_s), is the amount of reduction of the manufactured panel width at the rib tips compared to that in the perfect flexrib, and is expressed in inches. The measure of rib pitching, called pre-set (ΔV_s), is the distance from the tip of the unrestrained rib, i. e. without the mesh attached, to its theoretical position on the perfect flexrib which is measured in a direct parallel to the reflector axis, and is expressed in inches.

With all other physical characteristics and design details of the reflector fixed, the value of these two design variables will determine the actual configurations that the reflector surface will assume at the various orbit positions. Therefore, they can be used as a major design tool to:

- Minimize the worst case rf losses (i.e. the largest deviations from perfect flexrib) during mission
- Minimize the mean value of the losses over a single orbit for any particular time of the year or over the entire year
- Restrict the occurrence of the maximum loss to any particular orbit position (time of the day)

The final selection includes a trade-off between the relative values of these characteristics to the mission, from an overall system operation point of view.

The stiffness of the ribs in the direction perpendicular to the reflector surface is another variable that influences the elastic balance between mesh and ribs and, thus, the thermal deflections of the surface. However, there are other additional requirements that have to be satisfied by appropriate selection of rib shape and materials properties. The 1-g deployment requirement favors high stiffness of the rib in all directions since the reflector must successfully deploy and support itself in all three main orientations. The consideration of deployment reliability, minimum deployment envelope and high natural frequencies all require high stiffness values, particularly in the lateral (wrapping) direction of the ribs. In contrast, minimizing the stress level buildup in the stowed ribs requires a high flexibility, i.e. a low stiffness of the ribs in the lateral direction. The weight criterion dictates minimization of the rib stiffness in all directions.

The contradictory nature of these requirements requires that a complex optimization process be employed to develop the affected design details (number of ribs, rib shape, and material, values of pre-set and pre-tension, etc.) that will ensure that all the various design objectives are simultaneously satisfied. This procedure must also consider the design parameters, which, although not directly involved in the optimization process, influence the relevant characteristics and performance of the reflector, (e.g., thermal and structural properties of the hub, thermal controls employed on the hub, and ribs, etc.)

The optimization process consists of a successive reiteration of the various design analyses involved. The process starts with an initial choice of the optimization variables and changes them in the course of the process as required. This is done until a set of values is reached that will satisfy all requirements.

8.5.2 DESIGN OPTIMIZATION PROCESS

The rf gain of the flexrib reflector cannot be correlated with rms deviations in the same manner as that in normally used for standard solid surface reflectors. The reason is that the latter generally have surface errors randomly distributed over the surface, whereas the major flexrib surface deviations have a

definite systematic nature: both the approximation errors as well as the thermal deflections increase with radius. Therefore, the gain analysis is the only true verification that the reflector will produce the desired gain under all operational conditions. Nevertheless, a reasonably close relationship between gain (G) or gain degradation (ΔG) and surface rms has been shown to exist. This permits working in the design optimization process, at least in its preliminary phases, primarily with the rms values of surface deflections rather than the gain values which require lengthly and complex additional computer analyses.

These rms deflection values are used for conducting a number of parametric studies, to evaluate the effects of various design variables. Typically, the orbital average of the rms values is computed and plotted as a function of ΔV and ΔL_S for fixed values of the other parameters. Figure 8.5-1 illustrates such a parametric plot, which can be used to establish the corresponding ranges of ΔV and ΔL_S in which the mechanical tolerances applied to these dimensions will have the least effect on the rms values.

Plots of orbital rms histories for various values of ΔV and ΔL_S in the selected ranges will provide further performance details, specifically, the relative magnitudes of peak-gain losses, as well as their occurrence in time (orbit position) and also the periods of relatively high-gain conditions. This information is essential for making the trade-off decisions in this particular area.

Parametric curves of rms histories are plotted for a number of design parameters that require selection on the basis of their effect on reflector gain, i.e., rms history. Figure 8.5-2 shows, for example, the effects of various hub thermal gradient control methods.

Simultaneously, an optimization trade-off study is performed in the structural-dynamic area, determining the effects of rib size, shape, and material properties upon the reflector natural frequencies, deployment loads, rib stresses, one-g testability, and weight.

The parametric studies lead to a direct selection of many design variables (not involved in the design optimization processes) such as thermal controls. These studies also provide a definition of compatible selection ranges of the optimization variables.

The results are then used to formulate a candidate rib design, a tentative ΔV and ΔL_S selection and a hub design in sufficient detail to define its effects on reflector surface deviations and on the structural-dynamic problems.

The candidate design is then properly evaluated through the design analyses, including the use of the rf analysis to determine maximum and average losses and corresponding gain values. Additional design factors, such as mechanical tolerances, are also assessed and their effects included in the analysis.

If any of the specification requirements are not met, a suitable change in the selection of variables is made and the affected analyses are repeated. The process is continued until all requirements are simultaneously satisfied, and all variables and design details are specified.

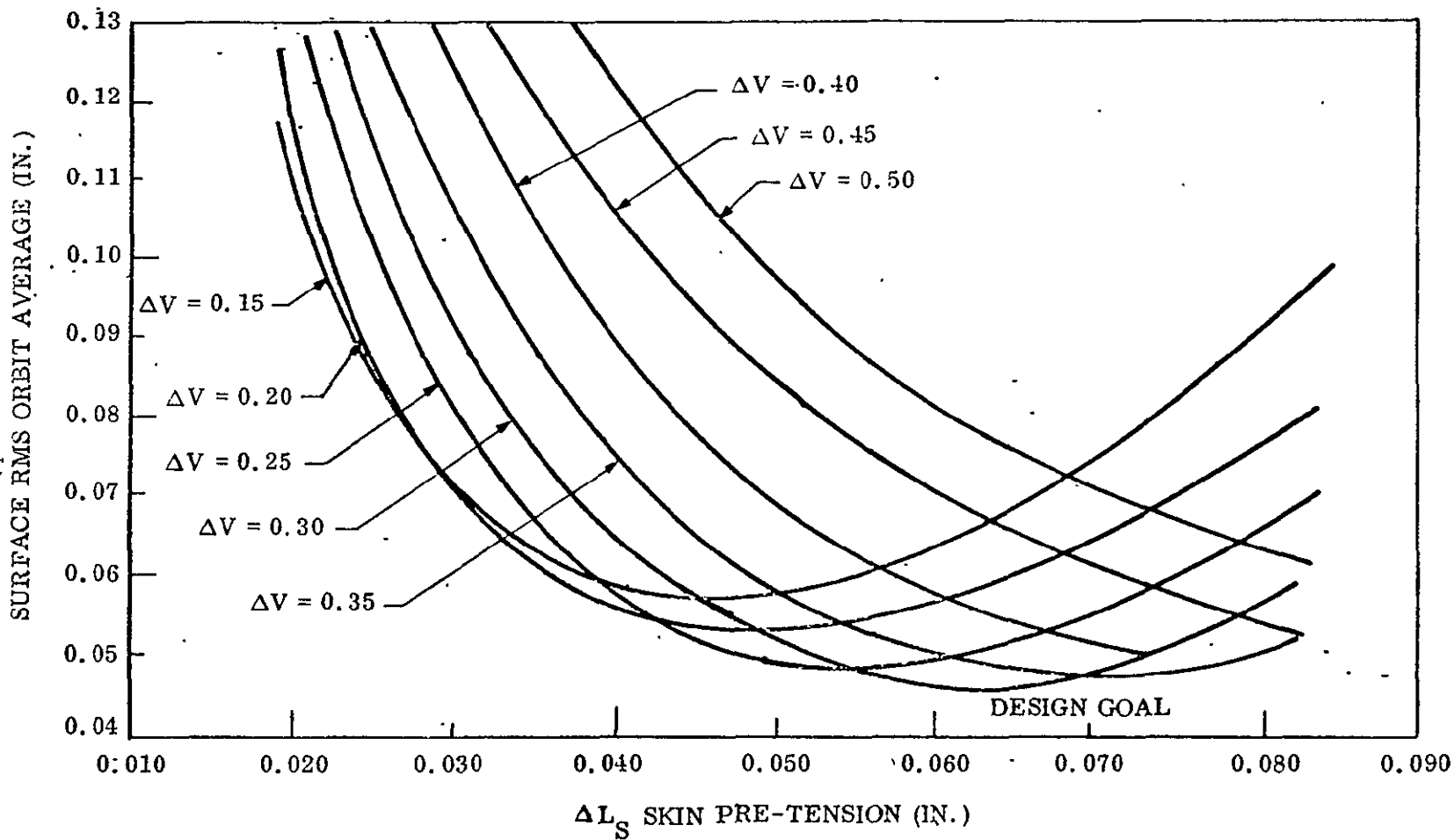


Figure 8.5-1. Typical Variable Optimization

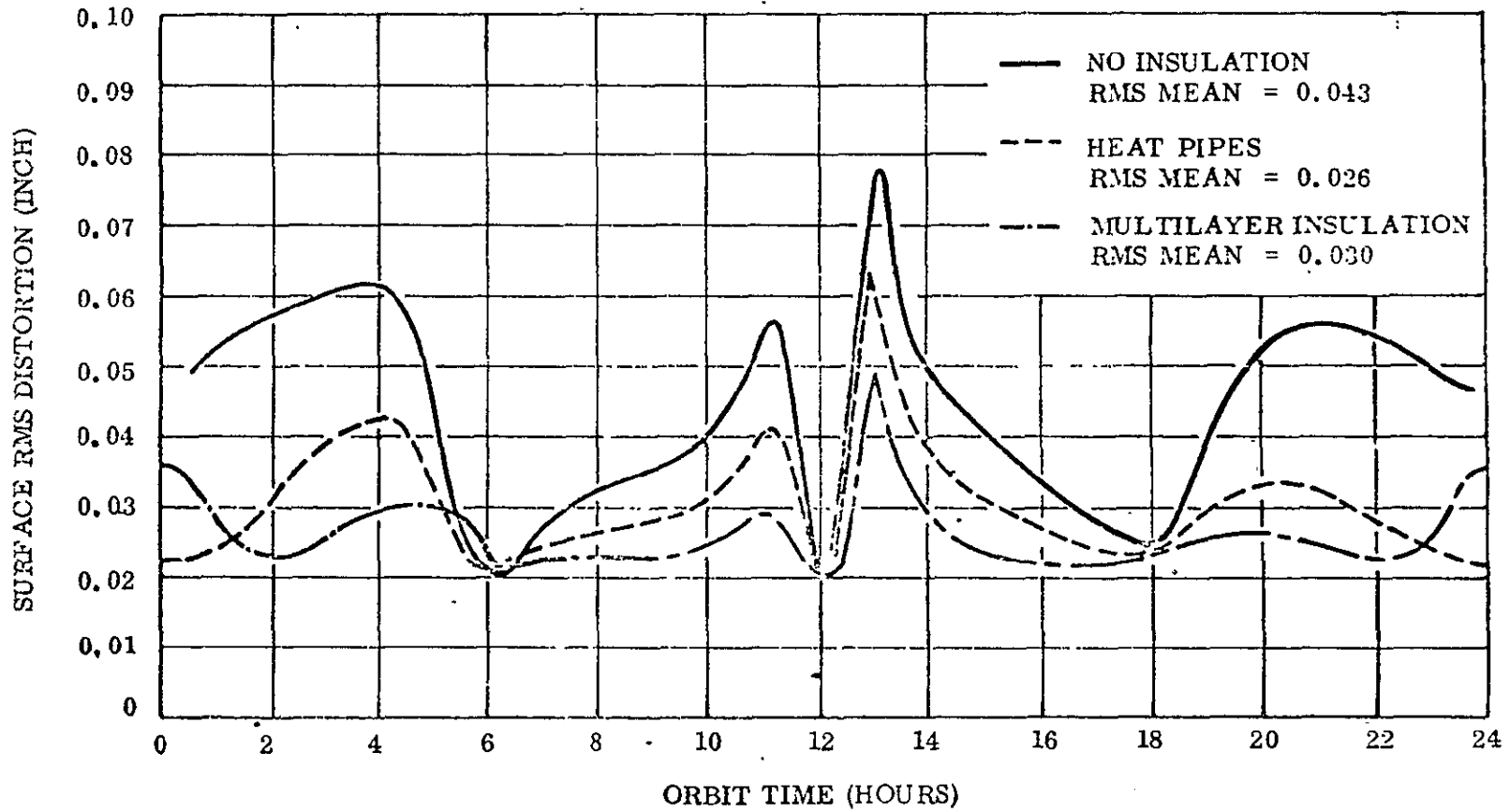


Figure 8.5-2. RMS Distortion History

8.5.4 FINAL DESIGN SELECTION

The performance of the reflector will be validated to a major extent, by the test program conducted on the completed reflector. Any discrepancies beyond the inherent inaccuracies involved in the analyses and excluding any specific effects or peculiarities of the test conditions will be resolved by tracing the discrepancies back to their causes and making appropriate corrections and modifications to the analyses.

A final design analysis will be performed in any area that may be affected by such changes. Any necessary modifications will be made to the reflector design if the performances predicted by the verified analyses are not with specification requirements. It is anticipated that any performance changes that may be required will be capable of being accomplished by merely changing the values of pre-set (ΔV) and pretension (ΔL_S).

8.6 MANUFACTURING PROCEDURE

8.6.1 COMPONENT PARTS FABRICATION

The ribs are made of 0.080 - inch thick 7178 aluminum alloy chemically milled to precise tapered thicknesses and formed into the desired shape. First, an accurate template establishing the physical shape of the rib flat pattern, will be made using computer data. This template will be used to make a routing tool, which will be used to cut out the flat blank for the ribs. The ribs will be formed on a common die to ensure the same physical shape in all ribs. Special care will be taken to minimize distortion due to forming stresses and heat treatment, thus ensuring that all rib blanks are identical prior to entering the chemical etching bath. During chemical etching, all 48 ribs will be held by a specially designed cage and lowered tip first into the bath at a controlled rate, thus resulting in uniform rib etching. Each rib will be the same size, shape, thickness, and weight and should therefore exhibit similar stiffness characteristics. A final rib contour fixture will be used, enabling the precise trim of the reflector side. A holding fixture will be used to position the hinge properly during attachment to the rib.

Raw panels of mesh will be chemically plated and treated, then cured in rigid framework. The panels will be tested for rf characteristics, and then trimmed to size and shape.

The 48 pie-shaped mesh panels will be bonded together with the aid of a reflector assembly fixture to form the parabolic-shaped mesh reflector. The fixture resembles the convex side of a parabola with the size and shape of the mesh reflector in a free (non-tension) state. Adjustments are provided to change the size of the fixture slightly, which in turn changes the size of the mesh reflector that is assembled upon it.

8.6.2 REFLECTOR ASSEMBLY AND ALIGNMENT

The final assembly and adjustments are performed on the reflector assembly fixture.

The assembly procedure will involve first adjusting the ribs to the original design value of ΔV by optically measuring the rib tip position prior to attaching it to the mesh. Next, the ribs will be forced down on the mesh assembly mold

to touch the mesh and will be attached to the latter. The assembly will then be released from the assembly mold on which the mesh surface had been fabricated, and the rib tip positions attained measured, using optical techniques. If they are not in the position predicted by the design, that means the mesh has not been made to the correct size. Therefore, the mesh pretension adjustments will be used to set the rib tips in their correct position without changing the rib pitch, i.e., the value of ΔV . Once this has been accomplished, indicating that both ΔV and ΔL_S have been set to their design values, the adjustments will be locked in position. Further changes will only be made to change ΔV or ΔL_S values. Any such changes will be recorded to know the actual ΔV and ΔL_S settings of the reflector at all times.

Installation of the hub thermal control blankets will involve the bonding of the fiberglass batting and velcro fasteners to the hub skin with an epoxy adhesive. The mating half of the fastener will be fabricated as part of the individual blanket modules. Each unit will be prefitted prior to final installation.

8.7 SPACECRAFT INTEGRATION

8.7.1 SPACECRAFT INTERFACE REQUIREMENTS

The spacecraft interface must be designed to accommodate the outline and mounting requirements of the stowed reflector shown in Figure 8.7-1. In addition, a minimum clearance must be maintained above the reflector, on the convex side to insure interference free deployment. This minimum required envelope is a cone with its apex at the center of the top surface of the reflector hub, and with its mantle 18 inches above the same reference surface at a diameter of 30 feet.

The structure supporting the reflector must have the required strength to safely support the reflector during all launch, orbital, and terrestrial (handling and test) loadings, and to withstand deployment torques of up to 7500 ft-lbs. (This includes a 15 percent margin above the maximum allowable peak value of deployment torques and moments specified for the reflector).

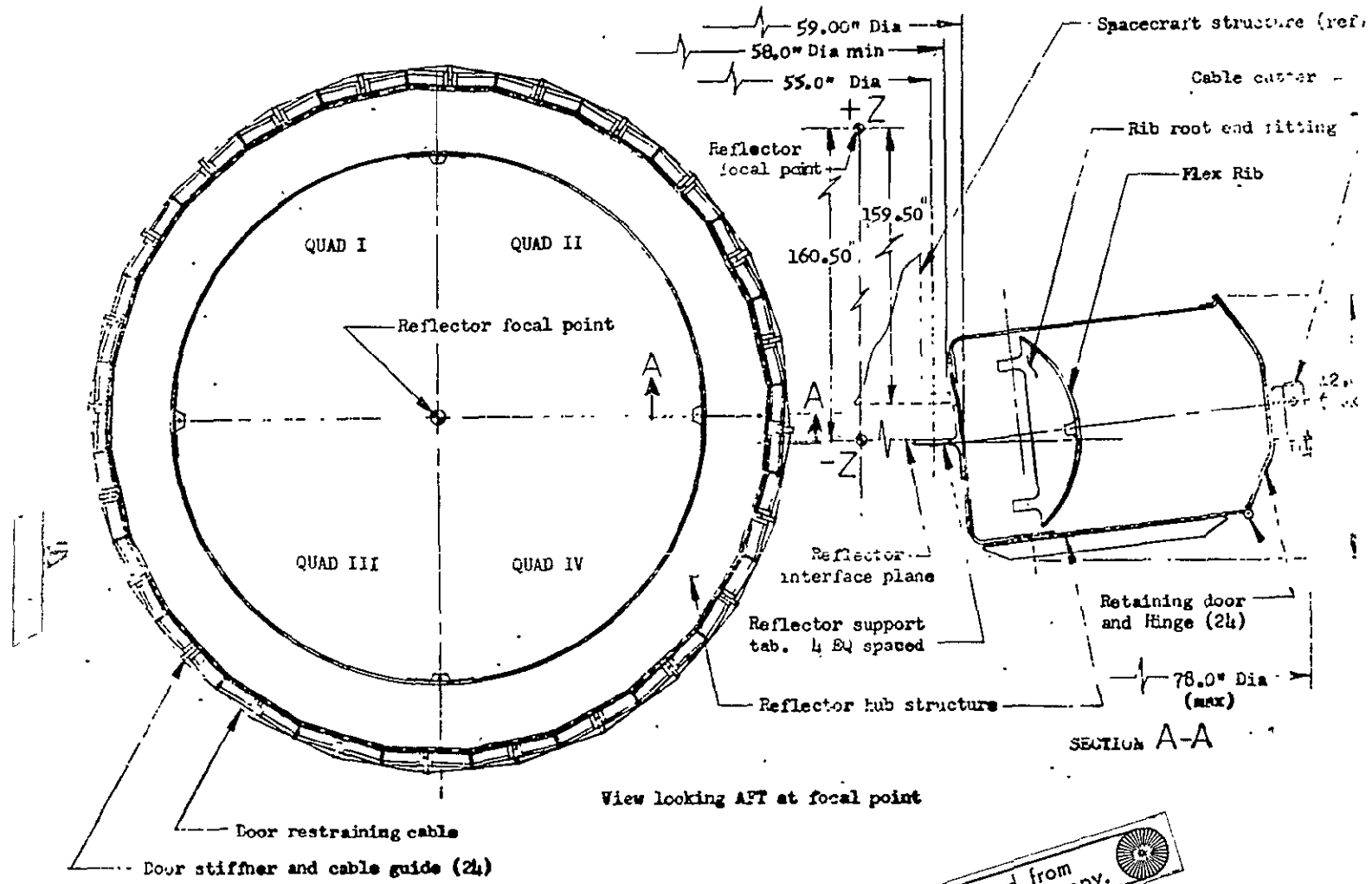
The spacecraft interface must be machined using the same master tool that will be used in machining the mating interface on the reflector hub.

The design of the electrical interfaces, i.e. the connectors for the deployment actuator power and the deployment indicator signals must be coordinated with LMSC to insure compatibility.

Reflector deployment initiation power must be simultaneously provided by two independent signal sources, to separate circuits at the interface connectors. Each source must provide a 20 to 28 V, 10 amp pulse of 10 msec duration, for firing the pyrotechnic cable cutters.

8.7.2 REFLECTOR ALIGNMENT WITH SPACECRAFT

Lateral alignment of the reflector with the spacecraft will be accomplished through use of the common interface fabrication master tool. The apex of the reflector paraboloid will be located at the center of the mounting interface defined by the master tool within a tolerance of 0.03 inches.



Reproduced from
best available copy.

Figure 8.7-1. Parabolic Reflector in Stowed Configuration

Angular alignment of the reflector axis onto the center of the composite feed will be accomplished using an optical alignment fixture, by differential shimming in the reflector-to-spacecraft interface underneath the four mounting lugs. This alignment fixture will consist of an autocollimation mirror supported at the center of the reflector hub by a rigid spider which will attach to the reflector hub using appropriate reference hard-points.

The procedure for aligning the reflector on the spacecraft will consist of the following steps:

- (a) The alignment fixture will be attached to the reflector, using the appropriate shims in the interface.
- (b) Sighting with a theodolite auto-collimated onto the mirror on the alignment fixture, the reflector will be aligned onto the center of the X-band feed horn of the composite feed sub-assembly. Shims will be provided at the four reflector mounting points as necessary for this purpose.
- (c) The feed-to-reflector distance will then be measured, and uniform shims provided under all four reflector mounting points to correct it to the required value.

The above mentioned feed to reflector distance will be that required for optimum RF performance of the reflector subsystem operating in conjunction with the composite feed subsystem. This distance will be established by an RF Integration Test performed on the prototype subsystems.